Investigations into the Chemistry of Highly Fluorinated Phosphorus Alkoxides

Sharifa Hussein

Doctor of Philosophy Degree

University of York

Department of Chemistry

September 2012

ABSTRACT

This thesis covers the diverse chemistry of fluorinated phosphorus alkoxides, which display Lewis basic, Lewis acidic, weakly coordinating anion or cation chemistry, depending on the number of substituents at the phosphorus centre. The chemistry of highly fluorinated phosphorus (III) alkoxides with the general formula $PR_{3-n}(OR^F)_n$ {R = Ph; OR^F = $C(CF_3)_3$, $CH(CF_3)_2$; n = 1 to 3} has been re-explored after initial work in the area from the late 1970s.[1,2] These are found to be useful as ligands with the combined properties of being both electron-poor and sterically bulky, an area in ligand space that to date is sparsely filled. In order to assess the steric properties of the ligands, Tolman "ligand cone angles" (θ) have been calculated for $[Ni(CO)_3L]$ and $[W(CO)_5L]$ complexes of each ligand from DFT optimised structures at the (RI-)BP86/SV(P) level and for $[Ru(\eta^5\text{-}C_5H_5)(NCMe)_{2-n}L_{1+n}]^+[PF_6]^-$ (n = 0, 1) and $[RhCl(CO)L_2]$ complexes from single-crystal X-ray diffraction data. The first structural characterisation of a metal complex with the tris(perfluoro-*t*-butyl)phosphite, $[Ru(\eta^5\text{-}C_5H_5)(NCMe)_2P\{OC(CF_3)_3\}_3]^+[PF_6]^-$ (θ = 195 °) is also reported. Structural analysis of $P\{OC(CF_3)_3\}_3$ suggests it is very rigid without significant conformational flexibility compared to the $P\{OC(CH_3)_3\}_3$ analogue. The electronic properties of these ligands were assessed using both a method suggested by Gusev involving the CO stretching frequencies and bond lengths of a [IrCpCOL] complex. The use of experimental data; $^1J_{PW}$, $^1J_{RhP}$, IR data from $[W(CO)_5L]$ and M-P bond lengths (M = Ru, Rh) from $[Ru(\eta^5\text{-}C_5H_5)(NCMe)_{2-n}L_{1+n}]^+[PF_6]^-$ (n = 0, 1), $[RhCl(CO)L_2]$ complexes were also employed.[3] Interestingly the fluorinated phosphites; $P\{OCH(CF_3)_2\}_3$ and $P\{OC(CF_3)_3\}_3$ are found to have similar electronic properties to the incredibly electron-poor PF_3 ligand, but with added steric bulk. In addition, preliminary investigations into the synthesis of highly fluorinated alkoxy-containing phosphonium cations which have the potential to form base resistant cations have been explored. For example, oxidation of highly fluorinated alkoxy-containing phosphorus (III) ligands have also been achieved, resulting in the formation of phosphonium cations such as $[MePPh_2OCH(CF_3)_2]^+[O_3SCF_3]^-$. In addition to new cations, the potential for P(V)-alkoxides to form new WCAs has been explored. For example, the synthesis of a novel suprafluorophosphate anion, $[P\{OCH(CF_3)_2\}_5F]^-$ has been investigated. This anion has been isolated as the following novel salts; $[Ag(NCMe)_4]^+[P\{OCH(CF_3)_2\}_5F]^-$, $[Na(NCMe)_6]^+[P\{OCH(CF_3)_2\}_5F]^-$, $[Ag(PR_3)_3]^+[P\{OCH(CF_3)_2\}_5F]^-$; R = Ph, ^{i}Pr, Me, and $[NEt_4]^+[P\{OCH(CF_3)_2\}_5F]^-$, some of which are even stable towards hydrolysis at room temperature. This suggests there is potential for the $[P\{OCH(CF_3)_2\}_5F]^-$ anion to be the next generation of $[PF_6]^-$ type anion.

TABLE OF CONTENTS

ABSTRACT I

TABLE OF CONTENTS II

LIST OF FIGURES X

LIST OF SCHEMES XIX

LIST OF TABLES XXIII

LIST OF EQUATIONS XXVI

ACKNOWLEDGEMENTS XXVII

DECLARATION XXVIII

1 INTRODUCTION 1

2 BULKY, ELECTRON-DEFICIENT PHOSPHORUS (III) LIGANDS 5

2.1 LITERATURE REVIEW 5

2.1.1 Review of Common Ligand Steric Descriptors 5

2.1.2 Review of Common Ligand Electronic Descriptors 14

2.1.3 Review of Stereoelectronic Maps of Phosphorus (III) Ligands 20

2.1.4 Known Bulky Electron Deficient Phosphorus (III) Ligands 22

2.1.5 Highly Fluorinated Phosphites 26

2.1.6 Hexafluoroisopropoxy Phosphite, $P\{OCH(CF_3)_2\}_3$, (**1**) in Catalysis 27

*2.1.6.1 Catalysis of the Diels-Alder [4+2] Cycloaddition with a **[Rh(I)]** Metal Centre 27*

*2.1.6.2 Catalytic C-C Coupling of (Hetero)Arenes with a **[Rh(I)]** Metal Centre 29*

2.1.6.3 Catalysis for the β Selective Functionalisation of Thiophene with a [Pd(II)] Metal Centre 31

*2.1.6.4 Catalytic Hydroformylation with a **[Rh(I)]** Metal Centre 33*

2.2 RESULTS AND DISCUSSION 34

2.2.1 Highly Fluorinated Phosphorus (III) Ligand Synthesis 34

2.2.2 Highly Fluorinated Phosphorus (III) Ligand Hydrolysis 38

2.2.3 Steric Properties of the Novel Bulky Electron Deficient Phosphorus (III) Ligands 41

2.2.3.1 Cone Angle Calculations (From Experimental and DFT Studies) 41

2.2.3.2 Single-Crystal XRD Structural Data for the Perfluoro-t-Butyl Phosphite, $P\{OC(CF_3)_3\}_3$, (2) *48*

2.2.3.3 Spacefill Models of DFT Optimised Free Ligands *49*

2.2.4 Electronic Properties of the Novel Bulky Electron-Deficient Phosphorus (III) Ligands 52

2.2.4.1 Electronic Properties Assessed Using the [CpIr(CO)L] Model Complex *52*

2.2.4.2 $^1J_{WP}$ Coupling Constants for $W(CO)_5L$ Complexes *60*

2.2.4.3 IR Data (Experimental and DFT) for$[W(CO)_5L]$ Complexes *65*

2.2.4.4 CO Force Field Calculations *68*

2.2.4.5 [Phosphenium – Phosphorus (III) Ligand] $^1J_{PP}$ Coupling Constants *72*

2.3 SUMMARY 74

2.4 FUTURE WORK 78

3 SYNTHESIS AND STRUCTURAL REACTIVITY OF METAL COMPLEXES OF LIGANDS (1) TO (6) 80

3.1 RHODIUM COMPLEXES 80

3.1.1 The Synthesis and Structural Chemistry of $[RhCl(CO)\{PPh_2OC(CF_3)_3\}_2]$, **[Rh(6)-2]** 80

3.1.2 IR Spectroscopic Analysis of *trans*-$[RhCl(CO)L_2]$ Complexes 84

3.1.3 $^{31}P\{^1H\}$ NMR Spectroscopic Data for *trans*-$[RhCl(CO)L_2]$ Complexes 86

3.2 RUTHENIUM COMPLEXES 88

3.2.1 The Synthesis and Structural Chemistry of Ruthenium Complexes 88

3.2.2 Comparisons of the Ruthenium Complexes with Structural Data in the CSD 100

3.2.3 Reactivity of $[Ru(\eta^5\text{-}C_5H_5)(NCMe)(Ph_2P\{OCH(CF_3)_2\})_2]^+[PF_6]^-$, **[Ru(5)-2]** 102

3.2.4 Reactivity of $[(\eta^5\text{-}C_5H_5)Ru(NCMe)_2(Ph_2P\{OCH(CF_3)_2\})]^+[PF_6]^-$, **[Ru(5)]** 110

3.2.5 Reactivity of $[(\eta^5\text{-}C_5H_5)Ru(NCMe)_2P\{OC(CF_3)_3\}_3]^+[PF_6]^-$, **[Ru(2)]** 112

3.3 PALLADIUM COMPLEXES 115

3.3.1 C-C Coupling Catalysis, The Heck-Mizoroki Reaction 115

3.3.2 $Pd(dba)L_2$ NMR Studies 119

3.4 SUMMARY AND FUTURE WORK 127

4 IN SEARCH OF PERFLUORINATED WEAKLY COORDINATING CATIONS. 129

4.1 LITERATURE REVIEW OF WEAKLY COORDINATING CATIONS 129

4.1.1 Weakly Coordinating Cations Designed for Ionic Liquids 129

4.1.2 Quaternary Phosphonium Cations Used for Ionic Liquids 131

4.1.3 Weakly Coordinating Cations Designed for Their Stability in Basic Conditions 132

4.1.4 Non-Fluorinated Alkoxy-Phosphonium Ions 137

4.1.4.1 The Michaelis-Arbusov Reaction 137

4.1.4.2 Neopentyl-Containing Phosphonium Intermediates 139

4.1.4.3 Tetramethoxyphosphonium Hexachloroantimonate 139

4.1.4.4 Tetraalkoxyphosphonium Tetrafluoroborate Salts 140

4.1.4.5 Trinorborn-1-yl Phosphonium Intermediates 141

4.1.5 Fluorinated Phosphonium Cations 143

4.1.6 Phosphonium Salts as Phase-Transfer Catalysts 146

4.1.7 Project Aims 147

4.2 RESULTS AND DISCUSSION 149

4.2.1 Phosphorus (III) Ligand Oxidation 149

4.2.2 Attempted Synthesis of $[P(OR^F)_4]^+$ from $[PX_4]^+$ Salts, (X = Cl, Br) 160

4.2.3 Attempted Synthesis of $[P(OR^F)_4]^+$ from One-Pot Reactions 161

4.2.4 Attempted Synthesis of $[P(OR^F)_4]^+$ from Lewis-Acid-Mediated Halide/Alkoxide Abstraction of $P\{OCH(CF_3)_2\}_{5-n}Cl_n$ (n = 0, 1) 163

4.2.5 Single-Crystal X-ray Diffraction Structure of $(CF_3)_3COH\cdots O=P\{OC(CF_3)_3\}_3$ 166

4.3 PHOSPHINE-PHOSPHENIUM CHEMISTRY 170

4.3.1 Background Literature 170

4.3.2 Fluorinated Phosphorus (III)-Phosphenium Salts 174

4.4 SUMMARY 180

4.5 FUTURE WORK: 185

5 SYNTHETIC AND STRUCTURAL CHEMISTRY OF P(V)-ALKOXIDE BASED LEWIS ACIDS AND WEAKLY COORDINATING ANIONS 187

5.1 LITERATURE REVIEW 187

5.1.1 Review on Weakly Coordinating Anions 187

5.1.1.1 Requirements for a Weakly Coordinating Anion 187

5.1.1.2 Applications of Weakly Coordinating Anions 188

5.1.1.3 Borate-Based Weakly Coordinating Anions 189

5.1.1.4 Carborane-Based Weakly Coordinating Anions 190

5.1.1.5 Teflate-Based Weakly Coordinating Anions 194

5.1.1.6 Fluorinated Alkoxy- and Aryloxy-Based Weakly Coordinating Anions ... 195

5.1.1.7 Lewis Acid-Based Weakly Coordinating Anions 197

5.1.2 Review of the Acyclic Pentakis(hexafluoroisopropoxy)phosphorane, $P\{OCH(CF_3)_2\}_5$ 198

5.2 RESULTS AND DISCUSSION 201

5.2.1 Simple Synthesis of the Acyclic Pentakis(hexafluoroisopropoxy)-phosphorane, $P\{OCH(CF_3)_2\}_5$, (**16**) 201

5.2.2 The Lewis Acidity of $P\{OCH(CF_3)_2\}_5$, (**16**) 203

5.2.3 Synthesis of the $[P\{OCH(CF_3)_2\}_5F]^-$ Silver Salts 204

5.2.4 Synthesis of the $[P\{OCH(CF_3)_2\}_5F]^-$ Sodium Salts 210

5.2.5 Synthesis of the Tetraethylammoinum Salt, $[NEt_4]^+[P\{OCH(CF_3)_2\}_5F]^-$, (**24**) 213

5.2.6 Observations of the Potential $[P\{OCH(CF_3)_2\}_6]^-$ Anion 216

5.2.7 Reactivity of the Novel Salts; $[Ag(NCMe)_4]^+[P\{OCH(CF_3)_2\}_5F]^-$, (**17**), $[Na(NCMe)_6]^+[P\{OCH(CF_3)_2\}_5F]^-$, (**18**), $[Ag(PPh_3)_3]^+[P\{OCH(CF_3)_2\}_5F]^-$, (**19**) 216

5.3 SUMMARY 222

5.4 FUTURE WORK 225

6 EXPERIMENTAL 226

6.1 EXPERIMENTAL DETAILS 226

6.2 SYNTHETIC METHODOLOGY FOR COMMON STARTING MATERIALS 229

6.2.1 Synthesis of Lithium Hexafluoroisopropoxide, $LiOCH(CF_3)_2$ 229

6.2.2 Synthesis of Lithium Perfluoro-*t*-butoxide, $LiOC(CF_3)_3$ 229

6.2.3 Synthesis of Sodium Hexafluoroisopropoxide, $NaOCH(CF_3)_2$ 230

6.2.4 Synthesis of Sodium Perfluoro-*t*-butoxide, $NaOC(CF_3)_3$ 230

6.3 SYNTHETIC METHODOLOGY FOR OTHER KNOWN MATERIALS 231

6.3.1 Synthesis of Dibenzylideneacetone Bis(triphenylphosphine)Palladium, $[(dba)Pd(PPh_3)_2]$ 231

6.3.2 Synthesis of Tungsten Pentacarbonyl Tetrahydrofuran, $W(CO)_5\{THF\}$ 231
6.3.3 Synthesis of Lithium tetra(perfluoro-*t*–butoxide) Aluminate, $LiAl\{OC(CF_3)_3\}_4$ 231
6.4 SYNTHETIC METHODOLOGY FOR THE ISOLATED MATERIALS 233
6.4.1 Synthesis of Tris(hexafluoroisopropoxy)phosphite, $P\{OCH(CF_3)_2\}_3$, (**1**) ... 233
6.4.2 Synthesis of Tris(perfluoro-*t*-butyl)phosphite, $P\{OC(CF_3)_3\}_3$, (**2**) 235
6.4.3 Synthesis of Bis(hexafluoroisopropoxy)phenylphosphonite, $PPh\{OCH(CF_3)_2\}_2$, (**3**) 237
6.4.4 Synthesis of Bis(perfluoro-*t*-butoxy)phenylphosphonite, $PPh\{OC(CF_3)_3\}_2$, (**4**) 239
6.4.5 Synthesis of Hexafluoroisopropoxydiphenylphosphinite, $PPh_2\{OCH(CF_3)_2\}$, (**5**) 241
6.4.6 Synthesis of Perfluoro-*t*-butoxydiphenylphosphinite, $PPh_2\{OC(CF_3)_3\}$, (**6**) 243
6.4.7 Perfluorinated-*t*-butoxypyrophosphite, $\{OC(CF_3)_3\}_2P\text{-}\mu O\text{-}P\{OC(CF_3)_3\}_2$, (**7**). 245
6.4.8 Synthesis of Tungsten pentacarbonyl tris(hexafluoroisopropoxy)phosphite, $[W(CO)_5P\{OCH(CF_3)_2\}_3]$, **[W(1)]** 246
6.4.9 Synthesis of Tungsten pentacarbonyl tris(perfluoro-*t*-butyl)phosphite, $[W(CO)_5P\{OC(CF_3)_3\}_3]$, **[W(2)]** 247
6.4.10 Synthesis of Tungsten pentacarbonyl (bis{hexafluoroisopropoxy} phenylphosphonite), $[W(CO)_5\{PhP(OCH\{CF_3\}_2)_2\}]$, **[W(3)]** 248
6.4.11 Synthesis of Tungsten pentacarbonyl (bis{perfluoro-*t*-butoxy}phenylphosphonite), $[W(CO)_5\{PhP(OC\{CF_3\}_3)_2\}]$, **[W(4)]** 249
6.4.12 Synthesis of Tungsten pentacarbonyl (hexafluoroisopropoxydiphenyl-phosphinite), $[W(CO)_5\{Ph_2POCH(CF_3)_2\}]$, **[W(5)]** 250
6.4.13 Synthesis of Tungsten pentacarbonyl (perfluoro-*t*-butoxydiphenylphosphinite), $[W(CO)_5PPh_2\{OC(CF_3)_3\}]$, **[W(6)]** 251
6.4.14 Synthesis of $(\eta^5\text{-}C_5H_5)Ru(P\{OCH(CF_3)_2\}_3)(NCCH_3)_2]^+[PF_6]^-$, **[Ru(1)]** 252
6.4.15 Synthesis of $[(\eta^5\text{-}C_5H_5)Ru(P\{OC(CF_3)_3\}_3)(NCCH_3)_2]^+[PF_6]^-$, **[Ru(2)]** 254
6.4.16 Synthesis of $[(\eta^5\text{-}C_5H_5)Ru(PhP\{OCH(CF_3)_2\}_2)(NCCH_3)_2]^+[PF_6]^-$, **[Ru(3)]** 256
6.4.17 Synthesis of $[(\eta^5\text{-}C_5H_5)Ru(PhP\{OCH(CF_3)_2\}_2)_2(NCCH_3)]^+[PF_6]^-$, **[Ru(3)-2]** ... 258
6.4.18 Synthesis of $(\eta^5\text{-}C_5H_5)Ru(PhP\{OC(CF_3)_2\}_2)(CH_3CN)_2]^+[PF_6]^-$, **[Ru(4)]** 260
6.4.19 Synthesis of $[(\eta^5\text{-}C_5H_5)Ru\{Ph_2POCH(CF_3)_2\}(CH_3CN)_2]^+[PF_6]^-$, **[Ru(5)]** ... 262

6.4.20 Synthesis of $[(\eta^5\text{-}C_5H_5)Ru\{Ph_2POCH(CF_3)_2\}_2(CH_3CN)]^+[PF_6]^-$, **[Ru(5)-2].....** 264
6.4.21 Synthesis of $[(\eta^5\text{-}C_5H_5)Ru(Ph_2P\{OC(CF_3)\}_3)(CH_3CN)_2]^+[PF_6]^-$, **[Ru(6)]** ...266
6.4.22 Synthesis of $[(\eta^5\text{-}C_5H_5)Ru(Ph_2P\{OC(CF_3)_2\})_2(CH_3CN)]^+[PF_6]^-$, **[Ru(6)-2 .....]** 268
6.4.23 Synthesis of *trans*-Bis(perfluoro-*t*-butylphosphite) Rhodium(I) Carbonyl Chloride, $Rh(CO)Cl(P\{OC(CF_3)_3\}_3)_2$, **[Rh(2)-2]** 270
6.4.24 Synthesis of *trans*-Bis{di(perfluoro-*t*-butoxy)phenylphosphonite} Rhodium (1) Carbonyl Chloride, $Rh(CO)Cl(PPh\{OC(CF_3)_3\}_2)_2$, **[Rh(4)-2]**.....271
6.4.25 Synthesis of *trans*-Bis{di(perfluoro-*t*-butoxy)diphenylphosphinite} Rhodium(I) Carbonyl Chloride, $Rh(CO)Cl(PPh_2\{OC(CF_3)_3\})_2$, **[Rh(6)-2]**.....272
6.4.26 Synthesis of Dibenzylideneacetone Bis(bis(hexafluoroisopropoxy phenylphosphonite) Palladium, $[(dba)Pd(PhP\{OCH(CF_3)_2\}_2)_2]$, **[Pd(3)-2]** 274
6.4.27 Synthesis of Dibenzylideneacetone Bis(hexafluoroisopropoxy diphenylphosphinite) Palladium, $[(dba)Pd\{Ph_2POCH(CF_3)_2\}_2]$, **[Pd(5)-2]**.....275
6.4.28 Synthesis of [1,1-Diphenyl-1-hexafluoroisopropoxy-1-methyl phosphonium Triflate, $[Ph_2P\{OCH(CF_3)_2\}Me]^+$ $[F_3CS(O)_2O]^-$, (**10**).....276
6.4.29 Synthesis of $[MePPh\{OCH(CF_3)_2\}_2]^+[OS(O)_2CF_3]^-$, (**11**).....278
6.4.30 Synthesis of $[PPh_2\text{-}P\{OCH(CF_3)_2\}_3]^+[AlCl_4]^-$, (**12**).....279
6.4.31 Synthesis of $[PPh_2\text{-}PPh\{OCH(CF_3)_2\}_2]^+[AlCl_4]^-$, (**13**).....280
6.4.32 Synthesis of $[PPh_2\text{-}PPh_2\{OCH(CF_3)_2\}]^+[AlCl_4]^-$, (**14**).....281
6.4.33 Synthesis of $[PPh_2\text{-}PPh_2\{OC(CF_3)_3\}]^+[AlCl_4]^-$, (**15**).....282
6.4.34 Synthesis of Pentakis(hexafluoroisopropoxy)phosphorane, $P\{OCH(CF_3)_2\}_5$, (**16**).....283
6.4.35 Synthesis of Tetrakis(acetonitrile)silver(I) monofluoropentakis-(hexafluoroisopropoxy)phosphate, $[Ag(NCMe)_4]^+[P\{OCH(CF_3)_2\}_5F]^-$, (**17**).....285
6.4.36 Synthesis of Hexakis(acetonitrile)sodium(I) monofluoropentakis-(hexafluoroisopropoxy)phosphate, $[Na(NCMe)_6]^+[P\{OCH(CF_3)_2\}_5F]^-$ (**18**).....287
6.4.37 Synthesis of Tris(triphenylphosphine)silver(I) monofluoropentakis-(hexafluoroisopropoxy)phosphate, $[Ag(PPh_3)_3]^+[P\{OCH(CF_3)_2\}_5F]^-$, (**19**).....289
6.4.38 Synthesis of Silver Tris(trimethylphosphine)silver(I) monofluoropentakis-(hexafluoroisopropoxy)phosphate, $[Ag(PMe_3)_3]^+[P\{OCH(CF_3)_2\}_5F]^-$, (**20**).....291
6.4.39 Synthesis of Tris(triisoproylphosphine)silver(I) monofluoro,pentakis-(hexafluoroisopropoxy)phosphate, $[Ag(P^iPr_3)_3]^+[P\{OCH(CF_3)_2\}_5F]^-$, (**21**).....293
6.4.40 Synthesis of $[Na(NCMe)_2(O{=}P\{OCH(CF_3)_2\}_3)]^+[P\{OCH(CF_3)_2\}_5F]^-$, (**22**)..... 295

6.4.41 Synthesis of Triethylamine Coordinated Sodium(I) monofluoro, pentakis-(hexafluoroisopropoxy) phosphate, $[Na(NEt_3)_n]^+[P\{OCH(CF_3)_2\}_5F]^-$, (**23**) 297
6.4.42 Synthesis of Tetraethylammonium monofluoropentakis-(hexafluoroisopropoxy)phosphate, $[NEt_4]^+[P\{OCH(CF_3)_2\}_5F]^-$, (**24**) 299
6.5 REACTION CONDITIONS EMPLOYED IN SEARCH OF $[P(OR^F)_4]^+$ CATIONS (CHAPTER 4) 301
6.5.1 Attempted Synthesis of $[P\{OC(CF_3)_3\}_4]^+[N\{S(O)_2CF_3\}_2]^-$, **[(8)][Tf$_2$N]** 301
6.5.2 Attempted Synthesis of $[P\{OC(CF_3)_3\}_4]^+[N\{S(O)_2CF_3\}_2]^-$, **[(8)][Tf$_2$N]** 301
6.5.3 Attempted Synthesis of $[P\{OC(CF_3)_3\}_4]^+[N\{S(O)_2CF_3\}_2]^-$, **[(8)][Tf$_2$N]** 302
6.5.4 Attempted Synthesis of $[P\{OCH(CF_3)_2\}_4]^+[PF_6]^-$, **[(9)][PF$_6$]** 303
6.5.5 Attempted Synthesis of $[P\{OCH(CF_3)_2\}_4]^+[Al\{OC(CF_3)_3\}_4]^-$, **[(9)][Al{OC(CF$_3$)$_3$}$_4$]** 305
6.5.6 Attempted Synthesis of $[P\{OC(CF_3)_2\}_4]^+[Al\{OC(CF_3)_3\}_4]^-$, **[(9)][Al{OC(CF$_3$)$_3$}$_4$]** 306
6.5.7 Attempted Synthesis of $[P\{OC(CF_3)_3\}_4]^+[P\{OCH(CF_3)_2\}_5F]^-$, **[(8)][P{OCH(CF$_3$)$_2$}$_5$F]** 306
6.5.8 Attempted Synthesis of $[P\{OCH(CF_3)_2\}_4]^+[AlCl_4]^-$, **[(9)][AlCl$_4$]** 307
6.5.9 Attempted Synthesis of $[P\{OCH(CF_3)_2\}_4]^+[AlCl_4]^-$, **[(9)][AlCl$_4$]** 307
6.5.10 Attempted Synthesis of $[P\{OCH(CF_3)_2\}_4]^+[AlCl_4]^-$, **[(9)][AlCl$_4$]** 308
6.6 REACTION CONDITIONS FOR P(III) LIGAND OXIDATION REACTIONS 310
6.6.1 Attempted Synthesis of $[BrP\{OC(CF_3)_3\}_3]^+[NO_2C_4H_4]^-$ 310
6.6.2 Attempted Synthesis of $[BrPPh_2\{OCH(CF_3)_2\}]^+[NO_2C_4H_4]^-$ 311
6.6.3 Synthesis of $[BrPPh_3]^+[NO_2C_4H_4]^-$ 311
6.7 REACTION CONDITIONS FOR $[PCL_4]^+[X]^-$ SYNTHESIS 312
6.7.1 Attempted Synthesis of $[PCl_4]^+[Tf_2N]^-$ 312
6.7.2 Attempted Synthesis of $[PCl_4]^+[PF_6]^-$ 312
6.7.3 Synthesis of $[PCl_4]^+[AlCl_4]^-$ 313
6.7.4 Attempted Synthesis of $[P\{OCH(CF_3)_2\}_4]^+[Al\{OCH(CF_3)_2\}_4]^-$, **[(9)][Al{OCH(CF$_3$)$_2$}$_4$]** 313
6.7.5 Attempted Synthesis of $[P\{OCH(CF_3)_2\}_4]^+[AlCl_4]^-$, **[(9)][Al{OCH(CF$_3$)$_2$}$_4$]** 313
6.7.6 Attempted Synthesis of $[P\{OCH(CF_3)_2\}_4]^+[AlCl_3Br]^-$, **[(9)][AlCl$_3$Br]** 314
6.7.7 Attempted Synthesis of $[P\{OC(CF_3)_3\}_4]^+[AlCl_4]^-$, **[(2)][AlCl$_4$]** 315
6.8 REACTION CONDITIONS FOR THE SYNTHESIS OF P(III)-LIGAND STABILISED DIPHENYLPHOSPHENIUM SALTS 316

6.8.1 Attempted Synthesis of $[PPh_2\text{-}PPh\{OC(CF_3)_3\}_2]^+[AlCl_4]^-$ 316
6.8.2 Attempted Synthesis of $[PPh_2\text{-}PPh_2\{OC(CF_3)_3\}]^+[OS(O)_2CF_3]^-$ 316
6.8.3 Attempted Synthesis of $[PPh_2\text{-}PPh_2\{OCH(CF_3)_2\}]^+[OS(O)_2CF_3]^-$ 317
6.8.4 Attempted Synthesis of $[PPh_2\text{-}PPh_2\{OCH(CF_3)_2\}]^+[GaCl_4]^-$ 317
6.8.5 Attempted Synthesis of $[PPh_2\text{-}PPh\{OCH(CF_3)_2\}_2]^+[GaCl_4]^-$ 318
6.8.6 Attempted Synthesis of $[PPh_2\text{-}P\{OCH(CF_3)_2\}_3]^+[GaCl_4]^-$ 318
6.8.7 Attempted Synthesis of $[PPh_2\text{-}PPh_2\{OC(CF_3)_3\}]^+[GaCl_4]^-$ 319
6.8.8 Crystal Structure of the Phosphonate-Alcohol Complex, $\{OC(CF_3)_3\}_3P{=}O\cdots HOC(CF_3)_3$ 319
6.9 REACTION CONDITIONS USED FOR "OTHER" REACTIONS DESCRIBED IN CHAPTER 5 321
6.9.1 Attempted Synthesis of $[\{Et_2O\}_2H]^+$ $[P\{OCH(CF_3)_2\}_5F]^-$ 321
6.9.2 Reactivity of $[Ag(NCMe)_4]^+[P\{OCH(CF_3)_2\}_5F]^-$, (**17**) with Ph_3CCl 321
6.9.3 Synthesis of $Ph_3COCH(CF_3)_2$ 322
6.9.4 Synthesis of $[PPh_3\text{-}CPh_3]^+[PF_6]^-$ 322
6.9.5 Reactivity of $[Ag(PPh_3)_3]^+[P\{OCH(CF_3)_2\}_5F]^-$, (**19**) with Ph_3CCl 322
6.9.6 Reactivity of $[Ag(PPh_3)_3]^+[P\{OCH(CF_3)_2\}_5F]^-$, (**19**) with MeI 323
6.9.7 Reactivity of $[Ag(PPh_3)_3]^+[P\{OCH(CF_3)_2\}_5F]^-$, (**19**) with $\{Et_2O\}_2HCl$ 324
6.9.8 Reactivity of $[Ag(PPh_3)_3]^+[P\{OCH(CF_3)_2\}_5F]^-$, (**19**) with Water 325
6.9.9 Attempted Synthesis of $[Na(NCMe)_6]^+[P\{OCH(CF_3)_2\}_6]^-$ 325
7 ABBREVIATIONS 327
8 REFERENCES 329

LIST OF FIGURES

Figure 1: Single-crystal X-ray diffraction structure of a tris(perfluoro-*t*-butyl)phosphite, (**2**) (left) and $[(\eta^5\text{-}C_5H_5)Ru(NCMe)_2\{P(OC\{CF_3\}_3)_3\}]^+[Na_4\{OC(CF_3)_3\}_4PF_6.MeCN]^-$, **[Ru(2)]** (right). Note anion omitted for clarity. 2

Figure 2: Single-crystal X-ray diffraction structure of $[MePPh_2\{OCH(CF_3)_2\}]^+[O_3SCF_3]^-$, (**10)** (left) and DFT optimised structure of $[PPh_2\text{-}PPh\{OC(CF_3)_3\}_2]^+$ (right). 3

Figure 3: Single-crystal X-ray diffraction structure of $P\{OCH(CF_3)_2\}_5$, (**16**) (left) and $[NEt_4]^+[P\{OCH(CF_3)_2\}_5F]^-$, (**24)** (right). 4

Figure 4: A) Diagrammatic representation of the Tolman cone angle used for symmetrical ligands.[20] B) Diagrammatic representation of half cone angles, used for ligands with different substituents.[20] Adapted from ref. 20. 6

Figure 5: Assumed conformation of phosphites by Tolman (A) and those observed from crystallographic data (B-D).[29] 8

Figure 6: Geometry used for computation of the He_8 steric parameter: the interaction energy between the phosphorus ligand (PA_3) and a ring of eight helium atoms. Figure adapted from ref. 32. 10

Figure 7: A) Definition of the Ne_{12} cone angle B) Examples of the PdL fragments at cone angles of 138 °, 178 ° and 218 °. Figure adapted from ref. 35 11

Figure 8: Definitions of the geometrical solid angle. Figure adapted from ref. 38. 12

Figure 9: The area of the ligand projection shadow used for the ligand solid angle can be seen and the metal is shown as a white sphere for easy visualisation.[37] 12

Figure 10: The electron donor-acceptor ligand properties of a CO ligand in the first example and a phosphorus (III) ligand in the second example. The orbital responsible for the acceptor properties of the phosphorus ligand may be the σ* antibonding orbital, the 3d-orbital or even a hybridisation of the two orbitals 15

Figure 11: a) Phosphorus (III) ligand with its lone pair b) V_{min} in the lone pair region.[53] 17

Figure 12: Two-layer ONIOM method. Here the inner hydrogen atoms are the link atoms.[65] 18

Figure 13: Repulsive steric interactions between the alkyne substituent R^2 and the bulky $P\{OCH(CF_3)_2\}_3$ ligand on Rh (I) catalyst allows only stereoselective products to form.[127] .. 29

Figure 14: Class of bulky, electron-deficient ligands synthesised. 34

Figure 15: Sodium perfluoro-*t*-butoxide clusters with coordinated diethyl ether solvent.[138] 36

Figure 16: Single-crystal X-ray structure of $(R^FO)_2P\text{-}\mu O\text{-}P(OR^F)_2$ {$R^F = C(CF_3)_3$}, (**7**) at 110 K. Extensive disorder (modelled over two equal positions) is present for all atoms except for those of one perfluoro-*t*-butoxy group in the structure. Only one position is shown (and

bond lengths and angles given for this) for clarity. Selected bond lengths (Å) and angles (°): P(1)-O(1) 1.589(9), P(1)-O(2) 1.637(9), P(1)-O(5) 1.63(5), P(2)-O(3) 1.611(8), P(2)-O(4) 1.643(9), P(2)-O(5) 1.62(4), P(1)-O(5)-P(2) 136(3), O(1)-P(1)-O(2) 93.6(4), O(1)-P(1)-O(5) 96(2), O(2)-P(1)-O(5) 96.2(9), O(3)-P(2)-O(4) 93.4(5), O(3)-P(2)-O(5) 101(2), O(4)-P(2)-O(5) 100.2(8). Crystal system: Orthorhombic. Space group: Pbca, 110 K, R_1 = 0.1170 (>2sigma(I)), wR_2 = 0.3379 (all data). 39
Figure 17: Crystal structure of $Rh(CO)_2Cl\{PPh_2OC(CF_3)_3\}_2$, **[Rh(6)-2]**, the starred (*) phenyl has a propeller arrangement increasing the P(1) ligand cone angle in comparison to that of the ligand with a P(2) centre. 43
Figure 18: Reduced cone angle for (**4**) in $[Ni(CO)_3PPh\{OC(CF_3)_3\}_2]$ (optimised by DFT, at the (RI-)BP86/SV(P) level) possibly due to a non-propeller configuration of the phenyl substituent on the ligand. Note CO ligands and Ni centre have been deleted for clarity. 44
Figure 19: The hexafluoroisopropoxy groups can change orientation; the O-R^F bond can point away from the phosphorus lone pair ("down"), O-R^F can bend so that is not parallel with the phosphorus lone pair ("side") or the O-R^F bond can point towards the lone pair ("up"). 45
Figure 20: Crystal structure of $[(\eta^5\text{-}C_5H_5)Ru(NCMe)(PPh\{OCH(CF_3)_2\}_2)_2]^+[PF_6]^-$, **[Ru(3)-2]**. One of the hexafluoroisopropoxy group points "down", O(4) and the other points "up", O(3). Note $[PF_6]^-$, MeCN, second $PPh\{OCH(CF_3)_2\}_2$ ligand and hydrogen atoms on the phenyl ring have been omitted for clarity. 45
Figure 21: Large cone angle for $P\{OCH(CF_3)_2\}_3$, (**1**), ligand on a nickel centre, $[Ni(CO)_3L]$ (optimised by DFT, at the (RI-)BP86/SV(P) level due to two P-O-R bonds pointing "up" towards the Ni centre. Note CO ligands have been omitted for clarity. 46
Figure 22: Smaller cone angles observed for **[Rh(1)-2]** in comparison to $[Ni(CO)_3P\{OCH(CF_3)_2\}_3]$, (XRD structure from ref. 133) due to O(1) and O(5) of the OR^F substituents pointing "down" away from the Rh centre. 46
Figure 23: Single X-ray crystal structure of perfluoro-*t*-butyl phosphite, $P\{OC(CF_3)_3\}_3$, (**2**). Extensive disorder (modelled over two positions, one "up" and "one" down" in the asymmetric unit) is present in the structure. Only one position is shown for clarity. Although disordered over two positions the incredible steric bulk on the ligand can be observed. Crystal system: monoclinic. Space group: C2/c. R_1= 0.1565 (>2sigma(I)), wR_2 = 0.4462. (all data). 48
Figure 24: Structures of aryl-phosphites found in the CSD, note the CSD names are presented below each structure. 49
Figure 25: $P\{OCH(CF_3)_2\}_3$, (**1**), A: top, B: bottom view of the ligand. 50
Figure 26: $P\{OC(CF_3)_3\}_3$, (**2**), A: top, B: bottom view of the ligand. 50
Figure 27: $PPh\{OCH(CF_3)_2\}_2$, (**3**), A: top, B: bottom view of the ligand. 50

Figure 28: PPh{OC(CF_3)$_3$}$_2$, (**4**), A: top, B: bottom view of the ligand. 51
Figure 29: PPh_2{OCH(CF_3)$_2$}, (**5**), A: top, B: bottom view of the ligand. 51
Figure 30: PPh_2{OC(CF_3)$_3$}, (**6**), A: top, B: bottom view of the ligand. 51
Figure 31: $^{31}P\{^1H\}$ NMR spectra overlay of all the [W(CO)$_5$L] successfully complexed with the following phosphorus (III) ligands, from bottom to top; [W(CO)$_5$P{OCH(CF_3)$_2$}$_3$] (note the downfield satellite is under a impurity peak), **[W(1)]**; [W(CO)$_5$P{OC(CF_3)$_3$}$_3$], **[W(2)]**; [W(CO)$_5$PhP{OCH(CF_3)$_2$}$_2$], **[W(3)]**; [W(CO)$_5$PhP{OC(CF_3)$_3$}$_2$], **[W(4)]**; [W(CO)$_5$Ph$_2$P{OCH(CF_3)$_2$}], **[W(5)]**; [W(CO)$_5$Ph$_2$P{OC(CF_3)$_3$}], **[W(6)]**. A multiplet is observed for uncoordinated P{OC(CF_3)$_3$}$_3$ ligand in the **[W(2)]** spectrum..... 61
Figure 32: Three IR stretches observed for CO ligands in [W(CO)$_5$L] complexes. 66
Figure 33: Definition of the CO-factored force constants in [M(CO)$_5$L] molecules. 68
Figure 34: Potential ionic ligands with charged substituents on the phenyl groups.[69] 78
Figure 35: Substituted phosphinite ligands, which allow for supramolecular interactions. .. 78
Figure 36: Potential bidentate pyrophosphite ligands. 79
Figure 37: Potential thionyl alkoxide ligands. 79
Figure 38: Single-crystal X-ray structure of [RhCl(CO){PPh$_2$OC(CF_3)$_3$}$_2$], **[Rh(6)-2]** at 110 K. Cl and CO positions are disordered; disordered parts omitted for clarity Thermal ellipsoids are drawn at the 50 % probability level. Selected interatomic distances (Å) and angles (˚): Rh(1)-P(1) = 2.2866(4), Rh(1)-P(2) = 2.3017(4), Rh(1)-Cl(1A) = 2.381(1), Rh(1)-C(1A) = 1.779(8), C(1A)-O(1A) = 1.15(1), P(1)-Rh-P(2) = 177.96(1), C(1A)-Rh-Cl(1A) = 169.68(5), P(1)-Rh(1)-Cl(1A) = 92.34(3), P(2)-Rh(1)-Cl(1A) = 87.22(3), C(1A)-Rh(1)-P(1) = 88.7(1), C(1A)-Rh(1)-P(2) = 91.6(1). Crystal system: tetragonal. Space group: P42/n. R_1: 0.0306 (all data), wR_2: 0.0645 (>2sigma(I)). 80
Figure 39: Histogram to show the range of P-Rh bond lengths in *trans*-[RhCl(CO)L$_2$] complexes with a number of phosphorus (III) ligands. Two series are displayed for the two different bond lengths (Å) for each phosphorus ligand found in the complex. 81
Figure 40: Molecular structure of [(η^5-C_5H_5)Ru(NCMe)$_2${P(OCH{CF_3}$_2$)$_2$}$_3$]$^+$[PF_6]$^-$, **[Ru(1)]** at 110 K. Hydrogen atoms and the second structure in the asymmetric unit omitted for clarity. Thermal ellipsoids are drawn at the 50 % probability level. Selected interatomic distances (Å) and angles (˚): Ru(1)-P(1) = 2.206(4), Ru(1)-N(1) = 2.05(1), Ru(1)-N(2) = 2.05(1), N(1)-Ru(1)-P(1) 89.0(3), N(2)-Ru(1)-P(1) 89.8(3), N(1)-Ru(1)-N(2) 86.5(4),O(3)-P(1)-O(2) = 95.3(5), O(1)-P(1)-O(2) = 95.8(5), O(1)-P(1)-O(3) = 101.7(5). Crystal system: triclinic. Space group: P-1. R_1: 0.1241 (all data) wR_2: 0.2653 (>2sigma(I)). Note high R_1 and wR_2 values as there is considerable disorder in the [PF_6]$^-$ anion and the Cp ring that has not been fully resolved. 88
Figure 41: Molecular structure of [(η^5-C_5H_5)Ru(NCMe)$_2${P(OC{CF_3}$_3$)$_3$}]$^+$[Na_4{OC(CF_3)$_3$}$_4$$PF_6$NCMe]$^-$, **[Ru(2)]** at 110 K.

Hydrogen atoms, parts and $[PF_6]^-$ anion omitted for clarity. Thermal ellipsoids are drawn at the 50 % probability level. Selected interatomic distances (Å) and angles (°): Ru(1)-P(1) = 2.233(1), Ru(1)-N(1) = 2.015(5), Ru(1)-N(2) = 2.071(4), N(1)-Ru(1)-P(1) = 94.0(1), N(2)-Ru(1)-P(1) = 93.2 (1), N(1)-Ru(1)-N(2) = 86.7 (1), O(1)-P(1)-O(2) = 98.4(3), O(1)-P(1)-O(3) = 97.8(3), O(2)-P(1)-O(3) = 96.2(4).Crystal system: monoclinic. Space group: $P2_1/n$. R_1: 0.0623 (all data), wR_2: 0.1677 (>2sigma(I)). 89

Figure 42: Molecular structure of $[(\eta^5\text{-}C_5H_5)Ru(NCMe)\{PPh(OCH\{CF_3\}_2)_2\}_2]^+[PF_6]^-$, **[Ru(3)-2]** at 110 K. Hydrogen atoms omitted for clarity. Thermal ellipsoids are drawn at the 50 % probability level. Selected interatomic distances (Å) and angles (°): Ru(1)-P(1) = 2.262(1), Ru(1)-P(2) = 2.265(1), Ru(1)-N(1) = 2.059(4), (1)-Ru(1)-P(1) = 92.7(1), P(1)-Ru(1)-P(2) = 96.31(4), P(1)-Ru(1)-P(2) = 94.5(1), O(2)-P(1)-O(1) =96.2(1), O(2)-P(1)-C(7) = 103.5(1), O(1)-P(1)-C(7) = 98.0(2), O(3)-P(2)-C(19) = 99.0(1), O(4)-P(2)-O(3) = 98.6(1), O(4)-P(2)-C(19) = 102.8(1). Crystal system: monoclinic. Space group: $P2_1/n$. R_1: 0.0557 (all data), wR_2: 0.0986 (>2sigma(I)). 89

Figure 43: Molecular structure of $[(\eta^5\text{-}C_5H_5)Ru(NCMe)_2\{PPh(OC\{CF_3\}_3)_2]^+[PF_6]^-$, **[Ru(4)]** at 110 K. Hydrogen atoms and parts omitted for clarity. Thermal ellipsoids are drawn at the 50 % probability level. Selected interatomic distances (Å) and angles (°): Ru(1)-P(1) = 2.254(6), Ru(1)-N(1) = 2.047(2), Ru(1)-N(2) = 2.061(2), N(1)-Ru(1)-P(1) = 94.77 (6), N(2)-Ru(1)-P(1) = 97.49 (6), N(1)-Ru(1)-N(2) = 86.63 (8), O(1)-P(1)-O(2) = 94.10(9), O(1)-P(1)-C(14) = 94.9(1), O(2)-P(1)-C(14) = 104.9(1). Crystal system: monoclinic. Space group: $P2_1/c$. R_1: 0.0401 (all data) wR_2: 0.0886 (>2sigma(I)) 90

Figure 44: Molecular structure of $[(\eta^5\text{-}C_5H_5)Ru(NCMe)_2\{PPh_2OCH(CF_3)_2\}]^+[PF_6]^-$, **[Ru(5)]** at 109.8 K. Hydrogen atoms omitted for clarity. Thermal ellipsoids are drawn at the 50 % probability level. Selected interatomic distances (Å) and angles (°): Ru(1)-P(1) = 2.2636(5), Ru(1)-N(1) = 2.2058(1), Ru(1)-N(2) = 2.2054(1), N(1)-Ru(1)-P(1) = 88.19(4), N(2)-Ru(1)-P(1) = 89.75(4), N(2)-Ru(1)-N(1) = 83.50(6), O(1)-P(1)-C(9) = 98.02(8), O(1)-P(1)-C(15) = 101.23(8), C(15)-P(1)-C(9) = 102.00(8).Crystal system: monclinic. Space group: $P2_1/c$. R_1: 0.0305 (all data), wR_2: 0.0709 (>2sigma(I)). 90

Figure 45: Molecular structure of $[(\eta^5\text{-}C_5H_5)Ru(NCMe)\{PPh_2OCH(CF_3)_2\}_2]^+[PF_6]^-$, **[Ru(5)-2]** at 110 K. Hydrogen atoms, second structure in asymmetric unit and solvent molecules omitted for clarity. Thermal ellipsoids are drawn at the 50 % probability level. Selected interatomic distances (Å) and angles (°): Ru(1)-N(1) = 2.046(4), Ru(1)-P(1) = 2.277(1), Ru(1)-P(2) = 2.276(1), N(1)-Ru(1)-P(1) = 91.5(1), N(1)-Ru(1)-P(2) = 94.5(1), P(2)-Ru(1)-P(1) = 98.97(4), O(1)-P(1)-C(9) = 102.8(1), O(1)-P(1)-C(15) = 101.9(1), C(15)-P(1)-C(9) = 104.8(2), O(2)-P(2)-C(24) = 95.6(1), O(2)-P(2)-C(24) = 95.6(1), O(2)-P(2)-C(30) = 101.5(1), C(30)-P(2)-C(24) = 102.8(2). Crystal system: orthorombic. Space group: $P2_12_12$. R_1: 0.0494, (all data), wR_2: 0.0989 (>2sigma(I)). 91

Figure 46: Molecular structure of $[(\eta^5\text{-}C_5H_5)Ru(NCMe)_2\{PPh_2OC(CF_3)_3\}]^+[PF_6]^-$, **[Ru(6)]** at 110 K. Hydrogen atoms and disorder omitted for clarity. The alkoxy group is disordered over two positions; the higher occupancy is shown here. Thermal ellipsoids are drawn at the 50 % probability level. Selected interatomic distances (Å) and angles (˚): Ru(1)-P(1) = 2.2628(9), Ru(1)-N(1) = 2.069(2), Ru(1)-N(2) = 2.065(3), N(1)-Ru(1)-P(1) = 94.53(8), N(1)-Ru(1)-N(2) = 84.9(1), P(1)-Ru-N(2) = 97.54(8), C(10)-P(1)-C(16) = 100.9(1), C(10)-P(1)-O(1) = 102.7(1), O(1)-P(1)-C(16) = 93.8(1), O(1)-P(1)-C(10) = 100.7 (1), C(10)-P(1)-C(16) = 105.5(1).Crystal system: monoclinic. Space group: $P2_1/c$. R_1: 0.0422 (all data), wR_2: 0.0895 (>2sigma(I)). 91

Figure 47: Molecular structure of $[(\eta^5\text{-}C_5H_5)Ru(NCMe)\{PPh_2OC(CF_3)_3\}_2]^+[PF_6]^-$, **[Ru(6)-2]** at 110 K. Hydrogen atoms, second structure from the asymmetric unit and solvent molecule omitted for clarity. Thermal ellipsoids are drawn at the 50 % probability level. Selected interatomic distances (Å) and angles (˚): Ru(1)-P(1) = 2.2882(9), Ru(1)-N(1) = 2.048(2), Ru(1)-N(2) = 2.2988(7), N(1)-Ru(1)-P(1) = 89.96(7), N(1)-Ru(1)-P(2) = 96.01(6), P(1)-Ru-P(2) = 99.07(3), O(2)-P(2)-C(32) = 104.2(1), O(2)-P(2)-C(26) = 100.7(1), C(32)-P(2)-C(26) = 109.0(1), O(1)-P(1)-C(10) = 100.7(1), C(10)-P(1)-C(16) = 105.5(1).Crystal system: monoclinic. Space group: $P2_1$. R_1: 0.0332 (all data), wR_2: 0.0785 (>2sigma(I)). 92

Figure 48: A chemdraw diagram and the single-crystal X-ray structure of the $[Na_4\{OC(CF_3)_3\}_4PF_6.NCMe]^-$ unusual counterion found in the single-crystal X-ray structure of **[Ru(2)]** at 110 K. Parts and cation omitted for clarity. Thermal ellipsoids are drawn at the 50 % probability level. Crystal system: monoclinic. Space group: $P2_1/n$. R_1: 0.0623 (all data), wR_2: 0.1677 (>2sigma(I)). 93

Figure 49: The hexafluoroisopropoxy groups can change orientation; the O-R bond can point away from the phosphorus lone pair (“down”), O-R can bend so that is not parallel with the phosphorus lone pair (side) or the O-R bond can point towards the lone pair (up). 94

Figure 50: Crystal structure of $[Rh(CO)_2Cl\{PPh_2OC(CF_3)_3\}_2]$, **[Rh(6)-2]** the starred (*) phenyl has a “propeller” arrangement increasing the ligand cone angle. 94

Figure 51: Histogram to show the range of Ru-P bond lengths (Å) in $[(\eta^5\text{-}Cp)Ru(P_1)(NCMe)_2]^+[Anion]^-$ and $[(\eta^5\text{-}Cp)Ru(P_1)(P_2)(NCMe)]^+[Anion]^-$complexes with a number of phosphorus (III) ligands. 100

Figure 52: A Chemdraw representation of the structure containing the shortest Ru-P bond length from a CSD search for a $[Ru(\eta^5\text{-}Cp)(P)_1(P)_2NCMe]^+$ fragment with $R_1 < 10$ %. The $Ru\text{-}P(OPh)_3$ bond has the shortest possible bond {2.22(2) Å} even though statistically it may be similar to the other $Ru\text{-}PPh_2R$ bond {2.34(3) Å}. CSD search name: QIFXIM. 101

Figure 53: A vinylidene with substituents R and R’, coordinated to a transition metal complex 102

Figure 54: The vinylidene (right) and acetylene (left) tautomers; both when free and coordinated to a transition metal. 103
Figure 55: $^{31}P\{^{1}H\}$ NMR spectra of $[(\eta^5\text{-}C_5H_5)Ru(NCMe)(Ph_2P\{OCH(CF_3)_2\})_2]^+[PF_6]^-$, **[Ru(5)-2]** and phenylacetylene , 150 to 190 ppm range. NMR spectra in overlay; a) after 15 minutes of reactions, b) 1 day, c) 1day heated at 50 ˚C, d) 2 days heated at 50 ˚C and e) 7 days heated at 50 ˚C. 105
Figure 56: $^{31}P\{^{1}H\}$ NMR of $[(\eta^5\text{-}C_5H_5)Ru(NCMe)(Ph_2P\{OCH(CF_3)_2\})_2]^+[PF_6]^-$, **[Ru(5)-2]** and phenylacetylene, 30 to -30 ppm range. NMR spectra in overlay; a) after 15 minutes of reactions, b) 1 day, c) 1 day heated at 50 ˚C, d) 2 days heated at 50 ˚C and e) 7 days heated at 50 ˚C. 106
Figure 57: Overlay of ^{19}F NMR spectra of disubstituted ruthenium complex, bottom spectra: a) **[Ru(5)-2]** top spectra: b) reaction **[Ru(5)-2]** with phenylacetylene. 107
Figure 58: ^{1}H NMR spectra overlay of **[Ru(5)-2]** and phenylacetylene. NMR overlay; after 15 minutes of reactions, 1 day, then 1 day heated at 50 ˚C, 2 days heated at 50 ˚C and 7 days heated at 50 ˚C. 108
Figure 59: $^{31}P\{^{1}H\}$ NMR spectrum of **[Ru(5)]** and phenylacetylene after 1 day, heated at 50 °C. Many new signals within the 55 to -30 ppm chemical shift range are observed. 110
Figure 60: ^{1}H NMR spectra of **[Ru(5)]** with after phenylacetylene after 1 day, heated at 50 °C. Many new phenyl-containing species formed in the aromatic region at 7-8 ppm. 111
Figure 61: Identified organic species using GS-MS from the reaction of phenylacetylene and **[Ru(5)]** in DCM solvent. 111
Figure 62: Proposed product formed *via* substitution of the fluorine atoms from the $[PF_6]^-$ anion with an alkoxy group on the $P\{OC(CF_3)_3\}_3$, (**2**) ligand. 113
Figure 63: ^{19}F NMR spectra overlay of **[Ru(2)]** after heating. NMR overlay: a) after 15 minutes, b) three days, d) 1 day heated at 43 °C and after six hours heated at 47 °C. A doublet of doublet of dectets grows in for the equatorial fluorine atoms of $[PF_5\{OC(CF_3)_3\}_2]$,which forms due to ligand exchange. 114
Figure 64: ^{19}F NMR spectrum of **[Ru(2)]** after heating, from bottom spectra to top: a) after 15 minutes, b) three days, d) 1 day heated at 43 °C and after six hours heated at 47 °C. A doublet of quintets grows in for the axial fluorine of $[PF_5\{OC(CF_3)_3\}_2]$,which forms due to ligand exchange. 115
Figure 65: A substituted dba ligand with a range of electron-donating or electron-withdrawing groups. 120
Figure 66: Overlay of the spectra from the variable temperature $^{31}P\{^{1}H\}$ NMR study over a 250-370 K temperature range for the **[Pd(5)-2] s**ystem. 123
Figure 67: Overlay of the spectra from the variable temperature $^{31}P\{^{1}H\}$ NMR study over a 250-370 K temperature range for the $[Pd\{PPh_3\}_2(dba)]$ system. 124

Figure 68: Schematic of a weakly bound PPh_3 ligand 124
Figure 69: $[Pd(P)_2(dba]$ system with the two different phosphorus environments labeled; A = near the η^2-bound dba substituent, B = near the majority of the bulk from the dba ligand. 126
Figure 70: Organic WCCs used in the preparation of ILs. A: alkylammonium, B: 1, 3-dialkylimidazolium, C: alkyltriazolium, D: alkylpyridinium and E: alkylphosphonium cations. 129
Figure 71: Born-Fajans-Haber cycle for the assessment of the melting (fusion) of a binary salt composed of complex ions ([A][X]), at temperature T, from lattice and solvation energies. Adapted from ref. 1. 130
Figure 72: Cations containing C-N-S^+ and S-N-P^+ backbones, all fully substituted with dialkyamino groups (NR_2). Adapted from ref. 22. 134
Figure 73: Phosphazenium ions of varying size with a range of alky groups. Adapted from ref. 17. 134
Figure 74: Imidazolium-type lipophilc cations, designed for phase-transfer applications, under drastic conditions; basic/nucleophilic media and high temperature. Adapted from ref. 18. 136
Figure 75: The steric bulk of the neopentyl groups on the phosphite slows completion of the Michaelis-Arbusov reaction, allowing the phosphonium intermediate to be observed by NMR spectroscopy..... 139
Figure 76: Tetraalkoxyphosphonium tetrafluoroborate salt synthesised from the trialkyoxonium salt.[26] 140
Figure 77: Trinorborn-1-yl phosphite compound.[24] 142
Figure 78: Diagram shows that the presence of phosphonium salts allows the picrate to transfer from the aqueous to the *fluorous* organic phase. Adapted from ref. 40..... 146
Figure 79: Weakly coordinating perfluorinated tetraalkoxyphosphonium target cation, (**8**). 147
Figure 80: Weakly coordinating ions due to the surface electrostatic repulsion..... 148
Figure 81: Molecular structure of $[MePPh_2\{OCH(CF_3)_2\}]^+[O_3SCF_3]^-$, (**10**). Two ionic pairs in each asymmetric unit, but one omitted for clarity. Thermal ellipsoids are drawn at the 50 % probability level. Crystal system: monoclinic. Space group: $P2_1/c$, R_1: 0.0388 (all data), wR_2: 0.0911 (>2sigma(I)). 153
Figure 82: Representation of the most significant compounds consisting of P-C-OH bonds. 155
Figure 83: $^{31}P\{^1H\}$ NMR spectra overlay for the reaction between $PPh\{OCH(CF_3)_2\}_2$, (**3**) and MeO_3SCF_3 in CD_2Cl_2 solvent to form (**11**); a) after addition of reagents at room temperature, b) after heating {12 hrs. at 50 ˚C}, c) after further heating {48 hrs. at 50 ˚C}. 159

Figure 84: ESI-MS spectra of correct mass and isotopic pattern for the $[P\{OC(CF_3)_3\}_4]^+$, (**8**) target cation on reaction with $PCl_3\{OC(CF_3)_3\}_2$ and the $[Ag(NCMe)_4]^+[P\{OCH(CF_3)_2\}_5F]^-$ ionic species, (**17**). 165
Figure 85: Molecular structure of $(CF_3)_3COH\cdots O=P\{OC(CF_3)_3\}_3$. Two $(CF_3)_3COH\cdots O=P\{OC(CF_3)_3\}_3$ molecules in each asymmetric unit but one omitted for clarity. Thermal ellipsoids are drawn at the 50 % probability level. Selected interatomic distances (Å) and angles (˚) for the above molecules; P(1)-O(1) = 1.570(3) , P(1)-O(2) = 1.576(3), P(1)-O(3) = 1.578(4), P(1)=O(4) = 1.434(3), O(4)-O(9) = 2.767(4), O(4)-P(1)-O(3) = 118.4(2), O(4)-P(1)-O(1) = 118.3(2), O(4)-P(1)-O(2) = 117.9(2), O(1)-P(1)-O(3) = 99.5(2), O(2)-P(1)-O(1) = 99.6(2), O(3)-P(1)-O(2) = 99.6(2). Crystal system: monoclinic. Space group: $P2_1/c$, R_1: 0.0569 (all data), wR_2: 0.1219 (>2sigma(I)). 167
Figure 86: A: Phosphenium ions are isolobal with singlet carbenes, B: Phosphenium ions can be stabilised by Lewis base coordination, C: The condensed phase isolated phosphenium salts is almost exclusively limited to phosphenium ions having at least one p-donor group at the phosphorus, such as NR_2. 170
Figure 87: Line drawings showing resonance forms of diamidophosphenium (top) and diphenylphosphenium (bottom) cations.[60] 171
Figure 88: Equilibrium favours the $[GaCl_3\text{-}PMe_2\text{-}PMe_2Cl]^+[GaCl_4]^-$ ionic material over the $[PMe_2]^+[GaCl_4]^-$ when excess $GaCl_3$ is added to the $[PMe_2\text{-}PMe_2Cl]^+[GaCl_4]^-$ phosphine-phosphenium adduct.[77] 174
Figure 89: DFT optimised structures at the (RI-)BP86/SV(P) level for the novel fluorinated ligand-phosphenium complexes. From the top left ligands (**5**), (**6**), (**3**), (**4**), (**1**) and (**2**) respectively. 178
Figure 90: Potential WCCs bearing perfluorinated alkoxy groups with nitrogen, antimony or sulphur centres. 186
Figure 91: Borate based WCAs.[299-301] 189
Figure 92: Carborane based WCAs. Adapted from ref. 228. 191
Figure 93: Teflate based WCAs.[330-333] 194
Figure 94: Perfluorinated-alkoxy aluminate and the dimeric perfluorinated-alkoxy aluminate WCA. [251, 263] 195
Figure 95: Lewis acidic based WCAs and the di-, tri- and tetra-nuclear antimony WCAs.[340, 341] 197
Figure 96: Molecular structure of $P\{OCH(CF_3)_2\}_5$, (**16**) at 150 K. Disordered parts and hydrogen atoms omitted for clarity. Thermal ellipsoids are drawn at the 50 % probability level. Selected interatomic distances (Å) and angles (˚):P(1)-O(1) = 1.679(2), P(1)-O(2) = 1.592(2), P(1)-O(3) = 1.590(3), P(1)-O(4) = 1.598(2), P(1)-O(5) = 1.666(2), average axial $P(1)\text{-}O_{(ax;\ 1,5)}$ = av. 1.673(2) Å, average equatorial $P\text{-}O_{(eq\ 2,3,4)}$ = av. 1.593(2) Å, O(4)-P(1)-

(O3) = 124.2(1), O(2)-P(1)-(O3) = 113.5(1), O(2)-P(1)-(O4) = 122.1(1), O(5)-P(1)-(O1) = 177.6(1). Crystal system: triclinic. Space group: P-1. R_1: 0.0493 (all data), wR_2: 0.1133 (>2sigma(I)). 202
Figure 97: Penta-alkoxy phosphorane containing a hexafluoroisopropoxy group found in a CSD search; GAWWIK. 202
Figure 98: The $^{31}P\{^1H\}$ NMR spectrum, range -144 to -150 ppm. The observed doublet, (-147.4 ppm, d, $^1J_{PF}$ = 818 Hz), for $[Ag(NCMe)_4]^+[P\{OCH(CF_3)_2\}_5F]^-$, (**17**) is found at a similar region to $[PF_6]^-$. 205
Figure 99: ^{19}F NMR spectrum, range -58 to -74 ppm. The observed doublet at -60.60 ppm (d, $^1J_{PF}$ = 818 Hz) for the P-F bond (*), a intense peak at -73.25 (s) for the equatorial alkoxy groups (eq) and a signal at -73.48 (br) for the axial alkoxy group (ax) of $[Ag(NCMe)_4]^+[P\{OCH(CF_3)_2\}_5F]^-$, (**17**)..... 206
Figure 100: Molecular structure of $[Ag(PPh_3)_3]^+[P\{OCH(CF_3)_2\}_5F]^-$ (**19**) at 110 K. Disordered parts and hydrogen atoms omitted for clarity. Thermal ellipsoids are drawn at the 50 % probability level. Selected interatomic distances (Å) and angles (˚): P(1)-F(1) = 1.627(6), P(1)-O(1) = 1.701(4), P(1)-O(2) = 1.693(2), P(1)-O(4) = 1.709(1), P(1)-O(5) = 1.690(1), average equatorial $P\text{-}O_{(1,2,4,5)}$ = av. 1.699(2), P(1)-O(3) = 1.704(3), F(1)-P(1)-O(3) = 176.8(2), O(1)-P(1)-O(4) = 90.6(2), O(4)-P(1)-O(5) = 93.8(3), O(5)-P(1)-O(2) = 86.2(3), O(2)-P(1)-O(1) = 89.4(2). Crystal system: monoclinic. Space group: $P2_1/c$. R_1: 0.0390 (all data), wR_2: 0.0901 (>2sigma(I)). 208
Figure 101: Spacefill representation of the anion in $[Ag(PPh_3)_3]^+[P\{OCH(CF_3)_2\}_5F]^-$ (**17**). Disorder omitted for clarity. F(1) atom labelled to visualise the steric bulk influence around this atom due to the bulky hexafluoroisopropoxy substituents on the phosphorus centre. .. 209
Figure 102: Molecular structure of $[P\{OCH(CF_3)_2\}_5F]^-[Na(NCMe)_2OP\{OCH(CF_3)_2\}_3]^+$, (**22**) at 110 K. Disorder and hydrogen atoms omitted for clarity. Thermal ellipsoids are drawn at the 50 % probability level. Selected interatomic distances (Å) and angles (˚): P(1)-O(1) = 1.698(2), P(1)-O(2) = 1.687(2), P(1)-O(4) = 1.688(2), P(1)-O(5) = 1.704(2), average equatorial $P\text{-}O_{(1,2,4,5)}$ = av. 1.694(2), axial P(1)-O(3) = 1.689(2), P(1)-F(1F) = 1.656(1), P(2)-O(6) 1.455(2) Å indicates this is a P=O, Na(1)-N(1) = 2.371(4), Na(1)-N(2) = 2.420(3), Na(1)-O(6) = 2.291(2), Na(1)-F(4) = 2.838(2), Na(1)-F(10) = 2.612(2), Na(1)-F(1F) = 2.218(2), O(6)-Na(1)-F(10) = 167.0(1), F(1F)-Na(1)-F(4) = 63.6(1), N(1)-Na(1)-N(2) = 105.5(1), F(1F)-Na(1)-N(1) = 104.4(1), F(4)-Na(1)-N(2) = 82.9(1), O(2)-P(1)-O(4) = 90.6(1), F(1)-P(1)-O(3) = 175.4(1), O(1)-P(1)-O(5) = 87.8(1), O(5)-P(1)-O(4) = 93.3(1), O(1)-P(1)-O(2) = 88.1(1). Crystal system: monoclinic Space group: $P2_1/n$. R_1: 0.0500 (all data), wR_2: 0.1253 (>2sigma(I)). 210

Figure 103: Spacefill diagram of $[P\{OCH(CF_3)_2\}_5F]^-[Na(NCMe)_2OP\{OCH(CF_3)_2\}_3]^+$, (**22**) highlights that the Na-F contact is present due to the small size of this ion allowing close contact. MeCN and $OP\{OCH(CF_3)_2\}_3$ ligands omitted for clarity. 212
Figure 104: Molecular structure of $[NEt_4]^+[P\{OCH(CF_3)_2\}_5F]^-$, (**24**) at 110 K. Disordered parts and hydrogen atoms omitted for clarity. Selected interatomic distances (Å) and angles (˚): P(1)-F(1) = 1.597(4), P(1)-O(1) = 1.672(3), P(1)-O(2) = 1.706(3), P(1)-O(3) = 1.715(3), P(1)-O(4) = 1.681(4), average equatorial $P\text{-}O_{(eq,\ 1,2,3,4)}$ = av. 1.694(3) Å, P(1)-O(5) = 1.722(4), O(2)-P(1)-O(1) = 88.5(1), O(5)-P(1)-F(1) = 172.6(2), O(3)-P(1)-O(4) = 94.3(2), O(2)-P(1)-O(3) = 88.6(2), O(4)-P(1)-O(1) = 88.6(1). Crystal system: triclinic. Space group: P-1. R_1: 0.0992 (all data), wR_2: 02829 (>2sigma(I)). 214
Figure 105: Phosphate anions with a greater number of fluoride groups. 225
Figure 106: Structure of common cations used for ILs..... 225
Figure 107: Double Schlenk vessel with Young valves and G4 frit plate. Measures are given in mm. Adapted from ref. 228. 226

LIST OF SCHEMES

Scheme 1: Chemical experiment using dissociation equilibrium constants, K_d to assess the steric parameters for phosphorus (III) ligands. 7
Scheme 2: Synthetic method by Brisdon *et al*. to yield known fluorinated phosphorus (III) ligands (R = Ph, ^{i}Pr; R^F = $\{C(CF_3)_3\}$, $\{CF(CF_3)_2\}_3$, cyclo-C_6F_{11}).[76] 22
Scheme 3: Synthesis fluorinated phosphorus (III) ligands reported by Caffyn *et al.*[90] 23
Scheme 4: Diels-Alder reaction of cyclopentadiene can give endo and exo isomer products. 28
Scheme 5: A possible mechanism for the cycloaddition reaction between a vinylallene with a terminal alkyne in the presence of a Rh(I)/$P\{OCH(CF_3)_2\}_3$ catalyst.[127] 29
Scheme 6: A possible mechanism for the rhodium catalysis of C-C coupling to form biaryl products, facilitated by $P\{OCH(CF_3)_2\}_3$, (**1**). Scheme adapted from ref. 132, 133. 30
Scheme 7: A possible mechanism for selective functionalisation at the less reactive β position of a thiophene in the presence of $PdCl_2$ (5 % mol) and $P\{OCH(CF_3)_2\}_3$ (10 % mol) catalytic system. Scheme adapted from ref. 135. 32
Scheme 8: Hydroformylation reaction, converts alkenes to aldehydes, giving two possible products.[30] 33
Scheme 9: Synthesis of a fluorinated phosphorus (III) ligand using the fluoroalcohol directly with triethylamine base in dry diethyl ether as the solvent. 35
Scheme 10: Synthesis of a fluorinated phosphorus (III) ligand, using sodium alkoxide ($NaOR^F$) in DCM solvent..... 35

Scheme 11: Synthesis of a phosphenium ion stabilised by fluorinated ligand, the example above uses ligand (**5**). 73
Scheme 12: Potential synthesis of chiral phosphorus (III) ligands. 79
Scheme 13: The three general mechanistic pathways for the formation of a vinyildene complex. 104
Scheme 14: Proposed products and intermediates for the reaction of **[Ru(5)-2]** with phenylacetylene 106
Scheme 15: The proposed mechanism for the cyclotrimerization of terminal alkynes in the presence of $[(\eta^5\text{-}C_5Me_5)RuCl]^+$ catalyst. Adapted from ref. 189. 109
Scheme 16: A tentative mechanism for the catalytic reaction between two phenylacetylene molecules with a ruthenium precursor to give a species A type product. Adapted from ref. 194. 112
Scheme 17: Two mechanistic pathways for the catalytic Heck cycle; either the cationic pathway from loss of X^- or the neutral pathway from loss of ligand. Figure adapted from ref. 202. 116
Scheme 18: Heck-Mizoroki reaction conditions, X = H, Me, OMe, Cl and L= PPh_3, $PPh_2OCH(CF_3)_2$, (**5**), $P\{OC(CF_3)_3\}_3$, (**2**) or no added ligand. 118
Scheme 19: Resonance form of 4-bromotoluene. 119
Scheme 20: The dba ligand was initially thought to be an innocent ligand and lead to the active palladium catalyst. 119
Scheme 21: Proposed intramolecular exchange of coordinated and uncoordinated double bonds of dba ligand (phenyl groups have been omitted for clarity). Adapted from ref. 217. 121
Scheme 22: Depicts that the presence of the π-acidic ligand, (**5**) at the Pd centre of **[Pd(5)-2]**. These reduce the electron-density, resulting in faster rotation around the dba-Pd bond. 122
Scheme 23: The dissociative pathway seems to be preferred over the associative reaction pathway for the exchange of the coordinated phosphorus (III) ligand (PR_3) with excess free ligand in the reaction mixture. 125
Scheme 24: Modes of decay of tetrakis(dialkylamino)phosphonium cations, paths 1-4. Adapted from ref. 17. 135
Scheme 25: The Michaelis-Arbusov mechanism. 137
Scheme 26: Synthesis of tetramethoxyphosphonium hexachloroantimonate. Adapted from ref. 27. 140
Scheme 27: Decomposition of the acyclic tetraalkoxyphosphonium salts form alkylfluorides and boron trifluoride complexes of the parent phosphate. [26] 140

Scheme 28: Phosphite reaction with α-halogenoketones goes *via* Michaelis-Arbusov (path a) or Perkow reaction (path b). Adapted from ref. 24. 141
Scheme 29: Alkylation of *fluorous* ponytail-containing phosphines with non-fluorinated reagents. Adapted from ref. 33. 144
Scheme 30: Alkylation of *fluorous* ponytail-containing phosphines with fluorinated reagents. Adapted from ref. 33. 145
Scheme 31: Attempted synthetic routes for highly fluorinated alkoxy-containing phosphonium ions. 149
Scheme 32: Possible outcomes of $P\{OC(CF_3)_3\}_3$, (**2**) reaction with NBS, A) ionic species, B) neutral species from oxidative addition and C) neutral species from ligand exchange of two molecules from B. 151
Scheme 33: The dibromophosphorane can brominate MeCN molecules to form the perfluorinated phosphite, **(2)**. 151
Scheme 34: Synthesis of the phosphonium salt $[MePPh_2OCH(CF_3)_2]^+[O_3SCF_3]^-$, (**10**). 152
Scheme 35: Reaction of PFP-hydroxyphosphine with methyl iodide.[50] 156
Scheme 36: Reaction of (HF)-hydroxyphosphine with methyl iodide. Adapted from ref. 50. 156
Scheme 37: Synthesis of 1, 2-oxaphosphetane. Adapted from ref. 50. 157
Scheme 38: Formation of phosphorane species from addition of $NaOCH(CF_3)_2$ to the $[PCl_4]^+[AlCl_4]^-$ ionic salt. 160
Scheme 39: Possible routes to the perfluorinated-*t*-butyl phosphite from phosphorus (V) species. 164
Scheme 40: Formation of a "melt", which can be further reacted for P-P bond formation. Adapted from ref. 78. 173
Scheme 41: Synthesis of novel fluorinated ligand stabilised phosphenium ions, the example above uses the $PPh_2\{OCH(CF_3)_2\}$, (**2**) ligand. 175
Scheme 42: Synthesis of the novel fluorinated ligand stabilised phosphenium complexes with trimethylsilyl triflate in place of the Lewis acidic $AlCl_3$. 176
Scheme 43: Potential synthetic methodology to the perfluorinated phosphonium cation, (**8**). 185
Scheme 44: The synthesis of trialkylsilyl carboranes.[273] 192
Scheme 45: The synthesis of anhydrous carborane acid.[273] 192
Scheme 46: The synthesis of alkyl carboranes.[273] 192
Scheme 47: Formation of tertiary cations from alkanes, using $[CH_3]^+[carborane]^-$. Adapted from ref. 273. 193
Scheme 48: The methylation of various weakly basic heteroatom substrates with $[CH_3]^+[carborane]^-$. Adapted from ref. 273. 193

Scheme 49: Decomposition of $[Bi(OTeF_5)_6]^-$ in MeCN solvent at room temperature. Adapted from ref. 331. 194
Scheme 50: Decomposition of $[Al\{OC(CF_3)_3\}_4]^-$, on reaction with highly electrophilic cations (E^+) *via* C-F activation, forming $[\{OC(CF_3)_3\}_3Al\text{-}F\text{-}Al\{OC(CF_3)_3\}_3]^-$.[339] 196
Scheme 51: Synthesis of the phosphorane *via* halogenation of the phosphite, followed by a metathesis reaction. 198
Scheme 52: The use of simple alkoxy groups on fluorine bonded phosphorane species result in their decomposition.[343-345] 199
Scheme 53: The synthesis of 2-arylamino-1, 1, 3, 3, 3-pentafluoropenes is achieved with the dehydrofluorination of N-hexafluoroisopropoxyanilines and not with the direct reaction of aniline and hexafluoropropene. Adapted from ref. 347. 200
Scheme 54: Simple synthetic preparation of the phosphorane, $P\{OCH(CF_3)_2\}_5$, (**16**). 201
Scheme 55: The (nearly) isodesmic reaction used to calculate FIAs in this study 203
Scheme 56: Simple synthesis of $[PF\{OCH(CF_3)_2\}_5]^-$ WCA, using $P\{OCH(CF_3)_2\}_5$, (**16**) and AgF. 205
Scheme 57: Synthesis of $[NEt_4]^+[P\{OCH(CF_3)_2\}_5F]^-$, (**24**). 214
Scheme 58: Methylation of the $[Ag(PPh_3)_3]^+[P\{OCH(CF_3)_2\}_5F]^-$, (**19**) salt to give the phosphonium salts. 217
Scheme 59: Reactivity of the $[Ag(PPh_3)_3]^+[P\{OCH(CF_3)_2\}_5F]^-$ salt, (**19**) and Ph_3CCl. 218
Scheme 60: Reactivity of the $[Ag(NCMe)_4]^+[P\{OCH(CF_3)_2\}_5F]^-$ salt, (**17**) and Ph_3CCl. 218
Scheme 61: Reactivity of the $[Ag(NCMe)_4]^+[P\{OCH(CF_3)_2\}_5F]^-$ salt, (**17**) and Ph_3CCl in excess AgF. 220

LIST OF TABLES

Table 1: Steric and electronic properties of selected ligands by Brisdon *et al. a:* For the complex [Rh(CO)Cl(P)$_2$]. *b and c:* Average and [observed] values. *d:* Calculated value taken from ref. 23, *e:* Data also from ref. 96. *f:* Data also from ref. 93. *g:* Data from ref. 20, 98 or 99. Table reproduced from ref. 95. 24

Table 2: $^{31}P\{^1H\}$, ^{19}F and ^1H NMR chemical shifts (δ/ppm) for (1) to (6). $^{31}P\{^1H\}$, NMR chemical shifts for the incompletely substituted phosphorus (III) products, * = ligands observed *in situ* only, all the rest have been isolated as pure products, [a] = selected ^1H NMR chemical shifts, for OC(H)(CF$_3$)$_2$ groups are only reported..... 37

Table 3: Hydrolysis products of the fluorinated ligands (**1**) to (**6**) observed by $^{31}P\{^1H\}$ NMR spectroscopy, * = hydrolysis product observed *in situ* only, all the rest have been identified by unit cell parameters of crystals suitable for X-ray diffraction analysis..... 39

Table 4: Comparison of ligand cone angles (θ/°) calculated using Tolman's method for DFT optimised at the (RI-)BP86/SV(P) level and XRD structures, where * = two molecules in unit cell so multiple cone angle values are calculated, # = values calculated for the ligand distorted over two positions, a = values from published structure from ref. 133, S = NCMe. 41

Table 5: P-O bond lengths for selected aryl phosphites found in the CSD..... 49

Table 6: Comparison of tungsten-phosphorus $^1J_{PW}$ coupling constants for a range of known [W(CO)$_5$L] complexes with **[W(1)]** to **[W(6)].** 64

Table 7: Experimental IR data of [W(CO)$_5$L] (**[W(1)]** to **[W(6)]**) complexes in comparison to other literature values, in order of increasing π-acidity, for the strongest intensity (E) ν_{CO} band. Note * = data extrapolated using systematic difference observed from experimental and DFT calculated at the (RI-)BP86/SV(P) level, [a] = extrapolated data from considering average difference between all the other ν_{CO} values and known (B$_1$) ν_{CO} . Complexes **[W(1)]** to **[W(6)]** are highlighted for clarity. 65

Table 8: DFT optimised [W(CO)$_5$L] at the (RI-)BP86/SV(P) level IR data of ligands (**1**) to (**6**), in order of increasing π-acidity for the strongest intensity (E) ν_{CO} band..... 67

Table 9: DFT optimised [Ni(CO)$_3$L] at the (RI-)BP86/SV(P) level IR data of all ligands (**1**) to (**6**), in order of increasing π-acidity. 67

Table 10: Calculated force field constants for a range of complexes [W(CO)$_5$L] (where L = phosphorus ligand) using experimentally found ν_{CO} values, extrapolated data used for all ν_{CO} modes of [W(CO)$_5$PhP{OC(CF$_3$)$_3$}$_2$], [W(CO)$_5$P{OC(CF$_3$)$_3$}$_3$]and the [W(CO)$_5$PF$_3$] (B1) ν_{CO} mode only..... 70

Table 11: Calculated force field constants for a range of complexes [W(CO)$_5$L] (where L = phosphorus ligand) using DFT calculated ν_{CO} values, at the (RI-)BP86/SV(P) Level..... 71

Table 12: Coupling constants, $^{1}J_{PP}$ for the [PPh_2-phosphorus (III) ligand]$^{+}$ adduct..... 73
Table 13: Rh-P bond lengths (Å) of selected crystal structures from a CSD search for *trans*-[$RhCl(CO)L_2$] complexes, where L = PPh_2X ligand with varying X substituents. Note the X substituent binds through to the phosphorus at the atom with the localized negative charge. 83
Table 14: The vibrational stretching frequencies ($\nu_{(CO)}$/cm^{-1}) of *trans*-[$RhCl(CO)L_2$] complexes, L = phosphorus (III) ligand. Complexes of ligands (**1**) to (**4**) and (**6**) are highlighted. 85
Table 15: $^{31}P\{^{1}H\}$ NMR spectroscopic data for *trans*-[$RhCl(CO)L_2$] complexes, L = phosphorus (III) ligand. Ligands (**1**), (**2**), (**4**) and (**6**) are highlighted. 87
Table 16: Substituent conformations for complexes with $P\{OCH(CF_3)_2\}_3$ (**1**). S = NCMe, $[A]^- = [PF_6]^-$..... 95
Table 17: Substituent conformations for complexes with $PPh\{OCH(CF_3)_2\}_2$, (**3**). S = NCMe, $[A]^- = [PF_6]^-$..... 96
Table 18: Substituent conformations for complexes with $PPh_2\{OCH(CF_3)_2\}$ (**5**). S = NCMe, $[A]^- = [PF_6]^-$..... 97
Table 19: Substituent conformations for complexes with $P\{OC(CF_3)_3\}_3$ (**2**). S = NCMe, $[A]^- = [PF_6]^-$..... 98
Table 20: Substituent conformations for complexes with $PPh\{OC(CF_3)_3\}_2$ (**4**). S = NCMe, $[A]^- = [PF_6]^-$..... 98
Table 21: Substituent conformations for complexes with $PPh_2\{OC(CF_3)_3\}$ (**6**). S = NCMe, $[A]^- = [PF_6]^-$..... 99
Table 22: Ruthenium-phosphorus bond lengths from crystallographic data for the ruthenium complexes with ligands (**1**) to (**6**) and others found from a CDS search of the $[Ru(\eta^5\text{-}Cp)P_1(NCMe)_2]^+$ fragment or [1] = from the JML group 2011/2012 masters student Steve McNicol's dissertation. * = shorter bond length than that found for any complexes from the CSD search. Bond lengths for ligands (**1**) to (**6**) are highlighted..... 102
Table 23: The Heck-Mizoroki reaction product percentage conversions to the alkene for the different ligand conditions (across the side) with different aryl halide substrates (across the top). These were calculated using GC-MS integrations. * = small amounts of stilbene and 1-methoxy-4-(1-phenyl-vinyl)-benzene present. # = small amounts of stilbene present. 118
Table 24: ^{31}P NMR (δ/ppm) data for selected phosphonium cations and their related phosphonates. Adapted from ref. 25. 138
Table 25: ^{31}P NMR (δ/ppm) data on *fluorous* ponytail-containing phosphonium cations.[33] 143
Table 26: Selected bond angles for the two phosphonium ions found in the asymmetric unit of the X-ray crystal structure of (**10**). * = carbon for methyl substituent. 153

Table 27: Selected bond distances for the two phosphonium ions found in the asymmetric unit of the X-ray crystal structure of (**10**). 153
Table 28: Summary of the $^{31}P\{^{1}H\}$ NMR and ESI-MS data for potential fluorinated phosphonium salts. 169
Table 29: The P-P (Å) bond lengths from the phosphine-phosphenium crystal structures. 174
Table 30: The $^{31}P\{^{1}H\}$ NMR (δ/ppm) data including the $^{1}J_{PP}$ values for all the novel fluorinated ligand-phosphenium complexes obtained. 176
Table 31: The P-P (Å) bond lengths of DFT optimised structures at the (RI-)BP86/SV(P) level for the novel fluorinated ligand-diphenylphosphenium complexes. 177
Table 32: FIA of the $P\{OCH(CF_3)_2\}_5$ phosphorane, (**16**) and other common Lewis acids. 204
Table 33: NMR shifts of $[P\{OCH(CF_3)_2\}_5F]^-$ anion with various ligands stabilising the metal cation. 207
Table 34: NMR shifts for various neutral and anionic hexafluoroisopropoxy-containing P(V) species. 219

LIST OF EQUATIONS

Equation 1: Mathematical description of a cone angle using half angles.[20] 6
Equation 2: Definition of the S4' parameter is the difference between ∠M-P-A and ∠A-P-A angles of a metal complex (M) with a phosphorus ligand (P) with substituents (A).[31] 9
Equation 3: Solid angle calculation, where A = shaded area caused by ligand shadow, r = radius of the sphere.[37] 12
Equation 4: Fractional solid angle.[37] 12
Equation 5: The ligand repulsive energy parameter.[9] 13
Equation 6: TEP method referenced to $P(^tBu)_3$, the most electron-donating ligand.[47] 16
Equation 7: Using reference point PH_3 V_{min}, the difference between this reference and PR_3 V_{min} can be taken as the combined effect of the electronic and steric effects of the PR_3 ligand.[53] 17
Equation 8: The steric effect of the PR_3 ligand (S_{eff}) can be defined as the difference between the V_{min} value of free PH_3 and the V_{min} value at the QM region of PR_3.[53] 18
Equation 9: The electronic effect of a phosphorus ligand (E_{eff}) can be defined as the difference between V_{min} (ONIOM, PR_3) and $V_{min}(PR_3)$.[53] 19
Equation 10: QALE property uses experimental data and stereoelectronic factors.[71] 21
Equation 11: Cotton-Kraihanzel force field assumption for (k_i) CO stretch–CO stretch interactions. 69
Equation 12: Calculation of the energy barrier for ligand exchange, $\Delta G^{\ddagger}$ ($Jmol^{-1}$). R = 8.314 ($Jmol^{-1}$) T_c = temperature of coalescence (K), σv = the difference in frequency for the separated signals (Hz). 123
Equation 13: The Gibbs free energy of the thermodynamic process of fusion. 130
Equation 14: Coulombs law. The magnitude of the electrostatic force (F) on a charge (q_1) due to the presence of a second charge (q_2), is given by the equation above, where *r* is the distance between the two charges and k_e is a proportionality constant, thus increasing r reduces the electrostatic force (F). 148

ACKNOWLEDGEMENTS

I would like to thank my supervisor Dr John Slattery for all his help and advice throughout my PhD. His enthusiastic approach has inspired me to be more creative and explore many avenues.

I would like to thank Adrian Whitwood, Rob Thatcher and Sam Hart for all their efforts in analysing all my air-sensitive crystals, Karl Heaton for the great mass spectrometry service he provides, Heather Fish for NMR help, Naser Jasim for his help drying solvents and Dr Robin Perutz for the IR related discussions.

I would like to thank the JMS project students over the years that have contributed to the work presented in this thesis; Rebecca Bibby for her catalysis work, Tim James for optimising the tungsten complexes presented, FlipFlop John for DFT calculations related to the palladium and phosphenium systems.

I would like to thank those from my early days as a PhD student; Mat Palframan and Pete Birch whom I shared a lab with from my days in D block, Cat Davies who was my mentor when I started out at York. Christine Welby for her support throughout her time at York, Christian Biewer for all the discussions and coffee breaks in the two years he was at York. I would like to thank the evolved JMS group and all JML group members, past and present for providing a friendly atmosphere and providing great banter. A special thanks to Neets, Lizzy, Rich and Lucy for proof reading chapters and their support throughout my writing up period; in particular Neets for her the motivational chats and Rich for his supply of fennel tea. DFT Dave for DFT related discussions and last minute calculations he ran for me and Dr Jason Lynam for being a great IPM, always making time to hear me out and for the chemicals that he probably doesn't realise I have used from his supplies. I would also like to thank Dan Smith for his help and advice in my last few weeks of writing up, Barbara Procacci my writing up buddy who shared the writing up experience with me, Ryan Mewis for helping me collate this thesis in a fancy way, the University of York for funding throughout my PhD and Mike Saunders for his help keeping me sane this last year with his continuous support.

Finally I would like to thank my Mum, Dad, Mussa, Salma, Hakeem, Hassam, Hasnen, Shazaad, Aaliya, Sajjad and especially my elder sister Mahrunisa for always giving me the strength and support throughout my studies. I will never be able to thank you enough. Love to my nephew Adam Ali and 1 day old new baby niece, without even knowing they are able to help me always see the bright side of life.

DECLARATION

This thesis is based on the work conducted by the author, in the Department of Chemistry of the University of York, during the period October 2008 to September 2012.

All the work described in the thesis is original except where indicated by special reference in the text and no part of this work has been submitted for any other degree either in the United Kingdom or overseas.

Any views expressed in this thesis are those of the author and in no way represent those of the University of York

Sharifa Hussein

21 September 2012

1 INTRODUCTION

The interests of this thesis focus on phosphorus compounds containing highly fluorinated alkoxy-groups. The chemical and physical properties of such species are very different in comparison to their hydrogen analogues. These include properties such as reduced nucleophilicity and enhanced thermal stability, making them attractive for their industrial use. The increased acidity of the fluoroalcohol species increases the rate of deprotonation *i.e.* CH_3CH_2OH pK_a = 15.9, CF_3CH_2OH pK_a = 12.8; $(CH_3)_2CHOH$ pK_a = 17.1, $(CF_3)_2CHOH$ pK_a = 9.3; $(CH_3)_3COH$ pK_a = 19.2, $(CF_3)_3C(CH_3)OH$ pK_a = 9.6, $(CF_3)_3COH$ pK_a = 5.4. It should be noted that the weaker acidity of the partially fluorinated alcohol is still much stronger than that of a non-fluorinated alcohol, by 6 to 9 pKa units.[4] This observed difference in acidity highlights the potential for significant changes in electronic properties at a phosphorus centre that is coordinated by highly fluorinated alkoxy-groups compared to a non-fluorinated analogue.

However, relatively few highly fluorinated alkoxy-containing phosphorus compounds have been made since the synthesis of the first fluoroalkoxy-containing phosphorus molecule, tris(2, 2 difluoroethyl)phosphate in 1909 by F. Swarts.[5] This is mainly because the synthesis of these molecules can be different to the classical routes to alkoxy-containing phosphorus compounds. To date, although some fluoroalkoxy-containing phosphorus species are known, they have not been used to their full potential and the synthetic routes to these species are often not very well developed. In particular, the perfluoro-*t*-butoxy {-$OC(CF_3)_3$} and the hexafluoroisopropoxy {-$OCH(CF_3)_2$} groups are used throughout the work discussed in this thesis. These were first studied in the late 1970's by Roschenthaler *et al.*[1] and Shreeve *et al.*[2] They investigated these particular fluorinated alkoxy groups on phosphorus centres, but the applications of such species were not explored.

The work presented in this thesis explores a wide variety of phosphorus species bearing highly fluorinated alkoxide-groups. Exploiting the different oxidation states of phosphorus; (III) and (V), both in their neutral and charged forms provides numerous potential uses and applications of such species that cover an extensive range, including Lewis acids, Lewis bases, cationic species and anionic species. This highlights the extreme effects a change in oxidation state, charge and the number of ligands can have to the function of a phosphorus-centred molecule.

The main aims of this project were to modernise previous findings in the area of fluorinated phosphorus alkoxides, by establishing suitable synthetic methods that are simple and can be

used routinely without specialised equipment (often required for fluorine chemistry). Investigation into understanding their unique chemical properties using a combination of experimental and theoretical methods were of key interest. This allowed for comparison to other related phosphorus species which are currently available and commonly used in commercial applications.

Highly fluorinated alkoxy-containing phosphorus (III) Lewis bases are found to be ideal for use as ligands, due to the availability of their lone pairs. Furthermore, the ability to "tune" the stereoelectronic properties of phosphorus (III) ligands by modification of the ligand substituents allows one to modify the properties of a metal complex to suit a particular application. Chapter 2 discusses in detail the steric and electronic properties of some novel fluorinated alkoxy-containing phosphorus (III) ligands. These ligands are found to be sterically bulky and electronically poor, a stereoelectronic combination that to date is sparsely filled in ligand space. Chapter 3 discusses the coordination chemistry of the novel fluorinated alkoxy-containing phosphorus (III) ligands, along with preliminary catalysis studies for these ligands. Relatively few applications of the hexafluoroisopropoxy-containing phosphorus (III) ligands have been explored in the literature. However, those reported indicate that the combination of their stereoelectronic properties allow for increased efficiency and selectively in some areas of catalysis. This thesis presents single-crystal X-ray diffraction data for a tris(perfluoro-*t*-butyl)phosphite, (**2**) and first structural evidence of a perfluorinated phosphite metal complex, see Figure 1.

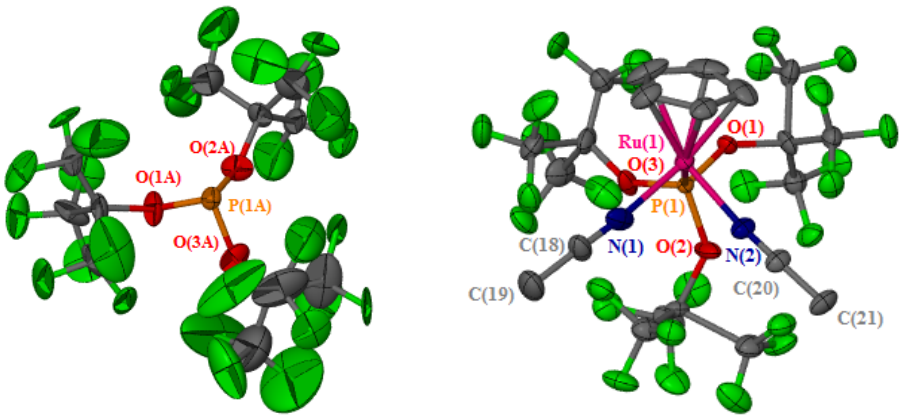

Figure 1: Single-crystal X-ray diffraction structure of a tris(perfluoro-*t*-butyl)phosphite, (2) (left) and $[(\eta^5\text{-}C_5H_5)Ru(NCMe)_2\{P(OC\{CF_3\}_3)_3\}]^+[Na_4\{OC(CF_3)_3\}_4PF_6.MeCN]^-$, [Ru(2)] (right). Note anion omitted for clarity.

Chapter 4 investigates the synthesis of cationic highly fluorinated alkoxy-containing phosphorus species. Oxidation of the highly fluorinated alkoxy-containing phosphorus (III) compounds leads to the formation of phosphonium cations *e.g.* $[MePPh_2\{OCH(CF_3)_2\}]^+[O_3SCF_3]^-$, (**10**), see Figure 2. Recent research has shown that the

quaternary phosphonium cations used for ILs have remarkable features, allowing them to be chemically and thermally very stable.[6, 7] Phosphonium salts have also attracted attention as *fluorous* phase-transfer catalysts, as well as ILs.[8, 9] The highly fluorinated alkoxy-containing phosphorus (III) ligands discussed in this thesis have also been utilised as stabilising ligands for highly electrophilic phosphenium cations, see Figure 2. The phosphorus (III)-phosphenium species that result from this have strong P-P bonds. The strength of the P-P interaction can be assessed using their $^{1}J_{PP}$ coupling constants.[10, 11] These can provide a gauge to understand the combined effects of the steric and electronic properties of such ligands and rank them in order of nucleophilicity.

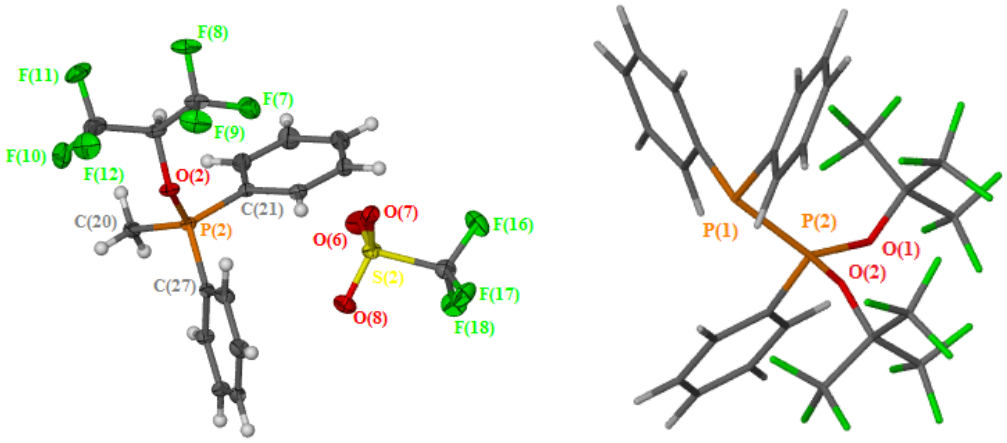

Figure 2: Single-crystal X-ray diffraction structure of $[MePPh_2\{OCH(CF_3)_2\}]^+[O_3SCF_3]^-$, (10) (left) and DFT optimised structure of $[PPh_2\text{-}PPh\{OC(CF_3)_3\}_2]^+$ (right).

Chapter 5 explores the use of highly fluorinated alkoxy-containing phosphorus species as strong Lewis acids and in WCA chemistry. Single-crystal X-ray diffraction of the pentakis(hexafluoroisopropoxy)phosphorane, (**16**) provides the first example of an X-ray crystal structure of a homoleptic fluorinated alkoxy phosphorane, see Figure 3. The fluoride-ion affinity (FIA) scale has been used to assess the Lewis acidity of this species. It is found that with a FIA of 437 kJ mol^{-1}, this phosphorane has a Lewis acidity in between that of $GaCl_3$ and $B(C_6F_5)$. This suggested that it was highly likely that (**16**) could react with anionic nucleophiles. In addition, the FIA calculations of (**16**) were found to be much higher than that of PF_5 (397 kJ mol^{-1}), implying that it was likely that this Lewis acid would easily abstract a fluoride to form a stable bulky anion, $[P\{OCH(CF_3)_2\}_5F]^-$ that is less susceptible to fluoride abstraction than $[PF_6]^-$. These fully saturated highly fluorinated alkoxy-containing phosphorus (V) compounds, $[P\{OCH(CF_3)_2\}_5F]^-$ have been successfully synthesised and investigated as WCAs, see Figure 3.

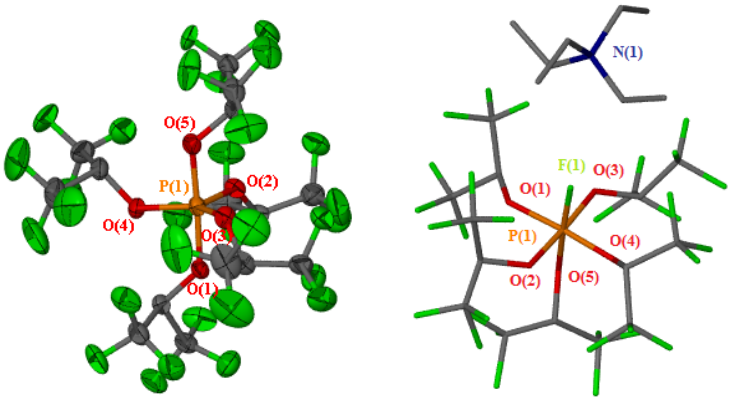

Figure 3: Single-crystal X-ray diffraction structure of $P\{OCH(CF_3)_2\}_5$, (16) (left) and $[NEt_4]^+[P\{OCH(CF_3)_2\}_5F]^-$, (24) (right).

The new generations of WCAs are key for stabilization of simple, but fundamentally important cations in the condensed phase and the generation of novel ILs. However, anions are either expensive, difficult to synthesise or unstable towards hydrolysis, making them unsuitable for industrial applications on a large scale. The monofluoropentakis(hexafluoroisopropoxy)phosphate anion salts investigated here are found to be both air- and moisture-stable, presumably from the combination of the steric bulk from the fluorinated alkoxy-groups, and coordinatively saturated phosphorus-centre. These anions are also relatively cheap to produce. WCAs are also of use in industrial scale olefin-polymerisation reactions and in electrochemistry.[12-14] More importantly large unsymmetrical, affordable, easy to prepare and air stable WCAs are useful for the synthesis of a range of room temperature ILs when paired with large cations. The low vapor pressure of such ILs make them ideal for replacing volatile organic solvents in industrial and laboratory processes as "green solvents". The ILs may even achieve selectivity by favoring specific transition states due to the ordering of the ions being different to that of solvent molecules.

Each results chapter within this thesis begins with a detailed literature review, followed by the results and discussion. A separate summary and future work section is discussed at the end of each chapter. Compounds that have been synthesised during this project are numbered in *bold type* in brackets, *e.g.* (**1**). Metal complexes of the ligands described in this thesis are numbered in *bold type* in square brackets containing the metal centre, the ligand and -2 if two ligands are coordinated to that particular centre *e.g.* **[Ru(6)-2]**. Only selected bond lengths and angles are presented for compounds that have been characterised using single-crystal X-ray crystallography during this project. For full data of these compounds, crystallographic CIF files are included on a disk that accompanies this thesis. Key data from the DFT calculations described in this thesis are also included on the disk.

2 BULKY, ELECTRON-DEFICIENT PHOSPHORUS (III) LIGANDS

2.1 LITERATURE REVIEW

2.1.1 Review of Common Ligand Steric Descriptors

Phosphorus (III)-centred Lewis bases are amongst the most commonly encountered ligands in coordination chemistry and homogeneous catalysis. The ability to "tune" the stereoelectronic properties of phosphorus (III) ligands by modification of the ligand substituents allows one to modify the properties of a metal complex to suit a particular application. For example, chiral phosphorus ligands can induce stereocontrol in asymmetric catalysis,[15, 16] electron-rich phosphines can accelerate the rate of oxidative addition in catalytic cycles where this is a limiting factor,[17, 18] and bulky ligands may facilitate phosphine loss, creating a vacant site for substrate binding or may impart selectivity by limiting access to the metal centre to certain molecules.[19]

In order to facilitate the application of phosphorus (III) ligands, certain parameters may be used to describe their stereoelectronic properties with varying degrees of complexity. Ligand "cone angles", S4' and He_8 parameters (all discussed below) are frequently used to describe the steric properties of a particular ligand.[20-23] Many studies have adapted these parameter methods to give computational ligand descriptors, keeping the methods up-to-date as science and technology continues to advance.[21] Computational methods are often preferred due to convenience. Such methods do not require the handling of toxic chemicals such as $Ni(CO)_4$. In addition, they can be calculated for a wide range of ligands; including those that are difficult to prepare or novel ligands where synthetic methods are unknown. A fundamental advantage of the use theoretical methods is that they can be calculated without any concerns regarding the purity of the compound. This is especially useful for establishing the properties of those compounds that are highly air-sensitive. Methods such as quantitative structure-activity relationship (QSAR), use computational methods to calculate many parameters to understand the ligand properties and then predict the experimental catalyst activities.[24] Although, there is no guarantee that the model includes all the important parameters, it does provide a starting point for the synthesis and screening for catalytic activity, as the virtual candidates can help narrow the initial search.[24]

Tolman's "ligand cone angle" (θ) is a concept that expresses the steric properties of phosphorus (III) ligands. Initially, this was a mechanical model, which relied on physical measurements from idealised space filling Corey-Pauling-Koltun (CPK) models using a

special jig and protractor.[25] In Tolman's words, "The steric parameter for symmetric ligands (all three substituents the same) is the apex angle of a cylindrical cone, centred at a distance of 2.28 Å (2.52 cm) from the centre of the P atom, which just touches the Van der Waals radii of the outermost atoms of the model", see **A** in Figure 4.[20] For values of θ above 180 ˚ a different method is in place, here the extent the angle passes over 180 ˚ is calculated (α). The total cone angle is then a sum of 180 + 2α. Cone angles of unsymmetrically substituted ligands have also been defined using half angles ($\theta_i/2$), this is the angle between the outermost atom of the ligand (S), the metal centre (M) and the phosphorus atom of the ligand (P) *e.g.* the S-M-P angle, see **B** in Figure 4 and Equation 1.[20]

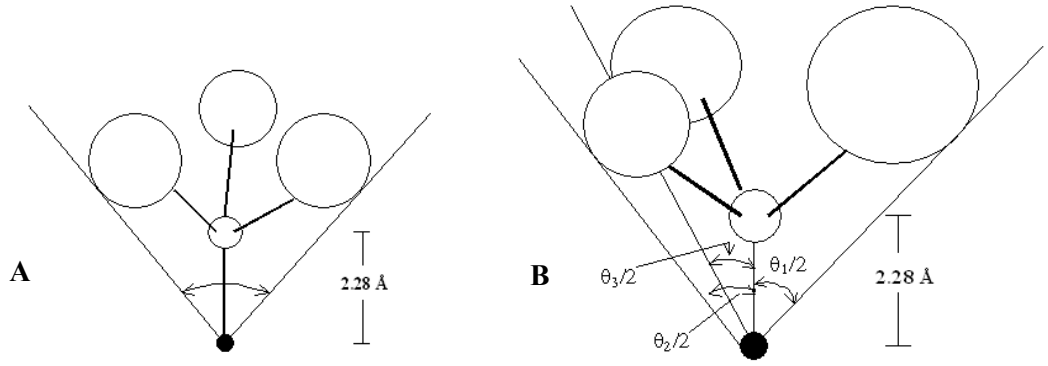

Figure 4: A) Diagrammatic representation of the Tolman cone angle used for symmetrical ligands.[20] B) Diagrammatic representation of half cone angles, used for ligands with different substituents.[20] Adapted from ref. [20].

$$\theta = 2/3 \sum_{i=1}^{3} \theta i/2$$

Equation 1: Mathematical description of a cone angle using half angles.[20]

Ligands are dynamic and are frequently conformationaly flexible; this can affect the cone angle values as the groups tend to move around. Minimum cone angles are calculated in this method to account for their flexibility, by "folding back" substituents that may rotate about the P-C bond so that the cone angle values are comparable. This is not a problem for ligands with a few degrees of freedom (*e.g.* PPh_3, PMe_3), or ligands such as $P(^tBu)_3$ with fixed geometry.[20] However, difficulty arises when minimising the cone angle of more conformationaly flexible ligands, as simply folding back substituents is not always appropriate. Chemical experiments using relative dissociation constants (K_d) for the reaction in Scheme 1 can be employed where difficulty arises with the mechanical model. Here the rates of dissociation show a steric effect. However, it seems that this is not sensitive to

changing *para*-substituents on aryl phosphites, and since phosphines dissociate much faster than phosphites of similar size, it is clear that their electronic effects are important too. Hence this is not an ideal model to compare the steric parameters of different classes of phosphorus (III) ligands.[26]

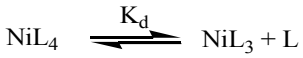

Scheme 1: Chemical experiment using dissociation equilibrium constants, K_d to assess the steric parameters for phosphorus (III) ligands.

Nevertheless, Tolman's cone angle method is widely used due to its strong correlations with experimental data[20] and has even been extended to amines.[25] Muller and Mingos have modernised the method by applying this calculation to crystallographic data, reducing assumption errors of a tetrahedral geometry from the inflexible spacefill models used initially (as in reality overcrowding can lead to distortions to lower energy conformations).[27] Muller and Mingos have discussed the variations of cone angles as a function of substituents and their conformations. They show normal distribution curves of the θ parameter for a range of crystal structures of the same phosphine.[21] They found that the triphenylphosphine cone angles in particular can "adjust to reflect the amount of space available in the complex".[21] This suggests that a whole range of ligand conformations need to be considered when understanding the ligands steric contributions in a particular system, as this clearly varies. Thus, looking at the minimum θ parameter as Tolman does, will not necessarily give a true appreciation of the ligands steric influence either when coordinated to a metal, or as a free ligand. It is however important to point out that it may be possible that none of the conformations found in the crystallographic data represent the true steric influence in solution. An average cone angle with standard deviation values for different environments is ideally required to truly compare phosphorus (III) ligands, and understand their potential steric bulk properties in any great detail.

Fundamental changes have been applied to Tolman's method to generate cone angles for phosphites. In some cases this increases θ by "up" to 25 °.[28] Initially it was assumed that the conformation was such that all P-O-R moieties were bent away from the phosphorus lone pair (see **A** in Figure 5) to give a minimum cone angle. Since this conformation had never been observed by X-ray analysis, it was thought that θ was underestimated for some phosphites. Crystallographic evidence[21] suggests most phosphites actually contain the conformations seen in **B**, **C** and in rare cases that of **D** in Figure 5.[29]

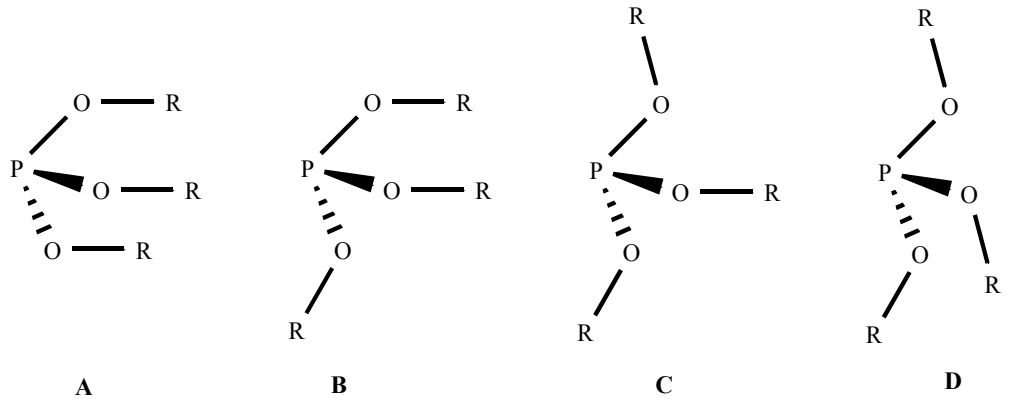

Figure 5: Assumed conformation of phosphites by Tolman (A) and those observed from crystallographic data (B-D).[29]

In addition Brown *et al.*[27] list other limitations of the cone angle method. These include:

i) Irregular Van der Waals surface formed from the outermost atoms on the phosphorus atom as substituents from ligands bound to the same metal can sometimes "mesh" with one another, causing closer packing than expected with the cone angle method.

ii) The values obtained from half-angle calculations of phosphorus ligands with different substituents may not be a great approximation, particularly when the substituents differ greatly.

iii) This method does not provide extensions to ligands such as sulfides, olefins and other ligands without three-fold axial symmetry.

A symmetric deformation coordinate parameter (S4') as an alternative measure of ligand steric bulk is described by Orpen *et al.*[22] This S4' parameter can be found by calculating the difference between ∠M-P-A and ∠A-P-A angles (see Equation 2) of a metal complex (M) with a phosphorus ligand (P) with substituents (A), where increased steric bulk causes a larger ∠A-P-A angle, hence a smaller ∠M-P-A angle.[23] Here, an inverse correlation occurs between S4' and the ligand steric bulk *i.e.* large S4' values correspond with small ligands (as S4' equals zero for perfect tetrahedral geometry around the phosphorus atom). The rhodium analogue of Vaska type complexes, [*trans*-$Rh(PR_3)_2(CO)Cl$], were used for this study as many of these have been structurally characterised and are of importance in catalysis (*i.e.* hydroformylation).[30]

$$S4' = \Sigma(\angle M\text{-}P\text{-}A_x) - \Sigma(\angle A_x\text{-}P\text{-}A_x), \text{ where } x = 1\text{-}3$$

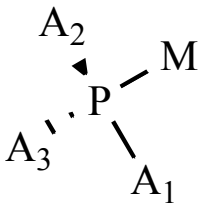

Equation 2: Definition of the S4' parameter is the difference between ∠M-P-A and ∠A-P-A angles of a metal complex (M) with a phosphorus ligand (P) with substituents (A).[31]

This method was used by Cundari *et al.*[23] to calculate S4' for ninety five phosphorus (III) ligands. Combined with an electronic parameter (SEP),[31] Cundari *et al.* developed a map of ligand space, discussed in Chapter 2.1.3. The advantages of this method include the ease of which S4' can be calculated from both X-ray crystallography databases and geometry optimised structures from computational methods.[23] However, there is a reduced accuracy for the modelling of phosphites (∠MPO tend to be too high and ∠OPO tend to be too low) when compared with the crystallographic data unlike that for the phosphines, hence any phosphite data should be analysed with caution. They conclude this may be due to the computational "difficulty in describing the accuracy of P-O versus P-C bonds".[23] However, it may be more likely that this is a cause of phosphites having added conformational flexibility than phosphines. In addition Cundari *et al.* [23] also report great discrepancy in the results of their mesityl phosphines *e.g.* $PMes_3$. This leads them to also suggest considerate caution when applying this S4' method to "extremely bulky phosphines".[23]

The He_8 model developed for the Ligand Knowledge Base concept (LKB) calculates the steric interaction energy (kcal mol^{-1}) between the phosphorus ligand and a fixed ring of eight helium atoms with a radius of 2.5 Å, see Figure 6.[32] The phosphorus centre is fixed to 2.28 Å above the centroid of this ring before optimisation of the structure.[32] This has been designed to mimic the steric interactions in an octahedral complex between the phosphorus (III) ligand and other *cis*-coordinated ligands (the He atoms are positioned where the *cis*-ligands would occur).[33] The phosphorus atom and the He_8 ring positions are fixed before optimisation, allowing the ligand bulk to adapt to the presence of the He_8 ring. In most cases, the conformational changes were not significantly different from the free ligand, however in some cases, optimisation from the free ligand failed and a different starting geometry, closer to that of a metal coordinated ligand had to be used.[33] This may not be a reliable comparison as coordinated ligand conformations are sensitive to both steric and electronic properties of different coordination environments. This approach can also overestimate the ligand size, as

the ligands will adapt their conformations to the available space in this specific environment.[33]

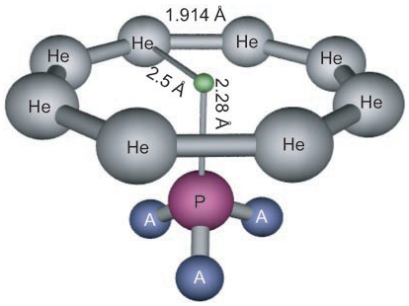

Figure 6: Geometry used for computation of the He_8 steric parameter: the interaction energy between the phosphorus ligand (PA_3) and a ring of eight helium atoms. Figure adapted from ref. [32].

This work shows high correlation with Tolman's cone angles as the energy increases with larger θ values, but deviation occurs for the significantly bulkier ligands.[32, 34] It is suggested the deviations are a result of the optimisations not necessarily minimising ligand size, whereas Tolman's cone angles calculate the smallest value by folding the substituents away from the metal centre.[20, 32, 34]

Another variation of this He_8 method has been proposed by Kozuch *et al.* where a Ne_{12} is used instead of He_8. Very few ligands were tested using this method, but those that were tested did vary greatly in their steric bulk influence.[32, 35] Kozuch *et al.* explain that by constraining distances and angles, "the neon ring could be opened like an umbrella, without altering the characteristics of the ligand". The only changes would be that of the cone angle, hence, this does not affect the ligand's inductive effects, see **A** in Figure 7.[32, 35] This method measures a cone angle between the tangents of the Van der Waals spheres of the Ne atoms with the vertex located at 2.28 Å from the phosphorus atom. The Ne_{12} ring moves along the phosphorus vertex, where a smaller ring is closer to the phosphorus centre and has a larger cone angle, see **B** in Figure 7.[32, 35] These type of steric descriptors allow calculations for a range of conformations (*i.e.* in a real system for a PPh_3 conformational energy landscape, different local minima and high energy transition states are found, these give areas of low/high effective cone angle) to understand the more dynamic aspects of a particular ligand, making them useful alternatives to Tolman's cone angles. It should be highlighted that the He_8/Ne_{12} methods do not account for the flexibility of real phosphines in the calculation. However, a range of calculations can be carried out on the different conformations to give an average value.[32, 35]

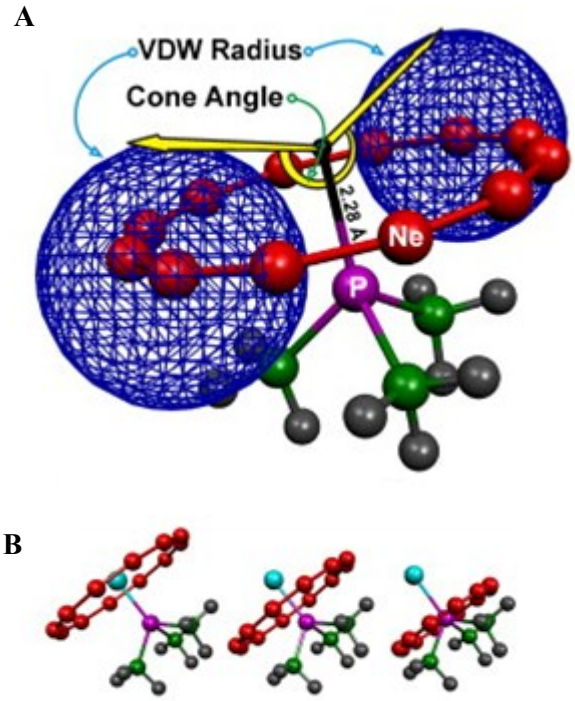

Figure 7: A) Definition of the Ne_{12} cone angle B) Examples of the PdL fragments at cone angles of 138 °, 178 ° and 218 °. Figure adapted from ref. [35].

Immirzi and Musco decided to generalise the cone angle model to three dimensions, giving a solid angle (Ω/measured in steradians, sr) by using single-crystal X-ray diffraction data.[36] The solid angle can be visualised if "the central metal of an organometallic complex is replaced with a light source, and each ligand casts a shadow on a sphere surrounding the molecule", see Figure 8.[37] This can be numerically given as the size of the shadowed area divided by the square of the radius of the sphere (see Equation 3), where Ω decreases as crowding around the metal centre increases.[37] If the entire sphere is covered with shadow, then the solid angle is 4π sr. Most often, the fractional solid angle, Ω_s, is more meaningful than the solid angle, see Equation 4.[37]

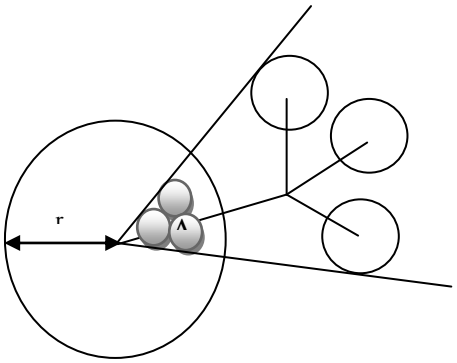

Figure 8: Definitions of the geometrical solid angle. Figure adapted from ref. [38].

$$\Omega = A/r^2$$

Equation 3: Solid angle calculation, where A = shaded area caused by ligand shadow, r = radius of the sphere.[37]

$$\Omega_s = \Omega/4\pi$$

Equation 4: Fractional solid angle.[37]

Figure 9 shows two views of projection of PPh_3 ligands onto a sphere of an arbitrary radius of 13 Å where the area of the ligand projection shadow used in the solid angle calculation can be easily identified.[37]

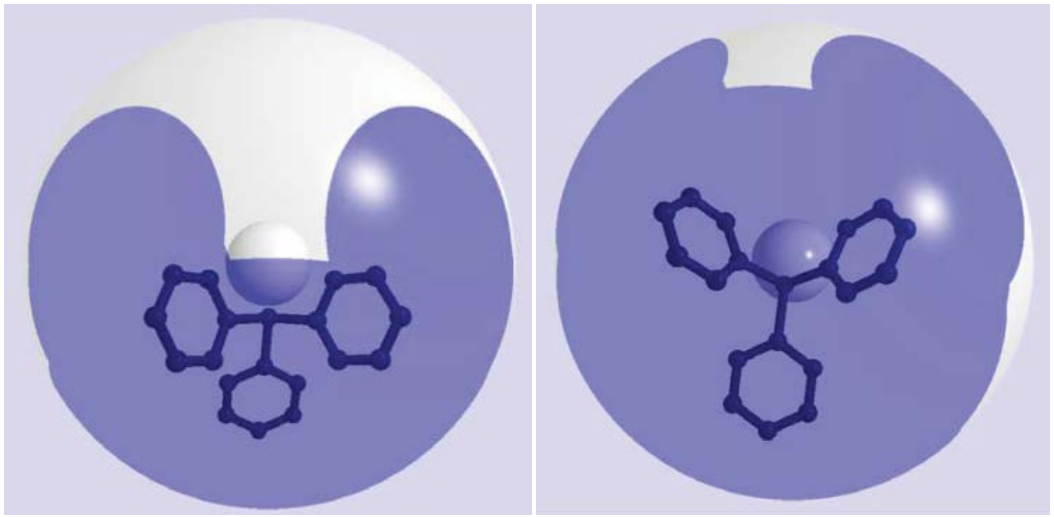

Figure 9: The area of the ligand projection shadow used for the ligand solid angle can be seen and the metal is shown as a white sphere for easy visualisation.[37]

This solid angle method was initially proposed as an alternative method to Tolman's angle when the molecular model was not applicable to several conformations of coordinated ligands. In addition, this method includes any intermeshing ability of adjacent ligands in crowded complexes by taking into account the dependence of the ligand's angular encumbrance (1/2 θ) on the orientation of the ligand itself about the metal-phosphorus bond. A computational method has also been developed and applied to alkyl and aryl groups as well as phosphorus (III) ligands and amines. In addition, the solid angle is thought to allow for more detailed information about the shape of the substituent as opposed to only noting the steric bulk.[39, 40] Unlike Tolman's cone angles, the solid angles are additive *e.g.* the total solid angle for the three spheres is the sum of the three individual solid angles.[24] However, most ligand substituents do not consist of simple spheres, but rather a collection of spheres where overlap is included. In order to obtain an accurate measure of ligand size, the overlap must be subtracted from the total solid angle.[24] Estimating the overlap of spheres poses difficulty and relies heavily on algorithms.[41]

The ligand repulsive energy parameter (E_R) is based on a molecular mechanics computational model of the ligand interacting with $[Cr(CO)_5]$,[27, 42] and therefore may be used for ligands where a reasonable molecular mechanics model can be calculated (values known for amines, arsines and thioethers as well as phosphorus ligands).[43-45] This is based on assumed force field parameters for an energy-minimised complex structure.[9] Free ligand conformations tend to differ to conformations of ligands in a complex; hence the latter are required for energy-minimised structure as a suitable starting point in computing E_R, this gives a much better estimation of the bound conformation of the ligand than in the cone angle method, where substituents are simply folded back.[9] The coordinates of the complex are frozen and the metal-ligand distance is varied and the repulsive Van der Waals energy is computed.[9] Variations of the repulsive Van der Waals energy ($dE_{VDW(repulsive)}$) and metal-ligand distance (d_r) represent the Van der Waals repulsive force acting between the ligand and the metal.[9] The product of the Van der Waals repulsive force and the equilibrium metal-ligand bond distance gives E_R (kcal mol^{-1}).[9]

$$E_R = r[dE_{VDW(repulsive)}/d_r]$$

Equation 5: The ligand repulsive energy parameter.[9]

This E_R parameter correlates well with Tolman's cone angles for phosphines, but differences occur when comparisons are extended for phosphites.[9] Since the oxygen lone pairs are explicitly accounted for in the E_R method, unlike in the CPK models used for the cone angle model, this could account for the observed differences.[9] In addition, this E_R method is likely

to provide an enhanced approximation for unsymmetrical as well as symmetrical ligands, unlike in the Tolman cone angle model.[9]

It is clear that steric bulk is an important property of ligands; the methods discussed above describe this well. However, as pointed out by Fey *et al.* "the detailed effect of ligand steric will depend on the anisotropy of the steric bulk, and this needs to be measured using more than one parameter".[46] Understanding conformational changes will however, allow for future ligands to be specifically chosen and designed to a specific task *e.g.* folding in will allow closer access of substrates to a metal centre or adopting a more bulky geometry and "protecting" the metal centre.[46]

2.1.2 Review of Common Ligand Electronic Descriptors

The electronic properties of ligands are equally important for understanding their reactivities. The Tolman electronic parameter (TEP) was an early method proposed for determining the electron donor/acceptor properties of phosphorus (III) ligands.[20, 47] This consisted of infrared spectroscopic measurements of the A_1 symmetric carbonyl stretching frequency, $\{\nu_{CO}\ (A_1)\}$ on a nickel centre, $Ni(CO)_3L$, in 0.05 M DCM solutions.[47] The work of Chatt and Hart,[48] first described the electron donor/acceptor properties of phosphorus (III) ligands, in which they observed dipole moments in $Ni(CO)_3L$ complexes to be smaller than expected for the complete donation of two electrons alone. Discussion remains on whether the orbitals utilised by the phosphorus (III) ligands which accept electron-density from the metal are P-R σ*-orbitals, P 3d-orbitals, or even a hybridised P-R σ*- and P 3d-orbital.[49] In studies by Orpen *et al.*, they show when analysing crystallographic data for multiple oxidation states of metal-phosphorus (III) ligands, that the M-P bond lengths increase on oxidising the metal, thus indicating a π-interaction is present. Reduction of the M-P π-interaction causes a decrease in the P-R bond length, suggesting the PR_3 π-orbital has P-R σ* character.[49]

Figure 10 below describes the bonding observed in electron donor-acceptor ligands; these can include CO, N_2, NO, alkenes and phosphorus (III) ligands. The first example shows the donor properties of the CO ligand *via* an σ-interaction to an empty metal d-orbital with its lone pair. In addition, a π-interaction due to its acceptor properties into its π* antibonding orbital is also possible. This increases the metal bond strength and can even be viewed as synergistic, as the stronger the σ-bond, the more electron-density is available to be pushed back on to the ligand *via* the π-bond. The second example shows the electron donor-acceptor properties of a phosphine ligand, where the σ* antibonding orbital overlaps with a filled

metal d-orbital *via* a π-interaction. This interaction is made stronger if the R group on the PR_3 is more electronegative, as this increases the 3p phosphorus-character, thus reducing the energy of the σ*-antibonding orbital.[49] The energies are better matched with the metal d-orbital; hence phosphites and fluorinated phosphorus ligands tend to be more π-acidic than standard phosphines as they contain orbitals of similar energies. It may also be argued that this trend is due to electron-withdrawing inductive effects of the substituents on the phosphorus 3d-orbital energies.[50]

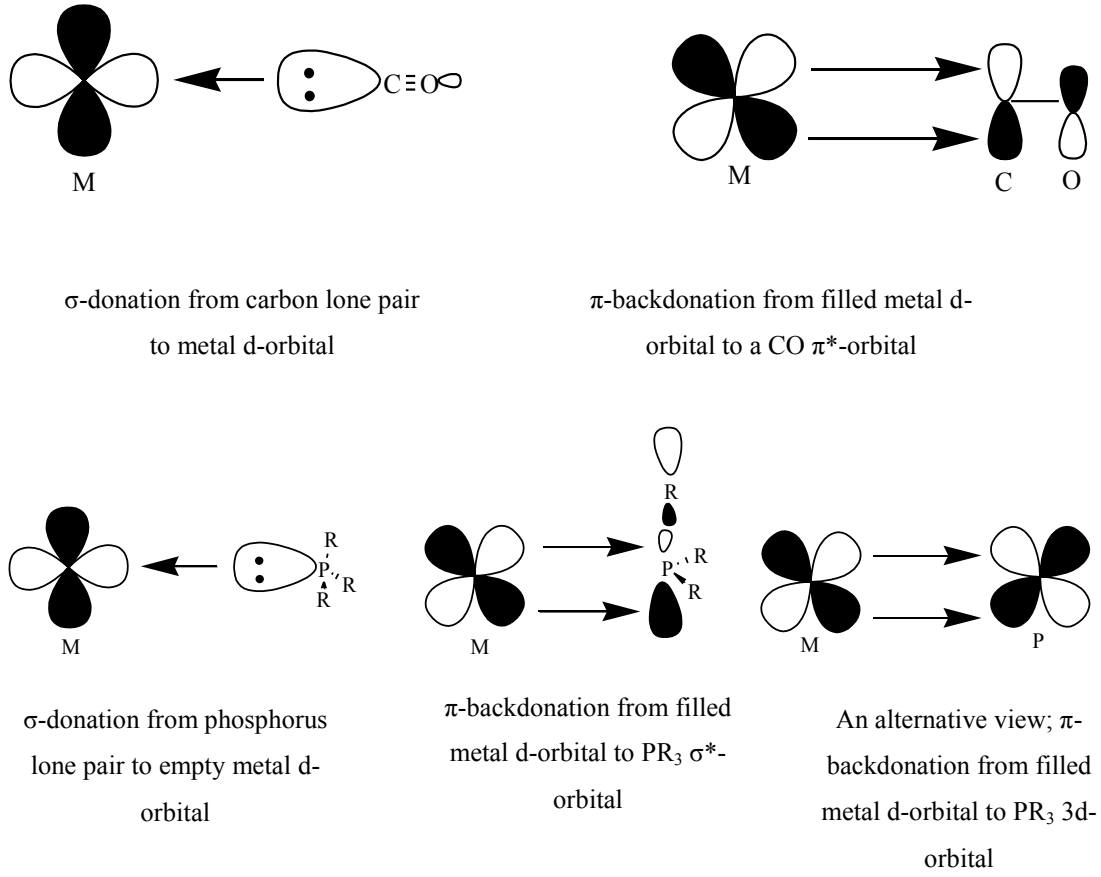

σ-donation from carbon lone pair to metal d-orbital

π-backdonation from filled metal d-orbital to a CO π*-orbital

σ-donation from phosphorus lone pair to empty metal d-orbital

π-backdonation from filled metal d-orbital to PR_3 σ*-orbital

An alternative view; π-backdonation from filled metal d-orbital to PR_3 3d-orbital

Figure 10: The electron donor-acceptor ligand properties of a CO ligand in the first example and a phosphorus (III) ligand in the second example. The orbital responsible for the acceptor properties of the phosphorus ligand may be the σ* antibonding orbital, the 3d-orbital or even a hybridisation of the two orbitals.

Tolman used this back-bonding argument and reasoned that using ν_{CO} (A_1) was a useful way to assess electron-density at the metal centre. Since donation from the metal centre to the CO ligand will decrease ν_{CO} due to population of the CO π* orbital, it was expected poor π-acceptors of a phosphorus (III) ligand would cause a lower ν_{CO} stretch.[47] A substituent additivity rule was also proposed, so predictions could be made for ν_{CO} (A_1) values of a $[Ni(CO)_3PX_1X_2X_3]$ complex by adding the contributions (χ_1) of the substituents (X_i).[47] The equation involves the value 2056.1 cm^{-1}, as this is the C≡O stretching frequency of $P(^tBu)_3$,

the most electron-donating ligand in the series, and so the scale can be set so $\chi_1 = 0$ for a ^{t}Bu substituent.

$$\nu_{CO}\,(A_1) = 2056.1 + \sum_{i=1}^{3} \chi i \text{ cm}^{-1}$$

Equation 6: TEP method referenced to P(^{t}Bu)$_3$, the most electron-donating ligand.[47]

This TEP method is useful in obtaining data for unavailable ligands or ligands too toxic to handle such as PH_3. This method is also useful for observing any trends in data sets *e.g.* an interesting observation showed the ν_{CO} (A_1) increased by 5 cm^{-1} for most groups following the insertion of oxygen between an organic group R and the phosphorus centre.[47] This indicates that the electronegative oxygen increases the electron acceptor properties of the phosphorus (III) ligands. However, there is not sufficient evidence to understand whether the increased ν_{CO} (A_1) values due to reduced electron-density on the nickel metal centre are as a result of reduced σ-donation or enhanced π-donation from the electron-withdrawing group. Disadvantages of this TEP method include using the very toxic, volatile [Ni(CO)$_4$] starting material to prepare the desired [Ni(CO)$_3$L] complexes, which then have to be stable enough to record IR spectra. Crabtree *et al.*[51] used computational methods to calculate ν_{CO} (A_1) values and overcome the toxicity and sensitivity problems. This computational electronic parameter (CEP) is of great advantage when designing novel ligands with specific properties for catalysis. Good correlations are observed between Crabtree's CEP and Tolman's TEP.[47, 51] Cundari has shown that semiempirical quantum mechanical (SEQM) methods are capable of achieving an accurate semiempirical electronic parameter (SEP) which can be computed much faster than using DFT methods.[31] This SEP method is not suited to nickel-based systems, therefore [W(L)(CO)$_5$], [Mo(L)(CO)$_5$], [Rh(L)(CO)$_2$Cl] systems were employed.[31] Optimisations were performed using crystallographic data with no disorder and no errors (R < 10 %) as input structures, and substituents on the ligands were modified for those where no data was found in the Cambridge Structural Database. A total of ninety five phosphorus (III) ligands have been electronically described using this SEP parameter for the [Rh(L)(CO)$_2$Cl] systems, including a range of exotic ligands, discussed below. It was found that the SEP is relatively independent of ligand conformation and correlates well with both computational CEP and experimental TEP, indicating the independent nature of the SEP and the metal environment to which the ligand is attached.[31]

Koga and Suresh proposed an alternative ligand electronic descriptor; this provides a quantitative measure of the σ-donating character of phosphines.[52] This method uses values of the molecular electrostatic potential minimum (V_{min}), which corresponds to the lone pair

region of several substituted phosphine ligands as determined by DFT calculations, see Figure 11.[52]

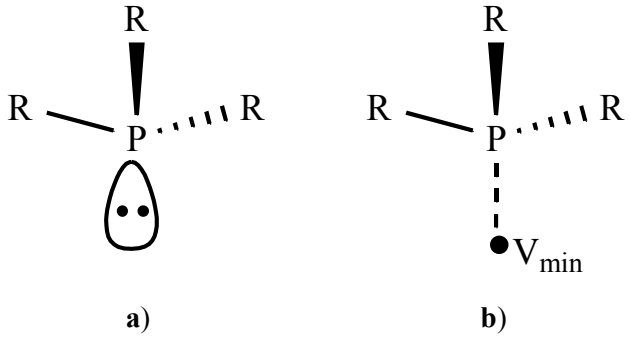

Figure 11: a) Phosphorus (III) ligand with its lone pair b) V_{min} in the lone pair region.[53]

Here the molecular electrostatic potential (MESP) is used, an important and widely used quantity for understanding molecular reactivity, intermolecular interactions, substituent effects and other chemical trends.[54-64] Koga and Suresh state that the simplest phosphine ligand PH_3 is generally described as an unsubstituted phosphine (V_{min} value is -28.22 kcal/mol).[52] Compared to this, an electron-donating substituent on a phosphine ligand has a more negative V_{min} due to an enhancement in the electron-density around the phosphorus lone pair region (*e.g.* PCy_3 V_{min} = -44.99 kcal/mol).[52] Similarly, an electron-withdrawing group has a more positive character of the V_{min} (*e.g.* $P\{CF_3\}_3$ V_{min} = -5.95 kcal/mol).[52] Both steric (bulkiness of the R group can alter the p character of the sp^3-hybridized lone pair orbital of the phosphorus) and electronic effects of the substituents on the phosphorus centre contribute to the electron-donating/withdrawing effects of the ligand, PR_3.[52] The combined electronic and steric effect (E_{eff} + S_{eff}) of a phosphorus ligand can be calculated with this method using Equation 7 below. Interestingly, they observe that all the phosphites studied have a negative value for E_{eff} + S_{eff} combined, indicating they have an electron-withdrawing nature due to the electronegative oxygen on the phosphorus centre, regardless of the extent of steric bulk from the R group.[52]

$$E_{eff} + S_{eff} = V_{min}(PH_3) - V_{min}(PR_3)$$

Equation 7: Using reference point PH_3 V_{min}, the difference between this reference and PR_3 V_{min} can be taken as the combined effect of the electronic and steric effects of the PR_3 ligand.[53]

The advantage of the method highlighted by Koga and Suresh is that it does not require the phosphorus (III)-metal complex or the protonated form of phosphine ligand for finding out the electron-donating properties. The free ligands can be used directly to obtain steric and

electronic properties. The theoretical study can be expanded further using a two-layer quantum mechanics (QM) - molecular mechanics (MM) optimization of phosphorus (III) ligands using the ONIOM method.[65] The QM inner layer is always constructed as PH_3, and the outer MM layer contains the substituents on the phosphorus ligand, see Figure 9.

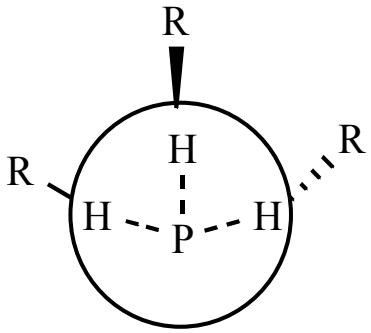

Figure 12: Two-layer ONIOM method. Here the inner hydrogen atoms are the link atoms.[65]

This is an effective method for separating the electronic and steric effect of the phosphorus ligands. The subtle variations in the electron distribution that arise as a result of the steric bulkiness as well as the conformational changes in the substituent groups is well reflected in the value of the MESP minimum (V_{min}) located in the QM region. Sterically bulky groups show a more negative V_{min} than a sterically less bulky group as the sp^3-hybridized lone pair orbital on the phosphorus atom will have increasingly more Lewis basic character as the bulkiness of the R group increases. Since the PH_3 is only considered using QM, the substituent electronic effects are not captured in the layered model, and any geometry changes are due to steric interactions between the substituents in the outer MM layer. The difference between the V_{min} value of free PH_3 and the V_{min} value at the QM region of PR_3 (as change in electron-density at the lone pair region is observed) is used as a measure of the steric effect of the PR_3 ligand (S_{eff}). Suresh has shown good linear correlation with their S_{eff} and the Tolman cone angles.[65]

$$S_{eff} = V_{min}(PH_3) - V_{min}(\text{ONIOM}, PR_3)$$

Equation 8: The steric effect of the PR_3 ligand (S_{eff}) can be defined as the difference between the V_{min} value of free PH_3 and the V_{min} value at the QM region of PR_3.[53]

Equations 7 and 8, described by Suresh *et al.* explain the electronic effect of a phosphorus ligand (E_{eff}), which can be defined as the difference between $V_{min}(\text{ONIOM}, PR_3)$ and $V_{min}(PR_3)$, see Equation 9.[53] This method can be used to describe the properties of ligands and to understand which ligands have substituents that make them electron-donating, yet the electronic effects are electron-withdrawing. For example $P(CF_3)_3$ remains electron-

withdrawing and can be explained by its high E_{eff} value or the E_{eff} value for PPh_3 is close to zero, but the ligand is electron-donating because of its positive value for S_{eff}.[53]

$$E_{eff} = V_{min}(ONIOM, PR_3) - V_{min}(PR_3)$$

Equation 9: The electronic effect of a phosphorus ligand (E_{eff}) can be defined as the difference between V_{min} (ONIOM, PR_3) and $V_{min}(PR_3)$.[53]

Suresh *et al.* conclude that the steric and electronic effects of a phosphorus ligand are "intermingled and nearly inseparable in every system, and therefore only the combined effect is always observed in their associated electronic properties".[53] The method describes an "effective way to assess the amount of steric-effect-induced electronic variations" of the phosphorus (III) ligands, and correlates well with S4' values for free phosphorus (III) ligands {described using similar approach to that for S4' of complexed phosphorus (III) ligands}.[53] Giering e*t al.*[66] have argued that a one-parameter V_{min}-based correlation for the electron-donating ability may not be accurate for a variety of phosphorus (III) ligands and not enough ligands (thirty three) have been studied in the original work to study any correlations with other methods. In addition, Suresh states that the interaction energy between the metallic moiety and the phosphine ligand would be proportional to the V_{min} value, if there is no significant back-bonding from the metal to the phosphine. This suggests that this method is not useful for π-acidic ligands. Conversely, Kühl[67] compared several approaches used for predicting the net electron-donating ability of phosphine ligands and stated that V_{min} values of the MESP are useful for calculating the electron-donating ability of a broad range of phosphorus (III) ligands and correlate well with TEP.

Guesev *et al.* proposed a similar method in 2009. This involved DFT calculations on [(η^5-C_5H_5)Ir(CO)L] complexes (where L is the desired ligand) to give CO stretching frequencies and optimised structures that give C-O bond lengths for the corresponding CO ligands attached.[3] The [(η^5-C_5H_5)Ir(CO)L] complex was chosen as it contains minimum ligand repulsion due to its low coordination number. This eliminates complications from vibrational coupling as it has one CO ligand only and has the CO at an ~90 ˚ angle to the desired ligand, thus avoiding any interference due to the *trans*-influence.[3] The key advantage of this method is that Gusev has shown that the use of this complex allows the comparison of a large range of different ligand classes, such as N-heterocyclic carbenes, alkenes and other nitrogen and oxygen containing ligands. This key feature makes this recent method more appealing than the other common gauges of the electronic properties, such as TEP, CEP, SEP described above.[31, 47, 51] The stretching frequencies, ν_{CO} obtained from these

calculations allow the comparison of ligand donor properties (lower energy ν_{CO} frequencies are associated with stronger donors and *vice versa*).

Other spectroscopic features such as metal-phosphorus coupling constants are also commonly used as indicators of the electronic properties of phosphorus (III) ligands, and have known to correlate with the original TEP.[68] The $^{1}J_{PSe}$ coupling constants of phosphine-selenides can also be used to assess the electronic properties of the phosphine, these are observed as satellites in the $^{31}P\{^{1}H\}$ NMR spectra. This coupling constant is related to the s-character of the lone pair of the phosphorus atom. The HOMO energy level is related to the phosphorus lone pair and is higher for phosphines with lower s-character in the lone pair; hence the electrons are more available for bonding and thus the phosphorus is a stronger σ-donor.[69] The $^{1}J_{PSe}$ coupling constant has an inverse relationship with the phosphines σ-donor ability; hence smaller $^{1}J_{PSe}$ coupling constants are observed for strong phosphine σ-donors.[69] Phosphine-selenide compounds can be prepared by heating the phosphine in toluene with excess selenium powder to increase the rate of oxidation. More severe conditions may be required for more π-acidic ligands.[70] In addition, the difference in chemical shift for the free phosphine and selenides phosphine can also give electronic information *i.e.* an upfield shift can indicate reduced deshielding of the phosphorus nucleus suggesting the $R_3P{=}Se$ resonance form is more likely than the ionic $R_3P^{+}\text{-}Se^{-}$.[70]

2.1.3 Review of Stereoelectronic Maps of Phosphorus (III) Ligands

Combined steric and electronic parameters can provide a stereoelectronic map of phosphine "ligand space". These can be used to link structure to function and aid in the design of ligands and complexes for particular applications. Such design principles are exemplified in concepts such as Ligand Knowledge Base (LKB), in which three hundred and forty eight monodentate phosphorus (III) ligands provide coverage of "ligand space".[32-34, 46] Fey *et al.* suggest that these studies bring research "closer to being able to rationally design and evaluate novel catalysts *in silico*, which should ultimately allow for targeted synthesis and efficient reaction optimisation."[33] Other examples of stereoelectronic maps can be found by Tolman (plot of TEP and θ)[20] and Suresh *et al.* (plot of E_{eff} and S_{eff}, where both positive E_{eff} and S_{eff} values indicate electron-donating effects {*i.e.* $P^{t}Bu_3$ is known to have the maximum steric effect in their studies} and both negative E_{eff} and S_{eff} values indicate electron-withdrawing effects {*i.e.* $P(CF_3)_3$ is known to have the highest E_{eff} in their studies}).[53] Another more complicated approach includes that by Giering *et al.* termed quantitative analysis of ligand effects (QALE). This method uses experimental data and stereoelectronic factors to generate a phosphorus ligand knowledge database of one hundred and thirty eight

ligands.[71] The QALE equation of the following; σ-donor capacity of the ligand (χ_d), Tolman's cone angle (θ), the steric threshold (θ_{st}), the switching function that turns on the steric term after the size of the ligand surpasses the steric threshold (λ), an extra electronic effect originally associated with the number of aromatic pendant groups but is now thought to be more general (E_{ar}), a measure of the π-acidity (π_p) and i which describes the number of hydrogens in $PZ_{3-i}H_i$, see Equation 10.

$$\text{QALE property} = a\,\chi_d + b(\theta - \theta_{st})\lambda + c\,E_{ar} + d\pi_p + e\,i + f$$

Equation 10: QALE property uses experimental data and stereoelectronic factors.[71]

As briefly described earlier Cundari *et al.* considered a map of ligand space derived from computed steric and electronic parameters and commented on the fact that a large proportion of work with phosphorus (III) ligands involves species that are relatively electron-rich.[23] The smaller proportion of work involving electron-poor phosphorus (III) ligands typically involve species that are relatively small, *i.e.* $P(CF_3)_3$.[23] Therefore, there exists a significant gap in ligand space corresponding to electron-poor, sterically bulky phosphorus (III) ligands which may be of use particularly for stabilisation of metals in low oxidation states that are coordinatively unsaturated.[72] Exploring novel ligands using the advantages of computational analysis, Cundari *et al.* were able to determine the properties of $P\{C(CF_3)_3\}_3$ and recommend this as a suitable ligand identified to fill the niche in the stereoelectronic phosphorus ligand map, in particular for its bulky steric properties in addition to its π-acidic properties.[23] Cundari *et al.* also predict that the phosphite equivalent $P\{OC(CF_3)_3\}_3$, would have similar electronic properties to $P\{C(CF_3)_3\}_3$, but sterically is much smaller, and suggest it is similar in size to $P(OCF_3)_3$.[23] DFT $[Ni(CO)_3L]$ optimised structures on BP86/SV[P] level of theory, allow for one to compare cone angle calculations for $P\{OC(CF_3)_3\}_3$ (discussed in further detail in Chapter 2.2.3.1) and $P(OCF_3)_3$. The values found are very different, due to the change in steric bulk. The bulky $P\{OC(CF_3)_3\}_3$ (θ = 195 °) ligand has a much larger cone angle than $P(OCF_3)_3$ (θ = 142 °). These calculations contradict the predictions by Cundari *et al.*, as it seems they have underestimated the potential steric influence of a $P\{OC(CF_3)_3\}_3$ ligand.[23] Giering *et al.* reported that the π-acidity of PF_3 to be five times that of $P(OR)_3$ and three times than that of PCl_3.[73, 74] They reveal $P(CF_3)_3$ is also very π-acidic and this π-acidic effect of the "fluorine atom is transmitted to the phosphorus through at least three bonds and appears to have vanished by five bonds".[71] It appears that intervening an ethylene $-CH_2$ group does insulate phosphorus from the extreme π-acidity from the electron-withdrawing fluorine atoms, hence can be used as a handle to fine tune the

electronic properties of the ligand. This allows *fluorous* phosphine ligands to be developed without significantly affecting the electronic properties.[71] Newman *et al.* have recently published new studies on a phosphinane ligand with moderate steric bulk (similar in cone angle to PCy_3) and similar electronic properties to a PPh_3 ligand.[75] However, it appears phosphorus (III) ligands require fluorinated groups to encompass extremely π-acidic electronic properties.

2.1.4 Known Bulky Electron Deficient Phosphorus (III) Ligands

Brisdon *et al*. have attempted to overcome the gap corresponding to electron-poor, sterically bulky phosphorus (III) ligands using air and moisture stable ligands such as R_2PR^F (R = Ph, ^{i}Pr; R^F = {$C(CF_3)_3$}, {$CF(CF_3)_2$}$_3$, cyclo-C_6F_{11}).[76] These have been synthesised from perfluoroalkyliodides which react with trimethylsilyl-containing phosphines to achieve higher yields of these materials than those from Grignard or lithium reagents used previously.[76, 77]

$$R_2PSiMe_3 + R^FI \rightarrow R_2PR^F + Me_3SiI$$

Scheme 2: Synthetic method by Brisdon *et al*. to yield known fluorinated phosphorus (III) ligands (R = Ph, ^{i}Pr; R^F = {$C(CF_3)_3$}, {$CF(CF_3)_2$}$_3$, cyclo-C_6F_{11}).[76]

These new species add to the few known fluorinated phosphorus (III) ligands that are available.[78] Examples mainly include the fluoroaryl phosphorus (III) ligands[78] and the rare perfluoroalkyl phosphorus (III) ligands; those containing -CF_3[79] and -CF_2CF_3[80] are the only ones studied in any detail. Roddick *et al.* reported a more practical synthesis compared to previous methods for bis(pentafluoroethyl)phosphines; $(C_2F_5)_2PR$ (R = C_2F_5, ^{t}Bu, Ph, Me and Et_2N).[80] Synthetic routes to trifluoromethyl-substituted phosphines such as $P(CF_3)_3$,[81] $P(CF_3)_n(R)_{3-n}$ (R = H, halide, alkyl, Ph, Et_2N)[81, 82] and $(CF_3)_2P(CR_2)(CR_2)P(CF_3)_2$ (R = H, F),[83] as well as some higher perfluoroalkyl derivatives have been established too.[84] However, the development of these ligands has been limited by the practical difficulties in the synthetic methodologies used *e.g.* the synthesis of $(C_2F_5)_2PR$ phosphines uses the $LiCF_2CF_3$ starting material. Although $LiCF_3$ is extremely unstable and rapidly eliminates LiF to form a difluorocarbene, even at temperatures below-100 ˚C, hence an alternative method was required for the synthesis of -CF_3 containing phosphines. The method utilised involved thermal addition of $(CF_3)_2P$-$P(CF_3)_2$ to ethylene[85] or 1,2-diiodethane.[86] However, this method was known to be tedious with many difficult separation steps. The latter three of the bis(pentafluoroethyl)phosphines were reported to have successfully complexed on a $[Mo(CO)_5L]$ centre, and only the $(C_2F_5)_2PMe$ ligand was coordinated to a $[Cr(CO)_5L]$ centre.

Essentially identical values of ν_{CO} (A_1) for the [$Mo(CO)_5\{(C_2F_5)_2PR\}$] complexes (R = Me, Ph, NMe_2) were found; 2089, 2088, and 2090 cm^{-1}, respectively. Roddick *et al.* concluded that the ν_{CO} (A_1) values are only "a rough indicator of changes in effective metal electron-density" and are "relatively insensitive to phosphine substituent effects", as shown by the small difference between ν_{CO} (A_1) for [$Mo(CO)_5(CF_3)_2PMe$] (ν_{CO} (A_1) = 2094 cm^{-1}) and [$Mo(CO)_5(CF_3)PMe_2$] (ν_{CO} (A_1) = 2086 cm^{-1}).[87] Roddick *et al.* place their bis(pentafluoroethyl)phosphines between that of [$Mo(CO)_5PMe_3$], [$Mo(CO)_5PPh_3$], [$Mo(CO)_5P(OMe)_3$] {ν_{CO} (A_1) = 2071, 2073, 2080 cm^{-1}, respectively}[88, 89] and that of the strong π-acceptor ligands PF_3 (ν_{CO} (A_1) = 2103 cm^{-1}) and $P(CF_3)_3$ (ν_{CO} (A_1) = 2104 cm^{-1}).[87] They describe these ligands to have "strong π-acceptor ability and steric influence, as well as chemical inertness and solubility in *fluorous* media afforded by the perfluoroalkyl substituents".[80] Caffyn *et al.* later reported the synthesis of these phosphorus (III) ligands using perfluoroalkyltrimethylsilanes with triphenylphosphites and CsF as an initiator.[90]

$$P(OPh)_3 + 3R^FSiMe_3 + 3CsF \rightarrow PR^F_3 + 3PhOSiMe_3$$

Scheme 3: Synthesis fluorinated phosphorus (III) ligands reported by Caffyn *et al.*[90]

Unfortunately, this synthetic method described by Caffyn *et al*. was limited due to the lack of available perfluoroalkyltrimethylsilanes or suitable perfluoroalkyl starting materials *i.e.* the Grignard and lithium reagents are either unstable or inaccessible. Thus, these types of phosphorus (III) ligands were previously only prepared using specialised methods, including direct fluorination using F_2 [91] or electrochemical fluorination of phosphines in anhydrous HF [92] *etc.* This highlights the importance of the work by Brisdon *et al.*, as they have allowed access to a range of novel phosphorus (III) ligands using a convenient route. These have not yet been studied in catalysis to appreciate their rare and specific properties which make them unusual in comparison to their hydrogen analogues.[76]

Perfluorovinyl-containing phosphines, $PR_{3-n}(vinyl^F)_n$ {R = Ph, NMe_2, NEt_2, OEt, ^{i}Pr, Cy, OBu; n = 1, 2; $vinyl^F$ = $CF{=}CF_2$, $CCl{=}CF_2$, $CF{=}CFH$, $CCCF_3$} and the chiral ^{n}BuPhP($CF{=}CF_2$) mostly synthesised by Brisdon *et al.* are also found to contain these rare stereoelectronic properties.[76, 77, 93-97] Coordination of these ligands has been investigated with a range of metal centres including square planar rhodium (I), platinum (II), and palladium (II) to provide a better understanding of their electronic (IR ν_{CO} stretches, and $^1J_{RhP}$ coupling constants) and steric properties (from crystal structures).[95] The electronic (IR ν_{CO} stretches) and steric properties (θ and S_4') are summarised in Table 1. The steric properties contain variations depending on their complex environment.

P(III) Ligand	*v(CO)[a] / cm^{-1}*	*Tolman Cone Angel[b] /°*	*S_4' [c] /°*
P^iPr_3	1950 [g]	160 [g]	35 [d]
PPh_3	1965 [g]	138 [g]	35 [d]
$PEt_2(CF=CF_2)$ [e]	1981	152	44
		[142, 157, 157, 154]	[45, 66, 30, 37]
$P^iPr_2(CF=CF_2)$	1981	165	34
		[168,166,160, 159, 169, 166, 165]	[32, 35, 35, 35, 30, 35, 39]
$PCy_2(CF=CF_2)$	1979	169	29
		[168, 170,168,170]	[31, 23, 34, 29]
$PPh_2(CF=CF_2)$ [f]	1989	163	34, 39 [d]
		[164, 162, 164, 160]	[38, 38, 36, 25]
$PPh(CF=CF_2)_2$	2002	161	39, 40 [d]
		[169, 163, 161, 150]	[44, 36, 38, 37]
$PPh_2(C_6F_5)$	1982 [g]	158 [g]	38 [d]
$PPh(C_6F_5)_2$	1996 [g]	171 [g]	38 [d]
$P(OMe)_3$	2006 [g]	107 [g]	63 [d]
$P(OPh)_3$	2016 [g]	128 [g]	76 [d]

Table 1: Steric and electronic properties of selected ligands by Brisdon *et al.* *a:* For the complex $[Rh(CO)Cl(P)_2]$. *b and c:* Average and [observed] values. *d:* Calculated value taken from ref. [23], *e:* Data also from ref. [96]. *f:* Data also from ref. [93]. *g:* Data from ref. [20], [98] or [99]. Table reproduced from ref. [95].

It appears that these perfluorovinyl groups are similar electronically to electron-withdrawing alkoxy groups (OR) but sterically smaller than that of a perfluorinated phenyl group (C_6F_5). However, in comparison to -C_6F_5, the perfluorovinyl groups are more electron-withdrawing.[77, 95] Brisdon *et al.* concluded that these fluorinated vinyl phosphines contain distinct properties between those of the hydrogen based phosphines (sterically demanding) and phosphites (electronically π-acidic).[95]

In 1994, Horvárth and Rábai introduced *fluorous* chemistry,[100] since then there has been considerable interest in the synthesis and application of species containing long perfluoroalkyl substituents (also known as *fluorous* ponytails).[101] Hope *et al.* studied in particular the steric and electronic implications of perfluoroalkyl substituents (*e.g.* CF_3, C_6F_{13})[102] on phosphorus (III) ligands {*e.g.* PPh_2R^F, $PPh(PR^F)_2$, $P(PR^F)_3$,

$(PR^F)_2CH_2CH_2(PR^F)_2\}$ designed to increase solubility of catalysts in non-traditional solvents such as *fluorous* solvents and supercritical CO_2.[102-111] The focus of their work initially looked at electronically insulating the phosphorus donor atom from the perfluoroalkyl substituents using a range of spacer units ($P\{Ph\}_{3-x}\{SR^F\}_x$, $P\{Ph\}_{3-x}\{OSR^F\}_x$, S = C_2H_4,[102] C_3H_6,[106] Ph,[106] *p*-Ph-CH_2) to give phosphorus (III) ligands with similar electronic properties to non-fluorinated ligands but with this enhanced solubility in *fluorous* solvents.[102] The enhanced solubility was required as a novel approach to catalyst-product separation due to the problems observed in homogeneous catalysis.[102] This approach consisted of utilising the thermomophism (temperature-dependent solubility) properties of *fluorous* media. The catalyst is dissolved in the *fluorous* solvent and the substrates in an organic solvent.[102] At elevated temperatures the system is homogenous allowing catalysis to occur, and on cooling the products and the catalyst are easily separated in the different phases allowing efficient catalyst recycling.[102] This approach has successfully been used in a range of catalytic reactions such as oxidation,[112, 113] C-C bond formation,[114] hydrogenation,[115] hydroboration[116, 117] and hydroformylation.[100, 101] Hope *et al.* confirmed that the aryl spacer unit is a better electronic insulator than the -C_2H_4 unit initially used, and found it was impossible to completely insulate the phosphorus atom, even when using the *p*-Ph-OCH_2 spacer unit.[106] They also confirmed a purely inductive electronic effect through the aryl ring is observed, whereby a *meta*-substituent has a greater effect than a *para*-substituent.[106] When considering the steric effect of the same *fluorous* ponytail positioned *meta* and *ortho* on the aryl spacer unit, it was found the *ortho* containing metal complexes have a larger steric influence. This resulted in the formation of the less thermodynamically favoured *trans*-$[PtCl_2L_2]$ complexes, over the *cis*-$[PtCl_2L_2]$ stereoisomer.[107] These findings will prove useful for ligand designing for future *fluorous* biphasic catalytic reactions, as they can be used for fine tuning the ligand properties. Recent work by Hope *et al.* has inverted their focus by exploiting the electronic influence of the *fluorous* ponytails on the phosphorus ligand centre rather than including spacer units to reduce the electron-withdrawing effects they induce. Many spectroscopic methods[109] have been used as well as theoretical calculations[111] to understand the properties of these *fluorous* ponytails ligands. Hydroformylation of olefins as discussed below (Chapter. 2.1.6.4) acquire better rates and regioselectivities to linear aldehydes if electron-withdrawing ligands are used on the rhodium catalyst in organic solvents.[118] In industry, cobalt-based catalysts are employed as the rhodium catalysts decompose at the high boiling points of the products, but these conditions are required for purification *via* distillation. However, the use of *fluorous* biphasic systems allows the advantages of homogenous catalysis, but heterogeneous product-catalyst separation. Studies of the use of these *fluorous* ponytails ligands in hydroformylation reactions by Hope *et al.* found that the more electron-withdrawing ligands afforded faster rates than electron-donating ligands; however, the

regioselectivity varies little with respect to changes in the ponytails.[111] It was also concluded that the drastic rates observed were not purely down to electronic effects, as the difference in solubility of the *fluorous* and non-*fluorous* ponytails was a key factor to these observations, in addition to the length of the ponytail.[103, 111] Hope *et al.* have also investigated incorporating perfluoroalkyl-derivatised biphenolic units to try and increase the stability (reduced hydrolysis and decomposition) of the catalyst in the hydroformylation reactions (particularly at the elevated temperatures).[105] However, it was found that these type of phosphorus ligands were extremely air- and moisture-sensitive making them impractical for use at an industrial scale.[105] The ligand design of these type of *fluorous* ponytail ligands is a difficult task, as it requires a fine balance between the stability of the ligand in air and moisture, but also this enhanced solubility in fluorinated solvents to utilise this biphasic approach.[105]

2.1.5 Highly Fluorinated Phosphites

In 1978, Roschenthaler *et al*. synthesised the hexafluoroisopropoxy phosphite, $P\{OCH(CF_3)_2\}_3$, (**1**) by reaction of the lithium salt, $Li[OCH(CF_3)_2]$ with phosphorus trichloride (PCl_3) or by reaction of hexafluoroisopropanol $\{HOCH(CF_3)_2\}$ with PCl_3 and triethylamine base (NEt_3).[2] Their focus, along with others who worked with $P\{OCH(CF_3)_2\}_3$, (**1**) was to use these as starting materials for the synthesis of the related phosphorane, P(V) species, rather than the ligand properties of the phosphite.[2, 119-123] Roschenthaler *et al*. suggested in their work that the perfluoro-*t*-butoxy $-OC(CF_3)_3$ group is far too bulky to allow more than two groups to be bonded to the central phosphorus atom.[2] Shreeve *et al.* contradicted this, as in 1979 they discovered that it was possible to react PCl_3 and phosphorus pentachloride (PCl_5) with perfluoro-*t*-butoxy hypochlorite $\{ClOC(CF_3)_3\}$ and displace all the chlorine atoms on the phosphorus to obtain the perfluoro-*t*-butyl phosphite, $P\{OC(CF_3)_3\}_3$, (**2**) and perfluoro-*t*-butyl phosphorane, $P\{OC(CF_3)_3\}_5$.[1] The phosphite reaction takes place quantitatively at 0 ˚C as the perfluoro-*t*-butoxy hypochlorite, $ClOC(CF_3)_3$ is condensed onto phosphorus trichloride, PCl_3. The phosphite was purified through sublimation under dynamic vacuum at 25 ˚C.[1] However, very little analytical data is presented for this phosphite, and there are no suggestions for its applications. In addition, the synthetic methodology involves the use of hypochlorite, making this method impracticable for routine use, due to having to handle contact poisons and highly corrosive chemicals; ClF and HF in the synthesis of the hypochlorite and chlorine gas, Cl_2 as a side product, which is a known corrosive toxic gas. Interestingly, no signs to date of $P\{OC(CF_3)_3\}_3$, (**2**) used as a ligand has been shown, except in one attempt to synthesise $[Cr(CO)_5P\{OC(CF_3)_3\}_3]$ by Shreeve *et al.* in

1983.[124] Here $[Cr(CO)_6]$ was heated in DCM to 60 ˚C for 2.75 hours with $P\{OC(CF_3)_3\}_3$, (**2**). Shreeve *et al.* describe that although CO evolved, it appears the higher molecular weight complex failed to give the desired $[Cr(CO)_5P\{OC(CF_3)_3\}_3]$ isolated product *via* sublimation. Shreeve *et al.* concluded that the reaction was complex due to several sites available for substitution.[124] Researching the ligand properties of $P\{OC(CF_3)_3\}_3$, (**2**) as well as the synthetic methodologies useful for routine use and expanding on the previous studies on this perfluorinated phosphite would be of great interest, in hope that this ligand could fulfil the gap in the stereoelectronic map described by Cundari *et al*.[23]

Since the synthesis of $P\{OCH(CF_3)_2\}_3$, (**1**), relatively few applications have been explored. One use of $P\{OCH(CF_3)_2\}_3$, (**1**) includes reacting this with a nucleoside, proceeding to form oligonucleotides as reported by Takaku *et al.*[125] The important aspect to note from this paper is that $P\{OCH(CF_3)_2\}_3$, (**1**) was synthesised using a similar method reported by Roschenthaler *et al*. with hexafluoroisopropanol, NEt_3 and PCl_3 in diethyl ether.[2] They report this as a modification of the procedure reported by Denney *et al. i.e.* they use excess hexafluoroisopropanol and triethylamine base so a 1:3.3 (PCl_3 : $HOCH(CF_3)_2/N(CH_3CH_2)_3$) ratio rather than a 1:3 ratio to achieve 80 % yields of the phosphite product.[119] In rare cases, $P\{OCH(CF_3)_2\}_3$, (**1**) has been used as a useful electron-deficient (π-acidic), bulky ligand in catalysis but these types of ligands are still relatively unexplored to their full extent.

2.1.6 Hexafluoroisopropoxy Phosphite, $P\{OCH(CF_3)_2\}_3$, (**1**) in Catalysis

Catalytic uses of the $P\{OCH(CF_3)_2\}_3$, (**1**) ligand have been found in cobalt clusters, $[(propargylium)Co_2(CO)_5(P\{OCH(CF_3)_2\}_3)]^+[BF_4]^-$. These can form diastereoselective carbon-carbon coupled products with mild nucleophiles (*i.e.* synthetically important trimethylsilyl propene), showing the importance of these types of ligands in asymmetric synthesis.[126] Oligomerization of isopropene catalysed by nickel complexes of $P\{OCH(CF_3)_2\}_3$, (**1**) ligand has also shown increased selectivity to cyclodimers (97 %). Here the electron-deficient ligand is thought to promote the head to head (at the iso-groups) coupling of the isopropene molecules.[122]

2.1.6.1 Catalysis of the Diels-Alder [4+2] Cycloaddition with a [Rh(I]) Metal Centre

The Diels-Alder [4+2] cycloaddition, is one of the most utilised methods in organic chemistry due to its prominent role in the construction of complex cyclic compounds.[127] A requirement for the Diels-Alder [4+2] cycloaddition to be effective (without the use of most severe conditions) is that the two substrates have complementary electronic properties (*i.e.*

electron-rich 1, 3-diene and electron-poor dienophile), both inter/intra-molecular reactions result in stereospecific construction of six membered rings.[127, 128] Diels-Alder reactions, intramolecular [4+2] cycloadditions between π-components that are electronically not well differentiated typically require high temperatures, with the additional difficulty of controlling the stereochemistry.[129]

Product selectivity is vital for efficient catalysis when a range of stereoisomers are available. This can be achieved by favouring a specific transition state. The Diels-Alder reaction between a cyclopentadiene and an electron-poor dienophile gives a clear example of the choice of selectivity.[130] The electron-poor substituent on the dienophile can point down (almost axial) from the ring giving an endo conformation, or almost equatorial from the ring, giving an exo conformation, see Scheme 4.

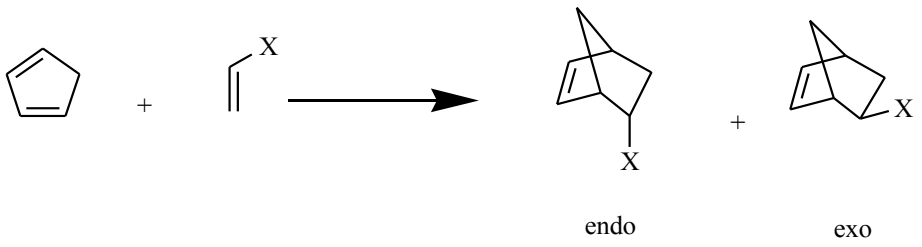

Scheme 4: Diels-Alder reaction of cyclopentadiene can give endo and exo isomer products.

Livinghouse *et al.* report that the use of electronically and sterically tuneable transition metal complexes can increase stereoselectivity with excellent efficiency in Diels-Alder reactions. They disclose that the use of Rh(I) complexes generated *in situ* from the chlorobis(cyclooctene)rhodium(I)dimer, $[(C_8H_{14})_2RhCl]_2$ with two or more equivalents of $P\{OCH(CF_3)_2\}_3$, (**1**) "possess superb activity as catalysts for intramolecular [4+2] cycloadditions".[131] In addition, these highly active catalyst systems were found to be effective at temperatures as low as 25 °C in specific solvent solutions.[128] Murakami *et al.*[127] also report complexation of unactivated substrates with no electron-withdrawing or electron-releasing substituents, prepared *in situ* from $[Rh(cod)_2]OTf$ (cod = 1,5 –cyclooctadiene) and $P\{OCH(CF_3)_2\}_3$, (**1**) with the unactivated substrates. They too report cycloaddition reactions taking place at low temperatures (20 °C) in the presence of the catalyst. This is also true for ethene which they call one of the most "sluggish" dienophiles.[127] However, it should be noted that only low yields are observed for this ethene dienophile.[127]

A mechanism is proposed for the cycloaddition reaction between a vinylallene with a terminal alkyne, see Scheme 5. This involves initial formation of a five-membered rhodacycle from the vinylallene substrate. A seven-membered rhodacycle is produced *via* C-C bond formation after coordination of the alkyne to the rhodium centre. The regiochemical

outcome observed with terminal alkynes is due to stereoselectivity as the alkyne is inserted into the Rh-C_{sp3} bond. The competing insertion with the alternative alkyne orientation would be disfavoured because of the repulsive steric interactions between the alkyne substituent R^2 and the bulky $P\{OCH(CF_3)_2\}_3$, (**1**) ligands on the rhodium metal centre, see Figure 13.[127]

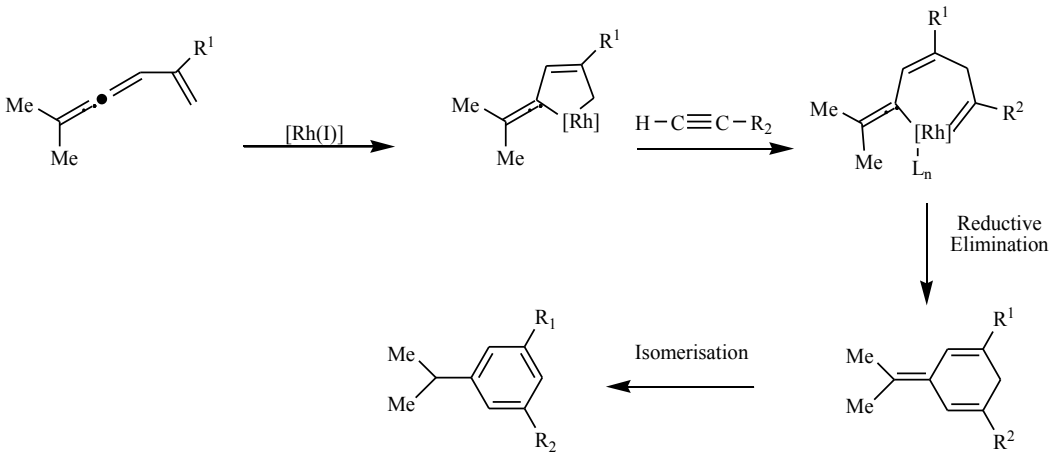

Scheme 5: A possible mechanism for the cycloaddition reaction between a vinylallene with a terminal alkyne in the presence of a Rh(I)/$P\{OCH(CF_3)_2\}_3$ catalyst.[127]

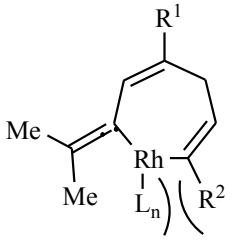

Figure 13: Repulsive steric interactions between the alkyne substituent R^2 and the bulky $P\{OCH(CF_3)_2\}_3$ ligand on Rh (I) catalyst allows only stereoselective products to form.[127]

Finally, reductive elimination followed by isomerisation completes the formation of the stereoselective substituted arenes.[127] The precise reason for the beneficial effect of employing electron-accepting ligands is not reported by Murakami *et al.*[127]

2.1.6.2 Catalytic C-C Coupling of (Hetero)Arenes with a [Rh(I)] Metal Centre

Recent evidence has shown that $[RhCl(CO)\{P(OCH\{CF_3\}_2)_3\}_2]$ works well as a catalyst in the presence of silver carbonate, Ag_2CO_3 to produce a range of biaryls in high yields from direct C-H coupling of (hetero)arenes and haloarenes.[132, 133, 134] The rhodium complex is highly stable in the solid state towards air and moisture. The high stability of the complex catalyst may be due to the effective steric shielding of the rhodium atom by its two bulky phosphite, $P\{OCH(CF_3)_2\}_3$, (**1**) ligands, as shown by their X-ray crystal structure.[132] The

mechanistic details of the catalytic cycle are not precisely known, yet a proposition has been made. This is summarised in the scheme below, where the initial step proceeds *via* ligand dissociation, most likely from the phosphite, $P\{OCH(CF_3)_2\}_3$, (**1**) which results in a coordinatively unsaturated [Rh(I)] species, **A** in Scheme 6.[132] It is this complex which follows the [Rh(I)]/[Rh(III)] redox cycle.[132, 133] The mechanism includes:

i) Oxidative addition of the iodoarene, Ar-I to the coordinatively unsaturated [Rh(I)] species, **A** in Scheme 6, as Ar-I loses I^- (to Ag^+) thus taking the aryl groups electron involved in the bond.[132, 133]

ii) Generation of cationic [arylrhodium(III)] species, **B** in Scheme 6 with the assistance of Ag_2CO_3.[132, 133]

iii) Electrophilic metalation (rhodation) of the other (hetero)arene, Ar-H, with **B** in Scheme 6, giving [diarylrhodium(III)] species, **C** in Scheme 6. [132, 133]

iv) Reductive elimination of biaryl product with the regeneration of **A** in Scheme 6, the [Rh(I)] species.[132, 133]

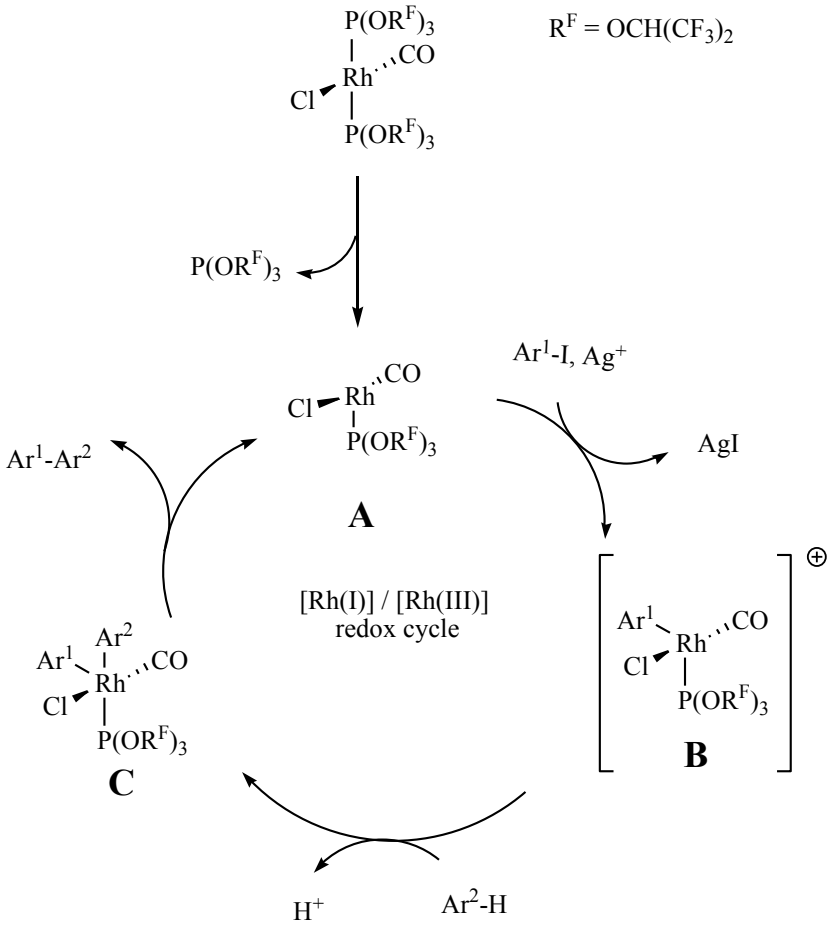

Scheme 6: A possible mechanism for the rhodium catalysis of C-C coupling to form biaryl products, facilitated by $P\{OCH(CF_3)_2\}_3$, (1). Scheme adapted from ref. [132, 133].

The electron acceptor ability of the phosphite is likely to have a beneficial effect on the rhodium centre. The phosphite can form an electron-deficient rhodium centre, hence facilitate in the electrophilic metalation, helping to stabilise the [Rh(I)] species, thus facilitating the reductive elimination step. The presence of the π-acidic phosphite group is key to the mechanism, as similar reactions with less π-accepting ligands such as $P(OC_6H_5)_3$ and $P\{OCH(CH_3)_2\}_3$ yielded lower amounts of the biaryl products.[132, 133] The ligand effects in this catalytical system suggest that strongly π-accepting ligands are required. The paper claims since $P\{OCH(CH_3)_2\}_3$ (θ = 130 °)[47] and $P\{OCH(CF_3)_2\}_3$, (**1**) are similar in size, the electronic nature of the ligand has the greatest effect on their catalysis rather than the steric properties of the ligand. However, the findings of this thesis suggests the cone angles of the two actually differ by 48 ° (using a DFT optimised $[Ni\{CO\}_3L]$ complex for $P\{OCH(CF_3)_2\}_3$, (**1**), discussed below), indicating steric effects have a more crucial role in the overall ligand property. This could be tested using $P\{OC(CF_3)_3\}_3$, (**2**) which is sterically larger (greater cone angle, as discussed later) than $P\{OCH(CF_3)_2\}_3$, (**1**) which was used by Itami *et al.*, but with similar electronic properties. Any difference observed in the yields would help to indicate that the steric contribution of the ligand also plays a part and that it is the combined properties of a bulky and electron-deficient ligand that are required. A universal catalyst that can directly arylate all heteroarenes as well as simple arenes is still to be developed, the use of $P\{OC(CF_3)_3\}_3$, (**2**) with its combined properties may be the way to achieve this type of catalyst formation.

2.1.6.3 Catalysis for the β Selective Functionalisation of Thiophene with a [Pd(II)] Metal Centre

More recently in 2010, Itami *et al.* showed that palladium (II) chloride, $[PdCl_2]$ (5 mol %) and $P\{OCH(CF_3)_2\}_3$, (**1**) (10 mol %) can be used *in situ* as a catalyst to achieve selective functionalisation at the less reactive β position of a thiophene, when both α and β positions are available.[134, 135] This is much simpler than the currently used multistep approach, containing α, β dibromination, α debromination and finally the organometallic cross coupling step, see Scheme 7. The paper highlights the use of the electron-withdrawing $P\{OCH(CF_3)_2\}_3$, (**1**) ligand being the cause of the β-selective (β: α = 86:14) arylation of the thiophenes. This is apparent as when the non-fluorinated $P\{OCH(CH_3)_2\}_3$ ligand is used, selectivity goes towards the α position (β: α = 30:70).[135] This paper also uses bis(hexafluoroisopropoxy) phenyl phosphonite, $PPh\{OCH(CF_3)_2\}_2$, (**3**) as a ligand to observe good β selectivity (β: α = 63:37), it should be highlighted that the use of the latter as a ligand is very rare in published literature, although synthesis has previously been reported.[135]

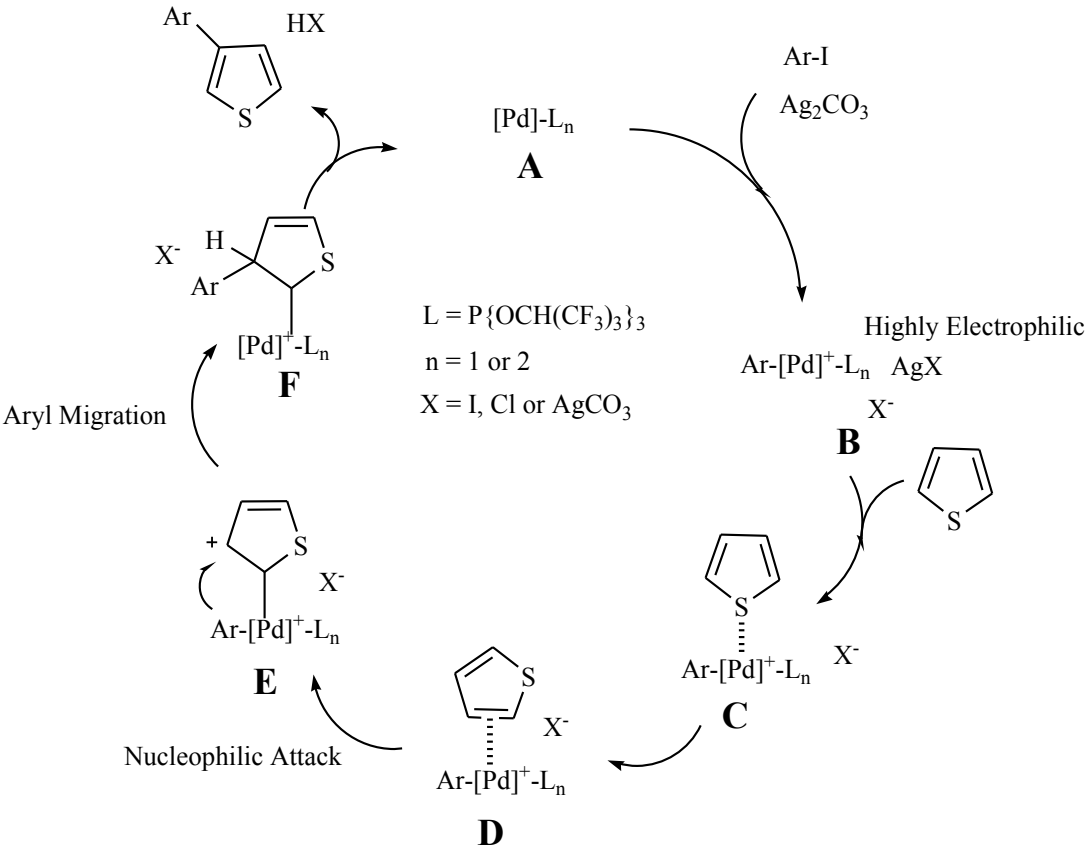

Scheme 7: A possible mechanism for selective functionalisation at the less reactive β position of a thiophene in the presence of $PdCl_2$ (5 % mol) and $P\{OCH(CF_3)_2\}_3$ (10 % mol) catalytic system. Scheme adapted from ref. [135].

A possible mechanism is published by comparing their catalytic system to that with the [Pd(0)]/[Pd(II)] system described by Fagnou and co-workers.[136] This involves:

i) Oxidative addition of the iodoarene (Ar-I) to the Pd complex, **A** in Scheme 7 [135]

ii) Silver-mediated generation of the cationic and electrophilic aryl palladium species, **B** in Scheme 7.[135]

iii) Coordination of the thiophene to Pd to give **C** and/or **D** in Scheme 7.[135]

iv) α Carbon-Pd bond formation to give **E** in Scheme 7.[135]

v) Migration of the aryl group from Pd to the β carbon atom to form a formal Ar-Pd insertion intermediate, **F** in Scheme 7.[135]

vi) Proton abstraction to produce a β-aryl thiophene with the regeneration of **A** in Scheme 7.[135]

It seems the β selectivity is a result of the weak thiophene-palladium interaction, which is likely promoted by the observed electronic preference for the extremely electron-withdrawing $P\{OCH(CF_3)_2\}_3$, (**1**) ligand.[135]

2.1.6.4 *Catalytic Hydroformylation with a [Rh(I)] Metal Centre*

Hydroformylation is another important process used in industry for the conversion of alkenes to aldehydes, which can be reacted further *e.g.* hydrogenated to form alcohols for use in detergents.[30] The alkene is usually treated with high pressure carbon monoxide and hydrogen at high temperatures. Transition metal catalysts are useful for this process, currently rhodium based catalysts with hydride and bulky phosphorus (III) ligands are used use to give normal (over iso) selective aldehydes, see Scheme 8 .[30]

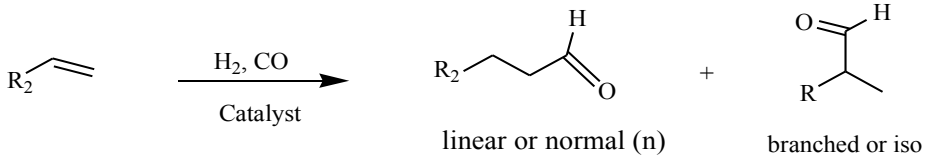

Scheme 8: Hydroformylation reaction, converts alkenes to aldehydes, giving two possible products.[30]

Electron-deficient, bulky ligands have been found to give very efficient [Rh(I)] hydroformylation catalysts.[137] In 1980, cyclooctadiene-rhodium (I) acetate in the dimer form, $[Rh(cod)_2OAc]_2$ (cod = 1,5 – cyclooctadiene and OAc = acetate) (1 eq.) was used with $P\{OCH(CF_3)_2\}_3$, (**1**) ligand (2 eq.) along with other phosphorus (III) ligands containing end $–CF_3$ groups. These were found to favour the normal aldehyde product over the iso selectivity, making these ligands also useful in this catalytic system.

As highlighted above, the versatility of these types of ligands to be used in many synthetic processes is possible. These ligands have the advantage of increasing the stereoselectivity in many catalytic reactions, allowing for significant potential for their use in the chemical industry. In addition, the ease of ligand design by changing the substituents at the phosphorus-centre makes them incredibly appealing to a range of catalytic reactions. Catalytic systems could be fine tuned, depending on the specific requirements once a library for this class of ligands is formed and their properties are fully explored.

2.2 RESULTS AND DISCUSSION

2.2.1 Highly Fluorinated Phosphorus (III) Ligand Synthesis

A series of phosphorus (III) ligands bearing highly fluorinated alkoxide substituents have been synthesised. Increased understanding of their stereoelectronic properties is achieved *via* a combination of experimental and theoretical methods. Ligands with the general formula $PR_{3-n}(OR^F)_n$ {R = Ph; OR^F = $C(CF_3)_3$, $CH(CF_3)_2$; n = 1, 2} are simple to synthesise and the fluorinated alkoxide groups impart both steric bulk, and considerable acceptor character to the ligands, making these useful candidates to fill the significant gap in ligand space corresponding to electron-poor, sterically bulky phosphorus (III) ligands, see Figure 14.[23] The steric and electronic properties of these species can be tuned by varying R and R^F to give a variety of ligands with different electronic and steric combinations. Most importantly, these reported methods allow easy access to the perfluoro-*t*-butyl phosphite, (**2**). This involves a synthetic methodology without the need for the hazardous preparations, as described in Chapter 2.1.5.

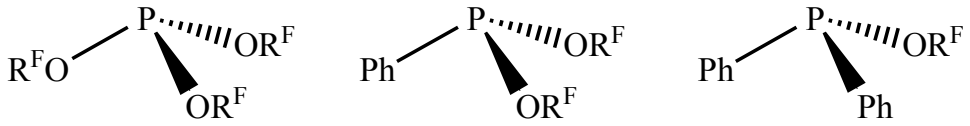

(**1**): $R^F = CH(CF_3)_2$ (**3**): $R^F = CH(CF_3)_2$ (**5**): $R^F = CH(CF_3)_2$
(**2**): $R^F = C(CF_3)_3$ (**4**): $R^F = C(CF_3)_3$ (**6**): $R^F = C(CF_3)_3$

Figure 14: Class of bulky, electron-deficient ligands synthesised.

Optimisation of the synthetic methodology in order to increase the yields and the purity of these ligands has been a key focus of this work. Previously reported methods in the literature include using triethylamine base, NEt_3, to deprotonate the fluoroalcohol, HOR^F. This gives the alkoxide, $^-OR^F$, which can displace the chloride atoms on the chlorophosphine starting reagent, PCl_3/PCl_2Ph/$PClPh_2$ *via* nucleophilic substitution (S_N2), forming the ligand product and triethylammonium chloride, $[Et_3NH]^+[Cl]^-$ as a side product. Compounds (**1**), (**3**) and (**5**) have previously been synthesised using the described method.[2, 119, 121, 132] Compound (**2**) has only been reported by Shreeve *et al.* using a method involving the hypochlorite described in Chapter 2.1.5.[1, 124] Compounds (**4**) and (**6**) are not found to have been reported previously and can be synthesised in a similar manner to methods described above, from the relevant chlorophosphine and perfluoro-*t*-butanol. Scheme 9 below describes the conditions for the synthesis of (**2**).

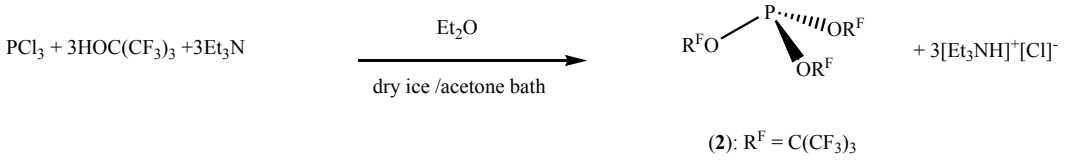

Scheme 9: Synthesis of a fluorinated phosphorus (III) ligand using the fluoroalcohol directly with triethylamine base in dry diethyl ether as the solvent.

However, using this method all the ligands required further purification after filtration as products of hydrolysis were evident in the $^{31}P\{^{1}H\}$ NMR spectra *e.g.* $O{=}P(OR^F)_2OH$. Purification was achieved *via* reduced-pressure distillation or sublimation onto a sublimation finger cooled to 77 K. The highest yield achieved was 84 % for the $PPh_2\{OCH(CF_3)_2\}$, (**5**) ligand. However, problems persisted with this method with reactions not going to completion as shown by $^{31}P\{^{1}H\}$ NMR spectroscopy. The addition of an extra 10 % NEt_3 and fluoroalcohol (HOR^F) did however allow the reaction to proceed to completion. Using this synthetic method, the purity of the ligands was affected by the formation of triethylammonium-alkoxide adducts; $[Et_3NH]^+[OC(CF_3)_3]^-$, $[Et_3NH]^+[H\{OC(CF_3)_3\}_2]^-$, $[Et_3NH]^+[OCH(CF_3)_3]^-$ and $[Et_3NH]^+[H\{OCH(CF_3)_2\}_2]^-$. Although these species themselves are interesting as potential new protic ionic liquids they are difficult to remove *via* reduced-pressure distillation/sublimation, as they decompose to form NEt_3 and HOR^F at temperatures below the boiling point of the ligands (even under reduced pressure) and these then co-distil with the ligands, eventually re-forming $[Et_3NH]^+[OR^F]^-$ salts in the reaction vessel. Further purification *via* a second distillation/sublimation step to remove these salts would complicate the method making it impractical for routine use.

An alternative synthetic method investigated included reacting sodium hydride (NaH) with the fluoroalcohols (HOR^F) to make the sodium alkoxide ($NaOR^F$) and hydrogen gas as a side product. This $NaOR^F$ could then be used for the synthesis of the ligands in DCM solvent by reaction with the relevant chlorophosphine; $PCl_3/PCl_2Ph/PClPh_2$. The reaction mixture required ultrasonic activation to increase the solubility of the $NaOR^F$, see Scheme 10 for an example of the synthesis of the tris(perfluoro-*t*-butyl)phosphite, (**2**), with this method.

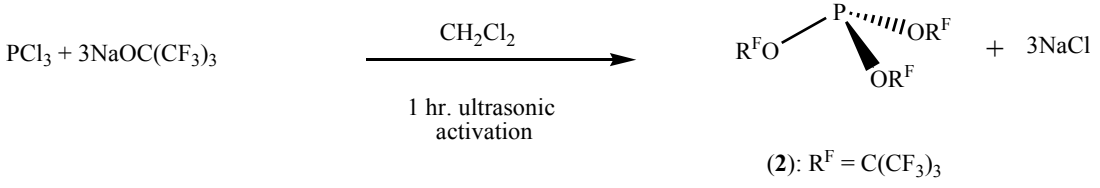

Scheme 10: Synthesis of a fluorinated phosphorus (III) ligand, using sodium alkoxide ($NaOR^F$) in DCM solvent.

Since the sodium chloride (NaCl) side product from this reaction is insoluble in DCM, it was removed by filtration under inert atmosphere. Celite was used to trap any fine sodium chloride particles that may have been broken down in the ultrasonic activation process. These reactions were carried out in ampoules sealed by grease-free J. Young's taps, as the grease joints in Schlenk tubes are affected by the ultrasonic activation treatment. The grease seal is disturbed, which can lead to the formation of many hydrolysis products (observed by $^{31}P\{^{1}H\}$ NMR spectroscopy, see Table 3). All six ligands can be synthesised using this method and include the advantage of no additional purification steps being required. The $^{31}P\{^{1}H\}$ NMR spectra of the ligands indicate high purity as they contain clear multiplets for the ligand signals only, and very minor signals (if any) for hydrolysis products. Molecular ion peaks have been found using EI-MS for ligands (**1**) to (**6**) to confirm their identity. In addition, ammonium-containing side products (which have been shown to be problematic to separate from the ligands) were not formed with the metal alkoxide method. Again, the addition of 10 % extra $NaOR^F$ led to successful reaction completion with this method. The $NaOR^F$ tend to form cubic clusters[138] (observed by ESI-MS, see Figure 15), this can affect the mass and change the stoichiometry of the reaction as diethyl ether molecules are known to coordinate. Conversely, if the $NaOR^F$ is dried sufficiently under vacuum, all the coordinated diethyl ether can be removed (assessed by elemental analysis). The use of excess $NaOR^F$ in the reaction mixture can affect the purity of the ligand if no further purification is applied. However, this excess $NaOR^F$ has not yet proved to inhibit the reactivities of these ligands. Although all compounds reported here can be purified by distillation {sublimation in the case of (**2**)}, it is found to be possible to use the ligands *in situ* as prepared in DCM solution, after filtration to remove NaCl.

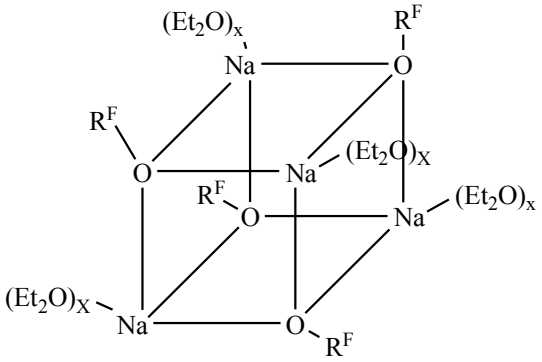

Figure 15: Sodium perfluoro-*t*-butoxide clusters with coordinated diethyl ether solvent.[138]

A description of the ligand composition, colour and $^{31}P\{^{1}H\}$ NMR chemical shifts can be found in Table 2, along with the $^{31}P\{^{1}H\}$ NMR chemical shift data for the mono- and di-

substituted products observed. While (**1**), (**3**), (**5**), (**4**) and (**6**) are liquids under standard conditions, (**2**) is a solid that crystallises readily from DCM solution (discussed in Chapter 2.2.3.2).

$^{31}P\{^1H\}$ NMR (δ/ppm)	*^{19}F NMR (δ/ppm)*	*^{1}H NMR [a] (δ/ppm)*	*Description*	*Ligand*
*217.0	-	NA	-	$P\{(OC(CF_3)_3\}Cl_2$
*191.0	-	NA	-	$P\{OC(CF_3)_3\}_2Cl$
190.0	-71.51	NA	colourless liquid	$PhP\{OC(CF_3)_3\}_2$, (**4**)
190.3	-74.48, -74.35	4.69	colourless liquid	$PhP\{OCH(CF_3)_2\}_2$, (**3**)
*187.0	-	-	colourless liquid	$P\{OCH(CF_3)_2\}Cl_2$
*186.0	-	NA	-	$PhP\{(OC(CF_3)_3\}Cl$
*171.0	-	-	colourless liquid	$P\{OCH(CF_3)_2\}_2Cl$
147.0	-72.12	NA	white solid	$P\{OC(CF_3)_3\}_3$, (**2**)
142.6	-78.50	4.75	colourless liquid	$Ph_2P\{OCH(CF_3)_2\}$, (**5**)
139.7	-74.32	4.92	colourless liquid	$P\{OCH(CF_3)_2\}_3$, (**1**)
*140.0	-	-	colourless liquid	$PhP\{OCH(CF_3)_2\}Cl$
132.3	-71.60	NA	colourless liquid	$Ph_2P\{OC(CF_3)_3\}$, (**6**)

Table 2: $^{31}P\{^1H\}$, ^{19}F and ^{1}H NMR chemical shifts (δ/ppm) for (1) to (6). $^{31}P\{^1H\}$, NMR chemical shifts for the incompletely substituted phosphorus (III) products, * = ligands observed *in situ* only, all the rest have been isolated as pure products, [a] = selected ^{1}H NMR chemical shifts, for $OC(H)(CF_3)_2$ groups are only reported.

The $^{31}P\{^1H\}$ NMR chemical shifts are known to relate to the atomic ionicity index, which in turn relates to the equilibrium electronegativity of an atom as it becomes part of a molecule.[139] This atomic ionicity is related to the deshielding effects observed in the $^{31}P\{^1H\}$ NMR spectra. This can be effective from a substituent atom that is at least four bonds away from the nuclear phosphorus. Generally, if one focuses purely on the electronic effects, it can be seen that as the electron-density on the phosphorus atom is reduced as the $^{31}P\{^1H\}$ NMR chemical shift increases.[139] In addition, Tolman states a more downfield $^{31}P\{^1H\}$ NMR chemical shift is seen with larger cone angles (*i.e.* $\delta_P = PH_3$, -240.0 ppm, θ = 87 °; PMe_3, -62.0 ppm, θ = 118 °; P^tBu_3, 63.3 ppm, θ = 182 °). This can explained due to larger SPS angles, as ligands with large substituents open out further; hence the steric bulk plays a key role too, suggesting both steric and electronic effects are important.[20] However, Tolman adds

that the chemical shifts are insensitive to the bulk of the alkyl groups of phosphites $P(O^iPr)_3$, δ_P = 137.5 ppm, θ = 130 °; $P(O^tBu)_3$, δ_P = 138.1 ppm, θ = 172 °}; the oxygens provide flexibility so that the OPO angles can remain essentially constant and so the phosphorus centre is insulated from the steric bulk of the R group by the oxygen atom.[20] Table 2 above shows that the data from the studies presented here agree with this statement. The incredibly bulky $P\{OC(CF_3)_3\}_3$, (**2**) ligand has a similar $^{31}P\{^1H\}$ NMR chemical shift value to that of $P\{OCH(CF_3)_2\}_3$, (**1**); δ_P = 147.0 ppm and 139.7 ppm respectively. This suggests that the steric effects are not a major contribution to the $^{31}P\{^1H\}$ NMR chemical shifts of phosphite ligands, due to their essentially constant OPO angle. The change in $^{31}P\{^1H\}$ NMR chemical shifts of the two fluorinated phosphites (Δδ = 7 ppm), is likely to be due to electronic effects. If the difference in chemical shift between these phosphites is purely electronic, then these data would suggest (**2**) has reduced electron-density around the phosphorus centre than (**1**). Using this approach, one can also imagine $P\{OC(CF_3)_3\}_2Cl$, $PhP\{OC(CF_3)_3\}_2$, (**4**), $PhP\{OCH(CF_3)_2\}_2$, (**3**) to have similar electronic character as all three contain $^{31}P\{^1H\}$ NMR chemical shifts at ~190 ppm (these are comparable as they all contain a similar structure; $P(OR^F)_2Z$, where Z = Cl or Ph). However, $PhP\{OCH(CF_3)_2\}Cl$ and $P\{OCH(CF_3)_2\}_3$, (**1**) contain similar $^{31}P\{^1H\}$ NMR chemical shift values; both come at ~140 ppm, but direct comparison of the electronic properties cannot be made with the $^{31}P\{^1H\}$ NMR chemical shift as one is a $P(OR^F)Z_2$ type species and the other a $P(OR^F)_3$ type species. The number of alkoxy groups can affect the steric influence due to a change in its SPS angle. Table 2 summarises that both steric (SPS angle opening) and electronic (electronegativity) effects contribute to the variation in the $^{31}P\{^1H\}$ NMR chemical shift values. However, it appears in the case of the fluorinated phosphites, $P(OR^F)_3$ the electronic effects have a greater contribution to $^{31}P\{^1H\}$ NMR chemical shifts, since the OPO angles remain essentially constant for a range of phosphites. This allows one to compare their $^{31}P\{^1H\}$ NMR chemical shifts of phosphorus ligands to gain an insight into their different electronic properties.

2.2.2 Highly Fluorinated Phosphorus (III) Ligand Hydrolysis

The free ligands (**1**) to (**6**) are susceptible to hydrolysis, but unlike with many electron-rich phosphorus (III) ligands, no evidence of oxidation in air at room temperature has been observed. This may be due to the reduced availability of the lone pair, as these ligands are π-acidic ligands. Difficulties associated with ligand oxidation makes the phosphine-selenide $^1J_{PSe}$ coupling constant method unsuitable for assessing the electronic properties of these ligands. Table 3 presents the hydrolysis products observed by $^{31}P\{^1H\}$ NMR spectroscopy in this study. A product of partial hydrolysis of ligand (**2**) where small amounts of water have

inadvertently entered the reaction vessel has been structurally characterised, phosphite $(R^FO)_2P\text{-}\mu O\text{-}P(OR^F)_2$ $\{R^F = C(CF_3)_3\}$, (**7**). This species gives some insight into the mechanism of hydrolysis. It also suggests the possibility that bidentate analogues of (**2**) may be accessible *via* a suitable synthetic route. The pyrophosphite, (**7**) has a characteristic multiplet at 135.0 ppm in the $^{31}P\{^1H\}$ NMR spectrum and crystals suitable for X-ray diffraction structural analysis could be grown from DCM solution, see Figure 16.

$^{31}P\{^1H\}$ NMR (δ/ppm)	**Description**	**Hydrolysis Product**
135.0	white solid	$\{OC(CF_3)_3\}_2P\text{-}\mu O\text{-}P\{OC(CF_3)_3\}_2$, (**7**)
*39.0	-	$Ph_2(O)POH$
*36.0	-	$Ph_2(O)PH$
29.0	white solid	$Ph_2(O)POP(O)Ph_2$
24.0	white solid	$Ph_2(O)PP(O)Ph_2$

Table 3: Hydrolysis products of the fluorinated ligands (1) to (6) observed by $^{31}P\{^1H\}$ NMR spectroscopy, * = hydrolysis product observed *in situ* only, all the rest have been identified by unit cell parameters of crystals suitable for X-ray diffraction analysis.

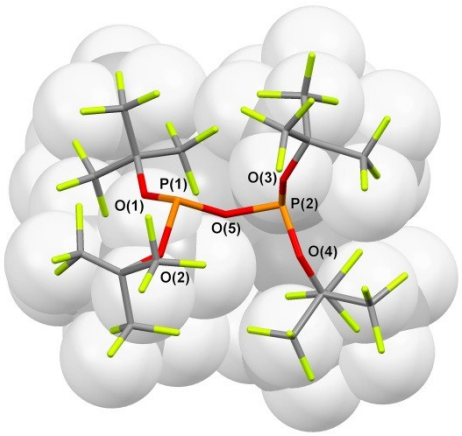

Figure 16: Single-crystal X-ray structure of $(R^FO)_2P\text{-}\mu O\text{-}P(OR^F)_2$ $\{R^F = C(CF_3)_3\}$, (7) at 110 K. Extensive disorder (modelled over two equal positions) is present for all atoms except for those of one perfluoro-*t*-butoxy group in the structure. Only one position is shown (and bond lengths and angles given for this) for clarity. Selected bond lengths (Å) and angles (°): P(1)-O(1) 1.589(9), P(1)-O(2) 1.637(9), P(1)-O(5) 1.63(5), P(2)-O(3) 1.611(8), P(2)-O(4) 1.643(9), P(2)-O(5) 1.62(4), P(1)-O(5)-P(2) 136(3), O(1)-P(1)-O(2) 93.6(4), O(1)-P(1)-O(5) 96(2), O(2)-P(1)-O(5) 96.2(9), O(3)-P(2)-O(4) 93.4(5), O(3)-P(2)-O(5) 101(2), O(4)-P(2)-O(5) 100.2(8). Crystal system: Orthorhombic. Space group: Pbca, 110 K, $R_1 = 0.1170$ (>2sigma(I)), $wR_2 = 0.3379$ (all data).

As with the single-crystal X-ray structure of (**2**) discussed in Chapter 2.2.3.2, all crystals of (**7**) are heavily disordered, even at 110 K. In the case of (**7**), the structure exhibited extensive

disorder such that all atoms except for those of one perfluoro-*t*-butoxy group were modelled in two positions with equal occupancy. It is notable when comparing the two forms, that the oxygen and phosphorus atoms occupy significantly positions but the perfluoro-*t*-butoxy sites are much closer to each other, hence the two forms present a very similar external surface to adjacent molecules. Within the disordered portion of the structure, the C-F bond-lengths within each perfluoro-*t*-butyl group were restrained to be equal as were the F-F distances. As the model is still relatively poor, an extensive structural description is not appropriate. However, the data serves to confirm structural connectivity and suggest that the phosphorus centres exhibit distorted pyramidal geometries (with smaller O-P-O angles than in an ideal tetrahedral geometry). In addition, the phosphorus lone pairs point in opposite directions to each other, presumably as a consequence of the steric bulk of the two large $-OC(CF_3)_3$ groups at each P. Structurally characterised examples of free, uncoordinated pyrophosphites are very rare. To the best of our knowledge only one previous example is present in the Cambridge Structural Database, the sterically congested pyrophosphite 6-[(2,4,8,10-tetrakis(1,1-dimethylethyl)-dibenzo[*d,f*][1,3,2]dioxaphosphepin-6-yl)oxy]-2,4,8,10-tetrakis(1,1-dimethylethyl)-dibenzo[*d,f*][1,3,2]-dioxaphosphepin reported by DeBellis *et al.*,[140] although structural data for a small number of metal complexes of these ligands have been reported. The single-crystal X-ray structure of the pyrophosphite reported by DeBellis *et al.* displays a similar phosphorus-oxygen core conformation to that shown by (**7**), with P-lone pairs pointing away from each other. Although any comparison of structural parameters is tentative, given the quality of the data for (**7**), it appears that the P-O distances and O-P-O angles in (**7**) are comparable to those reported by DeBellis (although any subtle effects due to the inclusion of fluorinated alkoxides would not be identifiable in these data).

2.2.3 Steric Properties of the Novel Bulky Electron Deficient Phosphorus (III) Ligands

2.2.3.1 Cone Angle Calculations (From Experimental and DFT Studies)

The Tolman "ligand cone angle" (θ) was chosen as the steric parameter to be used here, as unlike other methods, this represents bulky ligands along with phosphites well.[20] DFT optimised structures at the (RI-)BP86/SV(P) level for the nickel carbonyl complexes, $[Ni(CO)_3L]$ of the relevant ligands were used to compare the steric properties of ligands (**1**) to (**6**), see Table 4.[20]

L = Ligand	**θ ˚ $[Ni(CO)_3L]$ DFT**	**θ ˚ $[W(CO)_5L]$ DFT**	**θ ˚ $[Ru(\eta^5\text{-}C_5H_5)(S)_2L]^+$ $[PF_6]^-$ XRD**	**θ ˚ $[Ru(\eta^5\text{-}C_5H_5)S(L)_2]^+$ $[PF_6]^-$ XRD**	**θ ˚ $[RhCOClL_2]$ XRD**
$P\{OCH(CF_3)_2\}_3$ (**1**)	178	155	*160 and 157	No Complex	167[a] and 160[a]
$P\{OC(CF_3)_3\}_3$ (**2**)	195	180	[#]180 and 173	No Complex	-
$PPh\{OCH(CF_3)_2\}_2$ (**3**)	173	162	144	147 and 140	-
$PPh\{OC(CF_3)_3\}_2$ (**4**)	163	165	178	No Complex	-
$PPh_2OCH(CF_3)_2$ (**5**)	170	152	147	*158, 147, 142,142	-
$PPh_2OC(CF_3)_3$ (**6**)	170	163	164	*144, 144, 143,142	193 and 163

Table 4: Comparison of ligand cone angles (θ/˚) calculated using Tolman's method for DFT optimised at the (RI-)BP86/SV(P) level and XRD structures, where * = two molecules in unit cell so multiple cone angle values are calculated, # = values calculated for the ligand distorted over two positions, a = values from published structure from ref. [133], S = NCMe.

These calculations suggest a cone angle of 195 ˚ for the tris(perfluoro-*t*-butyl)phosphite, $P\{OC(CF_3)_3\}_3$, (**2**). This is large in comparison to the hydrogen analogue *t*-butyl phosphite, $P\{OC(CH_3)_3\}_3$ which has a cone angle of 172 ˚ and the *t*-butyl phosphine, $P\{C(CH_3)_3\}_3$ known as one of the highly sterically crowded ligands with a cone angle of 182 ˚. These θ values highlight the extent of the bulkiness of this tris(perfluoro-*t*-butyl)phosphite,

$P\{OC(CF_3)_3\}_3$, (**2**). Considering the electronic properites, these phosphorus (III) ligands could potentially be very useful π-acidic ligands, with similar properties to a carbonyl ligand, but in combination with steric bulk, which will change the reactivity of the metal complex.[23, 124, 126] The largest cone angle reported by Tolman is that of tri-mesityl phosphine, $PMes_3$ (θ = 212 °), others at the larger range include $P(C_6F_5)_3$ (θ = 184 °), $P(O\text{-}o\text{-}C_6H_3Me_2)_3$ (θ = 190 °) and P(o-Tol)$_3$ (θ = 194 °). However, these essentially consist of bulky phenyl groups which can be conformationaly flexible, depending on their environment, and can undergo many conformational changes (although $PMes_3$ is more limited to avoid steric clash of the methyl groups with the phosphorus lone pair) unlike the rigid tris(perfluoro-*t*-butyl)phosphite, $P\{OC(CF_3)_3\}_3$, (**2**). This suggests that the incredibly bulky (**2**) has a great deal of steric bulk without the flexibility to accommodate to specific environments. This gives (**2**) a steric property that is unusual to the current bulkier ligands available for catalysis, especially when combined with its π-acidic electronic properties (discussed below). In comparison, the hexafluoroisopropoxy phosphite, $P\{OCH(CF_3)_2\}_3$, (**1**), has a cone angle of 178 °, lower than $P\{OC(CF_3)_3\}_3$, (**2**), as expected due to the reduced bulk from the replacement of a -CF_3 group by a -H atom. The hydrogen analogue, $P(O^iPr)_3$ has a cone angle of 160 °, which again reinforces the added bulk achieved from exchanging the –CH_3 hydrogen atoms for fluorine atoms. $P\{OCH(CF_3)_2\}_3$, (**1**) allows access to a phosphorus (III) ligand of similar electronic property (discussed below) to PF_3 (θ = 104 °), but with additional steric bulk. The $P\{OCH(CF_3)_2\}_3$, (**1**) ligand also has some conformational flexibility unlike (**2**), allowing it to change its steric bulk effect depending on a specific environment, this making it more versatile for use in a range of metal centres with varying ligands coordinated. The Tolman cone angles (θ) confirm that the substitution of the fluorinated alkoxy groups {$OC(CF_3)_3$, $OCH(CF_3)_2$} for phenyl rings reduces the steric influence of the ligands (*i.e.* $P\{OCH(CF_3)_2\}_3$, (**1**), $PPh\{OCH(CF_3)_2\}_2$, (**3**) and $PPh_2OCH(CF_3)_2$, (**5**); θ = 178 °, 173 ° and 170 ° respectively). In comparison, although one would expect the cone angle values to be much greater for the perfluoro-*t*-butoxy group, this appears not to be the case for ligands (**4**) and (**6**), those substituted with a phenyl group. The $PPh_2OC(CF_3)_3$, (**6**) ligand has a cone angle of 170 ° same as that of the $PPh_2OCH(CF_3)_2$, (**5**) ligand, whereas the $PPh\{OC(CF_3)_3\}_2$, (**4**) ligand has a cone angle of 163 °, smaller than that of $PPh\{OCH(CF_3)_2\}_2$, (**3**) and $PPh_2OC(CF_3)_3$, (**6**). This is explained due to the conformational flexibility of the phenyl substituents, which adjust to each specific environment and the space available. This highlights an oversimplification in the Tolman parameter, from basing calculations on static optimised structures. The Tolman cone angle calculations come to their limitation here. However, it is a reasonable estimate as the majority of the time the molecule will be in this conformation. All the DFT optimisations are of the lowest energy conformation; hence the cone angles of the nickel complexes are likely to be consistent with

each other in terms of their steric bulk calculation. The calculations can give an estimate of the extent of steric bulk each ligand can provide, but in reality they are dynamic and conformationaly flexible. A clear example of the conformationally changes can be observed when calculating and comparing cone angles of the same ligand for a range of crystal structures. These include either different metal centres or similar metal centres but with different ligand environments, as shown from the results of Table 4.[21] The $PPh_2OC(CF_3)_3$, (**6**) ligand has successfully been complexed to ruthenium, $[Ru(\eta^5\text{-}C_5H_5)(NCMe)\{PPh_2OC(CF_3)_3\}_2]^+[PF_6]^-$, **[Ru(6)-2]** and rhodium, $[Rh(CO)Cl\{PPh_2OC(CF_3)_3\}_2]$, **[Rh(6)-2]** centres. Crystals suitable for X-ray structural analysis could be grown from DCM/hexane using a layering technique for both these complexes. The **[Ru(6)-2]** crystal structure contained two sets of ionic pairs in the unit cell, giving a structure with four ligands complexed to a ruthenium centre. The cone angle calculations of these four ligand conformations are fairly consistent; θ = 144 ˚, 144 ˚, 143 ˚ and 142 ˚, but much lower than that for the DFT nickel optimised structure (θ = 170 ˚). This demonstrates the flexibility of the steric influence on this ligand due to conformational changes of the phenyl groups. Single-crystal X-ray diffraction structural analysis of **[Rh(6)-2]** gave two cone angle values (θ = 193 ˚ and 163 ˚) for each coordinated ligand, showing very different steric effects of this flexible ligand, see Figure 17.

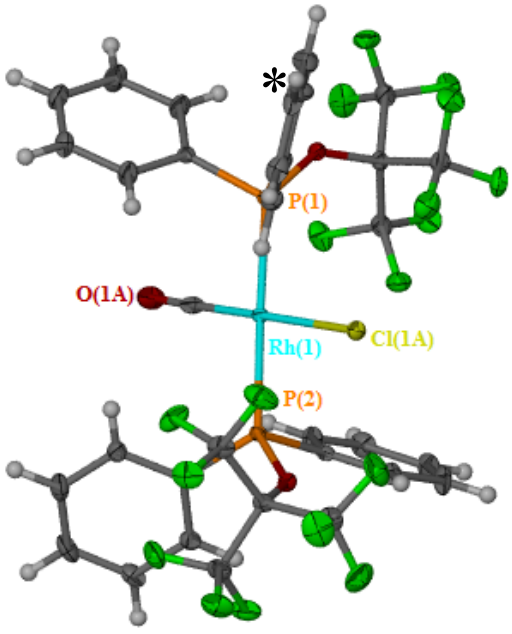

Figure 17: Crystal structure of $Rh(CO)_2Cl\{PPh_2OC(CF_3)_3\}_2$, [Rh(6)-2], the starred (*) phenyl has a propeller arrangement increasing the P(1) ligand cone angle in comparison to that of the ligand with a P(2) centre.

The P(1) ligand in the single-crystal X-ray diffraction structure in Figure 17 has a greater cone angle than that of the P(2) ligand. This can be due to phenyl ring (near the star)

arranging itself vertically (propeller like) in line with the Rh(1)-P(1) bond, so its C(1) hydrogen atom positions itself above 180 °. The P(2) ligand has a smaller cone angle, as both phenyl rings are positioned away from the metal centre and lie horizontally flat rather than strictly vertical, and thus avoiding any hydrogen atoms reaching beyond the metal centre, thus reducing its cone angle. This propeller-like positioning of the phenyl ring (discussed further in Chapter 3) seems key to maximising the cone angle and can be used to explain the reduced cone angle observed for the $PPh\{OC(CF_3)_3\}_2$, (**4**) ligand (θ = 163 °). Figure 18 shows that the conformation of the optimised $[Ni(CO)_3PPh\{OC(CF_3)_3\}_2]$ structure has a reduced θ value, since the phenyl ring is slightly tilted away from the propeller arrangement.

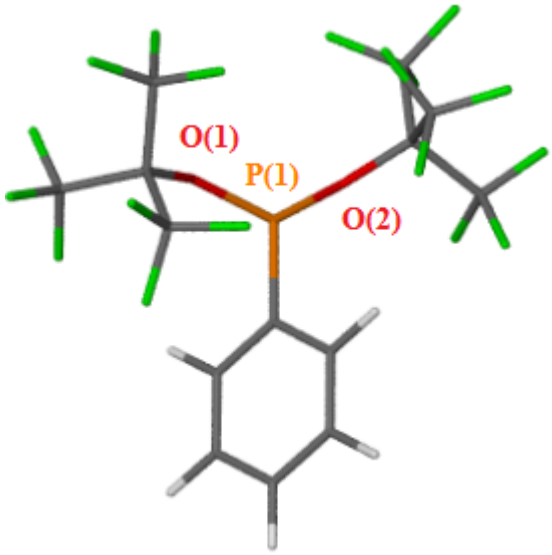

Figure 18: Reduced cone angle for (4) in $[Ni(CO)_3PPh\{OC(CF_3)_3\}_2]$ (optimised by DFT, at the (RI-)BP86/SV(P) level) possibly due to a non-propeller configuration of the phenyl substituent on the ligand. Note CO ligands and Ni centre have been deleted for clarity.

Finally, another example of the conformational changes of the substituents on a phosphorus ligand can be observed with that of $PPh\{OCH(CF_3)_2\}_2$, (**3**). The DFT nickel optimised, $[Ni(CO)_3PPh\{OCH(CF_3)_2\}_2]$ structure (θ = 173 °) of this ligand is higher than that of the two calculated **[Ru(3)-2]** (θ = 140 ° and 147 °). This can be due to the flexibility introduced through the oxygen of the alkoxy substituents; these can move the bulk of the hexafluoroisopropoxy groups in different orientations (*i.e.* "down", "side" or "up", see Figure 19) to reduce clashing, discussed further in Chapter 3. Figure 20 shows a crystal structure of **[Ru(3)-2]**. The hexafluoroisopropoxy groups are positioned in different orientations; one with the hydrogen pointing away from the phosphorus lone pair ("down") and the other pointing towards the lone pair ("up"). The "down" orientation reduces the cone angle, as the bulk from the fluorine atoms is spread out away from the metal centre.

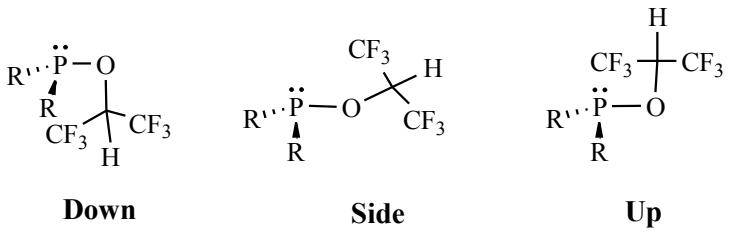

Figure 19: The hexafluoroisopropoxy groups can change orientation; the O-R^F bond can point away from the phosphorus lone pair ("down"), O-R^F can bend so that is not parallel with the phosphorus lone pair ("side") or the O-R^F bond can point towards the lone pair ("up").

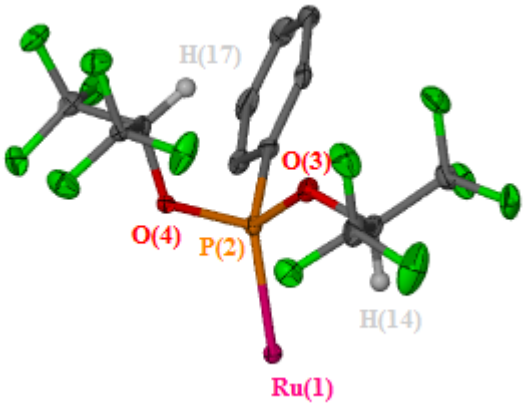

Figure 20: Crystal structure of $[(\eta^5\text{-}C_5H_5)Ru(NCMe)(PPh\{OCH(CF_3)_2\}_2)_2]^+[PF_6]^-$, [Ru(3)-2]. One of the hexafluoroisopropoxy group points "down", O(4) and the other points "up", O(3). Note $[PF_6]^-$, MeCN, second $PPh\{OCH(CF_3)_2\}_2$ ligand and hydrogen atoms on the phenyl ring have been omitted for clarity.

This flexibility of the hexafluoroisopropoxy groups allow for many orientations, these can in turn affect their steric influence. This is evident when studying the cone angles of the $P\{OCH(CF_3)_2\}_3$, (**1**), ligand. The DFT optimised $[Ni(CO)_3P\{OCH(CF_3)_2\}_3]$ complex has a much greater cone angle (θ = 178 °) than the two values calculated for the **[Rh(1)-2]** crystal structure (θ = 167 ° and 160 °). This is due to $[Ni(CO)_3P\{OCH(CF_3)_2\}_3]$ containing two P-O-R bonds pointing "up" towards the Ni centre, forming a large cone angle, see Figure 21. However, the crystal structure of **[Rh(1)-2]** consists of one P-O-R^F group pointing "down" in each of the ligand environments, hence the steric influence of this conformation is reduced, see Figure 22.

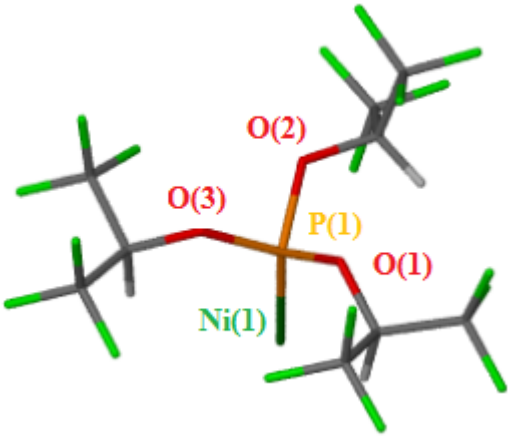

Figure 21: Large cone angle for $P\{OCH(CF_3)_2\}_3$, (1), ligand on a nickel centre, $[Ni(CO)_3L]$ (optimised by DFT, at the (RI-)BP86/SV(P) level due to two P-O-R bonds pointing "up" towards the Ni centre. Note CO ligands have been omitted for clarity.

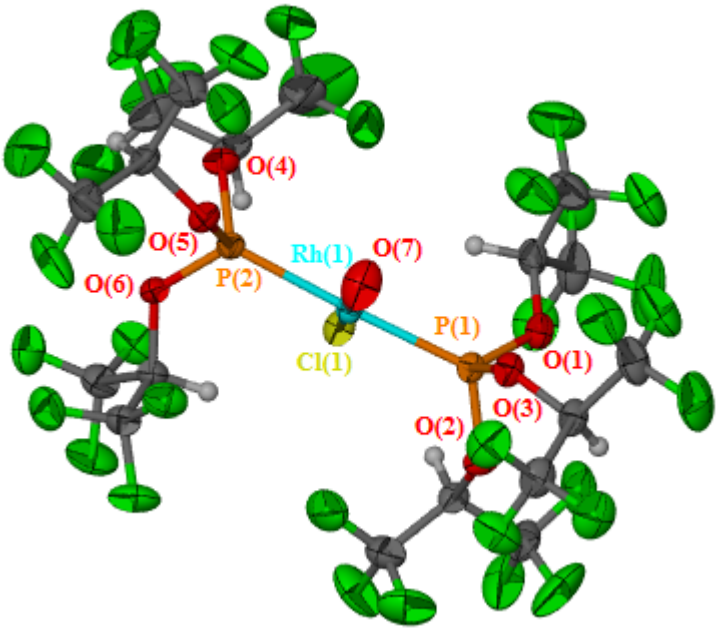

Figure 22: Smaller cone angles observed for [Rh(1)-2] in comparison to $[Ni(CO)_3P\{OCH(CF_3)_2\}_3]$, (XRD structure from ref. [133]) due to O(1) and O(5) of the OR^F substituents pointing "down" away from the Rh centre.

The cone angle calculations from DFT optimised structures of ligands (**1**) to (**6**) coordinated to a tungsten centre in a $[W(CO)_5L]$ complex environment are generally lower in comparison to the $[Ni(CO)_3L]$ environment. This is likely due to the octahedral geometry in $[W(CO)_5L]$ being significantly more crowded. This causes the ligands to pull in more, due to less available space. The rigid ligand (**2**) possesses a large θ value, as difficulty in closing this ligand occurs due to the significant steric repulsion. Conversely, ligand (**1**) can drastically reduce its θ value as it can bend its P-O-R^F groups so that they point "down" and

pull in the steric bulk closer. Similar observations are also made for the other ligands where both the phenyl and the alkoxy groups can orient themselves to give a range of conformations that reduce their cone angles in the area available around the octahedral tungsten centre. The ruthenium complexes have the smallest cone angles than that from all the other metal centres considered. This may be a result of the smaller ruthenium centre being crowded by the large cyclopentadienyl, in combination with MeCN and P(III) ligands that are close in space.

2.2.3.2 *Single-Crystal XRD Structural Data for the Perfluoro-t-Butyl Phosphite, P{OC(CF$_3$)$_3$}$_3$, (2)*

Significant disorder (even at low temperatures) appears to be present in crystals of (**2**) grown under a variety of conditions. However, it has been possible to obtain an X-ray crystal structure of this compound of suitable quality to establish structural connectivity, see Figure 23. The crystal structure shows that the ligand contains a distorted pyramidal phosphorus centre as the lone pair of the phosphorus centre pushes the perfluoro-*t*-butoxy groups away. A spacefilling representation of the structure of (**2**) clearly demonstrates the extreme steric bulk of this ligand, see Figure 23. The bulky perfluoro-*t*-butoxide substituents appear to have little room for conformational flexibility. This suggests that this phosphite should have a relatively rigid steric profile compared to many phosphites, where conformational flexibility allows the alkoxide groups at the phosphorus centre to adjust to the steric requirements of a metal complex.[29] As such, (**2**) may prove to be a useful bulky ligand, which is also very electron-poor.

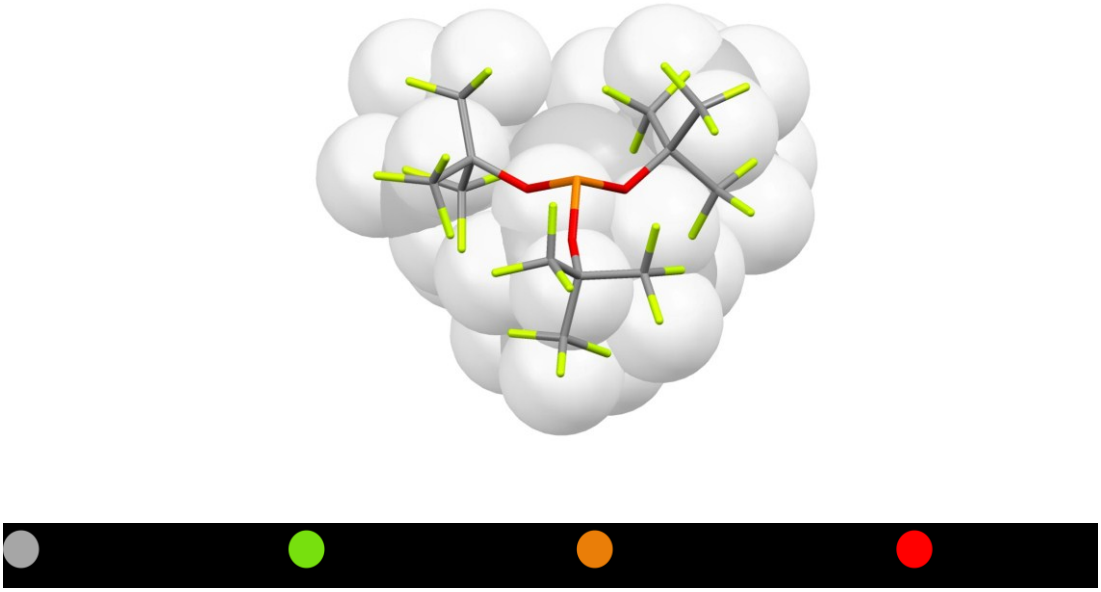

Figure 23: Single X-ray crystal structure of perfluoro-*t*-butyl phosphite, P{OC(CF$_3$)$_3$}$_3$, (2). Extensive disorder (modelled over two positions, one "up" and "one" down" in the asymmetric unit) is present in the structure. Only one position is shown for clarity. Although disordered over two positions the incredible steric bulk on the ligand can be observed. Crystal system: monoclinic. Space group: C2/c. R_1= 0.1565 (>2sigma(I)), wR_2 = 0.4462. (all data).

The P-O bond lengths for the phosphite, P{OC(CF$_3$)$_3$}$_3$, (**2**) are found to be; P(1A)–O(1A) = 1.61(1) Å, P(1A)–O(2A) = 1.62(1) Å, and P(1A)–O(3A) = 1.61(1) Å. Selected aryl phosphite crystal structures found from the CSD are shown in Figure 24 with their P-O bond lengths summarised in Table 5. The disorder in this structure and the relatively low precision of the bond lengths means a general conclusion can only be made. This being that the P-O

bond lengths are similar in length to aryl phosphites and the pyrophosphite, (**7**). The large errors on the $P\{OC(CF_3)_3\}_3$, (**2**) bond lengths makes it difficult to make comparisons between the fluorinated alkoxy groups and non-fluorinated groups.

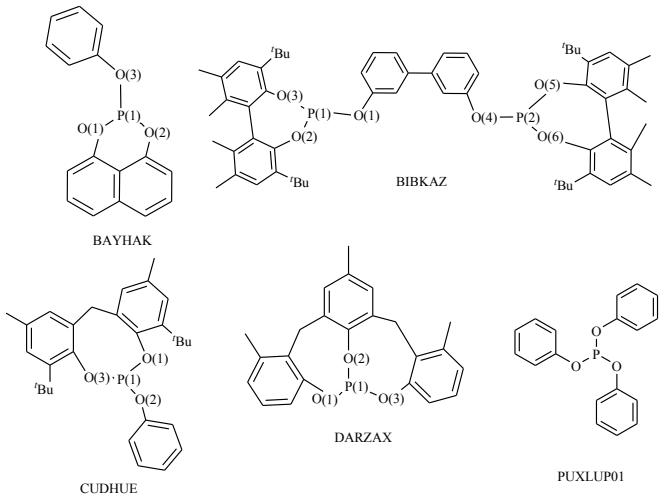

Figure 24: Structures of aryl-phosphites found in the CSD, note the CSD names are presented below each structure.

CSD Name	*Bond Length (Å)*	*Bond Length (Å)*	*Bond Length (Å)*
PUXLUP01	P(1)-O(1) = 1.611(8)	P(1)-O(2) = 1.60(1)	P(1)-O(3) = 1.600(9)
BAYHAK	P(1)-O(1) = 1.6050(4)	P(1)-O(2) = 1.6433(4)	P(1)-O(3) = 1.6568(7)
BIBKAZ	P(1)-O(1) = 1.628(1)	P(1)-O(2) = 1.617(2)	P(1)-O(3) = 1.639 (1)
BIBKAZ	P(2)-O(4) = 1.644(1)	P(2)-O(5) = 1.631(2)	P(2)-O(6) = 1.607 (2)
CUDHUE	P(1)-O(1) = 1.643(2)	P(1)-O(2) = 1.618(1)	P(1)-O(3) = 1.640 (2)
DARZAX	P(1)-O(1) = 1.618(2)	P(1)-O(2) = 1.623(2)	P(1)-O(3) = 1.625 (2)

Table 5: P-O bond lengths for selected aryl phosphites found in the CSD.

2.2.3.3 Spacefill Models of DFT Optimised Free Ligands

Spacefill models of the top and bottom views from looking down the lone pair vector are presented below, to give an idea of the steric bulk of these ligands. These were optimised using DFT calculations at the (RI-)BP86/SV(P) level.

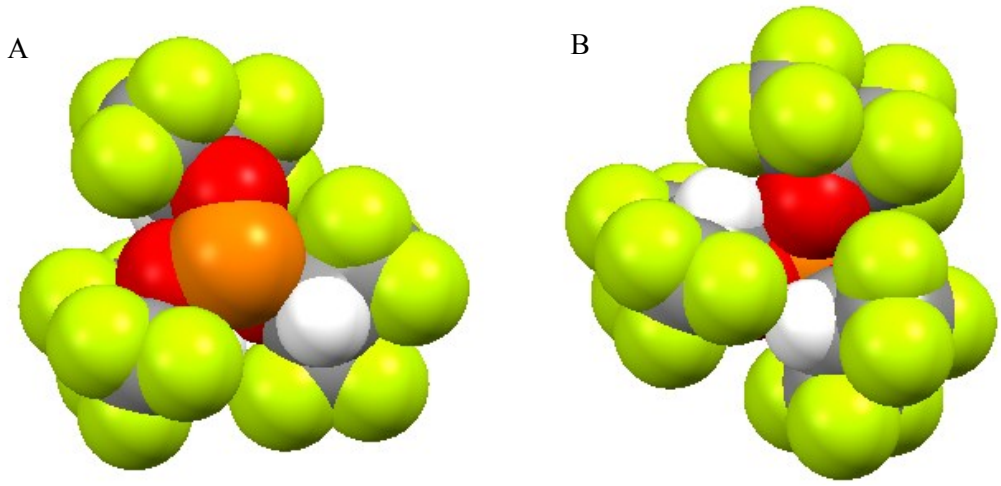

Figure 25: $P\{OCH(CF_3)_2\}_3$, (1), A: top, B: bottom view of the ligand.

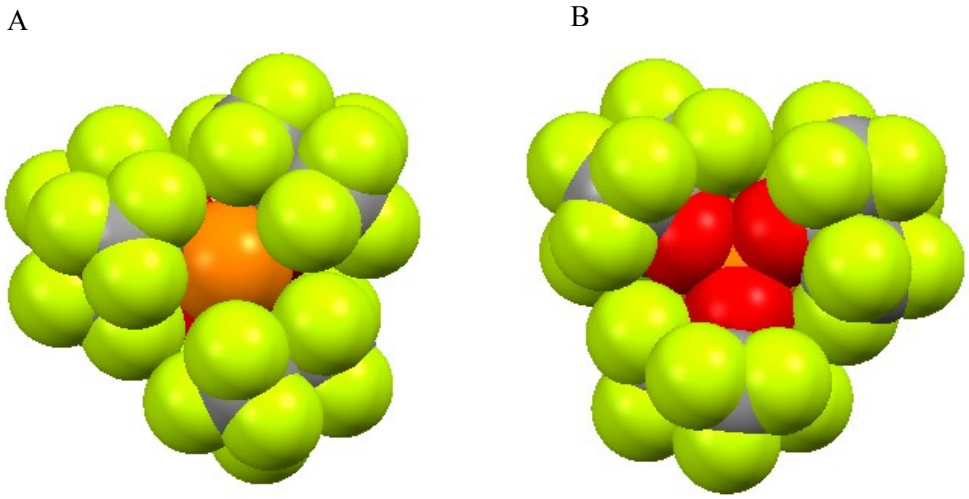

Figure 26: $P\{OC(CF_3)_3\}_3$, (2), A: top, B: bottom view of the ligand.

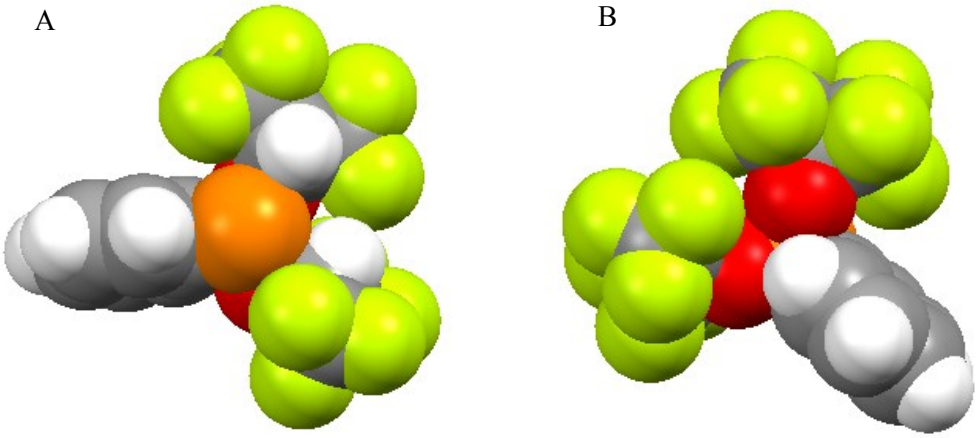

Figure 27: $PPh\{OCH(CF_3)_2\}_2$, (3), A: top, B: bottom view of the ligand.

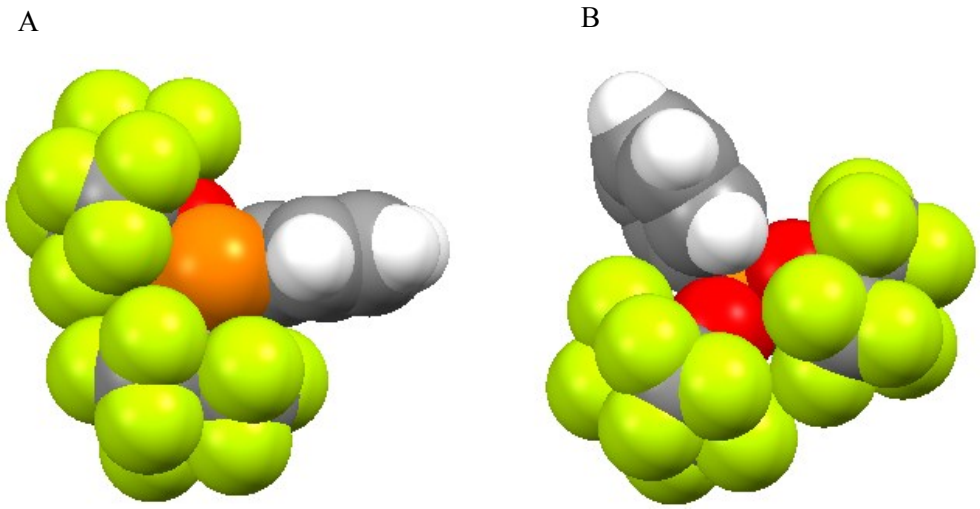

Figure 28: $PPh\{OC(CF_3)_3\}_2$, (4), A: top, B: bottom view of the ligand.

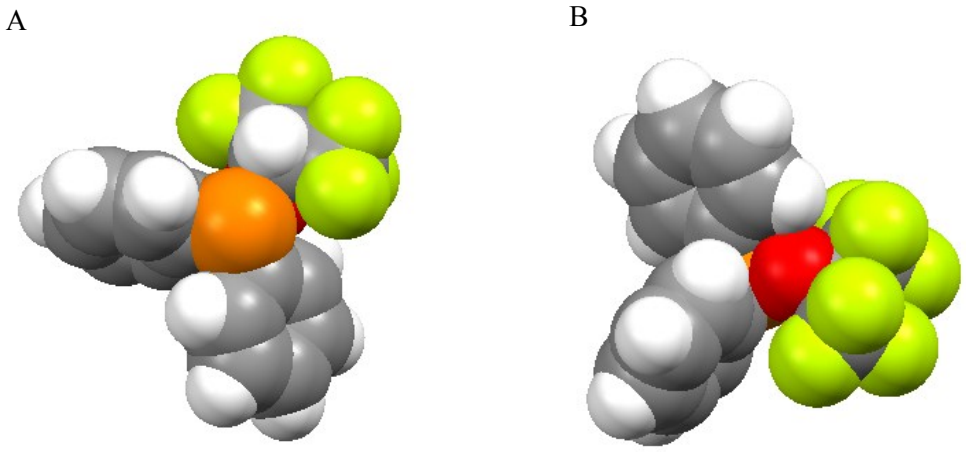

Figure 29: $PPh_2\{OCH(CF_3)_2\}$, (5), A: top, B: bottom view of the ligand.

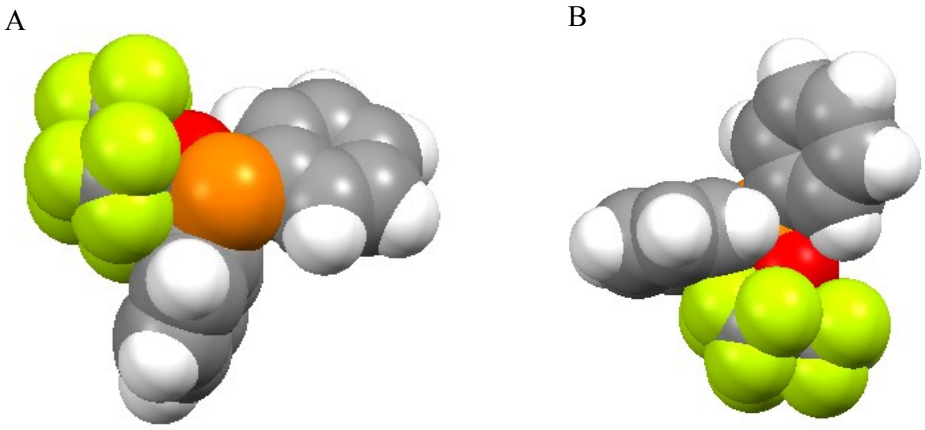

Figure 30: $PPh_2\{OC(CF_3)_3\}$, (6), A: top, B: bottom view of the ligand.

2.2.4 Electronic Properties of the Novel Bulky Electron-Deficient Phosphorus (III) Ligands

2.2.4.1 Electronic Properties Assessed Using the [CpIr(CO)L] Model Complex

The electronic properties of ligands (**1**) to (**6**) can be calculated using the method suggested by Gusev in 2009.[3] This involves DFT calculations of $[(\eta^5\text{-}C_5H_5)Ir(CO)L]$ complexes (where L is the desired ligand) to give CO stretching frequencies and optimised structures to give CO bond lengths for the attached corresponding CO ligands. All optimisations were performed at the (RI-)BP86/SV(P) level, followed by frequency calculations at the same level. All calculations were performed using the TURBOMOLE V5.10 package using the resolution of identity (RI) approximation. If the CO stretching frequencies and CO bond lengths are plotted on a graph, they should correlate; the lower the stretching frequency, the greater the CO bond length, since electron-density is placed into the anti-bonding molecular orbitals on the CO *via* back-bonding. The hydrogen and fluorinated phosphorus (III) analogues were calculated for a range of ligands *i.e.* PR_nOR_{3-n}, $PR_nOR^F_{3-n}$ {R = Mesityl, Ph, Me, H, NMe_2, F; OR = O^{t}Bu, O^{i}Pr; OR^F = $OC(CF_3)_3$, $OCH(CF_3)_2$; n = 0-3}, see Graph 1.

As expected, the non-fluorinated phosphorus (III) ligands show longer CO bond lengths and lower CO stretching frequencies. This can be attributed to their less π-acidic properties than the fluorinated phosphite analogues (shorter CO bond lengths and higher CO stretching frequencies). The ligands under study can be divided into three clusters; these being electron-donating, electron-neutral and electron-withdrawing ligands, in regards to their overall electronic character. Each cluster has examples of extreme cases, showing that a range of electronic properties are available from the class of ligands studied here.

The least π-acidic are the $PMes_2OR$ phosphinites; here the bulky mesityl groups contain electron-donating properties at the phosphorus centre due to greater inductive effects (+I). A direct comparison of $PMes_3$ and $P\{C_6(CF_3)_3H_2\}_3$ highlights a difference in ν_{CO} of ~21 cm^{-1}, this indicates that the groups on the phenyl ring have a crucial effect on the overall electronic properties of the ligand. Here, the electron-withdrawing effect (-I) of the CF_3 groups follow through on to the phosphorus centre, unlike in a mesityl substituent, where its CH_3 groups are electron-donating (+I) allowing the mesityl groups to transfer positive inductive effects on the phosphorus centre. The $PMes_2OR$ ligands seem to overcome the electron-withdrawing effects from the oxygen of the alkoxy group. It appears that the inductive effects from the R groups on the alkoxy substituents add to this electron-donating effect as a simple $PMes_3$ is not the least π-acidic. This may also be due to the extra steric bulk of the

third mesityl group causing conformational changes which in turn effect the electronic interactions between the mesityl substituents and the phosphorus centre. These bulky conformations can reduce orbital overlap with the iridium metal centre as the steric effects inhibit a close interaction. This is shown when comparing the Ir-P bond lengths for the optimised structures; $PMes_3$ = 2.34 Å, $PMes_2O^tBu$ = 2.29 Å, $PMes_2O^iPr$ = 2.28 Å.

Graph 1: CO bond length (Å) vs CO stretching frequency (cm^{-1}) for $[(\eta^5\text{-}C_5H_5)IrCOL]$, where L = Phosphorus (III) ligand, from DFT calculations on the (RI-)BP86/SV[P] level

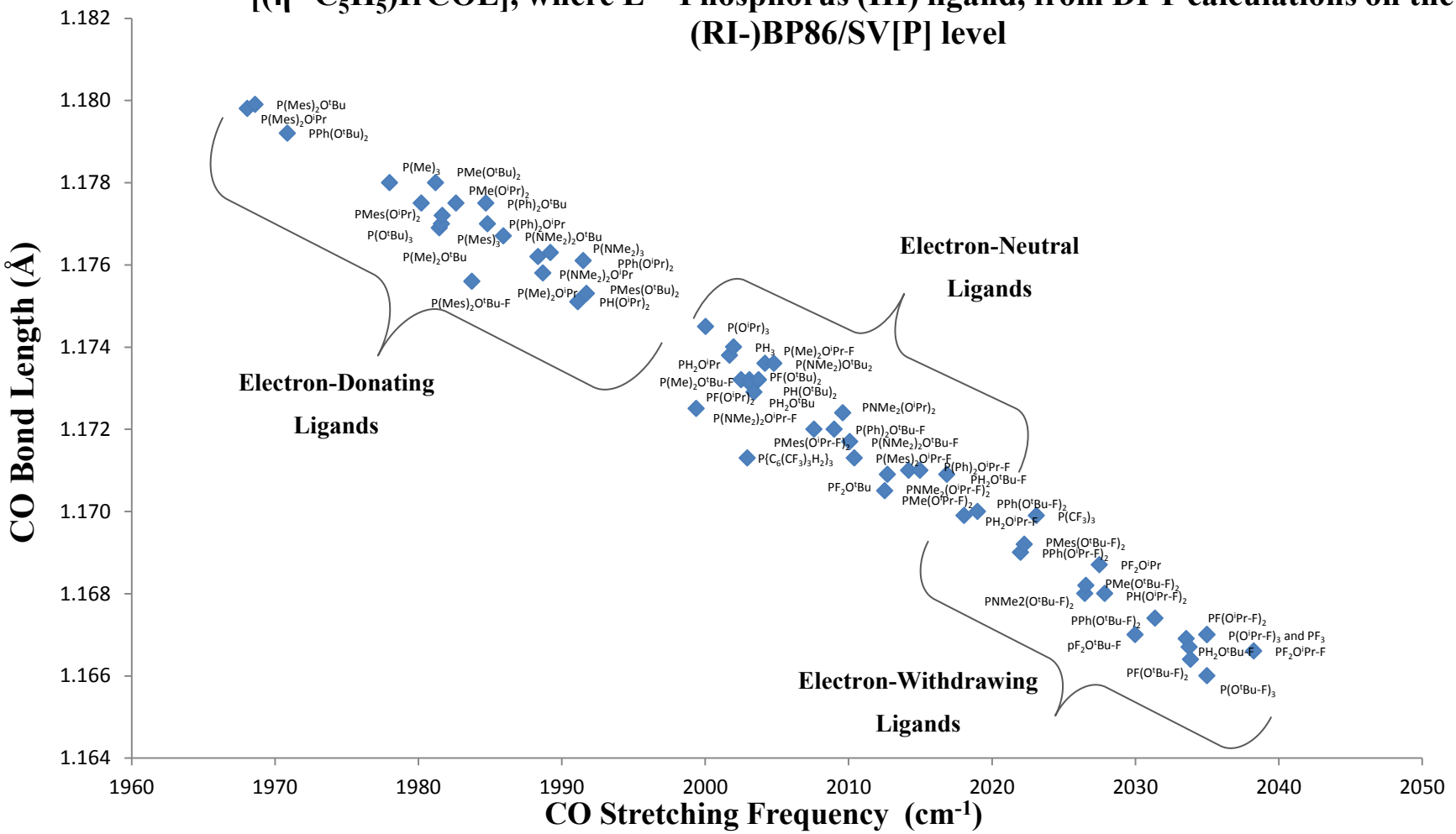

The $P\{NMe_2\}_3$ and $P\{NMe_2\}_2OR$ ligands are close to the region of the electron-donating groups. This can be explained due to mesomeric effects, since NMe_2 is a π-donor group. Donation of electron-density from the nitrogen to the phosphorus increases the donor strength for this ligand. Fluorinating the alkoxy substituents on ligands bearing NMe_2 groups increases the π-acidity beyond that of the simplest phosphine, PH_3, generally described as an unsubstituted phosphine (it contains no EDGs or EWGs). It can be thought that although an NMe_2 π-donor group is present, the electron-withdrawing fluorinated alkoxy groups can reduce the conjugation on the vacant phosphorus orbital as it pulls the electron-density towards itself, thus increasing the ligands π-acidity.

The difference in the inductive effects of an -O^{t}Bu and -O^{i}Pr group can be observed in two examples. Firstly, the $P(O^tBu)_3$ ν_{CO} is 19 cm^{-1} lower than ν_{CO} $P(O^iPr)_3$, suggesting the inductive effects increase due to a larger +I in the $P(O^tBu)_3$ case, placing it not that far from an alkyl phosphine, PMe_3; ν_{CO} = 1981.7 and 1978.0 cm^{-1} respectively. However, it should be noted that the $P(O^iPr)_3$ is lower than PH_3, suggesting the electron-withdrawing effects of the oxygen atoms present overcome any +I from the isopropyl group. This highlights that the phosphites with relatively smaller R groups tend to balance the positive inductive effects from the R group with any electronegative effects from the oxygen atom. Hence, they appear to cancel out and overall electronically the phosphites are similar to an unsubstituted phosphine, PH_3, but with considerably more steric bulk. Significant changes are observed in π-acidity for a $PPh(O^tBu)_2$ and $PPh(O^iPr)_2$ ligand; ν_{CO} = 1970.9 and 1991.5 cm^{-1} respectively. The PPh_2O^tBu and PPh_2O^iPr ligands are much closer in ν_{CO} stretching frequencies, suggesting the two phenyl substituents on each ligand majorly contribute to the overall electronic effect, likely through greater +I inductive effects. These PPh_2O^tBu/PPh_2O^iPr ligands lie in between the two extremes of the $PPh(O^tBu,)_2$ and $PPh(O^iPr)_2$ ligands on the electronic map, implying the overall inductive effects from the phenyl R group is less than that of a bulky -O^{t}Bu group, but greater than a -O^{i}Pr group. This emphasises that an alkoxy group can contribute to larger +I inductive effects than an aryl group, but only in extreme cases where increased electron donating ability is present.

The ligands clustering around PH_3 can be regarded as electronically neutral, as overall their electronic influence is neither strongly electron-donating nor electron-withdrawing. Gusev shows in his studies, that phosphites with small alkyl groups $P(OR)_3$ {R = Me, Et}, PPh_3 and PH_2Ph cluster around this electronic region. The calculations in this study show that as expected $PH(O^tBu)_2$, $PH_2(O^tBu)$ and $PH_2(O^iPr)$ also come in this region of the electronic map. This study also shows that substituents of very different electronic nature overall appear to give very neutral electronic properties, especially those with two strongly electron-

donating groups and one electron-withdrawing group *e.g.* $P\{NMe_2\}_2(O^tBu^F)$, $P\{NMe_2\}_2(O^iPr^F)$, $PMe_2(O^tBu^F)$, $PMe_2(O^iPr^F)$, $PPh_2(O^tBu^F)$, $PPh_2(O^iPr^F)$, $PF(O^tBu)_2$, $PF(O^iPr)_2$. Those ligands that contain strongly electron-donating groups and two alkoxy groups *e.g.* $PMe(O^iPr^F)_2$, $PMes(O^iPr^F)_2$, $P\{NMe_2\}(O^iPr^F)_2$, $P\{NMe_2\}(O^tBu)_2$ and $P\{NMe_2\}(O^iPr)_2$ are also found in this cluster as the electronic character appears to balance out to give very electronic neutral properties overall.

The cluster containing the electron-withdrawing ligands is the most interesting in the context of this work, as it shows a range of ligands of varying π-acidic electronic character. Very little focus in previous work using this method has been on π-acidic ligands.[3] Gusev presents only ligands such as PPh_2Cl, PCl_3, $P(CF_3)_3$ and PF_3 in this region.[3] The latter two are known as the most π-acidic phosphorus ligands presently studied in detail, but both of which are sterically small in "ligand space".[23] Direct P-F bonds on a phosphorus ligand introduce a level of π-acidity to the ligand, but the full induction effect of the fluorine atoms can be shielded by a carbon atom on the phosphorus in $P(CF_3)_3$ making it less π-acidic. The results in this thesis shows that $PF_2(O^iPr)$ appears at a ν_{CO} value that is ~3 cm^{-1} higher than $P(CF_3)_3$, suggesting similar electronic character. However, in the $PF_2(O^tBu)$ case the +I effects from the -^{t}Bu group surprisingly overcome the electron-withdrawing effects from the two P-F groups and reduces the π-acidity of the $PF_2(O^tBu)$ ligand by shifting it to ~9 cm^{-1} lower in ν_{CO} than that for the $P(CF_3)_3$ ligand. It may also be possible that the incredible steric bulk from the *t*-butyl group reduces sufficient orbital overlap, thus reducing its π-acidic properties.

The fluorinated phosphites $P\{OCH(CF_3)_2\}_3$, (**1**) and $P\{OC(CF_3)_3\}_3$, (**2**) are found to have similar electronic properties to PF_3. Interestingly, although one would expect $P\{OC(CF_3)_3\}_3$, (**2**) to have greater π-acidity than $P\{OCH(CF_3)_2\}_3$, (**1**) due to the extra CF_3 groups, the data suggest that in fact the electronic properties of the two ligands are similar. This is likely to be due to the steric bulk of $P\{OC(CF_3)_3\}_3$, (**2**), which may prevent a close approach of the ligand to the metal centre, thus reducing the metal-phosphorus orbital overlap and preventing metal-to-ligand back-donation. There is some evidence of this in the optimised Ir-P bond lengths; $[(\eta^5\text{-}C_5H_5)Ir(CO)P\{OCH(CF_3)_2\}_3]$ (2.194 Å), whereas $[(\eta^5\text{-}C_5H_5)Ir(CO)P\{OC(CF_3)_3\}_3]$ (2.198 Å), is a little longer. Another observation shows substituting the fluorinated alkoxy groups with phenyl groups bring the ligands' electronic properties closer to PH_3. This indicates there is potential for the electronic properties to be finely tuned to suit specific tasks, making them appealing for use in catalysis. The DFT calculations for three of these iridium complexes {of ligands (**1**), (**3**), (**5**)} were calculated by

the JMS group 2009/2010 MChem student, Paul Beet and three {of ligands (**2**), (**4**), (**6**)} were calculated by Dr John Slattery.

Graph 2 consists of a scatter graph showing the correlation of all the ligands calculated bearing one alkoxy substituent only {$PR_2(OR)$ and $PR_2(OR^F)$; R = Mesityl, Ph, Me, H, NMe_2, F; OR = O^{t}Bu, O^{i}Pr; OR^F = $OC(CF_3)_3$, $OCH(CF_3)_2$}. Reference points are added to the graph; PMe_3 an electron-donating ligand, PH_3 an electron-neutral ligand, $P(CF_3)_3$ and PF_3 the two most electron-withdrawing ligands most commonly used for the comparison of electronic properties for novel ligands.[47] These reference points allow one to understand the electronic properties of the calculated ligands from their positions on the graphs. The ligands with hydrogen substituents allow one to understand the consequence of fluorinating an alkoxy group on the ligands electronic effect *e.g.* $PH_2(O^tBu)$ (ν_{CO} = 2003.4 cm^{-1}); $PH_2(O^tBu^F)$ (ν_{CO} = 2016.9 cm^{-1}), and $PH_2(O^iPr)$ (ν_{CO} = 2001.7 cm^{-1}); $PH_2(O^iPr^F)$ (ν_{CO} = 2018.1 cm^{-1}). The increase in the ν_{CO} upon fluorination suggests that the ligands electron-withdrawing property increases, making them more π-acidic. The overall electronic property of ligands bearing highly electron-donating and electron-withdrawing ligands is a fine balance between the two extremes, grouping them close to the neutral ligands. Similarly Graph 3 consists of a scatter graph showing the correlation of all the ligands calculated bearing two alkoxy substituents {$PR(OR)_2$ and $PR(OR^F)_2$; R = Mesityl, Ph, Me, H, NMe_2, F; OR = O^{t}Bu, O^{i}Pr; OR^F = $OC(CF_3)_3$, $OCH(CF_3)_2$}.

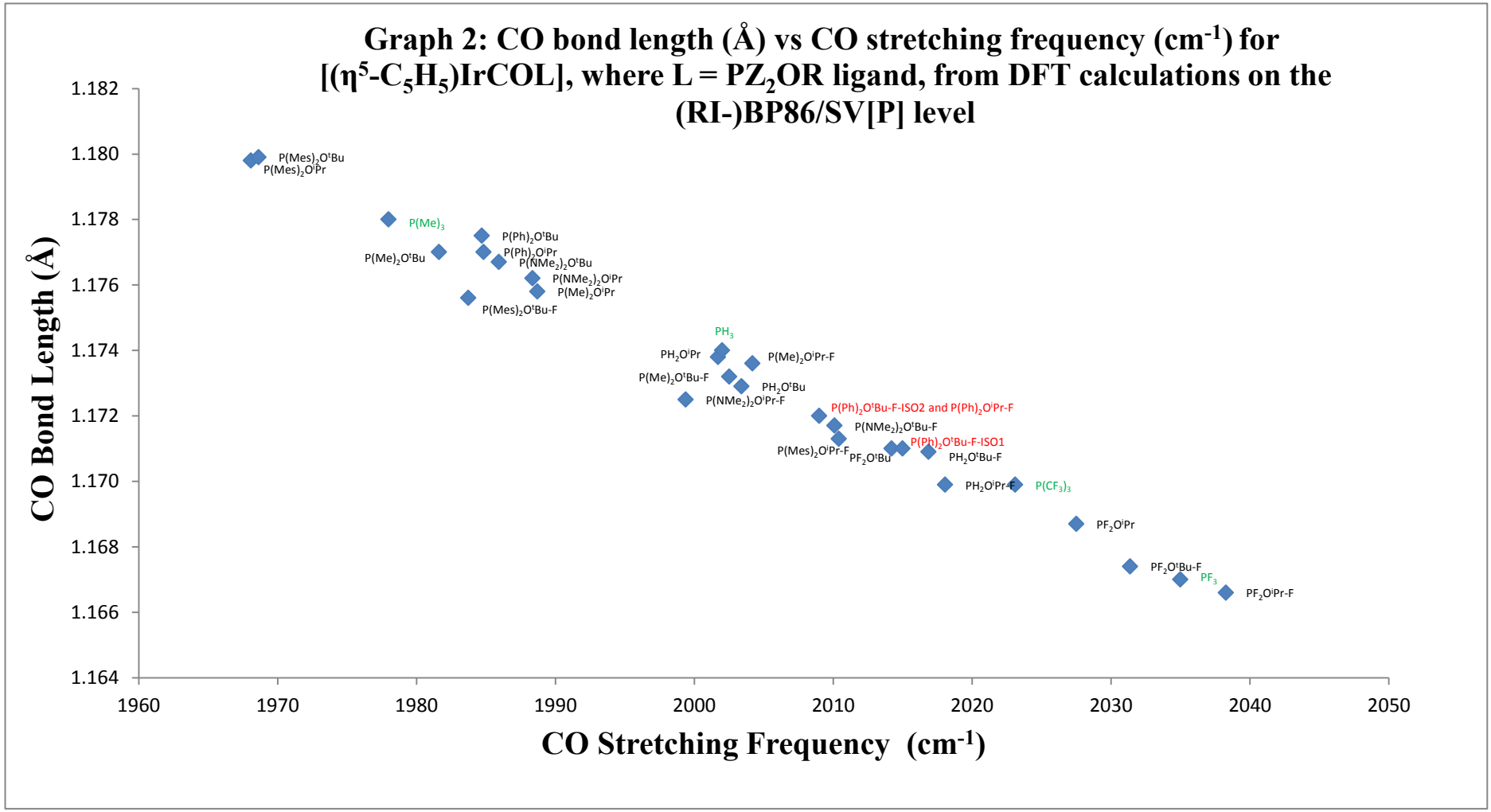
Graph 2: CO bond length (Å) vs CO stretching frequency (cm-1) for [(η5-C5H5)IrCOL], where L = PZ2OR ligand, from DFT calculations on the (RI-)BP86/SV[P] level
CO Bond Length (Å)
CO Stretching Frequency (cm-1)
1.182
1.180
1.178
1.176
1.174
1.172
1.170
1.168
1.166
1.164
1960
1970
1980
1990
2000
2010
2020
2030
2040
2050
P(Mes)2OtBu
P(Mes)2OiPr
P(Me)3
P(Ph)2OtBu
P(Ph)2OiPr
P(Me)2OtBu
P(NMe2)2OtBu
P(NMe2)2OiPr
P(Me)2OiPr
P(Mes)2OtBu-F
PH3
PH2OiPr
P(Me)2OiPr-F
P(Me)2OtBu-F
PH2OtBu
P(NMe2)2OiPr-F
P(Ph)2OtBu-F-ISO2 and P(Ph)2OiPr-F
P(NMe2)2OtBu-F
P(Ph)2OtBu-F-ISO1
P(Mes)2OiPr-F
PF2OtBu
PH2OtBu-F
PH2OiPr-F
P(CF3)3
PF2OiPr
PF2OtBu-F
PF3
PF2OiPr-F

Graph 3: CO bond length (Å) vs CO stretching frequency (cm^{-1}) for $[(\eta^5\text{-}C_5H_5)IrCOL]$, where L = $PZ(OR)_2$ ligand, from DFT calculations on the (RI-)BP86/SV[P] level

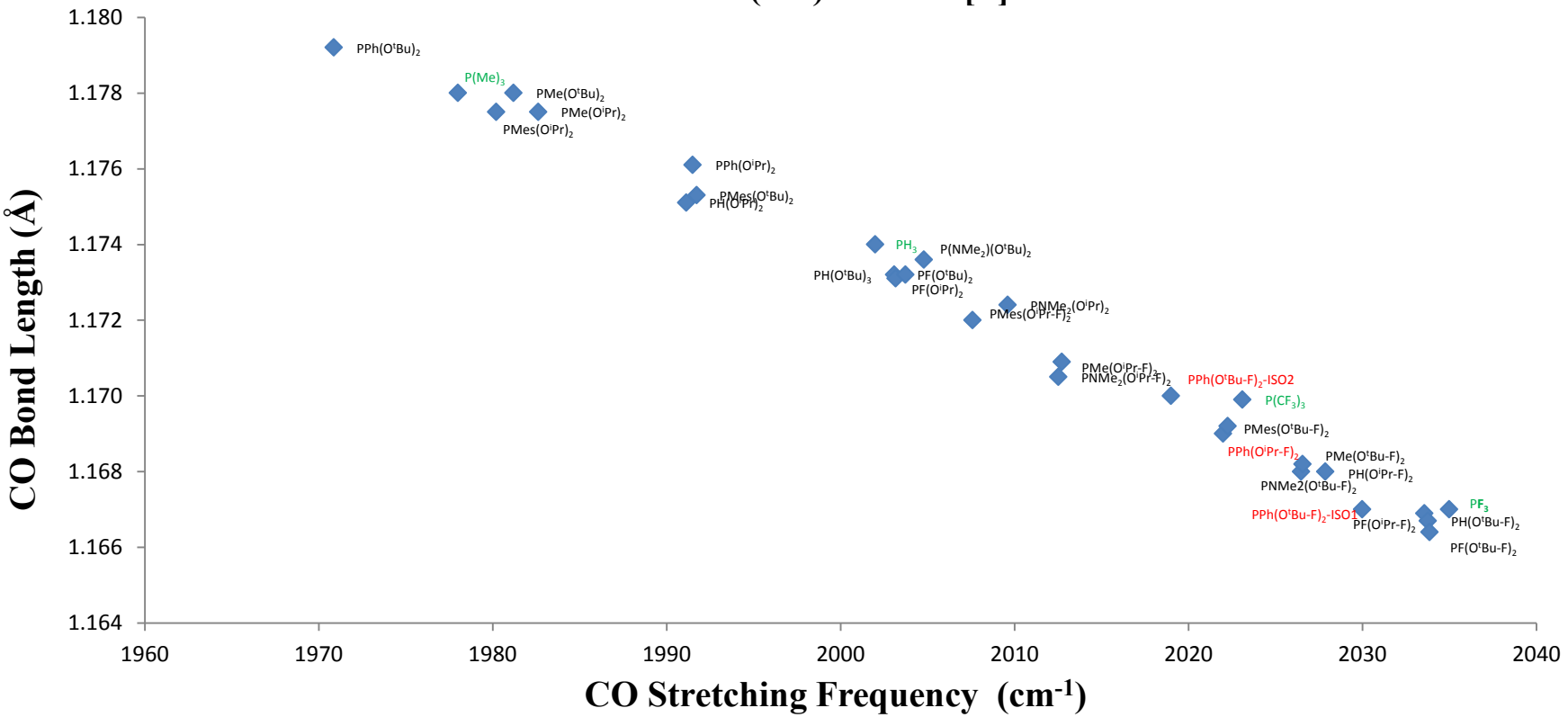

2.2.4.2 $^{1}J_{WP}$ Coupling Constants for $W(CO)_5L$ Complexes

All six ligands, (**1**) to (**6**) were successfully complexed to a tungsten pentacarbonyl metal centre, $[W(CO)_5L]$ {where L = (**1**) – (**6**)} by reaction of $[W(CO)_5(THF)]$ with the relevant ligand in tetrahydrofuran (THF) solution. The $^{31}P\{^{1}H\}$ NMR spectroscopic data for these complexes in THF, along with the carbonyl IR stretching frequencies (solution phase in THF/hexane) provide useful experimental data on the ligand electronic properties and are summarised in Table 6 and Table 7. Although coordination of all six synthesised ligands has been observed by a change in chemical shift and the presence of satellites in the $^{31}P\{^{1}H\}$ NMR spectra, only four have been isolated, after sublimation, see Figure 31. The sublimation purification step is required to remove excess $[W(CO)_6]$, which can dominate the carbonyl region of the IR spectra, making it difficult to obtain any useful IR characterisation data. The sublimation step requires around fifteen hours whilst heating to 80 °C, this in turn can lead to decomposition (from release of a CO ligand followed by subsequent degradation reactions) of these complexes. Hence, isolated $[W(CO)_5PPh\{OC(CF_3)_3\}_2]$ and $[W(CO)_5P\{OC(CF_3)_3\}_3]$ products were difficult to obtain. EI-MS confirms the purity {no $[W(CO)_6]$ molecular ion peaks after sublimation} for the remaining four ligands and the complexation of these isolated ligands to a tungsten metal centre ($[M]^+$ seen in all cases).

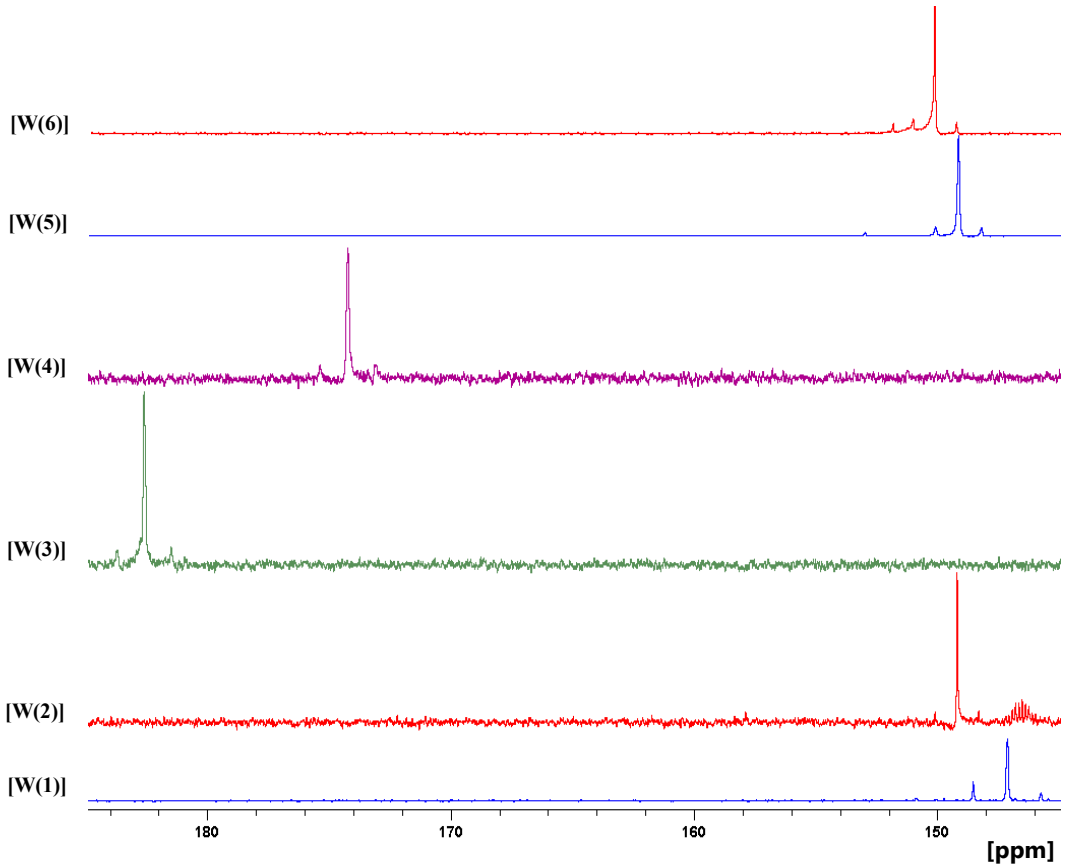

Figure 31: $^{31}P\{^{1}H\}$ NMR spectra overlay of all the $[W(CO)_5L]$ successfully complexed with the following phosphorus (III) ligands, from bottom to top; $[W(CO)_5P\{OCH(CF_3)_2\}_3]$ (note the downfield satellite is under a impurity peak), [W(1)]; $[W(CO)_5P\{OC(CF_3)_3\}_3]$, [W(2)]; $[W(CO)_5PhP\{OCH(CF_3)_2\}_2]$, [W(3)]; $[W(CO)_5PhP\{OC(CF_3)_3\}_2]$, [W(4)]; $[W(CO)_5Ph_2P\{OCH(CF_3)_2\}]$, [W(5)]; $[W(CO)_5Ph_2P\{OC(CF_3)_3\}]$, [W(6)]. A multiplet is observed for uncoordinated $P\{OC(CF_3)_3\}_3$ ligand in the [W(2)] spectrum.

It is important to note, that successful complexation was observed only when pure isolated ligands were used with $[W(CO)_5(THF)]$, synthesised from a known literature preparation method.[141] Problems occurred in the presence of DCM solvent and NaCl (present if the ligands are not filtered well). It is thought that these possibly activate and form $[W(CO)_5Cl]^-$ or similar species making it difficult for the ligand complexation. In addition, the $[W(CO)_5(THF)]$ intermediate is air-sensitive and can quickly decompose to form the $[W(CO)_6]$ starting material if left unused for too long. All samples were kept at low temperature (5 ˚C) and treated as air-sensitive to avoid decomposition. These complexes tend to form oxidised tungsten species and turn blue in colour (sometimes even black over time), from the original intense yellow/green colour. Additional peaks are also observed at around 105.0, 100.0 and 95.0 ppm in the $^{31}P\{^{1}H\}$ NMR spectra containing tungsten satellites if the samples are not treated as temperature, light and air-sensitive. These are likely to be oxidised phosphorus-tungsten complexes as hydrolysis of the complexed ligands can also occur. Using the data from the successful complexation of the hexafluoroisopropoxy-containing ligands, it seems the tungsten-phosphorus coupling constants ($^{1}J_{PW}$) seem to follow a trend. This can be explained; the larger the $^{1}J_{PW}$ value, then the greater the π-acidity

i.e. $P\{OCH(CF_3)_2\}_3$, (**1**) $^1J_{PW}$ = 451 Hz; $PhP\{OCH(CF_3)_2\}_2$, (**3**) $^1J_{PW}$ = 357 Hz; $Ph_2P\{OCH(CF_3)_2\}$, (**5**) $^1J_{PW}$ = 291 Hz.[20, 142] Previous studies show coupling constant values increase because the s-character contribution in the σ-bond increases.[143, 144] However, it is thought for $^1J_{PW}$ coupling constants a strengthening of the σ-bond by a synergic π-interaction or by contraction of the tungsten 6s-orbital increase the coupling by the Fermi mechanism, hence it can be a useful method to gage the π-acidity of phosphorus (III) ligands.[142] One may expect the perfluoro-*t*-butoxy ligands to be greater in π-acidity compared to the hexafluoroisopropoxy ligands; $PhP\{OC(CF_3)_3\}_2$, (**4**) and $Ph_2P\{OC(CF_3)_3\}$, (**6**) follow this trend as their coupling constants ($^1J_{PW}$) are higher than that for their hexafluoroisopropoxy analogues. These differ by ~10 Hz showing the extent of increased π-acidity of an extra CF_3 group. However, the steric contributions appear to play a critical part in the electronic reactivity. As the perfluoro-*t*-butyl phosphite, $P\{OC(CF_3)_3\}_3$, (**2**) has a much lower coupling constant than expected ($^1J_{PW}$ = 292 Hz). It is likely a poor overlap due to the incredible steric bulk is what affects the electronic effects (reducing its full potential as an extreme π-acidic ligand like PF_3). The structure of these complexes were optimised at the (RI-)BP86/SV(P) level and show evidence of the reduced orbital overlap in the W-P bond lengths; $[W(CO)_5P\{OCH(CF_3)_2\}_3]$ (2.482 Å), where as $[W(CO)_5P\{OC(CF_3)_3\}_3]$ (2.548 Å) is significantly longer. Considering the overall electronic effects, these phosphorus (III) ligands could potentially be very useful π-acid ligands due to their willingness to accept d-electrons from metals into their P-O σ* orbitals through metal-phosphorus back-bonding. This π-acidity is enhanced greatly by fluorinating the alkoxy-groups as the highly electronegative fluorine atoms reduce the electron-density on the phosphorus, but clearly the steric effects contribute to the overall π acceptor ability of the ligands. Table 6 compares a range of phosphorus (III) ligands where the $^1J_{PW}$ coupling constants are known from literature values.[20, 142, 144-150]

$^1J_{PW}$ (Hz)	Ligand	Reference
68.0	PH_2Li	[145]
150.9	$P(Me_3Si)_3$	[145]
200.0	$P(^nBu)_3$	[151]
215.2	PD_3	[150]
216.0	PH_3	[145]
216.5	PEt_3	[145]
225.0	PMe_3	[145]
230.6	$P(^n\text{octyl})_3$	[147]
233.0	$P(^iPr)_3$	[146]
235.0	$P(^nBu)_2Ph$	[151]
240.0	$PPh_2(^tBu)$, $PPh_2(^iPr)$, $PPh_2(Et)$	[151]
242.3	$P(^p\text{toly})_3$	[147]
243.0	PPh_3	[146]
245.0	$PPh_2(Me)$	[151]
245.2	$P\{C_6H_4\text{-}_4\text{-}CH_2CH_2(CF_2)_7CF_3\}_3$	[147]
248.8	$P\{CH_2CH_2(CF_2)_5CF_3\}_3$	[147]
250.0	$P(^nBu)Ph_2$, $PMe_2(CF_3)$	[151, 152]
267.0	$PH_2(Cl)$	[148]
269.0	$PH_2(OH)$	[148]
275.0	$PMe(CF_3)_2$	[139]
280.0	$PPh_2(OMe)$	[142]
284.4	$PH_2(F)$	[148]
291.0	$Ph_2P\{OCH(CF_3)_2\}$, **[W(5)]**	This work
292.0	$P\{OC(CF_3)_3\}_3$, **[W(2)]**	This work
300.0	$P(CF_3)_3$	[139]
304.0	$Ph_2P\{OC(CF_3)_3\}$, **[W(6)]**	This work
312.5	$PH(OH)_2$	[148]
313.0	$P(NMe_2)_3$	[146]
323.0	$PPh(OMe)_2$	[142]
334.0	PI_3	[149]

336.9	$P(H)Cl_2$	[148]
357.0	$PhP\{OCH(CF_3)_2\}_2$, **[W(3)]**	This work
361.0	P(H)(F)Cl	[148]
374.0	$PhP\{OC(CF_3)_3\}_2$, **[W(4)]**	This work
376.0	$P(H)F_2$	[148]
381.0	$P(O^iPr)_3$	[146]
390.0	$P(O^nBu)_3$	[142]
391.0	$P(OEt)_3$	[142]
398.0	$P(OMe)_3$, PBr_3	[142, 149]
416.0	$P(OPh)_3$	[146]
426.0	PCl_3	[149]
452.0	$P\{OCH(CF_3)_2\}_3$, **[W(1)]**	This work
496.3	PF_3	[150]

Table 6: Comparison of tungsten-phosphorus $^1J_{PW}$ coupling constants for a range of known $[W(CO)_5L]$ complexes with [W(1)] to [W(6)].

The $P\{OCH(CF_3)_2\}_3$, (**1**) ligand ($^1J_{PW}$ = 452.0 Hz) comes in between that of the most π-acidic phosphorus ligand known, PF_3 ($^1J_{PW}$ = 496.3 Hz) and $P(OPh)_3$ ($^1J_{PW}$ = 416.0 Hz) an electron-withdrawing phosphite due to little inductive effects from the R group. The other phosphites seem to follow the expected trend discussed in this work regarding the Gusev electronic scale, where increased inductive effects from the R group of a phosphite can reduce its overall π-acidity due to the electronegative oxygen atoms, *e.g.* $P(OMe)_3$, $^1J_{PW}$ = 398.0 Hz; $P(OEt)_3$, $^1J_{PW}$ = 391.0 Hz; $P(O^nBu)_3$, $^1J_{PW}$ = 390.0 Hz. Interestingly similar coupling constants values ($^1J_{PW}$) for $PhP\{OCH(CF_3)_2\}_2$, (**3**) with PHF_2 and $Ph_2P\{OCH(CF_3)_2\}$, (**5**) with PH_2F suggest these fluorinated ligands (**1**) to (**6**) have comparable electronic properties in-between PF_3 and PH_3 ligands, as discussed above with the Gusev electronic scale. Table 6 helps to understand that the electronic properties of $P\{OC(CF_3)_3\}_3$, (**2**) are similar to PH_2F when the reduced orbital overlap is considered, due to the incredible steric bulk it carries.

2.2.4.3 *IR Data (Experimental and DFT) for[W(CO)$_5$L] Complexes*

The [W(CO)$_5$L] complexes described earlier can also serve as probes of the electronic properties of ligands by analysis of their CO vibrational spectra. The IR data of the isolated tungsten complexes seem to follow the trend of increased π-acidity when more alkoxy groups are substituted on the phosphorus (III) ligands, see Table 7.

Reference	*Tungsten Complex (Experimental)*	*(A_1) ν_{CO} (cm^{-1})*	*(A_1) ν_{CO} (cm^{-1})*	*(E) ν_{CO} (cm^{-1})*	*(B) ν_{CO} (cm^{-1})*
[143]	[W(CO)$_5$PBu$_3$]	2070	1934	1934	1976
[143]	[W(CO)$_5$PPh$_3$]	2075	1942	1942	1980
[143]	[W(CO)$_5$P(OBu)$_3$]	2077	1944	1944	1977
[143]	[W(CO)$_5$P(OEt)$_3$]	2078	1945	1945	1976
[143]	[W(CO)$_5$P(OMe)$_3$]	2081	1952	1952	1980
This work	[W(CO)$_5$Ph$_2$P{OCH(CF$_3$)$_2$}]	2080	1968	1953	1992
This work	[W(CO)$_5$Ph$_2$P{OC(CF$_3$)$_3$}]	2081	1964	1954	1996
[143]	[W(CO)$_5$PCl$_3$]	2085	1960	1960	1990
This work	[W(CO)$_5$PhP{OCH(CF$_3$)$_2$}$_2$]	2088	1970	1962	2002
This work	[W(CO)$_5$PhP{OC(CF$_3$)$_3$}$_2$]	*2089	*1980	*1967	*1999
This work	[W(CO)$_5$P{OCH(CF$_3$)$_2$}$_3$]	2097	2002	1975	2017
[153]	[W(CO)$_5$PF$_3$]	2101	2005	1975	[a]2020
This work	[W(CO)$_5$P{OC(CF$_3$)$_3$}$_3$]	*2097	*1989	*1976	*2007

Table 7: Experimental IR data of [W(CO)$_5$L] ([W(1)] to [W(6)]) complexes in comparison to other literature values, in order of increasing π-acidity, for the strongest intensity (E) ν_{CO} band. Note * = data extrapolated using systematic difference observed from experimental and DFT calculated at the (RI-)BP86/SV(P) level, [a] = extrapolated data from considering average difference between all the other ν_{CO} values and known (B_1) ν_{CO} . Complexes [W(1)] to [W(6)] are highlighted for clarity.

Similarly to the DFT calculations for the [(η^5-C$_5$H$_5$)Ir(CO)L] complex discussed earlier, one can compare the CO stretching frequencies to that of a free CO with no back-bonding at ~2100 cm^{-1}. It appears that the greater number of fluorinated alkoxy groups on the phosphorus ligand, then the greater π-acidity of the ligand. The CO stretching frequencies for π-acidic ligands appear to be similar to a free CO, as less back-bonding is present from the metal to the CO ligand. This can be explained by donation of the electron-density from the tungsten metal d-orbitals into the P-O σ* (antibonding molecular orbitals) of the π-acidic

phosphorus (III) ligands. The octahedral $[W(CO)_5L]$ complex is based on C_{4V} symmetry (depending on the ligand), thus giving it three IR active bands ($E + 2A_1$). Figure 32 shows the three stretches observed; one symmetric and two antisymmetric stretches. Since the intensity of the IR peaks depends on the change in dipole caused by the specific stretch/bend, the symmetric stretch observed for the $[W(CO)_5L]$ complex is not the most reliable when looking for trends as the low intensity signal can be difficult to identify.

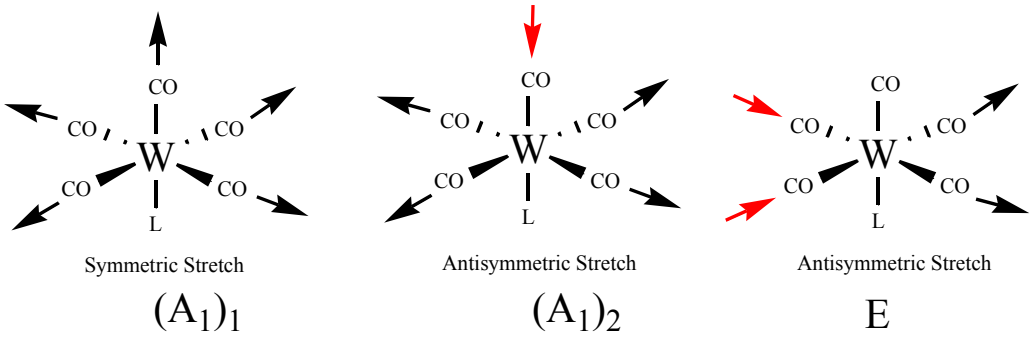

Figure 32: Three IR stretches observed for CO ligands in $[W(CO)_5L]$ complexes.

In addition, interactions between multiple CO ligands can split the vibrational bands, this can be useful in gaining structural information on the complexes *i.e.* when combined with group theory. The relative intensities of the vibrational bands can also help distinguish the specific structure *i.e.* A_1 equatorial mode should be weak at high frequency for a C_{4V} symmetry, while the A_1 axial and E mode appear at lower frequency (with the E mode being higher in frequency and more intense) in comparison. In addition, in cases where perfect C_{4V} symmetry is not achieved, it causes all the vibrational modes to be IR active, thus including the vibrational B_1 mode and splitting of the degeneracy of the E mode. It may be likely that in the observed ν_{CO} bands for the $[W(CO)_5L]$ complexes in this thesis, the coupling of the CO stretching motions to the phosphorus (III) ligand vibrational modes causes the B_1 mode to gain intensity without splitting of the degenerate E mode, hence the B_1 ν_{CO} is observed in the IR spectra.[154] Table 7 highlights that the range of electronic properties of ligands (**1**) to (**6**) from the experimentally obtained stretching frequencies are between that of $P(OMe)_3$ and PF_3. However, they are significantly more bulky making them relatively unusual compared to the the current phosphorus ligands. The order of π-acidity of these ligands agrees extremely well with the calculated stretching frequencies using DFT at the (RI-)BP86/SV(P) level (calculations performed by Tim James, a 2010/2011 MChem student of the JMS group), see Table 8.

Tungsten Complex (DFT)	*(A_1) ν_{CO} (cm^{-1})*	*(A_1) ν_{CO} (cm^{-1})*	*(E) ν_{CO} (cm^{-1})*	*(B) ν_{CO} (cm^{-1})*
$[W(CO)_5Ph_2P\{OCH(CF_3)_2\}]$	2088	1989	1983	1999
$[W(CO)_5Ph_2P\{OC(CF_3)_3\}]$	2090	1990	1984	1998
$[W(CO)_5PhP\{OCH(CF_3)_2\}_2]$	2094	1994	1990	2010
$[W(CO)_5PhP\{OC(CF_3)_3\}_2]$	2097	1999	1995	2004
$[W(CO)_5P\{OCH(CF_3)_2\}_3]$	2105	2006	2001	2020
$[W(CO)_5P\{OC(CF_3)_3\}_3]$	2105	2008	2006	2012

Table 8: DFT optimised $[W(CO)_5L]$ at the (RI-)BP86/SV(P) level IR data of ligands (1) to (6), in order of increasing π-acidity for the strongest intensity (E) ν_{CO} band.

Theoretical stretching frequencies of the $A_{1(CO)}$ for a $[Ni(CO)_3L]$ calculated at the (RI-)BP86/SV(P) level agrees well with the general trend of the experimental $[W(CO)_5L]$ complexes, see Table 9.

DFT optimised $[Ni(CO)_3L]$ Complex	*(A_1) ν_{CO} (cm^{-1})*
$[Ni(CO)_3Ph_2P\{OC(CF_3)_3\}]$	2037
$[Ni(CO)_3Ph_2P\{OCH(CF_3)_2\}]$	2038
$[Ni(CO)_3PhP\{OCH(CF_3)_2\}_2]$	2045
$[Ni(CO)_3PhP\{OC(CF_3)_3\}_2]$	2054
$[Ni(CO)_3P\{OCH(CF_3)_2\}_3]$	2058
$[Ni(CO)_3P\{OC(CF_3)_3\}_3]$	2063

Table 9: DFT optimised $[Ni(CO)_3L]$ at the (RI-)BP86/SV(P) level IR data of all ligands (1) to (6), in order of increasing π-acidity.

This suggests the π-acidity of the ligands is increased when a larger number of fluorinated alkoxy groups are present on the ligand *i.e.* phosphinite < phosphonite < phosphite. These results disagree with the electronic order that the $^1J_{PW}$ coupling constants, propose. The poor correlation can be explained due to increase in steric influence on $^1J_{PW}$, affecting the magnitudes and shifting away from purely electronic effects as the ligand size increases. Whereas, if one was to focus on the $^1J_{PW}$ values for the hexafluoroisopropoxy-containing ligands, then these agree well with the stretching frequencies. In addition, both experimental and theoretical stretching frequencies confirm that the $P\{OC(CF_3)_3\}_3$, (**2**) ligand has a similar π-acidity to the $P\{OCH(CF_3)_3\}_3$, (**1**) ligand. This is likely to be a cause of a reduced orbital

overlap with the metal d-orbital for the $P\{OC(CF_3)_3\}_3$, (**2**) ligand, due to its incredible steric bulk.

2.2.4.4 CO Force Field Calculations

Cotton-Kraihanzel force field, CKFF calculations[154] have been applied to the ν_{CO} tungsten-ligand stretches observed both experimentally and those extrapolated from DFT calculations. This method can give additional information on the nature and strength of the bonding in the complex and its structure.[154] In this case CKFF calculations can help understand the ligand effects on different CO force constants and assess coupling between these. This gives more data than analysis of a particular stretching frequency. The CKFF method is simplified as it omits anharmonicity and all coupling (they suggest small secondary effects of coupling to other oscillators are not as important) except CO-CO interaction constants, k_{CO-CO}. Figure 33 describes the CO-force constants; k_1 are for those CO ligands that are *trans* to the ligand (L) k_2 are for those CO ligands *cis* to L, k_t are for those CO-CO interactions that are *trans* to one another, k_c are for those CO-CO interactions that are *cis* to one another, where one is *cis* to L and the other *trans* to L, k_c' are for those CO-CO interactions that are *cis* to one another, where both CO ligands are *cis* to L.

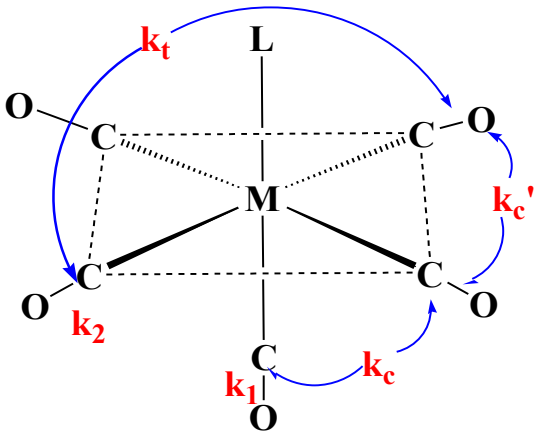

Figure 33: Definition of the CO-factored force constants in $[M(CO)_5L]$ molecules.

A series of assumptions are made in this CKFF calculation, these include[154]:

i) $k_t \sim 2k_c$, since a pair of *cis* CO groups share one dπ-orbital whereas *trans* CO groups share two, see Equation 11.[154]

ii) $k_i = k_c = k_c' = k_t/2$

Equation 11: Cotton-Kraihanzel force field assumption for (k_i) CO stretch–CO stretch interactions.

iii) Less π-acidic ligands give lower CO stretching force field constants and the CO ligands *cis* to these have higher stretching force field constants than those *trans* to such reduced π-acidic ligands, hence $k_2 > k_1$.[154]
iv) CO stretch-CO stretch interactions (k_i) should probably increase as a CO is replaced with reduced π-acidic ligands since more dπ-electron-density becomes available and should magnify the effects responsible for the CO stretch-CO stretch interaction constants.[154]

The latter can be explained further; as the stretching of a CO bond weakens the π-bond, the π* orbital reduces in energy so it matches that of the metal d-orbital. This causes increased metal-CO π-interaction causing a shift of the metal electron-density to this M-CO bond, hence decreasing the availability of electron-density to the other CO ligands. This in turn strengthens the C-O bond of the other CO ligands and increases their resistance to stretching, hence a positive coefficient is given for the force constants.[154]

It has been reported that the extent of π-bonding from a metal in the same group (*i.e.* Cr, Mo, W) are similar, hence they have force constants that are similar.[154] DFT calculations have been employed by Thiel and Jonas to describe force field constants and compare their results with those from the CKFF method. They conclude that the CKFF approach provides a good understanding of the trend in the C-O stretching force constants but does not give reliable CO_{cis}-CO_{trans} interaction constants.[155]

Karakas and Kaya suggest alternative calculations to CKFF, specifically for $[M(CO)_5L]$ complexes, which contain two fundamental vibrations belonging to the A_1 symmetry species. Here the CO_{ax}-CO_{eq} interaction constants are related to experimental ν_{CO} values. The CKFF method leads to an undetermined algebraic system when used on complexes that contain more than one fundamental vibration in the same nondegenerate irreducible representation.[156] Since the $[M(CO)_5L]$ complex has C_{4v} symmetry, there are two C-O stretching force constants (k_1 and k_2) and three CO-CO interaction constants (k_c, k_c' and k_t),

these are described in Figure 33. The necessary constraints were employed in this method along with an equation that uses the experimental ν_{CO} values before further direct C-O force field constants are calculated.[156]

[W(CO)$_5$L] Complex from Experimental ν_{CO}	k_1 *(N/m)*	k_2 *(N/m)*	k_t *(N/m)*	k_c' *(N/m)*	k_c *(N/m)*
[W(CO)$_5$PBu$_3$]	1555	1571	61	27	44
[W(CO)$_5$PPh$_3$]	1567	1582	58	28	43
[W(CO)$_5$P(OBu)$_3$]	1570	1583	56	30	43
[W(CO)$_5$P(OEt)$_3$]	1571	1584	56	31	43
[W(CO)$_5$P(OMe)$_3$]	1581	1592	53	31	42
[W(CO)$_5$PCl$_3$]	1593	1605	53	29	41
[W(CO)$_5$Ph$_2$P{OC(CF$_3$)$_3$}]	1596	1601	59	25	38
[W(CO)$_5$Ph$_2$P{OCH(CF$_3$)$_2$}]	1601	1599	58	27	37
[W(CO)$_5$PhP{OCH(CF$_3$)$_2$}$_2$]	1606	1613	58	26	39
[W(CO)$_5$PhP{OC(CF$_3$)$_3$}$_2$]$_{extrapolated}$	1619	1617	54	28	36
[W(CO)$_5$P{OC(CF$_3$)$_3$}$_3$] $_{extrapolated}$	1634	1631	53	28	36
[W(CO)$_5$P{OCH(CF$_3$)$_2$}$_3$]	1650	1635	59	25	31
[W(CO)$_5$PF$_3$]	1656	1638	62	26	32

Table 10: Calculated force field constants for a range of complexes [W(CO)$_5$L] (where L = phosphorus ligand) using experimentally found ν_{CO} values, extrapolated data used for all ν_{CO} modes of [W(CO)$_5$PhP{OC(CF$_3$)$_3$}$_2$], [W(CO)$_5$P{OC(CF$_3$)$_3$}$_3$]and the [W(CO)$_5$PF$_3$] (B1) ν_{CO} mode only.

The force field constants in Table 10 above show that $k_2 > k_1$ for those metal complexes containing less π-acidic ligands than CO (*i.e.* the obvious electron-donating PBu$_3$ and even π-acidic alkylated phosphites and PCl$_3$, as when competing with a *trans* CO ligand these are not classed as very π-acidic). Most interestingly, the force field constants calculated for ligands (**1**) to (**6**) can identify which of these are more π-acidic ligands than a CO ligand. These are recognized as those ligands where $k_1 > k_2$, which is the case for the PF$_3$ ligand. When analysing the results from the experimental obtained stretching frequencies all except [W(CO)$_5$Ph$_2$P{OC(CF$_3$)$_3$}] and [W(CO)$_5$PhP{OCH(CF$_3$)$_2$}$_2$] have values of $k_1 > k_2$. When considering the results obtained from DFT calculations, all except [W(CO)$_5$PhP{OCH(CF$_3$)$_2$}$_2$], [W(CO)$_5$P{OCH(CF$_3$)$_2$}$_3$] and [W(CO)$_5$P{OC(CF$_3$)$_3$}$_3$] have values of $k_1 > k_2$, see Table 11.

[W(CO)$_5$L] Complex from DFT ν_{CO}	*k_1 (N/m)*	*k_2 (N/m)*	*kt (N/m)*	*kc' (N/m)*	*kc (N/m)*
[W(CO)$_5$Ph$_2$P{OCH(CF$_3$)$_2$}]	1631	1630	41	29	33
[W(CO)$_5$Ph$_2$P{OC(CF$_3$)$_3$}]	1633	1631	41	30	33
[W(CO)$_5$PhP{OCH(CF$_3$)$_2$}$_2$]	1639	1642	43	27	33
[W(CO)$_5$PhP{OC(CF$_3$)$_3$}$_2$]	1647	1645	38	30	32
[W(CO)$_5$P{OCH(CF$_3$)$_2$}$_3$]	1658	1660	43	27	33
[W(CO)$_5$P{OC(CF$_3$)$_3$}$_3$]	1661	1661	35	31	32

Table 11: Calculated force field constants for a range of complexes [W(CO)$_5$L] (where L = phosphorus ligand) using DFT calculated ν_{CO} values, at the (RI-)BP86/SV(P) Level.

The force field results from the DFT calculations do suggest that although the P{OC(CF$_3$)$_3$}$_3$, (**2**) is not more π-acidic than a CO ligand, it is very similar as $k_1 = k_2$. These type of observations have been made in the literature for fluorophosphines {[(PF$_3$)$_2$Mo(CO)$_4$], ([PF{CF$_3$}$_2$)$_2$Mo(CO)$_4$] and [(PF$_2${CF$_3$})$_2$Mo(CO)$_4$]} and suggests the condition that $k_2 > k_1$ is not always a valid assumption, as stated in the CKFF method, as it is not the case that all ligands are less π-acidic than a CO ligand.[157] Although the magnitudes of the differences observed between k_1 and k_2 can potentially order the relative π-acidity of these ligands compared to a free CO ligand, the differences in the experimental and DFT calculated force constants suggests a more general conclusion can only be made, as the exact experimentally obtained frequencies for all six ligands are not known. This being ligands (**1**) to (**6**) are electronically different to others widely used in catalysis, as they are similar in π-acidity to a CO ligand, if not more π-acidic. In addition, the lack of sufficient orbital overlap due to steric bulk can reduce the overall π-acidity of the bulkier ligands with greater number of fluorinated alkoxy substituents. In general, the CO stretch - CO stretch interactions (k_i) seem to decrease, suggesting a more π-acidic ligand than CO is present, this being a result of less dπ-electron-density available, reducing the effects responsible for the CO stretch - CO stretch interaction constants.[154]

2.2.4.5 [Phosphenium – Phosphorus (III) Ligand] $^{1}J_{PP}$ Coupling Constants

It was thought that it may be possible to assess the electronic properties of these fluorinated ligands using direct phosphorus-phosphorus ($^{1}J_{PP}$) coupling constants. In order to achieve this, [phosphenium-phosphorus (III) ligand] cations were synthesised *via* methodologies described by Burford *et al.*[158] The main contribution to $^{1}J_{PP}$ coupling is from the through-space transmission of the Fermi contact term, which is mainly defined by the overlap of both phosphorus lone pairs.[159] The $^{1}J_{PP}$ coupling constant values can increase due to an increase in the s-character (due to the lone pair) contribution in the phosphorus hybrid orbital, which is involved in the phosphorus-phosphorus σ-bond.[160] Other influences on the $^{1}J_{PP}$ value include the energies of the molecular p_z orbitals, which change as the substituents on the phosphorus centre are altered. It should be noted, that changes in the SPS angle would affect the s-character contribution in the σ-bond as it corresponds with changes in hybridisation, thus steric interactions can compete with the electronic effects. This is shown by Nelson *et al.* in a plot of Tolman's substituent contributions (χ_1) as a measure of the phosphorus electron-density and $^{2}J_{PP}$ for a range of [LL'$PdCl_2$] complexes.[161] The magnitude of $^{2}J_{PP}$ is majorly affected by the electronegativity of the substituents bound to the phosphorus centre (*i.e.* a decrease in magnitude as the groups become less electronegative), but deviations in the correlation occur when steric effects contribute.[161] Keiter *et al.* use the QALE method described by Giering and Prock to show phosphorus-phosphorus coupling constants ($^{2}J_{PP}$) for ligands on a metal complex correlate strongly with the electronic properties (both χ and E_{ar}) of the phosphorus ligand, but are rather insensitive to their cone angles (θ).[162] They conclude that it is possible the steric threshold is present at greater θ values than those they used (largest θ they considered was 288°).[162] Their study also showed a strong negative correlation (*i.e.* larger $^{2}J_{PP}$ with lower pKa values, less basic ligands) between the pKa values based on proton dissociation from $[R_3PH]^+$ in polar aprotic media and $^{2}J_{PP}$ of *trans*-$[Fe(CO)_3LL']$ complexes for a range of phosphines. This correlation is in agreement with the general findings that the magnitude of $^{2}J_{PP}$ increases as the electronegativity of the substituents on the phosphorus increase and the proton affinities of the phosphine decreases.[162] Cone angle values were also plotted for these phosphines against $^{2}J_{PP}$ and pKa in a three-dimensional plot, but no significant correlations were found for the set of ligands considered.[162] It should be highlighted no phosphites have been used in the studies above but the general rule of increased $^{1}J_{PP}$ coupling constant for increased ligand π-acidity is used in the discussion below. The $^{1}J_{PP}$ coupling constant of the [phosphenium-phosphorus (III) ligand] complexes could be used as a novel method of gauging ligand electronic property, see Table 12.[163]

[PPh_2-Phosphorus (III) Ligand]$^+$ Adduct	*Doublets (δ/ppm) in the $^{31}P\{^1H\}$ NMR Spectra ($^1J_{PP}$ Hz)*
$[PPh_2\text{-}P\{OCH(CF_3)_2\}_3]^+$	97.9 (391) and 25.6 (392)
$[PPh_2\text{-}PhP\{OCH(CF_3)_2\}_2]^+$	71.7 (391) and 58.2 (391)
$[PPh_2\text{-}Ph_2P\{OC(CF_3)_3\}]^+$	89.0 (375) and -12.3 (375)
$[PPh_2\text{-}Ph_2P\{OCH(CF_3)_2\}]^+$	87.0 (362) and -16.2 (368)

Table 12: Coupling constants, $^1J_{PP}$ for the [PPh_2-phosphorus (III) ligand]$^+$ adduct.

Ligands (**1**) to (**6**) were used to stabilise the diphenylphosphenium cation, see Scheme 11. No stabilised phosphenium complexes were observed for $P\{OC(CF_3)_3\}_3$, (**2**) and $PhP\{OC(CF_3)_3\}_2$, (**4**), discussed further in Chapter 4.

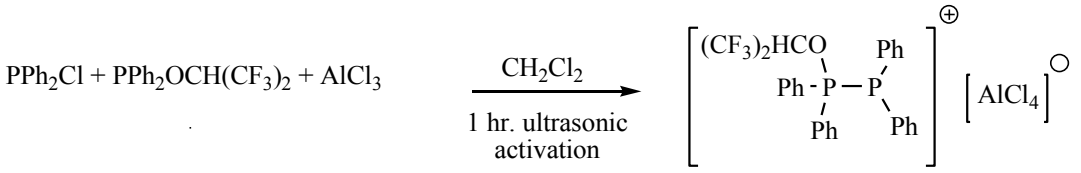

Scheme 11: Synthesis of a phosphenium ion stabilised by fluorinated ligand, the example above uses ligand (5).

The $PhP\{OCH(CF_3)_2\}_2$, (**3**) and $P\{OCH(CF_3)_2\}_3$, (**1**) ligands appears to have the largest $^1J_{PP}$ values (both around 391 Hz) suggesting these are the most π-acidic ligands of the series considered in Table 12. However, it is possible that the greater steric contributions in the phosphite $P\{OCH(CF_3)_2\}_3$, (**1**) and the perfluoro-*t*-butoxy ligands either reduce the orbital overlap thus reducing the strength of the P-P bond in these adducts, or the steric affects from these ligands are beyond the threshold, consequently diminishing the correlations between the $^1J_{PP}$ coupling constants and the π-acidity.

2.3 SUMMARY

A series of phosphorus (III) ligands bearing highly fluorinated alkoxide substituents, with the general formula $PR_{3-n}(OR^F)_n$ {R = Ph; OR^F = $C(CF_3)_3$, $CH(CF_3)_2$} have been synthesised. A simple synthetic route which leads to high purity products in high yields has been developed. This involves reaction of sodium alkoxide, $NaOR^F$ {OR^F = $C(CF_3)_3$, $CH(CF_3)_2$} with the relevant chlorophosphine; PCl_3/PCl_2Ph/$PClPh_2$ in DCM solvent (1 hr. ultrasonic activation), followed by an air-sensitive filtration to remove the NaCl salt. $^{31}P\{^1H\}$ NMR spectroscopy is used to indicate reaction completion and track the extent of hydrolysis after the filtration, this can help gauge whether further purification is required. Generally, it is possible to use the ligands *in situ* as prepared in DCM solution, after filtration. This method allows easy access to $P\{OC(CF_3)_3\}_3$, (**2**) without the need for extreme or hazardous preparations. All free ligands (**1**) to (**6**) are susceptible to hydrolysis, but unlike with many electron-rich phosphorus (III) ligands, no evidence of oxidation in air at room temperature has been observed.

The fluorinated alkoxide groups impart both steric bulk and significant acceptor character to the ligands. A detailed understanding of their combined stereoelectronic properties has been achieved *via* a combination of experimental and theoretical methods. The Tolman "ligand cone angle" (θ) was chosen as the steric parameter as unlike other methods this represents bulky ligands along with phosphites well.[20] DFT optimised structures at the (RI-)BP86/SV(P) level for $[Ni(CO)_3L]$ and $[W(CO)_5L]$ systems of the relevant ligands were used to compare the steric properties of ligands (**1**) to (**6**). The $[Ni(CO)_3L]$ systems allowed for comparisons to made with those calculated by Tolman. A cone angle much larger than that for the hydrogen analogue *t*-butyl phosphite, $P\{OC(CH_3)_3\}_3$ (θ =172 °) and the highly sterically crowded *t*-butyl phosphine, $P\{C(CH_3)_3\}_3$ (θ =182 °) was found for $P\{OC(CF_3)_3\}_3$, (**2**) (θ =195 °). Although this is not the largest cone angle reported in the literature, this ligand is very rigid without the flexibility to accommodate to specific environments. This gives the $P\{OC(CF_3)_3\}_3$, (**2**) ligand steric properties that are unusual compared to the bulkier ligands available for catalysis, as many of the ligands containing larger cone angels consist of bulky phenyl groups that can undergo many conformational changes *e.g.* $PMes_3$ (θ = 212 °), $P(C_6F_5)_3$ (θ = 184 °), $P(O\text{-}o\text{-}C_6H_3Me_2)_3$ (θ = 190 °) and P(o-Tol)$_3$ (θ = 194 °). The Tolman cone angle calculations confirm that the substitution of the fluorinated alkoxy groups, OR^F {OR^F = $OC(CF_3)_3$; $OCH(CF_3)_2$} for phenyl rings, reduces the steric influence of the ligands *i.e.* $P\{OCH(CF_3)_2\}_3$, (**1**), $PPh\{OCH(CF_3)_2\}_2$, (**3**) and $PPh_2OCH(CF_3)_2$, (**5**); θ = 178 °, 173 ° and 170 ° respectively. The over simplification in the Tolman parameter from basing calculations on static optimised structures is also observed with the cone angle calculations

for the DFT optimised structures. One would expect the cone angle values to be much greater for all the ligands containing the perfluoro-*t*-butoxy group. However, this appears not to be the case for the $PPh_2OC(CF_3)_3$, (**6**) ligand (θ = 170 °), which is the same as that of the $PPh_2OCH(CF_3)_2$, (**5**) ligand, and the $PPh\{OC(CF_3)_3\}_2$, (**4**) ligand (θ = 163 °), much smaller than that of the $PPh\{OCH(CF_3)_2\}_2$, (**3**) ligand and $PPh_2OC(CF_3)_3$, (**6**). This is explained due to the conformational flexibility of the phenyl substituents, which adjust to each specific environment and the available space. Conformational changes due to the flexibility of the oxygen of the alkoxy substituents were also discussed, as these can point in different directions which in turn affect the steric influence of the ligand. Comparison of cone angles of the same ligand for a range of different complex environments also demonstrates the importance of conformational changes. Most of the cone angle values calculated for ligands (**1**) to (**6**) in a $[W(CO)_5L]$ environment are lower in comparison to those in a $[Ni(CO)_3L]$ environment. The octahedral geometry in $[W(CO)_5L]$ is more crowded and likely to be a cause of the lower cone angles, as the ligands pull in more due to less available space. Similarly, all the cone angle calculations for ligands (**1**) to (**6**) in the $[Ru(\eta^5\text{-}C_5H_5)(NCMe)_{3-n}L_n]^+[PF_6]^-$ (n = 1, 2) environments from single-crystal X-ray diffraction data are also found to be lower, due to steric congestion around the ruthenium centre.

The electronic properties of these ligands were assessed using the method suggested by Gusev, involving DFT calculations.[3] All optimisations were performed at the (RI-)BP86/SV(P) level, followed by frequency calculations at the same level. The hydrogen and fluorinated phosphite analogues were calculated for a range of ligands *i.e.* PR_nOR_{3-n}, $PR_nOR^F_{3-n}$ {R = Mesityl, Ph, Me, H, NMe_2, F; OR = O^tBu, O^iPr; OR^F = $OC(CF_3)_3$, $OCH(CF_3)_2$; n = 0-3}. As expected, the non-fluorinated phosphites showed less π-acidic properties than the fluorinated phosphite analogues. The ligands under study could be divided into three clusters; these being electron-donating, electron neutral and electron-withdrawing ligands in regards to their overall electronic character. It was found that the inductive effects from the R groups on the alkoxy substituents added to their electron-donating property. Those with bulkier R groups were found in the electron-donating cluster. The phosphites with relatively smaller R groups balanced their positive inductive effects from their R groups with any electronegative effects from the oxygen atoms, so they appeared to cancel out and were overall electronically similar to an unsubstituted phosphine, PH_3. They were found in the electronically neutral cluster, as overall their electronic influence was found to be neither strongly electron-donating nor electron-withdrawing. Substituents of very different electronic nature, gave very neutral electronic properties overall *i.e.* $P\{NMe_2\}_2(O^tBu^F)$, $P\{NMe_2\}_2(O^iPr^F)$, $PMe_2(O^tBu^F)$, $PMe_2(O^iPr^F)$, $PPh_2(O^tBu^F)$, $PPh_2(O^iPr^F)$, $P\{NMe_2\}(O^tBu)_2$, $P\{NMe_2\}(O^iPr)_2$, $PF(O^tBu)_2$, $PF(O^iPr)_2$, $PMe(O^iPr^F)_2$,

$PMes(O^iPr^F)_2$, $P\{NMe_2\}(O^iPr^F)_2$. The cluster containing the electron-withdrawing ligands showed a range of ligands of varying π-acidic electronic character. It was found that strong +I effects from a -^{t}Bu group can overcome the strong electron-withdrawing effects from the two P-F groups in PF_2O^tBu, which reduces the π-acidity of this ligand. Although, it should be noted that it may be possible that the steric bulk form the -^{t}Bu group reduces sufficient orbital overlap, thus reducing its π-acidic properties. The fluorinated phosphites $P\{OCH(CF_3)_2\}_3$, (**1**) and $P\{OC(CF_3)_3\}_3$, (**2**) were found to have similar electronic properties to the PF_3 ligand. In addition, although one would expect $P\{OC(CF_3)_3\}_3$, (**2**) to have greater π-acidity than $P\{OCH(CF_3)_2\}_3$, (**1**) due to the extra CF_3 groups, the data suggests this is not the case. The $P\{OC(CF_3)_3\}_3$, (**2**) ligand may prevent a close approach of the ligand to the metal centre, thus reducing the metal-phosphorus orbital overlap and preventing metal-to-ligand back-donation. There is some evidence of this in the optimised Ir-P bond lengths; $[IrCp(CO)P\{OCH(CF_3)_2\}_3]$ (2.194 Å), where as $[IrCp(CO)P\{OC(CF_3)_3\}_3]$ (2.198 Å), is longer. It was also found that substituting the fluorinated alkoxy groups for phenyl groups brings the ligands' electronic properties closer to PH_3, but with considerably more steric bulk. This can be used as an electronic handle to fine tune the ligands to suit specific tasks making them appealing for their use in catalysis.

The $^{31}P\{^1H\}$ NMR spectroscopic analysis of $[W(CO)_5L]$ complexes of ligands (**1**) to (**6**) provided $^1J_{PW}$ coupling constants. These were used as an electronic gauge to assess the π-acidic properties of the complexed phosphorus (III) ligands. The larger the $^1J_{PW}$ value then the greater the π-acidity *i.e.* $P\{OCH(CF_3)_2\}_3$, (**1**) $^1J_{PW}$ = 451 Hz; $PhP\{OCH(CF_3)_2\}_2$, (**3**) $^1J_{PW}$ = 357 Hz; $Ph_2P\{OCH(CF_3)_2\}$, (**5**) $^1J_{PW}$ = 291 Hz.[20, 142] Similarly to the DFT calculations above, these $^1J_{PW}$ coupling constants showed that $P\{OC(CF_3)_3\}_3$, (**2**) ($^1J_{PW}$ = 292 Hz) had a much lower coupling constant than expected. The structures of these complexes were optimised at the (RI-)BP86/SV(P) level and showed evidence of reduced orbital overlap in the W-P bond lengths; $[W(CO)_5P\{OCH(CF_3)_2\}_3]$ (2.482 Å), where as $[W(CO)_5P\{OC(CF_3)_3\}_3]$ (2.548 Å), is longer. This suggested that a poor overlap due to the incredible steric bulk of $P\{OC(CF_3)_3\}_3$, (**2**), reduces its overlap with tungsten, leading to reduced back-donation. Similar $^1J_{PW}$ coupling constants values were observed for $PhP\{OCH(CF_3)_2\}_2$, (**3**) with PHF_2 and $Ph_2P\{OCH(CF_3)_2\}$, (**5**) with PH_2F. This suggests that these fluorinated ligands (**1**) to (**6**) have comparable electronic properties in-between PF_3 and PH_3 ligands, as discussed with the results from the Gusev calculations. In general the $^1J_{PW}$ coupling constants values indicate that the π-acidity of the ligands is enhanced greatly by fluorinating the alkoxy-groups. This is likely due to the highly electronegative fluorine atoms reducing the electron-density on the phosphorus and bringing their P-O σ* orbitals closer in energy to the tungsten metal-d orbital. This allows increased metal-phosphorus

back-bonding to occur. Comparisons of the $^1J_{PW}$ coupling constants of $[W(CO)_5L]$ complexes to other well known ligands showed that the other phosphites seemed to follow the expected trend as discussed in this work on the Gusev electronic scale. This being that the increased inductive effects from the R group of a phosphite can reduce its overall π-acidity due to the electronegative oxygen atoms *i.e.* $P(OMe)_3$, $^1J_{PW}$ = 398.0 Hz; $P(OEt)_3$, $^1J_{PW}$ = 391.0 Hz; $P(O^nBu)_3$, $^1J_{PW}$ = 390.0 Hz.

The experimentally obtained stretching frequencies from IR analysis of the isolated tungsten complexes seemed to follow the expected trend of increased π-acidity when more alkoxy groups are present on the phosphorus (III) ligand. The electronic properties of ligands (**1**) to (**6**) are between that of $P(OMe)_3$ and PF_3 if not similar, but of course with this additional steric bulk making them relatively unique compared to current phosphorus ligands. The order of π-acidity of these ligands agreed extremely well with the calculated stretching frequencies for $[W(CO)_5L]$ complexes, using DFT calculations at the (RI-)BP86/SV(P) level. Theoretical stretching frequencies for the $[Ni(CO)_3L]$ complexes calculated at the (RI-)BP86/SV(P) level were also in good agreement with the general trend of the experimental $[W(CO)_5L]$ complexes. This suggests that the π-acidity of the ligands is increased as a higher number of fluorinated alkoxy groups are present on the ligand *i.e.* phosphinite < phosphonite < phosphite. The observed correlation with the $^1J_{PW}$ coupling constants and the stretching frequencies differs slightly. The increase in steric influence for the bulkier ligands affects the $^1J_{PW}$ magnitudes, as it no longer acts as a gauge for purely the electronic effects once the ligand size increases beyond the steric threshold. The $^1J_{PW}$ coupling constants for the hexafluoroisopropoxy ligands are in good agreement with the IR stretching frequencies This may be because these are below the threshold where the steric contributions affect the $^1J_{PW}$ coupling constant values. Both experimental and theoretical stretching frequencies confirm that the $P\{OC(CF_3)_3\}_3$, (**2**) ligand has a similar π-acidity to the $P\{OCH(CF_3)_3\}_3$, (**1**) ligand. This is likely due to a reduced orbital overlap with the metal orbitals for the $P\{OC(CF_3)_3\}_3$, (**2**) ligand due to its incredible steric bulk. In addition, a general conclusion that ligands (**1**) to (**6**) are electronically different to others widely used in catalysis, as they are similar in π-acidity to a CO ligand if not more π-acidic, can be made for these systems from the results of the force Cotton-Kraihanzel force field analysis. Overall the detailed stereoelectronic analysis of the fluorinated ligands (**1**) to (**6**) indicates that they fulfil the intention of their synthesis, as they can add to the niche for bulky, electron-poor ligands.

2.4 FUTURE WORK

Future work could expand this library of bulky, electron-poor ligands and focus on varying the alky groups as well using a range of different fluorinated alkoxy groups, using a similar synthetic method *i.e.* $PR_n(OR^F)_{3-n}$; R = Mes, ^{t}Bu, Cy, ^{i}Pr, Me, Et, NMe_2; $OR^F = OC_6F_5$, $OCy\text{-}F_{11}$ *etc.* In addition, more exotic ligands could be explored with perhaps charged substituents on the phenyl groups to form ionic ligands, these could potentially further stabilise metal complexes through intramolecular, interligand ionic associative interactions, see Figure 34.[69]

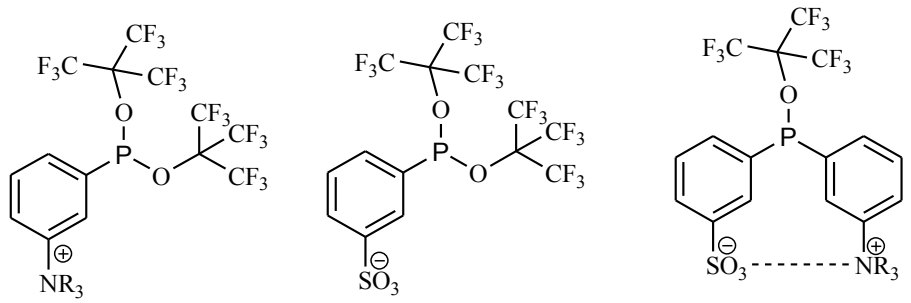

Figure 34: Potential ionic ligands with charged substituents on the phenyl groups.[69]

Supramolecular interactions can also be introduced on the ligands. These can self-assemble in the coordination sphere of a metal centre to generate ligand-ligand interactions. These can be used to form bidentate chelating ligands on complexation, similar to that found by Breit *et al*, see Figure 35.[164]

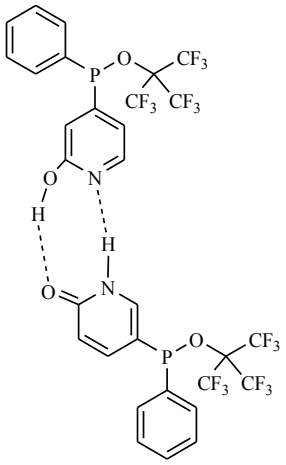

Figure 35: Substituted phosphinite ligands, which allow for supramolecular interactions.

Furthermore the pyrophosphite, $(R^FO)_2P\text{-}\mu O\text{-}P(OR^F)_2$ {$R^F = C(CF_3)_3$}, (**7**) could be explored as a bidentate ligand. Although a suitable synthetic methodology would be required, which could allow for a range of fluorinated alkoxy group-containing pyrophosphites to be discovered, see Figure 36.

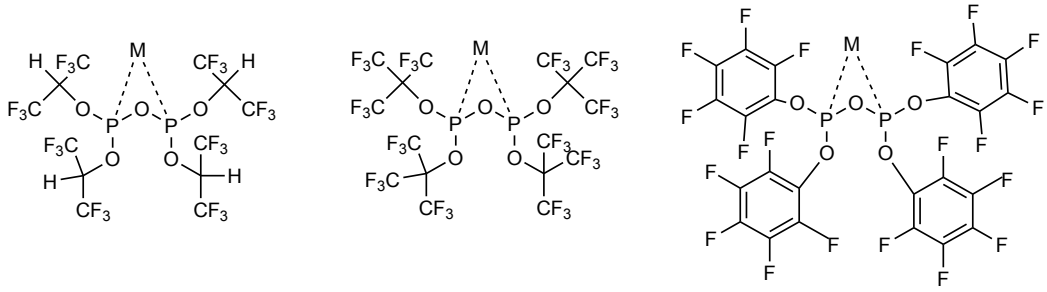

Figure 36: Potential bidentate pyrophosphite ligands.

Chirality could be introduced to the phosphorus (III) ligands with careful stoichiometric control with the metal alkoxides to form a range chiral phosphorus (III) compounds with potential use in catalysis for selective asymmetric synthesis of organic compounds, see Scheme 12. However, selective separation of the chiral isomers, or a synthetic method that favours one isomer would be required.

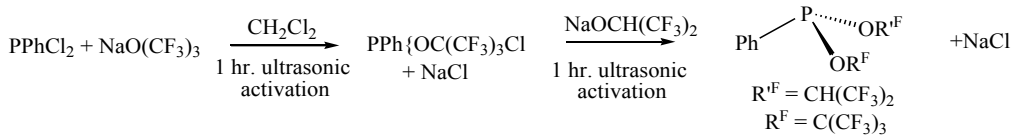

Scheme 12: Potential synthesis of chiral phosphorus (III) ligands.

Alternative ligands bearing fluorinated alkoxy substituents can also be explored in the future. Thionyl alkoxide groups could be of potential interest as they may act as possible bifunctional ligands, which can coordinate through the sulphur or the oxygen atom, depending on if the metal is hard or soft, see Figure 37.

$OR^F = OCH(CF_3)_3, OC(CF_3)_3, OC_6F_5$

Figure 37: Potential thionyl alkoxide ligands.

The data on ligands (**1**) to (**6**) investigated in the work of this thesis can be incorporated in the LKB for comparison to various ligands and to portray the availability of π-acidic, bulky ligands. In addition to development of the ligands, a theoretical approach for the dynamic assessment of the steric bulk of such ligands is clearly required, as current methods use static models only. Perhaps even development of a method for any metal, any environment and any ligand type is required to map the steric influence of all ligand types on one scale.

3 SYNTHESIS AND STRUCTURAL REACTIVITY OF METAL COMPLEXES OF LIGANDS (1) TO (6)

3.1 RHODIUM COMPLEXES

3.1.1 The Synthesis and Structural Chemistry of $[RhCl(CO)\{PPh_2OC(CF_3)_3\}_2]$, **[Rh(6)-2]**

The rhodium di-carbonyl chloride dimer, $[RhCl(CO)_2]_2$ (1 eq.) was reacted with the $PPh_2OC(CF_3)_3$, (**6**) ligand (2 eq.) in DCM solvent. The $[RhCl(CO)_2]_2$ complex in DCM solvent, gave a red coloured solution which turned orange instantly after the addition of $PPh_2OC(CF_3)_3$, (**6**). Bubbles were observed on addition, indicating release of CO. Crystals of $[RhCl(CO)\{PPh_2OC(CF_3)_3\}_2]$, **[Rh(6)-2]** suitable for single-crystal X-ray diffraction characterisation, were obtained by slow evaporation from a DCM solution, see Figure 38.

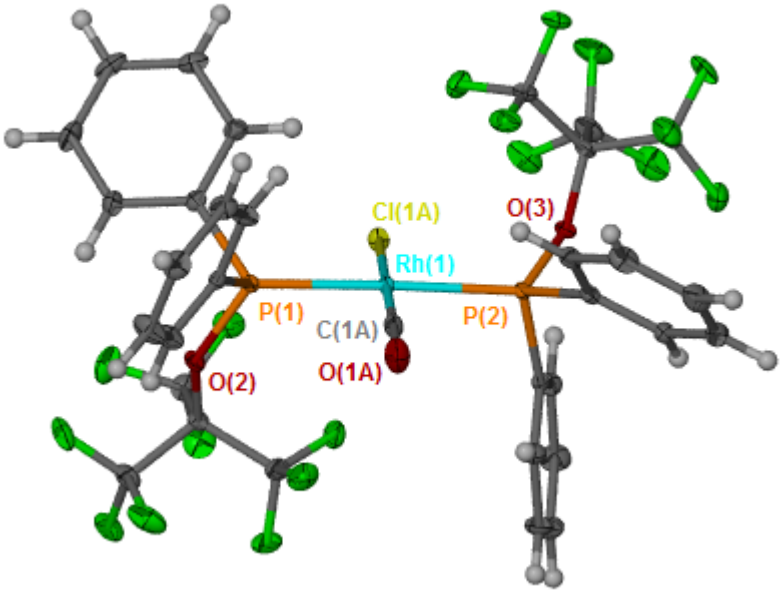

Figure 38: Single-crystal X-ray structure of $[RhCl(CO)\{PPh_2OC(CF_3)_3\}_2]$, [Rh(6)-2] at 110 K. Cl and CO positions are disordered; disordered parts omitted for clarity Thermal ellipsoids are drawn at the 50 % probability level. Selected interatomic distances (Å) and angles (°): Rh(1)-P(1) = 2.2866(4), Rh(1)-P(2) = 2.3017(4), Rh(1)-Cl(1A) = 2.381(1), Rh(1)-C(1A) = 1.779(8), C(1A)-O(1A) = 1.15(1), P(1)-Rh-P(2) = 177.96(1), C(1A)-Rh-Cl(1A) = 169.68(5), P(1)-Rh(1)-Cl(1A) = 92.34(3), P(2)-Rh(1)-Cl(1A) = 87.22(3), C(1A)-Rh(1)-P(1) = 88.7(1), C(1A)-Rh(1)-P(2) = 91.6(1). Crystal system: tetragonal. Space group: P42/n. R_1: 0.0306 (all data), wR_2: 0.0645 (>2sigma(I)).

The complex shows a slightly distorted square planar geometry around Rh, where the P-Rh-Cl angle for P(1) is slightly larger than ideal (92.3 °) and the P-Rh-C distance for P(1) slightly smaller than ideal (88.7 °), with the opposite trend being seen for P(2). The metal coordination geometry is similar to that obtained for a range of *trans*-phosphine complexes of the type [RhCl(CO)L_2], where L = phosphorus (III) ligand. These known structures were found and analysed using the Cambridge Structural Database (CSD); searching for a [RhCOClP_2] fragment with R_1 < 10 %.[165-168] They have the following mean values for the selected interatomic bond lengths; Rh-P_{mean} = 2.328 Å, Rh-Cl_{mean} = 2.386 Å, Rh-C_{mean} = 1.803 Å. Figure 39 highlights the extensive range of Rh-P bond lengths found for all types of phosphorus (III) ligands, including many bidentate phosphorus ligands as well as monodentate phosphines, phosphinites, phosphonites and phosphites. The average Rh-P bond distance for **[Rh(6)-2]** {2.295 Å, from Rh(1)-P(1) = 2.287(1), Rh(1)-P(2) = 2.302 (1)} is much shorter than the mean calculated value (2.328 Å), but not as short as some monodentate phosphite ligands such as $P(OPh)_3$ {average = 2.270 Å, WEXNAP; Rh(1)-P(1) = 2.265(1), Rh(1)-P(2) = 2.275(1)}, and $P\{OCH(CF_3)_2\}_3$, (**1**) {average = 2.258 Å, SENWAK; Rh(1)-P(1) = 2.260(1), Rh(1)-P(2) = 2.255(1)}. This can be explained by phosphites possibly having a more π-acidic character than phosphinites as discussed in Chapter 2. However, the bonding involved can be complicated and can also be shortened due to a balance of a stronger σ- and π-bond.

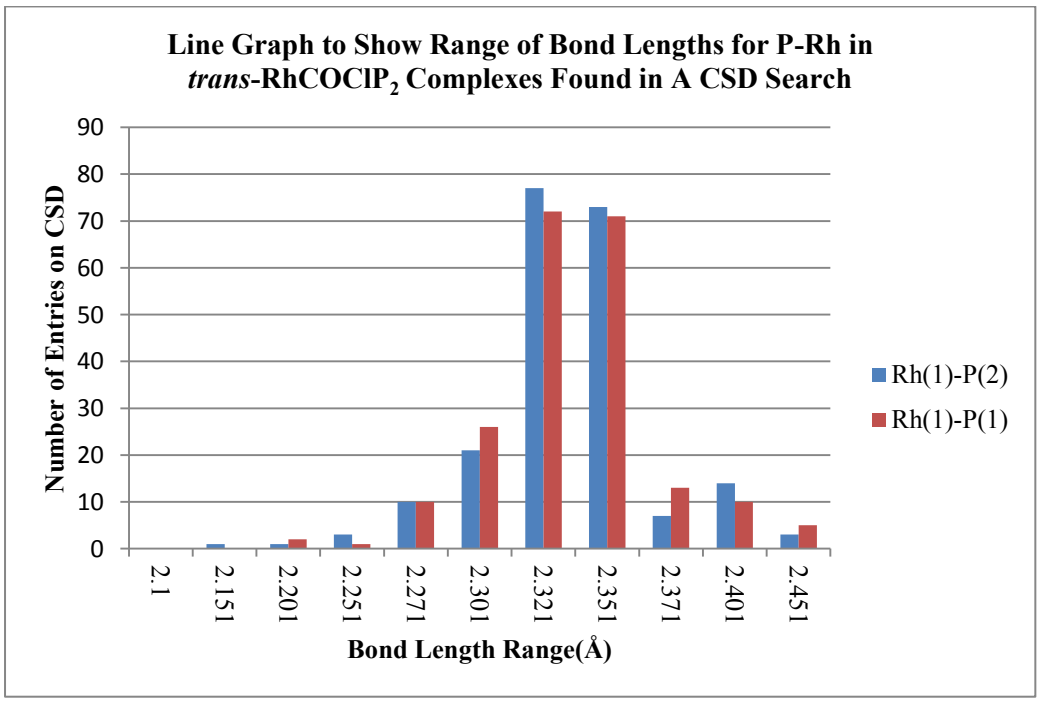

Figure 39: Histogram to show the range of P-Rh bond lengths in *trans*-[RhCl(CO)L_2] complexes with a number of phosphorus (III) ligands. Two series are displayed for the two different bond lengths (Å) for each phosphorus ligand found in the complex.

Most interestingly, **[Rh(6)-2]** contains the shortest Rh-P bond distance (Å) when compared to all the available crystal structures that have a monodentate phosphorus (III) ligand with a similar diphenyl-moiety *i.e. trans*-[RhCOClPPh$_2$X], where X can be any group, see Table 13. The perfluorinated alkoxy substituent is likely to induce a π-acidic effect on the ligand as electron-density is pulled towards the electronegative fluorine atoms and away from the phosphorus centre. This lowers the energy of its P-R σ* antibonding orbital, making it closer in energy to the metal 3d-orbital. This in turn allows more efficient π back-bonding. A fluorinated ponytail alkoxy-containing ligand, PPh$_2${O(CH$_2$)$_2$(CF$_2$)$_5$CF$_3$} is found to consist of similar Rh-P bond length to that of **[Rh(6)-2]**. The two -CH$_2$ spacer groups are designed to reduce the electronegative effects from the fluorinated ponytail as discussed in Chapter 2, but the Rh-P bond lengths suggest this is not the case. It appears the phosphorus centre of the PPh$_2${O(CH$_2$)$_2$(CF$_2$)$_5$CF$_3$} ligand must experience the full extent of the electronegative effects of the fluorinated groups like in that for the **[Rh(6)-2]**, see Table 13. The longest Rh-P bond lengths appear to have nitrogen-containing substituents in the ligands (*e.g.* PPh$_2${CH$_2$N(Ph)$_2$} and PPh$_2${C(-*o*-Ph-Cl)NHPh}), suggesting that the π-conjugation from the nitrogen lone pair to the P-R σ* antibonding orbital reduces the π-acidity of the phosphinite ligand, hence the longer bonds can be a cause of reduced back-bonding.

RhCl(CO)(PPh$_2$X)$_2$, X =	*P(2)-Rh(1)*	*P(1)-Rh(1)*	*CSD Name*
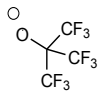	2.287(1)	2.302(1)	This work
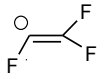	2.304(2)	2.297(3)	CISYEJ
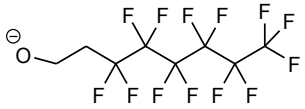	2.304(3)	2.298(3)	GOFVOM
-Ph	2.304(3)	2.363(3)	CTPRHC
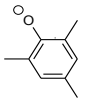	2.310(1)	2.320(1)	PARWEL
-Me	2.313(2)	2.321(2)	DABDAL
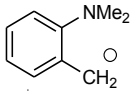	2.320(1)	2.320(1)	YEBVIL
	2.320(5)	2.313(5)	DIJQOC
-Et	2.321(1)	2.316(1)	SISXUO
	2.324(2)	2.322(2)	QAXHOM
-$CH_2N(Ph)_2$	2.324(3)	2.333(3)	TABZEB
-*o*-Ph-CF_3	2.327(1)	2.327(1)	ADIXIU
-*o*-Tol	2.327(1)	2.328(2)	WUPREE
-*o*-Ph-MeCOO	2.329(7)	2.329(8)	IJAKUZ
-*o*-Ph-OMe	2.331(1)	2.334(1)	QAKQIC
-CH_2Ph	2.336(1)	2.320(1)	WEFQAA
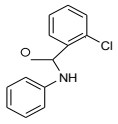	2.336(1)	2.333(1)	GUZPEW

Table 13: Rh-P bond lengths (Å) of selected crystal structures from a CSD search for *trans*-[RhCl(CO)L$_2$] complexes, where L = PPh$_2$X ligand with varying X substituents. Note the X substituent binds through to the phosphorus at the atom with the localized negative charge.

3.1.2 IR Spectroscopic Analysis of *trans*-[RhCl(CO)L_2] Complexes

Along with **[Rh(6)-2]**, other *trans*-[RhCl(CO)L_2] complexes of ligands containing perfluorinated-*t*-butoxy substituents *e.g.* PPh{$OC(CF_3)_3$}$_2$, (**4**) and P{$OC(CF_3)_3$}$_3$, (**2**) were also investigated, using a similar synthetic method. Table 14 compares the observed infrared stretching frequencies (ν_{CO}) of the *trans*-[RhCl(CO)L_2] complexes for the three ligands; (**2**), (**4**) and (**6**). Itami *et al.*[132] provide ν_{CO} data for two other ligands discussed in this thesis; PhP{$OCH(CF_3)_2$}$_2$, (**3**) and P{$OCH(CF_3)_2$}$_3$, (**1**). Comparisons are also made with some general phosphorus (III) ligands and those containing fluorinated ponytail groups from the work of Hope *et al.*[104, 106, 109, 111] As discussed in Chapter 2, a higher ν_{CO} value corresponds to increased π-acidity of the ligand. Table 14 highlights that the fluorinated ponytail-containing ligands synthesised by Hope *et al.* are not as π-acidic as ligands (**1**) to (**6**) presented in this thesis. The fluorinated ponytail-containing ligands are similar in electronic properties to the non-fluorinated ligands. The fluorinated ponytail-containing ligands have been designed to contain similar electronic properties to phosphites using spacer groups to shield the full effects from the fluorine atoms. However, the fluorinated substituents are required in the design to increase their solubility in *fluorous*-phases as discussed in Chapter 2.[104, 106, 109, 111] The most π-acidic ligand according to the ν_{CO} stretching frequency is P{$OC(CF_3)_3$}$_3$, (**2**), greater than P{$OCH(CF_3)_2$}$_3$, (**1**) by 5 cm^{-1}. The ν_{CO} values reported by Itami *et al.* [132] for P{$OCH(CH_3)_2$}$_3$ {ν_{CO} = 2002 cm^{-1}} and P{$OCH(CF_3)_2$}$_3$ {ν_{CO} = 2070 cm^{-1}}, again highlight the extensive effects of fluorination on the ligands' electronic properties.

trans-[RhCl(CO)L$_2$] Complexes, L =	*ν_{CO}, cm^{-1}*	*Reference*
PEt_3	1956	[109]
$PPh_2(C_6H_4\text{-}2\text{-}CF_3)$	1957	[104]
$PPh(Et)_2$	1960	[109]
PPh_3	1962/1983	[109, 132]
$PPh_2(C_6H_4\text{-}2\text{-}C_6F_{13})$	1965	[104]
$P(C_6H_4\text{-}4\text{-}CH_2CH_2C_6F_{13})_3$	1972	[111]
$P(C_6H_4\text{-}4.C_6H_{13})_3$	1975	[111]
$PPh_2(C_6H_4\text{-}3\text{-}C_6F_{13})$	1980	[104]
$PPh_2(CH_2CH_2C_6F_{13})$	1981	[109]
$PPh_2(C_6H_4\text{-}4\text{-}C_6F_{13})$	1982	[104]
$PPh(CH_2CH_2C_6F_{13})_2$	1983	[109]
$P(C_6H_4\text{-}4\text{-}C_6F_{13})_2Et$	1984	[109]
$PPh(C_6H_4\text{-}3\text{-}C_6F_{13})_2$	1984	[106]
$P(CH_2CH_2C_6F_{13})_3$	1990	[109]
PPh_2OEt	1990	[109]
$PPh_2(OCH_2CH_2C_6F_{13})$	1991	[109]
$P(C_6H_4\text{-}3\text{-}C_6F_{13})_3$	1992	[104]
$P(C_6H_4.4\text{-}C_6F_{13})_3$	1993	[109]
PPh_2OPh	1996	[109]
$P\{OCH(CH_3)_2\}_3$	2002	[132]
$P(OMe)_3$	2006	[109]
$PPh_2(OC_6H_4\text{-}4\text{-}C_6F_{13})$	2008	[109]
$PPh_2\{OC(CF_3)_3\}$, (**6**)	2009	This work
$PPh(OCH_2CH_2C_6F_{13})_2$	2013	[109]
$P(OPh)_3$	2016	[109]
$PPh\{OC(CF_3)_3\}_2$, (**4**)	2035	This work
$P(OCH_2CH_2C_6F_{13})_3$	2036	[109]
$PPh\{OCH(CF_3)_2\}_2$, (**3**)	2038	[132]
$P\{OCH(CF_3)_2\}_3$, (**1**)	2070	[132]
$P\{OC(CF_3)_3\}_3$, (**2**)	2075	This work

Table 14: The vibrational stretching frequencies ($\nu_{(CO)}$/cm^{-1}) of *trans*-[RhCl(CO)L$_2$] complexes, L = phosphorus (III) ligand. Complexes of ligands (1) to (4) and (6) are highlighted.

3.1.3 $^{31}P\{^{1}H\}$ NMR Spectroscopic Data for *trans*-[RhCl(CO)L_2] Complexes

The $^{1}J_{RhP}$ coupling constants can also be used as an indicator of the electronic properties of the phosphorus (III) ligand, where larger $^{1}J_{RhP}$ values are observed for increased π-acidity of the ligand. A large $^{1}J_{RhP}$ coupling constant is observed for **[Rh(2)-2]** ($^{1}J_{RhP}$ = 286 Hz). This is much larger than that for **[Rh(1)-2]** ($^{1}J_{RhP}$ = 224 Hz). All the *trans*-[RhCl(CO)L_2] complexes of the perfluoro-*t*-butoxy substituent-containing ligands have larger $^{1}J_{RhP}$ values than $P(OPh)_3$ ($^{1}J_{RhP}$ = 217 Hz) and $P(OCH_2CH_2C_6F_{13})_3$ ($^{1}J_{RhP}$ = 199 Hz). This highlights the difference in the π-acidity of the perfluoro-*t*-butoxy substituent-containing ligands, compared to the non-fluorinated phosphite ligands and fluorinated phosphites containing spacer groups. In addition, the change in $^{31}P\{^{1}H\}$ NMR chemical shift can provide information on the ligand properties. A change in the SPS angle (discussed in Chapter 2) upon coordination and the nature of the metal are key contributors to the $^{31}P\{^{1}H\}$ NMR chemical shifts ($\Delta = \delta_{complex} - \delta_{free}$) upon coordination.[169] A downfield shift (positive Δ) occurs with angle opening on coordination, whereas the magnitude of Δ is much less for larger ligands as the bulkier substituents on the phosphorus ligands are generally already orientated to reduce steric repulsion, hence a reduced angle opening is observed on coordination. Focussing purely on the phosphites in Table 15, the upfield shifts (negative Δ) on coordination suggests that the free ligands do not undergo an angle opening transition. This can be explained by the oxygen atom of the phosphites introducing extra flexibility, which already minimises the steric repulsion of the free ligand. Interestingly, the change in $^{31}P\{^{1}H\}$ NMR chemical shift values (Δ), also suggests from their similar magnitudes that all phosphites have a similar OPO angle, regardless of the size of the steric bulk on the alkyl group (*i.e.* **[Rh(1)-2]** and **[Rh(2)-2]** Δ = -16.9 for both complexes). Hence, phosphites are more similar in terms of their steric properties than phosphines with varying substituents.

trans-[RhCl(CO)L$_2$] Complexes, L =	*Ligand $^{31}P\{^1H\}$ NMR (δ/ppm)*	*trans-[RhCl(CO)L$_2$] $^{31}P\{^1H\}$ NMR (δ/ppm)*	*$\Delta^{31}P\{^1H\}$ NMR (δ/ppm)*	*$^1J_{RhP}$ (Hz)*	*Reference*
PEt_3	-20.4	23.6	44	117	[109]
$PPh(Et)_2$	-17.1	24.6	40.6	121	[109]
$P(CH_2CH_2C_6F_{13})_3$	-25	22.8	47.8	121	[109]
$PPh_2(CH_2CH_2C_6F_{13})$	-16	24.5	40.5	125	[109]
$PPh(CH_2CH_2C_6F_{13})_2$	-23	22.8	45.8	125	[109]
$P(C_6H_4\text{-}4\text{-}C_6F_{13})_2Et$	-10.8	27	37.8	126	[109]
$PPh_2(C_6H_4\text{-}3\text{-}C_6F_{13})$	-	-	34.5	128	[104]
PPh_3	-5	28.9	33.9	129	[109]
$P(C_6H_4.4\text{-}C_6F_{13})_3$	-6	30	36	131	[109]
$PPh_2(C_6H_4\text{-}2\text{-}CF_3)$	-	-	47.5	134	[104]
$PPh_2(C_6H_4\text{-}2\text{-}C_6F_{13})$	-	-	46.4	136	[104]
PPh_2OPh	111.1	123	11.9	143	[109]
$PPh_2\{OC(CF_3)_3\}$, (**6**)	132.3	142.3	10	154	This work
$PPh(OCH_2CH_2C_6F_{13})_2$	156.7	153.7	-3	167	[109]
$P(OMe)_3$	141.1	130.5	-10.6	195	[109]
$P(OCH_2CH_2C_6F_{13})_3$	139.4	128.7	-10.2	199	[109]
$P(OPh)_3$	127.8	115.2	-12.6	217	[109]
$P\{OCH(CF_3)_2\}_3$, (**1**)	140.2	123.3	-16.9	224	[132]
$PPh\{OC(CF_3)_3\}_2$, (**4**)	190	160.8	-29.2	285	This work
$P\{OC(CF_3)_3\}_3$, (**2**)	146.5	129.6	-16.9	286	This work

Table 15: $^{31}P\{^1H\}$ NMR spectroscopic data for *trans*-[RhCl(CO)L$_2$] complexes, L = phosphorus (III) ligand. Ligands (1), (2), (4) and (6) are highlighted.

3.2 RUTHENIUM COMPLEXES

3.2.1 The Synthesis and Structural Chemistry of Ruthenium Complexes

As discussed in Chapter 2, when calculating the ligand cone angles, successful complexation of the entire ligand series, (**1**) to (**6**) to a ruthenium metal centre, $[Ru(\eta^5\text{-}C_5H_5)(NCMe)_3]^+[PF_6]^-$ has been achieved. Successful crystallisation of these complexes has provided useful structural information. All crystals were grown by slow diffusion of hexane into a concentrated DCM solution of the complex. It should be noted; that although for the majority of the ligands the reaction was instant to yield the monosubstituted ruthenium complexes, for the disubstituted ruthenium complexes full conversion took up to three weeks at room temperature. In addition, it was observed that the $-CF_3$ groups for the hexafluoroisopropoxy substituent-containing ligands became inequivalent on complexation, as two fluorine multiplets were observed in the ^{19}F NMR spectrum. This may be due to atropisomerism, a cause of hindered rotation around either the P-O or O-C bond. All complexes with the perfluoro-*t*-butoxy substituents contained only one chemical shift for all three $-CF_3$ groups (as seen for the free ligands), suggesting they are equivalent due to faster rotation than that of the NMR time scale.

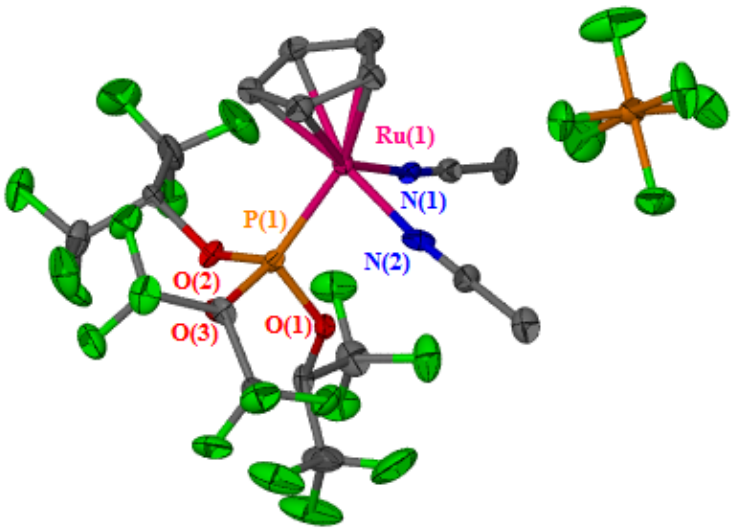

Figure 40: Molecular structure of $[(\eta^5\text{-}C_5H_5)Ru(NCMe)_2\{P(OCH\{CF_3\}_2)_2\}_3]^+[PF_6]^-$, [Ru(1)] at 110 K. Hydrogen atoms and the second structure in the asymmetric unit omitted for clarity. Thermal ellipsoids are drawn at the 50 % probability level. Selected interatomic distances (Å) and angles (°): Ru(1)-P(1) = 2.206(4), Ru(1)-N(1) = 2.05(1), Ru(1)-N(2) = 2.05(1), N(1)-Ru(1)-P(1) 89.0(3), N(2)-Ru(1)-P(1) 89.8(3), N(1)-Ru(1)-N(2) 86.5(4),O(3)-P(1)-O(2) = 95.3(5), O(1)-P(1)-O(2) = 95.8(5), O(1)-P(1)-O(3) = 101.7(5). Crystal system: triclinic. Space group: P-1. R_1: 0.1241 (all data) wR_2: 0.2653 (>2sigma(I)). Note high R_1 and wR_2 values as there is considerable disorder in the $[PF_6]^-$ anion and the Cp ring that has not been fully resolved.

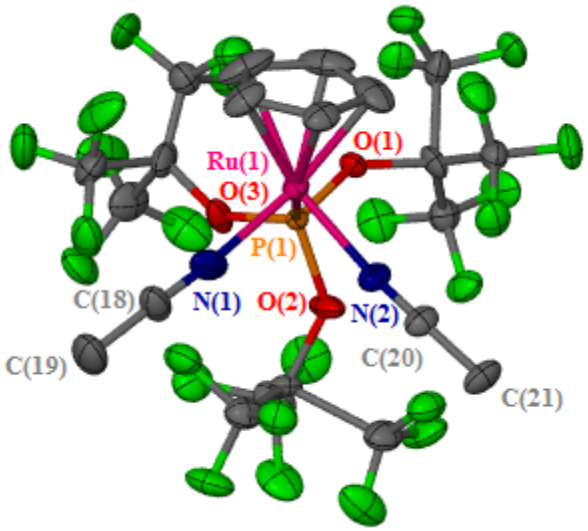

Figure 41: Molecular structure of $[(\eta^5\text{-}C_5H_5)Ru(NCMe)_2\{P(OC\{CF_3\}_3)_3\}]^+[Na_4\{OC(CF_3)_3\}_4PF_6NCMe]^-$, [Ru(2)] at 110 K. Hydrogen atoms, parts and $[PF_6]^-$ anion omitted for clarity. Thermal ellipsoids are drawn at the 50 % probability level. Selected interatomic distances (Å) and angles (°): Ru(1)-P(1) = 2.233(1), Ru(1)-N(1) = 2.015(5), Ru(1)-N(2) = 2.071(4), N(1)-Ru(1)-P(1) = 94.0(1), N(2)-Ru(1)-P(1) = 93.2 (1), N(1)-Ru(1)-N(2) = 86.7 (1), O(1)-P(1)-O(2) = 98.4(3), O(1)-P(1)-O(3) = 97.8(3), O(2)-P(1)-O(3) = 96.2(4).Crystal system: monoclinic. Space group: $P2_1/n$. R_1: 0.0623 (all data), wR_2: 0.1677 (>2sigma(I)).

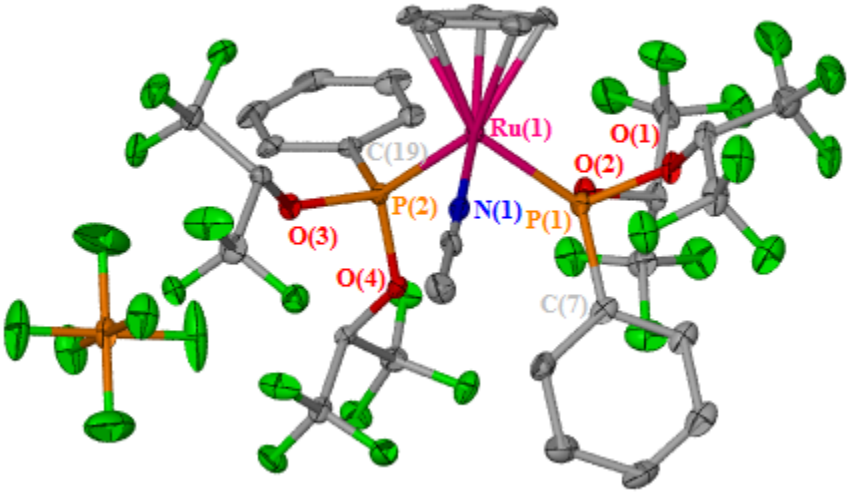

Figure 42: Molecular structure of $[(\eta^5\text{-}C_5H_5)Ru(NCMe)\{PPh(OCH\{CF_3\}_2)_2\}_2]^+[PF_6]^-$, [Ru(3)-2] at 110 K. Hydrogen atoms omitted for clarity. Thermal ellipsoids are drawn at the 50 % probability level. Selected interatomic distances (Å) and angles (°): Ru(1)-P(1) = 2.262(1), Ru(1)-P(2) = 2.265(1), Ru(1)-N(1) = 2.059(4), (1)-Ru(1)-P(1) = 92.7(1), P(1)-Ru(1)-P(2) = 96.31(4), P(1)-Ru(1)-P(2) = 94.5(1), O(2)-P(1)-O(1) =96.2(1), O(2)-P(1)-C(7) = 103.5(1), O(1)-P(1)-C(7) = 98.0(2), O(3)-P(2)-C(19) = 99.0(1), O(4)-P(2)-O(3) = 98.6(1), O(4)-P(2)-C(19) = 102.8(1). Crystal system: monoclinic. Space group: $P2_1/n$. R_1: 0.0557 (all data), wR_2: 0.0986 (>2sigma(I)).

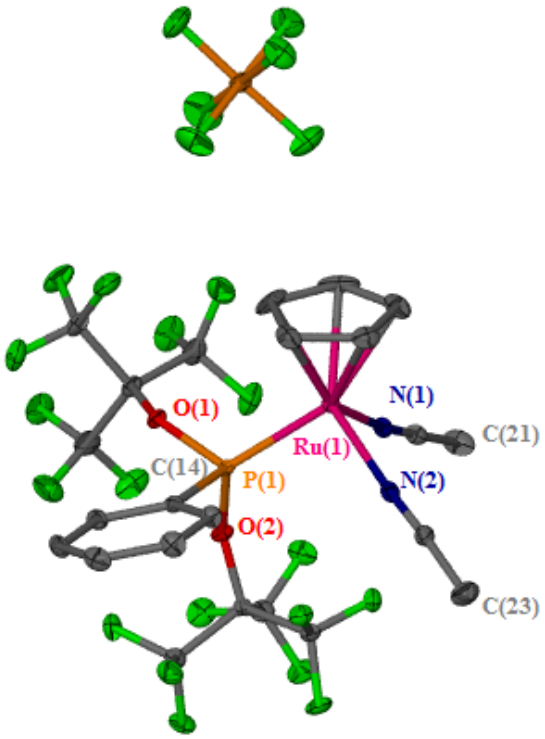

Figure 43: Molecular structure of $[(\eta^5\text{-}C_5H_5)Ru(NCMe)_2\{PPh(OC\{CF_3\}_3)_2\}]^+[PF_6]^-$, [Ru(4)] at 110 K. Hydrogen atoms and parts omitted for clarity. Thermal ellipsoids are drawn at the 50 % probability level. Selected interatomic distances (Å) and angles (°): Ru(1)-P(1) = 2.254(6), Ru(1)-N(1) = 2.047(2), Ru(1)-N(2) = 2.061(2), N(1)-Ru(1)-P(1) = 94.77 (6), N(2)-Ru(1)-P(1) = 97.49 (6), N(1)-Ru(1)-N(2) = 86.63 (8), O(1)-P(1)-O(2) = 94.10(9), O(1)-P(1)-C(14) = 94.9(1), O(2)-P(1)-C(14) = 104.9(1). Crystal system: monoclinic. Space group: $P2_1/c$. R_1: 0.0401 (all data) wR_2: 0.0886 (>2sigma(I)).

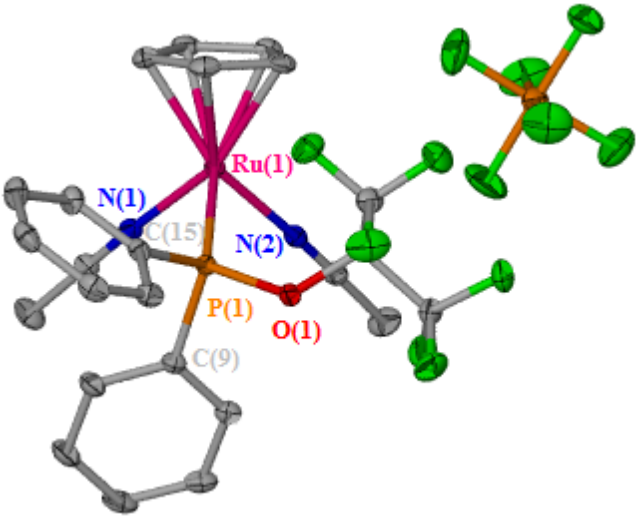

Figure 44: Molecular structure of $[(\eta^5\text{-}C_5H_5)Ru(NCMe)_2\{PPh_2OCH(CF_3)_2\}]^+[PF_6]^-$, [Ru(5)] at 109.8 K. Hydrogen atoms omitted for clarity. Thermal ellipsoids are drawn at the 50 % probability level. Selected interatomic distances (Å) and angles (°): Ru(1)-P(1) = 2.2636(5), Ru(1)-N(1) = 2.2058(1), Ru(1)-N(2) = 2.2054(1), N(1)-Ru(1)-P(1) = 88.19(4), N(2)-Ru(1)-P(1) = 89.75(4), N(2)-Ru(1)-N(1) = 83.50(6), O(1)-P(1)-C(9) = 98.02(8), O(1)-P(1)-C(15) = 101.23(8), C(15)-P(1)-C(9) = 102.00(8).Crystal system: monclinic. Space group: $P2_1/c$. R_1: 0.0305 (all data), wR_2: 0.0709 (>2sigma(I)).

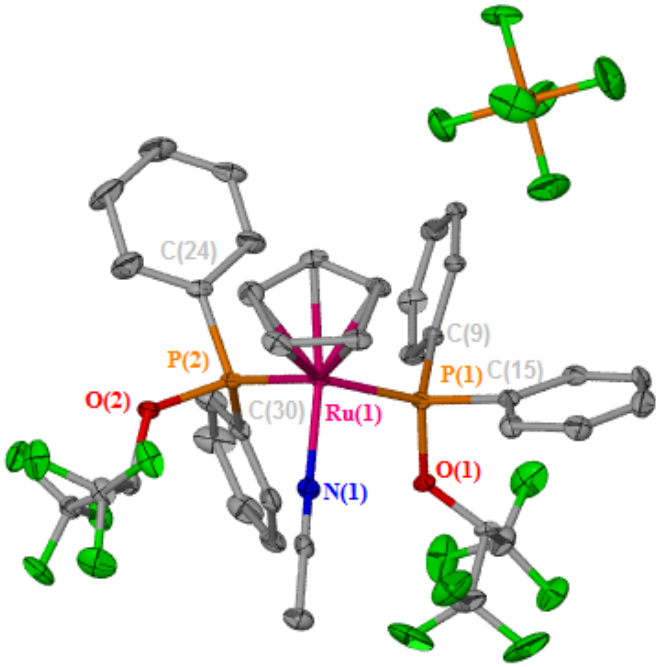

Figure 45: Molecular structure of $[(\eta^5\text{-}C_5H_5)Ru(NCMe)\{PPh_2OCH(CF_3)_2\}_2]^+[PF_6]^-$, [Ru(5)-2] at 110 K. Hydrogen atoms, second structure in asymmetric unit and solvent molecules omitted for clarity. Thermal ellipsoids are drawn at the 50 % probability level. Selected interatomic distances (Å) and angles (°): Ru(1)-N(1) = 2.046(4), Ru(1)-P(1) = 2.277(1), Ru(1)-P(2) = 2.276(1), N(1)-Ru(1)-P(1) = 91.5(1), N(1)-Ru(1)-P(2) = 94.5(1), P(2)-Ru(1)-P(1) = 98.97(4), O(1)-P(1)-C(9) = 102.8(1), O(1)-P(1)-C(15) = 101.9(1), C(15)-P(1)-C(9) = 104.8(2), O(2)-P(2)-C(24) = 95.6(1), O(2)-P(2)-C(24) = 95.6(1), O(2)-P(2)-C(30) = 101.5(1), C(30)-P(2)-C(24) = 102.8(2). Crystal system: orthorombic. Space group: $P2_12_12$. R_1: 0.0494, (all data), wR_2: 0.0989 (>2sigma(I)).

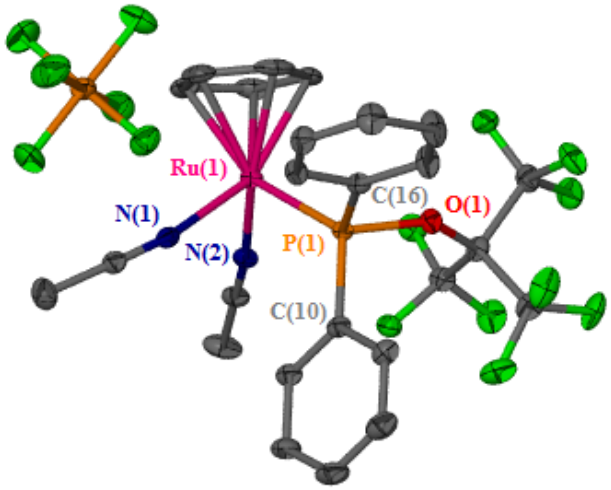

Figure 46: Molecular structure of $[(\eta^5\text{-}C_5H_5)Ru(NCMe)_2\{PPh_2OC(CF_3)_3\}]^+[PF_6]^-$, [Ru(6)] at 110 K. Hydrogen atoms and disorder omitted for clarity. The alkoxy group is disordered over two positions; the higher occupancy is shown here. Thermal ellipsoids are drawn at the 50 % probability level. Selected interatomic distances (Å) and angles (°): Ru(1)-P(1) = 2.2628(9), Ru(1)-N(1) = 2.069(2), Ru(1)-N(2) = 2.065(3), N(1)-Ru(1)-P(1) = 94.53(8), N(1)-Ru(1)-N(2) = 84.9(1), P(1)-Ru-N(2) = 97.54(8), C(10)-P(1)-C(16) = 100.9(1), C(10)-P(1)-O(1) = 102.7(1), O(1)-P(1)-C(16) = 93.8(1), O(1)-P(1)-C(10) = 100.7 (1), C(10)-P(1)-C(16) = 105.5(1).Crystal system: monoclinic. Space group: $P2_1/c$. R_1: 0.0422 (all data), wR_2: 0.0895 (>2sigma(I)).

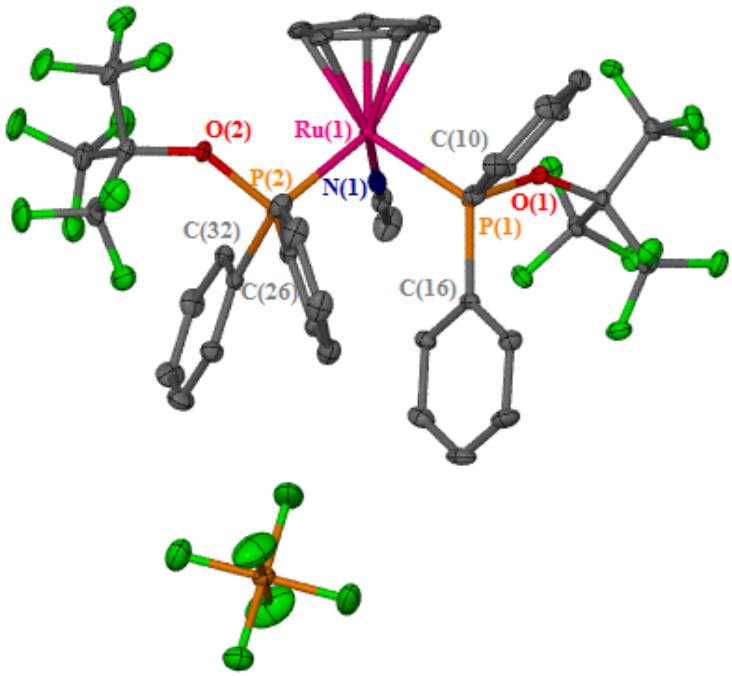

Figure 47: Molecular structure of $[(\eta^5\text{-}C_5H_5)Ru(NCMe)\{PPh_2OC(CF_3)_3\}_2]^+[PF_6]^-$, [Ru(6)-2] at 110 K. Hydrogen atoms, second structure from the asymmetric unit and solvent molecule omitted for clarity. Thermal ellipsoids are drawn at the 50 % probability level. Selected interatomic distances (Å) and angles (°): Ru(1)-P(1) = 2.2882(9), Ru(1)-N(1) = 2.048(2), Ru(1)-N(2) = 2.2988(7), N(1)-Ru(1)-P(1) = 89.96(7), N(1)-Ru(1)-P(2) = 96.01(6), P(1)-Ru-P(2) = 99.07(3), O(2)-P(2)-C(32) = 104.2(1), O(2)-P(2)-C(26) = 100.7(1), C(32)-P(2)-C(26) = 109.0(1), O(1)-P(1)-C(10) = 100.7(1), C(10)-P(1)-C(16) = 105.5(1).Crystal system: monoclinic. Space group: $P2_1$. R_1: 0.0332 (all data), wR_2: 0.0785 (>2sigma(I)).

All the $[(\eta^5\text{-}C_5H_5)Ru(NCMe)_{n-3}L_n]^+[PF_6]^-$ structures shown above have a distorted tetrahedral structure at the ruthenium if the cyclopentadienyl centroid is considered as one ligand. This is common for half-sandwich ruthenium complexes. The Ru-P bond lengths provide a good indication of the strength of the bond, which can in turn be related to the π-acidity of the coordinated ligand; the shorter the Ru-P bond then the more π-acidic the ligand, (discussed in further detail below). The SPS angles can be calculated from each crystal structure. Generally, these show that larger SPS angles are found for structures with less bulky ligands. This may be a result of the reduced ligand bulk, allowing the substituents on the phosphorus atom to push out further and open up in the available space around the metal-phosphorus bond. This is due to reduced phosphorus lone pair repulsion with the substituents on the phosphorus atom upon coordination of the ligand. Most the Ru-N bond lengths for the complexed acetonitrile groups are all very similar. This indicates the coordination of the acetonitrile groups is not significantly affected by the phosphorus ligand at the ruthenium metal centre.

The molecular structure of **[Ru(2)]** shown in Figure 41 contains the desired cation $[(\eta^5\text{-}C_5H_5)Ru(NCMe)_2\{P(OC\{CF_3\}_3)_3\}]^+$, but it crystallises as a salt with the unusual $[Na_4\{OC(CF_3)_3\}_4PF_6.NCMe]^-$ counterion, see Figure 48.

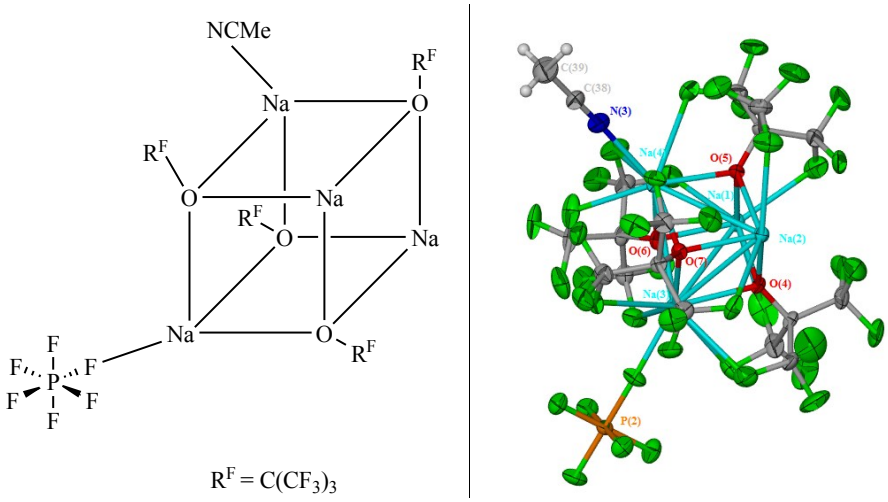

Figure 48: A chemdraw diagram and the single-crystal X-ray structure of the $[Na_4\{OC(CF_3)_3\}_4PF_6.NCMe]^-$ unusual counterion found in the single-crystal X-ray structure of [Ru(2)] at 110 K. Parts and cation omitted for clarity. Thermal ellipsoids are drawn at the 50 % probability level. Crystal system: monoclinic. Space group: $P2_1/n$. R_1: 0.0623 (all data), wR_2: 0.1677 (>2sigma(I)).

This anion results from the coordination of a $[PF_6]^-$ anion and a molecule of MeCN to a neutral sodium alkoxide cluster $[Na_4\{OC(CF_3)_3\}_4]$. Some $NaOC(CF_3)_3$ was present as a low concentration impurity in the sample of (**2**) used in this reaction. Cubic clusters are common structural forms in alkoxides of this type.[138] To the best of our knowledge compound **[Ru(2)]** is the first structurally characterised example of a metal complex of (**2**) and is indeed, again to the best of our knowledge, the first structurally characterised example of a metal complex of a perfluorinated phosphite. The basic structure of **[Ru(2)]** is as expected, similar to the other complexes described above. However, given the size of this ligand, the remarkably short Ru-P bond length (2.233 Å) is particularly noteworthy and may be an indication of relatively strong π-backdonation from Ru to P, discussed below. Another interesting feature in this structure is the marked asymmetry in the Ru-N bond lengths (2.015 and 2.071 Å), which appear in other complexes described here to be relatively insensitive to the nature of the ligand. Although the ligand is heavily disordered (rotation of CF_3 groups in the $-C(CF_3)_3$ substituents), it appears that there is a closer approach of one C-F bond from (**2**) to the C≡N bond of the coordinated MeCN that displays a particularly short Ru-N distance (2.015 Å) than is present for the MeCN that has a Ru-N distance that is more typical for the complexes described here (2.071 Å). It is possible that this asymmetry observed in the Ru-N bond distances is due to the weak intramolecular interactions in the solid-state rather than this being related to the nature of the metal to P-ligand interaction.

As discussed in Chapter 2, three typical conformations are found for the alkoxy substituents on the phosphorus ligand centres. These are described as; “up” which points towards the M-P bond (parallel with it, increasing the cone angle value), “side” where the alkoxy group bends away from the M-P bond and “down” which points away from the M-P bond (but still parallel with it, reducing the cone angle), see Figure 49.

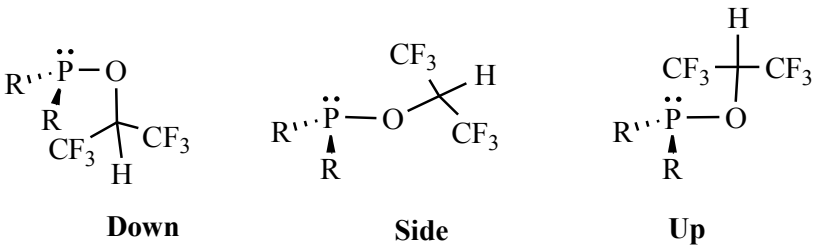

Figure 49: The hexafluoroisopropoxy groups can change orientation; the O-R bond can point away from the phosphorus lone pair (“down”), O-R can bend so that is not parallel with the phosphorus lone pair (side) or the O-R bond can point towards the lone pair (up).

In addition to the conformation of the alkoxy substituents, the phenyl rings also possess different conformations; “planar” (see non starred phenyl in Figure 50), perpendicular to the M-P-C bond, reducing the cone angle and “propeller” (see starred phenyl in Figure 50), in line with the M-P-C bond, which in turn increases the cone angle, as discussed in Chapter 2.

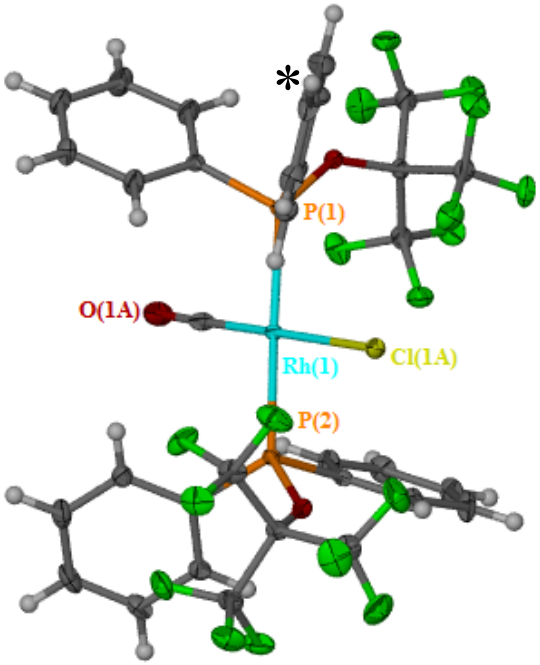

Figure 50: Crystal structure of $[Rh(CO)_2Cl\{PPh_2OC(CF_3)_3\}_2]$, [Rh(6)-2] the starred (*) phenyl has a “propeller” arrangement increasing the ligand cone angle.

The combination of the phenyl ring and alkoxy substituent conformations can be used to explain the variation of cone angles observed for each ligand type. The tables below

compare the various conformations found in the XRD {$[(\eta^5\text{-}C_5H_5)Ru(NCMe)_{n-3}L_n]^+[PF_6]^-$; n = 1 or 2, $[RhCOCl(L)_2]$} and DFT calculated {$[W(CO)_5L]$, $[Ni(CO)_3L]$} structures for ligands (**1**) to (**6**). Multiple cone angle values for the same $[(\eta^5\text{-}C_5H_5)Ru(NCMe)_{n-3}L_n]^+[PF_6]^-$ type complex, are due to either multiple complexes in the asymmetric unit and/or two coordinated ligands on the ruthenium centre, both with different conformations.

L= P{OCH(CF$_3$)$_2$}$_3$ (1)	***Alkoxide 1***	***Alkoxide 2***	***Alkoxide 3***	***θ°***
$[(\eta^5\text{-}C_5H_5)Ru(S)_2L]^+[A]^-$	Alkoxy up	Alkoxy down	Alkoxy side	160
$[(\eta^5\text{-}C_5H_5)Ru(S)_2L]^+[A]^-$	Alkoxy up	Alkoxy down	Alkoxy side	157
$[RhCOCl(L)_2]$	Alkoxy up	Alkoxy down	Alkoxy side	167
$[RhCOCl(L)_2]$	Alkoxy up	Alkoxy down	Alkoxy side	160
$[W(CO)_5L]$	Alkoxy up	Alkoxy down	Alkoxy side	155
$[Ni(CO)_3L]$	Alkoxy up	Alkoxy up	Alkoxy side	178

Table 16: Substituent conformations for complexes with P{OCH(CF$_3$)$_2$}$_3$ (1). S = NCMe, $[A]^- = [PF_6]^-$.

The conformations of the alkoxy substituents of (**1**) in the $[Ni(CO)_3L]$ complex consists of two pointing "up" and one to the "side", resulting in a cone angle of θ = 178 °. The **[Ru(1)]**, **[Rh(1)-2]** and $[W(CO)_5L]$ complexes in comparison consist of one alkoxy group pointing "up", one pointing "down" and one to the "side". This combination lowers the steric influence of P{OCH(CF$_3$)$_2$}$_3$, (**1**), resulting in lower cone angles (ranging between 155 ° – 167 °). While it can clearly be seen that conformational changes have a big impact on θ, this is evidently not the only factor.

L = PPh{OCH(CF$_3$)$_2$}$_2$, (3)	*Alkoxide 1*	*Alkoxide 2*	*Phenyl 1*	*θ°*
[(η^5-C$_5$H$_5$)RuS(L)$_2$]$^+$[A]$^-$	Alkoxy down	Alkoxy up	Phenyl propeller	147
[(η^5-C$_5$H$_5$)RuS(L)$_2$]$^+$[A]$^-$	Alkoxy down	Alkoxy side	Phenyl almost propeller	140
[Ni(CO)$_3$L]	Alkoxy up	Alkoxy side	Phenyl propeller	173
[W(CO)$_5$L]	Alkoxy up	Alkoxy side	Phenyl almost propeller	162

Table 17: Substituent conformations for complexes with PPh{OCH(CF$_3$)$_2$}$_2$, (3). S = NCMe, [A]$^-$ = [PF$_6$]$^-$.

Similarly, the substituents on (**3**) in the [Ni(CO)$_3$L] complex give rise to a cone angle of 173 °. This larger cone angle is likely to be an attribute of the phenyl ring occupying a "propeller" arrangement, in combination with one alkoxy group pointing "up" and one pointing to the "side". The cone angles of the ligand in **[Ru(3)-2]** have a much smaller cone angle than the [Ni(CO)$_3$L] complex, presumably due to having one alkoxy group pointing "down" rather than "up".

L = $PPh_2\{OCH(CF_3)_2$, (5)	*Alkoxide 1*	*Phenyl 1*	*Phenyl 2*	*θ°*
				147
$[(\eta^5\text{-}C_5H_5)Ru(S)_2L]^+[A]^-$	Alkoxy side	Phenyl almost propeller	Phenyl almost planar	
$[(\eta^5\text{-}C_5H_5)RuS(L)_2]^+[A]^-$	Alkoxy down	Phenyl almost propeller	Phenyl almost planar	143
$[(\eta^5\text{-}C_5H_5)RuS(L)_2]^+[A]^-$	Alkoxy down	Phenyl almost propeller	Phenyl almost planar	142
$[(\eta^5\text{-}C_5H_5)RuS(L)_2]^+[A]^-$	Alkoxy up	Phenyl almost propeller	Phenyl almost planar	144
$[(\eta^5\text{-}C_5H_5)RuS(L)_2]^+[A]^-$	Alkoxy side	Phenyl almost propeller	Phenyl almost planar	144
$[Ni(CO)_3L]$	Alkoxy side	Phenyl propeller	Phenyl almost planar	170
$[W(CO)_5L]$	Alkoxy up	Phenyl almost propeller	Phenyl almost planar	152

Table 18: Substituent conformations for complexes with $PPh_2\{OCH(CF_3)_2\}$ (5). S = NCMe, $[A]^- = [PF_6]^-$.

The cone angles found in **[Ru(5)]** and **[Ru(5)-2]** are all very similar, possibly due the phenyl rings all having similar arrangements in the asymmetric unit of the crystal structures. A larger cone angle is observed for the $[Ni(CO)_3L]$ complex, possibly due to one of the phenyl rings having a "propeller" arrangement.

L = P{OC(CF$_3$)$_3$}$_3$, (2),	*Alkoxide 1*	*Alkoxide 2*	*Alkoxide 3*	*θ°*
[(η^5-C$_5$H$_5$)Ru(S)$_2$L]$^+$[A]$^-$	Alkoxy side	Alkoxy side	Alkoxy side	180
[(η^5-C$_5$H$_5$)Ru(S)$_2$L]$^+$[A]$^-$	Alkoxy side	Alkoxy side	Alkoxy side	173
[Ni(CO)$_3$L]	Alkoxy side	Alkoxy side	Alkoxy side	195
[W(CO)$_5$L]	Alkoxy side	Alkoxy side	Alkoxy down	180

Table 19: Substituent conformations for complexes with P{OC(CF$_3$)$_3$}$_3$ (2). S = NCMe, [A]$^-$ = [PF$_6$]$^-$.

Although the alkoxide conformations in **[Ru(2)]** and [Ni(CO)$_3$L] all possess a "side" orientation, the cone angles differ greatly. The larger cone angle found in the [Ni(CO)$_3$L] complex is presumably due to the increased steric congestion at the smaller Ni centre in comparison to **[Ru(2)]** and [W(CO)$_5$L]. In addition, the optimised [W(CO)$_5$L] complex consists of one alkoxide substituent pointing "down", possibly due to the increased space at the octahedral centre. The cone angle for [W(CO)$_5$L] is smaller than that of the [Ni(CO)$_3$L] complex. However, [W(CO)$_5$L] and **[Ru(2)]** are found to contain cone angles of similar magnitudes, even though the alkoxide conformations are different. This highlights that other factors such as the size of the metal and it geometry can also affect the cone angles.

L = PPh{OC(CF$_3$)$_3$}$_2$, (4)	*Alkoxide 1*	*Alkoxide 2*	*Phenyl 1*	*θ°*
[(η^5-C$_5$H$_5$)Ru(S)$_2$L]$^+$[A]$^-$	Alkoxy side	Alkoxy side	Phenyl almost propeller	178
[Ni(CO)$_3$L]	Alkoxy up	Alkoxy down	Phenyl in-between	163
[W(CO)$_5$L]	Alkoxy down	Alkoxy up	Phenyl in-between	165

Table 20: Substituent conformations for complexes with PPh{OC(CF$_3$)$_3$}$_2$ (4). S = NCMe, [A]$^-$ = [PF$_6$]$^-$.

Complex **[Ru(4)]** has a much larger cone angle than in the calculated $[Ni(CO)_3L]$ or $[W(CO)_5L]$ complexes. Here the alkoxy groups are in the "side" conformation and the phenyl is almost in a "propeller-like" arrangement. The cone angle values are reduced in the $[Ni(CO)_3L]$ and $[W(CO)_5L]$ complexes, as the phenyl group tilts away from the "propeller" arrangement and the alkoxy substituent point "down", this reduces the steric congestion at the metal.

L = $PPh_2\{OC(CF_3)_3\}$, (6)	***Alkoxide 1***	***Phenyl 1***	***Phenyl 2***	***θ˚***
$[(\eta^5\text{-}C_5H_5)RuS(L)_2]^+[A]$	Alkoxy down	Phenyl planar	Phenyl almost propeller	158
$[(\eta^5\text{-}C_5H_5)RuS(L)_2]^+[A]^-$	Alkoxy down	Phenyl almost planar	Phenyl almost propeller	147
$[(\eta^5\text{-}C_5H_5)RuS(L)_2]^+[A]^-$	Alkoxy down	Phenyl almost planar	Phenyl almost propeller	142
$[(\eta^5\text{-}C_5H_5)RuS(L)_2]^+[A]^-$	Alkoxy down	Phenyl almost planar	Phenyl almost propeller	142
$[(\eta^5\text{-}C_5H_5)Ru(S)_2L]^+[A]^-$	Alkoxy side	Phenyl propeller	Phenyl almost propeller	164
$[RhCOCl(L)_2]$	Alkoxy up	Phenyl propeller	Phenyl almost propeller	193
$[RhCOCl(L)_2]$	Alkoxy side	Phenyl planar	Phenyl almost planar	163
$[Ni(CO)_3L]$	Alkoxy up	Phenyl planar	Phenyl almost propeller	170
$[W(CO)_5L]$	Alkoxy side	Phenyl almost planar	Phenyl almost propeller	163

Table 21: Substituent conformations for complexes with $PPh_2\{OC(CF_3)_3\}$ (6). S = NCMe, $[A]^- = [PF_6]^-$.

Interestingly, the two coordinated $PPh_2\{OC(CF_3)_3\}$, (**6**) ligands in **[Rh(6)-2]** show an incredible difference of 30 ˚ in their calculated cone angles. This can be an attribute of one of the coordinated ligands consisting of phenyl rings with the "propeller" arrangement (θ = 193 ˚) and the other consisting of "planar" arrangements (θ = 163 ˚). The larger cone angle is a likely cause of the alkoxy substituent possessing an "up" conformation, which in turn reduces the available space for the phenyl substituents, forcing them to be close to "propeller", rather than "planar".

In summary, it appears that the conformations with the alkoxy substituents possessing the "up" conformation give rise to the largest cone angles, followed then by the alkoxy "side" conformation. The alkoxy substituents possessing the "down "conformation give rise to the smallest cone angles as this allows for reduced steric congestion at the metal centre. The phenyl ring conformations are found to be more flexible and particularly when in the "propeller" conformation (as a result of interacting with either the "up" or "side" conformations of the alkoxy substituents) can significantly affect the cone angle, by increasing it. However, when the phenyl ring is in a "planar" conformation the cone angle is significantly reduced.

3.2.2 Comparisons of the Ruthenium Complexes with Structural Data in the CSD

A CSD search was carried out for a $[(\eta^5\text{-Cp})Ru(P_1)(P_2)(NCMe)]^+$ fragment with $R_1 < 10$ %.[165-168] Over one hundred and eighty structures were found with the required parameters, see Figure 51. The shortest Ru-P bond distance was found to be 2.22(2) Å, much shorter than the average 2.33 Å for all the structures found. This short bond length is found for a triphenylphosphite ligand coordinated to a substituted cyclopentadienyl ruthenium complex, see Figure 52.

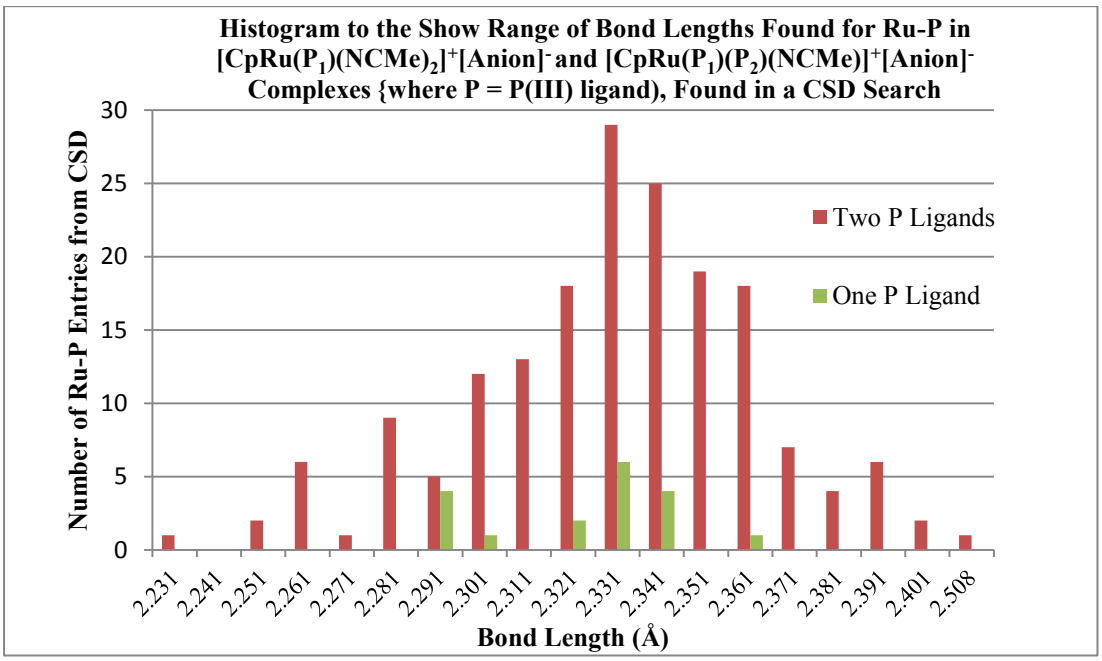

Figure 51: Histogram to show the range of Ru-P bond lengths (Å) in $[(\eta^5\text{-Cp})Ru(P_1)(NCMe)_2]^+[Anion]^-$ and $[(\eta^5\text{-Cp})Ru(P_1)(P_2)(NCMe)]^+[Anion]^-$complexes with a number of phosphorus (III) ligands.

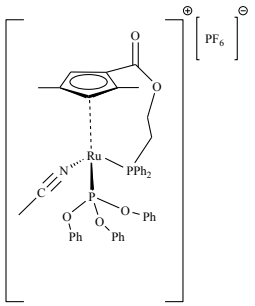

Figure 52: A Chemdraw representation of the structure containing the shortest Ru-P bond length from a CSD search for a $[Ru(\eta^5\text{-}Cp)(P)_1(P)_2NCMe]^+$ fragment with $R_1 < 10$ %. The Ru-$P(OPh)_3$ bond has the shortest possible bond {2.22(2) Å} even though statistically it may be similar to the other Ru-PPh_2R bond {2.34(3) Å}. CSD search name: QIFXIM.

The Ru-P distances for all the complexes presented in this thesis have bond lengths much shorter than the average half-sandwich ruthenium complexes; see Table 22. This suggests a significant extent of back-bonding is present between the ruthenium metal centre and the phosphorus (III) ligands (**1**) to (**6**). Table 22 suggests that the general order of π-acidity of the ligands is as follows; phosphinite < phosphonite < phosphite, which is in good agreement with the results discussed in Chapter 2. In addition, these Ru-P bond lengths also highlight the difference in electronic properties between the two phosphite ligands. The perfluorinated phosphite, $P\{OC(CF_3)_3\}_3$, (**2**) has a longer bond length than $P\{OCH(CF_3)_2\}_3$, (**1**) indicating this is not as π-acidic as one might expect due to its extra CF_3 group. This again is in good agreement from the conclusions of Chapter 2 and can be possibly an effect observed due to reduced orbital overlap from the greater steric bulk on the perfluorinated phosphite ligand, $P\{OC(CF_3)_3\}_3$, (**2**).

Ru –P (Å) in $[Ru(\eta^5\text{-}C_5H_5)(NCMe)_2L]^+$ $[PF_6]^-$, L =	*Ru –P (Å) in $[Ru(\eta^5\text{-}C_5H_5)(NCMe)L_2]^+$ $[PF_6]^-$, L =*
PCy_3, 2.359(1)	
$Ph_2PNC_5H_{10}$, 2.332(5)	
PPh_3, 2.321(4)	
PMe_3, 2.294(4)	
	$PPh_2\{OC(CF_3)_3\}$, (**6**), 2.2881(9) and 2.2988(7)
$Ph_2PNHC_3H_7$, 2.282(5)	
	$PPh_2\{OCH(CF_3)_2\}$, (**5**), 2.277(1) and 2.276(1)
Ph_2POCy, 2.276(7) [1]	
$Ph_2P\{OCH(CF_3)_2\}$, (**5**), 2.264(4)	
PPh_2Cl, 2.2640(5)[1]	
	$PPh\{OCH(CF_3)_2\}_2$, (**3**), 2.262(1) and 2.265(1)
$PPh\{OC(CF_3)_3\}_2$, (**4**), 2.254(6)	
$P\{OC(CF_3)_3\}_3$, (**2**), 2.233(1)	
$P\{OCH(CF_3)_2\}_3$, (**1**), 2.206(4)*	

Table 22: Ruthenium-phosphorus bond lengths from crystallographic data for the ruthenium complexes with ligands (1) to (6) and others found from a CDS search of the $[Ru(\eta^5\text{-}Cp)P_1(NCMe)_2]^+$ fragment or [1] = from the JML group 2011/2012 masters student Steve McNicol's dissertation. * = shorter bond length than that found for any complexes from the CSD search. Bond lengths for ligands (1) to (6) are highlighted.

3.2.3 Reactivity of $[Ru(\eta^5\text{-}C_5H_5)(NCMe)(Ph_2P\{OCH(CF_3)_2\})_2]^+[PF_6]^-$, **[Ru(5)-2]**

A vinylidene molecule is an example of a Fischer carbene ligand where the C_α atom is electrophilic, and the C_β atom is nucleophilic in nature, see Figure 53.

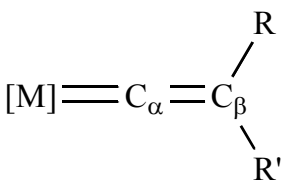

Figure 53: A vinylidene with substituents R and R', coordinated to a transition metal complex

In the gas phase, a vinylidene (:C=CH_2) is approximately 188 kJ mol^{-1} less stable than its acetylene (HC≡CH) tautomer.[170, 171] However, on coordination to a late transition metal centre, this stability is reversed, as shown by Hoffmann *e.g.* [Mn(η^5-C_5H_5)(C=CH_2)$(CO)_2$] is 146 kJ mol^{-1} more stable than a η^2–bound acetylene ligand, see Figure 54.[172]

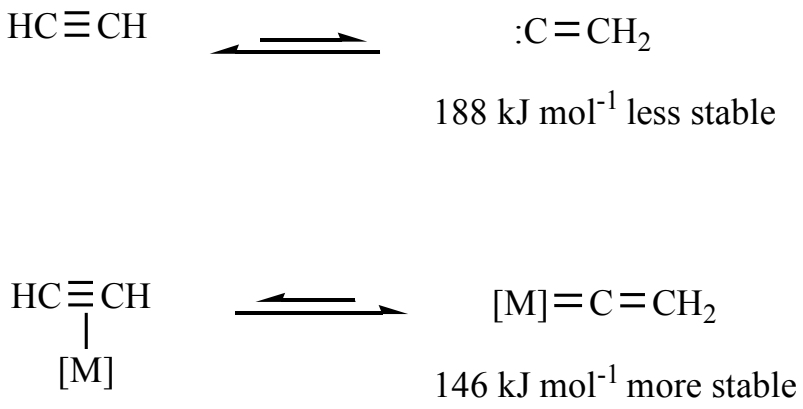

Figure 54: The vinylidene (right) and acetylene (left) tautomers; both when free and coordinated to a transition metal.

Similar half-sandwich ruthenium complexes to those discussed above are well known for their role in catalysis. For example, they can be used to promote carbon-carbon coupling of alkynes to give poylmerisation and cyclisation products.[173] The labile acetonitrile ligands on [(η^5-C_5H_5)Ru$(NCMe)_2L]^+[PF_6]^-$ or [(η^5-C_5H_5)Ru(NCMe)$(L)_2]^+[PF_6]^-$ provide access to 14-electron [(η^5-C_5H_5)RuL]$^+$ or 16-electron [(η^5-C_5H_5)Ru$(L)_2]^+$ fragments. These are known to react with alkynes to give vinylidene complexes[171] (see Figure 54) and metallacyclopentadienes,[174] which may be important intermediates in the catalytic activation of alkynes in a variety of reactions for the catalytic transformation of small organic molecules *e.g.* alkyne oligomerisaion, alkyne hydration[175, 176] or hydroamination *etc.* in the anti-Markovnikoff addition of various nucleophiles to alkynes.[177, 178]

Extensive theoretical and experimental studies have concluded that there are three general pathways for the formation of a vinylidene complex.[171, 179] The initial step in all three cases involves the coordination of the alkyne in a η^2-fashion; hence the metal precursor must possess a vacant coordination site, this can be generated from either dissociation of a labile ligand *e.g.* solvent molecule or a switch in the ligand bonding mode *e.g.* as seen for NO[180] or an acetate.[181, 182] Pathway 1 follows a concerted 1, 2-hydrogen migration *via* **A** in Scheme 13,[183] whereas pathway 2 follows an oxidative addition to give the alkynyl hydride complex **B** in Scheme 13, which then undergoes a 1, 3-hydrogen-migration to form the metal vinylidene complex.[184] The steric and electronic properties of the ligands on the metal centre and the nature of the metal itself are key contributors to the preferred pathway. In general, it

can be found that the more electron rich metal centres follow the formation of a vinylidene *via* pathway 2. This may be due to the intermediate **B** from Scheme 13 consisting of a Ru(IV) species that cannot be stabilized well by electron-poor ligands. Pathway 3 consists of a metal alkenyl ligand intermediate, see species **C** in Scheme 13. This occurs through insertion of an alkyne into a metal hydride bond.[185-187] In addition, the rate of vinyildene formation has found to be enhanced by electron-donating substituents on the considered alkynes.[179]

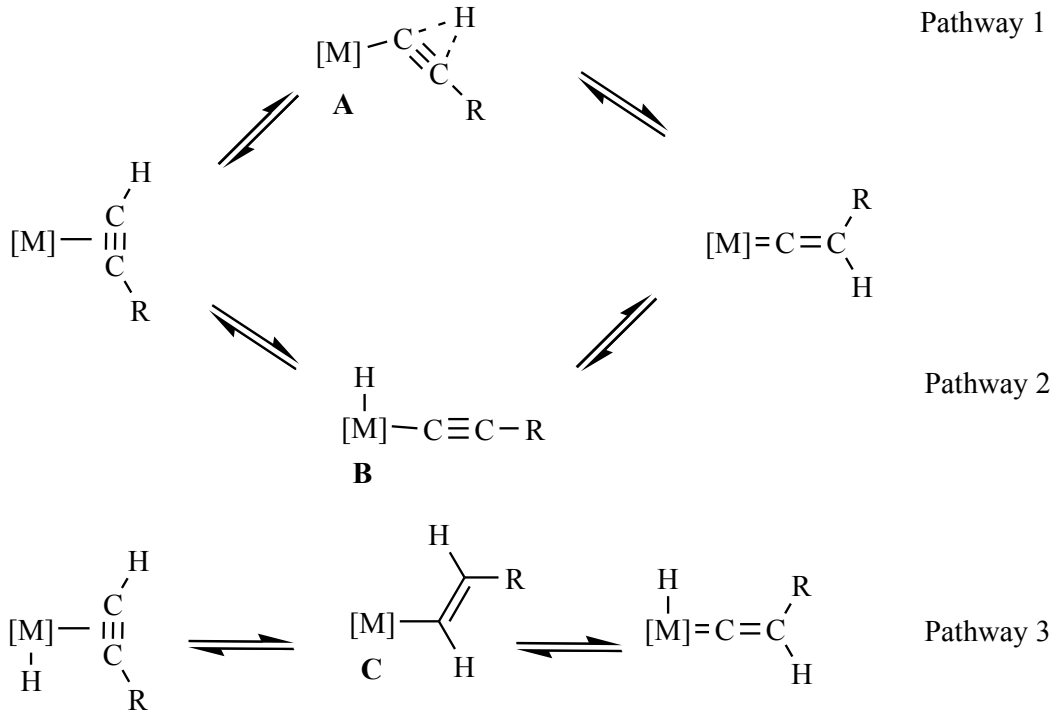

Scheme 13: The three general mechanistic pathways for the formation of a vinyildene complex.

The novel **[Ru(5)-2]** complex was reacted with 1 eq. phenylacetylene in DCM solvent, in anticipation of observing a possible vinylidene complex. No changes were observed in the $^{31}P\{^{1}H\}$ NMR spectrum of the reaction mixture after one day at room temperature. There is a possibility that the two bulky electron deficient ligands reduce the electron-density at the ruthenium metal centre, which in turn affects its reactivity with the phenylacetylene. Therefore an immediate η^2 alkyne-metal complex is not observed. However, the $^{31}P\{^{1}H\}$ changes after heating the reaction, see Figure 55. To rule out decomposition of **[Ru(5)-2]** at 50 ˚C, a control was run using isolated crystals of **[Ru(5)-2]** in the absence of phenylacetylene. No change was observed in the $^{31}P\{^{1}H\}$ NMR spectrum after heating the control sample of **[Ru(5)-2]** at 50 ˚C for two weeks, hence thermal decomposition is highly unlikely.

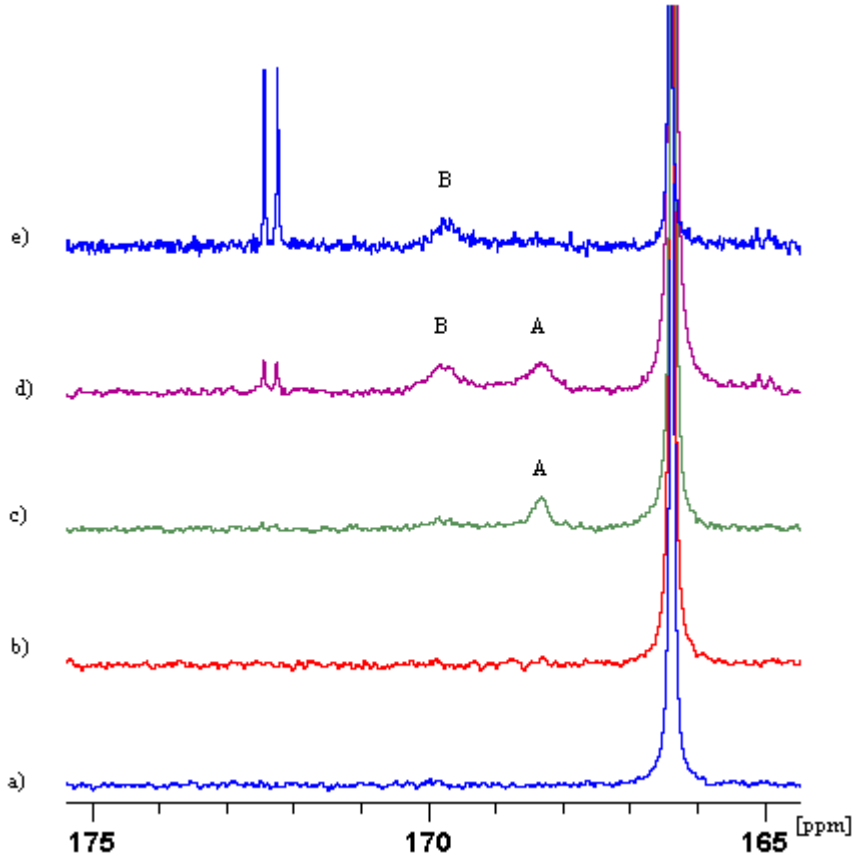

Figure 55: $^{31}P\{^{1}H\}$ NMR spectra of $[(\eta^5\text{-}C_5H_5)Ru(NCMe)(Ph_2P\{OCH(CF_3)_2\})_2]^+[PF_6]^-$, [Ru(5)-2] and phenylacetylene , 150 to 190 ppm range. NMR spectra in overlay; a) after 15 minutes of reactions, b) 1 day, c) 1day heated at 50 ˚C, d) 2 days heated at 50 ˚C and e) 7 days heated at 50 ˚C.

The phosphorus signal in **[Ru(5)-2]** at 168.1 ppm in the $^{31}P\{^{1}H\}$ NMR spectrum gradually converts to intermediate products; species A, δ_P = 169.7 ppm (br) and species B δ_P = 170.1 ppm (br). The signal for species B increases as species A diminishes, see Figure 55. Another explanation could be that the two broad peaks (A and B in Figure 55, spectra d) are due to slow vinylidene rotation around the Ru=C bond, so that the two $Ph_2P\{OCH(CF_3)_2\}$, (**5**) ligands appear to be in different environments. Over time these broad peaks convert to a doublet at δ_P = 173.7 ppm (J = 40 Hz). A 2D P-P COSY of this sample showed that the signal at δ_P = 173.7 ppm (d, J = 40 Hz) relates to a signal observed at δ_P = 23.0 ppm (d, J = 40 Hz), which also grows in over time, see Figure 56 below.

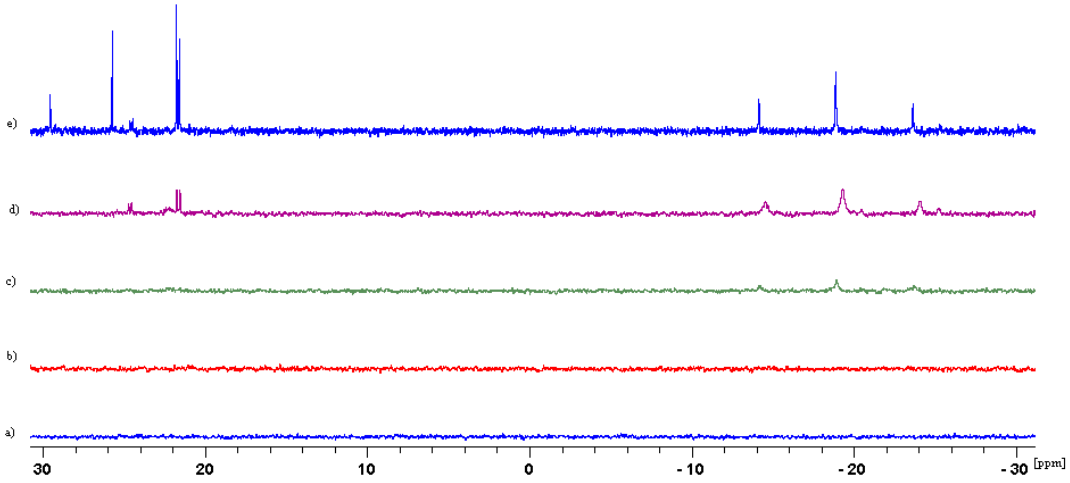

Figure 56: $^{31}P\{^{1}H\}$ NMR of $[(\eta^5\text{-}C_5H_5)Ru(NCMe)(Ph_2P\{OCH(CF_3)_2\})_2]^+[PF_6]^-$, [Ru(5)-2] and phenylacetylene, 30 to -30 ppm range. NMR spectra in overlay; a) after 15 minutes of reactions, b) 1 day, c) 1 day heated at 50 ˚C, d) 2 days heated at 50 ˚C and e) 7 days heated at 50 ˚C.

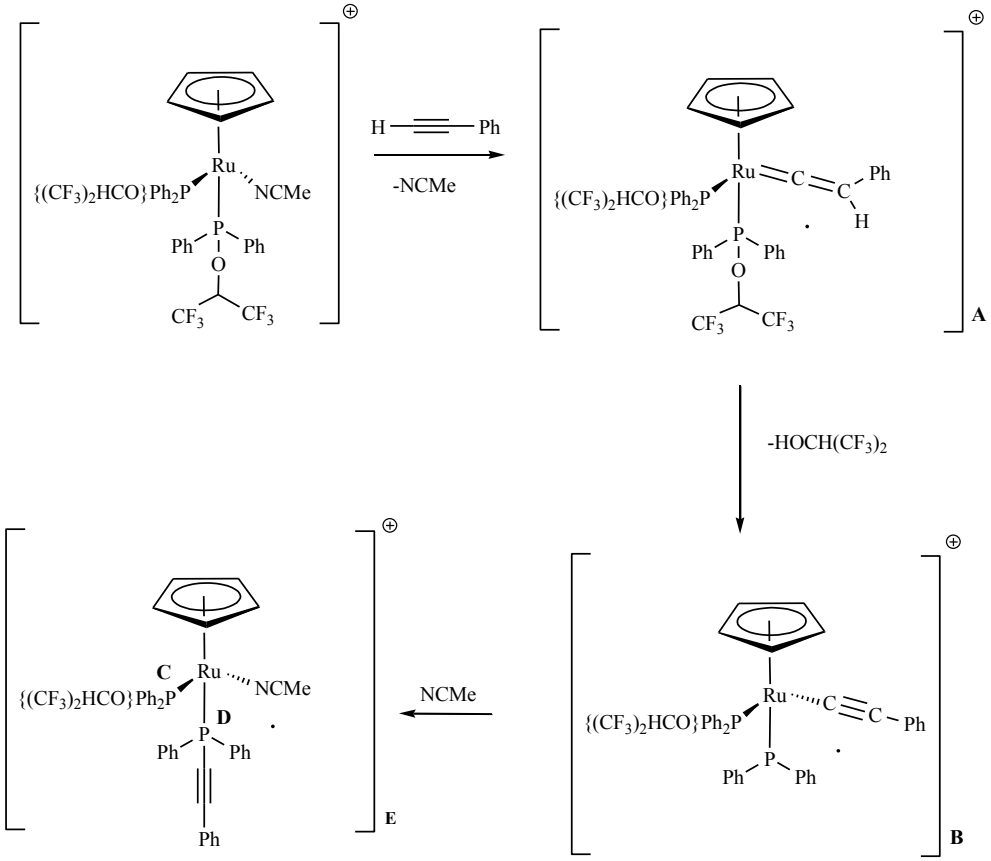

Scheme 14: Proposed products and intermediates for the reaction of [Ru(5)-2] with phenylacetylene.

Scheme 14 describes a possible explanation for the observed doublets in the $^{31}P\{^{1}H\}$ NMR spectra. On the addition of phenyacetylene, a vinylidene is formed at the ruthenium metal centre (**A**). This could potentially explain the broad peak observed at δ_P = 169.7 ppm in Figure 55. The vinylidene could undergo intramolecular deprotonation from the terminal

carbon to form the corresponding acetylide (**B**). This could potentially lead to the broad peak observed at δ_P = 170.1 in Figure 55. The hexafluoroisopropoxy group of one of the coordinated $Ph_2P\{OCH(CF_3)_2\}$ ligands could then dissociate and undergo protonation forming the hexafluoroisopropanol molecule (δ_F = -75.80, d, $^4J_{FH}$ = 6 Hz), shown in the ^{19}F NMR spectra in Figure 57, spectra b). This would produce a vacant site at the coordinated phosphorus ligand, allowing migration of the acetylide group, to form coordinated PPh_2CCPh type ligand, environment **D** in Scheme 14. This could potentially be related to the signal observed at δ_P = 23.0 ppm (d, $^2J_{PP}$ = 40 Hz), see Figure 56. The coordinated $Ph_2P\{OCH(CF_3)_2\}$ ligand (environment **C** in Scheme 14) could potentially be related to the signal observed at δ_P = 173.7 ppm ($^2J_{PP}$ = 40 Hz), see Figure 55. The $^{31}P\{^1H\}$ NMR spectra in Figure 56 also suggests $[PF_6]^-$ anion decomposition occurs after heating in the presence of trace amounts of water to form $O{=}P(OH)F_2$ (-17.9 ppm, t, $^1J_{PF}$ = 963 Hz).[188]

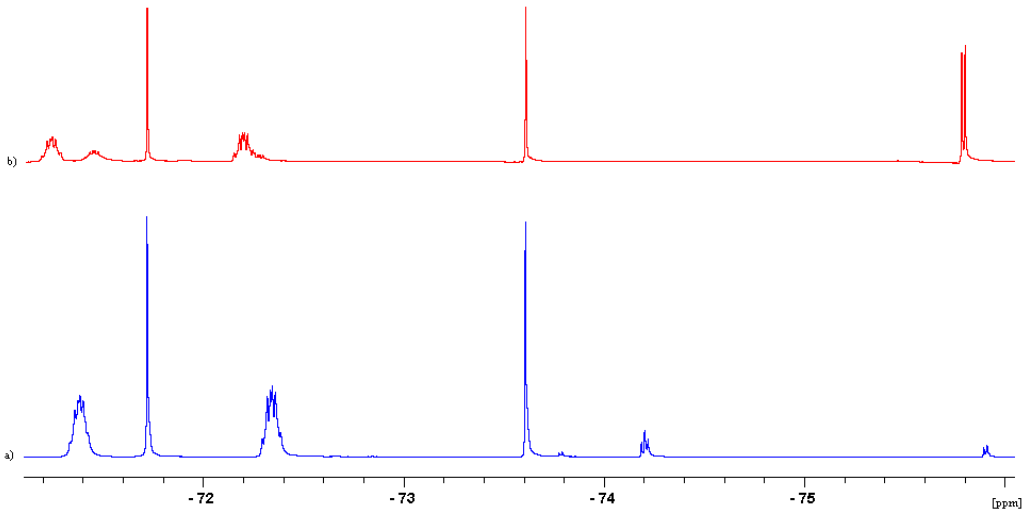

Figure 57: Overlay of ^{19}F NMR spectra of disubstituted ruthenium complex, bottom spectra: a) [Ru(5)-2] top spectra: b) reaction [Ru(5)-2] with phenylacetylene.

The ^{19}F NMR spectrum of **[Ru(5)-2]** (Figure 57 in spectrum a) shows a large doublet at 72.63 ppm ($^1J_{FP}$ = 717 Hz) for the $[PF_6]^-$ and two multiplets for the inequivalent CF_3 groups from the alkoxy groups at -71.38 and -72.34 ppm (both with $^4J_{FP}$ = *ca.* 5 Hz), presumably due to restricted rotation around the P-O bond at 298 K (anisotropy). After the addition of phenylacetylene and heating (7 days at 50 °C), a new set of multiplets of lower intensity are observed, see Figure 57, spectrum b). One of the multiplets is at similar chemical shift to that of **[Ru(5)-2]** at -72.25 ppm and the other is at -71.45 ppm. These new signals indicate a new metal-complex, likely to be species **E** in Scheme 14. In addition, a signal at δ_F = -75.80 ppm (d, $^4J_{FH}$ = 6 Hz) for the hexafluoroisopropanol and a signal for $O{=}P(OH)F_2$ (-83.33 ppm, d, $^1J_{FP}$ = 963 Hz) is observed.

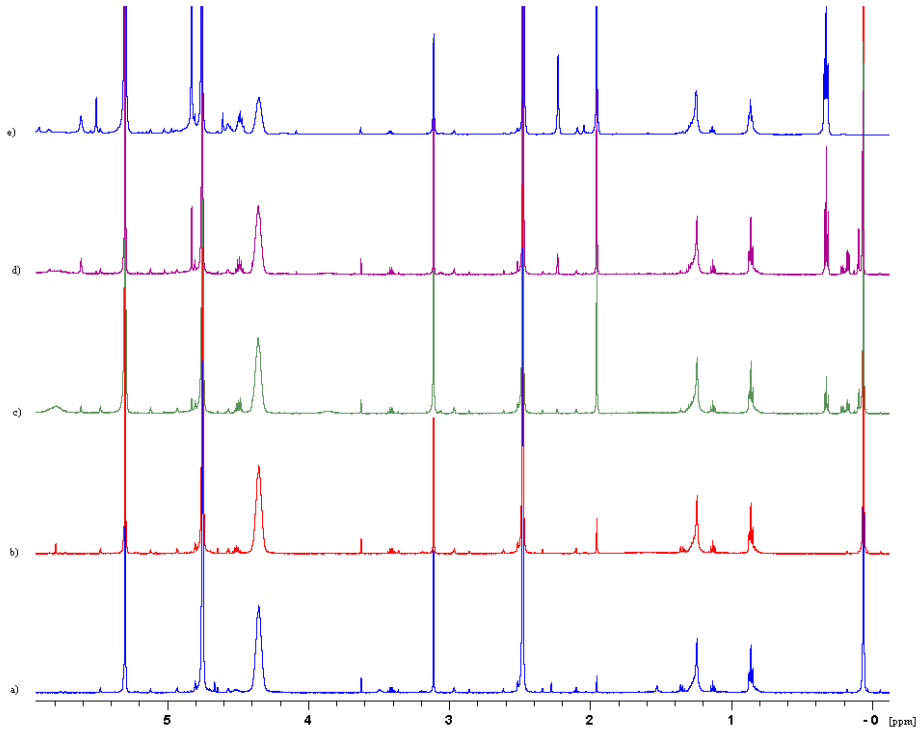

Figure 58: ^{1}H NMR spectra overlay of [Ru(5)-2] and phenylacetylene. NMR overlay; after 15 minutes of reactions, 1 day, then 1 day heated at 50 ˚C, 2 days heated at 50 ˚C and 7 days heated at 50 ˚C.

The ^{1}H NMR spectrum (see Figure 58) shows a signal at 2.46 ppm for the complexed acetonitrile ligand, but over time a peak at 1.97 ppm (s) grows in, which is likely to be free acetonitrile. The presence of free MeCN indicates that ligand substitution has taken place at the **[Ru(5)-2]** complex. Also a peak at 2.23 ppm (s) grows in, which is likely to be a new complex with acetonitrile bound as a ligand. The signal at 3.12 ppm (s) corresponds to the phenylacetylene terminal hydrogen, which reduces in intensity over time, indicating that transformation of the phenylacetylene must have taken place to form a new species related to the signals that grow in at 5.51 ppm (s), 5.62 ppm (s) and 0.3 ppm (t). In addition, a new signal at 4.57 ppm (m) is observed. This is likely to be a shift of the hydrogen atom of the hexafluoroisopropoxy group from the coordinated ligand (originally at 4.35 ppm) for the suggested species **E** in Scheme 14. A new signal at 4.84 ppm (s) is likely to be a new cyclopentadienyl environment (originally at 4.76 ppm) for the suggested species **E** in Scheme 14. Broad signals at 3.90 ppm and 5.80 ppm also grow in and disappears on further heating, see Figure 58, spectra c). Either of these may be the vinylidene proton resonance, related to the broad signal in the ^{31}P{^{1}H} NMR spectrum observed for species A (169.7 ppm, br), which also disappears on further heating.

A sample of this reaction mixture was analysed by GC-MS(EI), column: ZB5, 30 metres, 250 μm id, 0.25 μm film thickness; carrier gas (He) flow rate: 1ml/min; injector temperature: 280 ˚C; GC ramp: starting temperature 50˚C, ramped at 6 ˚C/min to 351 mins, run time 51 mins. Free $Ph_2P\{OCH(CF_3)_2\}$ ligand and many other ruthenium containing species *e.g.* ruthenocene, $[Ru(\eta^5\text{-}C_5H_5)_2]$ were detected. Most interestingly, there was evidence of a cyclotrimerization product, 1, 3 ,5 triphenyl benzene, see species **C** in Figure 61. This suggests the phenylacetylene is activated by a $[(\eta^5\text{-}C_5H_5)Ru(Ph_2P\{OCH(CF_3)_2\})_2]^+$ fragment and catalysis with the complex is possible. The scheme below describes a proposed mechanism found in the literature[189] for the formation of this cyclotrimerization organic product with a $[Ru(\eta^5\text{-}C_5Me_5)Cl]$ catalyst. This catalyst is formed as the additional cod (cod = 1, 5 cyclooctadiene) or triphenylphosphine ligands are cleaved prior to catalysis from the pre-catalysts $[Ru(\eta^5\text{-}C_5Me_5)Cl(cod)]$ and $[Ru(\eta^5\text{-}C_5Me_5)Cl(PPh_3)_2]$ respectively.[189] The terminal alkyne then coordinates *via* a η^2-fashion to give complexes I and II in Scheme 15. Complex II then rearranges to give a ruthenacyclopentatriene, of type III in Scheme 15. This reacts with additional terminal alkyne to give the aromatic [2+2+2] cyclisation products with regeneration of the $[Ru(\eta^5\text{-}C_5Me_5)Cl]$ catalyst. The mechanism has been investigated by computational studies, which agree with the proposed mechanism. Although, it should be noted that most the calculation were performed with the non-substituted ring, $[Ru(\eta^5\text{-}C_5H_5)Cl]$ catalyst.[190-193]

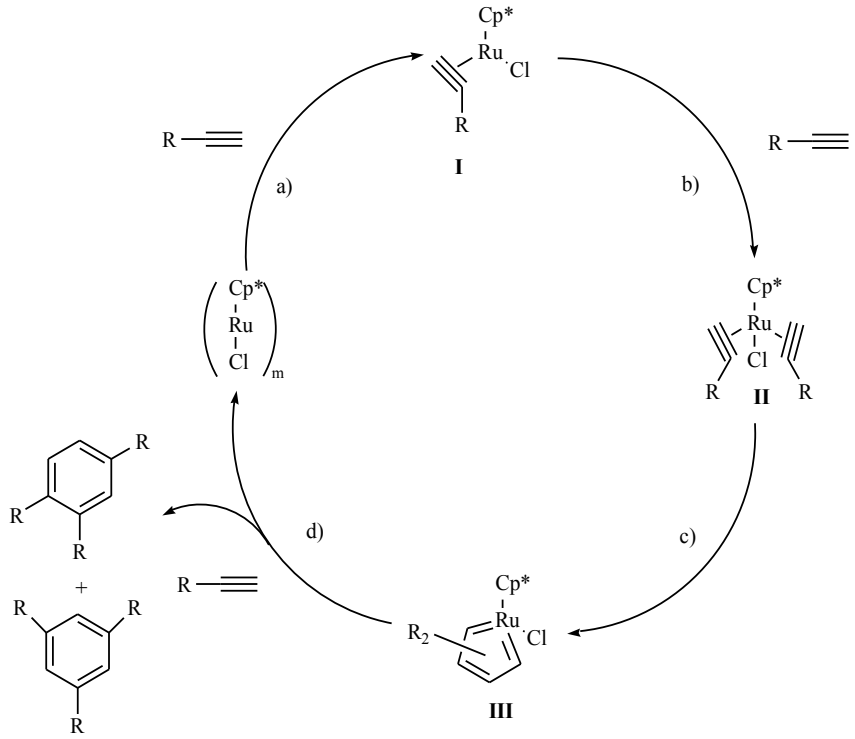

Scheme 15: The proposed mechanism for the cyclotrimerization of terminal alkynes in the presence of $[(\eta^5\text{-}C_5Me_5)RuCl]^+$ catalyst. Adapted from ref. [189].

In conclusion, the broad peaks observed in the $^{31}P\{^{1}H\}$ and ^{1}H NMR spectra suggests a vinylidene complex may have formed after heating this reaction mixture, since **[Ru(5)-2]** complex does not appear to activate the phenylacetylene at room temperature. This may be an effect of the reduced electron-density at the ruthenium metal centre due to the two coordinated $Ph_2P\{OCH(CF_3)_2\}$, (**5**) ligands. The formation of a vinylidene complex is consistent with the evidence from GC-MS(EI) for the cyclotrimerization organic product.

3.2.4 Reactivity of $[(\eta^5\text{-}C_5H_5)Ru(NCMe)_2(Ph_2P\{OCH(CF_3)_2\})]^+[PF_6]^-$, **[Ru(5)]**

The monosubstituted complex, $[(\eta^5\text{-}C_5H_5)Ru(NCMe)_2(Ph_2P\{OCH(CF_3)_2\})]^+[PF_6]^-$, **[Ru(5)]** contains two labile acetonitrile groups, therefore there are two potential alkyne coordination sites (as it provides the 14-electron $[(\eta^5\text{-}C_5H_5)Ru(Ph_2P\{OCH(CF_3)_2\})]^+$ fragment), and different electronic properties to that of the disubstituted **[Ru(5)-2]**; increased electron-density at the ruthenium metal centre. It was thought, that these properties would possibly assist the formation of a vinylidene complex and enhance the rate of the reaction.

The reaction of 1 eq. **[Ru(5)]** with 1 eq. phenylacetylene in DCM solvent (1 day of heating, 50 °C) showed the presence of a low intensity signal growing in at 169.8 ppm (s), in addition to a signal at 171.8 ppm (s) for **[Ru(5)]** and many peaks within the 55 to -30 ppm chemical shift range in the $^{31}P\{^{1}H\}$ NMR spectrum, see Figure 59.

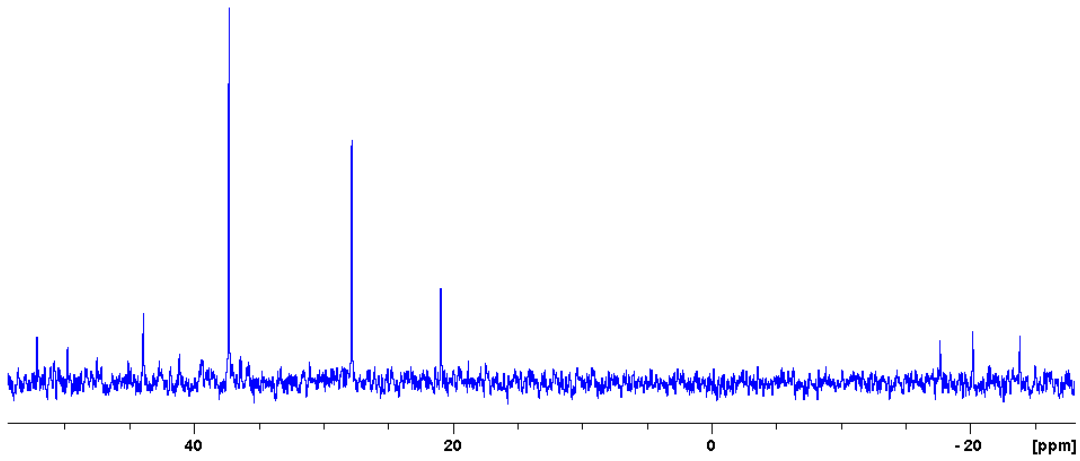

Figure 59: $^{31}P\{^{1}H\}$ NMR spectrum of [Ru(5)] and phenylacetylene after 1 day, heated at 50 °C. Many new signals within the 55 to -30 ppm chemical shift range are observed.

A sample of this reaction mixture was also analysed by GC-MS(EI) column: ZB5, 30 metres, 250 μm id, 0.25 μm film thickness; carrier gas (He) flow rate: 1ml/min; injector temperature: 280 ˚C; GC ramp: starting temperature 50 ˚C, ramped at 6 ˚C/min to 351 mins, run time 51 mins. This showed a mixture of alkyne oligomerisation products.

Cyclotrimerization[189] and cyclodimerization[194] of phenylacetylene had taken place, see Figure 61, product **C** and **A** respectively. The GC-MS(EI) data was also supported by the ^{1}H NMR spectrum, as many new species had grown in the aromatic region, see Figure 60 below.

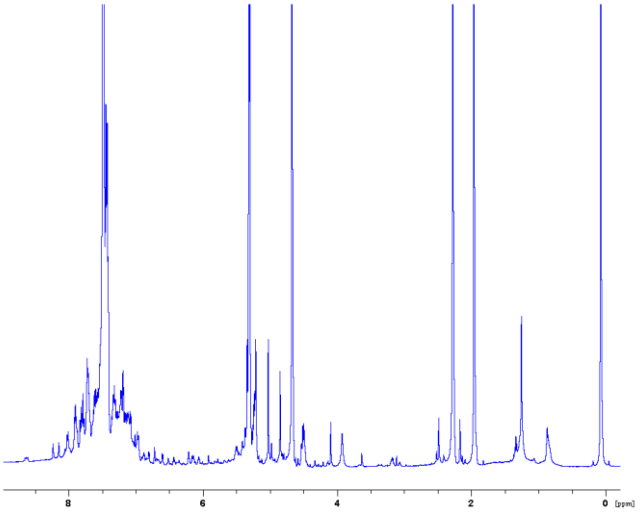

Figure 60: ^{1}H NMR spectra of [Ru(5)] with after phenylacetylene after 1 day, heated at 50 °C. Many new phenyl-containing species formed in the aromatic region at 7-8 ppm.

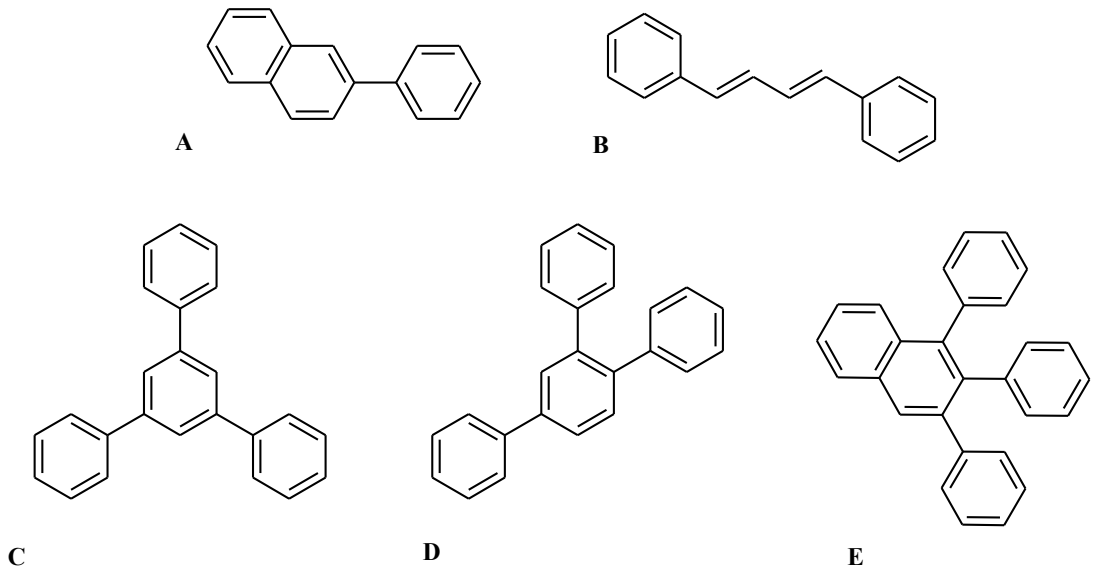

Figure 61: Identified organic species using GS-MS from the reaction of phenylacetylene and [Ru(5)] in DCM solvent.

Products **A**, **C** and **D** in Figure 61 {observed at 21.50, 33.20 and 30.70 minutes respectively by GC-MS(EI)} are relatively simple to rationalise as oligomerisation products, see Scheme 16 for a tentative mechanism for the synthesis of **A** in Figure 61. However, **B** and **E** proposed on the basis of MS ($[M]^{+}$) for GC signals at 22.20 and 33.50 minutes respectively,

are more difficult to explain, as they are not simple oligomerisation products. However, the observation of the organic products suggest $Ph_2P\{OCH(CF_3)_2\}$, (**5**) ligand can assist in the formation of a vinylidene species, provided there is sufficient electron-density and space around the ruthenium metal centre of the half-sandwich complex. Further work is required in this area to increase the selectivity of the catalytic products formed.

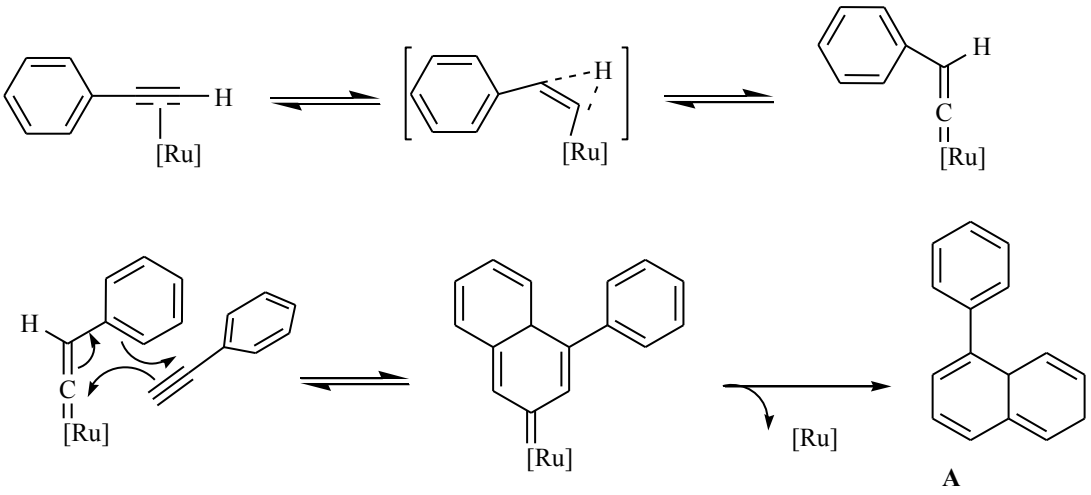

Scheme 16: A tentative mechanism for the catalytic reaction between two phenylacetylene molecules with a ruthenium precursor to give a species A type product. Adapted from ref. [194].

3.2.5 Reactivity of $[(\eta^5\text{-}C_5H_5)Ru(NCMe)_2P\{OC(CF_3)_3\}_3]^+[PF_6]^-$, **[Ru(2)]**

The **[Ru(2)]** complex was formed from reaction of ground $P\{OC(CF_3)_3\}_3$, (**2**) (2 eq.) with the $[(\eta^5\text{-}C_5H_5)Ru(NCMe)_3]^+[PF_6]^-$ precursor in DCM solvent (1 hr. ultrasonic activation). This new **[Ru(2)]** complex gave a peak at 117.1 ppm (s) in the $^{31}P\{^1H\}$ NMR spectrum. However, unreacted $P\{OC(CF_3)_3\}_3$, (**2**) was still present in the reaction mixture. Attempts to heat this reaction mixture overnight at 43 °C to react further with $P\{OC(CF_3)_3\}_3$, (**2**) caused the product peak of **[Ru(2)]** to diminish in the $^{31}P\{^1H\}$ NMR spectrum, as a new signal grew in at 120.7 ppm (d, J = 1252 Hz). ESI-MS indicated an intense peak, $[M]^+$ at 768.9 m/z, suggesting the presence of $[(\eta^5\text{-}C_5H_5)Ru(NCMe)_2(PF\{OC(CF_3)_3\}_2)]^+$. This is likely to be the new product in $^{31}P\{^1H\}$ NMR spectrum with strong P-F coupling. This seems to have formed due to exchange of the alkoxy groups of the **[Ru(2)]** complex with a fluoride from the $[PF_6]^-$ anion upon heating the reaction mixture, forming the $PF\{OC(CF_3)_3\}_2$ ligand, see Figure 62.

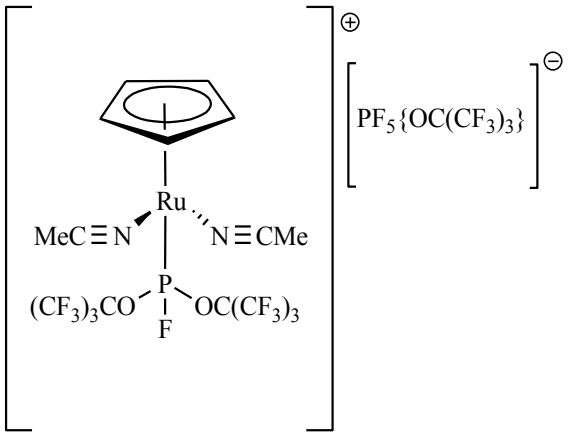

Figure 62: Proposed product formed *via* substitution of the fluorine atoms from the $[PF_6]^-$ anion with an alkoxy group on the $P\{OC(CF_3)_3\}_3$, (2) ligand.

The alkoxy group on the phosphorus-centre may have exchanged to reduce the steric bulk around the ruthenium complex. An ESI-MS spectra of the reaction mixture (in MeCN solution) has peaks at m/z of 576.9 and 360.9 in the negative mode, $[M]^-$ for $[PF_5\{OC(CF_3)_3\}]^-$ and $[PF_4\{OC(CF_3)_3\}_2]^-$ anions respectively. This suggests that fluoride-alkoxide exchange is taking place at the anion. The ^{19}F NMR spectrum shows a signal at -62.25 ppm (d, $^2J_{FP}$ = 746 Hz). This could be due to the four equivalent equatorial fluorine atoms on the $[PF_5\{OC(CF_3)_3\}_2]^-$ anion. This is split further into a doublet of doublets ($^2J_{FF}$ = 50 Hz) as the axial fluorine on the phosphorus is inequivalent due to the alkoxy group. These doublets of doublets are then coupled to the fluorine atoms in the alkoxy, $-OC(CF_3)_3$ groups splitting them into dectets ($^5J_{FF}$ = 6 Hz). However, due to inadequate signal to noise ratio, multiplets are observed rather than clear dectets, see Figure 63.

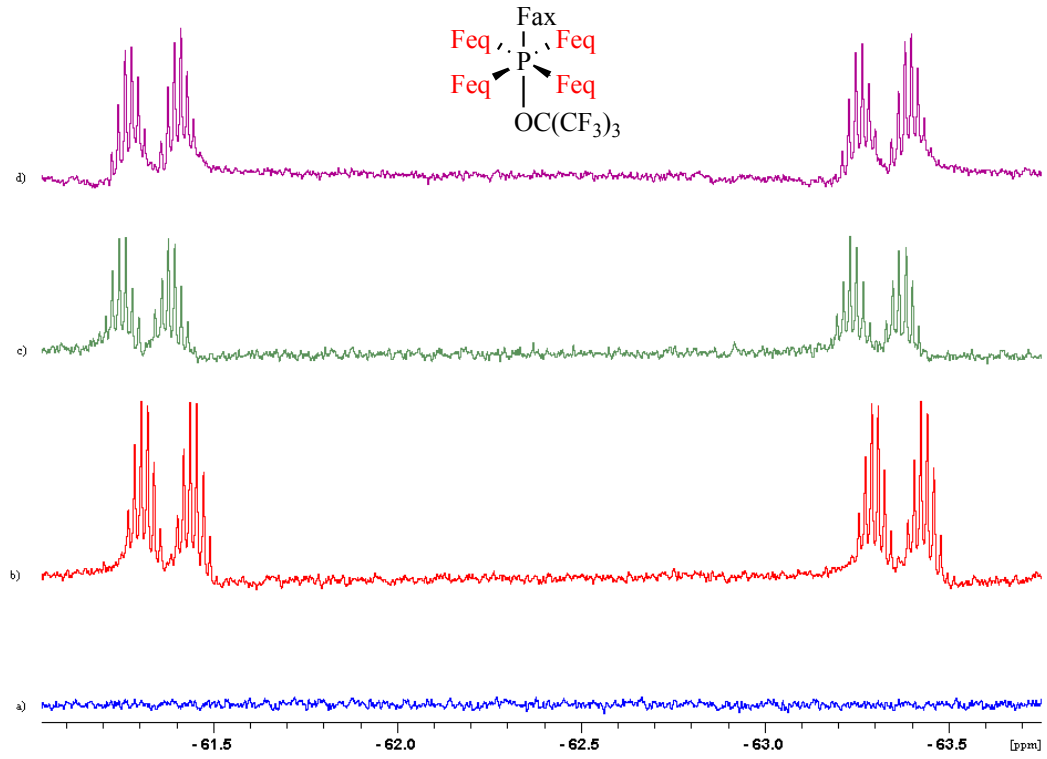

Figure 63: ^{19}F NMR spectra overlay of [Ru(2)] after heating. NMR overlay: a) after 15 minutes, b) three days, d) 1 day heated at 43 °C and after six hours heated at 47 °C. A doublet of doublet of dectets grows in for the equatorial fluorine atoms of $[PF_5\{OC(CF_3)_3\}_2]$,which forms due to ligand exchange.

The axial fluorine *trans* to the alkoxy group is coupled to the phosphorus centre ($^2J_{FP}$ = 700 Hz) and then to the four other fluorine atoms on the phosphorus centre ($^2J_{FF}$ = 50 Hz), forming a doublet of quintets. The signals for the axial fluorine should integrate to 1:4 to the doublet of doublet of dectets for the equatorial fluorine atoms. However, it was not possible to integrate the equatorial signals against the axial, as one of the axial quintets is hidden under the $[PF_6]^-$ signal, see Figure 64 below.

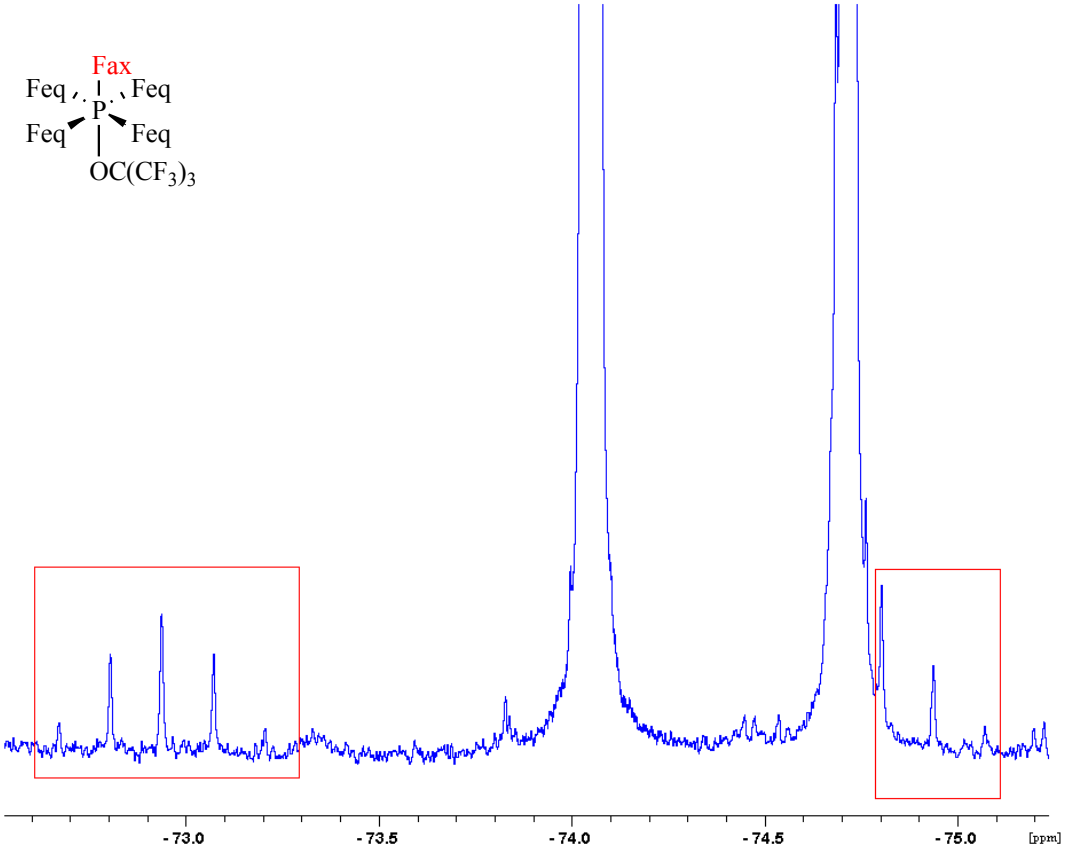

Figure 64: ^{19}F NMR spectrum of [Ru(2)] after heating, from bottom spectra to top: a) after 15 minutes, b) three days, d) 1 day heated at 43 °C and after six hours heated at 47 °C. A doublet of quintets grows in for the axial fluorine of $[PF_5\{OC(CF_3)_3\}_2]$,which forms due to ligand exchange.

3.3 PALLADIUM COMPLEXES

3.3.1 C-C Coupling Catalysis, The Heck-Mizoroki Reaction

In 2010, Professor Richard F. Heck, Professor Ei-ichi Negishi and Professor Akira Suzuki were all awarded the Nobel Prize in Chemistry for the development of methods for palladium catalysed formation of carbon-carbon bonds *via* cross-coupling reactions.[195-197] The palladium transition-metal complex is used to activate and assemble two organic molecules close in space *via* Pd-C bonds. This allows them to couple to one another and leads to the formation of a new carbon-carbon single bond. This discovery by the awarded organic chemists has had great impact on the development of new drugs,[198, 199] materials, natural product synthesis,[200, 201] agricultural chemicals and high technology materials that benefit society, as well as academic research in synthetic organic chemistry.

Palladium catalysed cross-coupling for C-C bond formation has advanced drastically with a range of palladium complexes with different ligands coordinated, which have been investigated as effective catalysts.[202] The Heck-Mizoroki reaction involves arylation of

alkenes. The catalytic cycle for the Heck-Mizoroki reaction can occur *via* either a cationic or neutral mechanistic pathway. Both consist of three fundamental steps; oxidative addition (**A** in Scheme 17), carbometallation, which proceeds through the formation of a π-complex (**B** in Scheme 17) and β-hydride elimination (**C** in Scheme 17).[202]

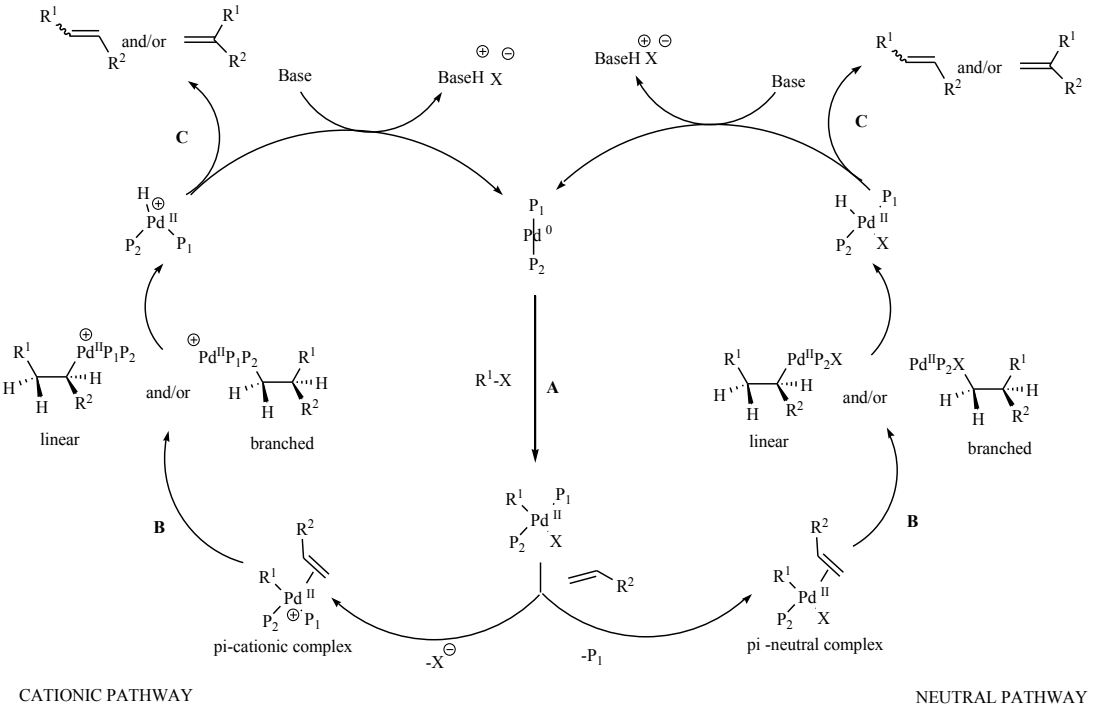

P_1 and P_2 = dippb, dipp, dippe, dppe, P(^{i}Pr)$_2$^{n}Bu, P(^{i}Pr)$_3$, PPh_3, P(^{t}Bu)$_3$, P(OTol)$_3$, P{OCH(CF_3)$_2$}$_3$, P($PC_6H_4CF_3$)$_3$, P($OC_6H_3{}^tBu_2$)$_3$.[202, 203]

R^1 = Ph, Ph_2CO, 4-Ph-(OHC), 4-Ph(CH_3), 4-$C_6H_4(NO_2)$.[203]

R^2 = Ph, Ph-(MeO), Ph(CH_3), Cy-(CH_3), Ph-(^{t}Bu)(CH_3), Ph-NH_2, CH_3-Ph-NH_2, CH_3O-Ph-NH_2, Cl-Ph-NH_2, NO_2-Ph-NH_2.[203, 204]

Scheme 17: Two mechanistic pathways for the catalytic Heck cycle; either the cationic pathway from loss of X^- or the neutral pathway from loss of ligand. Figure adapted from ref. [202].

The first step in the catalytic cycle is the oxidative addition of R^1-X, **A** in Scheme 17. The rate of the oxidative addition has been found to be sensitive to the nature of the R^1-X bond. The order of reactivity has been experimentally determined to be I > OTf > Br > Cl.[202] Traditionally electron-donating phosphorus (III) ligands are used, as these are thought to facilitate the oxidation addition step with the increased electron-density on the palladium metal centre. Electron-donating ligands tend to undergo a dissociation mechanism (discussed in the second step of the cycle); hence steric crowding is not an issue here. The second step,

B in Scheme 17, involves coordination of the alkene through its double bond on the Pd complex, forming a π-complex. The reaction conditions direct the exact mechanism. Dissociation of X leads to the cationic route and dissociation of a phosphine ligand leads to the neutral route (the most predominant route). Example of reaction conditions that proceed *via* the cationic route include those where X = OTf, as this has a weak Pd-OTf bond and can easily dissociate.[202] The presence of halide scavengers (*e.g.* Ag^+, Tl^+, or K^+) can also help direct this mechanistic route.[202] The *syn*-insertion of the complexed alkene in to the π-complex gives the σ-alkyl Pd(II) complexes. The R^1 group will either add to the β-carbon, yielding the linear product or add to the α-carbon, yielding the branched product. The regioselectivity of the product of this process depends on various factors, such as the nature of R^2, reaction conditions and the type of phosphine ligand used.[202] The last step involves a *syn*-β-hydride elimination, **C** in Scheme 17, yielding the organic product (may contain both regioisomers) and the hydridopalladium complex. Addition of a base can deprotonate this hydridopalladium complex after reductive elimination to regenerate the catalytically active $[Pd(0)L_2]$ species.[202] It should be noted that the cationic route gives rise to high levels of stereoselectivity as both ligands remain bound to the palladium metal centre.[202] The neutral pathway can suffer from reduced influence from the phosphine ligand. However, it should be highlighted that high levels of stereoselectivity has been observed with the neutral pathway in some exceptions that have been reported in literature.[202] In addition, the stereoelectronic properties of the ligands and substrates can also affect the enantioselectivity.

Rebecca Bibby, a JMS group 2010/2011 MChem student investigated the use of ligands (**2**) and (**5**) in the Heck-Mizoroki reaction. Bulky ligands are known to favor the reductive elimination step which give the organic product and the use of electron-poor ligands were thought to provide a different electronic influence on the catalytic cycle than those reported in literature. Investigations into the use of bidentate electron-poor phosphorus ligands for electron-rich olefins have already proved to be successful.[205] The Heck-Mizoroki reaction was studied using styrene as the alkene substrate and bromobenzene, 4-bromoanisole, 4-bromotoluene and 1-bromo-4-chlorobenzene as the aryl halide substrates, see Scheme 18. The four reactions were each carried out with a different ligand system; no added phosphorus ligand, PPh_3, $PPh_2\{OCH(CF_3)_2\}$, (**5**) and $P\{OC(CF_3)_3\}_3$, (**2**), hence a total of sixteen catalysis reactions were carried out, the product conversions of these are summarised in Table 23.

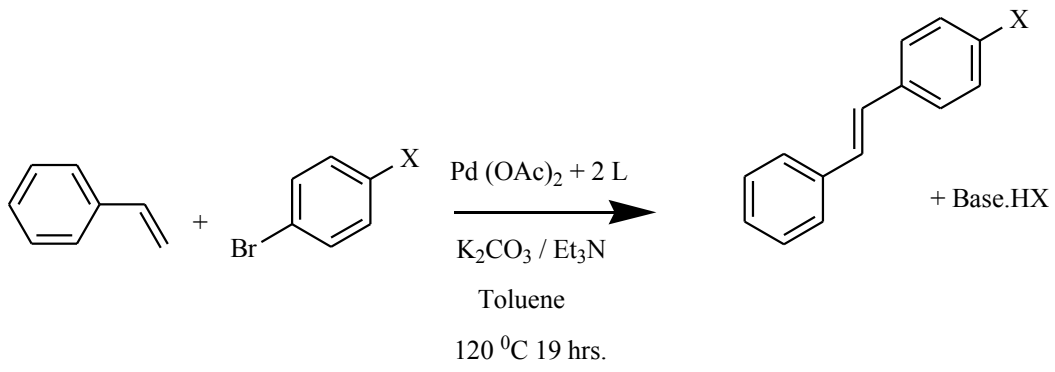

Scheme 18: Heck-Mizoroki reaction conditions, X = H, Me, OMe, Cl and L= PPh_3, $PPh_2OCH(CF_3)_2$, (5), $P\{OC(CF_3)_3\}_3$, (2) or no added ligand.

	Bromobenzene,	4-bromoanisole	4-bromotoluene	1-bromo-4-chlorobenzene
$Pd(OAc)_2$ Only	4 %	8 %	5 %	9 %
PPh_3	43 %	57 % *	30 %	23 % #
$PPh_2(OCH(CF_3)_2)$	48 %	41 %	68%	36 %
$P(OC(CF_3)_3)_3$	6 %	39 %	4%	24 %

Table 23: The Heck-Mizoroki reaction product percentage conversions to the alkene for the different ligand conditions (across the side) with different aryl halide substrates (across the top). These were calculated using GC-MS integrations. * = small amounts of stilbene and 1-methoxy-4-(1-phenyl-vinyl)-benzene present. # = small amounts of stilbene present.

In summary, the results showed that ligand $PPh_2\{OCH(CF_3)_2\}$, (**5**), consistently gave higher yields than a PPh_3 ligand, with the exception of the 4-bromoanisole case. Most interestingly, this $PPh_2\{OCH(CF_3)_2\}$, (**5**), ligand gave better selectivity *i.e.* fewer side products in all cases trialled, than that from a PPh_3 ligand. It may be likely that this is due to the increased bulk on the ligand $PPh_2\{OCH(CF_3)_2\}$, (**5**), compared to PPh_3, hence the dissociation of the ligand before the oxidative addition is much faster as the release of steric strain makes its thermodynamically more favorable. Difficulty of solubility of the solid sample used for $P\{OC(CF_3)_3\}_3$, (**2**), observed in all cases suggest no real conclusions can be made on the effectiveness of this ligand in this type of catalysis. Further work with this ligand is clearly required, where a range of solvents other than toluene is trialled, or the ligand is prepared in a specific solvent and used *in situ* while it is in solution. This study contradicts claims that the Heck-Mizoroki reaction is most efficient without the use of added phosphorus (III) ligands, as shown by the product percentage conversions for the $[Pd(OAc)_2]$ only case in Table 23.[206] However, it should be noted the change in conditions such as a different solvent and base from those reported in literature can be a cause of the observed results. The highest conversion is observed for the 4-bromotoluene aryl halide and $PPh_2\{OCH(CF_3)_2\}$, (**5**),

ligand. This suggests that the oxidative addition step is not the rate determining step, as if this was true then an electron-donating group like –Me in 4-bromotoluene would push electron-density into the conjugated system, see Scheme 19. This would presumably then allow the electronegative bromine atom to pull this electron-density towards itself, thus forming a stronger Ar-Br bond and deactivating it towards the oxidative addition step.

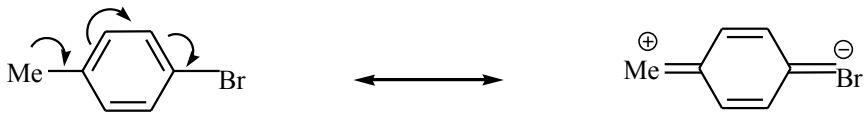

Scheme 19: Resonance form of 4-bromotoluene.

3.3.2 Pd(dba)L_2 NMR Studies

Coordination complexes of the form [Pd^0L_2] (where L = phosphine ligand) with alkenes[207, 208] or alkynes[209, 208] are well studied reagents found in palladium catalysed Heck, Sonogashira and Stille coupling processes.[17, 210] The active catalytic species found in these systems is the "low ligand moiety", [Pd^0L_2].[211] The kinetics of the first step of the catalytic cycle; the oxidative addition of aryl halides, has been found to be affected by the presence of such alkenes/alkynes. Complexation of the reactive [Pd^0L_2] to form unreactive [$Pd^0L_2(\eta^2$-alkene)]/[$Pd^0L_2(\eta^2$-alkyne)] results in slower oxidative additions as it decreases the concentration of the active catalyst, [Pd^0L_2]. Focusing on alkene complexes, [$Pd^0{}_2(dba)_3$] or [$Pd^0(dba)_2$] (dba = *trans*, *trans*-dibenzylidene-acetone) are often used as sources of Pd^0 complexes in many palladium catalysed reactions (*i.e.* Heck, Stille *etc.*). Amatore, Jutand *et al.* established that dba was a 'non-innocent' ligand in these types of systems.[211] Addition of two equivalents of the phosphine ligand does not simply result in the formation of the active catalyst, [Pd^0L_2] alone, as initially assumed, see Scheme 20.[211]

$$Pd(dba)_2 + 2\ L \longrightarrow PdL_2 + 2\ dba$$

Scheme 20: The dba ligand was initially thought to be an innocent ligand and lead to the active palladium catalyst.

It was initially believed that dba was a more weakly coordinating ligand than a phosphine, and hence should be easily displaced to give the active catalyst, [Pd^0L_2] in stoichiometric amounts.[211] This method was seen as advantageous as it uses [$Pd^0{}_2(dba)_3$] or [$Pd^0(dba)_2$]. Both are air stable complexes, hence easier to handle than the typical [$Pd^0(PPh_3)_4$] catalyst.[211] In addition, since only two equivalents of the phosphine, PPh_3 were required, this would be beneficial when using expensive chiral phosphine ligands *in situ*. Amatore, Jutand *et al.* identified that the process in Scheme 20 was oversimplified, since [$Pd^0(PPh_3)_4$]

appeared to be a more efficient catalyst when compared to four equivalents of phosphine, PPh_3 with $[Pd^0(dba)_2]$ and in some cases even more reactive than two equivalents of PPh_3 with $[Pd^0(dba)_2]$.[211] They found that almost six to eight equivalents of PPh_3 were required (dependent on the solvent), before the dba completely dissociated, suggesting this method is not so advantageous when using expensive phosphines.[211] However, it was concluded that in terms of reactivity of the oxidative addition, both systems proceed through the same [S-Pd^0L_2] (where S = solvent) intermediate. Any change in reactivity observed was due to dba being a stronger coordinating ligand than PPh_3 for the [S-Pd^0L_2] moiety, causing a decrease in the steady state concentrations of the active catalyst.[211] This contradicted the initial beliefs that dba was a weaker ligand than a phosphine and suggests dba acts as a 'non-innocent' ligand in these type of systems.[211] Fairlamb *et al.* later reported that the efficiency of palladium catalysed cross-coupling reactions can be affected by the electronic properties of the dba-Z ligand (where Z = substituents on the phenyl rings of the dba ligand), see Figure 65.[212]

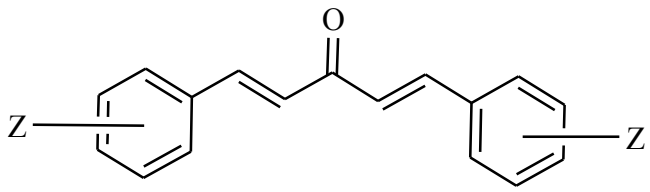

Z = CF_3, Br, Cl, F, H, Me, OMe,

Figure 65: A substituted dba ligand with a range of electron-donating or electron-withdrawing groups.

Fairlamb *et al.* found that electron-rich dba-z (*i.e.* substituted by electron-donating z groups) ligands favour high yields of cross-coupled product.[212] This was later found to be due to a decrease in dba affinity for [S-Pd^0L_2] species, when dba is electron-rich in comparison to π-acidic dba when electron-withdrawing z groups are present.[213, 214] The electron-rich dba leads to faster oxidative addition leading to increased catalytic activity. An alternative method for increasing the concentration of the active catalyst, $[Pd^0L_2]$ while using $[Pd^0{}_2(dba)_3]$ as the palladium source could prove to be successful if one was to focus on tuning the electronic properties of the coordinated phosphorus (III) ligands (L). Moderate π-acidic phosphorus (III) ligands, such as ligands (**3**) to (**6**) could be sufficiently σ-donating to coordinate to the palladium metal centre, but also sufficiently π-acidic to reduce the electron-density at the Pd^0 centre. This in turn could reduce the electron-density available for the dba ligand, and weaken the strength of the Pd-(η^2-dba) bond. This may be advantageous in the catalytic reaction, as it may increase the steady state concentrations of [S-Pd^0L_2] species, allowing for an increased rate of the oxidative addition.

Successful complexation of $PPh_2\{OCH(CF_3)_2\}$, (**5**) and $PPh\{OCH(CF_3)_2\}_2$, (**3**), two of the least π-acidic ligands of the series to a $[Pd_2(dba)_3]$ precursor was achieved in DCM solvent at room temperature. This was confirmed by $^{31}P\{^1H\}$ NMR spectra as peaks were observed for **[Pd(5)-2]** and **[Pd(2)-2]** at 150.8, 179.1 ppm respectively. LIFDI-MS of the correct mass for $[Pd(dba)L_2]$, $[M]^+$ was found for **[Pd(3)-2]** and **[Pd(5)-2]**. Although the reaction of $PPh_2\{OC(CF_3)_3\}$, (**6**) and $[Pd_2(dba)_3]$ was also trialled, the $^{31}P\{^1H\}$ NMR spectra were slightly complicated as many peaks were observed, making it difficult to identify **[Pd(6)-2]**. However, LIFDI-MS, $[M]^+$ confirmed that **[Pd(6)-2]** was present in the reaction mixture. Reaction with the $PPh\{OC(CF_3)_3\}_2$, (**4**) ligand did not lead to a new complex peak in the $^{31}P\{^1H\}$ NMR spectrum, only starting material was present. Presumably this ligand is simply not sufficiently σ-donating to coordinate to the palladium centre. The ^1H NMR spectra contain broad signals for the protons of the coordinated dba C=C bond and the non-coordinated C=C bond, which are superimposed by the aromatic protons of the dba and the phosphorus (III) ligand.[215] This broadening is due to several dynamic processes, such as rotational isomerism; exchange of the coordinated and the non-coordinated alkene ligands and rotation around the Pd-alkene axis; changing the face of coordination of the alkene, see Scheme 21.[215] In addition, some even believe that the metal can switch between coordinating the alkene carbon atoms and the oxygen atom of the ketone group.[216]

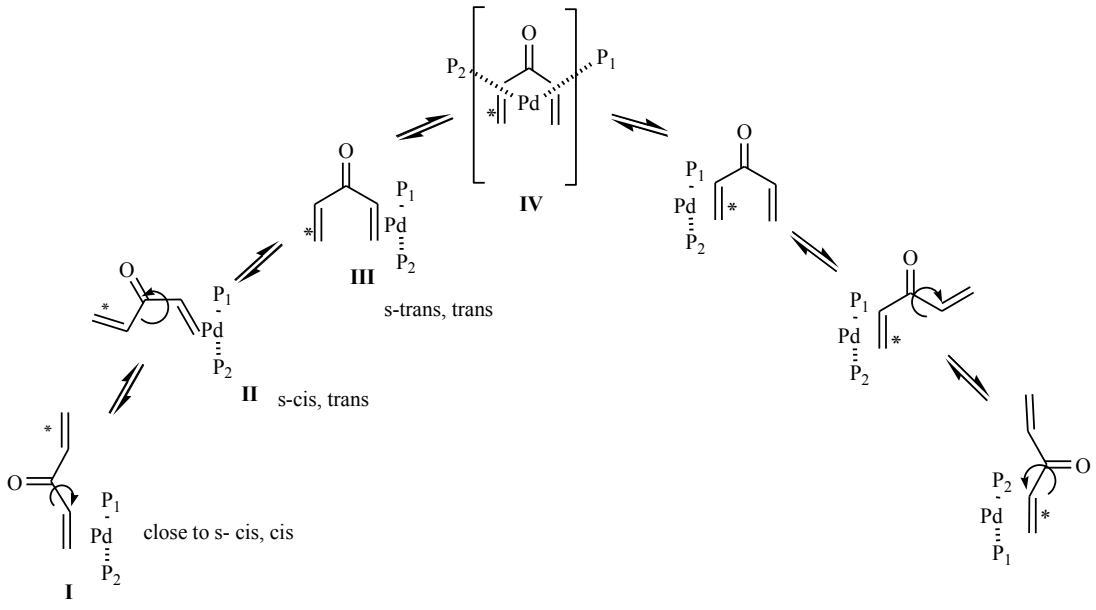

Scheme 21: Proposed intramolecular exchange of coordinated and uncoordinated double bonds of dba ligand (phenyl groups have been omitted for clarity). Adapted from ref. [217].

Most interestingly, the $^{31}P\{^1H\}$ NMR spectra for **[Pd(3)-2]** and **[Pd(5)-2]** are different to that observed for standard phosphine ligands (*e.g.* PPh_3) that have been investigated in the literature.[212-214] $[Pd(PPh_3)_2(dba)]$ shows two inequivalent phosphorus environments in the $^{31}P\{^1H\}$ NMR spectrum in dimethylformamide solvent, one for each PPh_3 bound ligand.

This is due to the unsymmetrically bound dba ligand which does not freely rotate on the NMR timescale. A strong Pd-dba bond is formed in this complex (as with other phosphines investigated in literature), due to the σ-donating properties of a PPh_3 ligand increasing the electron-density on the palladium metal centre. This allows for more available electron-density on the metal centre for π-back-bonding to the dba ligand. The increased metal-dba π-interaction reduces the extent of dba rotation and/or exchange (both inter- and intra-molecular). However, in the case of **[Pd(3)-2]** and **[Pd(5)-2]** only one $^{31}P\{^{1}H\}$ NMR environment is observed for the two ligands. This can be explained by the difference in the electronic properties of these ligands in comparison to phosphines; $PPh_2OCH(CF_3)_2$, (**5**) and $PPh\{OCH(CF_3)_2\}_2$, (**3**) are significantly more π-acidic and less σ-donating than a PPh_3 ligand. The π-acidic ligands tend to withdraw electron-density from the palladium metal centre and reduce the extent of back-bonding to the dba double bond, resulting in a weaker Pd-dba bond. This weaker Pd-dba bond is more prone to faster rotation and/or exchange of the dba, hence the two phosphorus environments of the bound π-acidic ligands appear to be equivalent on the NMR time scale at room temperature, see Scheme 22 and Figure 66 below.

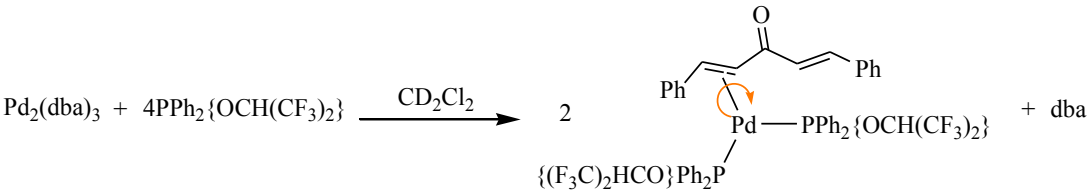

Scheme 22: Depicts that the presence of the π-acidic ligand, (5) at the Pd centre of [Pd(5)-2]. These reduce the electron-density, resulting in faster rotation around the dba-Pd bond.

In addition to dba rotation and/or exchange, the complexed phosphorus ligands can also exchange with free phosphorus ligands present in solution. The electronic properties of the phosphorus (III) ligand are crucial for the rate of the exchange processes. Variable temperature NMR studies (250-370 K) have been run on the **[Pd(5)-2]** and the $[Pd(PPh_3)_2(dba)]$ systems to allow for comparisons to be made.

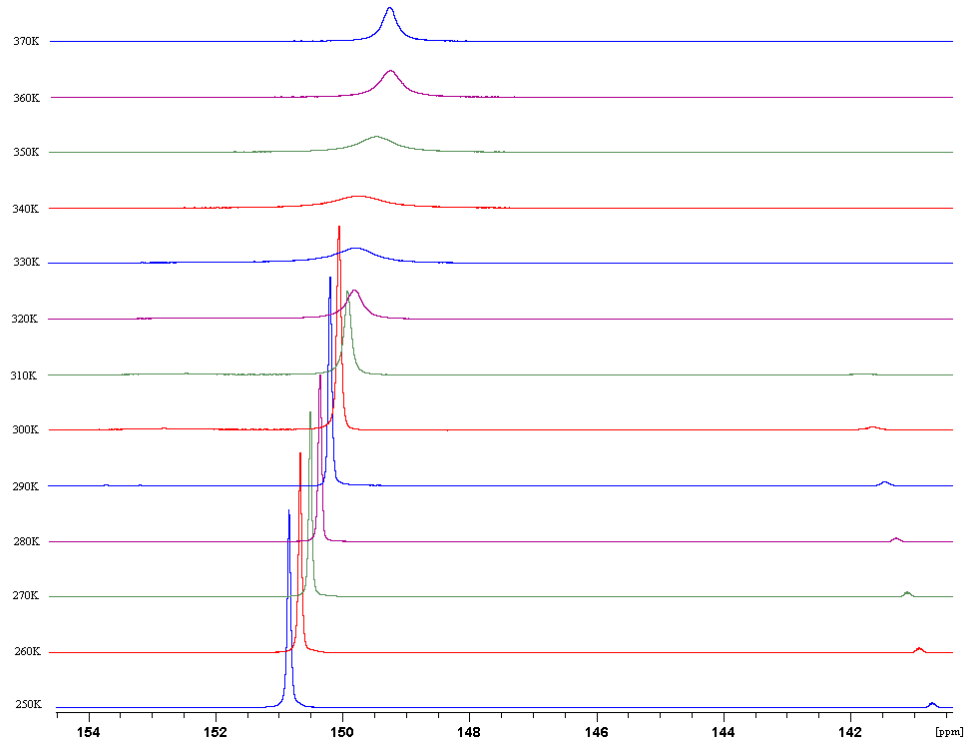

Figure 66: Overlay of the spectra from the variable temperature $^{31}P\{^{1}H\}$ NMR study over a 250-370 K temperature range for the [Pd(5)-2] system.

The $^{31}P\{^{1}H\}$ NMR spectra overlay from 250-370 K in Figure 66 shows coalescence of the free ligand signal (higher field) with the **[Pd(5)-2]** complex signal (lower field) at 330 K. The energy barrier for ligand exchange can be calculated using Equation 12, see below.

$$\Delta G^{\ddagger} \text{ (Jmol}^{-1}) = RT_c[22.96+\ln(T_c/\sigma v)]$$

Equation 12: Calculation of the energy barrier for ligand exchange, $\Delta G^{\ddagger}$ (Jmol^{-1}). R = 8.314 (Jmol^{-1}) T_c = temperature of coalescence (K), σv = the difference in frequency for the separated signals (Hz).

The $^{31}P\{^{1}H\}$ NMR spectra overlay (from 250-370 K) for the $[Pd(PPh_3)_2(dba)]$ complex in Figure 67 indicates that initially coalescence of the two signals for the complexed ligands occurs at 330 K ($\Delta G^{\ddagger 330}$ = 62 kJ mol^{-1}, 14.8 kcal mol^{-1}) due to dba ligand rotation/exchange.

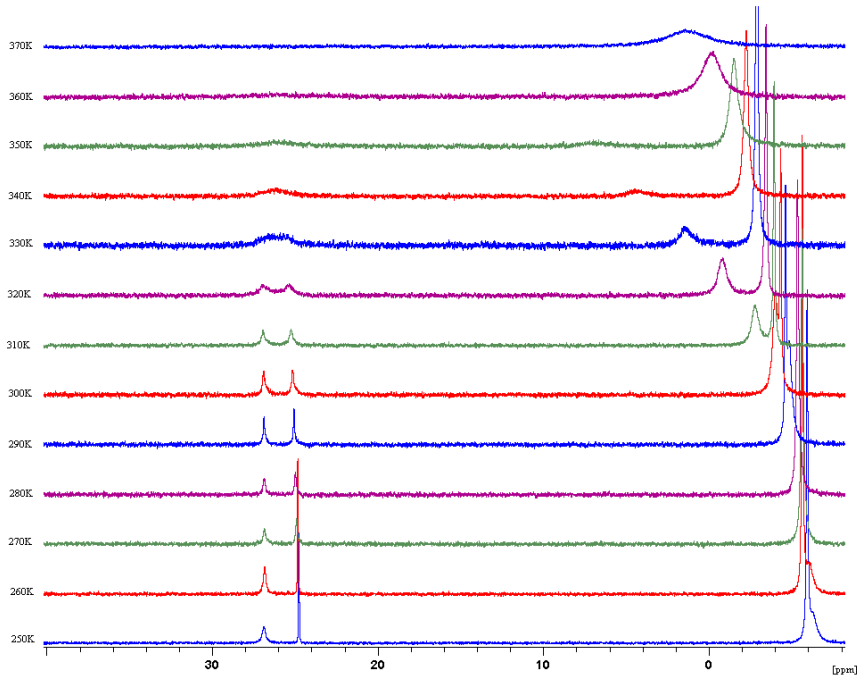

Figure 67: Overlay of the spectra from the variable temperature $^{31}P\{^{1}H\}$ NMR study over a 250-370 K temperature range for the $[Pd\{PPh_3\}_2(dba)]$ system.

Coalescence of the free PPh_3 ligand and the $[Pd(PPh_3)_2(dba)]$ follows this at 360 K ($\Delta G^{\ddagger 360}$ = 60 kJ mol^{-1}, 14.3 kcal mol^{-1}) due to phosphine exchange. Figure 67 shows that one of the complexed PPh_3 ligand signals is much sharper, hence there is preferential exchange between one of the coordinated PPh_3 ligands with free PPh_3 in solution. Furthermore, there is an additional broad peak near the chemical shift of the free PPh_3 ligand, observed more clearly at 310 K. This may be a signal for a weakly bound encounter complex as show in Figure 68.

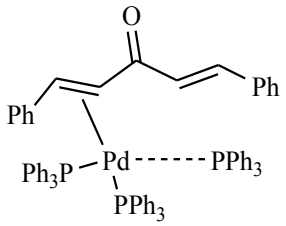

Figure 68: Schematic of a weakly bound PPh_3 ligand

The energy barrier for ligand exchange for the **[Pd(5)-2]** system ($\Delta G^{\ddagger 330}$ = 58 kJ mol^{-1}, 13.9 kcal mol^{-1}) can be compared to the $[Pd(PPh_3)_2(dba)]$ system ($\Delta G^{\ddagger 360}$ = 60 kJ mol^{-1}, 14.3 kcal mol^{-1}), discussed in detail below. DFT calculations at the (RI)BP86/SV(P)//(RI)PBE0/def2-TZVPP level, with a pseudo relativistic ECP's at palladium were performed in order to assist with the discussion of these observed activation parameters. The DFT calculations were carried out by John Cottom, the JMS group 2011/2012 Masters student. The calculations suggest that both systems undergo phosphorus (III) ligand exchange *via* a dissociative

pathway, hence the $\Delta S^{\ddagger}$ has a positive sign due to increased disorder on dissociation. The associative pathway was discarded, as a transition state was unattainable due to the steric crowding at the palladium metal centre, see Scheme 23.

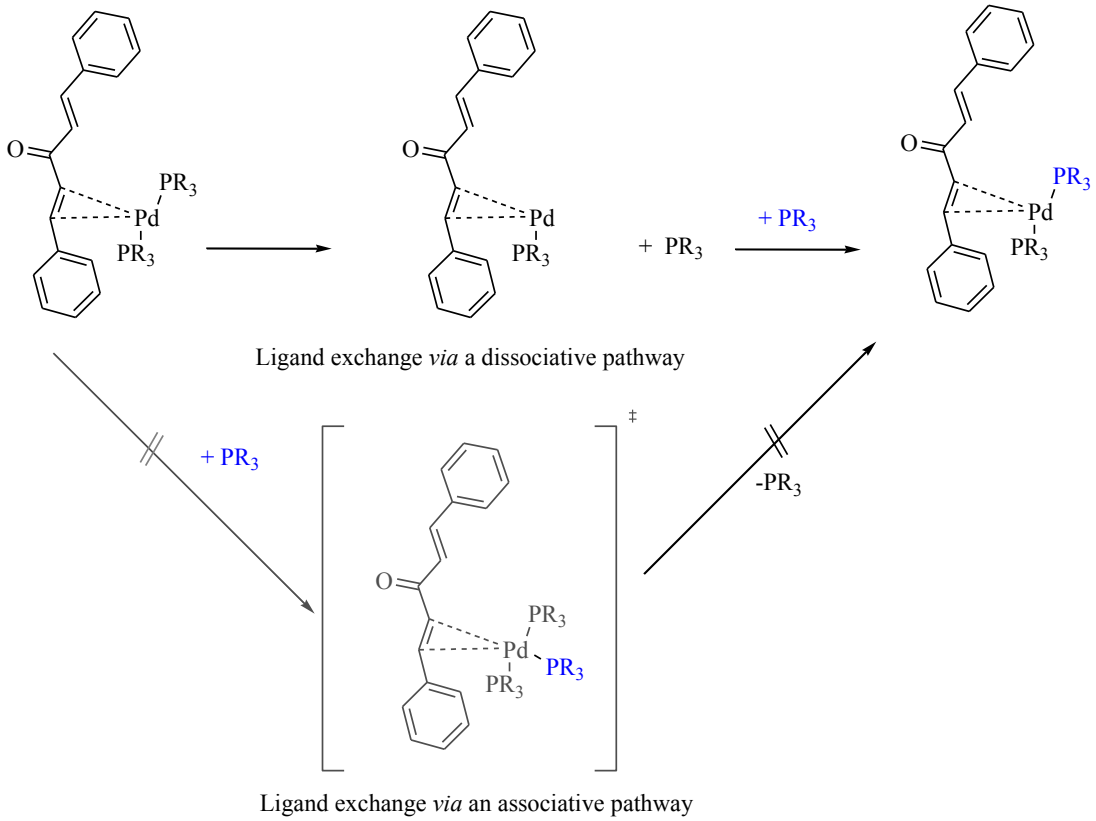

Scheme 23: The dissociative pathway seems to be preferred over the associative reaction pathway for the exchange of the coordinated phosphorus (III) ligand (PR_3) with excess free ligand in the reaction mixture.

Although the energy barrier for ligand exchange ($\Delta G^{\ddagger}$) for both systems considered are of similar magnitude, they are calculated at different temperatures. The **[Pd(5)-2]** system coalesces at a lower temperature than the $[Pd(PPh_3)_2(dba)]$ system. As stated above $\Delta S^{\ddagger}$ is positive, hence an assumption is made that it is similar in magnitude for both systems; **[Pd(5)-2]** and $[Pd(PPh_3)_2(dba)]$. Taking this into account, along with the different $\Delta G^{\ddagger}$ temperatures, this indicates that the $\Delta H^{\ddagger}$ for ligand exchange for the **[Pd(5)-2]** system is less positive than that found for the $[Pd(PPh_3)_2(dba)]$ system. This is consistent with the DFT calculations for the loss of a ligand L (L = PPh_3, $PPh_2OCH(CF_3)_2$}) on a $[Pd(L)_2(dba)]$ system {the calculated $\Delta H^{\ddagger}$ for [Pd(L)(dba)] + L relative to $[Pd(L)_2(dba)]$ is; 85 kJ mol^{-1} for L = $PPh_2OCH(CF_3)_2$ and 93 kJ mol^{-1} for L = PPh_3}. The less positive $\Delta H^{\ddagger}$ found for the **[Pd(5)-2]** system suggests that in this case the reduced σ-donor ability of (**5**) compared to PPh_3 results in a weaker M-P bond that is more easily broken. In addition, it may be possible that the greater extent of π-back-bonding present between the Pd-$PPh_2OCH(CF_3)_2$ bond as well as the Pd-dba bond could reduce the electron density at the palladium centre, allowing

for the greater stability of [Pd{$PPh_2OCH(CF_3)_2$}(dba)]. This highlights the different in electronic properties between the two systems, as a result of the two different ligands coordinated. It should be noted that the steric influence of the ligands may also play a significant role in stabilising the systems *i.e.* the bulkier ligand (**5**), requires less energy for complete dissociation due to this being sterically favourable for the system.

The $^{31}P\{^1H\}$ variable temperature NMR spectra (250-370 K) for the [$Pd(PPh_3)_2$(dba)] system indicate exchange of free and coordinated phosphorus ligands takes place preferentially at one position, see Figure 69. The broader peak found for the lower field complexed PPh_3 ligand environment in Figure 67 is due to preferential exchange of this coordinated ligand with free PPh_3. The phosphorus (III) ligand **A** in Figure 69 is near the η^2-bound dba substituent, whilst the phosphorus (III) ligand **B** in Figure 69 is near the majority of the bulk from the dba ligand.

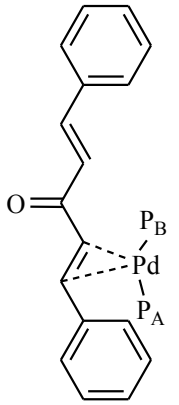

Figure 69: [$Pd(P)_2$(dba] system with the two different phosphorus environments labeled; A = near the η^2-bound dba substituent, B = near the majority of the bulk from the dba ligand.

The steric repulsion between this ligand **B** in Figure 69 and the dba favours loss of this ligand over ligand **A** in Figure 69. For this reason, preferential exchange is observed for ligand **B** in Figure 69; hence the higher field chemical shift value (26.90 ppm, br) at 250 K is broader. The lower field chemical shift (24.28 ppm, d, $^2J_{PP}$ = 7 Hz) for the other coordinated PPh_3 ligand is much sharper at 250 K due to loss of this ligand in environment **A** being less favourable, hence the slower rate of exchange of this ligand with free phosphine. Since the [$Pd(PPh_2OCH(CF_3)_2\}$(dba)] complex consists of one signal in the $^{31}P\{^1H\}$ NMR spectrum, even at 250 K, the preferential exchange is difficult to observe.

3.4 SUMMARY AND FUTURE WORK

The crystal structure of **[Rh(6)-2]** was compared to that of known structures containing monodentate phosphorus (III) ligands with a similar diphenyl-moiety in the CSD. The Rh-P bond lengths of **[Rh(6)-2]** are very short in comparison to others known, providing useful evidence that this perfluorinated alkoxy group greatly enhances the π-acidity of the phosphorus ligand. The ν_{CO} stretching frequencies and $^{1}J_{RhP}$ coupling constant of **[Rh(2)-2]**, **[Rh(4)-2]** and **[Rh(6)-2]** were compared to literature known rhodium complexes. These were found to be incredibly π-acidic, consistent with the DFT calculations from Chapter 2.

All six ligands (**1**) to (**6**) were also successfully coordinated to a ruthenium metal centre, by reaction with $[Ru(\eta^5\text{-}C_5H_5)(NCMe)_3]^+[PF_6]^-$. The majority of these were successfully characterised by single-crystal X-ray diffraction studies and gave useful structural information. As discussed in Chapter 2, cone angle calculations were of great benefit to appreciate the steric influence of these π-acidic ligands. Further investigation into their Ru-P bond lengths provided useful information on the strength of the bonds and the extent of their π-acidic character in comparison to similar structures found in the CSD. In general, it was found that the greater the number of alkoxy groups on the phosphorus centre and the greater extent of fluorination on the alkoxy group, then the more π-acidic the ligand. However, it should be highlighted that the perfluorinated phosphite, $P\{OC(CF_3)_3\}_3$, (**2**) complex has a reduced orbital overlap which results from the greater steric bulk. This hinders a close approach of ligand to metal and reduces its π-acidity in comparison to $P\{OCH(CF_3)_2\}_3$, (**1**).

The sub-stoichiometric reactivity of some of these novel ruthenium complexes was probed with phenylacetylene in DCM solvent and analysed using NMR spectroscopy and GC-MS(EI). Interestingly, a mixture of alkyne oligomerisation products; cyclotrimerization and cyclodimerization of the phenylacetylene had taken place after heating. This indicates catalytic activity does occur with these novel ruthenium complexes, although future work needs to focus on the selectivity of the reaction. In addition, it was observed that heating **[Ru(2)]** to higher temperatures, led to alkoxide/fluoride exchange of the coordinated ligand and the $[PF_6]^-$ anion.

Preliminary catalytic investigation into the use of (**2**), (**5**) ligands in the Pd-catalysed Heck-Mizoroki reaction found that (**5**) gave higher yields than PPh_3, for most substrates. Most interestingly, $PPh_2\{OCH(CF_3)_2\}$, (**5**), gave better selectivity *i.e.* fewer side products in all cases trialled, than in the case of PPh_3. This may be due to the increased bulk on the ligand $PPh_2\{OCH(CF_3)_2\}$, (**5**), compared to PPh_3, hence dissociation of the ligand before oxidative addition of the substrates is much faster as the release of steric strain makes its

thermodynamically more favorable. Further work with this ligand is clearly required, where a range of solvents other than toluene is trialled.

Successful complexation of $PPh_2\{OCH(CF_3)_2\}$, (**5**), $PPh\{OCH(CF_3)_2\}_2$, (**3**) and $PPh_2\{OC(CF_3)_3\}$, (**6**) to a $[Pd_2(dba)_3]$ precursor in DCM solvent gave $[Pd(dba)L_2]$ type species. This was confirmed by $^{31}P\{^1H\}$ NMR spectroscopy and LIFDI-MS. Most interestingly, the $^{31}P\{^1H\}$ NMR spectra for these type of species are found to be different to that of standard phosphine (*e.g.* PPh_3) ligands investigated in the literature.[212-214] Only one $^{31}P\{^1H\}$ NMR environment is observed for the two bound ligands. This can be explained by their difference in the electronic properties in comparison to common phosphines; $PPh_2OCH(CF_3)_2$, (**5**), $PPh\{OCH(CF_3)_2\}_2$, (**3**) and $PPh_2OC(CF_3)_3$, (**6**) are more π-acidic and less σ-donating than a PPh_3 ligand. The π-acidic ligands tend to withdraw electron-density from the palladium metal centre and reduce the extent of back-bonding to dba, resulting in a weaker Pd-dba bond. This weaker bond is more prone to faster rotation and/or exchange of the dba, hence the two phosphorus environments of the bound π-acidic ligands appear to be equivalent on an NMR time scale at room temperature. In addition to dba rotation or/and exchange, the complexed phosphorus ligands can also exchange with free phosphorus ligand in solution. The electronic properties of the phosphorus (III) ligand are crucial for the rate of the exchange processes. Variable temperature NMR studies (250-370 K) have been performed on the $[Pd(PPh_2\{OCH(CF_3)_2\})_2(dba)]$ system and comparisons have been with the $[Pd(PPh_3)_2(dba)]$ system. DFT calculations at the (RI)BP86/SV(P)//(RI)PBE0/def2-TZVPP level suggest that both systems undergo phosphorus (III) ligand exchange *via* a dissociative pathway. The energy barriers for ligand exchange ($\Delta G^{\ddagger}$) were calculated using the coalescence temperature values and it was found that the $\Delta H^{\ddagger}$ for the $[Pd\{PPh_2OCH(CF_3)_2\}_2(dba)]$ system is lower than that for the $[Pd(PPh_3)_2(dba)]$ system, which is consistent with the DFT calculations. This highlights the effects on similar systems with ligands of different steric and electronic nature.

This chapter has provided useful data to support the steric and electron properties discussed in Chapter 2. Evidently the metal complexes with the ligands (**1**) to (**6**) are simple to prepare and support the potential use of such ligands in catalysis. Further work in the use of these ligands in cross coupling reactions is required, as the results from the Heck-Mizoroki reaction show promising results with increased selectivity with the use of these bulky, electron-poor ligands. Future studies on the use of these ligands in hydroformylation reactions and others that specifically require bulky, electron-poor ligands for high turnover rates, as discussed in Chapter 2 would also be of key interest.

4 IN SEARCH OF PERFLUORINATED WEAKLY COORDINATING CATIONS

4.1 LITERATURE REVIEW OF WEAKLY COORDINATING CATIONS

4.1.1 Weakly Coordinating Cations Designed for Ionic Liquids

The development of weakly coordinating cations (WCCs) can be categorised into two main areas. These include "traditional" organic WCCs, which have been of particular interest in recent years due to their use in the preparation of ionic liquids (ILs), and perhaps the less commonly encountered WCCs, designed for their stability in basic conditions.

Alkylammonium, 1, 3- dialkylimidazolium, alkyltriazolium, alkylpyridinium and alkylphosphonium cations are the main class of organic cations used for ILs, see Figure 70.

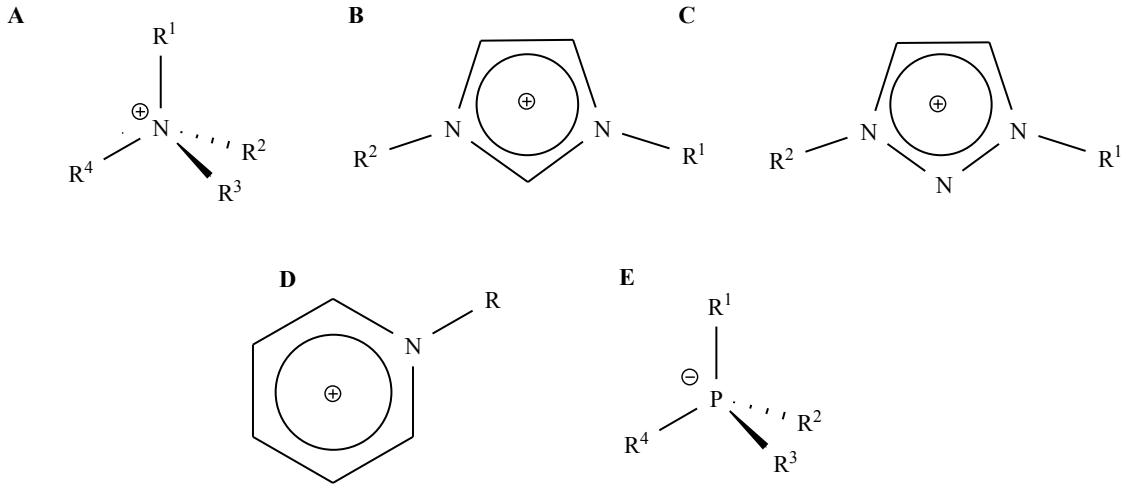

Figure 70: Organic WCCs used in the preparation of ILs. A: alkylammonium, B: 1, 3- dialkylimidazolium, C: alkyltriazolium, D: alkylpyridinium and E: alkylphosphonium cations.

These bulky asymmetric cations preclude good crystal packing when combined with anions where there is considerable delocalisation of charge over the molecular backbone, as this tends to decrease interionic interaction. Krossing *et al.* have used simple quantum chemical calculations based on lattice and solvation energies, in combination with a minimum of experimental data to understand why ILs favour the liquid state unlike the known classical salts.[218] Volume Based Thermodynamics and quantum chemical calculations are used to estimate the lattice free energies ($\Delta_{latt}G$).[218] The free energies of solvation ($\Delta_{solv}G$) of each ion in the bulk molten salts were also estimated using the COSMO solvation model and

experimentally determined dielectric constants.[218] These are used in the Born-Fajans-Harber cycle for the free energy of fusion to be calculated ($\Delta_{fus}G$) for a number of salts under standard ambient conditions, see Equation 13 and Figure 71.[218]

$$\Delta_{fus}G^{298K} = \Delta_{fus}H^{298K} - T\Delta_{fus}S^{298K}$$

Equation 13: The Gibbs free energy of the thermodynamic process of fusion.

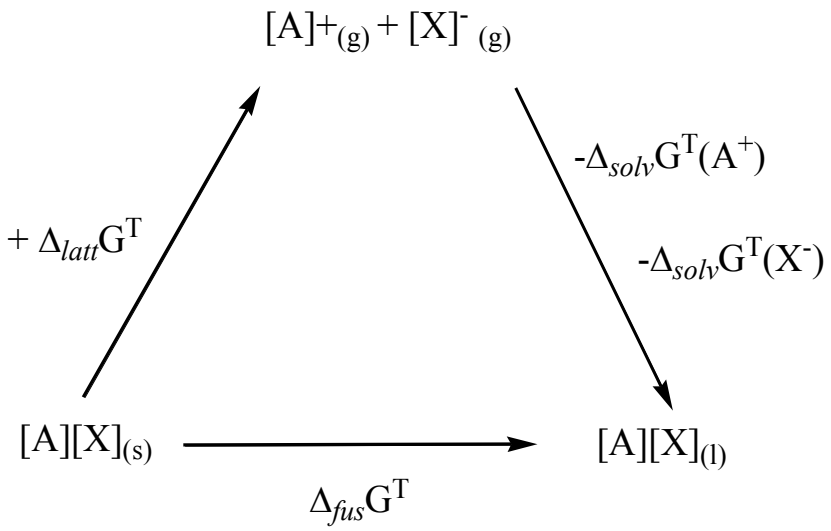

Figure 71: Born-Fajans-Haber cycle for the assessment of the melting (fusion) of a binary salt composed of complex ions ([A][X]), at temperature T, from lattice and solvation energies. Adapted from ref. [218].

All of the IL systems considered were estimated to have negative $\Delta_{fus}G°$ values, indicating that the liquid state is thermodynamically favourable under these conditions.[218] Krossing *et al.* presume these effects to be a result of the large size of the ions and their weakly coordinating nature which leads to small lattice enthalpies.[218] In addition, the conformational flexibility of the ions (particularly the cations) lead to large entropy changes, which favour the liquid state.[218]

Lengthening the alkyl chains on these cations can increase the hydrophobicity and viscosity of ILs. These can act as a handle to fine tune the ILs as, rather than simple fluids, they can be better understood as self organised phases. These phases consist of aggregated nonpolar and charged domains (almost surfactant-like) that form a dynamic network.[219] The different structural cations are useful in different ways, offering unique physical and chemical properties to the IL such as; solubility of organic and inorganic compounds, high ionic conductivity, high thermal stability and low flammability *etc*. As ILs may potentially become the new 'designer solvents', it is vital to fully understand the properties that the particular ions add to the ILs. Below a few of the identified properties of some of these organic WCCs are discussed to give an insight into how changing the cations can enhance the functionality of the IL.

Major room temperature ionic liquids (RTILs), used for electrochemical devices such as lithium batteries, include alkylammonium cation derivatives.[220] These have also been shown to be useful for neat lubricants or additives.[220] Features such as negligible volatility, flame retardancy, high thermal stability and better 'intrinsic performance' make them attractive for these functions.[220] Due to the better 'intrinsic performance' certain additives that are required to enhance performance of 'conventional lubricant formulations' can be avoided. These include avoiding additives such as; detergents (as ILs act like solvents), defoamers (as ILs' have ultra low vapour pressure) and anti-oxidants, (ILs' have high thermal stability in air).[220]

Studies have been carried out on the correlation between the molecular structures of alkylammonium and 1, 3- dialkylimidazolium cations and their physical properties. These include properties such as viscosity, thermal stability and wettability. Although it was found that 1, 3-dialkylimidazolium-based ILs outperformed the reference oils, their overall composition made them unsuitable as lubricants.[220] These 1, 3-dialkylimidazolium-based ILs were too viscous for most applications.[220] The alkylammonium ILs had the correct physical properties and the correct viscosities, the best candidate being $[(C_8H_{17})_3NH]^+[N(SO_2CF_3)_2]^-$.[220] In addition, studies showed that when mixed with mineral oils, the ILs showed reduced wear than that for either the base oil or neat IL.[220] This advocates the potential of ILs as lubricant additives. Their flexible molecular structures can guide future studies on tailoring application-orientated IL-based lubricants or additives.

4.1.2 Quaternary Phosphonium Cations Used for Ionic Liquids

Recent research has shown that the quaternary phosphonium cations used for ILs have remarkable features, allowing them to be chemically and thermally very stable. Initial research on phosphonium cations for ILs was based on large cationic structures, designed using tri-n-hexyl phosphine $(C_6H_{13})_3P$ derivatives.[6, 7] Due to their large molecular weights they tend to have high viscosities. However, low viscosity is a major requirement for electrochemical applications as this influences the ionic conductivity and mass transfer of solutes and mixtures.[221] Attempts were made to prepare RTILs based on quaternary phosphonium cations derived from tri-n-butylphosphine, P^nBu_3 with a variety of anions.[222] It was found that a combination of the phosphonium cations and a *bis*(trifluoromethanesulfonyl)imide, $[N(SO_2CF_3)_2]^-$ anion gave RTILs with low viscosity and thermal stablility.[222] However, the viscosity was still too high for electrochemical use. This led to investigations of the smaller phosphonium cations, in the hope of achieving lower viscosities. Quaternary phosphonium cations derived from triethylphosphine, PEt_3 paired

with the $[N(SO_2CF_3)_2]^-$ anion, along with phosphonium cations containing methoxylalkyl groups as well as straight chain alkyl groups, were employed.[221] Introducing alkoxy groups on the quaternary ammonium cations reduces both the melting point and the viscosity of the RTILs, using $[N(SO_2CF_3)_2]^-$ as the appropriate anion.[223-225] Although the effects of introducing a methoxy group on the phosphonium ion are not clarified fully, it can be explained similarly to that for the ammonium RTILs. It is thought that the electron donation from the methoxy group to the centred cationic nitrogen atom (N-O-Me) causes a decrease in the positive charge on the nitrogen cation. Hence, the electrostatic interaction between the cation and anion is weakened, resulting in a reduced melting point and lower viscosity for the RTILs.[223] Although symmetrical cations tend to have higher melting points than the unsymmetrical cations, the introduction of a methoxy group (R_3P-O-Me) lowers the melting point even if symmetrical groups are attached.[221] The introduction of methoxy groups on the phosphonium cations have established a new class of RTILs, which are lower in viscosity compared to the ammonium RTILs and can potentially be used as battery electrolytes, especially because of their non-flammable nature making them more durable and safer as electrolytic media.[226, 227] These methoxy-containing phosphonium cations have many properties that make them versatile cations, which can be exploited for many future applications. However, there is still room for more improvements in finding lower viscosity RTILs, an area where fluorinated phosphonium salts may be of use. Fluorinated ILs have recently been used as novel media for the generation of superhydrophobic coatings, but their full potential is yet to be fully explored.[8]

4.1.3 Weakly Coordinating Cations Designed for Their Stability in Basic Conditions

In contrast to those WCCs extensively studied in the applications of ILs, not much development has taken place in the last 10-20 years to develop the stability of WCCs in basic conditions. This is mainly due to conventional organic cations having limited base resistance (see common mechanisms for basic degradation in Scheme 24). The big exceptions are aminosulfonium, $[S(NR_2)_3]^+$, aminophosphonium, $[P(NR_2)_4]^+$ (R = Me, cyclohexane) and the poly-phosphazenium ions, *e.g.* $[P\{N{=}P(NR_2)_3\}_4]^+$.[228-232] These can be classed as "salts containing delocalised lipophilic cations", which are of high interest due to their stability and high performance in phase-transfer organic reactions. These type of reactions are run at high temperatures, often under strongly basic media, and in the presence of strong nucleophiles.[233] These type of WCCs even allow the formation of salts with unsolvated fluoride anions to yield the best approximation of "naked fluorides" possible and

probably the strongest stable metal-free bases known to date.[231, 234, 235] The aminosulfonium salts ($[S(NR_2)_3]^+$; R = alkyl chain of 1 to 20 carbons and each alkyl group has at least two α-hydrogen atoms) of the $[F_2Si(CH_3)_3]^-$ anion are highly soluble in organic solvents and have been useful for the synthesis of perfluorinated carbanions from perfluorinated alkenes.[228] The perfluorinated carbanions can form perfluoroalkyl halides on reaction with halogens and are even known as useful intermediates in the synthesis of fluorine-containing compounds. These fluorine-containing compounds have many commercial applications *e.g.* industrial solvents, dielectric and hydraulic fluids, pharmaceutical products, polymerization catalysts *etc*.[228] Perfluorinated alkoxides and perfluoroalkyl-mercaptides can also be synthesised in a similar manner using the carbonyl or thioepoxide compounds with $[S(NR_2)_3]^+[F_2Si(CH_3)_3]^-$ salts.[229] These are useful alternatives to the metal-salts as they are more soluble in organic solvents and are thermally stable *e.g.* $[CF_3O]^-[S\{N(CH_3)_2\}_3]^+$ is stable up to its melting point of 213 °C.[228,229]

Salts containing "delocalised lipophilic cations",[233] include species that contain C-N-P^+, C-N-S^+ and S-N-P^+ cationic backbones, all fully substituted with dialkyamino groups (NR_2), see Figure 72.[236] These salts are useful catalysts for solid-liquid phase-transfer halogen exchange with KF and chloroaromatic substrates. This process can be used on an industrial scale for the synthesis of selectively fluorinated aromatics, as these cations are more soluble in aprotic solvents in comparison to the metal-fluorides alone, even at elevated temperatures. The use of these cations as catalysts provides high fluorination rates and avoids the formation of by-products due to high temperatures. They have even been linked to the treatment of cancer, as these fluorinated organic species (synthesised from the use of the cations), are known to target the mitochondria of carcinoma cells, offering an effective treatment method.[233] The described cationic backbones consist of phosphoroaniminyl and guanidyl substituents, which are more electron donating than the NR_2 moiety,[230] thus reducing the electrophilicity of the centre atom which increases the stability of the onium salt under basic conditions.

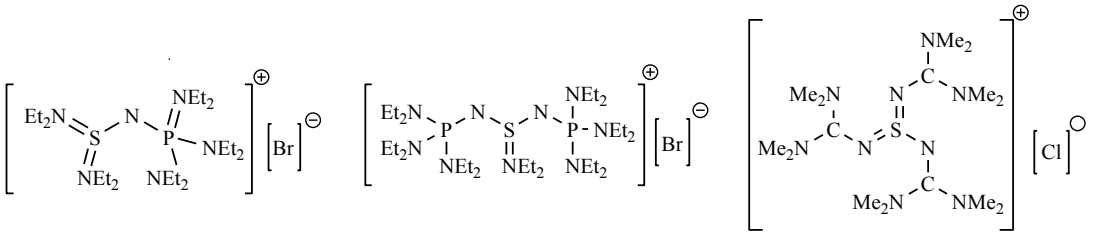

Figure 72: Cations containing C-N-S$^+$ and S-N-P$^+$ backbones, all fully substituted with dialkyamino groups (NR_2). Adapted from ref. [236].

Schwesinger *et al*.[231] describe the synthesis of a series of peralkylated polyaminophosphazenium cations. These exhibited amazing base resistance under phase-transfer conditions. This feature overcomes the limitations of instability of conventional organic cations used for catalysis, and the limited lipophilicity of resistant (metal) counterions. Research has been carried out to identify and develop phosphazenium cations with maximum base resistance. Alterations on the nature of the alkyl substituents on the nitrogen and the size of the conjugated system allowed a range of new potential structural designs for these WCCs, see Figure 73.[231]

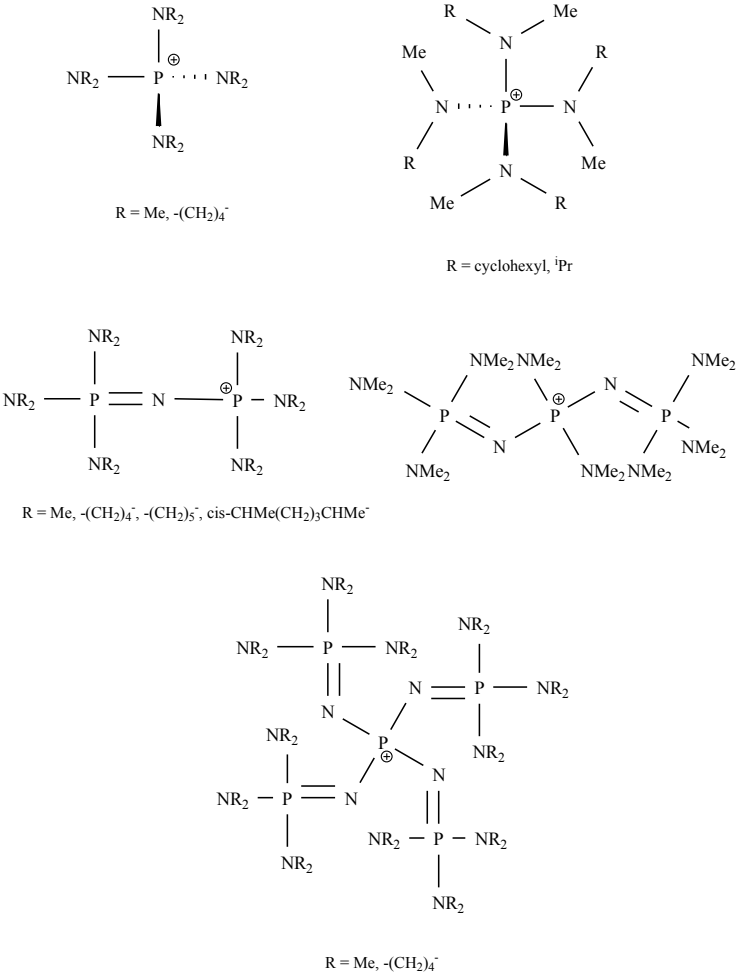

Figure 73: Phosphazenium ions of varying size with a range of alky groups. Adapted from ref. [231].

Schwesinger *et al.*[231] recognized that, in order to maximise the base resistance on the novel phosphazenium cations, it was essential to understand the potential paths of decay. Four paths are observed for tetrakis(dialkylamino) phosphonium ions, which can be related to most of the other phosphazenium ions and many other organic cations such as $[NR_4]^+$, see Scheme 24.

These are:

1) Hofmann degradation
2) Nucleophilic substitution on (alkyl-) carbon
3) β-Elimination with formation of an imine and a phosphorus acid amide
4) Hydrolysis by attack of hydroxide at the phosphorus atom (nucleophilic addition dependent on steric shielding at the phosphorus for other phosphazenium ions)

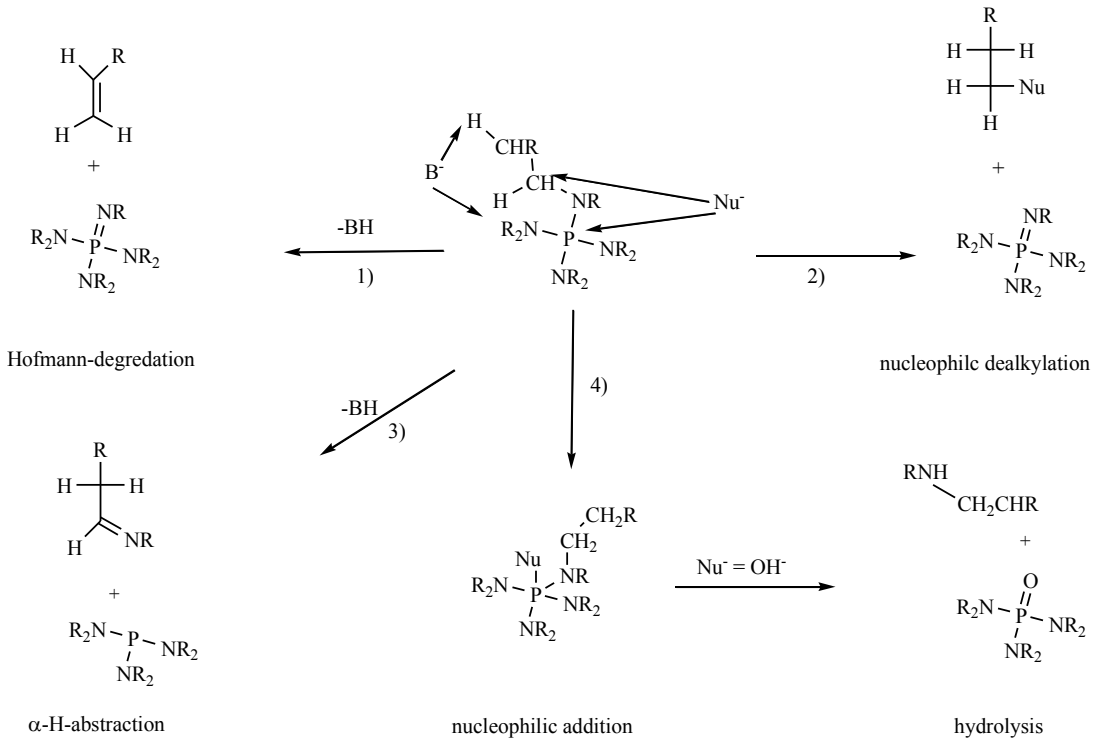

Scheme 24: Modes of decay of tetrakis(dialkylamino)phosphonium cations, paths 1-4. Adapted from ref. [231].

Stabilities of the phosphazenium cations were evaluated under phase transfer conditions by determining their half lives as chloride salts in the 50 % NaOH/50 % chlorobenzene system at 100 °C.[231] Increasing the basicity of the phosphazene *via* substitution of the amino groups for more electron donating nitrogen containing groups (*e.g.* pyrollidinyl) improves the stability of the cations by enhancing the resonance. Conclusions from this work suggested

that the phosphazenium cations were great WCCs offering several advantages as counter ions in reactions with strongly basic and/or strongly nucleophilic anions.[231] This ability to avoid decomposition *via* nucleophilic attack allows for high anionic (*i.e.* fluoride anion, F^-) reactivity. This is due to reduced interaction between the phosphazenium cations and the counter anion, making the anion more available. This is useful for catalysis where anionic sources are required for synthesis. However, these cations are still susceptible to deprotonation by strong bases, particularly by attack at the C-H bonds. In addition, the phosphazenium cations potentially exhibit dermal toxicity due to traces of hexaalkylphosphoramide.[232]

The search for alternative cationic designs without heavily relying on large high molecular weight dendritic networks for the delocalisation of the positive charge, led Lyapkalo *et al*. to study cations with the positive charge within an aromatic system, to impart additional stability and base resistance.[232] This aromaticity along with the "appropriately positioned donor substituent(s)" would provide efficient delocalisation of the positive charge, whilst bulky alky groups would offer the steric protection and avoid nucleophilic cleavage. This results in cations with high thermal stability.[232] These ideas were explored using imidazolium-type structures, see Figure 74.[232]

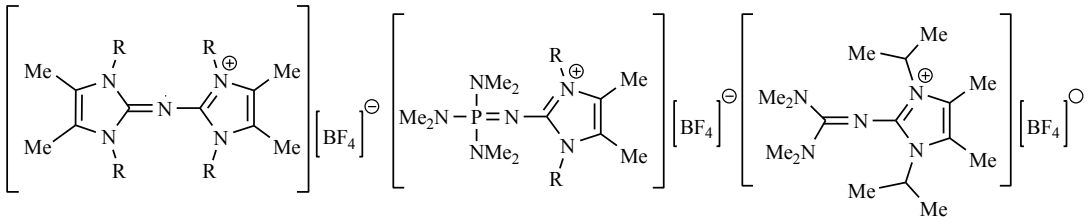

Figure 74: Imidazolium-type lipophilc cations, designed for phase-transfer applications, under drastic conditions; basic/nucleophilic media and high temperature. Adapted from ref. [232].

The imidazolium salts shown above in Figure 74 are stable and readily soluble in polar organic solvents.[232] Susceptibility to Hofmann degradation is strongly diminished due to the low charge density on the endocyclic nitrogen atoms or may be completely precluded, as in the case of the tetraneopentyl substituted cation **1**.[232] Cations **1** and **2** both show similar stabilities to that of the described P_5-phosphazenium cations by Schwesinger *et al.*[231] These imidazolium cations may potentially be combined with highly basic anions, specifically fluorides, alcoholates, and enolates to form useful new salts.

A literature search indicates that base-resistant cations and those that form ILs are currently available. However, there are few cations existing that are both base resistant and can form IL phases. Investigations into the synthesis of these types of cations, along with their physical and chemical reactivity were of key interest for this thesis. In particular, the use of highly fluorinated alkoxy substituents on phosphonium based cations. It was thought that these would not undergo decomposition *via* the common decay pathway; C-H activation. In addition, the bulky fluorinated alkoxy groups on the phosphonium centre would reduce the interionic interactions and hence be better for ILs. Fluorinated alkoxyphosphoranes were the main focus as they are simple to synthesise. These can act as scaffolds for the generation of these new fluorinated WCCs, designed with the potential to have the combined properties of current WCCs.

4.1.4 Non-Fluorinated Alkoxy-Phosphonium Ions

4.1.4.1 The Michaelis-Arbusov Reaction

The Michaelis-Arbusov reaction is one of the best known classical organophosphorus reactions. This is known for synthesis of a phosphonate {$OP(OR)_2R'$}, phosphinate {$OP(OR)R''R'$} or phosphine oxide ($OP(R'')_2R'$) from either the phosphite, $P(OR)_3$; phosphonite, $P(OR)_2R$; or phosphinite, $P(OR)R_2$, and alkyl halide ($R'X$) reactants.[237, 238] The general mechanistic details can be explained in two steps, see Scheme 25.

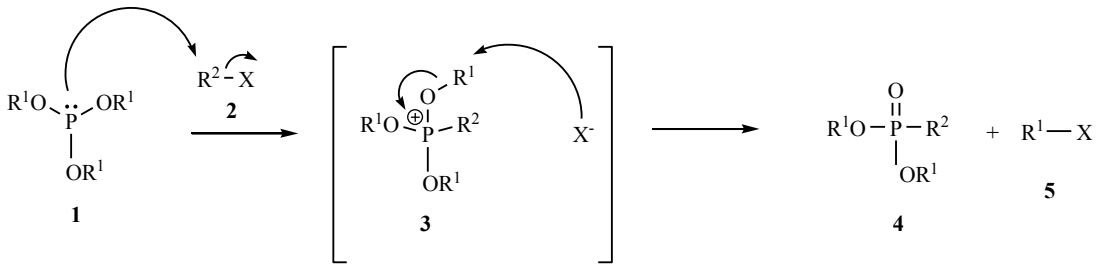

Scheme 25: The Michaelis-Arbusov mechanism.

The first step involves addition of an alkyl halide to a phosphite *via* an S_N2 reaction to give a phosphonium salt. This occurs through nucleophilic attack by the phosphite on the electrophilic alkyl (R') group of the alkyl halide, followed by loss of the halide to form an intermediate ionic complex. This intermediate product is unstable under the reaction conditions. This leads to the second step; cleavage of an O-alkyl bond to yield a new alkyl halide and the alkyl phosphonate.[4] This is initiated by the displaced halide anion, which reacts *via* another S_N2 reaction with the phosphonium intermediate to undergo dealkylation,

leaving the electrons to form a strong P=O bond.[238] Chiral phosphonium intermediates have been shown to proceed through to halide substitution with inversion of configuration, as expected by an S_N2 reaction.[5] However, these intermediates generally go through rapid dealkylation, and are therefore difficult to detect. For years the structures of the Michaelis-Arbusov intermediates were uncertain. It was thought they possibly existed as penta-coordinated phosphoranes and due to their partially ionic and partially covalent P-X bond character, were initially referred to as 'quasi-phosphonium salts'.[239] Through the use of ^{31}P NMR spectroscopy it is now clear that they exist as phosphonium salts (see Table 24) and molecular weight and conductivity measurements indicate ion pairs are present rather than dissociated ions.[238, 239]

Phosphonium Intermediate	***^{31}P NMR, (δ/ppm) X = Cl***	***^{31}P NMR, (δ/ppm) X = Br***	***^{31}P NMR, (δ/ppm) X = I***	***Phosphonate***	***^{31}P NMR, (δ/ppm)***
$[(PhO)_3PMeX]$	41	41	41	$(PhO)_2P(O)Me$	24
$[(PhO)_3PEtX]$	40	40	40	$(PhO)_2P(O)Et$	26.5
$[(PhO)_3PPr^nX]$	38	38	38	$(PhO)_2P(O)Pr^n$	26.5
$[(PhO)_3PPr^iX]$	38	38	38	$(PhO)_2P(O)Pr^i$	26
$[(PhO)_3PBu^nX]$	38	38	38	$(PhO)_2P(O)Bu^n$	26.5
$[(PhO)_3PBu^iX]$	38	38	38	$(PhO)_2P(O)Bu^i$	26
$[(PhO)_3P(CH_2Ph)X]$	30	30	-	$(PhO)_2P(O)(CH_2Ph)$	19
$[(Me_3C{\cdot}CH_2O)_3PMeX]$	-	54	54	$(Me_3C{\cdot}CH_2O)_2P(O)Me$	29.5

Table 24: ^{31}P NMR (δ/ppm) data for selected phosphonium cations and their related phosphonates. Adapted from ref. [239].

Table 24 shows that the ^{31}P NMR chemical shift values for the phosphonium intermediates are independent of the counter anion.[239] Hudson *et al.* highlight that a fine temperature balance is an essential requirement for the isolation of phosphonium intermediates. They found prolonged heating at temperatures up to 200 ˚C became necessary for the reaction, but this led to many side reactions and decomposition products, making it difficult to isolate the Michaelis-Arbusov intermediates.

4.1.4.2 Neopentyl-Containing Phosphonium Intermediates

Examples of relatively stable Michaelis-Arbusov intermediates have been observed as salts with sterically hindered neopentyl alkoxide groups at the phosphorus centre, see Figure 75. These are formed by reaction of the phosphite with halogenomethanes.[238, 240] Here nucleophilic attack by the halide ion is slowed down allowing NMR evidence of the alkoxy phosphonium salt to be collected, but isolation was still not possible.

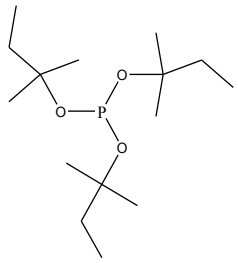

Figure 75: The steric bulk of the neopentyl groups on the phosphite slows completion of the Michaelis-Arbusov reaction, allowing the phosphonium intermediate to be observed by NMR spectroscopy.

4.1.4.3 Tetramethoxyphosphonium Hexachloroantimonate

Isolation of tetramethoxyphosphonium hexachloroantimonate was reported by Cohen.[241] Here trimethylphosphite and methylhypochlorite were reacted with antimony pentachloride, see **B** in Scheme 26. This led to the first isolation and characterisation of a tetraalkoxyphosphonium salt. This method has been used previously by Olah *et al.* for the successful isolation of unstable carbonium cations,[242] and by Hilgetag and Teichman for the preparation of tetraalkyoxythio-phosphonium salts.[243] Control reactions with trimethyl phosphite and antiomony pentachloride resulted in the formation of trimethoxymethyl phosphonium hexachloroantimonate in minor amounts, see **C** in Scheme 26. Hexachloroantimonate is a WCA which has reduced nucleophilicity compared to halide anions. This reduces the rate of the phosphonium decomposition reaction, which occurs rapidly in the presence of a chloride anion, see **A** in Scheme 26. However, Cohen did conclude that this method does not provide a general technique for the scavenging of such intermediates as no Perkow reaction intermediates were obtained when α-chloroacetone was used in place of the methyl hypochlorite.[241]

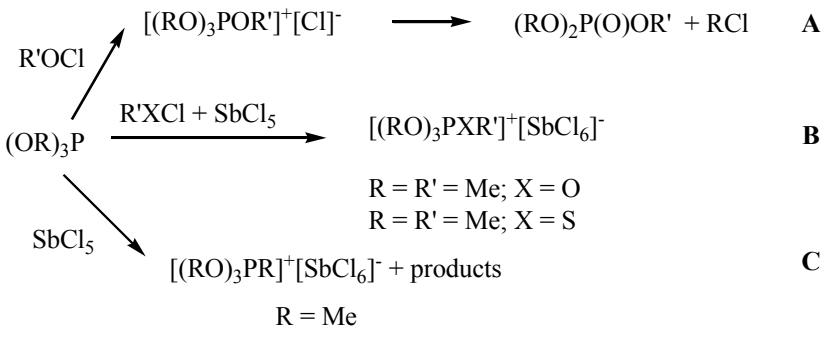

Scheme 26: Synthesis of tetramethoxyphosphonium hexachloroantimonate. Adapted from ref. [241].

4.1.4.4 Tetraalkoxyphosphonium Tetrafluoroborate Salts

Teichmann[244] and Nesterev[245] studied trialkyl-oxonium salt reactions with phosphates and phosphonates. This enabled them to gather evidence for the formation of relatively stable alkoxyphosphonium salts. Denney *et al.*[240] carried out similar work using phosphates and trialkyl-oxonium fluoroborates, R_3O^+-BF_4^- which, through alkylation form tetraalkoxyphosphonium tetrafluoroborate salts, see Figure 76.

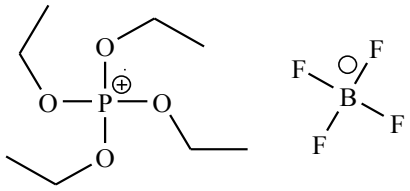

Figure 76: Tetraalkoxyphosphonium tetrafluoroborate salt synthesised from the trialkyoxonium salt.[240]

Acyclic tetraalkoxyphosphonium salts underwent slow decomposition at room temperature to give alkylfluorides and boron trifluoride complexes of the parent phosphate, see Scheme 27. Reactions of cyclic phosphates undergo Wagner-Meerwein rearrangement in which a group migrates to give carbonyl compounds.[240]

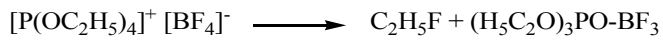

Scheme 27: Decomposition of the acyclic tetraalkoxyphosphonium salts form alkylfluorides and boron trifluoride complexes of the parent phosphate. [240]

Interestingly, the ^{31}P NMR chemical shifts for the tetraethoxyphosphonium fluoroborate, $[(H_3CH_2CO)_4P]^+[BF_4]^-$ (δ = 2.4 ppm) and the tetramethoxyphosphonium fluoroborate,

$[(H_3CO)_4P]^+[BF_4]^-$ (δ = -1.9 ppm) species are observed at similar chemical shifts to their phosphate analogues (δ = 1.0 ppm and -5.2 ppm respectively).

4.1.4.5 Trinorborn-1-yl Phosphonium Intermediates

Isomeric vinyl esters as well as β-keto-phosphonate/phosphinate/phosphine oxides from the Michaelis-Arbusov reaction are observed when phosphites are reacted with α-halogenoketones.[238] The Perkow reaction acts as an alternative process forming these isomeric vinyl esters, see **6** in Scheme 28.[238] The reaction pathway depends on attributes such as the nature of the halogen, the reaction medium and the reaction temperature. The mechanism of the Perkow reaction involves attack of the phosphorus at the carbonyl carbon atom followed by rapid migration of phosphorus from carbon to oxygen, giving a vinyloxyphosphonium species, see **5** in Scheme 28.[238] The final step is similar to the Michaelis-Arbusov where the phosphoryl bond is formed *via* dealkylation. The Perkow intermediates are less stable than the Michaelis-Arbusov intermediates; this may be due to the inductive effects of the additional electronegative oxygen atom attached to the phosphorus.[238]

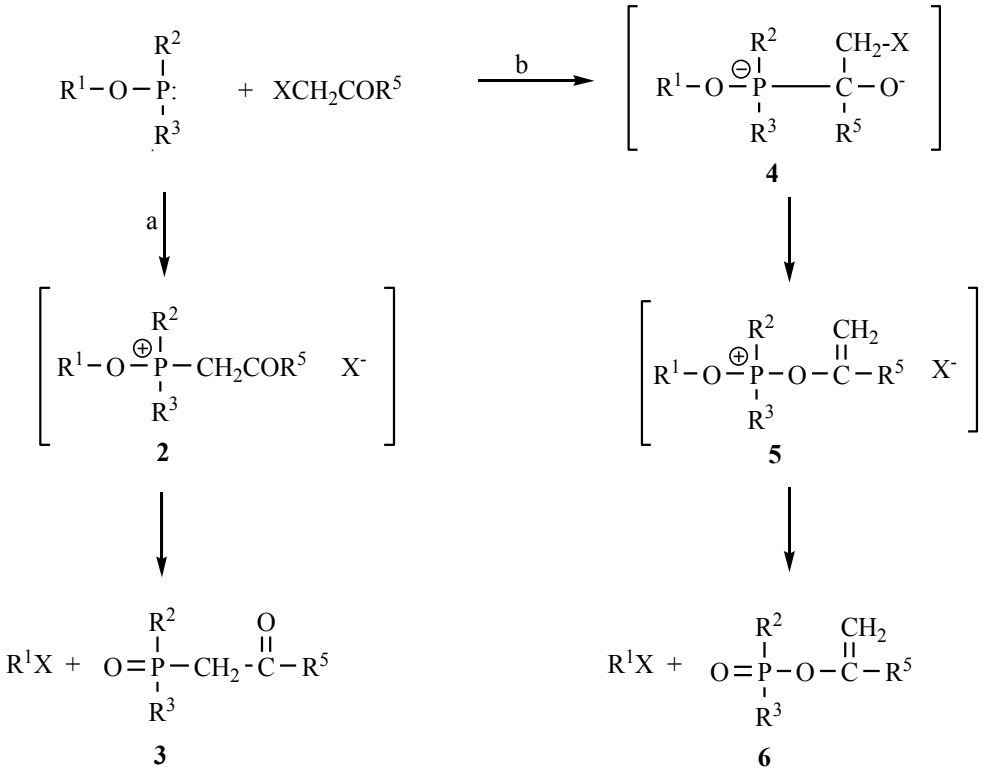

Scheme 28: Phosphite reaction with α-halogenoketones goes *via* Michaelis-Arbusov (path a) or Perkow reaction (path b). Adapted from ref. [238].

Hudson *et al.* synthesised a new trinorborn-1-yl phosphite, to enable isolation of stable intermediates for structural analysis, see Figure 77.[238] This trialkylphosphite reacts with α-halogenoketones to form stable quasiphosphonium intermediates *e.g.* $[P(OC_7H_{12})_3CH_3]^+[I]^-$ (δ_P = 36.9 ppm). This stability is due to the cage structure of the norbornyl group prohibiting S_N2 dealkylation. This can be explained by the bridgehead carbon atom being unable to form a planar configuration, making carbonium ion formation energetically unfavourable, thus forming quasiphosphonium ions with high thermal stability.[238] The trinorborn-1-yl phosphite is less reactive in comparison to an acyclic phosphite. It is not clear whether this is due to steric reasons as the S_N2 attack on the phosphorus is hindered by the bulky norborn-1-yloxy substituents. An alternative explanation could be due to electronic reasons (when the phosphorus centre has reduced nucleophilicity), as the conformation inhibits the inductive electron release from the tertiary carbon.[238] It is assumed that on decomposition the cation goes through carbon–oxygen fission *via* a S_N1 mechanism which is quite slow.[238, 240]

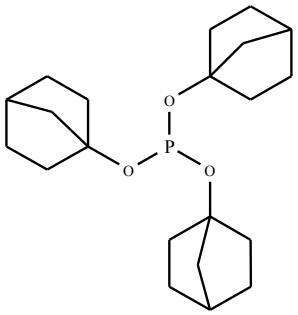

Figure 77: Trinorborn-1-yl phosphite compound.[238]

This trinorborn-1-yl phosphite was used to obtain the first stable Perkow intermediate, the first crystal X-ray structural characterisation of this material and the Michaelis-Arbusov intermediates, formed by reaction of the phosphite with α-halogenoketones.[238] Interestingly, it was observed that the lengths of the P-O-C bonds showed a degree of double bond character, this is explained by back donation from the oxygen atom to the phosphorus atom.[238] In addition, the ^{31}P NMR chemical shifts were higher field by 5 - 15 ppm than other related phosphonium ions, such as the neopentyl analogues *e.g.* $[P(OC_7H_{12})_3CH_3]^+[I]^-$ (δ_P = 36.9 ppm), $P(O^tBuCH_2)_3CH_3]^+[I]^-$ (δ_P = 54.0 ppm). This is justified through the steric bulk of the norbornenyl group causing distortion from an ideal tetrahedral geometry at the phosphorus, which influences the NMR chemical shifts.[238] Introducing electronegative substituents to the phosphite can also help increase the build up of the phosphonium intermediate, as this could avoid halide nucleophilic attack due to electron repulsion.[246] This paper suggests that non-fluorinated alkoxide groups on the Michaelis-Arbuzov intermediate are preferentially attacked compared to fluorinated substituents.[246] This indicates fluorination can be used to stabilise the cation by reducing the rate of nucleophilic attack due

to electronic repulsion of the halide anion and the electronegative fluorine atoms on the phosphonium intermediate.

4.1.5 Fluorinated Phosphonium Cations

Gladysz *et al.* describe the convenient synthesis of a variety of symmetrically- and unsymmetrically-substituted phosphonium salts that bear three to four *fluorous* ponytails, see Table 25.[247] A variety of alkylating agents are used, both *fluorous* and *non-fluorous e.g.* $PhCH_2Br$, $CH_3(CH_2)_3OSO_2CF_3$, $CF_3(CF_2)_5(CH_2)_2OSO_2CF_3$, $CF_3(CF_2)_5(CH_2)_2I$, $CF_3(CF_2)_7(CH_2)_2I$, $CF_3(CF_2)_5(CH_2)_2Br$. The *fluorous* alkylating agents are found to be less reactive than *non-fluorous* analogues,[248] hence higher temperatures are required *i.e.* 115 ˚C than that for any *non-fluorous* alkylating agents *i.e.* 45 ˚C for up to 60 hours. These alkylating agents are reacted with tertiary phosphines with *fluorous* ponytail substituents, see Scheme 29 and Scheme 30.[115-117, 247, 249]

Phosphonium Salt	***^{31}P NMR (δ/ppm)***
$[PhCH_2(CF_3\{CF_2\}_5\{CH_2\}_2)_3P]^+[Br]^-$	36.9
$[CH_3(CH_2)_3(CF_3\{CF_2\}_5\{CH_2\}_2)_3P]^+[CF_3SO_3]^-$	40.0
$[(CF_3\{CF_2\}_5\{CH_2\}_2)_4P]^+[CF_3SO_3]^-$	42.4
$[(CF_3\{CF_2\}_7\{CH_2\}_2)(CF_3\{CF_2\}_5\{CH_2\}_2)_3P]^+[I]^-$	40.4
$[(CF_3\{CF_2\}_7\{CH_2\}_2)_2(CF_3\{CF_2\}_5\{CH_2\}_2)_2P]^+[I]^-$	40.5
$[(CF_3\{CF_2\}_7\{CH_2\}_2)_4]^+[I]^-$	40.4
$[(CF_3\{CF_2\}_7\{CH_2\}_2)_4]^+[Br]^-$	40.3

Table 25: ^{31}P NMR (δ/ppm) data on *fluorous* ponytail-containing phosphonium cations.[247]

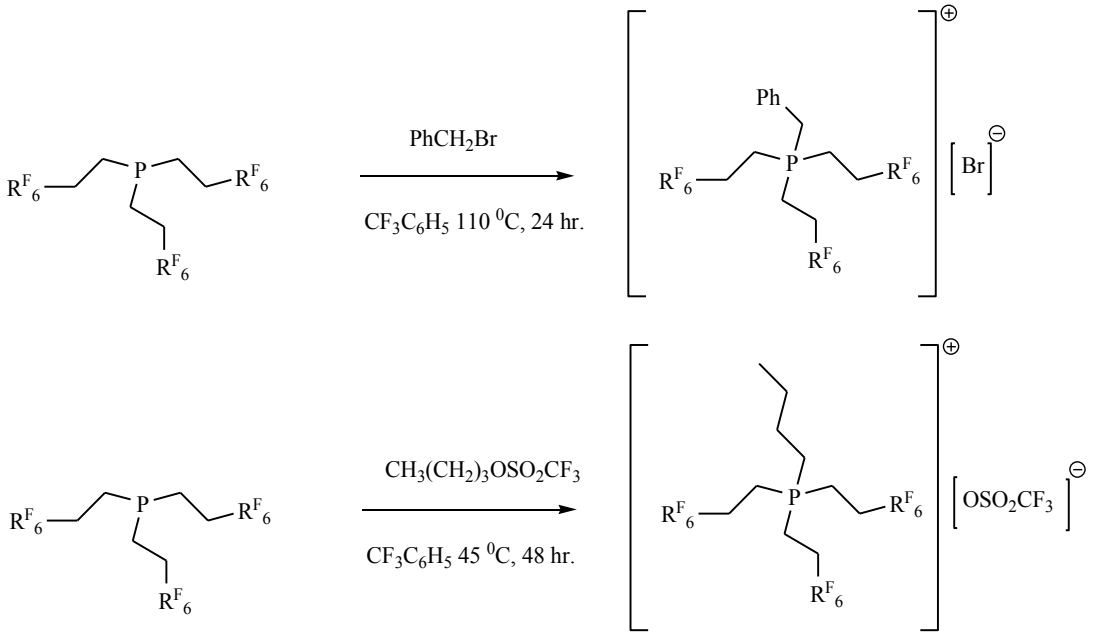

Scheme 29: Alkylation of *fluorous* ponytail-containing phosphines with non-fluorinated reagents. Adapted from ref. [247].

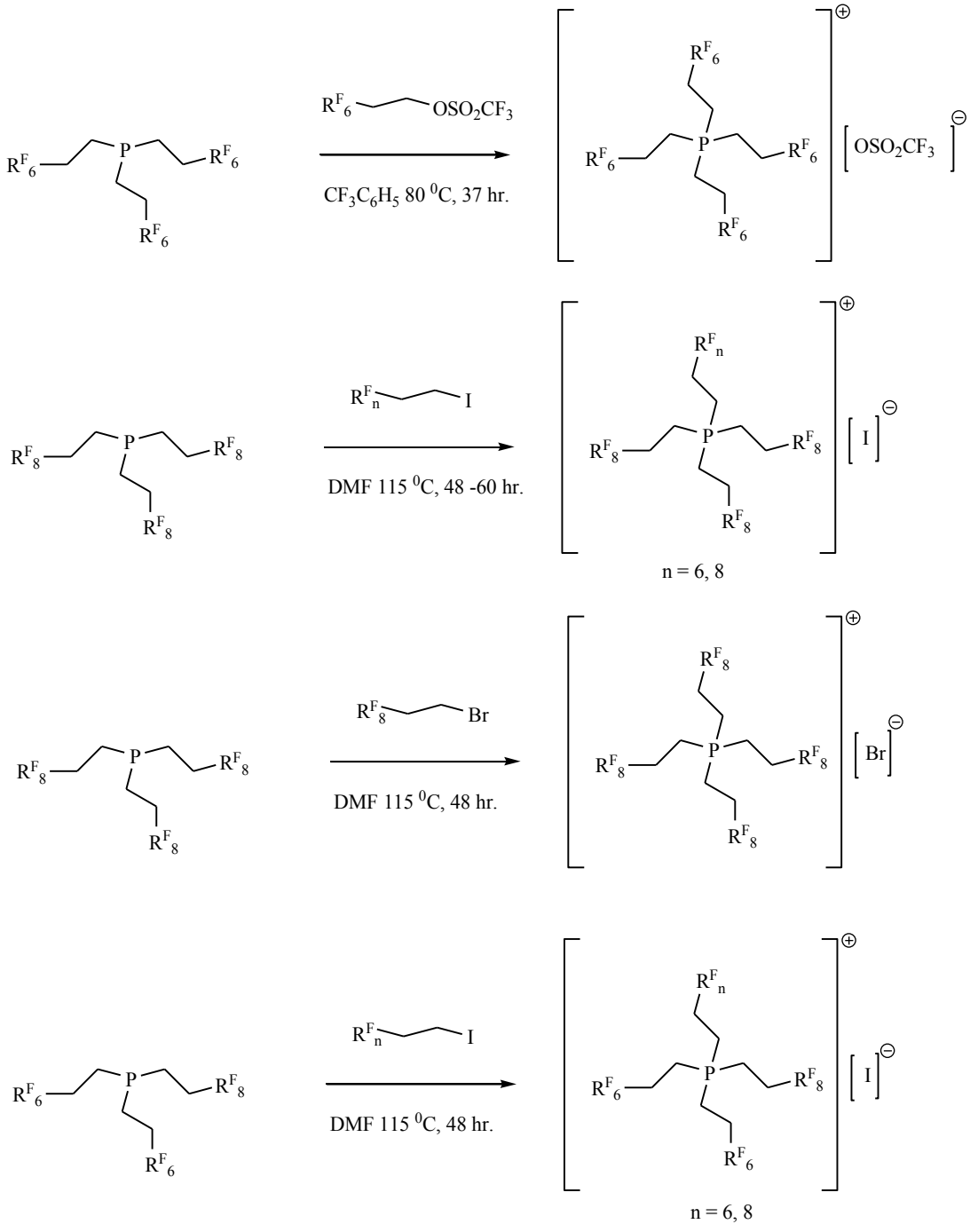

Scheme 30: Alkylation of *fluorous* ponytail-containing phosphines with fluorinated reagents. Adapted from ref. [247].

The phosphonium salts in Table 25 exhibit excellent thermal and air stabilities. Their melting points range from 43 to 110 ˚C, indicating that they are low melting salts (some classifiable as ILs).[247] Lower melting point temperatures were found when an iodide anion was exchanged with a bromide and when shorter *fluorous* ponytail substituents were present.[247] The higher melting points were found for the symmetrical cations *i.e.* four

identical *fluorous* ponytail substituents, as expected for ILs when comparing melting points of symmetrical to unsymmetrical cations.[247]

4.1.6 Phosphonium Salts as Phase-Transfer Catalysts

Phosphonium salts have also attracted attention as phase-transfer catalysts, as well as ILs.[8, 9] This has caused an interest in the development of new phosphonium salts and structure/property relationships.[247] This has recently moved towards *fluorous* phase-transfer catalysts. The essential role of a classical water/*fluorous* biphasic phase-transfer catalyst is to transfer an inorganic reagent from the aqueous phase into the *fluorous* phase. This can be observed using potassium picrate extraction experiments.[250] Here an aqueous solution of potassium picrate is stirred with a fluorinated solvent such as $CF_3C_6H_5$. The aqueous solution remains yellow due to the picrate anion and the fluorinated organic layer remains colourless. Addition of a phosphonium salt allows the picrate colour to transfer into the *fluorous* layer, indicating phase-transfer has taken place, see Figure 78. The efficiency of the picrate anion transfer can then be measured using UV-visible spectroscopy.[247]

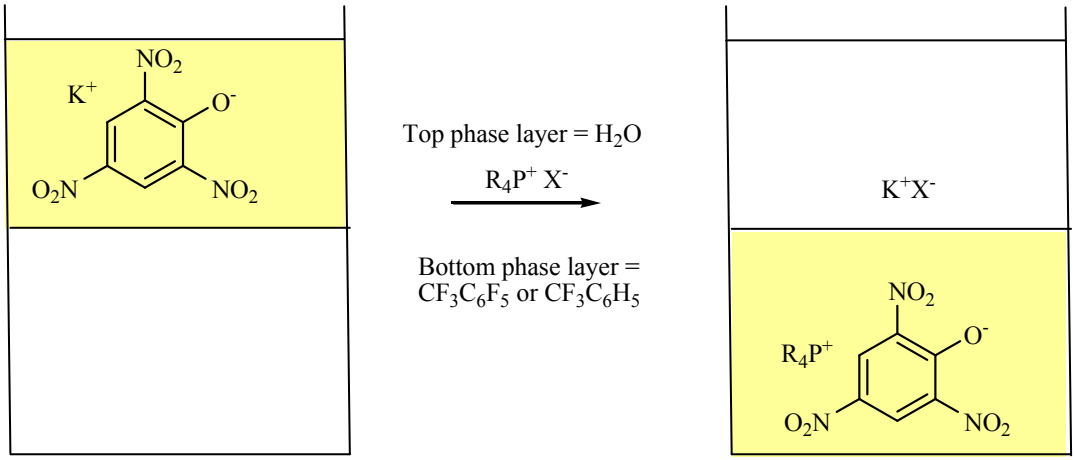

Figure 78: Diagram shows that the presence of phosphonium salts allows the picrate to transfer from the aqueous to the *fluorous* organic phase. Adapted from ref. [250].

Due to the success of non-fluorinated phosphonium salts as effective phase transfer catalysts (for anionic displacement reactions in organic solvents), similar studies have also been carried out with fluorinated phosphonium cations.[249] These fluorinated phosphonium salts were useful phase-transfer catalysts for systems involving fluorinated phases, *e.g.* C_6F_{14} and its isomers, which are some of the least polar solvents and can form biphasic systems with many solvents, including water and common organic solvents.[249] The fluorinated phosphonium ions considered by Gladysz *et al.* contain aliphatic groups with C-H bonds that

are susceptible to deprotonation and the formation of weak C-H···C-F interactions that may increase the strength of inter-ion interactions. This makes them unsuitable as WCCs for the stabilisation of reactive anions. Perfluorinated cations therefore, may offer some potential to improve WCC stability by blocking several of these decomposition routes and avoiding such interaction with C-H bonds as described above.

4.1.7 Project Aims

The simplest starting point to create a fundamentally different class of WCC is to take one of the most robust weakly coordinating anions, the fluorinated alkoxyaluminate, $[Al\{OC(CF_3)_3\}_4]^-$ and work on synthesising its isoelectronic cation using a phosphorus centre atom.[251, 252] This conceptually leads to the fluorinated alkoxyphosphonium ion $[P\{OC(CF_3)_3\}_4]^+$, (**8**), see Figure 79.

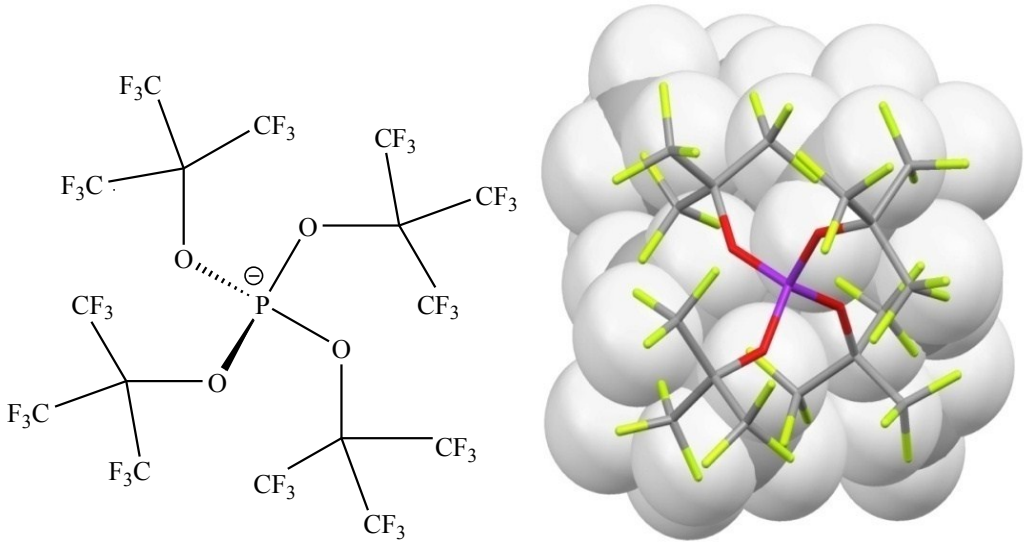

Figure 79: Weakly coordinating perfluorinated tetraalkoxyphosphonium target cation, (8).

Previous advances in WCA and WCC chemistry have generally relied on making larger cations (and anions in WCA chemistry) in order to reduce the Coulombic interactions between the anion and cation. Although it is known that increasing the size of an ion weakens the coordination,[253] there is a limit where increasing the size will have an reduced effect on its coordination ability. This is shown by Coulombs law, which is based on anions and cations attracting through electrostatic interaction, see Equation 14.

$$F = k_e (q_1 q_2 / r^2)$$

Equation 14: Coulombs law. The magnitude of the electrostatic force (F) on a charge (q_1) due to the presence of a second charge (q_2), is given by the equation above, where *r* is the distance between the two charges and k_e is a proportionality constant, thus increasing r reduces the electrostatic force (F).

The theory behind this perfluorinated alkoxyphosphonium, (**8**) being potentially a great WCC is down to the surface repulsion. The C-F bonds coat the cation with a partial negative charge, as the fluorine atoms are highly electronegative, thus pulling electron density towards them. This forms a polarised bonding situation with partial negative charges at the fluorine atoms. This allows the cation to appear to be similar to an anion at the surface (as anions are also often fluorinated at the surface), thus repelling any anions from getting too close, see Figure 80. Using surface repulsion to create a weakly coordinating ion has not yet been used, as currently the majority of ions have partial charges of the same sign at the core and at the surface.

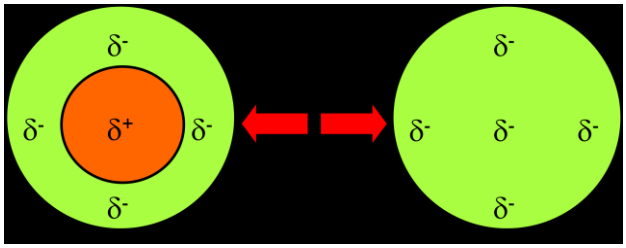

Figure 80: Weakly coordinating ions due to the surface electrostatic repulsion.

These fluorinated tetraalkoxyphosphonium ions can assist in the development of many research areas. In ILs they could serve as new cations potentially providing new properties due to the fluorination. They may have applications in high performance lubricants, as they will be weakly coordinating, consequently the ionic species will flow easily across each other, thus reducing the viscosity. Most interestingly are their uses in catalysis, with the potential that they will be able to stabilise reactive anions. The target cation, (**8**) will be resistant to attack from the anion and its bulkiness will avoid any nucleophilic attack, thus avoiding decomposition. Decomposition will also be avoided due to the cation being perfluorinated, as this avoids deprotonation providing stability in basic conditions. Other potential uses include background electrolytes in electrochemistry and to assist with the mobility of the ions in lithium batteries.[252]

4.2 RESULTS AND DISCUSSION

Various methods for the synthesis of the target cation (**8**), and related species were employed. These included oxidation of the phosphorus (III) ligands (**1**) to (**6**), in the hope that formation of the phosphonium salts would then allow for synthesis of related cations. Synthesis of the $[PX_4]^+$ (X = Cl, Br) cations were also trialled, followed by nucleophilic substitution of the X groups with metal alkoxides, MOR^F {M = Li, Na; OR^F = $OC(CF_3)_3$, $OCH(CF_3)_2$}. One pot reactions with PCl_5, MOR^F and a WCA salt, ligand redistribution of $P(OR^F)_2Cl_3$ species and alkoxy/chloride abstraction of phosphorane species were all investigated too, see Scheme 31. The findings of these methods explored are discussed in detail below.

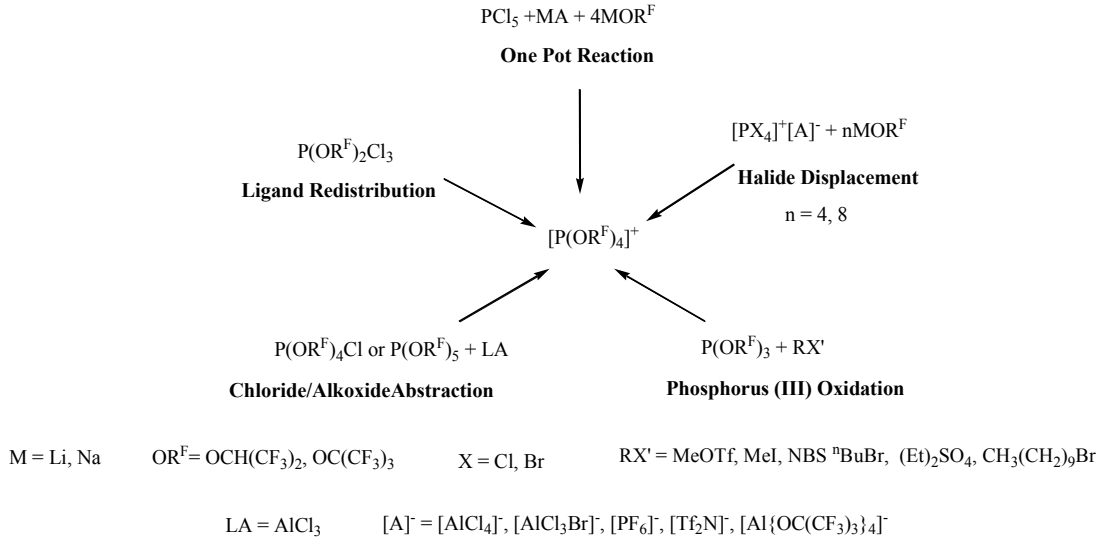

Scheme 31: Attempted synthetic routes for highly fluorinated alkoxy-containing phosphonium ions.

Most of the conclusions from the results are based on $^{31}P\{^1H\}$ NMR spectroscopy and ESI-MS. Although ^{19}F NMR spectroscopy has been used for analysis throughout this chapter, in many cases the complexity of the spectra makes it difficult to obtain reasonable conclusions from the data. The majority of the ^{19}F NMR spectra consist of many signals in the -60 to -80 ppm region of similar intensity, perhaps due to the increased sensitivity of this nucleus, making it difficult to identify the desired product peaks.

4.2.1 Phosphorus (III) Ligand Oxidation

The phosphorus (III) fluorinated alkoxy-containing ligands described in Chapter 2 can be useful precursors for the synthesis of phosphonium salts, *via* oxidation to phosphorus (V) cations using various oxidising reagents. *N*-bromosuccinimide (NBS) was purified by

recrystalisation from boiling water and the purity was confirmed by elemental CHN analysis; calculated, C: 27.13 %, H: 2.78 %, N: 7.91 %, observed, C: 26.94 %, H: 2.22 %, N: 7.69 %. The pure NBS reagent was reacted with tris(perfluoro-*t*-butyl)phosphite, $P\{OC(CF_3)_3\}_3$, (**2**) in both diethyl ether and MeCN solvents. Both reactions consistently gave a signal at -29.9 ppm (s) in the $^{31}P\{^1H\}$ NMR spectrum. This chemical shift is closer to the phosphorane region (*ca.* -100.0 to -20.0 ppm) rather than that expected for phosphorus cations (*ca.* -20.0 to 100.0 ppm). The ESI-MS positive mode spectrum (from MeCN solution) contained peaks for $[O=P\{OC(CF_3)_3\}_2]^+$ cations with varying number of MeCN molecules coordinated. In the negative mode a $[(O)_2P\{OC(CF_3)_3\}_2]^-$ anion was observed, and interestingly this compound was coordinated with either a MeCN molecule or a mono-, di-, tri-brominated MeCN molecule (CH_2BrCN, $CHBr_2CN$ and CBr_3CN respectively). The ESI-MS indicates the phosphate, $O=P\{OC(CF_3)_3\}_3$ is present in the reaction mixture, possibly as a result of the hydrolysis of the $[P\{OC(CF_3)_3\}_3Br]^+$ or $P\{OC(CF_3)_3\}_3(C_4H_4NO_2)_2$ (perhaps in the preparation of the MS sample). Both $^{31}P\{^1H\}$ NMR and ESI-MS suggest that a phosphorane species {either (**B**) or (**C**) in Scheme 32} is likely to have formed over the ionic species {(**A**) in Scheme 32}. This species (**B** in Scheme 32) is likely to have undergone ligand exchange with another phosphorane molecule, to form a phosphorane with two succinimide substituents, $P\{OC(CF_3)_3\}_3(C_4H_4NO_2)_2$ and a phosphorane with two bromine substituents, $P\{OC(CF_3)_3\}_3Br_2$, see (**C**) in Scheme 32. Although one would expect to observe two phosphorus environments in the $^{31}P\{^1H\}$ NMR spectrum, it appears from the ESI-MS evidence that the $P\{OC(CF_3)_3\}_3Br_2$ phosphorane can brominate MeCN molecules to form the brominated nitriles and (**2**). This appears more likely than direct bromination of MeCN by NBS, see Scheme 33. Hence, the -29.9 ppm chemical shift is likely to be for a phosphorane containing two succinate substituents, $P\{OC(CF_3)_3\}_3(C_4H_4NO_2)_2$.

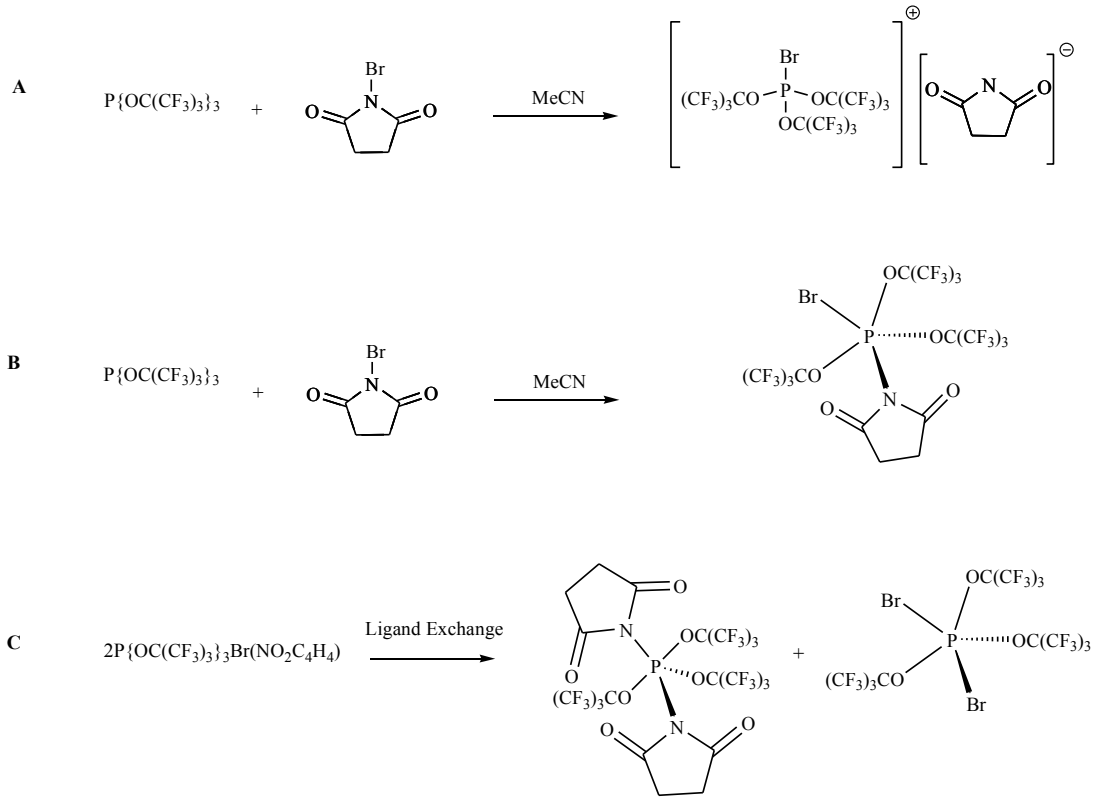

Scheme 32: Possible outcomes of $P\{OC(CF_3)_3\}_3$, (2) reaction with NBS, A) ionic species, B) neutral species from oxidative addition and C) neutral species from ligand exchange of two molecules from B.

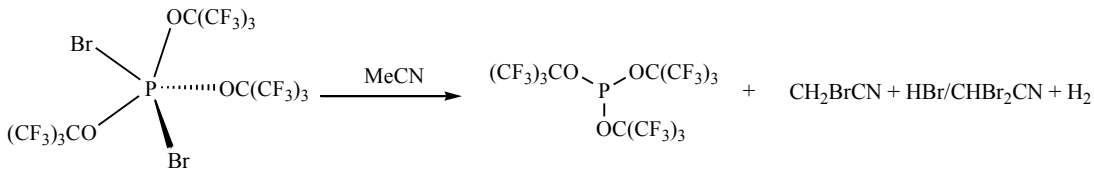

Scheme 33: The dibromophosphorane can brominate MeCN molecules to form the perfluorinated phosphite, (2).

Reaction of NBS with the $PPh_2OCH(CF_3)_2$, (**5**) ligand was also trialled, in the hope of gaining a better understanding of the products from the reaction of (**2**) and NBS. These were carried out in diethyl ether solvent (room temperature, 30 min. ultrasonic activation) and formed a pink/orange colour solution. The $^{31}P\{^1H\}$ NMR of this reaction mixture contained the free ligand, an intense peak at 39.1 ppm (s), and smaller peaks at 61.5 ppm (s) and 71.5 ppm (s). The intense peak at 39.1 ppm is likely to be the $[BrPPh_2OCH(CF_3)_2]^+$ cationic product. A similar reaction was trialled with triphenylphosphine in DCM solvent at room temperature. This initially gave peaks at 68.6 ppm (s) and 32.4 ppm (s) in the $^{31}P\{^1H\}$ NMR spectrum. However, after stirring over a weekend the $^{31}P\{^1H\}$ NMR spectrum of this reaction mixture consisted of only one peak at 48.2 ppm (s). This is most likely to be the $[PPh_3Br]^+[NC_4H_4O_2]^-$ product, as $[PPh_3Br]^+[BBr_4]^-$ has been reported as an ionic salt with the

$^{31}P\{^{1}H\}$ NMR spectrum consisting of a peak at δ = 49.0 ppm (s) in 25-oleum solution.[254] On addition of $NaOCH(CF_3)_2$ to the reaction mixture containing $[PPh_3Br]^+[NC_4H_4O_2]^-$, an intense peak at 31.5 ppm (s) and smaller peaks at 20.9 ppm (s) and -5.0 ppm (s) are observed in the $^{31}P\{^{1}H\}$ NMR spectrum. The latter is likely to be free triphenylphosphine. The ESI-MS (in MeCN solution) of this reaction mixture showed no bromine-containing species, suggesting that NaBr salt had precipitated out of solution. However, no cationic, $[PPh_3OCH(CF_3)_2]^+$ molecular ion was observed.

Methyl triflate has been found to be a useful methylating agent, as the triflate anion can stabilise the resulting phosphonium cations. Reaction with methyl triflate and $PPh_2OCH(CF_3)_2$, (**5**), (the most nucleophilic ligand of the six prepared in this thesis) leads to the formation of the phosphonium salt $[MePPh_2OCH(CF_3)_2]^+[O_3SCF_3]^-$, (**10**), see Scheme 34.

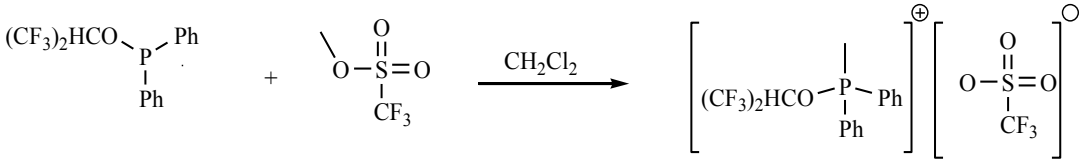

Scheme 34: Synthesis of the phosphonium salt $[MePPh_2OCH(CF_3)_2]^+[O_3SCF_3]^-$, (10).

This salt (**10**) has been isolated and fully characterised. The $^{31}P\{^{1}H\}$ NMR spectrum consists of a signal at 85.0 ppm (s) and the ^{19}F NMR consists of a signal at -73.54 ppm (d, $^{4}J_{FP}$ = 6 Hz). The ^{1}H NMR consists of a signal at 6.20 ppm (m), for the hexafluoroisopropoxy hydrogen split by the fluorine and the phosphorus atoms and a signal at 3.06 ppm (d, $^{2}J_{HP}$ = 13 Hz) for the methyl on the phosphonium cation {shifted from 4.10 ppm (s) for MeO_3SCF_3}. The ESI-MS positive mode has a molecular ion peak at 367.4 m/z and 883.8 m/z, for two cations with a triflate anion *i.e.* $[\{MePPh_2OCH(CF_3)_2\}_2O_3SCF_3]^+$. The negative mode has a peak at 149.0 m/z, $[M]^-$ consistent with the molecular ion of a triflate anion. The salt was stable enough to achieve elemental CHN analysis after manipulation in air; calculated, C: 39.54 %, H: 2.73 %, observed, C: 39.43 %, H: 2.96 %. This new salt has a melting point range of 101-103 ˚C, which is close to the border-line for claiming that this is a new IL. Crystals suitable for X-ray diffraction analysis were grown from a concentrated DCM solution, which was layered with hexane as an antisolvent, see Figure 81.

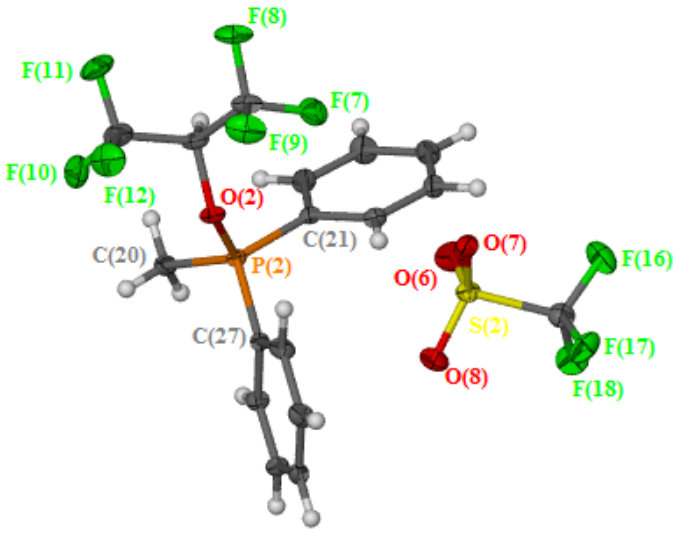

Figure 81: Molecular structure of $[MePPh_2\{OCH(CF_3)_2\}]^+[O_3SCF_3]^-$, (10). Two ionic pairs in each asymmetric unit, but one omitted for clarity. Thermal ellipsoids are drawn at the 50 % probability level. Crystal system: monoclinic. Space group: $P2_1/c$, R_1: 0.0388 (all data), wR_2: 0.0911 (>2sigma(I)).

Bond ***Cation 1***	***Angles (°):***	***Bond*** ***Cation 2***	***Angles (°):***
O(2)-P(2)-C(21)	109.76(7)	O(1)-P(1)-C(11)	99.58(7)
C(21)-P(2)-C(27)	112.00(8)	C(11)-P(1)-C(5)	110.78(9)
C(27)-P(2)-C*(20)	111.47(8)	C(5)-P(1)-C*(4)	110.38(8)
C*(20)-P(2)-O(2)	110.91(8)	C*(4)-P(1)-O(1)	110.31(8)

Table 26: Selected bond angles for the two phosphonium ions found in the asymmetric unit of the X-ray crystal structure of (10). * = carbon for methyl substituent.

Bond ***Cation 1***	***Distance (Å):***	***Bond*** ***Cation 2***	***Distance (Å):***
P(2)-O(2)	1.600(1)	P(1)-O(1)	1.597(1)
P(2)-C(20)	1.770(2)	P(1)-C(5)	1.778(2)
P(2)-C(27)	1.772(2)	P(1)-C(11)	1.780(2)
P(2)-C(21)	1.779(2)	P(1)-C(4)	1.765(2)

Table 27: Selected bond distances for the two phosphonium ions found in the asymmetric unit of the X-ray crystal structure of (10).

The $[MePPh_2\{OCH(CF_3)_2\}]^+[O_3SCF_3]^-$, (**10**) crystal structure indicates that the asymmetric unit consists of two independent ion pairs, both are very different structures. Cation 1 consists of a triflate behind the methyl substituent on the phosphonium ion and cation 2 with a triflate behind the alkoxy and phenyl substituents on the phosphonium ion. The orientation of the triflate anion in cation 2 appears to be approaching the phosphorus centre in a similar manner to that expected for an S_N2 type nucleophilic attack, since the alkoxy substituent is a better leaving group than a methyl substituent. Both pairs are ion separated species, as the distance between the phosphorus atom and the closest oxygen atom of the triflate anions; 4.7798(5) Å and 3.9634(5) Å, are greater than the sum of the VdW radii ($O_{1.52\ Å}$ +$P_{\ 1.80\ Å}$ = 3.32 Å) in both cases. The triflate anion has a dispersed negative charge over the entire anion molecule; hence this reduces the overall possibility of nucleophilic attack on the phosphonium ion, (**10**). The hexafluoroisopropoxy substituent in (**10**) is also likely to be a key structural feature of the cation. Both the steric bulk and any electronic repulsion from the fluorinated group can inhibit the triflate anion from getting too close and lead to cation decomposition. Table 26 indicates that the phosphonium ions in both ion-pairs show distorted tetrahedral geometries. Table 27 consists of the distances for the bonds directly with the phosphorus centre in both phosphonium ions. The P-O bonds for the phosphonium ions in both cases {1.600(1) Å and 1.597(1) Å} are of key interest as they are considerably shorter than the $P\text{-}O_{(ax)}$ bond distance for the pentakis(hexafluoroisopropoxy)phosphorane, $P\{OCH(CF_3)_2\}_5$, (**16**), but statistically the same as for the $P\text{-}O_{(eq)}$ {average $P\text{-}O_{(ax)}$ = 1.673(2) Å and average $P\text{-}O_{(eq)}$ = 1.593(2) Å}, discussed in Chapter 5. In comparison to the novel highly fluorinated WCA salt, $[Ag(PPh_3)_3]^+[P\{OCH(CF_3)_2\}_5F]^-$ (**19**) (discussed in further detail in Chapter 5), the phosphonium, (**10**) P-O bond distances are much shorter than both the equatorial and axial P-O bond lengths of (**19**); average $P\text{-}O_{(eq)}$ = 1.699(2) Å} and $P\text{-}O_{(ax)}$ = 1.704(3) Å. This suggests that the phosphonium, (**10**) P-O bond maybe more polarised $\{P(\delta^+)\text{-}O(\delta^-)\}$ and forms a stronger bond than the $P\text{-}O_{(ax)}$ bond for the neutral phosphorane, (**16**) and the negatively charged phosphorus anion, (**19**), both of which contain identical hexafluoroisopropoxy substituents. However, it is likely that the longer bond lengths found in the anion are due to a change in the polarity due to the presence of the direct P-F bond and the increased steric bulk around the phosphorus centre due to its distorted octahedral geometry. Although it may be expected for the phosphonium ion, (**10**) to have a shorter P-O bond length than the $P\text{-}O_{(eq)}$ bond lengths for the phosphorane, (**16**), this is not observed perhaps due to the electron releasing methyl substituent and the phenyl rings changing the electronic properties of the ion P-O bond polarity. A range of short contacts (less than the sum of the VdW radii – 0.2 Å) were also found with the molecules in the asymmetric unit. These included seven O···H-C interactions (2.082-2.471 Å, sum of the VdW radii of O and

H = 2.720 Å), and one C···O interaction (3.019 Å, sum of the VdW radii of C and O = 3.220 Å). The shortest O···H interaction (2.082 Å) found was between a triflate oxygen atom for the ion pair containing anion 1 and the hydrogen atom of the hexafluoroisopropoxy group on the phosphonium centre for the ion pair containing cation 2. It appears the highly fluorinated groups on the carbon atom polarise this C-H bond to form a hydrogen bond donor atom that is available for hydrogen bonding. The longest O···H interaction (2.471 Å) found was between a triflate oxygen atom for the ion pair containing anion 1 and a hydrogen atom of the methyl group on the phosphonium centre for the ion pair containing cation 2.

The $[MePPh_2OCH(CF_3)_2]^+[O_3SCF_3]^-$, (**10**) salt hydrolyses on addition of water to give the following peaks in the $^{31}P\{^1H\}$ NMR spectrum; δ = 40.7 (s), 36.6 (s), 34.6 (s), 34.3 (s) and 20.7 (s) ppm. These chemical shifts are similar to those found for $Ph_2(O)PP(O)Ph_2$ (δ_P = 25.0 ppm),[255] $Ph_2(O)POP(O)Ph_2$ (δ_P = 24.9 ppm),[256] $Ph_2(O)POH$ (δ_P = 39.3 ppm),[257] $O{=}PPh_2Me$ (δ_P = 30.6 ppm)[258] and $Ph_2(O)PH$ (δ_P = 23.9 ppm)[259] in various solvents.

The $[MePPh_2OCH(CF_3)_2]^+[I]^-$ ionic species is known in the literature but no crystal structure is available for comparison.[260] This phosphonium salt was studied in detail for the investigation of rearrangements of α-hydroxyalkylphosphines and α-hydroxyalkylphosphonium salts.[260] This was of interest due to the mechanistic and synthetic problems that occur in phosphorus chemistry as result of the behaviour of P-C-OH bonds under acidic and basic conditions.[260] Figure 82 consists of the structures of common compounds containing P-C-OH bonds.

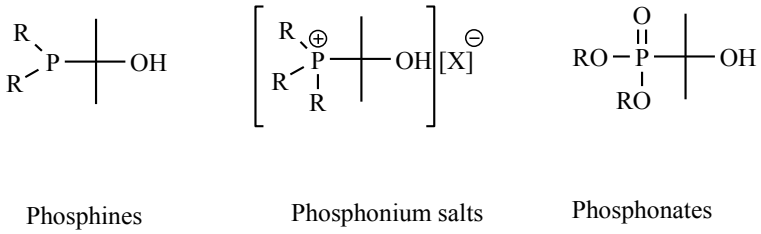

Figure 82: Representation of the most significant compounds consisting of P-C-OH bonds.

Evangelidou-Tsolis and Fausto describe that the reaction of pentafluorophenyl (PFP)-hydroxyphosphine with methyl iodide forms a relatively stable dialkyldiarylphosphonium salt without any molecular rearrangement, see Scheme 35.[260]

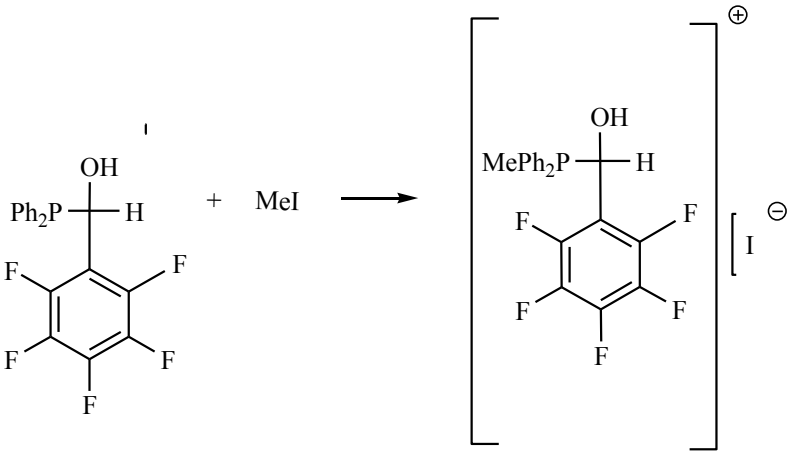

^{31}P NMR, d = -1.6 ppm ^{31}P NMR, d = 24.2 ppm

Scheme 35: Reaction of PFP-hydroxyphosphine with methyl iodide.[260]

However, alkylation of the hexafluoroisopropoxy (HF)-hydroxyphosphine with methyl iodide undergoes isomerisation *via* a molecular rearrangement to form an alkylalkoxydiarylphosphonium salt, $[RPPh_2OCH(CF_3)_2]^+[X]^-$ (R = H, X = I; R = Me, X = I; R= Ph, X = Br), see Scheme 36.[260]

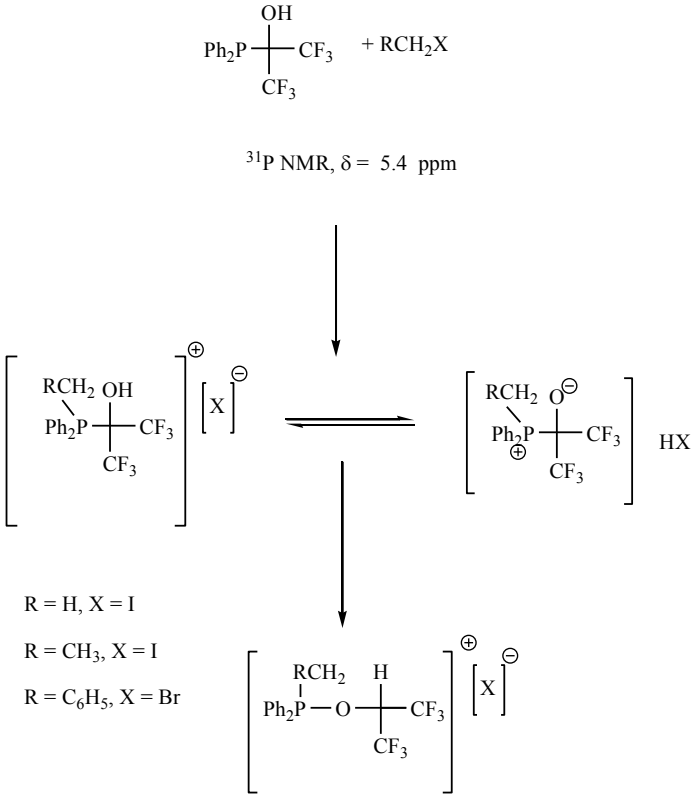

Scheme 36: Reaction of (HF)-hydroxyphosphine with methyl iodide. Adapted from ref. [260].

Dissociation of the dialkyldiarylphosphonium salts (see Scheme 36) into the phosphinite, $PPh_2OCH(CF_3)_2$, hexafluoroacetone, $(CF_3)_2CO$ and hydrogenhalide followed by recombination of the phosphinite and $(CF_3)_2CO$ to from a P-O-C- containing molecule has been excluded as a pathway. This is because no phosphonium product was observed when these reagents were reacted in a control reaction.[260] Interestingly, Evangelidou-Tsolis and Fausto report that these alkylalkoxydiarylphosphonium salts are stable towards the Michaelis-Arbuzov reaction as they to do not form P=O bonds, yet were unable to purify the salts to achieve elemental CHN analysis. The ^{31}P NMR spectroscopic analysis has been reported for the three $[RPPh_2OCH(CF_3)_2]^+[X]^-$ salts (R = H, X = I, δ_P = 85.0 ppm; R = Me, X = I, δ_P = 88.4 ppm; R= Ph, X = Br, δ_P = 80.1 ppm).[260] The $[MePPh_2OCH(CF_3)_2]^+[I]^-$ salt has a chemical shift value that is similar to the $[MePPh_2OCH(CF_3)_2]^+[O_3SCF_3]^-$ salt (δ = 84.9 ppm), suggesting the anion has little effect on their ^{31}P NMR chemical shift values. They have also been reported to form 1, 2-oxaphosphetanes with a 5 coordinate phosphorus atom when reacted with hexafluoroacetone, $(CF_3)_2CO$ in the presence of triethylamine, NEt_3, see Scheme 37.[260] These 1, 2-oxaphosphetanes are known as "Wittig-intermediates" are possibly derived from the intermediate alkoxydiphenyl-ylide, $Ph_2[(CF_3)_2CHO]P{=}CHR$. These are beneficial for synthesis on an industrial scale as the simple synthesis of 1, 2-oxaphosphetanes requires relatively high temperatures (*ca.* 150 °C) for complete reactant (phosphine and $(CF_3)_2CO$) conversion.

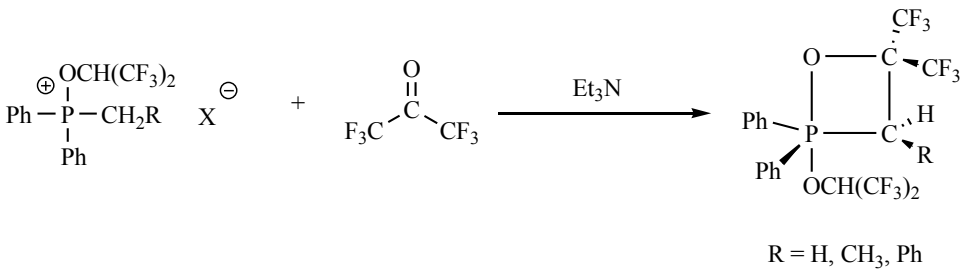

Scheme 37: Synthesis of 1, 2-oxaphosphetane. Adapted from ref. [260].

Interestingly, a melting point range of 120-125 °C has been reported for the $[MePPh_2OCH(CF_3)_2]^+[I]^-$ ionic salt.[260] This highlights the significance of altering the anion on the physical properties of such species. The triflate anion is more weakly coordinating than an iodide anion; hence the likely lower lattice enthalpy will lead to a lower melting point (101-103 °C), as observed.

Reaction of methyl triflate with $PPh\{OCH(CF_3)_2\}_2$, (**3**) shows evidence of the $[MePPh\{OCH(CF_3)_2\}_2]^+[O_3SCF_3]^-$, (**11**) salt in the $^{31}P\{^1H\}$ NMR spectrum (δ_P = ~90 ppm, dependent on reaction solvents). However, isolation of this salt is difficult. The reaction mixtures for the synthesis of $[MePPh\{OCH(CF_3)_2\}_2]^+[O_3SCF_3]^-$, (**11**) were heated in various

solvents, since no reaction was observed at room temperature. In addition, methyl iodide was also used in place of methyl triflate in toluene solvent and heated at 90 ˚C overnight. This showed no signs of the cation in the positive mode of ESI-MS and only a peak at 126.91 m/z for the molecular ion of an iodide anion in the negative mode. The $^{31}P\{^{1}H\}$ NMR consisted of new peaks at 32.5 ppm (s) and 24.7 ppm (s), as well as reduced intensity peaks for the free ligand $PPh\{OCH(CF_3)_2\}_2$, (**3**) peak. Either of these new peaks are in the chemical shift region for the possible Michaelis-Arbuzov product *i.e.* $(O)PMePhOCH(CF_3)$. Reaction with methyl triflate and $PPh\{OCH(CF_3)_2\}_2$, (**3**) in MeCN solvent, heated overnight at 80 ˚C, gave peaks at 86.7 ppm (s) and 62.2 ppm (s) in the $^{31}P\{^{1}H\}$ NMR spectrum and resulted in an intense yellow reaction mixture. Similarly, reaction with methyl triflate and $PPh\{OCH(CF_3)_2\}_2$, (**3**) in hexane gave a small peak at 85.7 ppm (s) and an intense multiplet for the free ligand (δ_P = 190.2 ppm) in the $^{31}P\{^{1}H\}$ NMR spectrum. This peak at ~86 ppm in the reaction mixtures of both MeCN and hexane solvent is likely to be the $[MePPh\{OCH(CF_3)_2\}_2]^+[O_3SCF_3]^-$, (**11**) product as it is of a similar chemical shift region to the $[MePPh_2OCH(CF_3)_2]^+[O_3SCF_3]^-$, (**10**) salt. The reaction mixture in hexane solvent was heated overnight at 66 ˚C which resulted in a loss of the potential product peak at 85.7 ppm (s) rather than increased conversion. The $^{31}P\{^{1}H\}$ NMR spectrum consisted of the free ligand and trace amounts of hydrolysis products (δ = 32.5 and 24.7 ppm). Repeating this reaction led to the observation of only a single peak at 24.7 ppm (s) in the $^{31}P\{^{1}H\}$ NMR spectrum as well as the free ligand. It was thought that the overnight heating at high temperatures was too harsh and the product could be possibly decomposing. A test reaction was carried with the synthesis of the $[MePPh_2OCH(CF_3)_2]^+[O_3SCF_3]^-$, (**10**) salt at similar conditions; heated at 90 ˚C overnight in toluene solvent. A peak was observed at 86.5 ppm (s) as well as an additional unidentifiable peak at 58.6 ppm (s) in the $^{31}P\{^{1}H\}$ NMR spectrum. This test reaction suggested these high temperatures are not too harsh for these type of cationic species, since the $[MePPh_2OCH(CF_3)_2]^+[O_3SCF_3]^-$, (**10**) salt can be observed in the reaction mixture by $^{31}P\{^{1}H\}$ NMR spectroscopy. The most successful reaction for the synthesis of $[MePPh\{OCH(CF_3)_2\}_2]^+[O_3SCF_3]^-$, (**11**) observed by $^{31}P\{^{1}H\}$ NMR spectroscopy involved heating in CD_2Cl_2 solvent. On addition of the reactants (0.2 mmol) in CD_2Cl_2 solvent (0.5 mL) at room temperature, a new signal at 92.4 ppm (s) was observed in the $^{31}P\{^{1}H\}$ NMR spectrum, in addition to the signal at 190.7 (m) for $PPh\{OCH(CF_3)_2\}_2$, (**3**). Following this, the same sample was heated (50 ˚C for 24 hrs.) followed by the $^{31}P\{^{1}H\}$ NMR analysis and further heating (50 ˚C for 48 hrs.) followed by the $^{31}P\{^{1}H\}$ NMR analysis. Although complete conversion was not observed, the signal did increase in intensity; see NMR overlay in Figure 83. Trace signals were also observed at 32.7 ppm (s) and 24.8 ppm (s), one of which is the possible Michaelis-Arbuzov product. The ^{1}H NMR spectra show the presence of a signal growing in at 3.22 (d, $^{2}J_{HP}$ = 13 Hz) for the methyl

group, [**Me**PPh{OCH$(CF_3)_2$}$_2$]$^+$ and a signal growing in at 6.27 (m) for the hexafluoroisopropoxy hydrogen atom, [MePPh{O**H**$(CF_3)_2$}$_2$]$^+$. The ^{19}F NMR spectra indicate two signals growing in at -74.05 (m) ppm and -73.79 (m) ppm. These are likely to be related to the phosphonium, product [MePPh{OCH(C**F**$_3)_2$}$_2$]$^+$, where restricted rotation around the P-O bond cause the -CF_3 groups to chemically in-equivalent. Interestingly removal of the solvent *in vacuo* (10^{-2} mbar) resulted in an oil. This may either suggest the phosphonium salt may not be a solid at room temperature or an impurity is present in the reaction mixture.

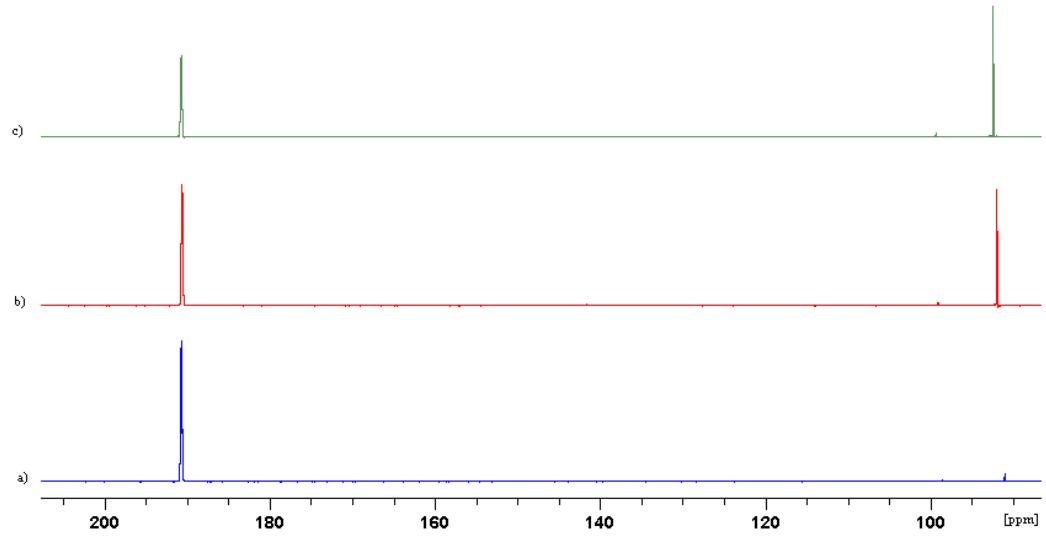

Figure 83: ^{31}P{^{1}H} NMR spectra overlay for the reaction between PPh{OCH$(CF_3)_2$}$_2$, (3) and MeO_3SCF_3 in CD_2Cl_2 solvent to form (11); a) after addition of reagents at room temperature, b) after heating {12 hrs. at 50 °C}, c) after further heating {48 hrs. at 50 °C}.

Reaction with methyl triflate and the other ligands trialled; P{OCH$(CF_3)_2$}$_3$, (**1**), P{OC$(CF_3)_3$}$_3$, (**2**), and PPh$_2${OC$(CF_3)_3$}, (**6**), showed no signs of reaction in the ^{31}P{^{1}H} NMR spectra, even after heating (only signals for the starting material and hydrolysis products were observed). It is likely that the reduced nucleophilicity of these ligands limits any reaction with the methyl triflate. In addition, solubility issues may have occurred with the P{OC$(CF_3)_3$}$_3$, (**2**) ligand, which is a crystalline solid at room temperature and only sparingly soluble in DCM solvent.

Overall, the oxidation reactions all show that the reaction conditions (such as the amount of heating and the temperature) need to be finely balanced. This balance requires the temperature to be sufficiently high to allow synthesis of the phosphonium salt. It is the low nucleophilicity of the fluorinated phosphorus ligands, which is desirable in terms of their ligand chemistry, but makes alkylation difficult. However, as well as increasing the reactivity of the ligand, the temperature has to be kept as low as possible to avoid

decomposition of the phosphonium intermediates to their Michaelis-Arbuzov products. The best methods to isolate the phosphonium salts require a WCA to stabilise them and inhibit fast decomposition. A potential reaction that may yield the target cation, but has not been trialled in this thesis (due to synthetic difficulty and toxicity issues) involves the reaction of $P\{OC(CF_3)_3\}_3$, (**2**), with the hypochlorite, $ClOC(CF_3)_3$ in the presence of a Lewis acid such as $SbCl_5$. The $SbCl_5$ may abstract the Cl^- from the hypochlorite to form a more stable $[SbCl_6]^-$ anion.[241] However, it is possible that the $SbCl_5$ may decompose the $P\{OC(CF_3)_3\}_3$, (**2**) ligand *via* ligand exchange reactions, forming P-Cl and Sb-$OC(CF_3)_3$ bonds or the $ClOC(CF_3)$ may oxidise (**2**) to form $P\{OC(CF_3)_3\}_4Cl$.

4.2.2 Attempted Synthesis of $[P(OR^F)_4]^+$ from $[PX_4]^+$ Salts, (X = Cl, Br)

Addition of $NaOCH(CF_3)_2$ (8 eq.) to a DCM solution of $[PCl_4]^+[AlCl_4]^-$ (1 hr. ultrasonic activation at room temperature) did not lead to the formation of $[P\{OCH(CF_3)_2\}_4]^+[Al\{OCH(CF_3)_2\}_4]^-$. The neutral $P\{OCH(CF_3)_2\}_5$ phosphorane was identified as the only phosphorus-containing species present in any significant concentration (by $^{31}P\{^1H\}$ NMR spectroscopy) in this reaction mixture, see Scheme 38. This indicates that the -$OCH(CF_3)_2$ groups are likely to not be sufficiently sterically bulky to avoid nucleophilic attack at the phosphonium centre of (**9**) by another $[OCH(CF_3)_2]^-$ ion.

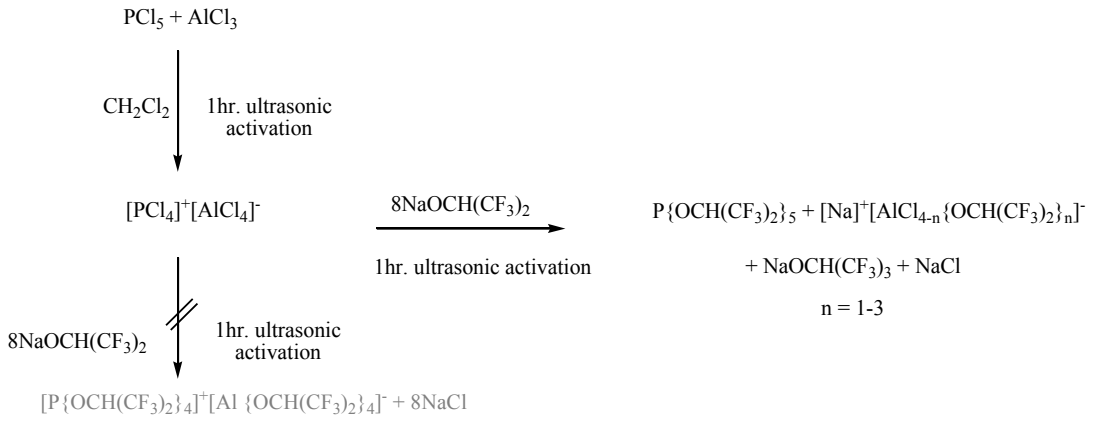

Scheme 38: Formation of phosphorane species from addition of $NaOCH(CF_3)_2$ to the $[PCl_4]^+[AlCl_4]^-$ ionic salt.

Similarly, on addition of less $NaOCH(CF_3)_2$ (4 eq.) to a DCM solution of $[PCl_4]^+[AlCl_4]^-$ (1 hr. ultrasonic activation at room temperature), the neutral phosphoranes $P\{OCH(CF_3)_2\}_5$, (**16**) and $P\{OCH(CF_3)_2\}_4Cl$ were observed in the $^{31}P\{^1H\}$ NMR spectrum, rather than the $[P\{OCH(CF_3)_2\}_4]^+[AlCl_4]^-$ ionic salt. On further addition of $AlCl_3$ (1 eq.) to this reaction, followed by 1 hr. ultrasonic activation led to the observation of a new peak at 0.0 ppm in the $^{31}P\{^1H\}$ NMR spectrum, in addition to the signal for (**16**). This signal at 0.0 ppm could

potentially be the $[P\{OCH(CF_3)_2\}_4]^+$, (**9**) cation, formed *via* a chloride abstraction from the $P\{OCH(CF_3)_2\}_4Cl$ species. However, although the molecular ion for $[AlCl_4]^-$ is present at 168.85 m/z, there are no signs of cation (**9**) in the ESI-MS (from MeCN solution). Reaction of $[PBr_4]^+[AlCl_3Br]^-$ with $NaOCH(CF_3)_2$ (4 eq.) in DCM also forms the neutral $P\{OCH(CF_3)_2\}_5$, (**16**) and $P\{OCH(CF_3)_2\}_4Br$ phosphoranes, observed by $^{31}P\{^1H\}$ NMR spectroscopy. In addition, a signal at -66.2 ppm (br) was also observed. This signal could be the $[PBr_4]^+$ cation. Interestingly, no sign of the $[AlCl_3Br]^-$ anion is present in the ESI-MS negative mode (from MeCN solution). The $[AlCl_4]^-$ molecular ion is however present at 168.85 m/z in low concentrations. The ESI-MS positive mode consist of intense signals at 865.1649, 947.1002 and 1049.2149 m/z, none of which are however the correct mass for the $[P\{OCH(CF_3)_2\}_4]^+$ cation, (**9**) .

The perfluoro-*t*-butoxy group is much bulkier than the hexafluoroisopropoxy group, hence, it is thought that it should give greater stability to any phosphonium cations with these groups as their substituents. The reaction of a DCM solution of $[PCl_4]^+[AlCl_4]^-$ with $NaOC(CF_3)_3$ (4 eq.) was trialled in the hope of synthesising $[P\{OC(CF_3)_3\}_4]^+[AlCl_4]^-$. The $^{31}P\{^1H\}$ NMR spectrum for this reaction mixture consisted of a range of signals. No signals were observed for the neutral phosphoranes, $P\{OC(CF_3)_3\}_4Cl$ or $P\{OC(CF_3)_3\}_5$. The observed signals included; δ_P 85.4 ppm (s), 61.8 ppm (s), 28.8 ppm (s) and -8.6 ppm (s). These are tentatively assigned as $[PCl_4]^+$, $[PCl_3\{OC(CF_3)_3\}]^+$, $[PCl_2\{OC(CF_3)_3\}_2]^+$, and $[PCl\{OC(CF_3)_3\}_3]^+$ salts respectively. These cations may form by a mixture of chloride and alkoxide exchange with both the anion and cation. Signals observed in the ^{19}F NMR spectra at -69.03 (s), -69.34 (s) and -69.74 (s) ppm may well correspond to the latter three cations respectively. However, ESI-MS of this sample (in MeCN solution) shows no signs of these cations in the positive mode, only intense peaks for $[Na_n\{OC(CF_3)_3\}_{n-1}]^+$ clusters with various amounts of diethyl ether solvent coordinated. These clusters are commonly seen when $NaOC(CF_3)_3$ is present in the sample and can swamp signals from the desired cations.

4.2.3 Attempted Synthesis of $[P(OR^F)_4]^+$ from One-Pot Reactions

Initial attempts to synthesise $[P\{OC(CF_3)_3\}_4]^+[A]^-$ using a one-pot method involved reaction of PCl_5 (1 eq.) with $LiOC(CF_3)_3$ (4 eq.) and $LiN\{O_2S(CF_3)\}_2$ (1 eq.). This reaction was trialled in various solvents and under a range of conditions. Reaction of these components in diethyl ether/DCM (25 %/75 %) for 2 hrs. showed evidence of $P\{OC(CF_3)_3\}_3$ (δ_P = 147.0 ppm), and weak signals for $P\{OC(CF_3)_3\}Cl_4$ (δ_P = -12.7 ppm), $P\{OC(CF_3)_3\}_2Cl_3$ (δ_P = -33.0 ppm), $(O)P\{OC(CF_3)_3\}_3$ (δ_P = -3.5 ppm) in the $^{31}P\{^1H\}$ NMR spectrum. In addition to these a weak signal at 6.9 ppm (s) was also observed in the $^{31}P\{^1H\}$ NMR spectrum, possibly for

the cation $[P\{OC(CF_3)_3\}_4]^+$, (**8**). On heating this reaction mixture (1 hr. at 50 ˚C), the $P\{OC(CF_3)_3\}_3$ signal disappeared and new signals appeared at -10.8 ppm (s) and -5.6 ppm (s), in addition to the presence of $P\{OC(CF_3)_3\}Cl_4$ (shifted to δ_P = -11.7 ppm), $P\{OC(CF_3)_3\}_2Cl_3$ (shifted to δ_P = -33.8 ppm), $O{=}P\{OC(CF_3)_3\}$ (δ_P = -3.9 ppm). The ^{19}F NMR spectrum for this reaction shows the presence of intense signals for $LiN\{O_2S(CF_3)\}_2$ (δ_F = -80.05 ppm) and $LiOC(CF_3)_3$ (δ_F = -75.57 ppm), and a smaller signal at -71.49 (d, J = 8 Hz). The latter grows in after heating and could be related to either of the new signals at δ_P = -10.8 ppm or δ_P = -5.6 ppm. These are within the expected chemical shift range for ^{31}P NMR spectroscopy found for cationic phosphorus compounds. However, ESI-MS was not useful for further analysis of the crude reaction mixtures, as it was crowded by many peaks originating from $[Li_n\{OC(CF_3)_3\}_{n-1}]^+$ or $[Li_n\{OC(CF_3)_3\}_{n+1}]^-$ clusters (in the positive and negative mode respectively), with various amounts of diethyl ether solvent coordinated. This made identification of other cationic (or anionic species) difficult.

A one-pot reaction similar to that described above was also carried out in neat diethyl ether solvent. Signals for $P\{OC(CF_3)_3\}_3$, (**2**) were observed in the $^{31}P\{^1H\}$ NMR spectrum for this reaction too. This suggests that either PCl_3 is formed from PCl_5 and solvent side reactions, which then reacts with the $LiOC(CF_3)_3$, or reductive elimination of the hypochlorite from $P\{OC(CF_3)_3\}_4Cl$ or the peroxide from $P\{OC(CF_3)_3\}_5$ takes place. On the removal of diethyl ether *in vacuo* (10^{-2} mbar) and the addition of MeCN to this reaction mixture new peaks were observed at 9.7 ppm (s) and 7.5 ppm (s). Either of these signals could potentially be for the cation $[P\{OC(CF_3)_3\}_4]^+$, (**8**). The phosphite was not found due to its reduced solubility in MeCN. Interestingly, ESI-MS analysis (MeCN solution) of the reaction mixture gave a molecular ion peak with the correct isotope pattern at 970.7 m/z in the positive mode for the target cation $[P\{OC(CF_3)_3\}_4]^+$. In addition, the molecular ion for $[N\{O_3S(CF_3)\}_2]^-$ at 279.9 m/z was found in the negative mode. However, isolation of this material was unsuccessful. This one pot reaction was repeated in MeCN (at room temperature for 16 hrs.). Signals were found at 2.5 ppm (s), -4.6 ppm (s, possibly for $O{=}P\{OC(CF_3)_3\}_3$), -12.5 ppm (s, possibly for $P\{OC(CF_3)_3\}Cl_4$) and -13.5 ppm (s) in the $^{31}P\{^1H\}$ NMR spectrum. Crystals grown from this reaction mixture, which were suitable for single-crystal X-ray diffraction studies, were found to contain $LiCl(MeCN)_n$ rather than a phosphorus-containing product. However, the observation of solvated LiCl suggests that metathesis has taken place. In addition, the ESI-MS positive mode showed a peak at 970.7 m/z for the target cation $[P\{OC(CF_3)_3\}_4]^+$.

4.2.4 Attempted Synthesis of $[P(OR^F)_4]^+$ from Lewis-Acid-Mediated Halide/Alkoxide Abstraction of $P\{OCH(CF_3)_2\}_{5-n}Cl_n$ (n = 0, 1)

The phosphorane, $P\{OCH(CF_3)_2\}_4Cl$ was synthesised by the addition of PCl_5 (53 mg, 1 mmol, 1 eq.) to $LiOCH(CF_3)_2$ (174 mg, 4 mmol, 4 eq.) in DCM. KPF_6 was added to this reaction mixture and ultrasonic activation was used to increase its solubility. The DCM solvent was removed *in vacuo* (10^{-2} mbar) and MeCN was added to help promote the formation of ionic phosphonium ions rather than neutral phosphorane species. This led to the mixture turning grey/pink in colour. The $^{31}P\{^1H\}$ NMR spectrum indicated the presence of $P\{OCH(CF_3)_2\}_4F$ (δ_P = -81.0 ppm, d, $^1J_{PF}$ = 803 Hz), KPF_6 (δ_P = -144.1 ppm, sept, $^1J_{PF}$ = 711 Hz), and $O{=}P\{OCH(CF_3)_2\}_3$ (δ_P = -3.3 ppm, s). This reaction mixture was left stirring for 2 days and the NMR analysis was repeated. The $^{31}P\{^1H\}$ NMR spectrum showed the presence of PF_5 (δ_P = 34.5 ppm, m, $^1J_{PF}$ = 1072 Hz), $(O)P\{OCH(CF_3)_2\}_3$ (-3.0 ppm, s), $P\{OCH(CF_3)_2\}_4F$ (-81.0 ppm, d, $^1J_{PF}$ = 803 Hz) and $[PF_2\{OCH(CF_3)_2\}_4]^-$ (-144.1 ppm, t, $^1J_{PF}$ = 710 Hz). Corresponding signals in the ^{19}F NMR spectrum were also identified for; PF_5 (δ_F = -88.00 ppm, d, $^1J_{FP}$ = 1072 Hz), $[PF_2\{OCH(CF_3)_2\}_4]^-$ (-56.00 ppm, d, $^1J_{FP}$ = 710 Hz), and $P\{OCH(CF_3)_2\}_4F$ (-72.30 ppm, d, $^1J_{FP}$ = 803 Hz). The ESI-MS (from MeCN solution) showed molecular ion peaks for $[PF\{OCH(CF_3)_2\}_5]^-$ (885.0 m/z), $[PF_2\{OCH(CF_3)_2\}_4]^-$ (737.1 m/z) and $[PF_3\{OCH(CF_3)_2\}_3]^-$ (589.3m/z) in the negative mode. It was only possible to observe signals in the positive mode for $[K_{n+1}(PF_6)_n]^+$ cluster cations. This suggests that chloride/fluoride or alkoxide/fluoride ligand exchange takes place. This can occur either from the neutral $P\{OCH(CF_3)_2\}_4Cl$/$P\{OCH(CF_3)_2\}_5$ phosphoranes, or an alternative mechanism suggests that the $[P\{OCH(CF_3)_2\}_4]^+[PF_6]^-$ is formed along with a KCl side product. This $[P\{OCH(CF_3)_2\}_4]^+[PF_6]^-$ ionic salt can react further to abstract a fluoride from $[PF_6]^-$ to yield PF_5 and $P\{OCH(CF_3)_2\}_4F$. The $P\{OCH(CF_3)_2\}_4F$ and PF_5 phosphoranes can then undergo fluoride/alkoxide ligand exchange processes. The $LiAl\{OC(CF_3)_3\}_4$ salt was also reacted with the neutral $P\{OCH(CF_3)_2\}_4Cl$ species in DCM solvent (1 hr. ultrasonic activation). It was thought that the $[Al\{OC(CF_3)_3\}_4]^-$ anion would better stabilise the $[P\{OCH(CF_3)_2\}_4]^+$ cation than the $[PF_6]^-$ anion. However, since this reaction was carried out in a PTFE J Young's tap NMR tube, filtration to remove the LiCl precipitate was difficult. This led to poor shimming being observed for the NMR sample, resulting in very broad peaks. The chemical shifts of these signals in the $^{31}P\{^1H\}$ NMR spectrum ($CDCl_3$ solvent) were observed at 6.2 ppm (br), -11.2 ppm (s), -18.2 ppm (s), -20.6 (s), -24.8 (s), -80.5 ppm (d, $^1J_{PF}$ = 784 Hz) for the $P\{OCH(CF_3)_2\}_4F$, -83.5 (s) for the $P\{OCH(CF_3)_2\}_5$ and an intense signal at -85.0 ppm (s). Fluorobenzene, PhF, solvent was added to this reaction in the hope of stabilising any cationic species by coordination of the Lewis acidic phosphorus centre by

the weak donor PhF *i.e.* in the hope of forming $[P\{OCH(CF_3)_2\}_4C_6H_5F]^+$. This strategy has been successful in stabilising Lewis super acids in previous studies.[261] In the $^{31}P\{^1H\}$ NMR spectrum signals were found at 5.5 (s), -10.8 (s), -78.7 (d, $^1J_{PF}$ = 790 Hz, suggesting this is a neutral P-F containing species), -81.9 ppm (d, $^1J_{PF}$ = 796 Hz, $P\{OCH(CF_3)_2\}_4F$), -83.8 (s, $P\{OCH(CF_3)_2\}_5$) and -84.0 ppm (s) after the addition of PhF solvent. The most noticeable difference upon changing the solvent, is the loss of the peak at -18.2 ppm (s) and an increase in intensity and a small change in chemical shift (to -10.8 ppm) for the peak at -11.2 ppm (s). Again only $[Li_{n+1}\{OCH(CF_3)_2\}_n]$ clusters were observed in the ESI-MS (from MeCN solution) positive mode. Abstraction of a chloride from the neutral $P\{OC(CF_3)_3\}_4Cl$ (δ_P = -58.1 ppm, s) species using $LiAl\{OC(CF_3)_3\}_4$ salt was attempted in diethyl ether solvent (1 hr. ultrasonic activation). However, the $^{31}P\{^1H\}$ NMR spectrum showed the presence of $P\{OC(CF_3)_3\}_3$, (**2**) and an intense signal at -34.0 ppm (s), possibly for $P\{OC(CF_3)_3\}_2Cl_3$, which seemed to convert to a signal at -10.0 ppm (s) with time, possibly for $P\{OC(CF_3)_3\}Cl_4$. Interestingly, ESI-MS (from MeCN solution) did show a molecular ion at 970.8 m/z, which could be the target cation $[P\{OC(CF_3)_3\}_4]^+$. The NMR spectroscopic evidence suggests that halogenated phosphoranes are present in solution, hence this cation may have formed by halide/alkoxide loss and ligand exchange upon ionisation in the mass spectrometer. The phosphite, (**2**) may have formed during these reactions *via* reductive elimination of the hypochlorite, $ClOC(CF_3)_3$ or the peroxide, $(CF_3)_3COOC(CF_3)_3$ from the phosphoranes, $P\{OC(CF_3)_3\}_4Cl$ or $P\{OC(CF_3)_3\}_5$, due to steric repulsion, see Scheme 39. Alternatively, the phosphoranes may behave as oxidising agents (towards the solvent or potentially $NaOR^F$) forming phosphorus (III) halides/alkoxides that go on to react further, see Scheme 39.

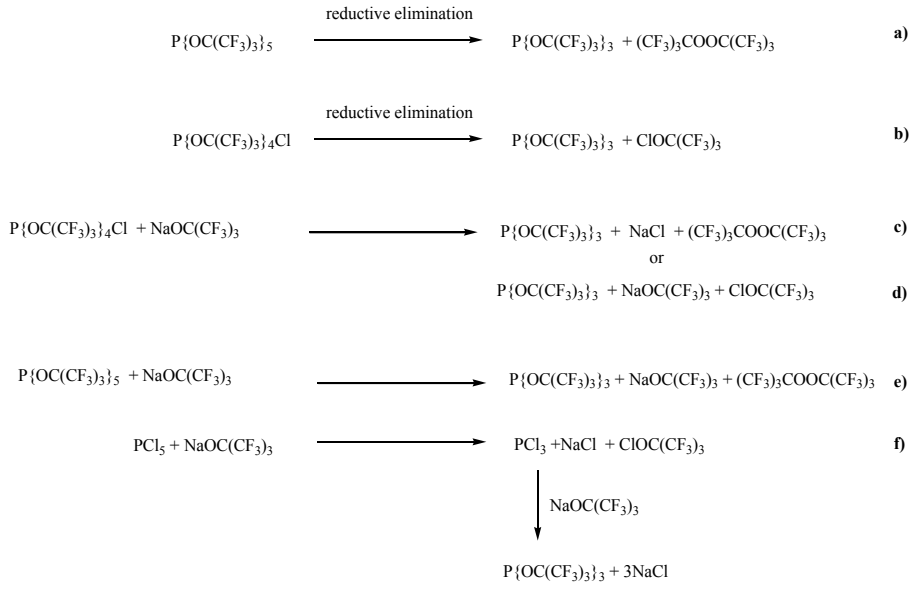

Scheme 39: Possible routes to the perfluorinated-*t*-butyl phosphite from phosphorus (V) species.

The synthesis of $PCl_3\{OC(CF_3)_3\}_2$ was often complicated as it was difficult to control the stoichiometry and avoid the formation of a range of alkoxy-substituted phosphoranes. Reaction of PCl_5 with $NaOC(CF_3)_3$ (2 eq.) in DCM solvent (1 hr. ultrasonic activation) was used as the standard method of preparation. However, the $P\{OC(CF_3)_3\}_3$ phosphite, (**2**) was found in many cases. In one case where $PCl_3\{OC(CF_3)_3\}_2$ was successfully made (δ_P = -34.1 ppm, s) the $[Ag(MeCN)_4]^+[P\{OCH(CF_3)_2\}_5F]^-$ ionic species (discussed in Chapter 5) was added to the reaction. This gave an intense peak at -3.7 ppm (s) in addition to the signal for $[P\{OCH(CF_3)_2\}_5F]^-$ (δ_P = 147.0 ppm, $^1J_{PF}$ = 818 Hz). ESI-MS (in MeCN solution) of this reaction mixture gave a molecular ion at 970.7 m/z for the $[P\{OC(CF_3)_3\}_4]^+$, (**8**) target cation, see Figure 84. It should be noted here that although the signal at δ_P = -3.7 ppm is within the correct chemical shift range for an expected phosphonium cation in the $^{31}P\{^1H\}$ NMR, it may also likely be the phosphate, $O{=}P\{OC(CF_3)_3\}_3$ (usually observed at -3 to -4 ppm, dependent on the solvent). This phosphate is the oxidation product for the perfluoro-*t*-butoxy substituted phosphorane, $P\{OC(CF_3)_3\}_nCl_{5-n}$ (n = 1-3). In addition, the observed cation in the ESI-MS may have formed in the gas phase *via* ligand redistribution, rather than in the condensed phase.

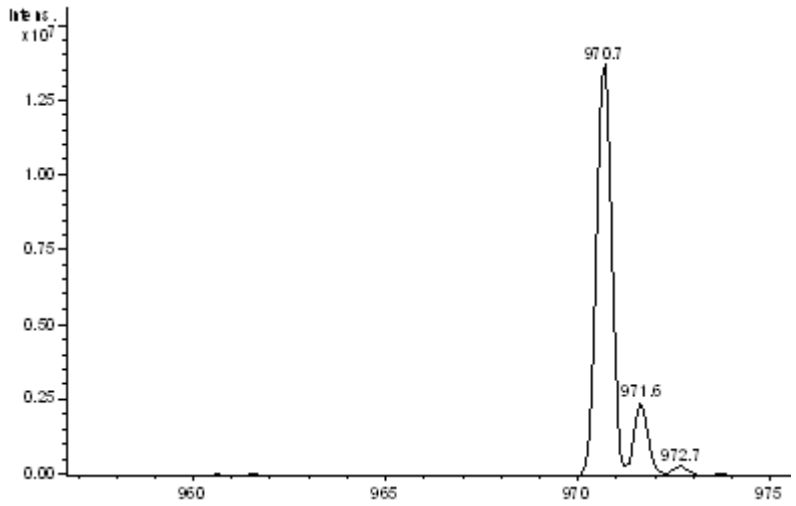

Figure 84: ESI-MS spectra of correct mass and isotopic pattern for the $[P\{OC(CF_3)_3\}_4]^+$, (8) target cation on reaction with $PCl_3\{OC(CF_3)_3\}_2$ and the $[Ag(NCMe)_4]^+[P\{OCH(CF_3)_2\}_5F]^-$ ionic species, (17).

Since the perfluoro-*t*-butoxy group repeatedly formed the phosphite, $P\{OC(CF_3)_3\}_3$, further investigations were focussed on improving the synthesis of a phosphonium cation with hexafluoroisopropoxy groups. A reaction with $P\{OCH(CF_3)_2\}_4Cl$ and $AlCl_3$ in PhF solvent (1 hr. ultrasonic activation) resulted in a signal at -16.5 ppm (s) in the $^{31}P\{^1H\}$ NMR spectrum. This reaction was promising as the NMR spectroscopy suggested very few side reactions had taken place. However, again ESI-MS showed only $[Na_{n+1}\{OCH(CF_3)_2\}_n]$ in the

positive mode. Repeating this reaction with the $AlCl_3$ and $P\{OCH(CF_3)_2\}_4Cl$ species in DCM solvent (1 hr. ultrasonic activation) gave an orange/peach colour reaction mixture. The $^{31}P\{^1H\}$ NMR spectrum had peaks at -81.8 (d, $^1J_{PF}$ = 795.0 Hz) for $P\{OCH(CF_3)_2\}_4F$, -21.7 (s), -16.2 (s) and an intense signal at 14.8 (s) ppm. Repeating the same reaction in DCM solvent again found peaks in the $^{31}P\{^1H\}$ NMR at -84.0 (s) for $P\{OCH(CF_3)_2\}_5$, -64.7 (s) for $P\{OCH(CF_3)_2\}_4Cl$, -21.7 (s) and 14.8 (s) ppm. This suggests that possibly either peaks at -21.7 ppm or 14.8 ppm could potentially be the cation as they are consistently observed.

Other attempts to synthesise the phosphonium cation included attempts to abstract an alkoxy, $-OCH(CF_3)_2$, group from the phosphorane, $P\{OCH(CF_3)_2\}_5$ with aluminium trichloride, $AlCl_3$ in DCM solution (1 hr. ultrasonic activation). A peak at -16.7 ppm (s) was observed in the $^{31}P\{^1H\}$ NMR spectrum, as well as that for the $P\{OCH(CF_3)_2\}_5$ at -84.1 ppm (s). This reaction was repeated and the $^{31}P\{^1H\}$ NMR consisted of two signals at -20.1 ppm (s) and -16.2 ppm (s). It was found that on further sonication the peak at -20.1 ppm (s) became more intense, this is consistent with the $^{31}P\{^1H\}$ NMR data for the reaction of $P\{OCH(CF_3)_2\}_4Cl$ and $AlCl_3$. It was thought that perhaps the cation required a Lewis base to stabilise it, hence PMe_3 was added to form a $[P\{OCH(CF_3)_2\}_4\text{-}PMe_3]^+$ adduct. However, the $^{31}P\{^1H\}$ NMR spectrum of this reaction found a signal at -4.1 ppm (s), likely to be the $O{=}P\{OCH(CF_3)_2\}_3$ and a signal at -84.0 ppm (s) for the $P\{OCH(CF_3)_2\}_5$. Trityl salts such as $[Ph_3C]^+[BF_4]^-$ and $[Ph_3C]^+[PF_6]^-$ were also reacted with the $P\{OCH(CF_3)_2\}_5$, (**16**) phosphorane to form $Ph_3COCH(CF_3)_2$ and the desired cation. However, these were found to show no changes in the $^{31}P\{^1H\}$ NMR spectra, suggesting no cation had formed, or if it had it had then reacted further with excess $NaOCH(CF_3)_2$ {present in the solution from the formation of (**16**)} to form the more stable neutral phosphorane, $P\{OCH(CF_3)_2\}_5$, (**16**) again.

4.2.5 Single-Crystal X-ray Diffraction Structure of $(CF_3)_3COH\cdots O{=}P\{OC(CF_3)_3\}_3$

The closest structural information for the target cation, $[P\{OC(CF_3)_3\}_4]^+$, (**8**) obtained is that of a phosphate with a perfluorinated alcohol molecule hydrogen bonded to the P=O oxygen atom, see Figure 85.

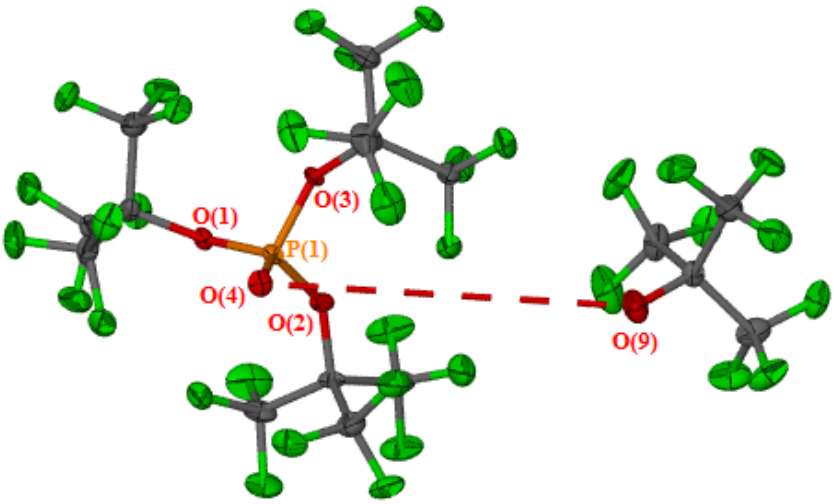

Figure 85: Molecular structure of $(CF_3)_3COH\cdots O{=}P\{OC(CF_3)_3\}_3$. Two $(CF_3)_3COH\cdots O{=}P\{OC(CF_3)_3\}_3$ molecules in each asymmetric unit but one omitted for clarity. Thermal ellipsoids are drawn at the 50 % probability level. Selected interatomic distances (Å) and angles (˚) for the above molecules; P(1)-O(1) = 1.570(3) , P(1)-O(2) = 1.576(3), P(1)-O(3) = 1.578(4), P(1)=O(4) = 1.434(3), O(4)-O(9) = 2.767(4), O(4)-P(1)-O(3) = 118.4(2), O(4)-P(1)-O(1) = 118.3(2), O(4)-P(1)-O(2) = 117.9(2), O(1)-P(1)-O(3) = 99.5(2), O(2)-P(1)-O(1) = 99.6(2), O(3)-P(1)-O(2) = 99.6(2). Crystal system: monoclinic. Space group: $P2_1/c$, R_1: 0.0569 (all data), wR_2: 0.1219 (>2sigma(I)).

This was crystallised from a reaction of PCl_5 and $LiOC(CF_3)_3$ (2 eq.) in DCM solvent. The phosphate, which was probably formed from hydrolysis of a $PCl_2\{OC(CF_3)_3\}_3$ type phosphorane, has a distorted tetrahedral symmetry. It seems the presence of the electron rich P=O bond pushes the other substituents down reducing the O-P-O bond angles to an average of 99.6 ˚ and increasing the O=P-O bond angle to an average of 118 ˚ from the ideal 109.5 ˚ for a tetrahedral structure. Finally the O···O distances between $(R^FO)_3P{=}\mathbf{O}\cdots H\text{-}\mathbf{O}R^F$ (where R^F = $C(CF_3)_3$) = O(4)···O(9) = 2.767(4) Å and O(8)···O(10) = 2.767(4) Å suggests that a strong H-bond is present. The O···O distance of water in the solid state for is 2.82 Å.[262] As the observed O···O distance in the crystal structure between the phosphate and the alcohol molecule is shorter than this, it suggests a relatively strong interaction is present. This is likely to be due to the strongly acidic character of the alcohol, $HOC(CF_3)_3$, which is enhanced compared to non-fluorinated alcohols, due to the electron withdrawing effects of the perfluoro-*t*-butoxy group.

These results provide tantalising evidence that the salts of both $[P\{OCH(CF_3)_2\}_4]^+$, (**9**) and $[P\{OC(CF_3)_3\}_4]^+$, (**8**) may have been observed in condensed phases, but the reaction mixtures are often complex and purification of products has proved difficult. Isolation of $[P\{OC(CF_3)_3\}_4]^+$, (**8**) free from phosphorus (III) products is of particular difficulty. The from phosphorus (III) products are likely to result from either reductive elimination of the hypochlorite, $ClOC(CF_3)_3$ or the peroxide, $(CF_3)_3COOC(CF_3)_3$ from the phosphoranes, $P\{OC(CF_3)_3\}_4Cl$, $P\{OC(CF_3)_3\}_5$, respectively due to steric repulsion. Alternatively, the

phosphoranes may behave as oxidising agents (towards the solvent or potentially $NaOR^F$) forming phosphorus (III) halides/alkoxides. The extreme sensitivity of these materials and related phosphoranes towards moisture, the potential for redox chemistry leading to phosphorus (III) products and the potential for ligand exchange (between phosphoranes, the cations themselves and between anions and cations) makes this system synthetically challenging. However, there is scope for future work to capitalise on these observations and it is hoped that the right conditions may be found to allow the isolation of these potentially very interesting materials. Table 28 summarises the $^{31}P\{^1H\}$ NMR spectroscopic data for potential observation of the phosphonium cations $[P\{OCH(CF_3)_2\}_4]^+$, (**9**) and $[P\{OC(CF_3)_3\}_4]^+$, (**8**), gathered from a range of experiments (as described above).

Salt	*Proposed $^{31}P\{^{1}H\}$ NMR resonance/s (δ/ppm)*	*ESI-MS (m/z)*
$[P\{OCH(CF_3)_2\}_4][AlCl_4]$	0 (in CH_2Cl_2)	No $[M]^+$ found
$[P\{OCH(CF_3)_2\}_4][Al\{OC(CF_3)_3\}_4]$	6.2 and -11.2 (in CH_2Cl_2)	$[Li_n\{OC(CF_3)_3\}_{n-1}]^+$
$[P\{OCH(CF_3)_2\}_4][Al\{OC(CF_3)_3\}_4]$	5.5 and -10.8 (in CH_2Cl_2/C_6H_5F)	$[Li_n\{OC(CF_3)_3\}_{n-1}]^+$
$[P\{OCH(CF_3)_2\}_4][AlCl_4]$	-21.7 and 14.8 (in CH_2Cl_2)	No $[M]^+$ found
$[P\{OCH(CF_3)_2\}_4][AlCl_4]$	-16.5 (in C_6H_5F)	$[Na_n\{OC(CF_3)_3\}_{n-1}]^+$
$[P\{OCH(CF_3)_2\}_4][AlCl_4]$	-16.7 (in CH_2Cl_2)	-
$[P\{OCH(CF_3)_2\}_4][AlCl_3\{OCH(CF_3)_2\}]$	-20.1 (in CH_2Cl_2)	-
$[P\{OC(CF_3)_3\}_4][N\{O_2S(CF_3)\}_2]$	6.9 (in Et_2O/CH_2Cl_2)	-
	heating leads to -10.8 and -5.6	$[Li_n\{OC(CF_3)_3\}_{n-1}]^+$
$[P\{OC(CF_3)_3\}_4][N\{O_2S(CF_3)\}_2]$	9.7 or 7.5 (in Et_2O/CH_3CN)	970.7 (positive), 279.9 (negative)
$[P\{OC(CF_3)_3\}_4][N\{O_2S(CF_3)\}_2]$	2.5 and -13.5 (in MeCN)	970.7 (positive)
$[P\{OC(CF_3)_3\}_4][Al\{OC(CF_3)_3\}_4]$	-10.0 (in Et_2O)	970.8 (positive)
$[PCl_3\{OC(CF_3)_3\}][AlCl_4]$	61.8 (in CH_2Cl_2)	$[Na_n\{OC(CF_3)_3\}_{n-1}]^+$
$[PCl_2\{OC(CF_3)_3\}_2][AlCl_4]$	28.8 (in CH_2Cl_2)	$[Na_n\{OC(CF_3)_3\}_{n-1}]^+$
$[PCl\{OC(CF_3)_3\}_3][AlCl_4]$	-8.6 (in CH_2Cl_2)	$[Na_n\{OC(CF_3)_3\}_{n-1}]^+$
$[P\{OC(CF_3)_3\}_4][P\{OCH(CF_3)_2\}_5F]$	-3.7 (in CH_2Cl_2/CH_3CN)	970.7 (positive)

Table 28: Summary of the $^{31}P\{^{1}H\}$ NMR and ESI-MS data for potential fluorinated phosphonium salts.

The $^{31}P\{^{1}H\}$ NMR chemical shifts from these reactions summarised in Table 28 are all within the expected region for phosphonium cations (*ca.* -20.0 to 100.0 ppm). However, it appears from literature that the high field NMR shifts are found in alky/halide phosphonium salts rather than tetraalkoxyphosphonium salts. The chemistry of non-fluorinated alkoxy phosphorus compounds is more developed, with a range of ^{31}P NMR chemical shift values identified in comparison to fluorinated alkoxy phosphorus compounds. Hence, one can compare the chemical shifts values of fluorinated phosphorus (III) and the fluorinated phosphorane compounds which are already known in literature and from the work of this thesis, to those found for non-fluorinated alkoxy compounds *i.e.* phosphorus (III)

compounds (*ca.* 90.0 to 250.0 ppm) and phosphoranes compounds (*ca.* -100.0 to -20.0 ppm). This comparison would suggest that the chemical shift values for fluorinated alkoxy phosphonium salts would be close to those observed for non-fluorinated alkoxy phosphonium salts. In addition, it can be summarised that the ^{31}P NMR chemical shifts for tetraalkoxyphosphonium salts are observed at similar chemical shifts to their phosphate analogues *i.e.* $[(CH_3CH_2O)_4P]^+[BF_4]^-$ (δ = 2.4 ppm) and $[(CH_3O)_4P]^+[BF_4]^-$ (δ = -1.9 ppm) species are observed at similar chemical shifts to their phosphate analogues (δ = 1.0 ppm and -5.2 ppm respectively). This would further indicate that tetraalkoxyphosphonium salts are more likely to appear at *ca.* 10.0 to -20.0 ppm. Since the phosphates, $O=P\{OCH(CF_3)_2\}_3$ and $O=P\{OC(CF_3)_3\}_3$ analogues for the phosphonium cations $[P\{OCH(CF_3)_2\}_4]^+$, (**9**) and $[P\{OC(CF_3)_3\}_4]^+$, (**8**) are known, this would suggest that the possible target cations (**8**) and (**9**) should be close to -3 to -4 ppm in the ^{31}P NMR spectrum.

4.3 PHOSPHINE-PHOSPHENIUM CHEMISTRY

4.3.1 Background Literature

Phosphenium ions ($[PR_2]^+$) are isolobal with singlet carbenes, see **A** in Figure 86. Their fundamental chemistry has been of interest for many years and they have found application as ligands in coordination chemistry, as building blocks in *catena*-phosphorus (P-P bonding) chemistry and they undergo a variety of interesting and potentially useful reactions with organic or inorganic substrates, including examples of C–H and even P_4 activation reactions.[251, 263-269] While phosphenium ions with a variety of substituents have been observed coordinated to a metal centre or stabilised by Lewis base coordination (*e.g.* **B** in Figure 86) the range of salts containing "free" $[PR_2]^+$ ions that have been isolated in condensed phases is almost exclusively limited to phosphenium ions having at least one π-donor group (usually $-NR_2$) at the phosphorus, see **C** in Figure 86.

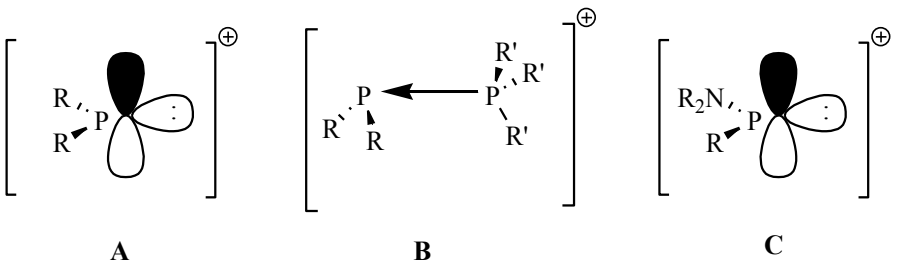

Figure 86: A: Phosphenium ions are isolobal with singlet carbenes, B: Phosphenium ions can be stabilised by Lewis base coordination, C: The condensed phase isolated phosphenium salts is almost exclusively limited to phosphenium ions having at least one p-donor group at the phosphorus, such as NR_2.

The diamidophosphenium cations are isolated as charge separated salts with a variety of anions, unlike the alkyl- or arylphosphenium cations.[266] The stability of $[(R_2N)_2P]^+$ cations is due to the donation of electron density from the amide lone pairs to the empty P_z orbital, which reduces the Lewis acidity of the free cation, see Figure 87. In comparison, the $[Ph_2P]^+$ cation has the potential for delocalisation of π-electron density from the aromatic rings to the empty p_z orbital, but this disrupts the aromatic π-system, hence is less favourable, see Figure 87.[270]

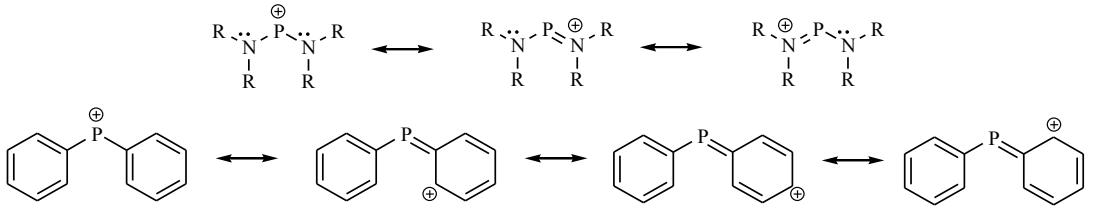

Figure 87: Line drawings showing resonance forms of diamidophosphenium (top) and diphenylphosphenium (bottom) cations.[270]

These features have a large effect on the acceptor chemistry of the two cations. The $[Ph_2P]^+$ cation forms donor-acceptor complexes with several phosphine ligands (PPh_3, PCy_3, PMe_3, $P(Cl)Ph_2$, DPPE and DPPH) and an N-heterocyclic carbene (NHC). However, this has not yet been isolated as a charge-separated salt of the free cation, whereas the $[(R_2N)_2P]^+$ cations only form complexes with strong σ-donors *e.g.* NHCs and PMe_3.[266, 271, 272]

The inability to synthesise salts of certain phosphenium ions is likely related to their highly electrophilic nature and the reactivity that this gives rise to. In recent years, WCA chemistry has revolutionised the study of highly electrophilic cations, and it is now possible to prepare salts of very reactive ions such as $[Me_3C]^+$ as stable salts "in a bottle".[252, 273-276] One might imagine that it is possible to use WCAs to stabilise "free" phosphenium ions with a range of substituents, even those that are highly electrophilic, but this appears not to be the case. Phosphenium ions that are not stabilised by π-donor substituents tend to form Lewis-acid-base adducts rather than "free" ions, even in the presence of the best WCAs. Understanding how the relative Lewis acidities of phosphenium ions change with different substituents at the phosphorus centre is crucial to understanding which cations are accessible as "free" ions. This can also act as a gauge for the σ-donating properties of the ligand, thus facilitating the design of ligands for particular applications *e.g.* in catalysis. The use of theoretical methods to design ligands in this way is of great interest *e.g.* in the use of ligand knowledge bases (LKB).[32-34, 46] Fluoride ion affinity (FIA) calculations are a simple way to gauge the relative Lewis acidities of phosphenium ions with different substituents, which can in turn be linked to the reactivity and the underlying electronic structure of these ions. By using FIAs rather

than other measures of Lewis acidity, it is straightforward to compare phosphenium ions with other Lewis acids, placing them on the general scale of Lewis acidity envisaged by Christe.[277] The Lewis acidity of these phospheniums can be reduced with π-donor substituents. Steric and inductive effects, which are less frequently discussed, can also affect the Lewis acidities of these ions. In addition, direct interaction between the phosphorus centre and more remote parts of the molecules can give rise to significant stabilisation in some cases (*i.e.* the F----- P contacts). In some cases steric effects are subtle, but in the case of very bulky ligands, FIAs can be dramatically reduced. This gives some hope that phosphenium ions that are currently unknown as "free" ions may yet be isolable without recourse to mesomeric stabilisation.[163]

Those stabilised by Lewis base coordination (*e.g.* **B** in Figure 86; R = Ph; R' = Ph, Cy, Me) have been studied in great detail by Burford *et al.*[158, 265, 278-282] They are referred to as phosphine-phosphenium donor-acceptor cationic complexes. Most current research on the interaction of neutral donors with phosphenium cations has involved either the $[Ph_2P]^+$ cation or the diamidophosphenium cations $[(R_2N)_2P]^+$. These phosphine-phosphenium donor-acceptor complexes contain homoatomic P-P coordinate bonds that are susceptible to ligand exchange reactions. A new P-P bond formation occurs on exchange, provided that the new ligand is more stabilising than the phosphine ligand in the phosphine-phosphenium complexes. This can be utilised to provide a versatile new synthetic method for the formation of P-P bonds.[265] This method can also be applied to other homoatomic coordination complexes *i.e.* stibine –stibenium salt.[283]

During the synthesis of the phosphine-phosphenium complexes, the Lewis-acid–base adducts are observed *i.e.* $R_2(Cl)P\text{-}ECl_3$; E = Al or Ga, in some cases. These tend to form for large substituents *i.e.* (R = ^{i}Pr, ^{t}Bu) on the phosphorus, as they hinder the chloride abstraction.[278] The chlorophosphine can also react with the solvent (the acidity of which is enhanced by the $GaCl_3$) and become protonated to give the $[R_2ClPH]^+$ species.[278] These Lewis acid–base adducts have been explored in the absence of solvents as RTILs, also known as molten mediums. These have found to be useful for P-P bond formations, when present in a mixture described by the authors as a "melt".[282] The "melt" consist of a variety of complex anions ($[Ga_2Cl_7]^-$ and $[Ga_3Cl_{10}]^-$) with the $[PPh_2\text{-}PPh_2Cl]^+$ cation and can be used with either $(PPh)_5$ to form a hexaphosphorus dication, or with gallium to form a $GaCl_3^-$-PPh_2^+-PPh_2^+- $GaCl_3^-$ diphosphane type species, see Scheme 40 below.[282]

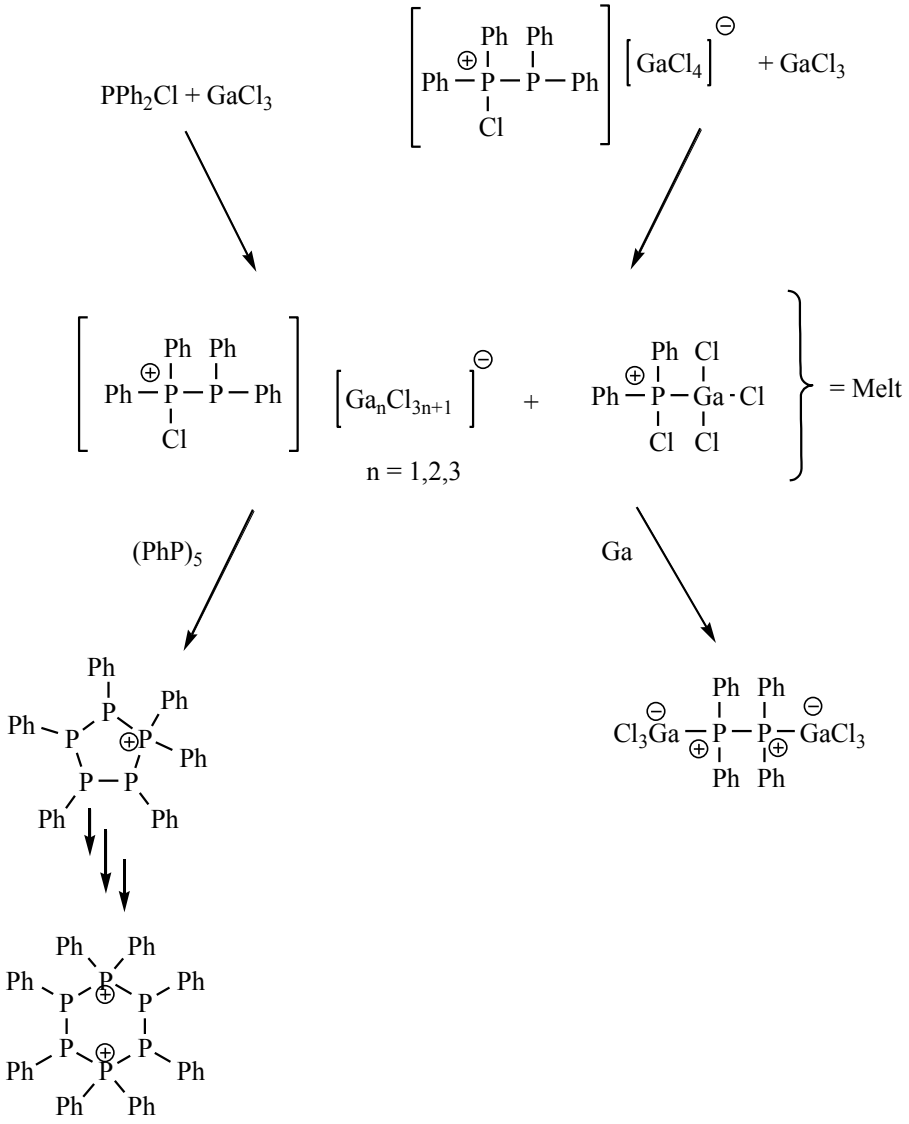

Scheme 40: Formation of a "melt", which can be further reacted for P-P bond formation. Adapted from ref. [282].

However, in most cases interaction with the Lewis acid ($AlCl_3$ or $GaCl_3$) and the chlorine centre of the $R_2(Cl)P$ species is preferred and often leads to heterolytic P-Cl cleavage to give the phosphenium salts.[266] Evidence for the anionic protection of phosphenium centres with N^{i}Pr substituents suggests a $[AlCl_4]^-$ aluminate or $[GaCl_4]^-$ gallate anion can better stabilise the cation than a $[BPh_4]^-$ anion.[280] The $[BPh_4]^-$ anion salt has been observed to react with chlorinated solvents, including the facile oxidative addition of DCM to the cation forming a phosphonium product.[280] It appears that the electron rich anions can protect the electrophilic centre of the cation, making them more susceptible to attack by the solvent as they now have a more "potent electrophilic reactivity than originally observed".[280] Long interatomic distances between counterions for these salts suggests that they are ionic in the solid state.[279] The use of trimethylsiyl triflate, $Me_3SiO_3SCF_3$ in place of a Lewis acid also successfully yields the $[PPh_2\text{-}PR_3]^+[O_3SCF_3]^-$ (R = Ph, Cy, Me) salts.[265] Crystal structures of the [PPh_2-

$PPh_3]^+$ cation with both the $[O_3SCF_3]^-$ and the $[GaCl_4]^-$ anions show that the P-P bond length is independent of the anion *i.e.* 2.230(1) Å and 2.220(6) Å respectively. Table 29 lists the bond lengths of known P-P bond lengths for arrange of phosphine-phosphenium reactions found in the literature.

$[PR_2$-P(III)$]^+[A]^-$	*P-P (Å)*	*Reference*
$[PPh_2\text{-}PPh_3]^+[O_3SCF_3]^-$	2.230(1)	[265]
$[PPh_2\text{-}PPh_3]^+[GaCl_4]^-$	2.220(6)	[265]
$[PPh_2\text{-}PCy_3]^+[O_3SCF_3]^-$	2.220(1)	[265]
$[PPh_2\text{-}PPh_2Cl]^+[GaCl_4]^-$	2.205(4)	[265]
$[PPh_2\text{-}PMe_3]^+[O_3SCF_3]^-$	2.187(2)	[265]
$[PPh_2\text{-dppm}]^+[O_3SCF_3]^-$	2.163(1)	[158]

Table 29: The P-P (Å) bond lengths from the phosphine-phosphenium crystal structures.

Attempts to isolate the "free" $[PMe_2]^+$ ion by Burford *et al*. led to the discovery of the $[GaCl_3\text{-}PMe_2\text{-}PMe_2Cl]^+[GaCl_4]^-$ ionic material.[281] A crystal structure of this material has been isolated, showing two adjacent tetracoordinate phosphorus centres, as it represents a PMe_2Cl moiety coordinated to a phosphenium $[PMe_2]^+$ moiety, which is in turn coordinated to a $GaCl_3$ molecule.[281] The melting point of the $[GaCl_3\text{-}PMe_2\text{-}PMe_2Cl]^+[GaCl_4]^-$ ionic material has a 78-80 °C range, suggesting this could be a potential new IL. The equilibrium favours this new cation in the presence of excess $GaCl_3$, as the lone pair on the phosphenium ion has a weak Lewis basicity towards $GaCl_3$, see Figure 88. The interaction with this quadrupolar gallium nucleus causes the ^{31}P NMR signal (-16 ppm, br) to broaden, while that for the $[PMe_2\text{-}PMe_2Cl]^+[GaCl_4]^-$ ionic species consists of a sharp doublet (-36 ppm, d).[281]

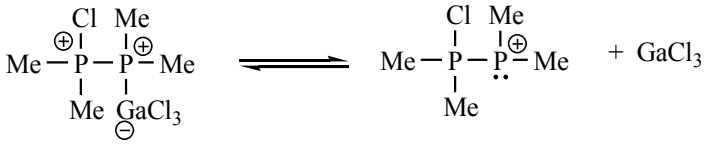

Figure 88: Equilibrium favours the $[GaCl_3\text{-}PMe_2\text{-}PMe_2Cl]^+[GaCl_4]^-$ ionic material over the $[PMe_2]^+[GaCl_4]^-$ when excess $GaCl_3$ is added to the $[PMe_2\text{-}PMe_2Cl]^+[GaCl_4]^-$ phosphine-phosphenium adduct.[281]

4.3.2 Fluorinated Phosphorus (III)-Phosphenium Salts

The phosphorus (III) ligands (**1**) to (**6**) described in this thesis have been used to stabilise diphenyl-phosphenium ions, $[PPh_2]^+$. These can be prepared using a strong Lewis acid, such as $AlCl_3$. This Lewis acid can abstract a chloride from the PPh_2Cl phosphine, to forms a diphenyl-phosphenium ion stabilised by a PPh_2Cl molecule. However, in the presence of a

more σ-donating ligand than PPh_2Cl, a new P-P bond can be formed *via* ligand exchange, see Scheme 41.

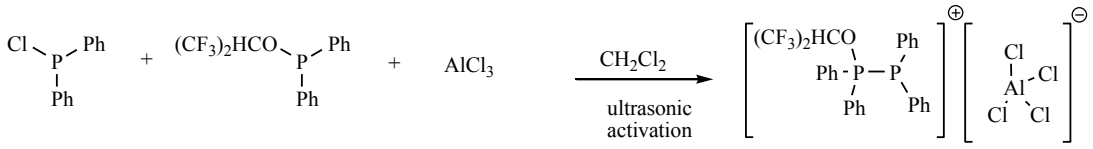

Scheme 41: Synthesis of novel fluorinated ligand stabilised phosphenium ions, the example above uses the $PPh_2\{OCH(CF_3)_2\}$, (2) ligand.

All the ligands except the poorly nucleophilic tris(perfluoro-*t*-butyl)phosphite, $P\{OC(CF_3)_3\}_3$, (**2**) and $PhP\{OC(CF_3)_3\}_2$, (**4**) successfully stabilised the diphenyl-phosphenium ions, see Table 30 for $^{31}P\{^1H\}$ NMR data. In the case of the $P\{OC(CF_3)_3\}_3$, (**2**) ligand, only the free ligand and a PPh_2Cl-$AlCl_3$ adduct (δ_P = 41.2 ppm) was observed in the spectra. The large steric influence of the $P\{OC(CF_3)_3\}_3$, (**2**) phosphite or the reduced nucleophilicity in comparison to PPh_2Cl, or a combination of both these properties is likely to inhibit the formation of a novel donor-acceptor cationic complex with (**2**). On removal of the solvent, oily products were observed for all the novel ligand-stabilised-phosphenium complexes. In the presence of the $PhP\{OC(CF_3)_3\}_2$, (**4**) ligand (δ_P = 190.4 ppm), a PPh_2Cl-$AlCl_3$ adduct (δ_P = 41.5 ppm) and the $[PPh_2\text{-}PPh_2Cl]^+[AlCl_4]^-$ (δ_P = 1.0, d, $^1J_{PP}$ = 394 Hz and 74.0, d, $^1J_{PP}$ = 391 Hz ppm), were also observed in the spectra. In addition to this, weaker intensity signals were observed at 75.5 (s), 62.6 (s) and 55.3 (s) ppm. The chemical shifts at 75.5 (s) and 55.3 (s) ppm can be assigned as potentially the $PPh\{OC(CF_3)_3\}_2$-$AlCl_3$ and $PPhCl\{OC(CF_3)_3\}$-$AlCl_3$ adducts respectively. The chemical shift at 62.6 (s) may tentatively be assigned as the $PPhCl_2$-$AlCl_3$ adduct, found in the literature to appear at 69.1 ppm in DCM solvent.[284] However the latter adduct is interestingly found to have different chemical shift values dependent on the exact stoichiometry used. $PPhCl_2$ (1 eq.) with $AlCl_3$ (1 eq) in DCM is believed to potentially form the adduct with resonances at 112.1 (s) and 84.3 (s) ppm.[284] The reaction of $PPhCl_2$ (1 eq.) with $AlCl_3$ (2 eq.) in DCM consists of only one resonance at 69.1 (s) ppm and reaction of reaction of $PPhCl_2$ (2 eq.) with $AlCl_3$ (1 eq.) in DCM consists of one resonance at 110.9 (s) ppm.[284]

Synthesis of the phosphorus (III)-phosphenium complexes was trialled with trimethylsilyl triflate, $Me_3SiO_3SCF_3$ rather than the Lewis acidic $AlCl_3$. However, even after heating (50 °C, 7 hours) no reaction seemed to have taken place. Product signals of very weak intensity were observed in the $^{31}P\{^1H\}$ NMR spectra after the reaction mixture was placed *in vacuo*, to remove the Me_3SiCl side product, see Scheme 42.

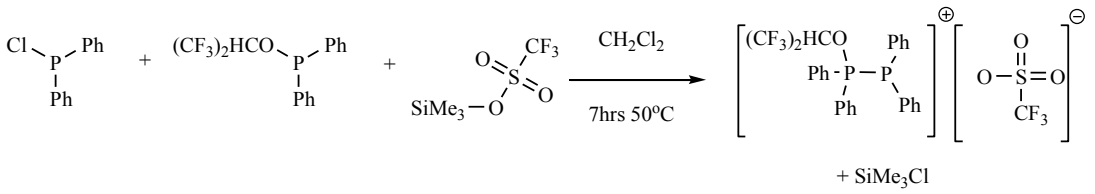

Scheme 42: Synthesis of the novel fluorinated ligand stabilised phosphenium complexes with trimethylsilyl triflate in place of the Lewis acidic $AlCl_3$.

The signals were very broad, suggesting fast exchange with other species in the reaction mixture was taking place. Many unknown peaks were observed in the $^{31}P\{^{1}H\}$ NMR spectra, suggesting this method was not as selective as the $AlCl_3$ method. It was thought some of the additional peaks could be due to oxidation of the ligand to give $[Me_3SiPR_3]^+[O_3SCF]^-$ type species (R = $OCH(CF_3)_2$, $OC(CF_3)_3$, Ph). However, reaction of $Ph_2P\{OCH(CF_3)_2\}$, (**5**) with $Me_3SiO_3SCF_3$ in DCM solvent gave no new products in the $^{31}P\{^{1}H\}$ NMR spectra. The Lewis acidic $GaCl_3$ was also trialled in place of $AlCl_3$, but although the reagent was more soluble in DCM solvent and required no ultrasonic activation, again product selectivity was an issue as a range of doublets was observed in the $^{31}P\{^{1}H\}$ NMR spectra. It has been reported that a strong P-P interaction tends to have a larger $^{1}J_{PP}$ coupling constant.[10, 11] Table 30 presents the $^{1}J_{PP}$ values along with the chemical shifts for all the novel fluorinated ligand-phosphenium complexes obtained.

$[PPh_2$-P(III) Ligand$]^+$ $[AlCl_4]^-$	*$^{31}P\{^{1}H\}$ NMR (δ/ppm)*
$P\{OCH(CF_3)_2\}_3$, (**1**)	87.0 (d, 363) and -16.3 (d, 370)
$PhP\{OCH(CF_3)_2\}_2$, (**3**)	71.7 (d, 393) and 58.2 (d, 393)
$Ph_2P\{OCH(CF_3)_2\}$, (**5**)	87.0 (d, 364) and -16.2 (d, 370)
$Ph_2P\{OC(CF_3)_3\}$,(**6**)	89.1 (d, 375) and -12.2 (d, 375)

Table 30: The $^{31}P\{^{1}H\}$ NMR (δ/ppm) data including the $^{1}J_{PP}$ values for all the novel fluorinated ligand-phosphenium complexes obtained.

The high field chemical shift values are likely for the tetracoordiante phosphonium-like environment and the low field chemical shift values for the tricoordinate phosphine-like environment. If one was to use to use the $^{1}J_{PP}$ coupling constants to determine the strengths of the P-P bonds, then it would appear that the $PhP\{OCH(CF_3)_2\}_2$, (**3**) ligand forms the strongest bond with the phosphenium cation. This ligand may have the correct steric and electronic properties to allow for sufficient σ-donation to the $[PPh_2]^+$ cation. The remaining

three ligands (**1**), (**5**), and (**6**) all have $^{1}J_{PP}$ coupling constant values of a similar magnitude. DFT optimised structures performed at the (RI-)BP86/SV(P) level allow for the P-P bond distances to be compared for the six ligand systems (**1**) to **(6)**. The results are consistent with the $^{1}J_{PP}$ coupling constants, suggesting the $PhP\{OCH(CF_3)_2\}_2$, (**3**) ligand has the strongest P-P bond (2.258 Å). The DFT study also indicates that the $P\{OC(CF_3)_3\}_3$, (**2**) ligand does not form a Lewis donor-acceptor adduct with the $[PPh_2]^+$ cation, as no P-P bond (5.217 Å between the uncoordinated two molecules) is found after various attempts in many orientations. This is consistent with the experimental results from any synthetic attempts for the formation of this species. The P-P bond distances from this DFT study did however indicate that the $P\{OCH(CF_3)_2\}_3$, (**1**) ligand adduct has a very similar bond length to the $PhP\{OCH(CF_3)_2\}_2$, (**3**) adduct, see Table 31.

$[PPh_2$-P(III)$]^+$	*P-P (Å)*
$[PPh_2\text{-}PhP\{OCH(CF_3)_2\}_2]^+$	2.258
$[PPh_2\text{-}P\{OCH(CF_3)_2\}_3]^+$	2.259
$[PPh_2\text{-}Ph_2P\{OCH(CF_3)_2\}]^+$	2.267
$[PPh_2\text{-}Ph_2P\{OC(CF_3)_3\}]^+$	2.302
$[PPh_2\text{-}PhP\{OC(CF_3)_3\}_2]^+$	2.316
$[PPh_2\text{-}P\{OC(CF_3)_3\}_3]^+$	5.217

Table 31: The P-P (Å) bond lengths of DFT optimised structures at the (RI-)BP86/SV(P) level for the novel fluorinated ligand-diphenylphosphenium complexes.

Interestingly the DFT calculations suggest a phosphenium-phosphonite complex can form for the $PhP\{OC(CF_3)_3\}_2$, (**4**) ligand, as a bond length of 2.316 Å is observed. Slightly longer P-P bond lengths are observed for both the adducts with the ligands containing the perfluoro-*t*-butoxy groups; $PhP\{OC(CF_3)_3\}_2$, (**4**) and $Ph_2P\{OC(CF_3)_3\}$, (**6**). This may be an attribute due to the perfluoro-*t*-butoxy groups being less flexible and having a greater steric influence, leading to reduced orbital overlap with the phosphorus ligand lone pair and the phosphenium p_z orbital. Figure 89 represents the optimised structures for each ligand (**1**) to (**6**) with a $-PPh_2$ fragment.

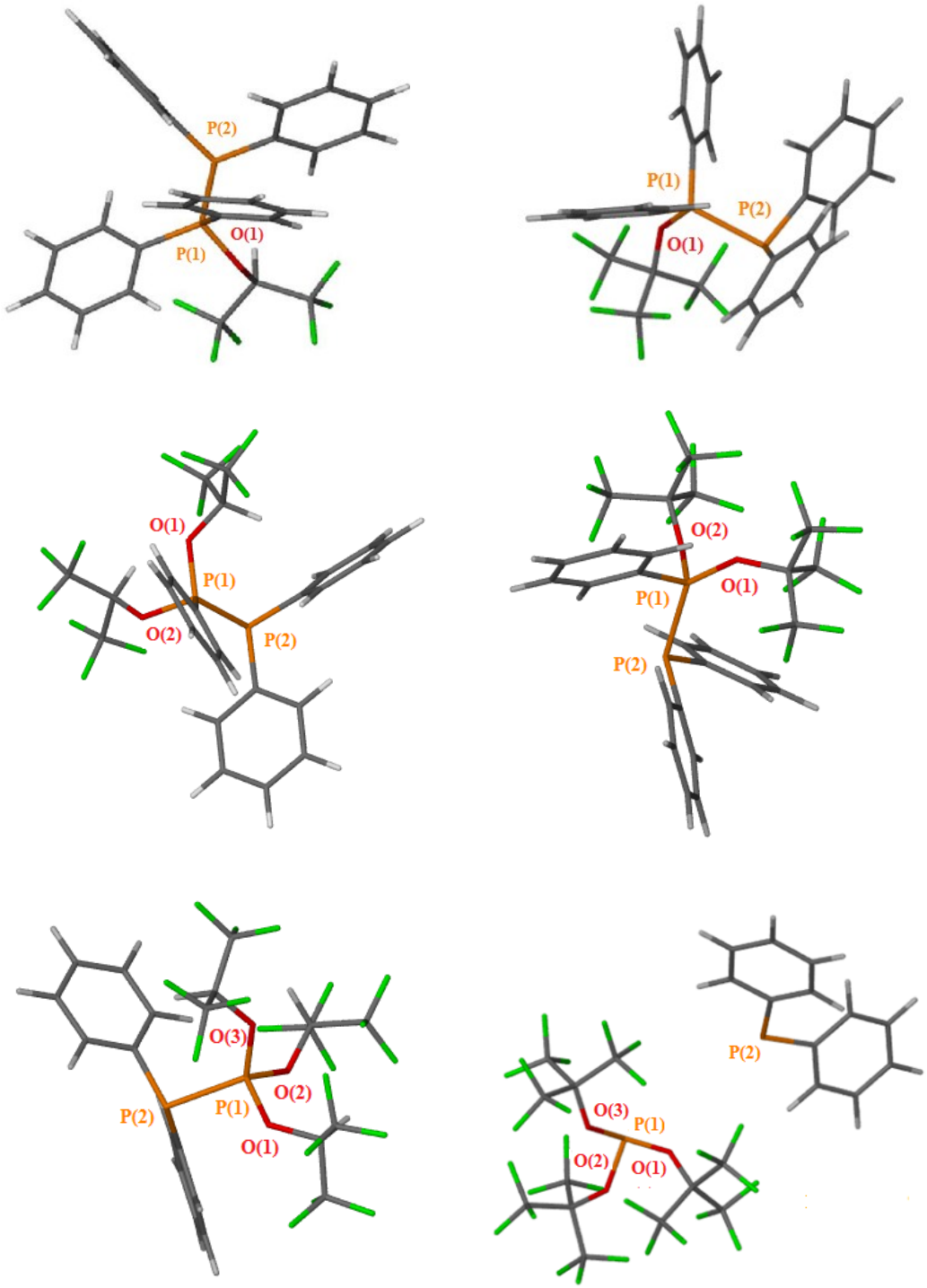

Figure 89: DFT optimised structures at the (RI-)BP86/SV(P) level for the novel fluorinated ligand-phosphenium complexes. From the top left ligands (5), (6), (3), (4), (1) and (2) respectively.

Interestingly reaction of the $Ph_2P\{OCH(CF_3)_2\}$, (**5**) ligand with $AlCl_3$ alone in DCM solvent also gave the ligand-stabilised phosphenium ion, $[PPh_2\text{-}Ph_2P\{OCH(CF_3)_2\},]^+$ as well as the $Ph_2P\{OCH(CF_3)_2\}$-$AlCl_3$ adduct. The ligand-stabilised phosphenium ion was observed by both $^{31}P\{^1H\}$ NMR and ESI-MS (537.1 m/z for the $[M]^+$). This suggests a hexafluoroisopropoxy group can be abstracted by $AlCl_3$ to form an $[AlCl_3\{OCH(CF_3)_2\}]^-$ anion. However, attempts to abstract an alkoxy group from either the $P\{OCH(CF_3)_2\}_3$, (**1**) and $P\{OC(CF_3)_3\}_3$, (**2**) phosphite ligands to give $[P(OR^F)_2\text{-}P(OR^F)_3]^+$ type species were unsuccessful. It is thought the $P\{OC(CF_3)_3\}_3$, (**2**) phosphite cannot provide sufficient σ-donation to stabilise the cationic phosphenium species. However, in the $P\{OCH(CF_3)_2\}_3$, (**1**) case, although no doublets were observed for the ligand stabilised phosphenium ion in the $^{31}P\{^1H\}$ NMR spectra, signals for the $P\{OC(CF_3)_3\}_2Cl$ and $P\{OC(CF_3)_3\}Cl_2$ species were observed. This suggests alkoxy/chloride exchange had taken place rather than alkoxy abstraction, forming the $Al\{OC(CF_3)_3\}_2Cl$ and $Al\{OC(CF_3)_3\}Cl_2$ species too. Other attempts to form $[P(OR^F)_2\text{-}P(OR^F)_3]^+$ type species, involved the reaction of $P\{OC(CF_3)_3\}_2Cl$, $P\{OCH(CF_3)_2\}_3$, (**1**) and $AlCl_3$ in DCM solvent. However, again only alkoxy/chloride exchange (*e.g.* PCl_3, δ_P = 220.0 ppm; $P\{OC(CF_3)_3\}_2Cl$, δ_P = 216.0 ppm; $P\{OC(CF_3)_3\}Cl_2$ δ_P = 191.0 ppm; $P\{OCH(CF_3)_2\}_2Cl$, δ_P = 187.0 ppm; $P\{OCH(CF_3)_2\}Cl_2$ δ_P = 170.0 ppm; $P\{OCH(CF_3)_2\}_3$, δ_P = 140.0 ppm) and adduct formation, $P\{OCH(CF_3)_2\}_3$-$AlCl_3$ (δ_P = 68.0 ppm) was observed.

4.4 SUMMARY

Although WCCs that are base-resistant and WCCs that form ILs are currently available, there are few cations that are both base resistant and form IL phases. Investigations into the synthesis of these types of cations with the use of highly fluorinated alkoxy substituents on phosphonium based cations were of key interest for this thesis. In particular perfluorinated cations were investigated as these have the advantage to avoid any decomposition *via* C-H activation, the common decay pathway of phosphonium salts. In addition, the bulky fluorinated alkoxy groups on the phosphonium centre would reduce the interionic interactions (and hence be better for ILs). Previous advances in WCA and WCC chemistry have generally relied on making larger cations (and anions in WCA chemistry) in order to reduce Coulombic interactions between the anion and cation. Although it is known that increasing the size of an ion weakens the coordination,[253] there is a limit where increasing the size will have little effect on its coordination ability, as shown by Coulombs law. The perfluorinated-alkoxyphosphonium ion $[P\{OC(CF_3)_3\}_4]^+$, (**8**) is thought to have good potential as a WCC, due to the surface repulsion formed by a partial negative charge from the C-F bonds that coat the cation. The formation of (**8**) has found to be synthetically challenging. Various methods for the synthesis of (**8**) and related species, $[P\{OCH(CF_3)_2\}_4]^+$, (**9**) were employed. These included oxidation of the phosphorus (III) ligands (**1**) to (**6**). *N*-bromosuccinimide (NBS) was trialled as a halogenation reagent with $P\{OC(CF_3)_3\}_3$, (**2**). The reaction proceeds consistently to a product with the same chemical shift (δ_P = -29.9 ppm, s), even with the use of different solvents (diethyl ether and MeCN). The chemical shift is closer to the phosphorane region (*ca.* -100.0 to -20.0 ppm) rather than that expected for phosphorus cations (*ca.* -20.0 to 100.0 ppm). However, the results are promising as they indicate that halogenation is potentially possible for (**2**). This may provide a possible route to the synthesis of bulky perfluoro-*t*-butoxy substituent-containing cations

Methyl triflate has been found to be useful for the synthesis of phosphonium cations *via* methylation of (**3**) and (**5**). This is a likely effect of the triflate anion providing stabilisation of the phosphonium cations formed by the triflate anion. Reaction with methyl triflate and $PPh_2OCH(CF_3)_2$, (**5**), (the most nucleophilic ligand of the six prepared in this thesis) leads to the formation of the phosphonium salt $[MePPh_2OCH(CF_3)_2]^+[O_3SCF_3]^-$, (**10**). This salt has been successfully isolated and crystals suitable for single-crystal X-ray diffraction analysis were grown. Interestingly, this new salt has a melting point range of 101-103 ˚C, which is border line for a potential new IL and lower than that reported for the known $[MePPh_2OCH(CF_3)_2]^+[I]^-$ ionic salt (mp = 120-125 ˚C).[260] The $[MePPh_2OCH(CF_3)_2]^+[O_3SCF_3]^-$, (**10**) salt has been found to be moisture-sensitive. Reaction

of methyl triflate with $PPh\{OCH(CF_3)_2\}_2$, (**3**) showed evidence of the $[MePPh\{OCH(CF_3)_2\}_2]^+[O_3SCF_3]^-$, (**11**) salt in the $^{31}P\{^1H\}$ NMR spectrum (δ_P = ~86 ppm, dependent on reaction solvents) after heating the reaction mixture. However isolation of this salt is difficult. The $^{31}P\{^1H\}$ NMR spectra indicates that signals close to that expected for $(O)PMePhOCH(CF_3)$ are present, suggesting this ionic salt is not stable towards the Michaelis-Arbusov reaction. Perhaps another stronger WCA is required to isolate this product, as this would reduce anionic interaction and further stabilise the reactive phosphonium ion and inhibit the Michaelis-Arbusov reaction. Methylation using methyl triflate with the other ligands trialled *e.g.* $P\{OCH(CF_3)_2\}_3$, (**1**), $P\{OC(CF_3)_3\}_3$, (**2**), and $PPh_2\{OC(CF_3)_3\}$, (**6**), showed no evidence of the phosphonium salts in the $^{31}P\{^1H\}$ NMR spectra. It is likely that the reduced nucleophilicity of these ligands (as discussed in Chapter 2) limits any reaction with the methyl triflate. It is clear from the methylation reactions that a temperature balance is required; it must be sufficiently high enough to allow synthesis of the phosphonium salt but as low as possible to avoid decomposition to the Michaelis-Arbuzov products. Perhaps the use of a WCA would sufficiently to stabilise the phosphonium cations and reduce the rate of decomposition, so isolation can be achieved.

The one pot reactions trialled with PCl_5, $MOC(CF_3)_3$ (M = Li, Na) and $LiN\{O_2S(CF_3)\}_2$ were also found to have reduced selectivity, as many products were observed by $^{31}P\{^1H\}$ NMR spectroscopy. These included $P\{OC(CF_3)_3\}_3$, $P\{OC(CF_3)_3\}Cl_4$, $P\{OC(CF_3)_3\}_2Cl_3$, $(O)P\{OC(CF_3)_3\}_3$ type species. In addition, ESI-MS was not useful for analysis of crude reaction mixtures, as it was crowded by many peaks originating from $[Li_n\{OC(CF_3)_3\}_{n-1}]^+$ or $[Li_n\{OC(CF_3)_3\}_{n+1}]^-$ clusters (in the positive and negative mode respectively), with various amounts of diethyl ether solvent coordinated. This made identification of other cationic (or anionic species) difficult. However, one reaction mixture contained signals at 9.7 ppm (s) and 7.5 ppm (s) in the $^{31}P\{^1H\}$ NMR spectrum. These could possibly be for the target cation $[P\{OC(CF_3)_3\}_4]^+$, (**8**). Interestingly, a molecular ion peak with the correct isotope pattern was observed at 970.7 m/z in the ESI-MS positive mode for the target cation $[P\{OC(CF_3)_3\}_4]^+$ and the molecular ion for $[N\{O_3S(CF_3)\}_2]^-$ at 279.9 m/z in the negative mode, but isolation of this material was unsuccessful due to the presence of a range of impurity products. This suggests that this synthetic route is inefficient and perhaps overcomplicates the isolation of $[P\{OC(CF_3)_3\}_4]^+$, (**8**) making it unsuitable. Similarly the ligand redistribution reactions of $P\{OC(CF_3)_3\}_2Cl_3$ are perhaps thermodynamically unfavourable without the presence of a WCA. It has been shown that the fluoride substituents of a $[PF_6]^-$ anion tend to exchange with the alkoxide/chloride substituents and it is thought that if the ionic isolation $[P\{OC(CF_3)_3\}_4]^+[PCl_6]^-$ was formed, then this too would exchange or form the more stable phosphorane species due to inadequate stabilisation from the $[PCl_6]^-$ anion.

Syntheses of the $[PX_4]^+$ (X = Cl, Br) cations were also trialled *via* abstraction of a halide from PX_5 (X = Cl, Br) with $AlCl_3$, a strong Lewis acid, to give $[PCl_4]^+[AlCl_4]^-$ and $[PBr_4]^+[AlCl_4]^-$ salts. These were used for further reactions *in situ* for reactions involving nucleophilic substitution of the X groups with metal alkoxides, MOR^F {M = Li, Na; OR^F = $OC(CF_3)_3$, $OCH(CF_3)_2$}. The -$OCH(CF_3)_2$ groups were found to be sterically insufficient to avoid nucleophilic attack at the phosphonium centre of (**9**) by another $[OCH(CF_3)_2]$- ion, as only formation of the phosphorane, $P\{OCH(CF_3)_2\}_5$, (**16**) was consistently observed by $^{31}P\{^1H\}$ NMR spectroscopy. Similar reactions with the bulkier perfluoro-*t*-butoxy group consisted of a range of signals. Although no signals were observed for the neutral phosphoranes, $P\{OC(CF_3)_3\}_4Cl$, or $P\{OC(CF_3)_3\}_5$, (**16**). The observed signals included; δ_P 85.4 ppm (s), 61.8 ppm (s), 28.8 ppm (s) and -8.6 ppm (s). These are tentatively assigned as $[PCl_4]^+$, $[PCl_3\{OC(CF_3)_3\}]^+$, $[PCl_2\{OC(CF_3)_3\}_2]^+$, and $[PCl\{OC(CF_3)_3\}_3]^+$ salts respectively. These cations may form by a mixture of chloride and alkoxide exchange with both the anion and cation. These results look promising and suggest the extra steric bulk of the -$OC(CF_3)_3$ group prevent formation of phosphoranes and this synthetic route may potentially prove to be very useful for the formation of $[P\{OC(CF_3)_3\}_4]^+$, (**8**).

Lewis-acid-mediated halide/alkoxide abstraction from $P\{OCH(CF_3)_2\}_{5-n}Cl_n$ phosphoranes were also explored. Fluorinated alkoxyphosphoranes were of main focus as they are simple to synthesise and it was hoped that these could act as scaffolds for the generation of these new fluorinated WCCs. However, reaction of $P\{OCH(CF_3)_2\}_4Cl$ with KPF_6 were found to form phosphoranes of the type PF_5 and $P\{OCH(CF_3)_2\}_4F$ *via* chloride/fluoride or alkoxide/fluoride ligand exchange. Reactions of $P\{OCH(CF_3)_2\}_4Cl$ with $LiAl\{OC(CF_3)_3\}_4$ also formed the $P\{OCH(CF_3)_2\}_4F$ species. However, additional signals that could potentially relate to the $[P\{OCH(CF_3)_2\}_4]^+$, (**9**) cation were observed in the $^{31}P\{^1H\}$ NMR spectrum. Isolation of any potential cation *via* fluorobenzene stabilisation *i.e.* $[P\{OCH(CF_3)_2\}_4C_6H_5F]^+$ was unsuccessful. Again ESI-MS (from MeCN solution) in the positive mode was dominated by $[Li_{n+1}\{OCH(CF_3)_2\}_n]$ clusters. Abstraction of a chloride from the neutral $P\{OC(CF_3)_3\}_4Cl$ species was also attempted but the synthesis of the phosphorane proved to be difficult. The reactions consistently formed $P\{OC(CF_3)_3\}_3$, (**2**). The phosphite, (**2**) may have formed during these reactions *via* reductive elimination of the hypochlorite, $ClOC(CF_3)_3$ or the peroxide, $(CF_3)_3COOC(CF_3)_3$ from the phosphoranes, $P\{OC(CF_3)_3\}_4Cl$ or $P\{OC(CF_3)_3\}_5$, to reduce steric strain on the phosphorus centre from the incredibly bulky substituents. Alternatively, the phosphoranes may behave as oxidising agents (towards the solvent or potentially $NaOR^F$) forming phosphorus (III) halides/alkoxides that go on to react further. Attempts to synthesise the phosphonium cation *via* abstraction of an alkoxy, -$OCH(CF_3)_2$, group from the phosphorane, $P\{OCH(CF_3)_2\}_5$ with the Lewis acidic $AlCl_3$ gave

a signal at -20.1 ppm (s) in the $^{31}P\{^{1}H\}$ NMR, this is consistent with the $^{31}P\{^{1}H\}$ NMR data for the reaction of $P\{OCH(CF_3)_2\}_4Cl$ and $AlCl_3$. This method seems to potentially be a useful approach for the isolation $[P\{OCH(CF_3)_2\}_4]^+$, (**9**) without the presence of excess $MOCH(CF_3)_2$ (M = Li, Na) to form the phosphorane. Future work with the right Lewis acid *i.e.* the bulky $Al(OCH(CF_3)_2)_3$ or $Al(OC(CF_3)_3)_3$, may prove to be successful in its isolation, due to greater stabilisation from a better WCA.

These results suggest that the salts of both $[P\{OCH(CF_3)_2\}_4]^+$, (**9**) and $[P\{OC(CF_3)_3\}_4]^+$, (**8**) may have been observed in condensed phases, but the reaction mixtures are often complex and purification of products has proved difficult. The extreme sensitivity of these materials, and related phosphoranes, towards moisture, the potential for redox chemistry leading to phosphorus (III) products and the potential for ligand exchange (between phosphoranes, the cations themselves and between anions and cations) makes this system synthetically challenging. However, there is scope for future work to capitalise on these observations and it is hoped that the right conditions may be found to allow the isolation of these potentially very interesting materials.

Finally, the phosphorus (III) ligands (**1**), (**3**), (**5**) and (**6**) described in this thesis have been used to stabilise diphenyl-phosphenium ions, $[PPh_2]^+$ forming P-P bond *via* ligand exchange. The $^{1}J_{PP}$ coupling constants were used to determine the strengths of the P-P bonds. The $P\{OCH(CF_3)_2\}_3$, (**1**) and $PhP\{OCH(CF_3)_2\}_2$, (**3**) ligands were found to form the strongest bonds with the phosphenium cation. This is probably an effect of $PhP\{OCH(CF_3)_2\}_2$, (**3**) containing the correct balance in terms of both steric and electron properties, whereas although $P\{OCH(CF_3)_2\}_3$, (**1**) ligand has a greater π-acidic nature the steric bulk is likely to reduce sufficient P-P overlap for the formation of a stronger bond. The remaining three ligands (**1**), (**5**), and (**6**) all have $^{1}J_{PP}$ coupling constant values of a similar magnitude. DFT optimised structures performed at the (RI-)BP86/SV(P) level were used to compare the strengths of the P-P bond distances with the $^{1}J_{PP}$ coupling constants. These results were found to be consistent suggesting the $P\{OCH(CF_3)_2\}_3$, (**1**) ligand and $PhP\{OCH(CF_3)_2\}_2$, (**3**) ligand have the strongest P-P bonds (2.259 Å) and 2.258 Å respectively). The DFT study also indicates that the $P\{OC(CF_3)_3\}_3$, (**2**) ligand does not form a Lewis donor-acceptor adduct with the $[PPh_2]^+$ cation, as no P-P bond (5.217 Å between the uncoordinated two molecules) is found after various attempts in many orientations. Slightly longer P-P bond lengths are observed for both the adducts with the ligands containing the perfluoro-*t*-butoxy groups; $PhP\{OC(CF_3)_3\}_2$, (**4**) and $Ph_2P\{OC(CF_3)_3\}$, (**6**). This may be an attribute due to the perfluoro-*t*-butoxy groups being less flexible and having a greater steric influence, again leading to reduced orbital overlap with the phosphorus ligand lone pair and the phosphenium

p_z orbital. Reaction of $Ph_2P\{OCH(CF_3)_2\}$, (**5**) with $AlCl_3$ in DCM solvent also gave the ligand stabilised phosphenium ion, $[PPh_2\text{-}Ph_2P\{OCH(CF_3)_2\},]^+$ as well as the $Ph_2P\{OCH(CF_3)_2\}\text{-}AlCl_3$ adduct. This suggests an hexafluoroisopropoxy group can be abstracted from the ligand by $AlCl_3$ to form an $[AlCl_3\{OCH(CF_3)_2\}]^-$ anion. However, attempts to abstract an alkoxy group from either the $P\{OCH(CF_3)_2\}_3$, (**1**) and $P\{OC(CF_3)_3\}_3$, (**2**) phosphite ligands to give $[P(OR^f)_2\text{-}P(OR^f)_3]^+$ type species were unsuccessful. Alkoxy/chloride exchange had taken place rather than alkoxy abstraction, forming $P\{OC(CF_3)_3\}_2Cl$ and $P\{OC(CF_3)_3\}Cl_2$ species.

4.5 FUTURE WORK:

Investigations into the synthesis of fluorinated phosphonium cations have provided a greater understanding of the conditions required for their isolation and a taste of the type of synthetic procedures that could potentially lead to these ions in the condensed phase in the future. Halogenation of the fluorinated phosphites (**1**) and (**2**) could be investigated further, in particular with the use of bromine, Br_2. Although there is potential that this may lead to the phosphorane, $P(OR^F)_3Br_2$, perhaps with the use of a WCA silver salt *i.e.* $Ag[Al\{OC(CF_3)_3\}_4]$, this could inhibit $P(OR^F)_3Br_2$ formation and favour $[P(OR^F)_3Br]^+[WCA]^-$ salt formation, see **A** in Scheme 43. Other potential synthetic routes include the use of the phosphite with the corresponding hypochlorite and antimony pentachloride to provide a better stabilising WCA than a chloride anion, see, **B** in Scheme 43. Similar type of reaction could also be trialled with the fluorinated phosphite, fluorinated peroxide and a strong Lewis acid *i.e.* $Al\{OC(CF_3)_3\}_3$, see **C** in Scheme 43. Other possible solutions involve synthesis of the oxonium fluoro-borates salts and reacting these with the phosphates, see **D** in Scheme 43.

A $P\{OC(CF_3)_3\}_3 + Br_2 + Ag[Al\{OC(CF_3)_3\}_4] \longrightarrow [P\{OC(CF_3)_3\}_3Br]^+[Al\{OC(CF_3)_3\}_4]^- + AgBr$

B $P\{OC(CF_3)_3\}_3 + ClOC(CF_3)_3 + SbCl_5 \longrightarrow [P\{OC(CF_3)_3\}_4]^+[SbCl_6]^-$

C $P\{OC(CF_3)_3\}_3 + (CF_3)_3COOC(CF_3)_3 + Al\{OC(CF_3)_3\}_3 \longrightarrow [P\{OC(CF_3)_3\}_4]^+[Al\{OC(CF_3\}_3\}_4]^-$

D $O{=}P\{OC(CF_3)_3\}_3 + [O\{C(CF_3)_3\}_3]^+[BF_4]^- \longrightarrow [P\{OC(CF_3)_3\}_4]^+[BF_4]^- + O\{C(CF_3)_3\}_2$

Scheme 43: Potential synthetic methodology to the perfluorinated phosphonium cation, (8).

ESI-MS is found not to be very useful for the identification of the target cations (**8**) and (**9**). The spectra tend to either be dominated by metal alkoxide clusters with coordinated solvent molecules, phosphonium cations are observed from ionisation of neutral compounds and ligand scrambling in the gas phase, making it difficult to understand if the synthesis has been achieved in the condensed phase. NMR spectroscopy, in particular $^{31}P\{^1H\}$ NMR spectroscopy is a key analytical technique for identification of any product peaks. However, since many signals are observed in the expected regions, perhaps calculated chemical shift values using computational chemistry *i.e.* DFT routes may provide a greater understanding on the important chemical shifts. Similarly to the theoretical route, the synthesis of the target cations (**8**) and (**9**) could be explored practically with the carborane anions. Although these

are expensive, difficult to prepare and would not be used on large scale synthesis, they may provide the required chemical shifts which in turn could be used for comparisons when analysing the NMR data from the other (less expensive) synthetic routes described above.

Investigations in search of a fluorinated WCC could also be explored with a range other cationic centres bearing fluorinated alkoxy groups. Antimony, similar to phosphorus would also lead to a cation isoelectronic to the WCA aluminate known. Fluorinated ammonium salts and sulfonium could also be investigated, see Figure 90.

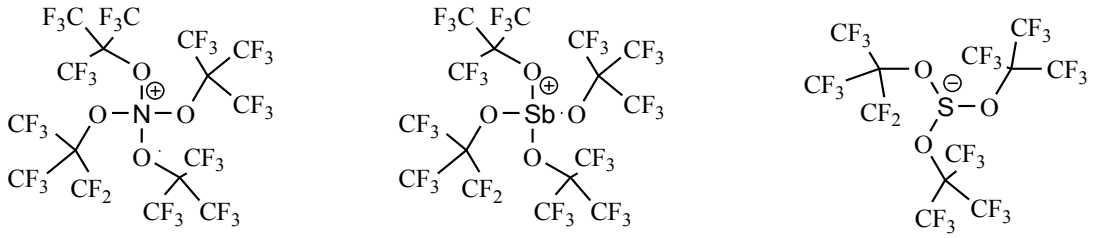

Figure 90: Potential WCCs bearing perfluorinated alkoxy groups with nitrogen, antimony or sulphur centres.

Further work could also be focussed on exploring the properties and isolating of the fluorinated alkoxy-containing phosphonium salts synthesised from alkylation of the phosphorus (III) ligands. Understanding their properties would assist in finding potential applications for these types of ions.

5 SYNTHETIC AND STRUCTURAL CHEMISTRY OF P(V)-ALKOXIDE BASED LEWIS ACIDS AND WEAKLY COORDINATING ANIONS

5.1 LITERATURE REVIEW

5.1.1 Review on Weakly Coordinating Anions

5.1.1.1 Requirements for a Weakly Coordinating Anion

Traditional halide anions, (X^- = F^-, Cl^-, Br^-, I^-) have been extensively used as counter anions as they are affordable and easily available. However, they are known to be strongly coordinating due to their small size (volumes = 25-72 $Å^3$) and high charge density. These were later replaced in some applications by complex anions such as $[NO_3]^-$, $[BF_4]^-$, $[ClO_4]^-$, $[AlX_4]^-$ (X = Cl to I), $[MF_6]^-$ (M = P, As, Sb *etc.*), $[O_3SCF_3]^-$ or $[N(SO_2CF_3)_2]^-$. These occupy much larger volumes, as big as 232 $Å^3$ for the bis(trifluoromethanesulfonyl)imide, $[N(SO_2CF_3)_2]^-$ anion. They are often fluorinated so that they are weakly basic and resistant to electrophilic attack, making them ideal for stabilizing electrophilic cations and for reducing interionic interactions (as found in ILs). These complex anions are generally considered to be the first generation of weakly coordinating anions (WCAs). Much larger and more complex anions have also been published in search of a "non-coordinating" anion. These include; $[CB_{11}H_6Cl_6]^-$ (volume = 392 $Å^3$), $[B(C_6F_5)_4]^-$ (volume = 623 $Å^3$), $[Al\{OC(CF_3)_3\}_4]^-$ (volume = 758 $Å^3$); and are known as the new generation of WCAs, sometimes referred to as "superweak anions".[285] These are discussed in more detail later in this chapter, along with their isolated salts. The new generations of WCAs are key for stabilization of simple, but fundamentally important cations in condensed phases. These cations previously may only have been observed in the gas phase, *i.e.* inside a mass spectrometer, or *in silico* with quantum chemical calculations (usually in the gas phase at 0 K). In addition, calculations of gas phase cations when paired with weak Lewis bases to give Lewis acid-base complexes are useful. However, there are problems when obtaining structural information from such calculations, such as shallow potential energy wells on extended potential energy surfaces.[286] Krossing *et al.* have identified that the general requirement for designing a new WCA is "the delocalization of the negative charge over a large area of non-nucleophilic and chemically robust moieties".[252] This can exchange a few strongly coordinating interactions for many weak interactions over the increased surface area of the WCA. Krossing *et al.* highlight that the most basic site on an anion is the limits of the coordination ability, and if it is sterically accessible, this can be the cause of anion decomposition.[252] A fine balance is required between the donor strengths of the WCA and the solvent. It is important to avoid

coordination of the solvent to the cation and/or to the anion itself, this is where the limits of WCA chemistry lie. A suitable solvent that does not coordinate to the WCA would prevent WCA decomposition in solution. The solid state WCA salts can be stable for days at high ambient temperature. However, this stability of the WCA salt in solution is still a key challenge in this field today.[286]

5.1.1.2 Applications of Weakly Coordinating Anions

WCAs have many possible applications. These include catalysis where "naked" metal ions, *e.g.* $[Li]^+$ and $[Ag]^+$ are required as catalytically active species. The air and moisture stable $[Ag(PPh_3)]^+[CB_{11}H_6Br_6]^-$ salt used in hetero Diels-Alder reactions is one example of WCA use in catalysis. Low catalyst loadings are required for this salt compared to that of salts with classical anions.[287] Industrial scale olefin-polymerization reactions are another example of a key area of catalysis that require WCAs.[288] Specifically designed cationic transition metal complexes (catalyst precursors) and main-group organometallic compounds (cocatalysts) are employed in such reactions to allow for exceptional control over the polymer microstructure, the generation of new polymer architectures, and the development of new polymerization reactions.[288] The catalytically active cations for the polymerization of ethylene include $[(Cp)_2MMe]^+$; M = Ti, Zr. The cocatalyst, which becomes an anion after the activation process, stabilizes the cationic catalyst *via* weak coordination and prevents its decomposition. However, Lewis base coordination to the cation suppresses catalytic activity. Therefore, the Lewis basicity of the anion must be balanced sterically and electronically with the Lewis acidity of the cation to obtain ion-paired catalysts with optimal stability and activity. Hence, anion engineering is imperative to afford better control of catalyst solubility and stability, as well as morphological behavior of the resulting polymers. Examples of cocatalysts used include borate and aluminate activators such as $[Ph_3C]^+[B(C_6F_5)_4]^-$,[289] $[HNRR'_2]^+[B(C_6F_5)_4]^-$,[290] and $[Ph_3C]^+[Al(C_6F_5)_4]^-$ respectively.[291] Functionalized fluoroarylborate salts *i.e.* $[B(C_6F_4SiR_3)_4]^-$; $SiR_3 = {}^iPr_3Si$, ${}^tBuMe_2Si$,[292] have been found to be more advantageous cocatalysts. This is due to their improved solubility, thermal stability, isolability, and the ease of characterization of the resulting cationic complexes, as well as high catalytic efficiencies. Other WCAs used for this type of catalysis include $[Ph_3C]^+[M(OC_6F_5)_6]^-$; M = Nb[293] and Ta[294] salts, but these have been found to show eventual decomposition *via* $-OC_6F_5$ transfer to the cationic metal centre catalyst. A bidentate fluoroarylborate-based activator structure, $[Ph_3C]^+[B(F_4C_6\text{-}C_6F_4)_2]^-$ has proven to be even more effective for ethylene polymerization when combined with the zirconocene dimethyls than the $[B(C_6F_5)_4]^-$ based and functionalized borate-based activators.[295]

Electrochemistry also benefits from the development of WCAs, as larger and more robust WCAs that are stable towards oxidized species can avoid complications with the voltammetric scans.[12-14] WCAs can also be paired with large unsymmetrical cations to give ionic liquids (ILs). The low vapor pressure of such ILs make them ideal for replacing volatile organic solvents in industrial and laboratory processes as "green solvents". The ability to tune the properties of ILs by changing their component ions is key to their success. Hence, greater variety of anion-cation combinations will expand the library of ILs and allow for a variety of differing properties such as hydrophobicity and viscosity, each suited for specific applications.[296] Electrolytes for lithium-ion batteries also rely on stable anions. It appears that to increase the conductance of lithium-ion batteries, the size (small is desired due to higher mobility), and coordinating ability (WCA is desired) of the anion are two key factors. Other key factors include; stability towards hydrolysis, affordability, non-toxicity and the availability of an easy preparation method. However, investigations into lithium-ion batteries have found high conductivities when using large aluminate[297] and borate-based[298] WCAs. This suggests that the desired small size for the stable anions is not a key requirement, as the smaller anions tend to coordinate more strongly and form ion pairs which reduce conductivity. Conversely, the larger anions reduce conductivity due to higher viscosities; hence a fine balance of the coordination ability and viscosity is required for suitable lithium-ion batteries anions.[299]

5.1.1.3 Borate-Based Weakly Coordinating Anions

Borate-based anions include $[B(C_6F_5)_4]^-$ and $[B(Ar^F)_4]^-$ {Ar^F = -C_6H_3- 3, 5 $(R^F)_2$; R^F = n-C_6F_{13}[300], n-C_4F_9[301], 2-C_3F_7[301]} type WCAs, see Figure 91.[302] These were developed from the $[B(C_6H_5)_4]^-$ anion, which is much larger than the $[BF_4]^-$ anion. However, the ease of hydrolysis of the $[B(C_6H_5)_4]^-$ anion and the ease of cleaving of a phenyl group and the strong η^6 coordination of a phenyl group led to introducing fluorination to these types of anions.

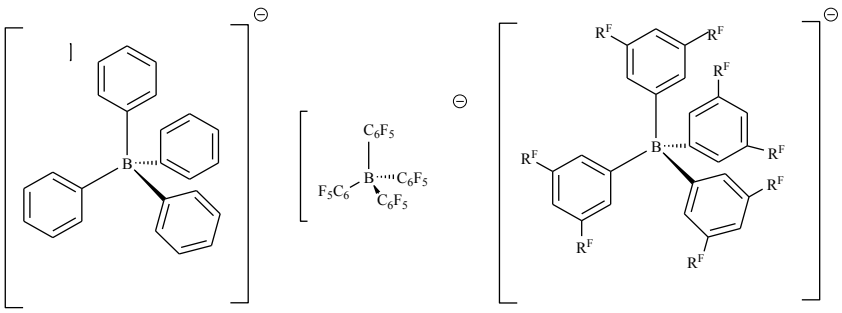

R^F = n-C_6F_{13}[300], n-C_4F_9[301], 2-C_3F_7[301]

Figure 91: Borate based WCAs.[300-302]

Although simple CF_3 groups were initially used,[303] the lack of solubility in hydrocarbon solvents brought about the use of a range of perfluoroalkyl substituents on aryl groups, $[B(Ar^F)_4]^-$. These can be useful in cationic transition metal catalysis and are compatible with *fluorous* biphasic recycling techniques.[300] Further modifications on $[B(Ar^F)_4]^-$ type WCAs involved reacting two equivalents of the WCA with a hard nucleophile, such as CN^-,[304] $C_3N_2H_3^-$ (imidazolyl)[305, 306] or NH_2^-(hydrogen bonding between this NH_2 and C-F from the Ar^F substituent provides extra thermal-stability),[307, 308] to yield a dimeric borate *i.e.* $[(Ar^F)_3B(\mu\text{-}CN)B(Ar^F)_3]^-$. These dimeric borates are stable enough to produce $[H(OEt_2)_2]^+$ and $[CPh_3]^+$ salts which do not decompose when exposed to air.[308] It should be noted that the $[B(CF_3)_4]^-$ anion, although small, is relatively stable and less coordinating than the $[Nb(OTeF_5)_6]^-$, $[B(OTeF_5)_4]^-$, and $[Sb_2F_{11}]^-$ anions (all three are known as WCAs and are discussed in detail below).[309] Although the $[B(CF_3)_4]^-$ anion is incompatible with the extremely reactive cations such as $[SiEt_3]^+$ and $[Al^iPr_2]^+$, the $[BF_3(CF_3)]^-$ and $[BF(CF_3)_3]^-$ derivatives are favorable as electrolytes for lithium-ion batteries when in the form of their corresponding lithium salts.[310-321] A disadvantage of the $[B(Ar^F)_4]^-$ anions, is that they tend to form salts which are oils rather than isolable crystalline ILs. This is likely a cause of $[B(Ar^F)_4]^-$ anions being almost spherical and disordered with the lack of a dipole moment.[307] In addition, highly electrophilic species of lighter metal elements that are coordinatively unsaturated or which are not stabilised by π-ligands have a strong tendency to attack the $[B(Ar^F)_4]^-$ counter anions. These borate anions tend to exchange with the metal substituents and form $M(Ar^F)_n$ and BR_3 species (R = Me, Et; M = Al, Zn, n = 3, 2 respectively).[307]

5.1.1.4 Carborane-Based Weakly Coordinating Anions

In 1986, the remarkably stable boron cluster framework of monocarborane anions such as the icosahedral, $[CB_{11}H_{12}]^-$ (a discrete ion with perfect I_h symmetry) were introduced as the "least coordinating anions", see Figure 92.[322] The lack of lone pairs and π-electrons in this anion gives it a very low nucleophilicity, allowing it to be very weakly coordinating. The icosahedral framework requires high energy for the disruption of the cluster, giving the structure additional stability to act as an inert counter anion.[275] In addition, derivatization at the carbon atoms and halogenation at the boron atoms (forming the hexahalo derivatives $[CB_{11}H_6X_6]^-$) give the carborane WCAs versatility. This allows variation in their properties such as solubility, inertness and stability towards oxidation allowing tailoring to specific applications.[275] The inertness is found to increase with the extent of halogenation, presumably because halide substituents can help with the distribution of the charge and create a layer that protects the CB_{11} core from chemical attack *via* electron repulsion.[273]

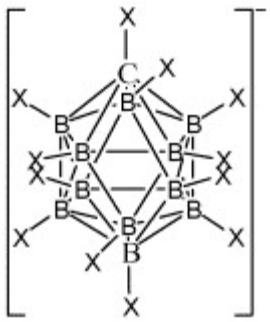

Figure 92: Carborane based WCAs. Adapted from ref. [286].

Many techniques are employed to measure the coordinating abilities of such WCAs. The average carbonyl stretching frequency, ν_{CO} of $FeCp(CO)_2A$, (where A = anionic ligand) can be used to quantify the cationic character of the $[FeCp(CO)_2]^{\delta+}$ moiety.[323] Increasing ν_{CO} correlates with diminished π-back-bonding, which in turn relates to increasing cationic character of the $[FeCp(CO)_2]^{\delta+}$ moiety. These studies showed that the hexabromocarborane, $[CB_{11}H_6Br_6]^-$ Fe complexes (ν_{CO} = 2108 cm^{-1}) are more cationic than the $[SbF_6]^-$ Fe complexes (ν_{CO} = 2050 cm^{-1}). The $[CB_{11}H_{12}]^-$ Fe complex (ν_{CO} = 2049 cm^{-1}) has a similar extent of π-back-bonding to that of the $[SbF_6]^-$ Fe complex (ν_{CO} = 2050 cm^{-1}), suggesting the WCAs are similar in terms of their coordinating ability. The $[CB_{11}Me_{12}]^-$ Fe complex (ν_{CO} = 2098 cm^{-1}) has increased π-back-bonding than the $[CB_{11}H_6Br_6]^-$ Fe complex (ν_{CO} = 2108 cm^{-1}). This suggests the $[CB_{11}Me_{12}]^-$ Fe complex is less cationic than the $[CB_{11}H_6Br_6]^-$ Fe complex, hence $[CB_{11}H_6Br_6]^-$ is a better WCA than $[CB_{11}Me_{12}]^-$. This implies that the bonding pair in a σ-complex can be a better electron donor than a traditional lone pair.[275] Another gauge for the coordination ability of anions uses the downfield ^{29}Si NMR chemical shift of silyl species, $^{i}Pr_3SiA$.[324] This method suggests the hexachlorocarborane, $[CB_{11}H_6Cl_6]^-$ WCA (^{29}Si = 115 ppm) is the most WCA in the series with the hexabromocarborane, $[CB_{11}H_6Br_6]^-$ (^{29}Si = 110 ppm) anion close to this. This is likely to be an effect of the decrease in polarisability of the halide causing a decrease in anion basicity.[324] This study highlights that the anions considered, have basicity similar to toluene (^{29}Si = 107 ppm),[324] hence competition between anion and solvent should always be considered.[275]

The carborane anions are useful for protonating/alkylating/silylating many weakly basic molecules such as benzene, C_{60}, phosphabenzenes, phosphazenes, Xe *etc.*[273] These type of reactions have been found to be more difficult when using the traditional triflate reagents as the products can react in undesired ways with the triflate nucleophile.[273] The inertness of the

carborane anions prevents them from undergoing oxidation or nucleophilic attack, a key problematic step observed in previous attempts to protonate weakly basic species.[273] The trityl carborane salt is used in the synthesis of the trialkylsilyl carboranes. The trityl cation can abstract a hydride from the silane to form the desired product, see Scheme 44. Low basicity solvents such as benzene and toluene are required for this synthesis.

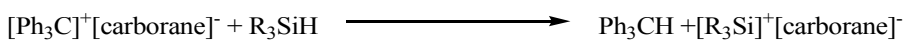

Scheme 44: The synthesis of trialkylsilyl carboranes.[273]

Although the trialkylsilyl carboranes are covalent compounds, they react in a similar manner to free silylium ions[325] and can even silylate many substrates that are inert to trialkylsilyl triflates *e.g.* phosphazenes at a nitrogen atom to give $[R_3Si(N_3P_3Cl_6)]^+[carborane]^-$ salts.[326] These silylated cations are found to be useful catalysts for ring-opening polymerisation at room temperature, unlike the Lewis acid catalysis which is achieved in a melt at 200 °C.[326]

Anhydrous carborane acids can be prepared with these trialkylsilyl carborane salts and condensed HCl, see Scheme 45. Unlike the triflate salts, these can be used to protonate benzene to form benzenium salts, $[C_6H_7]^+[carborane]^-$ which are stable enough to be studied by X-ray crystallography. Remarkably these salts have also been known to protonate fullerenes, C_{60}.

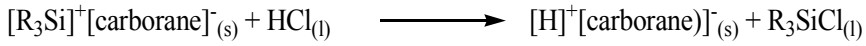

Scheme 45: The synthesis of anhydrous carborane acid.[273]

Alkyl carboranes can also be synthesized using the triethylsilylium carborane precursor and reacting this with an alkyl triflate, see Scheme 46.[327, 328] The preparative reaction of alkyl carboranes is frequently carried out *in situ* with its intended substrate, due to its high reactivity.

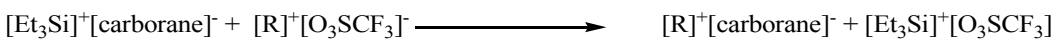

Scheme 46: The synthesis of alkyl carboranes.[273]

Hexane solvent can react with the WCA carborane salt, $[CH_3]^+[(CHB_{11}Cl_{11})]^-$ to form the methyl-cyclopentyl carbocation, see Scheme 47. In a similar manner butane or higher hydrocarbons can react with carborane WCA salts to form tertiary carbocations with enhanced stability, allowing for the reactive intermediates to be studied by X-ray crystallography at room temperature.[274]

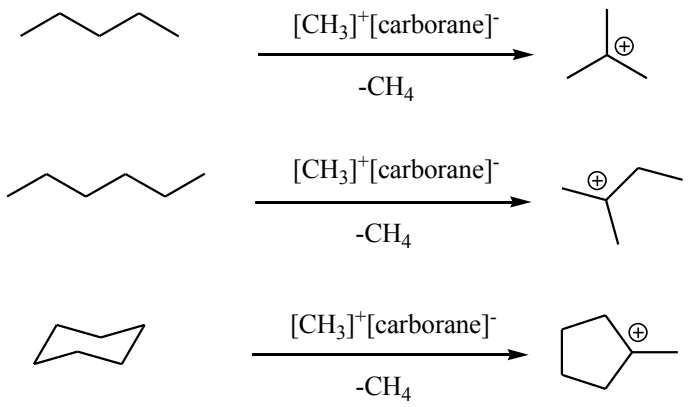

Scheme 47: Formation of tertiary cations from alkanes, using $[CH_3]^+[carborane]^-$. Adapted from ref. [273].

The methyl carboranes have also been found to be useful for the electrophilic alkylations of the weakly basic nitrogen atom of phosphazenes,[326] the weakly basic phosphorus atom of phosphabenzenes[328] and the synthesis of hexamethylhydrazinium(II) $[Me_3N\text{-}NMe_3]^{2+}$ cation, see Scheme 48.[329] This ion is a rare case of stable dication formation with formal positive charges on the adjacent nitrogen atoms.

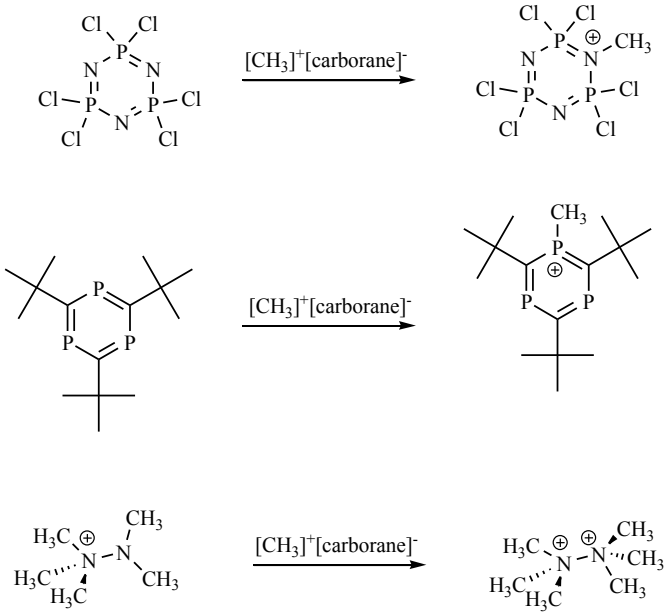

Scheme 48: The methylation of various weakly basic heteroatom substrates with $[CH_3]^+[carborane]^-$. Adapted from ref. [273].

However, challenges in this area include finding suitable solvents and keeping them dry. Despite the advantages of the halogenated carborane anions having the most WCA character and being chemically robust, they are not widely used. This is due to the lack of availability of these for bulk use. An expensive and time consuming synthetic procedure is required for carborane anion synthesis. This involves multiple steps with extremely toxic chemicals such as decarborane, HCl and the formation of HCN gas, which must be dealt with appropriately, along with the use of Me_2SO_4, a known carcinogen, which is also required in the

synthesis.[273] In addition, some of the best weakly coordinating carborane anions have even been found to be explosive *e.g.* $[CB_{11}(CF_3)_{12}]^-$.[330]

5.1.1.5 Teflate-Based Weakly Coordinating Anions

Another class of WCAs are developed from replacing the small fluorine atoms in $[BF_4]^-$ and $[MF_6]^-$ (M = As, Sb, Bi, Nb) with large teflate, $-OTeF_5$ substituents (similar to a F atom as they are hard and very electronegative)[331] to give $[B(OTeF_5)_4]^-$,[331] and $[M(OTeF_5)_6]^-$ (M = As,[332] Sb,[333, 334] Bi,[332] Nb[334, 335]) type WCAs, see Figure 93.

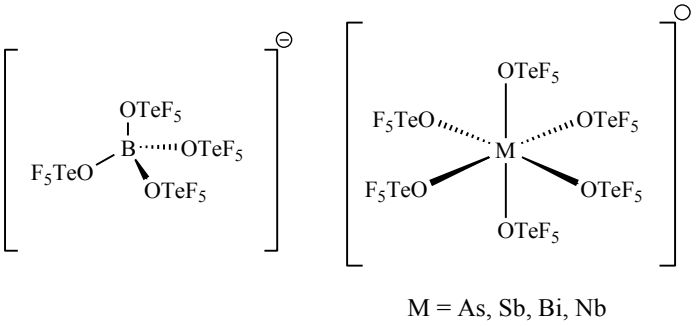

Figure 93: Teflate based WCAs.[331-334]

The negative charge of the anion is dispersed over many more fluorine atoms, reducing the basicity of the anion. The teflate, $-OTeF_5$ substituent is inert to the loss of a fluoride or fluorine atom. However, the $[B(OTeF_5)_4]^-$ anion is less stable than the $[M(OTeF_5)_6]^-$ anions described above, as it can lose a $-OTeF_5$ group in the presence of strong electrophiles such as $[SiR_3]^+$ or $[Ag]^+$.[331] The $[B(OTeF_5)_4]^-$ anion and a similar $[Pd(OTeF_5)_4]^{2-}$ anion have been found to compete with coordinated solvent molecules on metal cation centres by coordination through their oxygen or fluorine atoms.[332] It appears from the literature reports that the $[Sb(OTeF_5)_6]^-$ anion is the most stable of the series, as tetramethylammonium salts of $[M(OTeF_5)_6]^-$ (M = As, Bi, Nb) are found to decompose at room temperature in solvents such as MeCN and SO_2ClF, see Scheme 49. In addition the sterically more hindered octahedral $[Sb(OTeF_5)_6]^-$ anion inhibits oxygen interactions with the metal cation, hence only weak $[M]^+\cdots F\cdots Te$ interactions are present. However, the teflate anions are all moisture sensitive and all decompose rapidly in the presence of water to liberate HF making them difficult to handle routinely.[332]

$$[Bi(OTeF_5)_6]^- \xrightarrow{MeCN,\ 25\ ^0C} [BiO(OTeF_5)_4]^- + F_5TeOTeF_5$$

Scheme 49: Decomposition of $[Bi(OTeF_5)_6]^-$ in MeCN solvent at room temperature. Adapted from ref. [332].

5.1.1.6 *Fluorinated Alkoxy- and Aryloxy-Based Weakly Coordinating Anions*

Polyfluorinated alkoxy- (OR^F) and aryloxy- (OAr^F) metallates with B(III), Al(III), Nb(V), Ta(V), Y(III) and La(III) as the metal centres have also been used for WCA synthesis. These are affordable and easily synthesised, even on a large scale and are now available commercially. However, it seems the aryloxy-metallates have the tendency to bond through their oxygen atoms, as well as their C-F bonds. In addition, the anions are susceptible to OAr^F abstraction, leading to anion decomposition. This turns the attention to perfluorinated alkoxy-metallates, where substituents such as the perfluoro-*t*-butoxy groups, $-OC(CF_3)_3$ are sterically demanding and prevent any bonding through the oxygen atoms due to the shear steric bulk making it inaccessible. These types of substituents have led to the synthesis of alkoxy-aluminates *i.e.* $[Al\{OC(CF_3)_3\}_4]^-$ which are stable towards hydrolysis due to the steric shielding of the oxygen atom and electronic stabilization from the perfluorination, see Figure 94. The weakly coordinating nature of $[Al\{OC(CF_3)_3\}_4]^-$ is evident from the range of silver adducts of very weak Lewis bases such as P_4,[263, 336] S_8[337] and C_2H_4[338] and salts of highly electrophilic cations[251] *i.e.* $[PX_4]^+$ and $[CI_3]^+$ that can be formed. The lithium alkoxy-aluminate salts have been used in catalysis[339] and as electrolytes.[297] Overall, this $[Al\{OC(CF_3)_3\}_4]^-$ WCA is commercially available, easy to prepare and stable towards water and aqueous HNO_3, as well as being a robust WCA that can introduce the stabilisation of highly electrophilic cations. In addition, the perfluorinated anion excludes C-H activation as a decomposition pathway, and its silver salts are easily soluble in DCM at room temperature, making anion displacement very simple. However, the perfluorinated alcohol can be expensive to use on a large scale and the symmetrical anion is not very useful for the formation of new IL phases with low temperature melting points. In addition, Krossing *et al.* found that although $[Al\{OC(CF_3)_3\}_4]^-$ is a remarkably stable WCA, repeated decomposition to $[\{OC(CF_3)_3\}_3Al\text{-}F\text{-}Al\{OC(CF_3)_3\}_3]^-$ is observed when reacted with very electrophilic cations such as $[P_2X_5]^+$ (X = Br and I) at temperatures above -20 °C, see Figure 94.[251, 263]

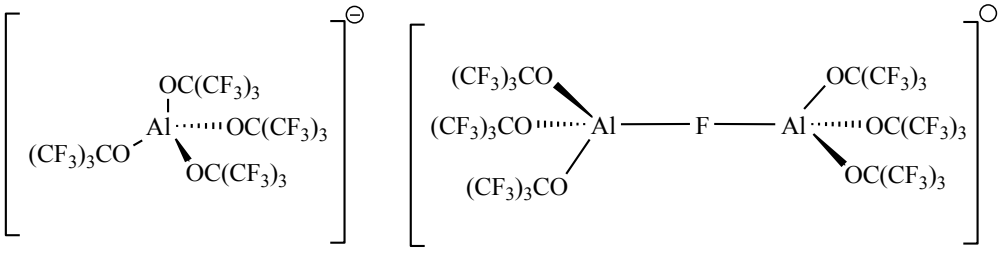

Figure 94: Perfluorinated-alkoxy aluminate and the dimeric perfluorinated-alkoxy aluminate WCA. [251, 263]

This anion, $[\{OC(CF_3)_3\}_3Al\text{-}F\text{-}Al\{OC(CF_3)_3\}_3]^-$ is found to be more stable than $[Al\{OC(CF_3)_3\}_4]^-$,[263, 264] as its negative charge is dispersed over fifty-four peripheral C-F bonds opposed to thirty-six for $[Al\{OC(CF_3)_3\}_4]^-$. Hence, this anion is presented by Krossing *et al.* as the weakest coordinating anion known that can be prepared simply.[286] The decomposition of the perfluorinated aluminate anion, $[Al\{OC(CF_3)_3\}_4]^-$, is thought to be caused by C-F activation in the presence of highly electrophilic cations (E^+).[340] The potential reaction mechanism for this type of decomposition could occur *via* loss of either a fluoride from the alkoxy group to the E^+, or loss of the entire alkoxy group to the E^+, see Step 1 in Scheme 50. Both mechanisms lead to the formation of a perfluorinated aluminate compound, $Al\{OC(CF_3)_3\}_3$ which has a Lewis superacidic nature, discussed in Chapter 5.2.2. This can then react further due to its Lewis superacidic nature with another $[Al\{OC(CF_3)_3\}_4]^-$ anion. This again undergoes C-F activation *via* loss of one of the alkoxy groups to form a perfluorinated epoxide, an anion with a direct Al-F bond, $[Al\{OC(CF_3)_3\}_3F]^-$ and another $Al\{OC(CF_3)_3\}_3$ molecule. The $[Al\{OC(CF_3)_3\}_3F]^-$ anion and the $Al\{OC(CF_3)_3\}_3$ Lewis superacid can then react to form the stable fluoride bridged anion, $[\{OC(CF_3)_3\}_3Al\text{-}F\text{-}Al\{OC(CF_3)_3\}_3]^-$, see Step 2 in Scheme 50.

Step 1

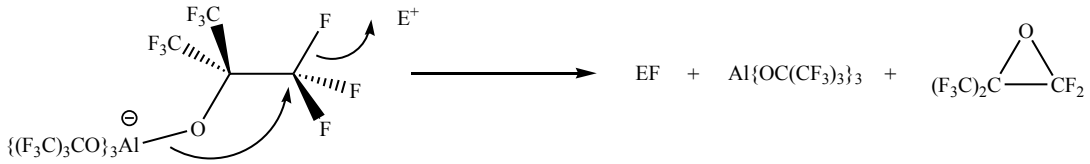

or

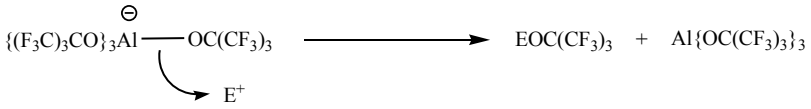

Step 2

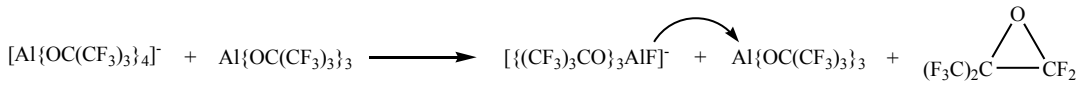

Scheme 50: Decomposition of $[Al\{OC(CF_3)_3\}_4]^-$, on reaction with highly electrophilic cations (E^+) *via* C-F activation, forming $[\{OC(CF_3)_3\}_3Al\text{-}F\text{-}Al\{OC(CF_3)_3\}_3]^-$.[340]

5.1.1.7 *Lewis Acid-Based Weakly Coordinating Anions*

Another synthetic route to WCAs involves abstracting an ionic fragment from a substrate *e.g.* AgF, using a strong Lewis acid. These type of Lewis acids include AsF_5 and SbF_5 which can form $[MF_6]^-$ anions. These can also form di-, tri- and tetra-nuclear ions by reacting $[MF_6]^-$ anions with excess MF_5 Lewis acid, see Figure 95.

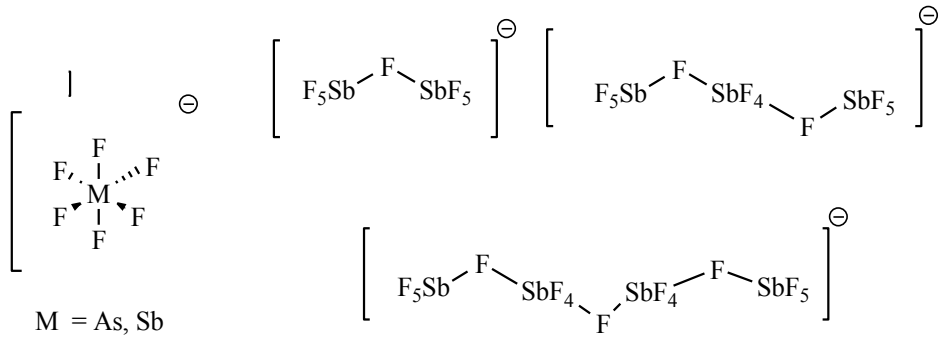

Figure 95: Lewis acidic based WCAs and the di-, tri- and tetra-nuclear antimony WCAs.[341, 342]

These multinuclear fluoro-metallate based WCAs are significantly more weakly coordinating and exhibit greater stability towards electrophiles than $[MF_6]^-$ anions. These weakly Lewis basic salts make cations such as $[Au(Xe)_4]^+$ accessible when paired with $[Sb_2F_{11}]^-$,[342] note only $[Au(Xe)_n]^+[SbF_6]^-$ (n = 1, 2) is possible with the mononuclear WCA.[341] The strength of some Lewis acids has been measured using quantum chemical calculations of their fluoride ion affinity (FIA), discussed in detail below.[277, 343] It appears from these calculations that AuF_5 is the strongest Lewis acid followed by SbF_5 and AlF_3. However, AuF_5 forms AuF_3 and F_2 when dissolved in anhydrous HF, due to its high reactivity.[23] Therefore, SbF_5 is the strongest Lewis acid of those considered in the calculations, which can be applied without the decomposition of the WCA due to increased reactivity.[23]

A "Lewis superacid" is a term that can be used to describe Lewis acids that have higher FIAs than the best conventional Lewis acid, SbF_5.[261] Krossing *et al.* report $Al\{OC(CF_3)_3\}_3$ as a Lewis superacid.[261] The replacement of the monoatomic ligands like F with electronegative polyatomic perfluoro-*t*-butoxy groups, $-OC(CF_3)_3$ leads to an increase in Lewis acidity. In addition, the steric bulk from the $-OC(CF_3)_3$ group prevents the alane from dimerizing. However, the isolation of $Al\{OC(CF_3)_3\}_3$ from toluene, DCM, pentane, or hexane was found to be difficult.[261] This was a result of self-decomposition of $Al\{OC(CF_3)_3\}_3$ by C-F activation (due to the Lewis superacidic nature) and formation of Al-F bonds.[261]

To avoid the internal coordination of $Al\{OC(CF_3)_3\}_3$ with its own fluorine atoms, fluorobenzene was used as a solvent. This gave the $PhF\rightarrow Al\{OC(CF_3)_3\}_3$ adduct, stabilising the Lewis acid and allowing its isolation as a solid material.[261] This is the first neutral Lewis acid that coordinates to the weak fluorobenzene nucleophile *via* the fluorine atom and is stable at room temperature. This adduct is useful as it can be further reacted as part of the *in situ* synthesis of known WCAs, *e.g.* $[Al\{OC(CF_3)_3\}_3F]^-$ and $[\{(CF_3)_3CO\}_3AlFAl\{OC(CF_3)_3\}_3]^-$.[252]

Although WCAs useful for stabilising electrophilic cations are available, they are expensive to synthesise making their use on an industrial scale inefficient. The cheaper alternatives available tend to be symmetrical and are not applicable to the synthesis of IL phases with low temperature melting points. These requirements highlight that this area still needs development. In specific, an unsymmetrical WCA (for use in ILs) with a simple preparation using affordable reagents for mass production would potentially be of great use.

5.1.2 Review of the Acyclic Pentakis(hexafluoroisopropoxy)phosphorane, $P\{OCH(CF_3)_2\}_5$

The acyclic pentakis(hexafluoroisopropoxy)phosphorane, $P\{OCH(CF_3)_2\}_5$, (**16**), has been known since 1978 when it was first reported by Roschenthaler *et al*.[2] However its reactivity, in particular its Lewis acidic properties have not been studied previously. The synthesis involved halogenation (using either Br_2 or Cl_2) of the tris(hexafluoroisopropoxy)phosphite, $P\{OCH(CF_3)_2\}_3$, (**1**), (prepared from methods described in Chapter 2). Nucleophilic displacement of the halophosphorane, $X_2P\{OCH(CF_3)_2\}_3$ (X = Cl or Br) with two equivalents of the lithium alkoxide, $LiOCH(CF_3)_2$ yields the pentakis(hexafluoroisopropoxy)phosphorane, $P\{OCH(CF_3)_2\}_5$ product, (**16**), see Scheme 51.[2]

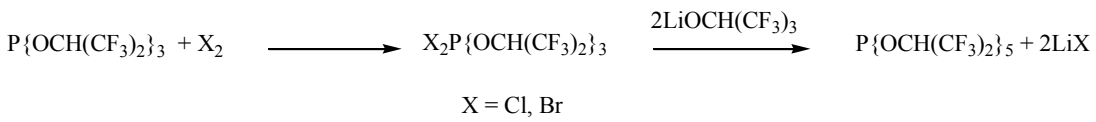

Scheme 51: Synthesis of the phosphorane *via* halogenation of the phosphite, followed by a metathesis reaction.

The phosphorane product, $P\{OCH(CF_3)_2\}_5$, (**16**) can undergo hydrolysis to give the phosphate, $O=P\{OCH(CF_3)_2\}_3$ and two equivalents of the hexafluoroisopropanol, $HOCH(CF_3)_2$.[2] Soon after, Roschenthaler *et al.* published variations of the hexafluoroisopropoxy-containing phosphorane species *i.e.* $PR\{OCH(CF_3)_2\}_4$,

$PRF_2\{OCH(CF_3)_2\}_2$ (R = Me, Ph) and $PMe_2\{OCH(CF_3)_2\}_3$, $P(CF_3)_2\{OCH(CF_3)_2\}_3$, $PPhF\{OCH(CF_3)_2\}_3$ and $PPhF_3\{OCH(CF_3)_2\}$. All of which were identified by NMR spectroscopy as the investigation of the fluorine-bonded oxyphosphoranes continued.[121] Roschenthaler *et al.* were interested in using the electronegative hexafluoroisopropoxy groups to stabilise fluorine bonded phosphorane species that were otherwise found to be unstable. These phosphorane species are known to decompose and form phosphoryl species when simple alkoxy groups are used, see Scheme 52.[344-346]

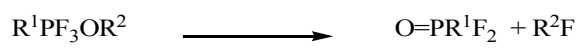

Scheme 52: The use of simple alkoxy groups on fluorine bonded phosphorane species result in their decomposition.[344-346]

Denney *et al.* investigated the fluxionality of $P\{OCH(CF_3)_2\}_5$, (**16**), using ^{19}F variable-temperature NMR studies. This species can undergo Berry pseudorotation in a similar way to other phosphorane species.[119] They concluded it was not possible to separate the equatorial and apical ^{19}F NMR signals for (**16**) even at 178.15 K, suggesting the fluxionality is much faster than the NMR time scale. However, they did observe broadening at 178.15 K in $CFCl_3CD_2Cl_2$ solvent, suggesting slowing of the intramolecular ligand reorganization. They also highlight that it appears the rate of Berry pseudorotation in acyclic pentakis(alkoxy)phosphoranes has never been observed to slow sufficiently to separate the equatorial and apical signals. They suggest the most likely candidate for this would be the acyclic pentakis(perfluoro-*t*-butoxy)phosphorane, $P\{OC(CF_3)_3\}_5$, prepared by Shreeve *et al.*, possibly due to slower ligand reorganization with the bulkier $-OC(CF_3)_3$ groups.[1] The synthetic method used by Shreeve *et al.* for the synthesis of $P\{OC(CF_3)_3\}_5$, involves nucleophilic displacement (S_N2) of all the chlorine atoms of PCl_5 using the perfluoro-*t*-butoxy hypochlorite, $ClOC(CF_3)_3$ at 25 °C.[1] Similarly to (**16**), the $P\{OC(CF_3)_3\}_5$ compound has also been found to be very hygroscopic and decomposes to the phosphate, $O=P\{OC(CF_3)_3\}_3$.[1] Shreeve *et al.* report that this synthetic method gives near to quantitative yields with a simpler method of isolation relative to that reported by Denney *et al*.[119] However, as discussed in Chapter 2, the hypochlorite is formed from handling highly corrosive chemicals *e.g.* ClF and HF and the phosphorane synthesis involves production of chlorine gas as a side product, making the method proposed by Shreeve *et al.* impractical for many chemical labs without special equipment. In addition, no application of (**16**) has been explored or suggested in any published work, as only their synthesis and stability had been previously investigated.[123, 347] A similar phosphorane, $Ph_3P\{OCH(CF_3)_2\}_2$ has however been reported as a useful reagent to introduce a trifluoromethyl, $-CF_3$ group into a desired position of heterocycles that have useful biological properties.[348] For example, anilines (*e.g.* $PhNH_2$, toly-NH_2) have been found to react with this $Ph_3P\{OCH(CF_3)_2\}_2$ phosphorane to form N-

hexafluoroisopropoxyanilines.[348] These can undergo dehydrofluorination with a suitable base *e.g.* triethylamine, potassium *tert*-butoxide *etc.* to form 2-arylamino-1, 1, 3, 3, 3-pentafluoropenes, see Scheme 53.[348] This is a useful method as this product is impossible to form from the direct synthesis of aniline with hexafluoropropene, CF_3-CF=CF_2, due to preferred attack by the nucleophiles considered at the terminal -CF_2 group, Scheme 53 below.[348]

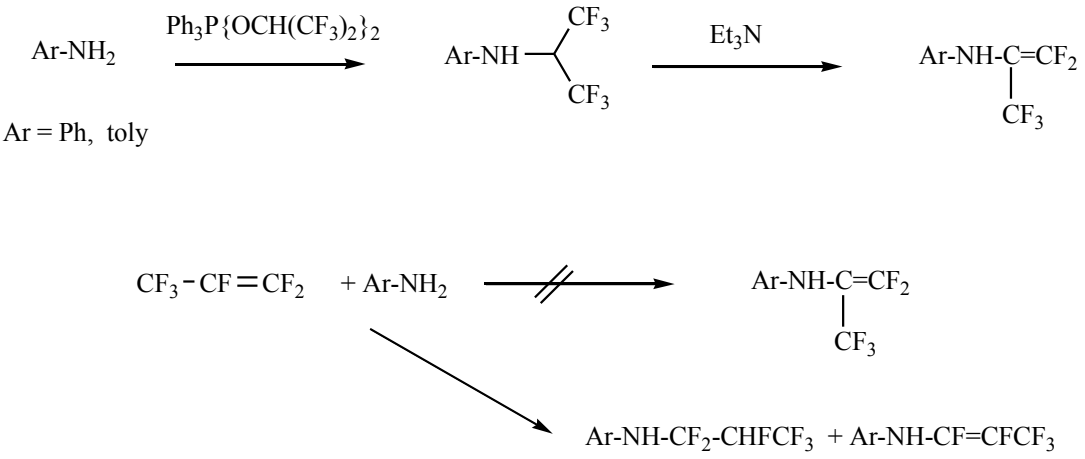

Scheme 53: The synthesis of 2-arylamino-1, 1, 3, 3, 3-pentafluoropenes is achieved with the dehydrofluorination of N-hexafluoroisopropoxyanilines and not with the direct reaction of aniline and hexafluoropropene. Adapted from ref. [348].

5.2 RESULTS AND DISCUSSION

5.2.1 Simple Synthesis of the Acyclic Pentakis(hexafluoroisopropoxy)-phosphorane, $P\{OCH(CF_3)_2\}_5$, (**16**)

The work presented in this thesis extends the investigation into the synthesis of the pentakis(hexafluoroisopropoxy)phosphorane, $P\{OCH(CF_3)_2\}_5$, (**16**). Additional information on its properties and its application are also discussed.

Simple preparation of (**16**) can be achieved without the use of hypochlorite or halogenation. Reaction of PCl_5 with sodium hexafluoroisopropoxide (both are solids which can be easily handled in the glovebox) in DCM solvent (with *ca.* 1 hr. ultrasonic activation) leads to the formation of (**16**) with qualitative conversion observed by $^{31}P\{^1H\}$ NMR spectroscopy, see Scheme 54. After completion, a simple filtration under inert-atmosphere is required to remove the NaCl side product. A sample of (**16**) can be purified by crystallisation from DCM, but is not suitable for purification by sublimation ($1x10^{-1}$ mbar, 50 ˚C, 4 hrs followed by a 70 ˚C, 7 hrs.).

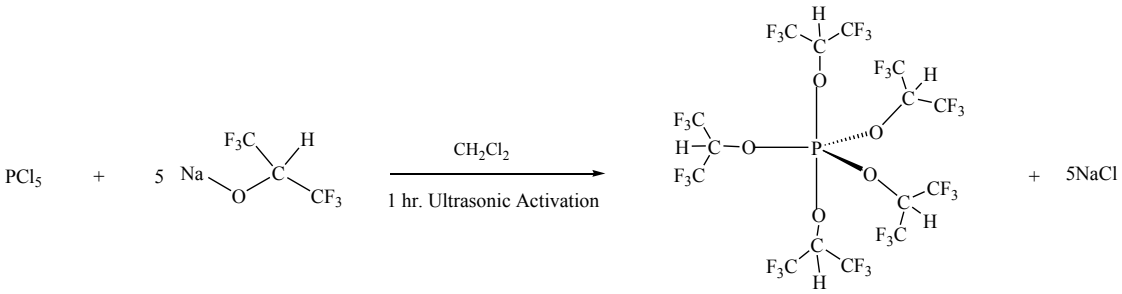

Scheme 54: Simple synthetic preparation of the phosphorane, $P\{OCH(CF_3)_2\}_5$, (16).

Crystals of (**16**) have been obtained from a DCM solution *via* slow cooling at 4 ˚C (this is achieved by placing a Schlenk tube containing the $P\{OCH(CF_3)_2\}_5$ solution in a dewar of ethanol *ca.* 200 ml at room temperature and transferring the dewar and sample to refrigeration at 4 ˚C). Single-crystal X-ray diffraction data were collected at 150 K as crystals of (**16**) underwent a phase change which destroyed the crystals at 110 K.

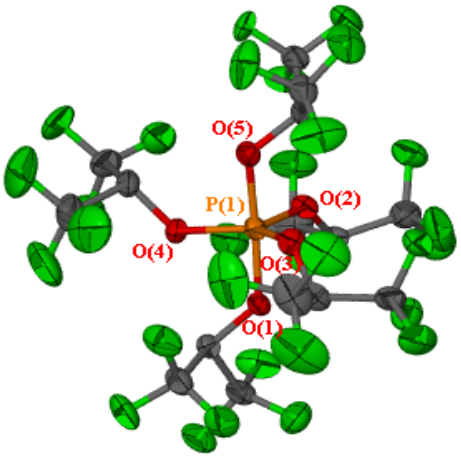

Figure 96: Molecular structure of $P\{OCH(CF_3)_2\}_5$, (16) at 150 K. Disordered parts and hydrogen atoms omitted for clarity. Thermal ellipsoids are drawn at the 50 % probability level. Selected interatomic distances (Å) and angles (˚):P(1)-O(1) = 1.679(2), P(1)-O(2) = 1.592(2), P(1)-O(3) = 1.590(3), P(1)-O(4) = 1.598(2), P(1)-O(5) = 1.666(2), average axial $P(1)-O_{(ax;\ 1,5)}$ = av. 1.673(2) Å, average equatorial $P-O_{(eq\ 2,3,4)}$ = av. 1.593(2) Å, O(4)-P(1)-(O3) = 124.2(1), O(2)-P(1)-(O3) = 113.5(1), O(2)-P(1)-(O4) = 122.1(1), O(5)-P(1)-(O1) = 177.6(1). Crystal system: triclinic. Space group: P-1. R_1: 0.0493 (all data), wR_2: 0.1133 (>2sigma(I)).

The single-crystal X-ray structure of (**16**) has a distorted trigonal bipyramidal structure, with the equatorial O-P-O angles deviating slightly from the 120 ˚ bond angle expected for a perfect trigonal bipyramidal geometry; O(4)-P(1)-(O3) = 124.2(1) ˚, O(2)-P(1)-(O3) = 113.5(1) ˚, O(2)-P(1)-(O4) = 122.1(1) ˚. Similarly the axial O-P-O bond angle deviates slightly from the 180 ˚ bond angle expected for perfect trigonal bipyramidal geometry; O(5)-P(1)-(O1) = 177.6(1) ˚. The average axial P-O bond length = 1.673(2) Å for (**16**) is greater than the average equatorial P-O bond length = 1.593(2) Å. This is the first example of an X-ray crystal structure of a homoleptic fluorinated alkoxy phosphorane; hence comparisons to similar fluorinated alkoxy-containing phosphoranes cannot be made. A penta-alkoxy phosphorane containing one $-OCH(CF_3)_2$ group of the type described in Figure 97 has been found in the CSD.

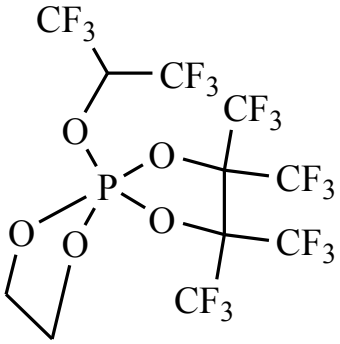

Figure 97: Penta-alkoxy phosphorane containing a hexafluoroisopropoxy group found in a CSD search; GAWWIK.

The P-O bond length for the -OCH(CF_3)$_2$ group in the structure in Figure 97; 1.596(3) Å, is similar to the average equatorial P-O bond length for (**16**). Comparisons can be made to that of the known homoleptic aryloxy/alkoxy phosphorane structures for P(OPh)$_5$ and P(OCy)$_5$, found from the CSD with the names PPHOXP and ACEZOX respectively. The average P-O bond lengths for the axial and equatorial groups can be compared to those for (**16**). The P(OCy)$_5$ bond lengths; P-O$_{(ax)}$ = 1.653(1) Å, 1.675(2) Å, average P-O$_{(ax)}$ = 1.664 Å, P-O$_{(eq)}$ = 1.611(3) Å, 1.602(2) Å, 1.608(2) Å, average P-O$_{(eq)}$ 1.607 Å, and P(OPh)$_5$ bond lengths; P-O$_{(ax)}$ = 1.6609(1) Å, 1.6639(9) Å, average P-O$_{(ax)}$ = 1.6624 Å, P-O$_{(eq)}$ = 1.6005(7) Å, 1.5717(9) Å, 1.572(1) Å, average P-O$_{(eq)}$ 1.602 Å, are found to be of similar magnitude to that for (**16**).

Attempts to slow down the Berry pseudorotation by cooling a CD_2Cl_2 solution of (**16**) to 220 K were unsuccessful {as (**16**) crystallises out of solution rapidly at 260 K, leading to low intensity signals observed in the NMR spectra}. This is consistent with the findings of Denney *et al*.[119]

5.2.2 The Lewis Acidity of P{OCH(CF_3)$_2$}$_5$, (**16**)

The FIA of a Lewis acid (A) is defined as the enthalpy change (under standard conditions) associated with the heterolytic cleavage of an A–F bond to give A^+ and F^-. A more positive FIA is associated with a stronger Lewis acid. FIA calculations were performed using Christe's method by Dr John Slattery.[277] The enthalpy change for the (nearly) isodesmic reaction (see Scheme 55) was calculated at the (RI-)MP2/def2-TZVPP level.[163] The use of a (nearly) isodesmic reaction improves the accuracy of these calculations by error cancellation and avoids the need to calculate free F^- in the gas phase. The table includes selected FIA data from previous studies that serves to put the FIA data presented here for (**16**) into context.

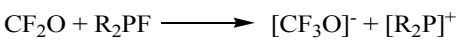

Scheme 55: The (nearly) isodesmic reaction used to calculate FIAs in this study

Compound	*FIA (kJ mol^{-1})*
SiF_4	308
BF_3	338
PF_5	397
BCl_3	405
$GaCl_3$	432
$P\{OCH(CF_3)_2\}_5$, (**16**)	437
$B(C_6F_5)_3$	444
$AlCl_3$	457
SbF_5	489
$Al\{OC(CF_3)_3\}_3$	537
$B(OTeF_5)_3$	550
$As(OTeF_5)_5$	593
$Sb(OTeF_5)_5$	633
$CB_{11}F_{11}$	716

Table 32: FIA of the $P\{OCH(CF_3)_2\}_5$ phosphorane, (16) and other common Lewis acids.

Since the FIA of (**16**) (437 kJ mol^{-1}) is much higher than that of PF_5 (397 kJ mol^{-1}), it was likely that this Lewis acid would easily react with sources of fluoride to form a stable bulky anion, $[P\{OCH(CF_3)_2\}_5F]^-$. The FIA calculations indicate that (**16**) lies between the Lewis acid character of $GaCl_3$ and $B(C_6F_5)_3$. This indicates there is high potential that (**16**) could be used to form WCAs with similar coordinating ability to that of the gallate and borate WCAs.

5.2.3 Synthesis of the $[P\{OCH(CF_3)_2\}_5F]^-$ Silver Salts

In attempt to synthesise a potential new WCA; $[P\{OCH(CF_3)_2\}_5F]^-$, initial reactions were trialled with AgF and (**16**) in MeCN solvent (*ca.* 1 hr. ultrasonic activation), see Scheme 56.

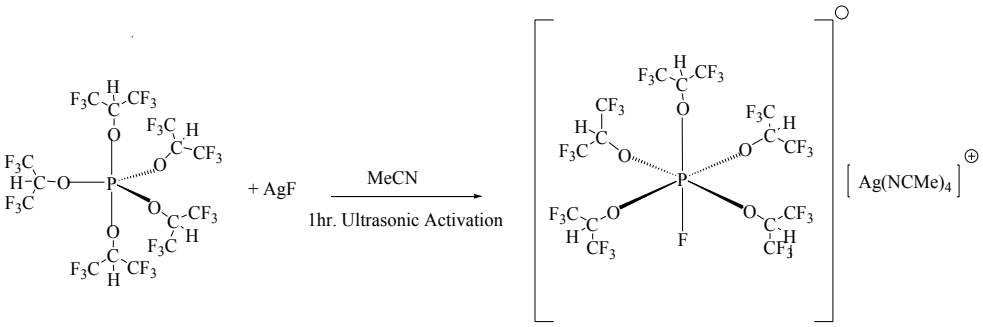

(**16**) (**17**)

Scheme 56: Simple synthesis of $[PF\{OCH(CF_3)_2\}_5]^-$ WCA, using $P\{OCH(CF_3)_2\}_5$, (16) and AgF.

An intense doublet was observed in the $^{31}P\{^1H\}$ NMR spectrum with a large coupling constant (-147.4 ppm, d, $^1J_{PF}$ = 818 Hz), in a similar region to $[PF_6]^-$ (-143.0 ppm, d, $^1J_{PF}$ = 711 Hz), see Figure 98. The ^{19}F NMR spectrum consists of a noticeable doublet at -60.60 ppm (d, $^1J_{PF}$ = 818 Hz) for the fluorine bond directly to the phosphorus centre, a signal at -73.25 (s) for the equatorial alkoxy groups and a signal at -73.48 (br) for the axial alkoxy group, see Figure 99.

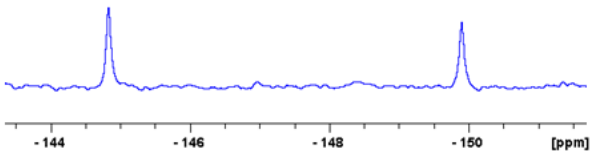

Figure 98: The $^{31}P\{^1H\}$ NMR spectrum, range -144 to -150 ppm. The observed doublet, (-147.4 ppm, d, $^1J_{PF}$ = 818 Hz), for $[Ag(NCMe)_4]^+[P\{OCH(CF_3)_2\}_5F]^-$, (17) is found at a similar region to $[PF_6]^-$.

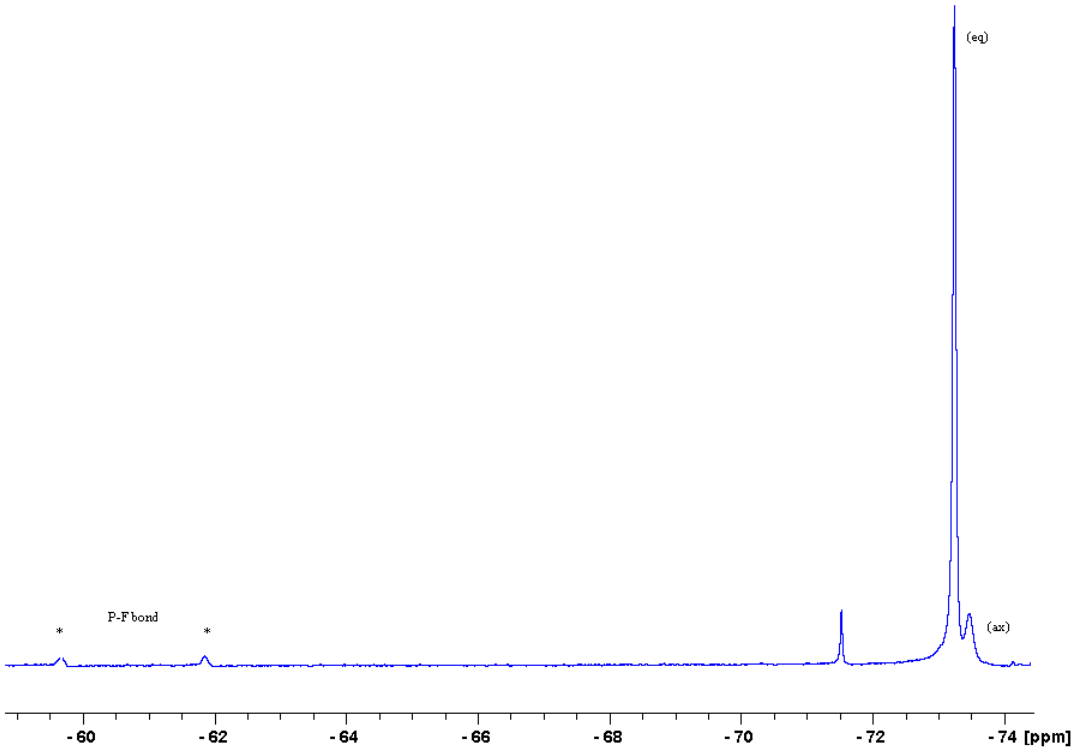

Figure 99: ^{19}F NMR spectrum, range -58 to -74 ppm. The observed doublet at -60.60 ppm (d, $^{1}J_{PF}$ = 818 Hz) for the P-F bond (*), a intense peak at -73.25 (s) for the equatorial alkoxy groups (eq) and a signal at -73.48 (br) for the axial alkoxy group (ax) of $[Ag(NCMe)_4]^+[P\{OCH(CF_3)_2\}_5F]^-$, (17).

The ESI-MS (MeCN solution) showed a signal at 885.0 m/z in the negative mode for the bulky $[P\{OCH(CF_3)_2\}_5F]^-$ anion, $[M]^-$. This is the first synthesis of this type of anion, and first signs of potential application of the Lewis acidic $P\{OCH(CF_3)_2\}_5$, (**16**), phosphorane. Formation of the $[P\{OCH(CF_3)_2\}_5F]^-$ anion using the NaF and (**16**) in MeCN solvent (*ca.* 1 hr. ultrasonic activation) is also successful. Essentially identical NMR peaks are observed for the $[P\{OCH(CF_3)_2\}_5F]^-$ anion with the Ag and Na cations as their MeCN solvates; the cations are likely to be $[Ag(NCMe)_4]^+$, (**17**) and $[Na(NCMe)_6]^+$, (**18**). These are similar to the NMR data for the $[Ag(PR_3)_3]^+$ $[P\{OCH(CF_3)_2\}_5F]^-$ (R = Ph, Me, ^{i}Pr) salts discussed below; (**19**), (**20**) and (**21**) respectively. This suggests that in solution the salts are essentially ion separated, as one would expect a metal/ligand dependent P-F chemical shift if this was involved in M---F-P interaction (*i.e.* no M---F contacts, M = Ag or Na). Crystals of $[Ag(NCMe)_4]^+[P\{OCH(CF_3)_2\}_5F]^-$, (**17**) were grown from a very concentrated, oily MeCN solution, stored under the vapour pressure of the solvent at -16 °C. However, after many attempts the crystals were found to be plates that were always too thin for single-crystal X-ray diffraction. The crystallisation of this product is however useful for isolation of (**17**) and can be used as a purification step. In addition, these isolated ionic crystals may be used as a precursor for a source of the WCA *via* a simple metathesis reaction.

Phosphorus (III) ligands can be used in place of MeCN to coordinate and stabilise the Ag metal cation. These type of ionic species can be formed *in situ* with (**16**), AgF and the relevant phosphine (3 eq., PR_3; R = Ph, Me, ^{i}Pr) in DCM solvent, see Table 33. The X-ray crystallographic data of a triphenylphosphine stabilised Ag^+ salt of (**19**) grown from slow evaporation of the DCM solvent shows three ligands coordinated to the Ag^+ in a trigonal planar coordination geometry, see Figure 100. The trimethylphosphine and triisopropylphosphine stabilised Ag^+ salts of the $[P\{OCH(CF_3)_2\}_5F]^-$ anion have also been prepared in a similar manner, (**20**) and (**21**) respectively. Control reactions in DCM solvent with (**16**) and AgF showed that no $[P\{OCH(CF_3)_2\}_5F]^-$ anion was observed in the $^{31}P\{^{1}H\}$ NMR spectra, even after long periods of ultrasonic activation (24 hrs.). This indicated that DCM is not sufficiently basic to stabilise the Ag^+ with this WCA.

[E]$^+$[P{OCH(CF$_3$)$_2$}$_5$F]$^-$, E =	***$^{31}P\{^{1}H\}$ NMR (δ/ppm)***	***^{19}F NMR (δ/ppm)***
$[Ag(NCMe)_4]^+$, (**17**)	-147.4 (d, $^{1}J_{PF}$ = 818 Hz)	-60.60 (d, $^{1}J_{PF}$ = 818 Hz), -73.00 (s), -73.48 (br)
$[Na(NCMe)_6]^+$, (**18**)	-147.4 (d, $^{1}J_{PF}$ = 820 Hz)	-60.21 (d, $^{1}J_{PF}$ = 820 Hz), -72.75 (s), -73.00 (br)
$[Ag(PPh_3)_3]^+$, (**19**)	12.1 (PPh_3), -147.6 (d, $^{1}J_{PF}$ = 818 Hz)	-59.85 (d, $^{1}J_{PF}$ = 818 Hz), -72.83, (s), -73.10 (br)
$[Ag(PMe_3)_3]^+$, (**20**)	-49.1 (PMe_3), -147.7 (d, $^{1}J_{PF}$ = 818 Hz)	-60.07 (d, $^{1}J_{PF}$ = 818 Hz), -72.70 (s), -73.00 (br)
$[Ag(P^{i}Pr_3)_3]^+$, (**21**)	44.9 ($P^{i}Pr_3$), -147.7 (d, $^{1}J_{PF}$ = 818 Hz)	-59.95 (d, $^{1}J_{PF}$ = 818 Hz), -72.72 (s), -72.95 (br)

Table 33: NMR shifts of $[P\{OCH(CF_3)_2\}_5F]^-$ anion with various ligands stabilising the metal cation.

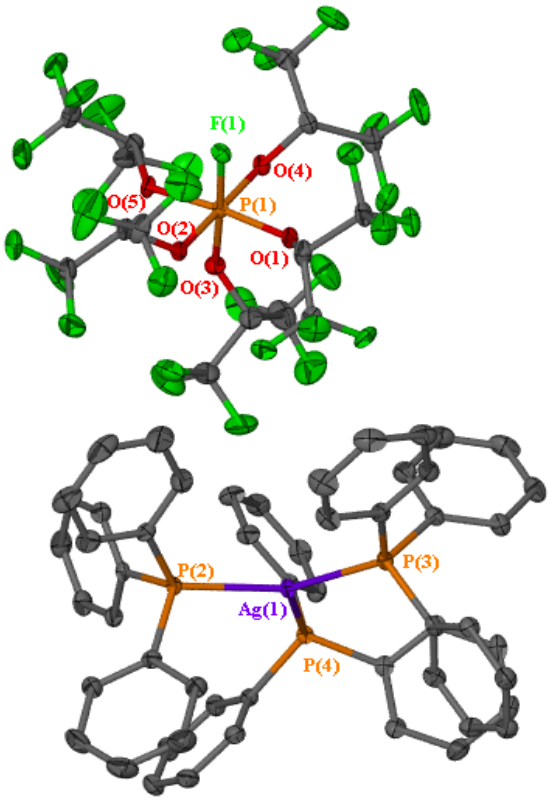

Figure 100: Molecular structure of $[Ag(PPh_3)_3]^+[P\{OCH(CF_3)_2\}_5F]^-$ (19) at 110 K. Disordered parts and hydrogen atoms omitted for clarity. Thermal ellipsoids are drawn at the 50 % probability level. Selected interatomic distances (Å) and angles (˚): P(1)-F(1) = 1.627(6), P(1)-O(1) = 1.701(4), P(1)-O(2) = 1.693(2), P(1)-O(4) = 1.709(1), P(1)-O(5) = 1.690(1), average equatorial P-$O_{(1,2,4,5)}$ = av. 1.699(2), P(1)-O(3) = 1.704(3), F(1)-P(1)-O(3) = 176.8(2), O(1)-P(1)-O(4) = 90.6(2), O(4)-P(1)-O(5) = 93.8(3), O(5)-P(1)-O(2) = 86.2(3), O(2)-P(1)-O(1) = 89.4(2). Crystal system: monoclinic. Space group: $P2_1/c$. R_1: 0.0390 (all data), wR_2: 0.0901 (>2sigma(I)).

On addition of fluoride to the pentakis(hexafluoroisopropoxy)phosphorane, (**16**) the axial bonds elongate and the equatorial bonds contract to change the trigonal bipyramidal geometry to a distorted octahedral geometry, as shown by the X-ray diffraction crystal structure, see Figure 100. The F(1)-P(1)-O(3) = 176.8(1) ˚ angle deviates slightly from 180 ˚ and the O(1)-P(1)-O(4) = 90.6(2) ˚, O(4)-P(1)-O(5) = 93.8(3) ˚, O(5)-P(1)-O(2) = 86.2(3) ˚, O(2)-P(1)-O(1) = 89.4(2) ˚ angles deviate slightly from 90 ˚, the angles of which describe a perfect octahedral structure. The P-O bond distances, P-$O_{(ax)}$ = 1.704(3) Å, average P-$O_{(eq)}$ = 1.699(2) Å, are longer than those found for $P\{OCH(CF_3)_2\}_5$, (**16**); average P-$O_{(ax)}$ = 1.673(2) Å and average P-$O_{(eq)}$ = 1.593(2) Å. The presence of the direct P-F bond is likely to reduce the overall bonding character of each bond, forming weaker P-O bonds. The P(1)-F(1) = 1.627(6) Å bond is found to be much longer than that found for the average P-F bond in $[N^nBu_4]^+[PF_6]^-$, CSD name; NOFKEY02; average 1.593(1) Å. Although the FIA calculations indicate that (**16**) is a stronger Lewis acid than PF_5, the longer bond maybe due to perhaps a weak anion-cation interaction in this salt. Three short contacts (less than the sum of VdW radii – 0.2 Å) were also found between the ions in crystal structure. These were all C-F···H-

C interactions (2.427-2.458 Å, sum of the VdW radii of F and H = 2.990 Å) between the phenyl hydrogen atoms of one of the triphenylphosphine molecules stabilising the Ag^+ cation. No C-H interactions were found with the P-F bond, even though this is likely to be one of the most basic sites on the anion. This is likely due to the P-F bond being crowded by the bulky hexafluoroisopropoxy groups that inhibit close enough approach for interactions, see Figure 101. This highlights that the anion can be weakly coordinating due to its steric influence when paired with cations stabilised by donor groups such as PPh_3. All bond lengths, angles and short interactions discussed were found using the atoms with the higher occupancy (58 %). Disorder was present in the axial hexafluoroisoproxy group and in two of the equatorial hexafluoroisoproxy groups, as they are packed over two positions.

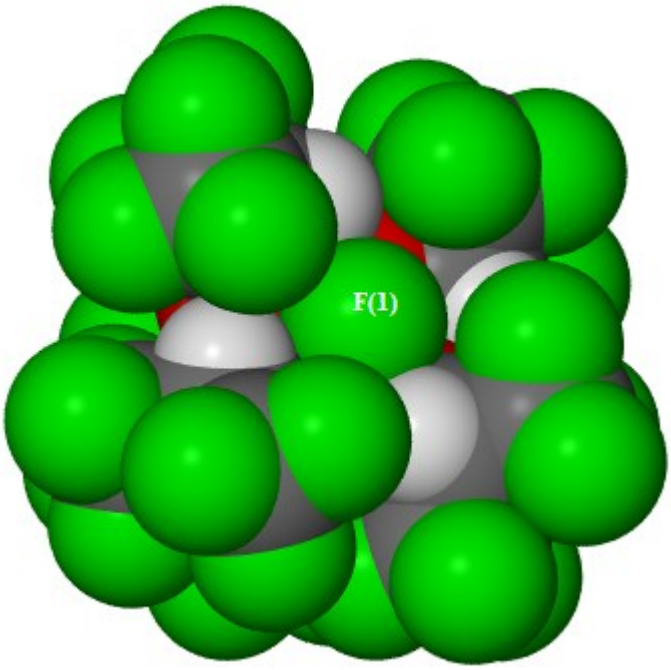

Figure 101: Spacefill representation of the anion in $[Ag(PPh_3)_3]^+[P\{OCH(CF_3)_2\}_5F]^-$ (17). Disorder omitted for clarity. F(1) atom labelled to visualise the steric bulk influence around this atom due to the bulky hexafluoroisopropoxy substituents on the phosphorus centre.

Fluoride addition to the $P\{OCH(CF_3)_2\}_4Cl$, phosphorane with AgF in DCM solvent (*ca.* 1 hr. ultrasonic activation) forms the $P\{OCH(CF_3)_2\}_4F$ phosphorane rather than a $[P\{OCH(CF_3)_2\}_4FCl]^-$ anion. This is likely due either to the $P\{OCH(CF_3)_2\}_4Cl$ phosphorane being less Lewis acidic or the large lattice energy of AgCl, which has a low solubility in the DCM solvent.

5.2.4 Synthesis of the $[P\{OCH(CF_3)_2\}_5F]^-$ Sodium Salts

As discussed above MeCN can solvate Na^+ and form the $[P\{OCH(CF_3)_2\}_5F]^-$ anion. Efforts to crystallize $[Na(NCMe)_6]^+[P\{OCH(CF_3)_2\}_5F]^-$, (**18**) for structural determination by single-crystal X-ray diffraction have been unsuccessful. However, a Na^+ salt of the $[P\{OCH(CF_3)_2\}_5F]^-$ anion has been structurally characterised by single-crystal X-ray diffraction. This was crystallised from a reaction mixture containing (**16**) and AgF in a DCM/MeCN (1:5) solvent mixture (1hr. ultrasonic activation). Slow diffusion of toluene in to a concentrated sample of this reaction mixture (after filtration) stored at -16 °C led to the formation of crystals of $[P\{OCH(CF_3)_2\}_5F]^-[Na(NCMe)_2O{=}P\{OCH(CF_3)_2\}_3]^+$, (**22**), see **Error! Reference source not found.**.

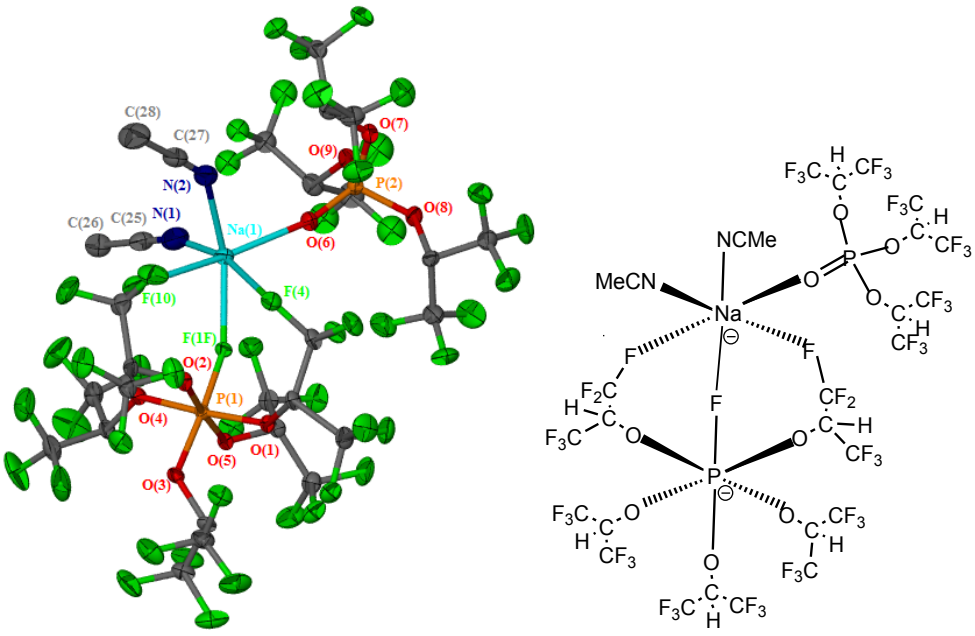

: Molecular structure of $[P\{OCH(CF_3)_2\}_5F]^-[Na(NCMe)_2OP\{OCH(CF_3)_2\}_3]^+$, (22)at 110 K. Disorder and hydrogen atoms omitted for clarity. Thermal ellipsoids are drawn at the 50 % probability level. Selected interatomic distances (Å) and angles (°): P(1)-O(1) = 1.698(2), P(1)-O(2) = 1.687(2), P(1)-O(4) = 1.688(2), P(1)-O(5) = 1.704(2), average equatorial P-$O_{(1,2,4,5)}$ = av. 1.694(2), axial P(1)-O(3) = 1.689(2), P(1)-F(1F) = 1.656(1), P(2)-O(6) 1.455(2) Å indicates this is a P=O, Na(1)-N(1) = 2.371(4), Na(1)-N(2) = 2.420(3), Na(1)-O(6) = 2.291(2), Na(1)-F(4) = 2.838(2), Na(1)-F(10) = 2.612(2), Na(1)-F(1F) = 2.218(2), O(6)-Na(1)-F(10) = 167.0(1), F(1F)-Na(1)-F(4) = 63.6(1), N(1)-Na(1)-N(2) = 105.5(1), F(1F)-Na(1)-N(1) = 104.4(1), F(4)-Na(1)-N(2) = 82.9(1), O(2)-P(1)-O(4) = 90.6(1), F(1)-P(1)-O(3) = 175.4(1), O(1)-P(1)-O(5) = 87.8(1), O(5)-P(1)-O(4) = 93.3(1), O(1)-P(1)-O(2) = 88.1(1). Crystal system: monoclinic Space group: $P2_1/n$. R_1: 0.0500 (all data), wR_2: 0.1253 (>2sigma(I)).

The crystal structure indicates that the Na^+ present forms an anion-coordinated species. This Na^+ must originate from residual unreacted sodium alkoxide, $NaOCH(CF_3)_2$, present in the reaction mixture of in the (**16**). The structure also contains a phosphate, $O{=}P\{OCH(CF_3)_2\}_3$

coordinated to the Na^+ along with two coordinated MeCN molecules. The phosphate is present in low concentration in the reaction mixture from the hydrolysis of the phosphorane. Interestingly, the XRD structure in **Error! Reference source not found.** shows that the WCA coordinates through the CF_3 fluorine atoms of the $OCH(CF_3)_2$ groups, rather than their most basic site (the alkoxide oxygen atoms) which appear to be accessible without much steric congestion. The Na^+ has a distorted octahedral geometry, which is completed with C-F···Na contacts from the $[P\{OCH(CF_3)_2\}_5F]^-$ anion, one from the P-F bond and two from the alkoxide groups (C-F bonds).

In the anion the F(1)-P(1)-O(3) = 175.4(1) ˚ angle deviates slightly from 180 ˚ and the O(2)-P(1)-O(4) = 90.6(1) ˚, O(1)-P(1)-O(5) = 87.8(1) ˚, O(5)-P(1)-O(4) = 93.3(1) ˚, O(1)-P(1)-O(2) = 88.1(1) ˚ angles deviate slightly from 90 ˚, the angles of which describe a perfect octahedral structure. The axial O-P bond distance P(1)-O(3) = 1.689(2) Å is longer then that found for $P\{OCH(CF_3)_2\}_5$, (**16**); average $P\text{-}O_{(ax)}$ = 1.673(2) Å, but shorter than the ion separated species in $[Ag(PPh_3)_3]^+[P\{OCH(CF_3)_2\}_5F]^-$, (**19**); $P\text{-}O_{(ax)}$ = 1.704(3) Å and $[NEt_4]^+[P\{OCH(CF_3)_2\}_5F]^-$, (**24**), $P\text{-}O_{(ax)}$ = 1.722(4) Å, discussed below. The average equatorial $P\text{-}O_{(ax)}$ = 1.694(2) Å is longer than that found for (**16**); average $P\text{-}O_{(eq)}$ = 1.593(2) Å, but statistically the same for those found in (**19**); $P\text{-}O_{(ax)}$ = 1.699(2) Å and (**24**); $P\text{-}O_{(ax)}$ = 1.694(3) Å.

As shown in Figure 101 the P-F bond in the $[P\{OCH(CF_3)_2\}_5F]^-$ anion is crowded by the bulky hexafluoroisopropoxy groups, these can inhibit close approach for interactions with this fluorine atom. However, the $[P\{OCH(CF_3)_2\}_5F]^-[Na(NCMe)_2OP\{OCH(CF_3)_2\}_3]^+$, (**22**) crystal structure indicates that small ions like a sodium ion can interact strongly with this fluorine atom from the P-F bond and form a strong bond; Na(1)-F(1F) = 2.218(2) Å, see Figure 102. It appears the strong electrostatic interaction with the partially stabilised sodium ion allows this close contact to be favourable. The fluorine atoms from the hexafluoroisopropoxy substituents can also interact with the sodium atom, although these are weaker than the Na-F-P interaction; Na(1)-F(4) = 2.838(2) Å, Na(1)-F(10) = 2.612(2) Å.

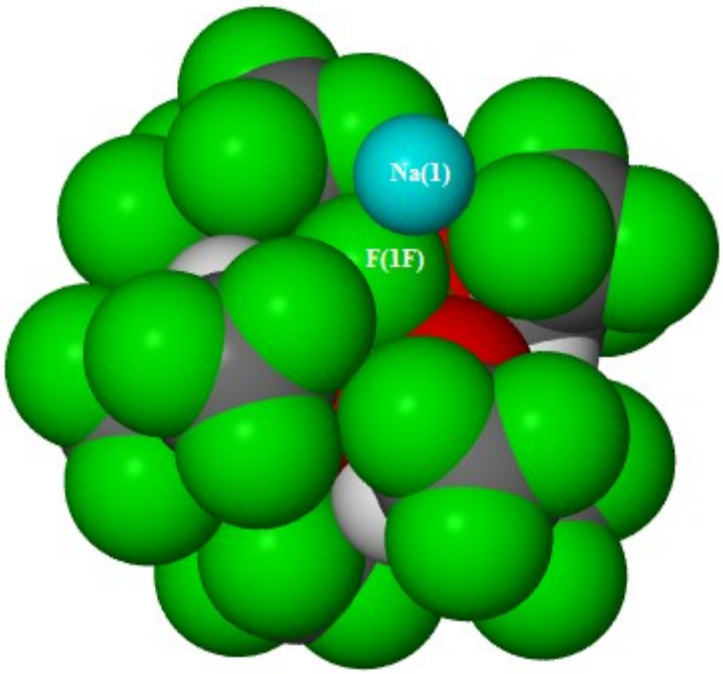

Figure 102: Spacefill diagram of $[P\{OCH(CF_3)_2\}_5F]^-[Na(NCMe)_2OP\{OCH(CF_3)_2\}_3]^+$, (22) highlights that the Na-F contact is present due to the small size of this ion allowing close contact. MeCN and $OP\{OCH(CF_3)_2\}_3$ ligands omitted for clarity.

It appears for this structure the P-F bond is significantly larger; P(1)-F(1F) = 1.656(1) Å than the average P-F bond in $[N^nBu_4]^+[PF_6]^-$, CSD name; NOFKEY02; average 1.593(1) Å. This P(1)-F(1F) bond is also greater than those found in (**19**); P-F = 1.627(6) and (**24**), P-F = P(1)-F(1) = 1.597(4). This is likely due to coordination to the Na^+. The longer P-F bond is accompanied by a shorter P-$O_{(ax)}$ bond length as phosphorus binds to the axial alkoxide more strongly to compensate for the weakened P-F interaction. Two short contacts (less than the sum of VdW radii – 0.2 Å) were found with the molecule in the asymmetric unit. One C-F··F-C interactions (2.732 Å, sum of the VdW radii of F and F = 2.940 Å), and one C-F··H-C interaction (2.414 Å, sum of the VdW radii of F and H = 2.990 Å). The C-F··H-C interaction found was between the acetonitrile hydrogen atoms with the outer fluorine atoms of the anion.

The $O=P\{OCH(CF_3)_2\}_3$ species coordinated to the sodium forms a strong Na-O=P interaction; Na(1)-O(6) = 2.291(2) Å. Although this is much longer than the average Na-O=P bond found in $[Na\{OP(Ph)_3\}_4]^+[PF_6]^-$; 2.226(1) Å, CSD name; AJIZEY. The P=O bond in this crystal structure; P(2)-O(6) 1.455(2) Å, is much shorter than the average P=O bonds found in $[Na\{OP(Ph)_3\}_4]^+[PF_6]^-$; 1.491(1) Å. This highlights that the high electron withdrawing nature of each hexafluoroisopropoxy group further polarises the phosphorus atom to form a shorter double bond with the oxygen atom. The presence of strongly

electron-withdrawing groups reduces the donor ability of the oxygen atom towards the sodium ion, hence increasing its Na-O bond length compared to ligands such as $O=P(Ph)_3$.

Formation of the anion in the presence of triethylamine base was also trialled. This involved the addition of $P\{OCH(CF_3)_2\}_5$, (**16**), NaF and triethylamine in DCM solvent (*ca.* 1 hr. ultrasonic activation). The anion was observed by ESI-MS (884.9387 m/s, $[M]^-$) of the reaction mixture. The $^{31}P\{^1H\}$NMR consisted of a doublet at -147.6 ppm (d, $^1J_{PF}$ = 818 Hz, [**P**$\{OCH(CF_3)_2\}_5F$]) and the ^{19}F NMR also consisted of signals at -73.03 (br, axial [$P\{OCH(C\mathbf{F}_3)_2\}_5F]^-$), -72.69 (s, equatorial [$P\{OCH(C\mathbf{F}_3)_2\}_5F]^-$) and -58.48 (d, $^1J_{FP}$ = 818 Hz, [$P\{OCH(CF_3)_2\}_5\mathbf{F}]^-$) ppm, confirming the presence of anion. The ^1H NMR indicated the presence of excess triethylamine; 0.88 (t, $^3J_{HH}$ = 7Hz, $\mathbf{Et}_3$), 2.38 (q, $^3J_{HH}$ = 7Hz, $\mathbf{Et}_3$) ppm and coordinated triethylamine; 1.33 (m, $[Na(N\mathbf{Et}_3)_n]^+$), 3.46 (m, $[Na(N\mathbf{Et}_3)_n]^+$) ppm.

5.2.5 Synthesis of the Tetraethylammoinum Salt, $[NEt_4]^+[P\{OCH(CF_3)_2\}_5F]^-$, (**24**)

One of the potential applications of these anions is in IL chemistry, so the synthesis of organic cation salts of $[P\{OCH(CF_3)_2\}_5F]^-$ were attempted in order to explore the possibility of forming IL phases. Reaction of $P\{OCH(CF_3)_2\}_5$, (**16**) with NEt_4Br and AgF in DCM solvent (*ca.* 1 hr. ultrasonic activation) followed by filtration through Celite and removal of the DCM solvent *in vacuo* gave a white solid, see Scheme 57. After an air-sensitive filtration through Celite and removal of the DCM solvent *in vacuo* a white solid product was obtained. The $^{31}P\{^1H\}$ NMR spectrum consists of an intense signal at -147.5 ppm (d, $^1J_{PF}$ = 818 Hz), indicating the presence of the $[P\{OCH(CF_3)_2\}_5F]^-$ anion. The ^{19}F NMR spectrum supports this, consisting of low intensity signals at -59.68 ppm (d, $^1J_{FP}$ = 818 Hz) and -72.98 ppm (br) for the alkoxy substituent axial to the fluorine atom. A higher intensity signal is also observed at -72.71 (s), for the four alkoxy groups equatorial to the fluorine atom on the phosphorus centre. In addition, the ESI-MS shows a signal at 884.9 m/z in the negative mode for the $[P\{OCH(CF_3)_2\}_5F]^-$ anion, $[M]^-$ and 130.1 m/z in the positive mode for the $[NEt_4]^+$ cation, $[M]^+$. The melting point of this material was determined to be 118 °C. This is higher than that required for an IL, but is lower than that seen for many $[NEt_4]^+$ salts; $[NEt_4]^+[BF_4]^-$ = 365-368 °C, $[NEt_4]^+[PF_6]^-$ = >300 °C, $[NEt_4]^+[Br]^-$ = 285 °C, $[NEt_4]^+[OTf]^-$ = 161-163 °C, suggesting that alternating the cation may significantly lower this to form potentially new ILs with this WCA. Crystallisation was achieved by slow diffusion of pentane into a concentrated sample of $[NEt_4]^+[P\{OCH(CF_3)_2\}_5F]^-$, (**24**).

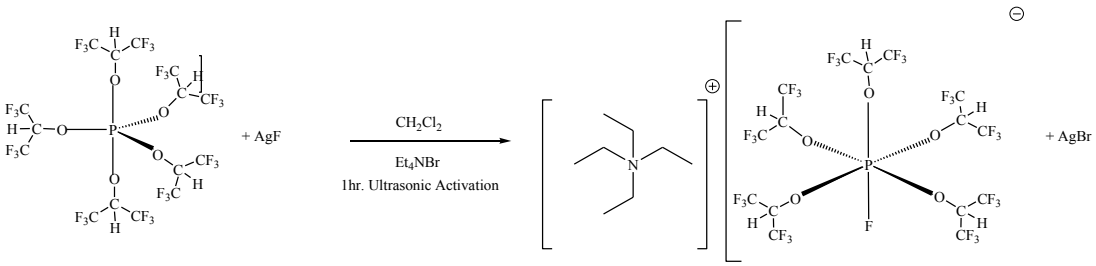

Scheme 57: Synthesis of $[NEt_4]^+[P\{OCH(CF_3)_2\}_5F]^-$, (24).

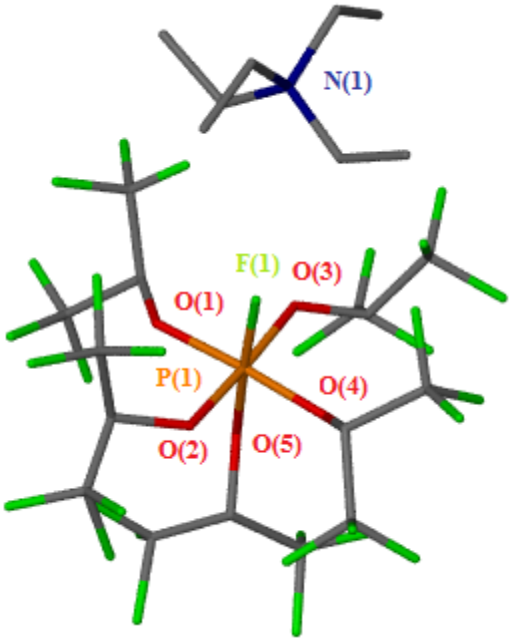

Figure 103: Molecular structure of $[NEt_4]^+[P\{OCH(CF_3)_2\}_5F]^-$, (24) at 110 K. Disordered parts and hydrogen atoms omitted for clarity. Selected interatomic distances (Å) and angles (˚): P(1)-F(1) = 1.597(4), P(1)-O(1) = 1.672(3), P(1)-O(2) = 1.706(3), P(1)-O(3) = 1.715(3), P(1)-O(4) = 1.681(4), average equatorial P-$O_{(eq, 1,2,3,4)}$ = av. 1.694(3) Å, P(1)-O(5) = 1.722(4), O(2)-P(1)-O(1) = 88.5(1), O(5)-P(1)-F(1) = 172.6(2), O(3)-P(1)-O(4) = 94.3(2), O(2)-P(1)-O(3) = 88.6(2), O(4)-P(1)-O(1) = 88.6(1). Crystal system: triclinic. Space group: P-1. R_1: 0.0992 (all data), wR_2: 02829 (>2sigma(I)).

The single-crystal X-ray diffraction structure of $[NEt_4]^+[P\{OCH(CF_3)_2\}_5F]^-$, (**24**) is shown in Figure 103. The anion is disordered over two positions (7:3 ratio of occupancy), all bond lengths, angles and short interactions were considered only for the position with the highest occupancy (70 %). Two "NEt_2" fragments, each with a nitrogen atom with ½ occupancy are also found in the asymmetric unit to balance the charge of the anion. Each cation position contains disordered Et groups (over two sites, each with 50 % occupancy). Short interactions are not discussed for this structure due to the complexity of the disorder. Similar to $[Ag(PPh_3)_3]^+[P\{OCH(CF_3)_2\}_5F]^-$, (**19**). The O(5)-P(1)-F(1) = 172.6(2) ˚ angle deviates from 180 ˚ and the O(2)-P(1)-O(1) = 88.5(2) ˚, O(3)-P(1)-O(4) = 94.3(2) ˚, O(2)-P(1)-O(3) = 88.6(2) ˚, O(4)-P(1)-O(1) = 88.6(2) ˚angles deviate from 90 ˚, the angles of which describe a

perfect octahedral structure. The axial P-O bond distance is longer; P-$O_{(ax)}$ = 1.722(4) than that found for P{$OCH(CF_3)_2$}$_5$, (**16**); average P-$O_{(ax)}$ = 1.673(2) Å and $[Ag(PPh_3)_3]^+[P\{OCH(CF_3)_2\}_5F]^-$, (**19**); P-$O_{(ax)}$ = 1.704(3) Å. The average equatorial P-$O_{(eq)}$ = 1.694(3) Å is similar to the average equatorial P-$O_{(eq)}$ of (**16**); average P-$O_{(eq)}$ = 1.593(2) Å, and that of (**19**); P-$O_{(ax)}$ = 1.699(2) Å. It appears that for this structure the P-F bond distance; P(1)-F(1) = 1.597(4) Å, is statistically the same as that found for a the average P-F bond in $[N^nBu_4]^+[PF_6]^-$, CSD name; NOFKEY02; average 1.593(1) Å. As discussed above (**16**) is found to have greater Lewis acidic property than PF_5 from the FIA calculations, hence a shorter P-F bond is expected. However, with the combination of steric effects, the reduced P-F orbital overlap is likely to cause longer bonds than that expected from a purely electronic point of view.

The P-F and P-$O_{(ax)}$ bond distances can be used to gauge how weakly coordinating the ion pairs are by indicating how ion separated these species are *i.e.* most deviation from P{$OCH(CF_3)_2$}$_5$, (**16**). The order of P-$O_{(ax)}$ bond distances increasing in size are as follows; (**16**), average P-$O_{(ax)}$ = 1.673(2) Å, $[Na(NCMe)_2OP\{OCH(CF_3)_2\}_3]^+[P\{OCH(CF_3)_2\}_5F]^-$, (**22**), P(1)-O(3) = 1.689(2) Å, $[Ag(PPh_3)_3]^+[P\{OCH(CF_3)_2\}_5F]^-$, (**19**), P-$O_{(ax)}$ = 1.704(3) Å and $[NEt_4]^+[P\{OCH(CF_3)_2\}_5F]^-$, (**24**), P-$O_{(ax)}$ = 1.722(4), Å. It appears that as the P-$O_{(ax)}$ bond distance increases for the anions, the P-F bond distance decreases and becomes closer to that of a $[PF_6]^-$ anion; (**22**), P(1)-F(1F) = 1.656(1) Å, (**19**), P(1)-F(1) = 1.627(6) Å, (**24**), P(1)-F(1) = 1.597(4) Å, $[N^nBu_4]^+[PF_6]^-$, CSD name; NOFKEY02; average P-F = 1.593(1) Å. This suggests that (**24**) has a weaker anion-cation interaction than (**22**) and (**19**).

5.2.6 Observations of the Potential $[P\{OCH(CF_3)_2\}_6]^-$ Anion

An intense signal was observed at around -146.9 ppm (s) in the $^{31}P\{^1H\}$ NMR spectra in a number of these reactions. ESI-MS of all the $P\{OCH(CF_3)_2\}_5$ species and some of the $[P\{OCH(CF_3)_2\}_5F]^-$ species in the negative mode have a found mass of 1032.94 m/z, as well as that for the molecular ion of the $[P\{OCH(CF_3)_2\}_5F]^-$ ionic species. Both the ESI-MS (in the negative mode, $[M]^-$) and $^{31}P\{^1H\}$ NMR spectroscopy (singlet in the expected region) suggest potential evidence of a hexa(hexafluoroisopropoxy)phosphate ionic species, $[P\{OCH(CF_3)_2\}_6]^-$. Denney *et al.* reported this type of species as very unstable and any attempts to synthesise these gave signals at -87 (s) and -109 (s) ppm in the $^{31}P\{^1H\}$ NMR spectra.[119] They suggested either chemical shift could be for the $[P\{OCH(CF_3)_2\}_6]^-$ anion as they were unable to confirm that they had made this species. However, the findings from this thesis suggest the chemical shift around -146.9 (s) ppm is similar to that of the $[P\{OCH(CF_3)_2\}_5F]^-$ and $[PF_6]^-$ ionic species, suggesting Denney *et al.* did not observe the $[P\{OCH(CF_3)_2\}_6]^-$ in their attempts. It should also be noted that a simple reaction with $P\{OCH(CF_3)_2\}_5$ and $NaOCH(CF_3)_2$ was trialled in DCM and MeCN solution, but did not lead to any new signals in the $^{31}P\{^1H\}$ NMR spectrum. This unstable $[P\{OCH(CF_3)_2\}_6]^-$ anion is potentially an interesting anion but requires the correct type of WCC in order to isolate it in the condensed phase and inhibit decomposition by alkoxide loss.

5.2.7 Reactivity of the Novel Salts; $[Ag(NCMe)_4]^+[P\{OCH(CF_3)_2\}_5F]^-$, (**17**), $[Na(NCMe)_6]^+[P\{OCH(CF_3)_2\}_5F]^-$, (**18**), $[Ag(PPh_3)_3]^+[P\{OCH(CF_3)_2\}_5F]^-$, (**19**)

The $[Ag(PPh_3)_3]^+[P\{OCH(CF_3)_2\}_5F]^-$, (**19**) salt was found to be stable towards moisture in the air when exposed for fifteen minutes, as well as water from a D_2O NMR test. The D_2O NMR test consisted of the addition of 0.4 mL of D_2O solvent to a small spatula full of (**19**). Salt (**19**) was found to be insoluble in D_2O solvent, therefore wet THF solvent was added and the sample was analysed by $^{31}P\{^1H\}$, ^{19}F and ^1H NMR spectroscopy. The solubility of (**19**) in D_2O/THF was poor. However, the characteristic peaks of the $[P\{OCH(CF_3)_2\}_5F]^-$ anion were present in the ^{19}F NMR spectrum. There was no evidence of hydrolysis of the $[P\{OCH(CF_3)_2\}_5F]^-$ anion to $O{=}P\{OCH(CF_3)_2\}_3$. This suggest hydrolysis does not readily occur at room temperature, unlike the air- and moisture-sensitive phosphorane (**16**), which decomposes rapidly to form $O{=}P\{OCH(CF_3)_2\}_3$. Similar observations are made for the stability of $[Ag(NCMe)_4]^+[P\{OCH(CF_3)_2\}_5F]^-$, (**17**) towards moisture in the air. One may expect the silver salt to be light sensitive but (**19**) is found to be stable after weeks of

exposure to natural light. The reactivity of the (**19**) was also probed. Excess methyl iodide was added to a DCM solution of (**19**). The $^{31}P\{^{1}H\}$ NMR spectrum consisted of a intense signal at 21.8 ppm (s), which is assigned as a $[PPh_3Me]^+$ cation (δ_P = 21.5 ppm).[349] A weaker intensity signal was also observed at -147.5 ppm (d, $^{1}J_{PF}$ = 818 Hz), indicating the presence of the $[P\{OCH(CF_3)_2\}_5F]^-$ anion. The higher intensity $[PPh_3Me]^+$ cation is likely due to a 3:1 ratio of the triphenylphosphine to the $[P\{OCH(CF_3)_2\}_5F]^-$ WCA. The excess $[PPh_3Me]^+$ may be present as the iodide salt in solution, see Scheme 58. There was no evidence in the $^{31}P\{^{1}H\}$ NMR of any cationic $[Ag(PPh_3)_3]^+$ species (δ_P = 12.1 ppm, s) in this reaction, suggesting 100 % methylation.

$$[Ag(PPh_3)_3]^+[P\{OCH(CF_3)_2\}_5F]^- + MeI \xrightarrow{CH_2Cl_2} [PPh_3Me]^+[P\{OCH(CF_3)_2\}_5F]^- + AgI + 2[PPh_3Me]^+[I]^-$$

Scheme 58: Methylation of the $[Ag(PPh_3)_3]^+[P\{OCH(CF_3)_2\}_5F]^-$, (19) salt to give the phosphonium salts.

The silver iodide side product is soluble in DCM, hence purification of $[PPh_3Me]^+[P\{OCH(CF_3)_2\}_5F]^-$ was difficult. Slow diffusion of hexane into the DCM solution led to crystal growth. The crystal structure consisted of the $[PPh_3Me]^+$ cation, but with a $[I_4Ag_3]^-$ anion. The CSD contains a similar ionic species; $([PPh_3Me]^+)_2[I_3Ag]^{2-}$, CSD name; SESXAP, consisting of a shorter Ag--I chain and a double negative charge.[350] Furthermore a $[I_8Ag_4]^-$ anion chain was also found in the CSD. This can be paired with various cations *i.e.* $[PPh_4]^+$ and $[AsPh_4]^+$, with the following CSD names; KEWDUL and KEWFAT respectively.

Interestingly, the addition of trityl chloride to (**19**) gave rise to new peaks in the $^{31}P\{^{1}H\}$ NMR spectrum at 28.7 (s) and 27.6 (s) ppm. Slow diffusion of hexane into this DCM solution gave crystals which were found to be a $(PPh_3)_2Ag_2Cl_2$ salt {a similar $(PPh_3)_4Ag_2Cl_2$ species is present in the CSD}. The observation of this silver chloride species indicates metathesis has taken place and the trityl cationic species is generated in solution, which may go on to react further. A simple reaction with $[Ph_3C]^+[PF_6]^-$ and PPh_3 in DCM solution formed a $[Ph_3C\text{-}PPh_3]^+[PF_6]^-$ species with a new chemical shift at 24.9 (s) ppm in the $^{31}P\{^{1}H\}$ NMR spectrum. Although the chemical shifts differ, it is possible that $[Ph_3C\text{-}PPh_3]^+[P\{OCH(CF_3)_2\}_5F]^-$ may have been formed in the reaction of trityl chloride and $[Ag(PPh_3)_3]^+[P\{OCH(CF_3)_2\}_5F]^-$ discussed above. The $^{31}P\{^{1}H\}$ NMR spectrum of the mother liquor consists of an intense signal at 27.6 (s) ppm, suggesting this is for the potential $[Ph_3C\text{-}PPh_3]^+$ cation and the signal at 28.7 (s) ppm for the $(PPh_3)_2Ag_2Cl_2$ salt, see Scheme 59.

Scheme 59: Reactivity of the $[Ag(PPh_3)_3]^+[P\{OCH(CF_3)_2\}_5F]^-$ salt, (19) and Ph_3CCl.

However, no sign of free triphenylphosphine is present in the $^{31}P\{^1H\}$ NMR spectrum, causing a stoichiometric imbalance in the above reaction. It may be likely that the majority of the salt contains a $(PPh_3)_4Ag_2Cl_2$ type species, which is more commonly known and the single-crystal obtained for X-ray diffraction analysis was a small component in the reaction mixture. Nevertheless, this reaction formed a $[Ph_3C\text{-}PPh_3]^+$ cationic species and did not lead to anion decomposition. In contrast, reaction of the trityl chloride with (**17**) in DCM (*ca.* 1 hr. ultrasonic activation) showed that the anion decomposes to $PF\{OCH(CF_3)_2\}_4$ (δ_P = 81.8 ppm, d, $^1J_{PF}$ = 794 Hz) and trityl alkoxide, $Ph_3COCH(CF_3)_2$ (δ_F = -72.30 ppm, d, $^3J_{FH}$ = 7 Hz), as the electrophilic cation abstracts an alkoxy group from the anion, see Scheme 60. This gives some insight into the stability of this anion; H_2O stable, but not necessarily stable towards electrophiles that can abstract an alkoxy group.

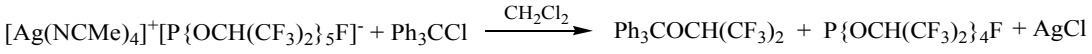

Scheme 60: Reactivity of the $[Ag(NCMe)_4]^+[P\{OCH(CF_3)_2\}_5F]^-$ salt, (17) and Ph_3CCl.

An interesting observation was made upon addition of excess trityl chloride and excess AgF with (**17**) in MeCN solvent (*ca.* 1 hr. ultrasonic activation). The AgF continues to fluorinate the phosphorane formed from the abstraction of the alkoxy species by the trityl chloride. The trityl chloride also continues to abstract an alkoxy group to give the phosphorane and this cycle repeats itself until the stable $[PF_6]^-$ anion is formed, see Scheme 61. Removal of the MeCN solvent and addition of DCM solvent before the addition of the trityl chloride would avoid continuous fluorination of the phosphorane. This would inhibit the series of reactions, as the DCM cannot stabilise the Ag ion *via* solvent stabilisation to form the silver salt. Controlled reactions in this way is one potential route to the synthesis of mixed fluoro-alkoxy phosphate WCAs *e.g.* $[P\{OCH(CF_3)_2\}_{4/3}F_{2/3}]^-$. Table 34 summarises the $^{31}P\{^1H\}$ NMR chemical shifts and ^{19}F NMR chemical shifts of key hexafluoroisopropoxy-containing phosphorane and phosphate species identified.

P(V) Species Identified	*$^{31}P\{^{1}H\}$ NMR (δ/ppm)*	*^{19}F NMR (δ/ppm)*
$P\{OCH(CF_3)_2\}_5$,	-84.0 (s)	-73.42 (br, Hz)
$[P\{OCH(CF_3)_2\}_5F]^-$	-147.4 (d, $^1J_{PF}$ = 818 Hz)	-60.50 (d, $^1J_{PF}$ = 818 Hz), -72.90 (s), -73.10 (br)
$PF\{OCH(CF_3)_2\}_4$	-81.8 (d, $^1J_{PF}$ = 794 Hz)	-68.55 (d, $^1J_{PF}$ 780 Hz), -73.57 (s),
$[P\{OCH(CF_3)_2\}_4F_2]^-$	-146.8 (t, $^1J_{PF}$ = 782 Hz)	-
$PF_2\{OCH(CF_3)_2\}_3$	-80.1 (t, $^1J_{PF}$ = 786 Hz)	

Table 34: NMR shifts for various neutral and anionic hexafluoroisopropoxy-containing P(V) species.

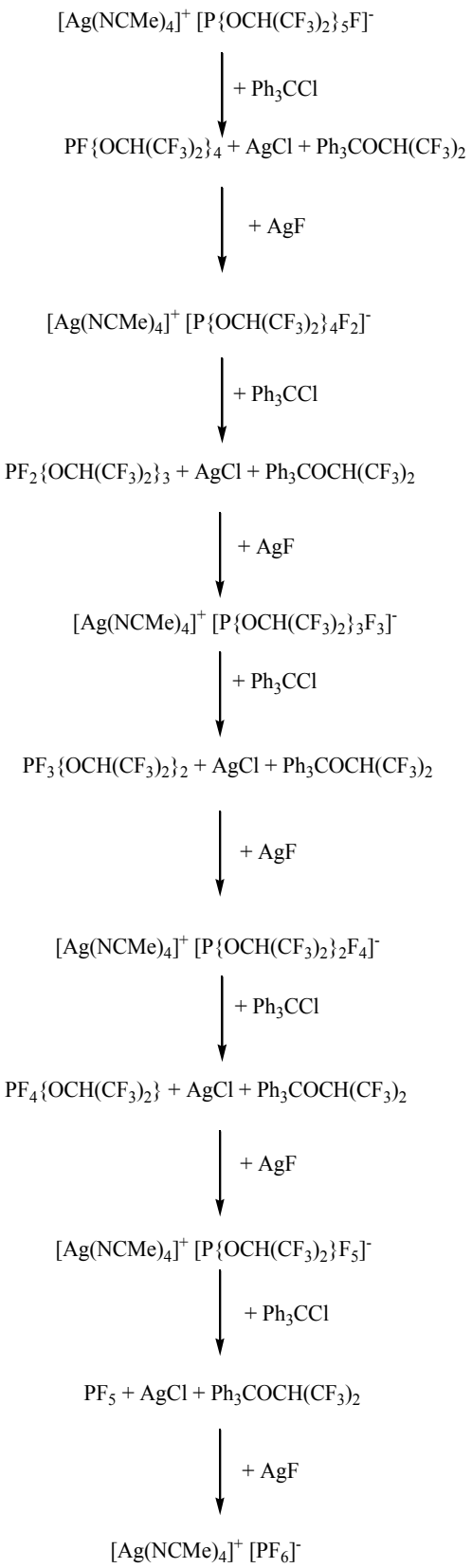

Scheme 61: Reactivity of the $[Ag(NCMe)_4]^+[P\{OCH(CF_3)_2\}_5F]^-$ salt, (17) and Ph_3CCl in excess AgF.

Stabilisation reactions of the cationic $[H(Et_2O)_2]^+$ with the $[P\{OCH(CF_3)_2\}_5F]^-$ WCA were also trialled. Initially (**16**), NaF and $HCl(Et_2O)_2$ were dissolved in DCM solvent. However, the $^{31}P\{^1H\}$ NMR spectrum showed no signals for the $[P\{OCH(CF_3)_2\}_5F]^-$ anion. It appears the $HCl(Et_2O)_2$ protonates the alkoxide to form the hexafluoroisopropanol, $HOCH(CF_3)_2$ and the $P\{OCH(CF_3)_2\}_4Cl$ phosphorane. Addition of $HCl(Et_2O)_2$ to either $[Na(NCMe)_6]^+[P\{OCH(CF_3)_2\}_5F]^-$, (**18**) or $[Ag(NCMe)_4]^+[P\{OCH(CF_3)_2\}_5F]^-$, (**17**) previously prepared ionic species results in anion decomposition. Reaction of $HCl(Et_2O)_2$ with $[Ag(PPh_3)_3]^+[P\{OCH(CF_3)_2\}_5F]^-$ (**19**) was also trialled, but again anion decomposition occurred. Slow diffusion of hexane into a concentrated DCM solution of the reaction mixture gave crystals of the $Ag_4Cl_4\{PPh_3\}_4$ cluster, suggesting metathesis occurred. This indicates that the new $[P\{OCH(CF_3)_2\}_5F]^-$ anion is not stable towards highly electrophilic cations such as $[H(Et_2O)_2]^+$. The $[P\{OCH(CF_3)_2\}_5F]^-$ WCA is likely to be more useful for the synthesis of novel low temperature ILs, due to its dipole moment and asymmetric structure. The stability of the anion towards water and its easy and affordable synthetic methodology are key advantages for this anion for industrial use. There is even potential use of this anion as an electrolyte, but the redox chemistry must be probed first.

5.3 SUMMARY

WCA chemistry has expanded over the recent years and includes a variety of structures such as; borate-based anions, carborane-based anions, teflate-based anions, poly- or perfluorinated alkoxy-, (OR^F) and aryloxy-, (OAr^F) metallates and those that originate from Lewis acidic compounds. The carborane-based anions are known as the "least coordinating anions" especially the halogenated carborane-based anions, due to distribution of the negative charge over the halide substituents. Development of these anions has allowed for the isolation of very electrophilic cations *e.g.* $[SiEt_3]^+$ and $[Al^iPr_2]^+$, $[PX_4]^+$ and $[CI_3]^+$ as well as silver adducts of very weakly Lewis bases such as P_4,[263, 336] S_8[337] and C_2H_4[338] and the protonation/alkylation/silyation of many weakly basic molecules *e.g.* benzene, C_{60}, phosphabenzenes and phosphazenes, Xe *etc*.[273] The general requirements for WCAs identified by Krossing *et al.* consists of the delocalization of the negative charge over a large area, reduced nucleophilicity and chemically robust moieties to avoid rapid decomposition.[252] The diversity in the applications of WCAs makes them significant for continuous development. Industrial scale olefin-polymerisation reactions is one example of catalysis where WCAs are useful to afford better control of catalyst solubility and stability.[288] WCAs can also be paired with large unsymmetrical cations to form a range of ILs[296] or for their use in electrochemistry and as electrolytes for lithium-ion batteries.

However, challenges with the carborane-based anions include their lack of availability for bulk use, due to an expensive and time consuming synthetic procedure involving the use of very toxic chemicals. In addition, some of the carborane-based WCAs have been found to be explosive *e.g.* $[CB_{11}(CF_3)_{12}]^-$.[330] The teflate-based anions are also not widely used as they can decompose rapidly in the presence of water to liberate HF, making them difficult to handle routinely. The poly- or perfluorinated aryloxy-, (OAr^F) metallate anions are susceptible to OAr^F abstraction, leading to anion decomposition. The perfluorinated alkoxy-metallates *e.g.* $[Al\{OC(CF_3)_3\}_4]^-$ are stable towards hydrolysis, due to the steric shielding of the oxygen atom and electronic stabilization from the perfluorination. Although this $[Al\{OC(CF_3)_3\}_4]^-$ WCA is robust and commercially available, the perfluorinated alcohol can be expensive to use on a large scale. This WCA also undergoes decomposition to a $[\{OC(CF_3)_3\}_3Al\text{-}F\text{-}Al\{OC(CF_3)_3\}_3]^-$ type anion when reacted with very electrophilic cations such as $[P_2X_5]^+$ (X = Br and I). This highlights that although WCAs useful for stabilising electrophilic cations are available, they are expensive to synthesise, making their use on an industrial scale inefficient. The cheaper alternatives available tend to be symmetrical and are not of use for IL phases with low temperature melting points. The current available WCAs

do not fulfil both criteria required for the use of these WCAs in ILs *i.e.* unsymmetrical and prepared from an affordable and simple synthetic method for mass use.

The acyclic pentakis(hexafluoroisopropoxy)phosphorane, $P\{OCH(CF_3)_2\}_5$, (**16**) was first reported with its method of synthesis in 1978, by Roschenthaler *et al*. This phosphorane, (**16**) is known to be air- and moisture-sensitive as it decomposes rapidly to form the phosphate, $O=P\{OCH(CF_3)_2\}_3$. However, this phosphorane has not been explored for any applications.[2] The work presented in this thesis extends the investigation into the synthesis to provide a simpler method with the use of less toxic chemicals. Furthermore, quantitative analysis on the Lewis acidity using a FIA scale is also discussed. The results indicate (**16**) lies between the Lewis acid character of $GaCl_3$ and $B(C_6F_5)_3$. Single-crystal X-ray diffraction analysis of (**16**) has also been obtained. This is the first example of an X-ray crystal structure of a homoleptic fluorinated alkoxy phosphorane. Comparisons to the X-ray crystallographic structure of $P(OCy)_5$ indicates that (**16**) has increased polarisation of the P-O bond, resulting in shorter bond lengths.

In addition, application of this phosphorane for the synthesis of a novel bulky anion, $[P\{OCH(CF_3)_2\}_5F]^-$ that is stable towards hydrolysis has been investigated. This has been found with the following novel ionic salts; $[Ag(NCMe)_4]^+[P\{OCH(CF_3)_2\}_5F]^-$, (**17**), $[Na(NCMe)_6]^+[P\{OCH(CF_3)_2\}_5F]^-$, (**18**), $[Ag(PR_3)_3]^+[P\{OCH(CF_3)_2\}_5F]^-$; PR_3; R = Ph, Me, ^{i}Pr; (**19**) , (**20**) and (**21**) respectively, $[Na(NEt_3)_6]^+[P\{OCH(CF_3)_2\}_5F]^-$ (**23**), $[NEt_4]^+[P\{OCH(CF_3)_2\}_5F]$, (**24**). The ionic salts of (**19**) and (**24**) have been characterised by single-crystal X-ray diffraction and are found to be stable towards hydrolysis at room temperature. The similar NMR data for all the $[P\{OCH(CF_3)_2\}_5F]^-$ salts suggest that in solution the ion pair is separated, indicating that this may be a potential new WCA similar to WCAs such as $[PF_6]^-$and $[BF_4]^-$, but with additional steric bulk. Crystallization of a sodium ion consisting of an octahedral type geometry, coordinated to three fluorine atoms of the $[P\{OCH(CF_3)_2\}_5F]^-$ anion, two MeCN molecules and a phosphate, $O=P\{OCH(CF_3)_2\}_3$ has been structurally characterised by single-crystal X-ray diffraction. This indicates, that although the anion has found to be ion separated, it can also coordinate through the CF_3 fluorine atoms of the $OCH(CF_3)_2$ groups. Interestingly, although their most basic site at the oxygen atoms appears to be accessible without much steric congestion the CF_3, fluorine atoms are preferred. The X-ray crystallographic structures obtained can also be used gauge how weakly coordinating the ion pairs are, to indicate how ion separated these species are *i.e.* most deviation of the $P\text{-}O_{(ax)}$ bond lengths from the phosphorane, (**16**) and most similar P-F bond lengths to that of a $[PF_6]^-$ anion. The following order is established with this method, from least anion separated to most ion separated salts;

$[Na(NCMe)_2OP\{OCH(CF_3)_2\}_3]^+[P\{OCH(CF_3)_2\}_5F]^-$; (**22**), $[Ag(PPh_3)_3]^+[P\{OCH(CF_3)_2\}_5F]^-$; (**19**) and $[NEt_4]^+[P\{OCH(CF_3)_2\}_5F]^-$; (**24**).

The reactivity of $[Ag(PPh_3)_3]^+[P\{OCH(CF_3)_2\}_5F]^-$, (**19**) was also probed with the addition of reagents *e.g.* methyl iodide or trityl chloride in DCM solvent. The results were promising as anion decomposition did not occur in either case. However, $[Ag(NCMe)_4]^+[PF\{OCH(CF_3)_2\}_5]^-$, (**17**) does undergo decomposition to $PF\{OCH(CF_3)_2\}_4$ on the addition of trityl chloride, as the electrophilic cation abstracts an alkoxy group from the anion. The addition of $HCl(Et_2O)_2$ protonates the alkoxide to form the hexafluoroisopropanol, $HOCH(CF_3)_2$ and the $P\{OCH(CF_3)_2\}_4Cl$ phosphorane. This concludes that although the novel anion is H_2O stable, it is not necessarily stable towards all electrophiles, as some of the more electrophilic ones can abstract an alkoxy group. A better use of the $[P\{OCH(CF_3)_2\}_5F]^-$ WCA includes the synthesis of novel low temperature ILs. The asymmetric structure, its dipole moment, and simple synthesis from affordable reagents make this an attractive candidate the preparation of novel IL phases.

Finally, observations by $^{31}P\{^1H\}$ NMR spectroscopy and ESI-MS have been discussed for the novel hexa(hexafluoroisopropoxy)phosphate anionic species, $[P\{OCH(CF_3)_2\}_6]^-$ in the condensed phase. Isolation has not yet been achieved for this anionic species, but perhaps with the correct type of WCC this is potentially an interesting anion for the future.

5.4 FUTURE WORK

Similar anions to that of $[P\{OCH(CF_3)_2\}_5F]^-$ are of key interest. These may include the synthesis of anions with greater fluorination, $[P\{OCH(CF_3)_2\}_{6-n}F_n]^-$ (n = 1-5), see Figure 104. These will change the properties, forming anions that lie in-between $[PF_6]^-$ and $[P\{OCH(CF_3)_2\}_{6-n}F_n]^-$.

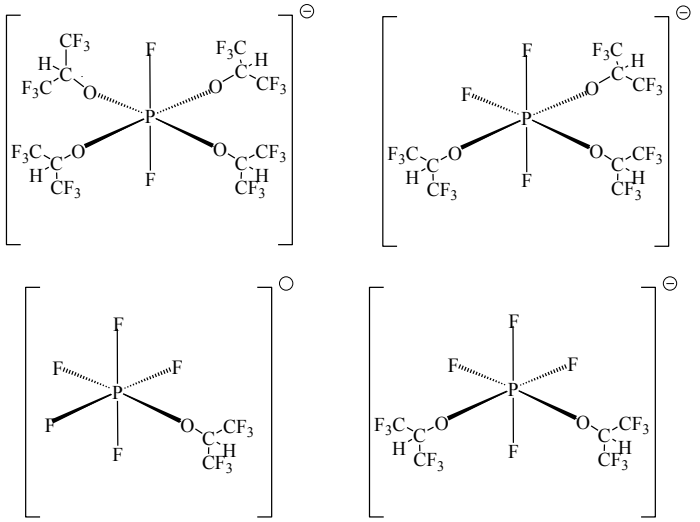

Figure 104: Phosphate anions with a greater number of fluoride groups.

A range of varying fluorinated alkoxy or fluorinated alky groups may also be considered *e.g.* OC_6F_5, $OCH_2(CF_3)$, OCF_2CF_3, $(CF_2)_3CF_3$, $(CF_2)_9CF_3$. These anions are potentially similar in terms of coordination ability to that of the weakly coordinating borates but affordable for bulk use. These can also be classed as bulkier alternatives to $[PF_6]^-$ anions. These anions are potentially of greater advantage for the synthesis of low melting point ILs, due to their unsymmetrical structures. These can be paired with various cations commonly used for ILs, Figure 105 provides a few examples of such cations. Investigations into the physical properties of salts with these types of anions may also provide key information that may even direct their potential applications in catalysis.

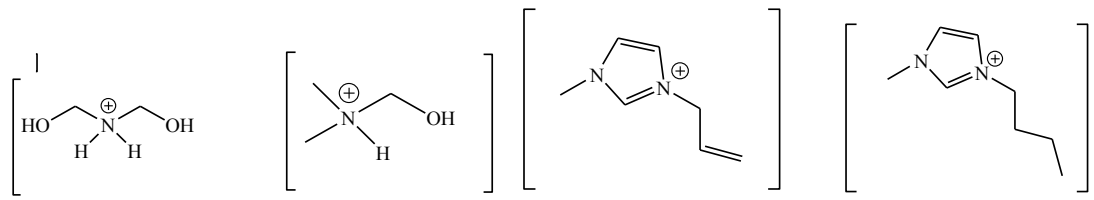

Figure 105: Structure of common cations used for ILs.

6 EXPERIMENTAL

6.1 EXPERIMENTAL DETAILS

The majority of the compounds prepared in this thesis were air- and moisture-sensitive. They were either handled using Schlenk line (10^{-2} mbar vacuum) techniques or inside an MBraun Unilab glove box, both of which contained oxygen-free nitrogen gas only. Reactions were carried out in Schlenk tubes, round bottom flasks with adaptor taps, J. Young's ampoules fitted with PTFE J Young's taps or specially designed double Schlenk tubes for inert-atmosphere filtration, see Figure 106.

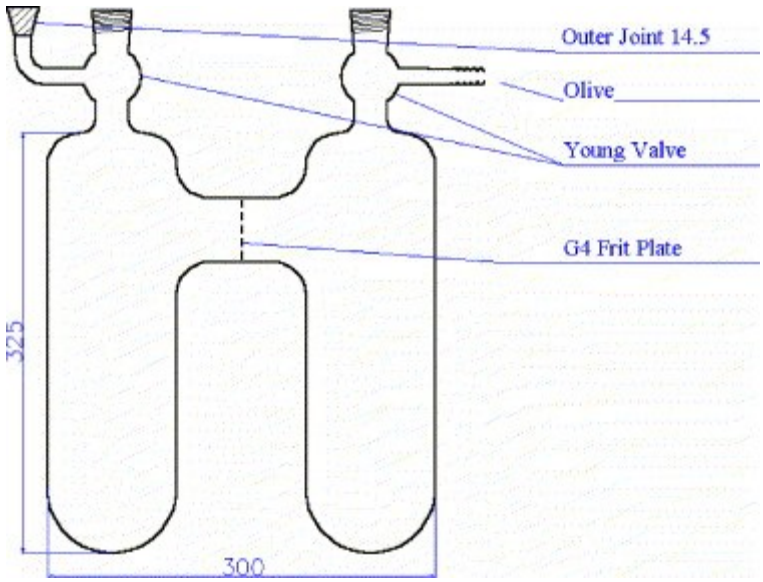

Figure 106: Double Schlenk vessel with Young valves and G4 frit plate. Measures are given in mm. Adapted from ref. [286].

These were all evacuated while being heated and then purged with dry, oxygen-free nitrogen gas (this repeated three times) to ensure they were air- and moisture-free. Chemicals were added to the reaction vessels through a rubber septum using a nitrogen-purged syringe or using a positive nitrogen pressure with no rubber septum or glass stopper. Inert-atmosphere filtrations involved the use of a sintered glass tube attached to a Schlenk tube. A 2 cm depth of Celite was packed in the sintered tube and dried well under vacuum to remove any traces of water. After purging with nitrogen and heating under vacuum (three times), the set up was ready for PTFE canula transfer of the reaction mixture through to the sintered tube. After filtration, 3 x 5 mL (unless stated otherwise) of the chosen solvent was used to wash the product through to the Schlenk tube.

All reagents were purchased from commercial sources, unless their preparation is described in this thesis. Solid reagents were dried under vacuum with gentle heating, unless described otherwise below, and then stored in the glove box. Any liquid reagents were dried using an appropriate drying agent, distilled and stored in glass Young's tubes under nitrogen and sealed with PTFE J Young's taps. Fluoroalcohols were dried using 4 Å molecular sieves and then distilled. Triethylamine was dried with calcium hydride and distilled. The majority of solvents were brought as "anhydrous" and were further dried using Innovation Technologies anhydrous engineering solvent purification system and used within one month of dispensing. Diethyl ether, THF and MeCN were dried with sodium wire under argon, distilled and transferred using a canula into glass Young's flasks.

Infrared (IR) spectra were recorded on a Thermo-Nicolet Avator 370 FTIR spectrometer using CsCl solution cells for sample insertion at *ca.* 200 mg/mL concentration. A Unicam RS 10000E FTIR instrument, averaging 16 scans at resolution 1 cm^{-1} was used with a SensIR ATR-IR accessory for solid samples.

Nuclear magnetic resonance (NMR) spectroscopy samples were prepared using deuterated solvents (*e.g.* $CDCl_3$), which were previously dried over 4 Å molecular sieves and then freeze-thaw degassed. Samples were made up in NMR tubes under nitrogen using either Schlenk line techniques or the glove box and sealed with lab film to keep them air-tight for short periods. NMR spectra were recorded on a Jeol EXC400 (frequencies operating at 161.8 MHz for ^{31}P, 376.2 MHz for ^{19}F and 100.5 for ^{13}C) spectrometer. All ^{1}H NMR and ^{13}C NMR chemical shifts are reported in ppm (δ) relative to trimethylsilane and referenced using the chemical shifts of residual protio solvent resonances (DCM-D_2, δ 5.32, chloroform-D_3, δ 7.26) to internal solvent peaks. The $^{31}P\{^{1}H\}$ NMR spectra were referenced to external H_3PO_4 and ^{19}F NMR to external $CFCl_3$. Delta software was used to interpret the results. A Bruker AVANCE 500 (frequencies operating at 202.5 MHz for ^{31}P, 470.7 MHz for ^{19}F and 130.3 MHz for ^{27}Al) spectrometer was used for selected samples, which were made up in Young's NMR tubes fitted with PTFE J Young's taps using CD_2Cl_2 that was previously dried over CaH_2 and degassed (with three freeze-pump-thaw cycles).

Single-crystal X-ray diffraction quality crystals were removed from the mother liquor under argon and run on either a Bruker Smart Apex diffractrometer, equipped with a 3-circle goniometer, 2 kW with a Mo-K_α X-ray source (λ = 0.71073 Å) and SMART CCD detector. Diffractrometer control, data collection and initial unit-cell determination was performed using SMART. Frame integration and unit-cell refinement was carried out using Saint+. Absorption corrections were applied by SADABS (v 2.03, Sheldrick). An Oxford Diffraction SuperNova, Single source at offset, Eos diffractometer was used for some

samples. Here Olex 2.20 was used to solve the structures with the XS21 structure solution program. Samples were run at low temperature (typically 110 K) using liquid nitrogen cooling. Mercury and Xseed software was used to interpret the results.

Electrospray ionisation mass spectrometry (ESI) analysis was performed on an Esquire 6000 instrument using Data Analysis software to interpret results. Unless otherwise stated below, samples were made up in dry MeCN (0.5 mg/mL). Other mass spectrometry measurements (LIFDI, EI, GS-MS) were performed on a Waters Micromass GCT Premier orthogonal time-of-flight instrument set to one scan per second with resolution power of 6000 fwhm and equipped with a LIFDI probe from LINDEN GmbH. MASLYNX software and the NIST library of known fragmentation patterns was used to identify compounds from GC-MS.

Elemental analysis was performed using an Exeter Analytical Inc. CE 440 analyser.

Photochemical reactions at room temperature were performed in Pyrex Schlenk tubes by using a Phillips 125 W medium-pressure mercury vapour lamp with a water filter (5 cm).

Quantum chemical calculations were performed with the TURBOMOLE V5.10 package using the resolution of identity (RI) approximation.[351-361] Initial optimisations were performed at the (RI-)BP86/SV(P) level, followed by frequency calculations at the same level In calculations involving Pd a 28 electron quasi-relativistic ECP replaced the core electron of Pd. No symmetry constraints were applied during optimisations.

6.2 SYNTHETIC METHODOLOGY FOR COMMON STARTING MATERIALS

6.2.1 Synthesis of Lithium Hexafluoroisopropoxide, $LiOCH(CF_3)_2$

To 30 mL of stirring diethyl ether, hexafluoroisopropanol (2 mL, 19 mmol, 1eq.) was added under an inert-nitrogen atmosphere. To this, 2.5 mol/dm n-butyl lithium in hexane (7.6 mL, 19 mmol, 1 eq.) was added dropwise. The reaction mixture was cooled in liquid nitrogen after addition of approximately 1 mL n-butyl lithium/hexane solution, to maintain a low temperature. The solvent and any butane by-product were removed *in vacuo* (10^{-2} mbar) to give a white solid product.

Yield: 3.14 g (95 %)

^{1}H NMR (295 K, 400 MHz, $CDCl_3$): δ_H = 4.27 (m, LiOC**H**$\{CF_3\}_2$) ppm.

^{19}F NMR (295 K, 376.2 MHz, $CDCl_3$): δ_F = -77.43 (d, $^{3}J_{FH}$ = 4 Hz, LiOCH$\{C\mathbf{F}_3\}_2$) ppm.

Elemental analysis: $LiOCH(CF_3)_2$; calculated C(20.69) H(0.58), observed C(21.48) H(1.10). The observed values are close to that calculated for $\{Et_2O\}_{0.06}Li\{OCH(CF_3)_2\}$; calculated C(21.79) H(0.90), suggesting a small amount of diethyl ether remained coordinated to the product after drying.

6.2.2 Synthesis of Lithium Perfluoro-*t*-butoxide, $LiOC(CF_3)_3$

To 30 mL of stirring diethyl ether, perfluorinated-*t*-butanol (2 mL, 13.8 mmol, 1 eq.) was added under an inert-nitrogen atmosphere. To this, 2.5 mol/dm n-butyl lithium in hexane (5.52 mL, 13.8 mmol, 1 eq.) was added dropwise. The reaction mixture was cooled in liquid nitrogen after addition of approximately 1 mL n-butyl lithium/hexane solution, to maintain a low temperature. The solvent and any butane by-product were removed *in vacuo* (10^{-2} mbar) to give a white solid.

Yield: 3.21 g (96 %)

^{19}F NMR (295 K, 376.2 MHz, $CDCl_3$): δ_F = -75.60 (s, LiOC$\{C\mathbf{F}_3\}_3$) ppm.

^{13}C NMR (295 K, 100.5 MHz, $CDCl_3$): δ_C = 83.0 (m, LiO**C**$\{CF_3\}_3$), 122.8 (q, $^{1}J_{CF}$, = 295 Hz, LiOC$\{\mathbf{C}F_3\}_3$) ppm.

Elemental analysis: $LiOC(CF_3)_3$; calculated C(19.83), H(0.00), observed C(19.57) H(0.16).

6.2.3 Synthesis of Sodium Hexafluoroisopropoxide, $NaOCH(CF_3)_2$

To 30 mL of stirring diethyl ether in a Schlenk tube, sodium hydride (0.48 g, 20 mmol, 1 eq.) was added and then the mixture was cooled in liquid nitrogen. To this, hexafluoroisopropanol (2 mL, 20 mmol, 1 eq.) was added and allowed to stir for an hour whilst warming to room temperature. The solvent was removed *in vacuo* (10^{-2} mbar) to give a white solid product.

Yield: 5.61 g (95 %)

^{1}H NMR (295 K, 400 MHz, $CDCl_3$): $\delta_H = 4.32$ (d, $^3J_{HF} = 6$ Hz, $NaOC\mathbf{H}\{CF_3\}_2$) ppm.

^{19}F NMR (295 K, 376.2 MHz, $CDCl_3$): $\delta_F = -79.67$ (d, $^3J_{FH} = 6$ Hz, $NaOCH\{C\mathbf{F}_3\}_2$) ppm.

Elemental analysis: $NaOCH(CF_3)_2$; calculated C(18.95) H(0.53), observed C(18.73) H(0.65) .

6.2.4 Synthesis of Sodium Perfluoro-*t*-butoxide, $NaOC(CF_3)_3$

To 30 mL of stirring diethyl ether in a Schlenk tube, sodium hydride (0.48 g, 20 mmol, 1 eq.) was added and then the mixture was cooled in liquid nitrogen. To this, perfluorinated-*t*-butanol (2.79 mL, 20 mmol, 1 eq.) was added and allowed to stir for an hour whilst warming to room temperature. The solvent was removed *in vacuo* (10^{-2} mbar) to give a white solid product.

Yield: 5.07 g (98 %)

^{19}F NMR (295 K, 376.2 MHz, $CDCl_3$): $\delta_F = -78.74$ (s, $NaOC\{C\mathbf{F}_3\}_3$) ppm.

Elemental analysis: $NaOC(CF_3)_3$; calculated C(18.61) H(0.00), observed C(18.08) H(0.17). The lower C % and higher H % may be due to the presence of a small amount of NaH if complete NaH conversion was not achieved.

6.3 SYNTHETIC METHODOLOGY FOR OTHER KNOWN MATERIALS

6.3.1 Synthesis of Dibenzylideneacetone Bis(triphenylphosphine)Palladium, [(dba)Pd(PPh_3)$_2$]

Tris(dibenzylideneacetone)palladium, $Pd_2(dba)_3$ (46 mg, 0.05 mmol, 1 eq.) and deuterated toluene, C_7D_8 (0.6 mL) were added to a PTFE J Young's tap NMR tube in an inert-atmosphere glovebox. Triphenylphosphine, PPh_3 (52 mg, 0.20 mmol, 4 eq.) was added to this and the mixture immediately analysed using NMR spectroscopy The product was treated as air- and light-sensitive and stored in an inert-atmosphere glove box.

$^{31}P\{^1H\}$ NMR (295 K, 161.8 MHz, C_7D_8): δ_P = -2.64 (s, **P**Ph_3), 24.8 (s, Pd(dba){**P**$Ph_3\}_2$), 27.0 (s, Pd(dba){**P**$Ph_3\}_{22}$) ppm.

^1H NMR (295 K, 400 MHz, C_7D_8): δ_H = 7.80-6.90 (m, P**Ph**$_3$ and dba) ppm. The coordinated alkene protons from the dba ligand are presumably fluxional and are not observed.

6.3.2 Synthesis of Tungsten Pentacarbonyl Tetrahydrofuran, $W(CO)_5${THF}

THF (30 mL) was added to a Schlenk tube containing tungsten hexacarbonyl, $W(CO)_6$ (1.056 g, 3 mmol, 1 eq.). The Schlenk tube was sealed under the vapour pressure of THF, to avoid over pressurising the Schlenk tube on the release of CO. This was then irradiated under a UV lamp (5 hrs.). Irradiation is complete after the insoluble $W(CO)_6$ is no longer observed. The Schlenk tube was then connected to the Schlenk line and opened to nitrogen, to allow for any small amounts of CO to release into the fume hood (a CO alarm is used as a precaution). The reaction mixture is an intense yellow colour solution.

IR (THF/hexane solution cell): $\nu_{(CO)}$[cm^{-1}]: 2014, 1930, 1892. A peak is also present at 1974 for the $W(CO)_6$ impurity.

6.3.3 Synthesis of Lithium tetra(perfluoro-*t*–butoxide) Aluminate, $LiAl\{OC(CF_3)_3\}_4$

Fresh $LiAlH_4$ in a 1 M solution in 100 mL diethyl ether was bought from Sigma Aldrich. This was dried at 80 °C in a water bath *in vacuo*. The solid was then well ground and dried *in vacuo* until no further changes in mass were observed (3 days) giving 3.1 g (82%) white solid $LiAlH_4$. In a 500 mL round bottom flask, the fresh $LiAlH_4$ (1.94 g, 50 mmol, 1 eq.) was

added. Perfluorinated-*t*-butanol (28.6 mL, 205 mmol, 4.1 eq.) and dry hexane (200 mL) *via* a canula transfer were added to the round bottom flask. This was put on reflux (70 °C, 24 hrs.) under a nitrogen atmosphere. A double condenser attached to a cooling system was used to cool the condenser to -20 °C. A 1:1 mix of water (6 L) and ethylene glycol (6 L) was used for the cooling system. The diethyl ether was then removed *in vacuo* to yield a solid white powder.

^{27}Al NMR (295 K, 130.3 MHz, D_2O):): δ_{Al} = 34.2, (s, Li**Al**$\{OC(CF_3)_3\}_4$), 10.0 (s, Li**Al**H$\{OC(CF_3)_3\}_3$) ppm.

^{19}F NMR (295 K, 376.2 MHz, D_2O): δ_F = -79.41 (s, possible LiAlH$\{OC(C\mathbf{F}_3)_3\}_3$), -80.46 (br, LiAl$\{OC(C\mathbf{F}_3)_3\}_4$) ppm.

6.4 SYNTHETIC METHODOLOGY FOR THE ISOLATED MATERIALS

6.4.1 Synthesis of Tris(hexafluoroisopropoxy)phosphite, P{OCH(CF$_3$)$_2$}$_3$, (**1**)

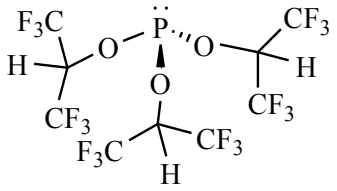

Sodium hexafluoroisopropoxide, NaOCH(CF$_3$)$_2$ (2.85 g, 15 mmol, 3.3 eq.) was added to a J Young's ampoule in an inert-atmosphere glovebox. DCM (30 mL) was added to this on a Schlenk line, followed by phosphorus trichloride, PCl_3 (0.61 g, 4.50 mmol, 1 eq.), added dropwise, followed by heating (40 °C, 24 hrs.). $^{31}P\{^1H\}$ NMR spectroscopy indicated full conversion to (**1**). The reaction mixture was then filtered through Celite under an inert-atmosphere to remove NaCl. This filtrate was washed with DCM (3 x 5 mL) and was analysed by NMR spectroscopy to check for purity and any hydrolysis products. The clear liquid product was isolated by removing the DCM *in vacuo* (10^{-2} mbar). Further purification from trace NaCl and hydrolysis impurities was achieved *via* a reduced pressure transfer (80 °C at 1.5 x10^{-1} mbar for 40 min.) of the liquid product to a dry J Young's ampoule. However, no satisfactory elemental analysis could be obtained due to the presence of impurities; possibly a combination of excess NaOCH(CF$_3$)$_2$ present due to sublimation of this material in the reduced pressure transfer and hydrolysis products, these may occur during the elemental analysis experimental procedure.

Yield: 360 mg (15 %)

^{1}H NMR (295 K, 400 MHz, CDCl$_3$): δ_H = 4.92 (m, P{OC**H**(CF$_3$)$_2$}$_3$) ppm.

A peak at 4.44 ppm (m, $^3J_{HF}$ = 6 Hz, NaOCH(CF$_3$)$_2$,) was also observed.

^{31}P{^{1}H} NMR (295 K, 161.8 MHz, CDCl$_3$): δ_P = 140.0 (m, $^4J_{PF}$ = 6 Hz, **P**{OCH(CF$_3$)$_2$}$_3$) ppm.

^{19}F NMR (295 K, 376.2 MHz, CDCl$_3$): δ_F = -74.32 (t, $^4J_{FP}$= 6 Hz, P{OCH(C**F**$_3$)$_2$}$_3$) ppm.

A peak at -79.34 ppm (d, $^3J_{FH}$ = 6 Hz, NaOCH(CF$_3$)$_2$,) was also observed.

^{13}C NMR (295 K, 100.5 MHz, CDCl$_3$): δ_C = 70.0 (sept of d, $^2J_{CF}$ = 35.32 Hz, P{O**C**H(CF$_3$)$_2$}$_3$), 120.2 (d of q, $^1J_{CF}$ = 285 Hz, $^2J_{CP}$ = 9 Hz, P{OCH(**C**F$_3$)$_2$}$_3$) ppm.

The NMR spectra of this material also showed the presence of a small amount of vacuum grease and DCM.

IR (in CH_2Cl_2 solution): $\nu_{(CF)}[cm^{-1}]$: 1080, 1088, 1207, 1223, 1231, 1297, 1374.

EI-MS (MeCN): m/z observed = 531.9521, $[M]^+$ (calculated 531.9532 m/z for $P\{OCH(CF_3)_2\}_3$, -2.1 ppm).

6.4.2 Synthesis of Tris(perfluoro-*t*-butyl)phosphite, P{OC(CF$_3$)$_3$}$_3$, (**2**)

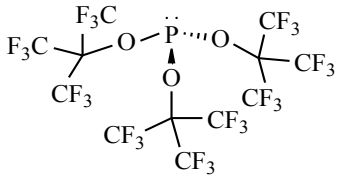

Sodium perfluoro-*t*-butoxide, NaOC(CF$_3$)$_3$ (3.87 g, 15 mmol, 3.3 eq.), was added to a J Young's ampoule in an inert-atmosphere glovebox. DCM (30 mL) was added to this on a Schlenk line, followed by phosphorus trichloride, PCl$_3$ (0.61 g, 4.5 mmol, 1 eq.), added dropwise. The mixture was ultrasonically activated for 24 hours. ^{31}P{^{1}H} NMR spectroscopy indicated full conversion to (**2**). The reaction mixture was then filtered through Celite under an inert-atmosphere to remove NaCl. This filtrate was washed with DCM (3 x 5 mL) and was analysed by NMR spectroscopy to check for purity and any hydrolysis products. The white solid product was isolated by removing the DCM *in vacuo* (10^{-2} mbar). Further purification from trace NaCl and hydrolysis impurities was achieved *via* sublimation (80 ˚C at 1.5 x10^{-1} mbar for 3 hrs.).

Yield: 1.32 g (40 %)

^{31}P{^{1}H } NMR (295 K, 161.8 MHz, CDCl$_3$): δ_P = 146.8 (m, $^4J_{PF}$ = 22 Hz, **P**{OC(CF$_3$)$_3$}$_3$) ppm.

Lower intensity signals were also observed at -9.6 (s), -4.6 (s, O=**P**{H}{OC(CF$_3$)$_3$}$_2$), 6.7 (s), 128.3 (m, J = 24 Hz), 136.6 (m, $^4J_{PF}$ = 25 Hz, {OC(CF$_3$)$_3$}$_2$**P**-μO-**P**{OC(CF$_3$)$_3$}$_2$.) ppm.

^{19}F NMR (295 K, 376.2 MHz, CDCl$_3$): δ_F = -72.12 (d, $^4J_{FP}$ = 22 Hz, P{OC(C**F**$_3$)$_3$}$_3$) ppm.

Lower intensity peaks were also observed at -75.82 (s, HOC(C**F**$_3$)$_3$), -72.69 (d, $^4J_{FP}$ = 24 Hz, {OC(C**F**$_3$)$_3$}$_2$P-μO-P{OC(C**F**$_3$)$_3$}$_2$) ppm.

^{13}C NMR (295 K, 100.5 MHz, CDCl$_3$): δ_C = 78.5 (m, P{O**C**(CF$_3$)$_3$}$_3$), 118.7 (q, $^1J_{CF}$ = 295 Hz, P{OC(**C**F$_3$)$_3$}$_3$) ppm.

A signal at 120.1(q, $^1J_{CF}$ = 291 Hz) ppm is also observed, this could be for either the HOC(**C**F$_3$)$_3$) or the {OC(**C**F$_3$)$_3$}$_2$P-μO-P{OC(**C**F$_3$)$_3$}$_2$).

The NMR spectra of this material also showed the presence of a small amount of vacuum grease, diethyl ether and [Et$_3$NH]$^+$[Cl]$^-$.

IR (ATR-ITR $\nu_{(CF)}$[cm^{-1}]: 727, 820, 852, 975, 975, 1109, 1189, 1247, 1305.

EI-MS (MeCN): m/z observed = mass 735.9171, $[M]^+$ (calculated 735.9154 m/z, for $P\{OC(CF_3)_3\}_3$, 2.3 ppm).

Elemental analysis: $P\{OC(CF_3)_3\}_3$: calculated C(19.57) , observed C(18.61). The sample may have partially hydrolysed to form pyrophosphite, $\{(CF_3)_3CO\}_2P\text{-}O\text{-}P\{OC(CF_3)_3\}_2$ impurities.

Single-Crystal X-ray Diffraction Measurements: Crystal size: 0.45 x 0.39 x 0.07 mm, $C_{12}F_{27}O_3P$, M = 736.09, monoclinic, a = 10.4392(4) Å, b = 18.0578(8) Å, c = 22.6156(15) Å, β = 89.527(6)°, V = 4263.1(4) Å^3, T = 110 K, space group C2/c (no. 15), Z = 8, μ(MoKα) = 0.382, Dc = 2.294 mg/mm^3, 11450 reflections measured, 3062 unique (R_{int} = 0.0412) which were used in all calculations. The final wR_2 was 0.4462 (all data) and R_1 was 0.1565 (>2sigma(I)).

6.4.3 Synthesis of Bis(hexafluoroisopropoxy)phenylphosphonite, $PPh\{OCH(CF_3)_2\}_2$, (**3**)

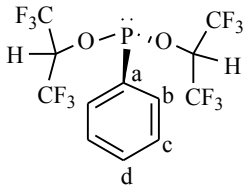

Sodium hexafluoroisopropoxide, $NaOCH(CF_3)_2$ (1.90 g, 10 mmol, 2 eq.), was added to a J Young's ampoule in an inert-atmosphere glovebox. DCM (10 mL) was added to this on a Schlenk line, followed by dichlorophenylphosphine, $PPhCl_2$ (0.90 g, 5 mmol, 1 eq.) added dropwise. The mixture was ultrasonically activated for 1 hour. $^{31}P\{^1H\}$ NMR spectroscopy indicated full conversion to (**3**). Following $^{31}P\{^1H\}$ NMR spectroscopic analysis, which indicated incomplete conversion, extra $NaOCH(CF_3)_2$ (200 mg, 1.05 mmol, 0.2 eq.), was added to the mixture. The stoichiometry was likely out due to coordinated diethyl ether in the sample of $NaOCH(CF_3)_2$ used (based on ^1H NMR spectroscopy). The reaction mixture was then filtered through Celite under an inert-atmosphere to remove NaCl. This filtrate was washed with DCM (3 x 5 mL) and was analysed by NMR spectroscopy to check for purity and any hydrolysis products. The clear liquid product could be isolated by removing the DCM *in vacuo* (10^{-2} mbar). Further purification from trace NaCl and hydrolysis impurities was achieved *via* a reduced pressure transfer (80 °C at 1.5 x10^{-1} mbar for 40 min.) of the liquid product to a dry J Young's ampoule. However, no satisfactory elemental analysis could be obtained due to the presence of impurities; possibly a combination of excess $NaOCH(CF_3)_2$ present due to sublimation of this material in the reduced pressure transfer and hydrolysis products, these may occur during the elemental analysis experimental procedure.

Yield: 1.7 g (77 %)

^{1}H NMR (295 K, 400 MHz, $CDCl_3$): δ_H = 4.69 (m, 2H, $^3J_{HF}$ = 5 Hz, $PPh\{OC\mathbf{H}(CF_3)_2\}_2$), 7.39 – 7.98 (m, 5H, $P\mathbf{Ph}\{OCH(CF_3)_2\}_2$) ppm.

A peak at 4.40 (br, $NaOCH(C\mathbf{F}_3)_2$) ppm was also observed.

$^{31}P\{^1H\}$ NMR (295 K, 161.8 MHz, $CDCl_3$): δ_P = 190.3 (m, $\mathbf{P}Ph\{OCH(CF_3)_2\}_2$) ppm.

^{19}F NMR (295 K, 376.2 MHz, $CDCl_3$): δ_F = -74.48 (br, 6F, $PPh\{OCH(C\mathbf{F}_3)_2\}_2$), -74.35 (br, 6F, $PPh\{OCH(C\mathbf{F}_3)_2\}_2$) ppm. Note two environments observed for each CF_3 group in the ^{19}F

NMR, possibly due to atropisomers forming due to hindered rotation around either the P-O or O-C bond.

A peak at -79.87 (br, NaOCH($C\mathbf{F}_3$)$_2$) ppm was also observed.

^{13}C NMR (295 K, 100.5 MHz, $CDCl_3$): δ_C = 74.1 (sept of d, $^2J_{CF}$ = 33 Hz, $^2J_{CP}$ = 15 Hz, PPh{O**C**H(CF_3)$_2$}$_2$), 120.9 (d of q, $^1J_{CF}$ = 284 Hz, $^2J_{CP}$ = 8.48 Hz, PPh{OCH(**C**F_3)$_2$}$_2$), 129.1 (d, $^3J_{CP}$ = 7.7 Hz, phenyl-c), 129.9 (d, $^1J_{CP}$ = 24.9 Hz, phenyl-a), 132.7 (s, phenyl-d), 136.1 (d, $^2J_{CP}$ = 13.8 Hz, phenyl-e) ppm.

EI-MS (MeCN): m/z observed = 441.9989, $[M]^+$ (calculated 441.9992 m/z for PhP{OCH(CF_3)$_2$}$_2$, -0.7 ppm).

6.4.4 Synthesis of Bis(perfluoro-*t*-butoxy)phenylphosphonite, $PPh\{OC(CF_3)_3\}_2$, (**4**)

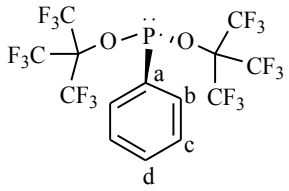

Sodium perfluoro-*t*-butoxide, $NaOC(CF_3)_3$ (2.58 g, 10 mmol, 2 eq.), was added to a J Young's ampoule in an inert-atmosphere glovebox. DCM (10 mL) was added to this on a Schlenk line, followed by dichlorophenylphosphine, $PPhCl_2$ (0.90 g, 5 mmol, 1 eq.) added dropwise. The mixture was ultrasonically activated for 1 hour. Following $^{31}P\{^1H\}$ NMR spectroscopic analysis, which indicated incomplete conversion, extra $NaOC(CF_3)_3$ (200 mg, 0.8 mmol, 0.08 eq.), was added to the mixture. The stoichiometry was likely out due to coordinated diethyl ether in the sample of $NaOC(CF_3)_3$ used (based on ^1H NMR spectroscopy). The reaction mixture was then filtered through Celite under an inert-atmosphere to remove NaCl. This filtrate was washed with DCM (3 x 5 mL) and was analysed by NMR spectroscopy to check for purity and any hydrolysis products. The clear liquid product could be isolated by removing the DCM *in vacuo* (10^{-2} mbar). Further purification from trace NaCl and hydrolysis impurities was achieved *via* a reduced pressure transfer (80 °C at 1.5 x10^{-1} mbar for 40 min.) of the liquid product to a dry J Young's ampoule.

Yield: 2.74 g (78 %)

^{1}H NMR (295 K, 400 MHz, CD_2Cl_2): δ_H = 7.30 – 8.05 (m, P**Ph**$\{OC(CF_3)_3\}_2$) ppm.

$^{31}P\{^1H\}$ NMR (295 K, 161.8 MHz, CD_2Cl_2): δ_P = 190.5 (m, $^4J_{PF}$ = 22 Hz, **P**$Ph\{OC(CF_3)_3\}_2$) ppm.

^{19}F NMR (295 K, 376.2 MHz, CD_2Cl_2): δ_F = -71.51 (d, $^4J_{FP}$ = 22 Hz, $PPh\{OC(CF_3)_3\}_2$) ppm.

A lower intensity peak at -78.38 (br, $NaOC\{CF_3\}_3$) ppm was also observed.

^{13}C NMR (295 K, 100.5 MHz, CD_2Cl_2): δ_C = 79.7 (m, $PPh\{OC(CF_3)_3\}_2$), 119.7 (q, $^1J_{CF}$ = 294 Hz, $PPh\{OC(CF_3)_3\}_2$), 128.8 (d, $^3J_{CP}$ = 9 Hz, phenyl-c), 129.3 (d, $^1J_{CP}$ = 33 Hz, phenyl-a), 133.4 (s, phenyl-d), 139.2 (d, $^2J_{CP}$ = 21 Hz, phenyl-b) ppm.

The NMR spectra of this material also showed the presence of a small amount of vacuum grease.

EI-MS (MeCN): m/z observed = 577.9740 $[M]^+$ (calculated 577.9740 m/z for $PhP\{OC(CF_3)_3\}_2$, 0.0 ppm).

Elemental analysis: $PhP\{OC(CF_3)_3\}_2$ calculated C(28.96) H(0.86), observed C(29.07) H(0.87)

6.4.5 Synthesis of Hexafluoroisopropoxydiphenylphosphinite, $PPh_2\{OCH(CF_3)_2\}$, (**5**)

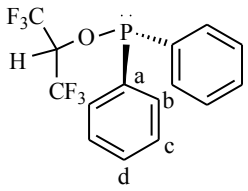

Sodium hexafluoroisopropoxide, $NaOCH(CF_3)_2$ (950 g, 5 mmol, 1 eq.), was added to a J Young's ampoule in an inert-atmosphere glovebox. DCM (10 mL) was added to this on a Schlenk line, followed by chlorodiphenylphosphine, PPh_2Cl (1.1 g, 5 mmol, 1 eq.) added dropwise. The mixture was ultrasonically activated for 1 hour. $^{31}P\{^1H\}$ NMR spectroscopy indicated full conversion (**5**). The reaction mixture was then filtered through Celite under an inert-atmosphere to remove NaCl. This filtrate was washed with DCM (3 x 5 mL) and was analysed by NMR spectroscopy to check for purity and any hydrolysis products. The clear liquid product could be isolated by removing the DCM *in vacuo* (10^{-2} mbar). Further purification from trace NaCl and hydrolysis impurities was achieved *via* a reduced pressure transfer (80 ˚C at 1.5 x10^{-1} mbar for 40 min.) of the liquid product to a dry J Young's ampoule. However, no satisfactory elemental analysis could be obtained due to the presence of impurities; possibly a combination of excess $NaOCH(CF_3)_2$ present due to sublimation of this material in the reduced pressure transfer and hydrolysis products, these may occur during the elemental analysis experimental procedure.

Yield: 1.61 g (84 %)

^{1}H NMR (295 K, 400 MHz, $CDCl_3$): δ_H = 4.75 (m, 1H, $^3J_{HF}$ = 5 Hz, $^3J_{HP}$ = 2 Hz, $PPh_2\{OC\mathbf{H}(CF_3)_2\}$), 7.23 -7.93 (m, 10H, $P\mathbf{Ph_2}\{OCH(CF_3)_2\}$) ppm.

$^{31}P\{^1H\}$ NMR (295 K, 161.8 MHz, $CDCl_3$): δ_P = 142.6 (m, $^4J_{PF}$ = 7 Hz, $\mathbf{P}Ph_2\{OCH(CF_3)_2\}$) ppm.

A lower intensity peak was also observed at 40.8 (s) ppm.

^{19}F NMR (295 K, 376.2 MHz, $CDCl_3$): δ_F = -78.50 (d, 6F, $^4J_{FP}$ = 21 Hz, $PPh_2\{OCH(C\mathbf{F}_3)_2\}$) ppm.

A peak at -78.05 (s) and -80.22 (d, $NaOCH(CF_3)_2$) ppm was also observed.

^{13}C NMR (295 K, 100.5 MHz, $CDCl_3$): δ_C = 76.7 (sept of d, $^2J_{CF}$ = 34 Hz, $^2J_{CP}$ = 25 Hz, $PPh_2\{O\mathbf{C}H(CF_3)_2\}$), 121.4 (q, $^1J_{CF}$ = 284 Hz, $PPh_2\{OCH(\mathbf{C}F_3)_2\}$), 128.5 (d, $^3J_{CP}$ = 8 Hz,

phenyl-c), 130.3 (s, phenyl-d), 130.7 (d, $^{1}J_{CP}$ = 23 Hz, phenyl-a), 139.5 (d, $^{2}J_{CP}$ =15 Hz, phenyl-b) ppm.

Lower intensity peaks were observed at 133.2 (d, J= 3 Hz) and 131.5 (d, J= 11 Hz) ppm.

EI-MS (MeCN): m/z observed = 352.0449, $[M]^{+}$ (calculated 352.0452 m/z for $Ph_2P\{OCH(CF_3)_2\}$,-0.9 ppm).

6.4.6 Synthesis of Perfluoro-*t*-butoxydiphenylphosphinite, $PPh_2\{OC(CF_3)_3\}$, (**6**)

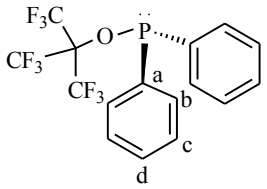

Sodium perfluoro-*t*-butoxide, $NaOC(CF_3)_3$ (1.29 g, 5 mmol, 1 eq.), was added to a J Young's ampoule in an inert-atmosphere glovebox. DCM (10 mL) was added to this on a Schlenk line, followed by chlorodiphenylphosphine, PPh_2Cl (1.1 g, 5 mmol, 1 eq.) added dropwise. The mixture was ultrasonically activated for 1 hour. $^{31}P\{^1H\}$ NMR spectroscopy indicated full conversion to (**6**). Following $^{31}P\{^1H\}$ NMR spectroscopic analysis, which indicated incomplete conversion, extra $NaOC(CF_3)_3$ (100 mg, 0.4 mmol, 0.08 eq.), was added to the mixture. The stoichiometry was likely out due to coordinated diethyl ether in the sample of $NaOC(CF_3)_3$ used (based on ^1H NMR spectroscopy). The reaction mixture was then filtered through Celite under an inert-atmosphere to remove NaCl. This filtrate was washed with DCM (3 x 5 mL) and was analysed by NMR spectroscopy to check the purity and any hydrolysis of the products. The clear liquid product could be isolated by removing the DCM *in vacuo* (10^{-2} mbar). Further purification from trace NaCl and hydrolysis impurities was achieved *via* a reduced pressure transfer (80 ˚C at 1.5 $x10^{-1}$ mbar for 1 hr.) of the liquid product to dry J Young's ampoule. However, no satisfactory elemental analysis could be obtained due to the presence of impurities; possibly a combination of excess $NaOC(CF_3)_3$ present due to sublimation of this material in the reduced pressure transfer and hydrolysis products, these may occur during the elemental analysis experimental procedure.

Yield: 1.69 g (80 %)

^{1}H NMR (295 K, 400 MHz, $CDCl_3$): δ_H = 7.21-7.84 (m, $P\mathbf{Ph_2}\{OC(CF_3)_3\}$) ppm.

$^{31}P\{^1H\}$ NMR (295 K, 161.8 MHz, $CDCl_3$): δ_P = 132.3 ppm (m, $^4J_{PF}$ = 22 Hz, $\mathbf{P}Ph_2\{OC(CF_3)_3\}$) ppm.

^{19}F NMR (295 K, 376.2 MHz, $CDCl_3$): δ_F = -71.60 (d, $^4J_{FP}$ = 22 Hz, $PPh_2\{OC(C\mathbf{F}_3)_3\}$) ppm.

A lower intensity peak at -78.74 ppm ($NaOC\{CF_3\}_3$) was also observed.

^{13}C NMR (295 K, 100.5 MHz, $CDCl_3$): δ_C = 80.0 (dec of d, $^2J_{CF}$ = 31 Hz, $^2J_{CP}$ = 6 Hz), 120.4 (q, $^1J_{CF}$ = 292 Hz, $PPh_2\{OC(\mathbf{C}F_3)_2\}$), 128.7 (d, $^3J_{CP}$ = 8 Hz, phenyl-c), 130.2 (s,

phenyl-d), 130.3 (d, $^{1}J_{CP}$ = 24 Hz, phenyl-a), 133.3 (s, phenyl-d), 139.6 (d, $^{2}J_{CP}$ = 18 Hz, phenyl-b) ppm.

EI-MS (MeCN): m/z observed = 420.0328, $[M]^{+}$ (calculated 420.0326 m/z for $Ph_2P\{OC(CF_3)_3$, 0.5 ppm).

6.4.7 Perfluorinated-*t*-butoxypyrophosphite, {OC(CF$_3$)$_3$}$_2$P-μO-P{OC(CF$_3$)$_3$}$_2$, (**7**)

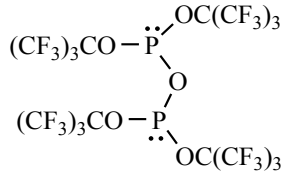

Partial hydrolysis of (**2**) formed crystals of (**7**). A synthetic procedure for this potential bidentate ligand has not been investigated for the purpose of this thesis.

^{31}P{^{1}H} NMR (295 K, 161.8 MHz, CDCl$_3$): δ_P = 135.0 ppm (m, {OC(CF$_3$)$_3$}$_2$**P**-μO-**P**{OC(CF$_3$)$_3$}$_2$) ppm.

Single-Crystal X-ray Diffraction Measurements: $C_{16}F_{36}O_5P_2$, M = 1018.10, orthorhombic, crystal size/mm = 0.23 × 0.13 × 0.09, a = 10.207(3) Å, b = 21.988(5) Å, c = 27.080(7) Å, U = 6078(3) Å^3, T = 110(2) K, space group Pbca (no. 61), Z = 8, μ(MoKα) = 0.398, ρ_{calc} mg/mm^3 = 2.225, 60023 reflections measured, 7536 unique (R_{int} = 0.0443) which were used in all calculations. The final $wR(F_2)$ was 0.3813 (all data).

6.4.8 Synthesis of Tungsten pentacarbonyl tris(hexafluoroisopropoxy)phosphite, $[W(CO)_5P\{OCH(CF_3)_2\}_3]$, **[W(1)]**

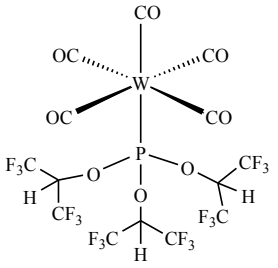

A solution of $W(CO)_5THF$ (prepared according to experimental section 6.3.2) was added to tris(hexafluoroisopropoxy)phosphite (532 mg, 1 mmol, 1 eq.) in a J Young's ampoule and the mixture was stirred at room temperature for 1 hr. $^{31}P\{^1H\}$ NMR spectroscopy was used to assess reaction completion. The solvent was removed *in vacuo* (10^{-2} mbar) and the resulting solid was redissolved in THF to precipitate any $W(CO)_6$. This insoluble $W(CO)_6$ was removed by filtration through Celite under an inert-atmosphere. The filtrate was washed with THF (3 x 5 mL). The solvent was again removed *in vacuo* (10^{-2} mbar) and any remaining $W(CO)_6$ removed by sublimation on to a sublimation finger cooled to 77 K under vacuum (1.5 x 10^{-1} mbar at 70 °C). The sublimation was repeated twice for 5 hours each time. The product was dark brown/black in colour, and was stored in an inert-atmosphere glove box at -16 °C.

^{1}H NMR (295 K, 400 MHz, $CDCl_3$): δ_H = 5.4 (br, $W(CO)_5\{P(OCH\{CF_3\}_2)_3\}$) ppm.

$^{31}P\{^1H\}$ NMR (295 K, 161.8 MHz, $CDCl_3$): δ_P = 147.1 (s, $^1J_{PW}$ = 452 Hz, $W(CO)_5\{P(OCH\{CF_3\}_2)_3\}$) ppm.

A peak at 142.4 (s) ppm was also observed.

^{19}F NMR (295 K, 376.2 MHz, $CDCl_3$): δ_F = -73.95, (br,$W(CO)_5\{P(OCH\{CF_3\}_2)_3\}$) ppm.

A peak at -76.71 (m) ppm was also observed; this is likely to be $NaOCH\{CF_3\}_2$.

The NMR spectra of this material also showed the presence of vacuum grease and THF.

IR (hexane solution): $\nu_{(CO)}$[cm^{-1}]: 1975, 2002, 2017, 2097.

EI-MS (C_4H_8O): m/z observed = 855.9062, $[M]^+$ (calculated 855.8788 m/z for $^{184}W(CO)_5\{P(OCH\{CF_3\}_2)_3\}$, 32 ppm).

6.4.9 Synthesis of Tungsten pentacarbonyl tris(perfluoro-*t*-butyl)phosphite, $[W(CO)_5P\{OC(CF_3)_3\}_3]$, **[W(2)]**

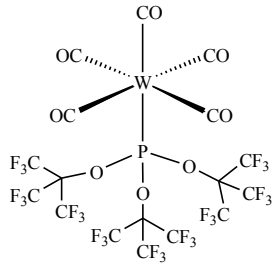

A solution of $W(CO)_5THF$ (prepared according to experimental section 6.3.2) was added to tris(perfluoro-*t*-butyl)phosphite, (736 mg, 1 mmol, 1 eq.) in 5 mL DCM and 5 mL fluorobenzene (to increase the solubility of the ligand) in a J Young's ampoule. The reaction mixture was stirred at room temperature for 1 hr. $^{31}P\{^1H\}$ NMR spectroscopy was used to assess reaction completion. The solvent was removed *in vacuo* (10^{-2} mbar) and the resulting solid was redissolved in THF to precipitate any $W(CO)_6$. This insoluble $W(CO)_6$ was removed by filtration through Celite under inert-atmosphere. The filtrate was washed with THF (3 x 5 mL). The solvent was again removed *in vacuo* (10^{-2} mbar) and any remaining $W(CO)_6$ removed by sublimation on to a sublimation finger cooled to 77 K under vacuum (1.5 x 10^{-1} mbar at 70 °C). The sublimation was repeated twice for 5 hours each time. The product was dark brown/black in colour, and was stored in an inert-atmosphere glove box at -16 °C.

$^{31}P\{^1H\}$ NMR (295 K, 161.8 MHz, $CDCl_3$): δ_P = 149.9 (s, $^1J_{PW}$ = 292 Hz, $W(CO)_5\{\mathbf{P}(OC\{CF_3\}_3)_3\}$) ppm.

Peaks at -15.2 (s), 3.9 (s), 19.2 (s), 38.2 (s), 104.5 (s) ppm were also observed.

^{19}F NMR (295 K, 376.2 MHz, $CDCl_3$): δ_F = -75.37 (s, $W(CO)_5\{P(OC\{C\mathbf{F_3}\}_3)_3\}$) ppm.

Peaks at -76.86 (d, J = 7 Hz), -73.50 (d, J = 6 Hz), -74.64 (d, J = 6 Hz) ppm were also observed.

The NMR spectra of this material also showed the presence of free $P\{OC(CF_3)_3\}_3$ ligand, vacuum grease and solvents; THF, DCM, fluorobenzene.

6.4.10 Synthesis of Tungsten pentacarbonyl (bis{hexafluoroisopropoxy} phenylphosphonite), $[W(CO)_5\{PhP(OCH\{CF_3\}_2)_2\}]$, **[W(3)]**

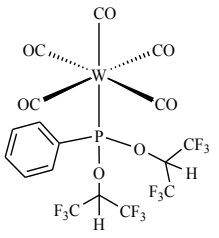

A solution of $W(CO)_5THF$ (prepared according to experimental section 6.3.2) was added to bis(hexafluoroisopropoxy)phenylphosphonite (580 mg, 1 mmol, 1 eq.) in a J Young's ampoule and the mixture was stirred at room temperature for 1 hr. $^{31}P\{^1H\}$ NMR spectroscopy was used to assess reaction completion. The solvent was removed *in vacuo* (10^{-2} mbar) and the resulting solid was redissolved in THF to precipitate any $W(CO)_6$. This insoluble $W(CO)_6$ was removed by filtration through Celite under inert-atmosphere. The filtrate was washed with THF (3 x 5 mL). The solvent was again removed *in vacuo* (10^{-2} mbar) and the any remaining $W(CO)_6$ removed by sublimation on to a sublimation finger cooled to 77 K under vacuum (1.5 x 10^{-1} mbar at 70 °C). The sublimation was repeated twice for 5 hours each time. The product was dark brown/black in colour in colour, and was stored in an inert-atmosphere glove box at -16 °C.

^{1}H NMR (295 K, 400 MHz, $CDCl_3$): δ_H = 4.60 (m, $W(CO)_5\{PhP(OC\mathbf{H}\{CF_3\}_2)_2\}\}$,), 7.20 (m, $W(CO)_5\{\mathbf{Ph}P(OCH\{CF_3\}_2)_2\}$) ppm.

$^{31}P\{^1H\}$ NMR (295 K, 161.8 MHz, $CDCl_3$): δ_P = 182.6 (s, $W(CO)_5\{Ph\mathbf{P}(OCH\{CF_3\}_2)_2\}$, $^1J_{PW}$ 357 Hz) ppm.

^{19}F NMR (295 K, 376.2 MHz, $CDCl_3$): δ_F = -74.07 (br, $W(CO)_5\{PhP(OCH\{C\mathbf{F_3}\}_2)_2\}$) ppm.

The NMR spectra of this material also showed the presence of a small amount of vacuum grease and THF.

IR (hexane solution): $\nu_{(CO)}[cm^{-1}]$: 1962, 1970, 2002, 2088.

EI-MS (C_4H_8O): m/z observed = 598.9344, $[M]^+$ (calculated 598.9316 m/z for $^{184}W(CO)_5\{PhP(OCH\{CF_3\}_2)_2\}$, 4.7 ppm).

6.4.11 Synthesis of Tungsten pentacarbonyl (bis{perfluoro-*t*-butoxy}phenylphosphonite), [W(CO)$_5${PhP(OC{CF$_3$}$_3$)$_2$}], **[W(4)]**

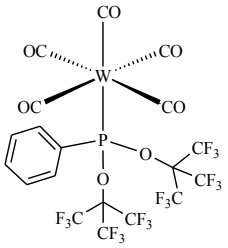

A solution of W(CO)$_5$THF (prepared according to experimental section 6.3.2) was added to bis(perfluoro-*t*-butoxy)phenylphosphonite (435 mg, 1 mmol, 1 eq.) in a J Young's ampoule and the mixture was stirred at room temperature for 1 hr. ^{31}P{^{1}H} NMR spectroscopy was used to assess reaction completion. The solvent was removed *in vacuo* (10^{-2} mbar) and the resulting solid was redissolved in THF to precipitate out any W(CO)$_6$. This insoluble W(CO)$_6$ was removed by filtration through Celite under inert-atmosphere. The filtrate was washed with 3 x 5 mL THF. The solvent was again removed *in vacuo* (10^{-2} mbar) and the any remaining W(CO)$_6$ was removed by sublimation on to a sublimation finger cooled to 77 K under vacuum (1.5 x 10^{-1} mbar at 70 °C). The sublimation was repeated twice for 5 hours each time, in order to remove all W(CO)$_6$ from the product. The product was dark brown in colour, and was stored in an inert-atmosphere glove box at -16 °C.

^{1}H NMR (295 K, 400 MHz, CDCl$_3$): δ_H = 7.17-7.96 (m, W(CO)$_5${**Ph**P(OC{CF$_3$}$_3$)$_2$}) ppm.

^{31}P{^{1}H} NMR (295 K, 161.8 MHz, CDCl$_3$): δ_P = 174.2 (s, $^1J_{PW}$ 374 Hz, W(CO)$_5${Ph**P**(OC{CF$_3$}$_3$)$_2$}) ppm.

^{19}F NMR (295 K, 376.2 MHz, CDCl$_3$): δ_F = -70.33 (br, W(CO)$_5${PhP(OC{C**F$_3$**}$_3$)$_2$}) ppm.

A peak at -75.31 (br) ppm was also observed, likely to be NaOC{CF$_3$}$_3$.

The NMR spectra of this material also showed the presence of free PhP(OC{CF$_3$}$_3$)$_2$ ligand, vacuum grease and THF.

EI-MS (C$_4$H$_8$O): m/z observed = 901.8964, [M]$^+$ (calculated 901.8995 m/z for ^{184}W(CO)$_5${PhP(OC{CF$_3$}$_3$)$_2$}, -3.4 ppm).

6.4.12 Synthesis of Tungsten pentacarbonyl (hexafluoroisopropoxydiphenyl-phosphinite), $[W(CO)_5\{Ph_2POCH(CF_3)_2\}]$, **[W(5)]**

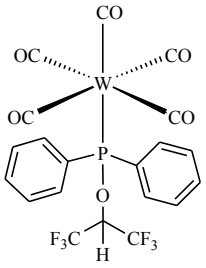

A solution of $W(CO)_5THF$ (prepared according to experimental section 6.3.2 was added to (hexafluoroisopropoxydiphenyl)phosphinite (352 mg, 1 mmol, 1 eq.) in a J Young's ampoule and the mixture was stirred at room temperature for 1 hr. $^{31}P\{^1H\}$ NMR spectroscopy was used to assess reaction completion. The solvent was removed *in vacuo* (10^{-2} mbar) and the resulting solid was redissolved in THF to precipitate any $W(CO)_6$. This insoluble $W(CO)_6$ was removed by filtration through Celite under inert-atmosphere. The filtrate was washed with THF (3 x 5 mL). The solvent was again removed *in vacuo* (10^{-2} mbar) and the any remaining $W(CO)_6$ was removed by sublimation onto a sublimation finger cooled to 77 K under vacuum (1.5 x 10^{-1} mbar at 70 °C). The sublimation was repeated twice for 5 hours each time. The product was dark brown in colour, and was stored in an inert-atmosphere glove box at -16 °C.

^{1}H NMR (295 K, 400 MHz, $CDCl_3$): δ_H = 4.69 (m, $W(CO)_5\{Ph_2P(OC\mathbf{H}\{CF_3\}_2)\}$), 7.26 - 7.71 (m, $W(CO)_5\{\mathbf{Ph}_2P(OCH\{CF_3\}_2)\}$) ppm.

$^{31}P\{^1H\}$ NMR (295 K, 161.8 MHz, $CDCl_3$): δ_P = 150.1 (s, $^1J_{PW}$ 291 Hz, $W(CO)_5\{Ph_2\mathbf{P}(OCH\{CF_3\}_2)\}$) ppm.

Lower intensity peaks at 106.7 (s), 105.0 (s), 99.6 (s) ppm were also observed

^{19}F NMR (295 K, 376.2 MHz, $CDCl_3$): δ_F = -73.05 (d, $^4J_{FP}$ = 6 Hz, $W(CO)_5\{PhP(OCH\{C\mathbf{F_3}\}_2)_2\}$) ppm.

A lower intensity peak was also observed at -72.90 (d, $^4J_{FP}$ = 6 Hz) ppm.

The NMR spectra of this material also showed the presence of vacuum grease and THF.

IR (hexane solution): $\nu_{(CO)}$[cm^{-1}]: 1953, 1968, 1992, 2080.

EI-MS (C_4H_8O): m/z observed = 675.9678, $[M]^+$ (calculated 675.9707 m/z for $^{184}W(CO)_5\{Ph_2P(OCH\{CF_3\}_2)\}$, -4.3 ppm).

6.4.13 Synthesis of Tungsten pentacarbonyl (perfluoro-*t*-butoxydiphenylphosphinite), $[W(CO)_5PPh_2\{OC(CF_3)_3\}]$, **[W(6)]**

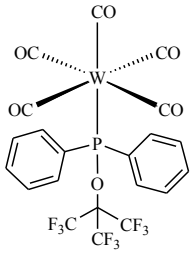

A solution of $W(CO)_5THF$ (prepared according to experimental section 6.3.2) was added to (perfluoro-*t*-butoxy)diphenylphosphinite (420 mg, 1 mmol, 1 eq.) in a J Young's ampoule and the mixture was stirred at room temperature for 1 hr. $^{31}P\{^1H\}$ NMR spectroscopy was used to assess reaction completion. The solvent was removed *in vacuo* (10^{-2} mbar) and the resulting solid was redissolved in THF to precipitate any $W(CO)_6$. This insoluble $W(CO)_6$ was removed by filtration through Celite under inert-atmosphere. The filtrate was washed with THF (3 x 5 mL). The solvent was again removed *in vacuo* (10^{-2} mbar) and the any remaining $W(CO)_6$ was removed by sublimation on to a sublimation finger cooled to 77 K under vacuum (1.5 x 10^{-1} mbar at 70 °C). The sublimation was repeated twice for 5 hours each time. The product was dark brown in colour, and was stored in an inert-atmosphere glove box at -16 °C.

^{1}H NMR (295 K, 400 MHz, $CDCl_3$): δ_H = 7.6-7.2 (m, $W(CO)_5\{\mathbf{Ph}_2P(OC\{CF_3\}_3)\}$) ppm.

$^{31}P\{^1H\}$ NMR (295 K, 161.8 MHz, $CDCl_3$): δ_P = 149.2 (s, $^1J_{PW}$ = 304 Hz, $W(CO)_5\{Ph_2\mathbf{P}(OC\{CF_3\}_3)\}$) ppm.

Peaks were also observed at 15.9 (d, J = 98 Hz), 36.8 (d, J = 91 Hz), 102.9 (s, $^1J_{PW}$ = 278 Hz), 107.3 (s, $^1J_{PW}$ = 214 Hz) ppm.

^{19}F NMR (295 K, 376.2 MHz, $CDCl_3$): δ_F = -69.79 (d, $^4J_{FP}$ = 3 Hz, $W(CO)_5\{Ph_2P(OC\{C\mathbf{F}_3\}_3)\}$) ppm.

Lower intensity peaks were also observed at -74.18 (s), -70.78 (s), -70.30 (m) ppm.

The NMR spectra of this material also showed the presence of vacuum grease and THF.

IR (hexane solution): $\nu_{(CO)}$[cm^{-1}]: 1954, 1964, 1996, 2081.

EI-MS (C_4H_8O): m/z observed = 6743.9594, $[M]^+$ (calculated 6743.9581 m/z for $^{184}W(CO)_5\{Ph_2P(OC\{CF_3\}_3)\}$, 1.7 ppm).

6.4.14 Synthesis of $(\eta^5\text{-}C_5H_5)Ru(P\{OCH(CF_3)_2\}_3)(NCCH_3)_2]^+[PF_6]^-$, **[Ru(1)]**

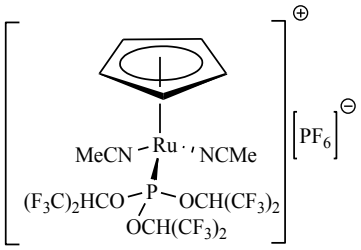

Tris(acetonitrile)(η^5-cyclopentadienyl)ruthenium(II) hexafluorophosphate, $[(\eta^5\text{-}C_5H_5)Ru(NCMe)_3][PF_6]^-$ (25 mg, 0.058 mmol, 1 eq.), deuterated CD_2Cl_2 (0.1 mL) and DCM (0.4 mL) were added to a PTFE J Young's tap NMR tube in an inert-atmosphere glovebox. Tris(hexafluoroisopropoxy)phosphite (27 mg, 0.051 mmol, 1 eq.) was added to this and the reaction was then monitored by $^{31}P\{^1H\}$ NMR spectroscopy. The reaction mixture was then layered with hexane and left to crystallise. The mother liquor was removed (any free ligand is removed this way) *via* a canula transfer and the remaining crystalline material was washed with hexane, followed by another canula transfer to remove any solvent. The crystalline product in the NMR tube was then dried *in vacuo* (at 1.5 x 10^{-2} mbar, for 30 min. at room temperature) on the Schlenk line. The yellow/brown crystalline product was treated as air-sensitive and stored in an inert-atmosphere glove box.

^{1}H NMR (295 K, 400 MHz, $CDCl_3$): δ_H = 2.40 (br, $[(\eta^5\text{-}C_5H_5)Ru(P\{OCH(CF_3)_2\}_3)(NCC\mathbf{H_3})_2]^+$), 4.24 (br, $[(\eta^5\text{-}C_5\mathbf{H_5})Ru(P\{OCH(CF_3)_2\}_3)(NCCH_3)_2]^+$), 4.83 (m, $[(\eta^5\text{-}C_5H_5)Ru(P\{OC\mathbf{H}(CF_3)_3)(NCCH_3)_2]^+$) ppm. Satisfactorily integration values could not be obtained.

A low intensity peak at 2.36 (s) ppm was also observed for the $[(\eta^5\text{-}C_5\mathbf{H_5})Ru(NCCH_3)_3]^+$ starting material, the Cp environment is likely to be under the broad peaks observed at 4.24 ppm.

$^{31}P\{^1H\}$ NMR (295 K, 161.8 MHz, $CDCl_3$):): δ_P= -143.0 (sept, $^1J_{PF}$ = 711.0 Hz, $[\mathbf{P}F_6]^-$), 162.1 (s, $[(\eta^5\text{-}C_5H_5)Ru(\mathbf{P}\{OCH(CF_3)_2\}_3)(NCCH_3)_2]^+$) ppm.

^{19}F NMR (295 K, 376.2 MHz, CD_2Cl_2): δ_F = -72.96 (d, $^1J_{PF}$ = 711.0 Hz, $[P\mathbf{F_6}]^-$), -73.81 (m, $[(\eta^5\text{-}C_5H_5)Ru(P\{OCH(C\mathbf{F}_3)_2\}_3)(NCCH_3)_2]^+$, -74.03 (m, $[(\eta^5\text{-}C_5H_5)Ru(P\{OCH(C\mathbf{F}_3)_2\}_3)_2(NCCH_3)_2]^+$) ppm. Two environments were observed for each CF_3 group in the ^{19}F NMR, possibly indicating atropisomerism due to hindered rotation around either the P-O or O-C bond.

Peaks at-73.50 (d, J = 5 Hz, P{OCH(C**F**$_3$)$_2$}$_3$), -74.41(d, J = 5 Hz) and -75.97(d, J = 6 Hz) ppm were also observed.

The NMR spectra of this material also showed the presence of a small amount of vacuum grease, DCM and MeCN.

EI-MS (MeCN): m/z observed 1091.9679, $[M]^+$ (calculated 1091.9745 m/z for $[(\eta^5\text{-}C_5H_5)\,^{102}Ru(P\{OCH(CF_3)_2\}_3)(NCCH_3)_2]^+$, -6.1 ppm). Observed 144.9647 m/z, $[M]^-$ (calculated 144.9649 m/z for $[PF_6]^-$, -1.0 ppm).

Single-Crystal X-ray Diffraction Measurements: $C_{18}H_{14}F_{24}N_2O_3P_2Ru$, M = 925.32, triclinic, crystal size/mm = 0.15 × 0.10 × 0.04, a = 10.4552(4) Å, b = 10.4722(4) Å, c = 27.5932(13) Å, α = 89.016(4)°, β = 89.614(4)°, γ = 87.978(3)°, V = 3018.8(2) Å^3, T = 110.00(10) K, space group P-1 (no. 2), Z = 4, μ(Mo Kα) = 0.801, ρ_{calc}mg/mm^3 2.036,17515 reflections measured, 10684 unique (R_{int} = 0.0312) which were used in all calculations. The final wR_2 was 0.2653 (all data) and R_1 was 0.1241 (>2sigma(I)).

6.4.15 Synthesis of $[(\eta^5\text{-}C_5H_5)Ru(P\{OC(CF_3)_3\}_3)(NCCH_3)_2]^+[PF_6]^-$, **[Ru(2)]**

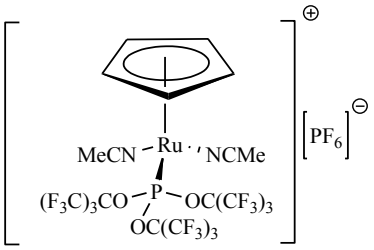

Tris(acetonitrile)(η^5-cyclopentadienyl)ruthenium(II) hexafluorophosphate, $[(\eta^5\text{-}C_5H_5)Ru(NCMe)_3][PF_6]^-$ (25 mg, 0.058 mmol, 1 eq.), deuterated CD_2Cl_2 (0.1 mL) and DCM (0.4 mL) were added to a PTFE J Young's tap NMR tube in an inert-atmosphere glovebox. Perfluoro-*t*–butyl-phosphite (368 mg, 0.5 mmol, 10 eq.) in 10 mL DCM solution was added to this and the reaction was then monitored by $^{31}P\{^1H\}$ NMR spectroscopy to follow the reaction. The reaction mixture was then layered with hexane and left to crystallise. The mother liquor was removed (any free ligand is removed this way) *via* a canula transfer and remaining crystalline material was then washed with hexane, followed by another canula transfer to remove any solvent. The crystalline product in the NMR tube was then dried *in vacuo* (at 1.5 x 10^{-2} mbar, for 30 min. at room temperature) on the Schlenk line. The yellow/brown crystalline product was treated as air-sensitive and stored in an inert-atmosphere glove box.

^{1}H NMR (295 K, 400 MHz, $CDCl_3$): δ_H = 2.20 (d, $^4J_{HP}$ = 2 Hz, either $[(\eta^5\text{-}C_5H_5)Ru(P\{OC(CF_3)_3\}_3)(NCC\mathbf{H_3})_2]^+$ or $[(\eta^5\text{-}C_5H_5)Ru(P\{OC(CF_3)_3\}_2Cl)(NCC\mathbf{H_3})_2]^+$), 2.42 (d, $^4J_{HP}$ = 2 Hz, either $[(\eta^5\text{-}C_5H_5)Ru(P\{OC(CF_3)_3\}_3)(NCC\mathbf{H_3})_2]^+$ or $[(\eta^5\text{-}C_5H_5)Ru(P\{OC(CF_3)_3\}_2Cl)(NCC\mathbf{H_3})_2]^+$, 4.50 (s, either $[(\eta^5\text{-}C_5\mathbf{H}_5)Ru(P\{OC(CF_3)_3\}_3)(NCCH_3)_2]^+$ or $[(\eta^5\text{-}C_5\mathbf{H}_5)Ru(P\{OC(CF_3)_3\}_2Cl)(NCCH_3)_2]^+$), 4.86 (s, either $[(\eta^5\text{-}C_5\mathbf{H}_5)Ru(P\{OC(CF_3)_3\}_3)(NCCH_3)_2]^+$ or $[(\eta^5\text{-}C_5\mathbf{H}_5)Ru(P\{OC(CF_3)_3\}_2Cl)(NCCH_3)_2]^+$) ppm. Satisfactorily integration values could not be obtained.

Lower intensity signals were also found at 4.98 (J = 2 Hz) and 4.99 (J = 1 Hz) ppm.

$^{31}P\{^1H\}$ NMR (295 K, 161.8 MHz, $CDCl_3$): δ_P = -143.00 (sept, $[\mathbf{P}F_6]^-$ $^1J_{PF}$ = 711.0 Hz), 117.1 (s, $[(\eta^5\text{-}C_5H_5)Ru(\mathbf{P}\{OC(CF_3)_2\}_3)(NCCH_3)_2]^+$), 138.9 (s, $[(\eta^5\text{-}C_5H_5)Ru(\mathbf{P}\{OC(CF_3)_2\}_2Cl)(NCCH_3)_2]^+$) ppm.

^{19}F NMR (295 K, 376.2 MHz, CD_2Cl_2): δ_F = -72.97 (d, 6F, $^1J_{PF}$ = 711 Hz, $[P\mathbf{F_6}]^-$), -71.05 (s, either $[(\eta^5\text{-}C_5H_5)Ru(P\{OC(C\mathbf{F}_3)_3\}_3)(NCCH_3)_2]^+$ or $[(\eta^5\text{-}$

C_5H_5)Ru(P{OC(C**F**$_3$)$_3$}$_2$Cl)(NCCH$_3$)$_2$]$^+$), -71.07 (s, either [(η^5-C_5**H**$_5$)Ru(P{OC(CF$_3$)$_3$}$_3$)(NCCH$_3$)$_2$]$^+$ or [(η^5-C_5**H**$_5$)Ru(P{OC(CF$_3$)$_3$}$_2$Cl)(NCCH$_3$)$_2$]$^+$) ppm.

Signals were also found at -78.17 (br, HOC(C**F**$_3$)$_3$}$_3$), -74.65 (br), -71.32 (d, $^1J_{FP}$ = 22 Hz, P{OC(C**F**$_3$)$_3$}$_3$), -70.15 (s), -69.99 (d, J = 3 Hz).

The NMR spectra of this material also showed the presence of vacuum grease, DCM, triethylamine from the preparation of (**2**), [(η^5-C_5H_5)Ru(NCCH$_3$)$_3$]$^+$[PF$_6$]$^-$and MeCN.

IR (solution cell in CH_2Cl_2): $\nu_{(CN)}$[cm^{-1}]: 2962 and 2926.

EI-MS (MeCN): m/z observed 784.9028 m/z , [M]$^+$ (calculated 784.8998 m/z for [(η^5-C_5H_5) ^{102}Ru(P{OC(CF$_3$)$_2$}$_2$Cl)(NCCH$_3$)$_2$]$^+$, -6.1 ppm). Observed 144.9650 m/z: [M]$^-$ (calculated 144.9647 m/z for [PF$_6$]$^-$, -1.0 ppm). No evidence of **[Ru(2)]** in ESI-MS.

Single-Crystal X-ray Diffraction Measurements: $C_{39}H_{14}F_{69}N_3Na_4O_7P_2Ru$, M = 2202.50, monoclinic, Crystal size/mm = 0.30 × 0.29 × 0.11, a = 18.6301(10) Å, b = 20.1555(7) Å, c = 20.1269(9) Å, β = 114.317(6)°, V = 6887.1(5) Å^3, T = 110.00(14) K, space group P2$_1$/n (no. 14), Z = 4, μ(MoKα) = 0.536, ρ_{calc}mg/mm^3 = 2.124, 32707 reflections measured, 15805 unique (R_{int} = 0.0350) which were used in all calculations. The final wR_2 was 0.1677 (all data) and R_1 was 0.0623 (>2sigma(I)).

6.4.16 Synthesis of $[(\eta^5\text{-}C_5H_5)Ru(PhP\{OCH(CF_3)_2\}_2)(NCCH_3)_2]^+[PF_6]^-$, **[Ru(3)]**

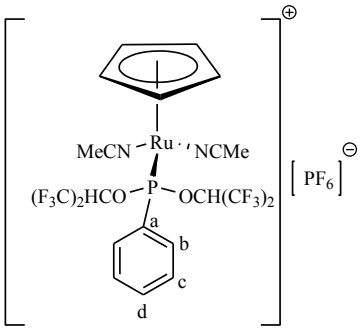

Tris(acetonitrile)(η^5-cyclopentadienyl)ruthenium(II) hexafluorophosphate, $[(\eta^5\text{-}C_5H_5)Ru(NCMe)_3][PF_6]^-$ (25 mg, 0.058 mmol, 1 eq.), deuterated CD_2Cl_2 (0.1 mL) and DCM (0.4 mL) were added to a PTFE J Young's tap NMR tube in an inert-atmosphere glovebox. Bis(hexafluoroisopropoxy)phenylphosphonite (20 mg, 0.045 mmol, 0.8 eq.) was added to this and the reaction was then monitored by $^{31}P\{^1H\}$ NMR spectroscopy to follow the reaction. The reaction mixture was then layered with hexane and left to crystallise. The mother liquor was removed (any free ligand is removed this way) *via* a canula transfer and remaining crystalline material was then washed with hexane, followed by another canula transfer to remove any solvent. The crystalline product in the NMR tube was then dried *in vacuo* (at 1.5 x 10^{-2} mbar, for 30 min. at room temperature) on the Schlenk line. The yellow/brown crystalline product was treated as air-sensitive and stored in an inert-atmosphere glove box.

Yield: 33 mg (68 %)

^{1}H NMR (295 K, 400 MHz, $CDCl_3$): δ_H = 2.37 (d, 6H, $^4J_{HP}$ = 1 Hz, $[(\eta^5\text{-}C_5H_5)Ru(PhP\{OCH(CF_3)_2\}_2)(NCC\mathbf{H}_3)_2]^+$), 4.72 (s, 5H, $[(\eta^5\text{-}C_5\mathbf{H_5})Ru(PhP\{OCH(CF_3)_2\}_2)(NCCH_3)_2]^+$), 4.83 (sept, 2H, $^3J_{HF}$ = 6 Hz $[(\eta^5\text{-}C_5H_5)Ru(PhP\{OC\mathbf{H}(CF_3)_2\}_2)(NCCH_3)_2]^+$), 7.56-7.82 (m, 5H, $[(\eta^5\text{-}C_5H_5)Ru(\mathbf{Ph}P\{OCH(CF_3)_2\}_2)(NCCH_3)_2]^+$) ppm.

$^{31}P\{^1H\}$ NMR (295 K, 161.8 MHz, $CDCl_3$):): δ_P= -143.0 (sept, $^1J_{PF}$ = 711 Hz, $[\mathbf{P}F_6]^-$), 199.8 (s, $[(\eta^5\text{-}C_5H_5)Ru(Ph\mathbf{P}\{OCH(CF_3)_2\}_2)(NCCH_3)_2]^+$) ppm.

^{19}F NMR (295 K, 376.2 MHz, CD_2Cl_2): δ_F = -73.59 (m, 3F, $[(\eta^5\text{-}C_5H_5)Ru(PhP\{OCH(C\mathbf{F}_3)_2\}_2)(NCCH_3)_2]^+$), -73.38 (m, 3F, $[(\eta^5\text{-}C_5H_5)Ru(PhP\{OCH(C\mathbf{F}_3)_2\}_2)(NCCH_3)_2]^+$), -72.93 (d, 6F, $^1J_{PF}$ = 711 Hz, $[P\mathbf{F_6}]^-$) ppm. Two

environments were observed for each CF_3 group in the ^{19}F NMR, possibly indicating atropisomerism due to hindered rotation around either the P-O or O-C bond.

^{13}C NMR (295 K, 100.5 MHz, $CDCl_3$): δ_C = 3.6 (d, $^4J_{HP}$ = 9 Hz, [(η^5-C_5H_5)Ru(PhP{OCH(CF_3)$_2$}$_2$)(NC**C**H$_3$)$_2$]$^+$), 72.9 (m, [(η^5-C_5H_5)Ru(PhP{O**C**H(CF_3)$_2$}$_2$)(NCCH$_3$)$_2$]$^+$), 80.2 (d, $^2J_{CP}$ = 3 Hz, [(η^5-**C**$_5H_5$)Ru(PhP{OCH(CF_3)$_2$}$_2$)(NCCH$_3$)$_2$]$^+$), 120.5 (q, $^1J_{CF}$ = 282 Hz, [(η^5-C_5H_5)Ru(PhP{OCH(**C**F$_3$)$_2$}$_2$)(NCCH$_3$)$_2$]$^+$), 129.0 (s, [(η^5-C_5H_5)Ru(PhP{OCH(CF_3)$_2$}$_2$)(N**C**CH$_3$)$_2$]$^+$), 129.6 (d, $^3J_{CP}$ = 12 Hz, phenyl-c), 130.7 (d, $^2J_{CP}$ = 16 Hz, phenyl-b), 133.3 (d, $^1J_{CP}$ = 58 Hz, phenyl-a) 133.8 (d, $^4J_{CP}$ = 2 Hz, phenyl-d) ppm.

The NMR spectra of this material also showed the presence of a small amount of vacuum grease, the [(η^5-C_5H_5)Ru(NCCH$_3$)$_3$]$^+$[PF_6]$^-$ starting material and DCM.

ESI-MS (MeCN): m/z observed mass = 690.9921, [M]$^+$ (calculated mass 690.9958 m/z for [(η^5- C_5H_5)^{102}Ru{PhP{OCH(CF_3)**$_2$**}$_2$(NCCH$_3$)$_2$]$^+$, 4.9 ppm). m/z observed mass = 144.9651, [M]$^-$(calculated mass 144.9647 m/z for [PF_6]$^-$, -2.8 ppm).

6.4.17 Synthesis of $[(\eta^5\text{-}C_5H_5)Ru(PhP\{OCH(CF_3)_2\}_2)_2(NCCH_3)]^+[PF_6]^-$, **[Ru(3)-2]**

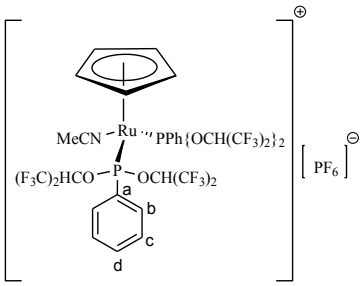

Tris(acetonitrile)(η^5-cyclopentadienyl)ruthenium(II) hexafluorophosphate, $[(\eta^5\text{-}C_5H_5)Ru(NCMe)_3][PF_6]^-$ (25 mg, 0.058 mmol, 1 eq.), deuterated CD_2Cl_2 (0.1 mL) and DCM (0.4 mL) were added to a PTFE J Young's tap NMR tube in an inert-atmosphere glovebox. Bis(hexafluoroisopropoxy)phenylphosphonite (44 mg, 0.100 mmol, 1.72 eq.) was added to this and the reaction was then monitored by $^{31}P\{^1H\}$ NMR spectroscopy to follow the reaction. The reaction mixture was then layered with hexane and left to crystallise. The mother liquor was removed (any free ligand is removed this way) *via* a canula transfer and remaining crystalline material was then washed with hexane, followed by another canula transfer to remove any solvent. The crystalline product in the NMR tube was then dried *in vacuo* (at 1.5 x 10^{-2} mbar, for 30 min. at room temperature) on the Schlenk line. The yellow crystalline product was treated as air-sensitive and stored in an inert-atmosphere glove box.

Yield: 40 mg (79 %)

^{1}H NMR (295 K, 400 MHz, $CDCl_3$): δ_H = 2.41 (br, $[(\eta^5\text{-}C_5H_5)Ru(PhP\{OCH(CF_3)_2\}_2)_2(NCC\mathbf{H_3})]^+$), 4.75 (s, $[(\eta^5\text{-}C_5\mathbf{H_5})$, $Ru(PhP\{OCH(CF_3)_2\}_2)_2(NCCH_3)]^+$), 4.86 (sept, $^3J_{HF}$ = 6 Hz $[(\eta^5\text{-}C_5H_5)Ru(PhP\{OC\mathbf{H}(CF_3)_2\}_2)_2(NCCH_3)]^+$), 7.61-7.82 (m, $[(\eta^5\text{-}C_5H_5)Ru(\mathbf{Ph}P\{OCH(CF_3)_2\}_2)_2(NCCH_3)]^+$) ppm. Satisfactorily integration values could not be obtained.

$^{31}P\{^1H\}$ NMR (295 K, 161.8 MHz, $CDCl_3$):): δ_P= -143.0 (sept, $^1J_{PF}$ = 711 Hz, $[\mathbf{P}F_6]^-$), 199.8 (s, $[(\eta^5\text{- }C_5H_5)Ru(Ph\mathbf{P}\{OCH(CF_3)_2\}_2)_2(NCCH_3)]^+$) ppm.

^{19}F NMR (295 K, 376.2 MHz, CD_2Cl_2): δ_F = -73.59 (m, 6F, $[(\eta^5\text{-}C_5H_5)Ru(PhP\{OCH(C\mathbf{F}_3)_2\}_2)_2(NCCH_3)]^+$), -73.38 (m, 6F, $[(\eta^5\text{-}C_5H_5)Ru(PhP\{OCH(C\mathbf{F}_3)_2\}_2)_2$ $(NCCH_3)]^+$), 72.01 (d, 6F, $^1J_{PF}$ = 711 Hz, $[P\mathbf{F_6}]^-$) ppm. Two environments were observed for each CF_3 group in the ^{19}F NMR, possibly indicating atropisomerism due to hindered rotation around either the P-O or O-C bond.

^{13}C NMR (295 K, 100.5 MHz, $CDCl_3$): δ_C = 4.0 (s, [(η^5-C_5H_5)Ru(PhP{OCH(CF_3)$_2$}$_2$)$_2$(NC**C**H_3)]$^+$), 73.0 (m, [(η^5-C_5H_5)Ru(PhP{O**C**H(CF_3)$_2$}$_2$)$_2$(NCCH$_3$)]$^+$), 80.4 (d, $^2J_{CP}$ = 4 Hz, [(η^5-**C**$_5H_5$)Ru(PhP{OCH(CF_3)$_2$}$_2$)$_2$(NCCH$_3$)]$^+$), 120.6 (q, $^1J_{CF}$ = 282 Hz, [(η^5-C_5H_5)Ru(PhP{OC(**C**F_3)$_3$}$_2$)$_2$(NCCH$_3$)]$^+$), 129.2 (s, [(η^5-C_5H_5)Ru(PhP{OC(CF_3)$_3$}$_2$)$_2$(N**C**CH$_3$)]$^+$), 129.8 (d, $^3J_{CP}$ = 12 Hz, phenyl-c), 130.9 (d, $^2J_{CP}$ = 16 Hz, phenyl-b), 133.4 (d, $^1J_{CP}$ = 58 Hz, phenyl-a), 134.1 (d, $^4J_{CP}$ = 2 Hz, phenyl-d) ppm.

The NMR spectra of this material also showed the presence of a small amount of vacuum grease, DCM and MeCN. The integration values were difficult to obtain for this sample.

IR (CH_2Cl_2 solution): $\nu_{(CN)}$[cm^{-1}]: 2197.

ESI-MS (MeCN): m/z observed mass = 1091.9679, [M]$^+$ (calculated mass 1091.9745 m/z for [(η^5-C_5H_5)^{102}Ru{Ph_2POCH(CF_3)**$_2$**}$_2$(NCCH$_3$)]$^+$, -6.1 ppm). m/z observed mass = 144.9647, [M]$^-$ (calculated mass 144.9649 m/z for [PF_6]$^-$, -1.0 ppm).

Elemental Analysis: [(η^5-C_5H_5)Ru{Ph_2POCH(CF_3)$_2$}$_2$(NCCH$_3$)]$^+$ [PF_6]$^-$: calculated C(30.11) H(1.79) N(1.13), observed C(30.43) H(2.14) N(1.13).

Single-Crystal X-ray Diffraction Measurements: $C_{31}H_{22}F_{30}NO_4P_3Ru$, M = 1236.48, monoclinic, crystal size/mm = 0.10 × 0.05 × 0.03, a = 10.7469(4) Å, b = 15.2241(10) Å, c = 24.7282(7) Å, β = 90.521(3)°, U = 4045.7(3) Å^3, T = 110.00(10) K, space group P2$_1$/n (no. 14), Z = 4, μ(Mo Kα) = 0.686, ρ_{calc}mg/mm^3 = 2.030, 13750 reflections measured, 8175 unique (R_{int} = 0.0379) which were used in all calculations. The final $wR(F_2)$ was 0.0986 (all data).

6.4.18 Synthesis of $(\eta^5\text{-}C_5H_5)Ru(PhP\{OC(CF_3)_2\}_2)(CH_3CN)_2]^+[PF_6]^-$, **[Ru(4)]**

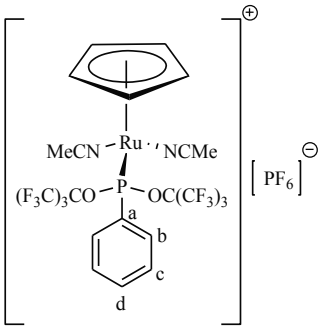

Tris(acetonitrile)(η^5-cyclopentadienyl)ruthenium(II) hexafluorophosphate, $[(\eta^5\text{-}C_5H_5)Ru(NCMe)_3][PF_6]^-$ (25 mg, 0.058 mmol, 1 eq.), deuterated CD_2Cl_2 (0.1 mL) and DCM (0.4 mL) were added to a PTFE J Young's tap NMR tube in an inert-atmosphere glovebox. Bis(perfluoro-*t*-butoxy)phenylphosphonite (34 mg, 0.059 mmol, 1 eq.) was added to this and the reaction was then monitored by $^{31}P\{^1H\}$ NMR spectroscopy to follow the reaction. The reaction mixture was then layered with hexane and left to crystallise. The mother liquor was removed (any free ligand is removed this way) *via* a canula transfer and remaining crystalline material was then washed with hexane, followed by another canula transfer to remove any solvent. The crystalline product in the NMR tube was then dried *in vacuo* (at 1.5 x 10^{-2} mbar, for 30 min. at room temperature) on the Schlenk line. The yellow crystalline product was treated as air-sensitive and stored in an inert-atmosphere glove box.

Yield: 19 mg (45 %)

^{1}H NMR (295 K, 400 MHz, CD_2Cl_2): δ_H = 2.44 (d, 6H, $^4J_{HP}$ = 1 Hz, $[(\eta^5\text{-}C_5H_5)Ru(PhP\{OC(CF_3)_3\}_2)(NCC\mathbf{H}_3)_2]^+$), 4.74 (m, 5H, $[(\eta^5\text{-}C_5\mathbf{H}_5)Ru(PhP\{OC(CF_3)_3\}_2)(NCCH_3)_2]^+$), 7.47-7.95 (m, 5H, $[(\eta^5\text{-}C_5H_5)Ru(\mathbf{Ph}P\{OC(CF_3)_3\}_2)(NCCH_3)_2]^+$) ppm.

$^{31}P\{^1H\}$ NMR (295 K, 161.8 MHz, CD_2Cl_2): δ_P = -143.0 (sept, $^1J_{PF}$ = 711 Hz, $[\mathbf{P}F_6]^-$), 192.2 (s, $[(\eta^5\text{-}C_5H_5)Ru(Ph\mathbf{P}\{OC(CF_3)_3\}_2)(NCCH_3)_2]^+$ ppm.

^{19}F NMR (295 K, 376.2 MHz, CD_2Cl_2): δ_F = -73.05 (d, 6F, $^1J_{PF}$ 711 Hz, $[PF_6]^-$), -70.48 (br, 18F, $[(\eta^5\text{-}C_5H_5)Ru(PhP\{OC(C\mathbf{F}_3)_3\}_2)(NCCH_3)_2]^+$ ppm.

^{13}C NMR (295 K, 100.5 MHz, CD_2Cl_2): δ_C = 4.0 (s, $[(\eta^5\text{-}C_5H_5)Ru(PhP\{OC(CF_3)_3\}_2)(NC\mathbf{C}H_3)_2]^+$), 81.8 (d, $^2J_{CP}$ = 4 Hz, $[(\eta^5\text{-}\mathbf{C_5}H_5)Ru(PhP\{OC(CF_3)_3\}_2)(NCCH_3)_2]^+$), 119.7 (q, $^1J_{CF}$ = 286 Hz, $[(\eta^5\text{-}C_5H_5)Ru(PhP\{OC(\mathbf{C}F_3)_3\}_2)(NCCH_3)_2]^+$), 128.8 (d, $^3J_{CP}$ = 12 Hz, phenyl-c), 129.1 (s, $[(\eta^5\text{-}$

C_5H_5)Ru(PhP{OC(CF_3)$_3$}$_2$)(N**C**CH_3)$_2$]$^+$), 131.7 (d, $^2J_{CP}$ = 20 Hz, phenyl-b), 134.1 (d, $^4J_{CP}$ = 2 Hz, phenyl-d), 139.3 (d, $^1J_{CP}$ = 48 Hz, phenyl-a) ppm.

IR (CH_2Cl_2 solution): $\nu_{(CN)}$[cm^{-1}]: 2197 and 2092.

EI-MS (MeCN): m/z, observed mass = 826.9706, $[M]^+$ (calculated mass 826.9694 m/z for [(η^5- C_5H_5) ^{102}Ru(PhP{OC(**C**F_3)$_3$}$_2$)(NCCH_3)$_2$]$^+$, 0.4 ppm), m/z observed mass = 144.9647, $[M]^-$ (calculated mass 144.9653 m/z for $[PF_6]^-$, -3.7ppm).

Elemental Analysis: [(η^5-C_5H_5)Ru(PhP{OC(**C**F_3)$_3$}$_2$)(NCCH_3)$_2$]$^+$[PF_6]$^-$: calculated C(28.40) H(1.66) N(2.88), observed C(28.29) H(1.69) N(3.08).

Single-Crystal X-ray Diffraction Measurements: $C_{23}H_{16}F_{24}N_2O_2P_2Ru$, M = 971.39, monoclinic, crystal size/mm = 0.25 × 0.13 × 0.06, a = 18.5185(9) Å, b = 8.9595(6) Å, c = 20.1750(19) Å, β = 107.424(8)°, U = 3193.7(4) Å^3, T = 110.0 K, space group $P2_1/c$ (no. 14), Z = 4, μ(Mo Kα) = 0.761, ρ_{calc}mg/mm^3 = 2.020, 20806 reflections measured, 10160 unique (R_{int} = 0.0277) which were used in all calculations. The final $wR(F_2)$ was 0.0886 (all data).

6.4.19 Synthesis of $[(\eta^5\text{-}C_5H_5)Ru\{Ph_2POCH(CF_3)_2\}(CH_3CN)_2]^+[PF_6]^-$, **[Ru(5)]**

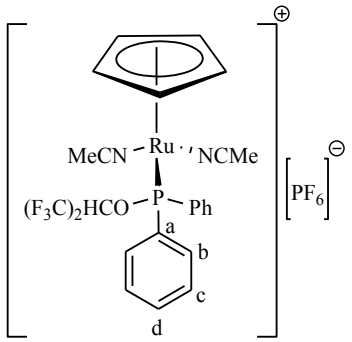

Tris(acetonitrile)(η^5-cyclopentadienyl)ruthenium(II) hexafluorophosphate, $[(\eta^5\text{-}C_5H_5)Ru(NCMe)_3][PF_6]^-$ (25 mg, 0.058 mmol, 1 eq.), deuterated CD_2Cl_2 (0.1 mL) and DCM (0.4 mL) were added to a PTFE J Young's tap NMR tube in an inert-atmosphere glovebox. Hexafluoroisopropoxydiphenylphosphinite (16 mg, 0.045 mmol, 0.8 eq.) was added to this and the reaction was then monitored by $^{31}P\{^1H\}$ NMR spectroscopy to follow the reaction. The reaction mixture was then layered with hexane and left to crystallise. The mother liquor was removed (any free ligand is removed this way) *via* a canula transfer and remaining crystalline material was then washed with hexane, followed by another canula transfer to remove any solvent. The crystalline product in the NMR tube was then dried *in vacuo* (at 1.5 x 10^{-2} mbar, for 30 min. at room temperature) on the Schlenk line. The yellow crystalline product was treated as air-sensitive and stored in an inert-atmosphere glove box.

Yield: 20 mg (58 %)

^{1}H NMR (295 K, 400 MHz, $CDCl_3$): δ_H = 2.30 (d, $^4J_{HP}$ = 6H, $[(\eta^5\text{-}C_5H_5)Ru\{Ph_2POCH(CF_3)_2\}(NCC\mathbf{H}_3)_2]^+$), 4.67 (s, 4H, $[(\eta^5\text{-}C_5\mathbf{H}_5)Ru\{Ph_2POCH(CF_3)_2\}(NCCH_3)_2]^+$), 7.22-7.92 (m, 10H, $[(\eta^5\text{-}C_5H_5)Ru\{\mathbf{Ph}_2POCH(CF_3)_2\}(NCCH_3)_2]^+$) ppm.

The $[(\eta^5\text{-}C_5H_5)Ru\{Ph_2POC\mathbf{H}(CF_3)_2\}(NCCH_3)_2]^+$ signal is likely to be under the intense DCM peak.

$^{31}P\{^1H\}$ NMR (295 K, 161.8 MHz, CD_2Cl_2): δ_P = -143.0 (sept, $^1J_{PF}$ = 711Hz, $[\mathbf{P}F_6]^-$), 171.7 (s, $[(\eta^5\text{-}C_5H_5)Ru\{Ph_2\mathbf{P}OCH(CF_3)_2\}(NCCH_3)_2]^+$), ppm.

^{19}F NMR (295 K, 376.2 MHz, CD_2Cl_2): δ_F = -72.75 (d, 6F, $^1J_{PF}$ = 6 Hz, $[(\eta^5\text{-}C_5H_5)Ru\{Ph_2POCH(C\mathbf{F}_3)_2\}(NCCH_3)_2]^+$), -72.59 (d, 6F, $^1J_{PF}$ = 711 Hz, $[P\mathbf{F}_6]^-$) ppm.

^{13}C NMR (295 K, 100.5 MHz, $CDCl_3$): δ_C = 3.9 (s, [(η^5-C_5H_5)Ru(Ph_2P{$OCH(CF_3)_2$})($NC\mathbf{C}H_3)_2$]$^+$), 73.7 (m, [(η^5-C_5H_5)Ru(Ph_2P{$O\mathbf{C}H(CF_3)_2$})($NC\mathbf{C}H_3)_2$]$^+$), 79.6 (d, $^2J_{CP}$ = 3 Hz, [(η^5-$\mathbf{C_5}H_5$)Ru(Ph_2P{$OCH(CF_3)_2$})($NCCH_3)_2$]$^+$), 128.5 ($^3J_{CP}$ = 11 phenyl-c), 129.7 (s, [(η^5-C_5H_5)Ru(Ph_2P{$OCH(CF_3)_2$}$_2$)($N\mathbf{C}CH_3)_2$]$^+$), 130.7 (d, $^2J_{CP}$ = 13 Hz, phenyl-b), 131.4 (d, $^4J_{CP}$ = 2 Hz, phenyl-d), 137.5 (d, $^1J_{CP}$ = 51 Hz, phenyl-a) ppm.

The NMR spectra of this material also showed the presence of a small amount of vacuum grease, triethylamine and DCM.

EI-MS (MeCN): m/z observed mass = 601.0410, $[M]^+$, (calculated mass 601.0418 m/z , for [(η^5-C_5H_5) ^{102}Ru{$Ph_2POCH(CF_3)_2$}($NCCH_3)_2$]$^+$, 0.3 ppm), m/z observed mass = 144.96475, $[M]^-$ (calculated mass 144.9647 m/z, for $[PF_6]^-$, 1.9 ppm).

Single-Crystal X-ray Diffraction Measurements: $C_{24}H_{22}N_2OF_6PRu$, M = 745.45, monoclinic, crystal size/mm = 0.18 × 0.14 × 0.10, a = 9.63854(12) Å, b = 20.5208(2) Å, c = 14.27507(18) Å, β = 98.4968(11)°, U = 2792.49(6) Å^3, T = 109.8 K, space group $P2_1/c$ (no. 14), Z = 4, μ(Mo Kα) = 0.779, ρ_{calc}mg/mm^3 = 1.773, 14407 reflections measured, 8130 unique (R_{int} = 0.0224) which were used in all calculations. The final $wR(F_2)$ was 0.0709 (all data).

6.4.20 Synthesis of $[(\eta^5\text{-}C_5H_5)Ru\{Ph_2POCH(CF_3)_2\}_2(CH_3CN)]^+[PF_6]^-$, **[Ru(5)-2]**

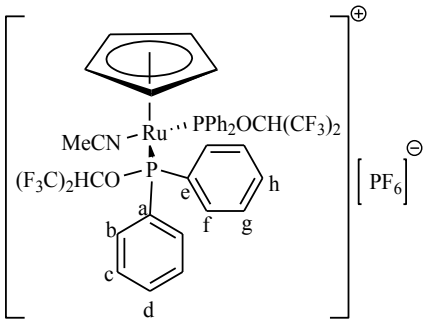

Tris(acetonitrile)(η^5-cyclopentadienyl)ruthenium(II) hexafluorophosphate, $[(\eta^5\text{-}C_5H_5)Ru(NCMe)_3][PF_6]^-$ (25 mg, 0.058 mmol, 1 eq.), deuterated CD_2Cl_2 (0.1 mL) and DCM (0.4 mL) were added to a PTFE J Young's tap NMR tube in an inert-atmosphere glovebox. Hexafluoroisopropoxydiphenylphosphinite (41 mg, 0.116 mmol, 2 eq.) was added to this and the reaction was then monitored by $^{31}P\{^1H\}$ NMR spectroscopy to follow the reaction. The reaction mixture was then layered with hexane and left to crystallise. The mother liquor was removed (any free ligand is removed this way) *via* a canula transfer and remaining crystalline material was then washed with hexane, followed by another canula transfer to remove any solvent. The crystalline product in the NMR tube was then dried *in vacuo* (at 1.5 x 10^{-2} mbar, for 30 min. at room temperature) on the Schlenk line. The yellow crystalline product was treated as air-sensitive and stored in an inert-atmosphere glove box.

Yield: 54 mg (80 %)

^{1}H NMR (295 K, 400 MHz, $CDCl_3$): δ_H = 2.51 (s, 3H, $[(\eta^5\text{-}C_5H_5)Ru\{Ph_2POCH(CF_3)_2\}_2(NCC\mathbf{H}_3)]^+$), 4.36 (br, 2H, $[(\eta^5\text{-}C_5H_5)Ru\{Ph_2POC\mathbf{H}(CF_3)_2\}_2(NCCH_3)]^+$), 4.76 (s, 5H, $[(\eta^5\text{-}C_5\mathbf{H}_5)Ru\{Ph_2POCH(CF_3)_2\}_2(NCCH_3)]^+$), 6.84-7.64 (m, 20H, $[(\eta^5\text{-}C_5H_5)Ru\{\mathbf{Ph}_2POCH(CF_3)_2\}_2(NCCH_3)]^+$) ppm.

$^{31}P\{^1H\}$ NMR (295 K, 161.8 MHz, CD_2Cl_2): δ_P = -143.0 (sept, $^1J_{PF}$ = 711Hz, $[\mathbf{P}F_6]^-$), 167.7 (s, $[(\eta^5\text{-}C_5H_5)Ru\{Ph_2\mathbf{P}OCH(CF_3)_2\}_2(NCCH_3)]^+$) ppm.

^{19}F NMR (295 K, 376.2 MHz, CD_2Cl_2): δ_F = -73.03 (d, 6F, $^1J_{PF}$ = 711 Hz, $[P\mathbf{F}_6]^-$), -72.69 (m, 6F, $[(\eta^5\text{-}C_5H_5)Ru\{Ph_2POCH(C\mathbf{F}_3)_2\}_2(NCCH_3)]^+$), -72.40 (br, 6F, $[(\eta^5\text{-}C_5H_5)Ru\{Ph_2POCH(C\mathbf{F}_3)_2\}_2(NCCH_3)]^+$), -71.73 (m, 6F, $[(\eta^5\text{-}C_5H_5)Ru\{Ph_2POCH(C\mathbf{F}_3)_2\}_2(NCCH_3)]^+$) ppm. Two environments were observed for each CF_3 group in the ^{19}F NMR, possibly indicating atropisomerism due to hindered rotation around either the P-O or O-C bond.

Lower intensity peaks at 74.52 (t, J = 6 Hz) and 74.10 (d, J = 6 Hz) were also observed.

^{13}C NMR (295 K, 100.5 MHz, $CDCl_3$): δ_C = 4.7 (s, [(η^5-C_5H_5)Ru{$Ph_2POCH(CF_3)_2$}$_2$($NC\mathbf{C}H_3$)]$^+$), 72.1 (m, [(η^5-C_5H_5)Ru{$Ph_2PO\mathbf{C}H(CF_3)_2$}$_2$($NCCH_3$)]$^+$), 86.0 (t, [($\eta^5$-$\mathbf{C}_5H_5$)Ru{$Ph_2POCH(CF_3)_2$}$_2$($NCCH_3$)]$^+$), 122.2 (m, part coupling of 284 Hz for $^1J_{CF}$ coupling and of 24 Hz for $^4J_{CF}$ coupling, [(η^5-C_5H_5)Ru{$Ph_2POCH(\mathbf{C}F_3)_2$}$_2$($NCCH_3$)]$^+$), 128.6 (t , $^3J_{CP}$ = 5 Hz, phenyl-c or -g), 129.4 (t, $^3J_{CP}$ = 5 Hz, phenyl-c or -g), 130.7 (t, $^2J_{CP}$ = 7 Hz, phenyl-b or -f), 131.8 (s, phenyl-d or -h), 132.4 (t, $^2J_{CP}$ = 6 Hz, phenyl-b or -f), 133.1 (s, phenyl -d or -h), 135.1 (t, $^1J_{CP}$ = 24 Hz, phenyl-a or-e), 138.1 (t, $^1J_{CP}$ = 24 Hz, phenyl-a or -e).

A lower intensity peaks at 29.9 (s) ppm was also observed.

The NMR spectra of this material also showed the presence of a small amount of vacuum grease, DCM and MeCN.

IR (CH_2Cl_2 solution): $\nu_{(CN)}$[cm^{-1}]: 2249, 1270.

EI-MS (CH_2Cl_2): m/z , observed mass = 912.0608, $[M]^+$ (calculated mass 912.0597 m/z, for [(η^5-C_5H_5) ^{102}Ru{$Ph_2POCH(CF_3)_2$}$_2$($NCCH_3$)]$^+$, 1.1 ppm), m/z observed mass = 144.9647 m/z, $[M]^-$ (calculated mass 144.9647 m/z for $[PF_6]^-$, 0.4 ppm).

Single-Crystal X-ray Diffraction Measurements: $C_{37.75}H_{31.5}Cl_{1.5}F_{18}NO_2P_3Ru$, M = 1120.29, orthorhombic, crystal size/mm = 0.18 × 0.14 × 0.10, a = 40.3432(9) Å, b = 20.6710(3) Å, c = 10.37245(15) Å, V = 8650.0(3) Å^3, T = 109.95(10) K, space group $P2_12_12$ (no. 18), Z = 8, μ(Mo Kα) = 0.680, ρ_{calc} mg/mm^3 =1.721, 25970 reflections measured, 19289 unique (R_{int} = 0.0233) which were used in all calculations. The final wR_2 was 0.0989 (all data) and R_1 was 0.0494 (>2sigma(I)).

6.4.21 Synthesis of $[(\eta^5\text{-}C_5H_5)Ru(Ph_2P\{OC(CF_3)\}_3)(CH_3CN)_2]^+[PF_6]^-$, **[Ru(6)]**

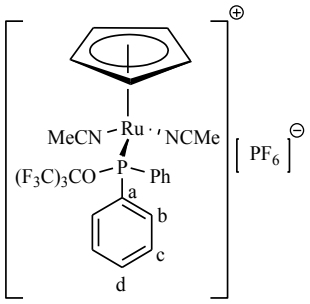

Tris(acetonitrile)(η^5-cyclopentadienyl)ruthenium(II) hexafluorophosphate, $[(\eta^5\text{-}C_5H_5)Ru(NCMe)_3][PF_6]^-$ (25 mg, 0.058 mmol, 1 eq.), deuterated CD_2Cl_2 (0.1 mL) and DCM (0.4 mL) were added to a PTFE J Young's tap NMR tube in an inert-atmosphere glovebox. Perfluoro-*t*-butoxydiphenylphosphinite (21 mg, 0.050 mmol, 0.9 eq.) was added to this and the reaction was then monitored by $^{31}P\{^1H\}$ NMR spectroscopy to follow the reaction. The reaction mixture was then layered with hexane and left to crystallise. The mother liquor was removed (any free ligand is removed this way) *via* a canula transfer and remaining crystalline material was then washed with hexane, followed by another canula transfer to remove any solvent. The crystalline product in the NMR tube was then dried *in vacuo* (at 1.5 x 10^{-2} mbar, for 30 min. at room temperature) on the Schlenk line. The yellow crystalline product was treated as air-sensitive and stored in an inert-atmosphere glove box.

Yield: 33 mg (70 %)

^{1}H NMR (295 K, 400 MHz, $CDCl_3$): δ_H = 2.38 (d, 6H, $^4J_{HF}$ = 1 Hz, $[(\eta^5\text{-}C_5H_5)Ru(Ph_2P\{OC(CF_3)_3\})(NCC\mathbf{H_3})_2]^+$), 4.49 (br, 4.3H, $[(\eta^5\text{-}C_5\mathbf{H}_5)Ru(Ph_2P\{OC(CF_3)_3\})(NCCH_3)_2]^+$), 7.26-7.95 (m, 10H, $[(\eta^5\text{-}C_5H_5)Ru(\mathbf{Ph}_2P\{OC(CF_3)_3\})(NCCH_3)_2]^+$) ppm. Integration values for (η^5- C_5H_5) are out from the expected 5H, due to a longer relaxation delay being required in the NMR experiment for this sample.

Lower intensity signals were also observed at 2.50 (br), 2.53 (s), 4.26 (s), 4.82 (s), 5.13 (s) and 4.72 ppm.

$^{31}P\{^1H\}$ NMR (295 K, 161.8 MHz, $CDCl_3$):): δ_P = -143.0 (sept, $^1J_{PF}$ = 711 Hz, $[\mathbf{P}F_6]^-$), 167.2 (br, $[(\eta^5\text{-}C_5H_5)Ru(Ph_2\mathbf{P}\{OC(CF_3)_3\})(NCCH_3)_2]^+$), ppm.

^{19}F NMR (295 K, 376.2 MHz, CD_2Cl_2): δ_F = 72.95 (d, 6F, $^1J_{FP}$ = 711 Hz, $[P\mathbf{F}_6]^-$), -70.43 (s, $[(\eta^5\text{-}C_5H_5)Ru(Ph_2P\{OC(C\mathbf{F}_3)_3\})(NCCH_3)_2]^+$) ppm.

A lower intensity peaks was also observed at -69.46 (d, J = 2 Hz) ppm.

^{13}C NMR (295 K, 100.5 MHz, $CDCl_3$): δ_C = 3.44 (s, [(η^5-C_5H_5)Ru(Ph_2P{$OC(CF_3)_3$})($NC\mathbf{C}H_3)_2$]$^+$), 79.35 (d, $^2J_{CP}$ = 3 Hz, [(η^5-$\mathbf{C}_5H_5$)Ru(Ph_2P{$OC(CF_3)_3$})($NCCH_3)_2$]$^+$), 119.5 (q, $^1J_{CF}$ = 292 Hz, [(η^5-C_5H_5)Ru(Ph_2P{$OC(\mathbf{C}F_3)_3$})($NCCH_3)_2$]$^+$), 127.9 (d, $^3J_{CP}$ = 11 Hz, phenyl-c), 130.9 (d, $^2J_{CP}$ = 16 Hz), 128.7 (s, [(η^5-C_5H_5)Ru(Ph_2P{$OC(CF_3)_3$})($N\mathbf{C}CH_3)_2$), 129.8 (d, $^3J_{CP}$ = 12 Hz), 130.9 (d, $^2J_{CP}$ = 16 Hz, phenyl-b), 133.4 (d, $^1J_{CP}$ = 58 Hz, phenyl-a) 134.1 (d, $^4J_{CP}$ = 2 Hz, phenyl-d) ppm.

The NMR spectra of this material also showed the presence of a small amount of vacuum grease, triethylamine and MeCN.

EI-MS (MeCN): m/z observed mass = 669.0269, $[M]^+$, (calculated mass 669.0292 m/z , for [(η^5-C_5H_5)^{102}Ru{$Ph_2POC(CF_3)_3$}($NCCH_3)_2$]$^+$, 2.9 ppm), m/z observed mass = 144.9638, $[M]^-$ (calculated mass 144.9647 m/z, for $[PF_6]^-$, 6.6 ppm).

Single-Crystal X-ray Diffraction Measurements: $C_{25}H_{21}F_{15}N_2OP_2Ru$, M = 813.45, monoclinic, crystal size/mm = 0.26 × 0.14 × 0.07, a = 20.3714(8) Å, b = 10.0333(3) Å, c = 15.0658(4) Å, β = 98.655(3)°, V = 3044.26(17) Å^3, T = 110.00(10) K, space group $P2_1/c$ (no. 14), Z = 4, μ(Mo Kα) = 0.736, ρ_{calc} mg/mm^3 = 1.775, 26610 reflections measured, 7116 unique (R_{int} = 0.0393) which were used in all calculations. The final wR_2 was 0.0895 (all data) and R_1 was 0.0422 (>2sigma(I)).

6.4.22 Synthesis of $[(\eta^5\text{-}C_5H_5)Ru(Ph_2P\{OC(CF_3)_2\})_2(CH_3CN)]^+[PF_6]^-$, **[Ru(6)-2]**

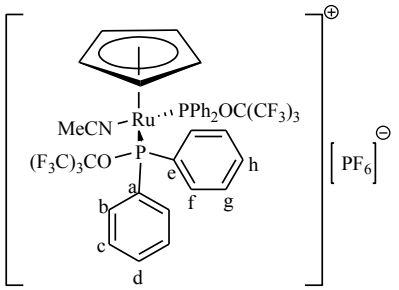

Tris(acetonitrile)(η^5-cyclopentadienyl)ruthenium(II) hexafluorophosphate, $[(\eta^5\text{-}C_5H_5)Ru(NCMe)_3][PF_6]^-$ (25 mg, 0.058 mmol, 1 eq.), deuterated CD_2Cl_2 (0.1 mL) and DCM (0.4 mL) were added to a PTFE J Young's tap NMR tube in an inert-atmosphere glovebox. Perfluoro-*t*-butoxydiphenylphosphinite ligand (49 mg, 0.116 mmol, 2 eq.) was added to this and the reaction was then monitored by $^{31}P\{^1H\}$ NMR spectroscopy to follow the reaction. The reaction mixture was then layered with hexane and left to crystallise. The mother liquor was removed (any free ligand is removed this way) *via* a canula transfer and remaining crystalline material was then washed with hexane, followed by another canula transfer to remove any solvent. The crystalline product in the NMR tube was then dried *in vacuo* (at 1.5 x 10^{-2} mbar, for 30 min. at room temperature) on the Schlenk line. The yellow crystalline product was treated as air-sensitive and stored in an inert-atmosphere glove box.

Yield: 30 mg (63 %)

^{1}H NMR (295 K, 400 MHz, CD_2Cl_2): δ_H = 1.97 (br, $[(\eta^5\text{-}C_5H_5)Ru(Ph_2P\{OC(CF_3)_3\})(NCC\mathbf{H_3})_2]^+$), 4.92 (br, $[(\eta^5\text{-}C_5\mathbf{H}_5)Ru(Ph_2P\{OC(CF_3)_3\})(NCCH_3)_2]^+$), 6.54-7.97 (m, $[(\eta^5\text{-}C_5H_5)Ru(\mathbf{Ph}_2P\{OC(CF_3)_3\})(NCCH_3)_2]^+$) ppm. Integration values are difficult to obtain as this sample is impure.

$^{31}P\{^1H\}$ NMR (295 K, 161.8 MHz, CD_2Cl_2):): δ_P= -143.0 (sept, $^1J_{PF}$ = 711 Hz, $[\mathbf{P}F_6]^-$), 184.6 (s, $[(\eta^5\text{-}C_5H_5)Ru(Ph_2\mathbf{P}\{OC(CF_3)_3\})_2(NCCH_3)]^+$) ppm.

A lower intensity signal at 135.7 (s) ppm was also present. This may indicate the presence of (**7**) in the NMR sample.

^{19}F NMR (295 K, 376.2 MHz, CD_2Cl_2): δ_F = -69.07 (s, $[(\eta^5\text{-}C_5H_5)Ru(Ph_2P\{OC(C\mathbf{F}_3)_3\})_2(NCCH_3)]^+$), -73.00 ppm.

^{13}C NMR (295 K, 100.5 MHz, CD_2Cl_2): δ_C = 3.8 (s, [(η^5-C_5H_5)Ru{$Ph_2POC(CF_3)_3$}$_2$($NC\mathbf{C}H_3$)]$^+$), 72.1 (m, [(η^5-C_5H_5)Ru{$Ph_2PO\mathbf{C}H(CF_3)_2$}$_2$($NCCH_3$)]$^+$), 84.9 (t, [($\eta^5$-$\mathbf{C}_5H_5$)Ru{$Ph_2POC(CF_3)_3$}$_2$($NCCH_3$)]$^+$), 120.0 (q, $^1J_{CF}$ = 294 Hz, [(η^5-C_5H_5)Ru{$Ph_2POC(\mathbf{C}F_3)_3$}$_2$($NCCH_3$)]$^+$), 128.7 (t, $^3J_{CP}$ = 5 Hz, η^5-C_5H_5)Ru{$Ph_2POC(CF_3)_3$}$_2$($N\mathbf{C}CH_3$)]$^+$) (129.2 (s, phenyl-c or -g), 129.3 (s, phenyl-c or -g), 130.7 (br, phenyl-b or -f), 131.0 (br, phenyl-b or -f), 132.7 (s, phenyl-d or -h), 133.1 (s, phenyl-d or -h), 132.8 (t, $^1J_{CP}$ = 8 Hz, phenyl-a or -e), 133.5 (s, phenyl-d or -h), 138.1 (t, $^1J_{CP}$ = 24 Hz, phenyl-a or -e), 133.9 (t, $^1J_{CP}$ = 8 Hz, phenyl-a or -e) ppm.

The NMR spectra of this material also showed the presence of uncoordinated $Ph_2P\{OC(CF_3)_3\}$, (**6**) ligand, trace amounts of the monosubstituted **[Ru(6)]** complex, a small amount of vacuum grease, DCM and hexane.

EI-MS (MeCN): m/z observed mass = 1048.0315, $[M]^+$, (calculated mass 601.0418 m/z , for [(η^5-C_5H_5)^{102}Ru{$Ph_2POC(CF_3)_3$}$_2$($NCCH_3$)$_2$]$^+$, 3.8 ppm), m/z observed mass = 144.9641 $[M]^-$ (calculated mass 144.9647 m/z, for $[PF_6]^-$, 4.5 ppm).

Single-Crystal X-ray Diffraction Measurements: $C_{79}H_{58}Cl_2F_{48}N_2O_4P_6Ru_2$, M = 2470.13, monoclinic, crystal size/mm = 0.28 × 0.21 × 0.14, a = 10.3645(4) Å, b = 20.080(5) Å, c = 21.6973(10) Å, β = 90.649(5)°, V = 4515.2(13) Å^3, T = 110.00(10) K, space group $P2_1$ (no. 4), Z = 2, μ(Mo Kα) = 0.650, ρ_{calc} mg/mm^3 = 1.817, 43684 reflections measured, 25200 unique (R_{int} = 0.0261) which were used in all calculations. The final wR_2 was 0.0785 (all data) and R_1 was 0.0332 (>2sigma(I)).

6.4.23 Synthesis of *trans*-Bis(perfluoro-*t*-butylphosphite) Rhodium(I) Carbonyl Chloride, $Rh(CO)Cl(P\{OC(CF_3)_3\}_3)_2$, **[Rh(2)-2]**

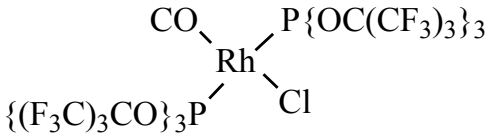

Di-μ-chloro-tetra-carbonyl dirhodium, $[Rh(CO)_2Cl]_2$ (19.44 mg, 0.05 mmol, 1 eq.) and CD_2Cl_2 (0.7 mL) were added to a PTFE J Young's tap NMR tube in an inert-atmosphere glovebox. To this, well ground tris(perfluoro-*t*-butyl)phosphite, $P\{OC(CF_3)_3\}_3$ (73.6 mg, 0.1 mmol, 2 eq.) was added. THF (0.4 mL) was added to increase the solubility of the phosphite ligand, followed by 30 min. ultrasonic activation at room temperature. The reaction mixture was then heated overnight at 50 ˚C. $^{31}P\{^1H\}$ NMR spectroscopy was used to monitor reaction completion. Further heating did not complete the conversion of this reaction, as uncoordinated ligand was still present in the NMR spectra.

$^{31}P\{^1H\}$ NMR (295 K, 161.8 MHz, $CDCl_3$): δ_P = 129.6 (br d, $^1J_{PRh}$ = 286 Hz, $Rh(CO)Cl(\mathbf{P}\{OC(CF_3)_3\}_3)$ ppm. Peaks are likely to be broad due to the fluorine coupling or possible ligand exchange.

^{19}F NMR (295 K, 376.2 MHz, $CDCl_3$): δ_F = -70.57 (br, $Rh(CO)Cl(\mathbf{P}\{OC(CF_3)_3\}_3)$ ppm.

The NMR spectra of this material also showed the presence of free $P\{OC(CF_3)_3\}_3$ ligand and $[(CH_3CH_2)_3NH]^+[OC(CF_3)_3]^-$ from the ligand synthesis.

IR (solution cell in CH_2Cl_2): $\nu_{(CO)}[cm^{-1}]$: 2075.

6.4.24 Synthesis of *trans*-Bis{di(perfluoro-*t*-butoxy)phenylphosphonite} Rhodium (1) Carbonyl Chloride, $Rh(CO)Cl(PPh\{OC(CF_3)_3\}_2)_2$, **[Rh(4)-2]**

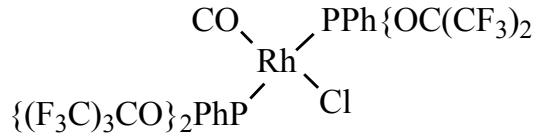

Di-μ-chloro-tetra-carbonyl dirhodium, $[Rh(CO)_2Cl]_2$ (19.44 mg, 0.05 mmol, 1 eq.) and CD_2Cl_2 (0.7 mL) were added to a PTFE J Young's tap NMR tube in an inert-atmosphere glovebox. To this, bis(perfluoro-*t*-butoxy)phenylphosphonite, $PPh\{OC(CF_3)_3\}_2$, (60 mg, 0.1 mmol, 2 eq.) was added. The red $[Rh(CO)_2Cl]_2$ solution turned orange instantly, and bubbles were observed, indicating that the reaction had occurred. The reaction mixture was then layered with hexane and left to crystallise. The mother liquor was removed *via* a canula transfer on the Schlenk line. The crystalline material was then washed with hexane, followed by another canula transfer to remove the solvent. The crystalline product in the NMR tube was dried *in vacuo* (1.5×10^{-2} mbar, for 30 min. at room temperature) on the Schlenk line. The orange crystalline product was treated as air-sensitive and stored in an inert-atmosphere glove box.

^{1}H NMR (295 K, 500 MHz, $CDCl_3$): δ_H = 7.36-8.22 (m, $Rh(CO)Cl(\mathbf{Ph}P\{OC(CF_3)_3\}_2)$ ppm.

$^{31}P\{^1H\}$ NMR (295 K, 500MHz, CD_2Cl_2): δ_P = 160.8 (br d, $^1J_{PRh}$ = 285 Hz, $Rh(CO)Cl(Ph\mathbf{P}\{OC(CF_3)_3\}_2)$ ppm. Peaks are likely to be broad due to fluorine coupling.

A peak at 9.2 (s) ppm was also observed.

The NMR sample of this material also contained free $PPh\{OC(CF_3)_3\}_2$ ligand and residual $[(CH_3CH_2)_3NH]^+[OC(CF_3)_3]^-$ the ligand synthesis.

IR (solution cell in CH_2Cl_2): $\nu_{(CO)}[cm^{-1}]$: 2035.

6.4.25 Synthesis of *trans*-Bis{di(perfluoro-*t*-butoxy)diphenylphosphinite} Rhodium(I) Carbonyl Chloride, $Rh(CO)Cl(PPh_2\{OC(CF_3)_3\})_2$, **[Rh(6)-2]**

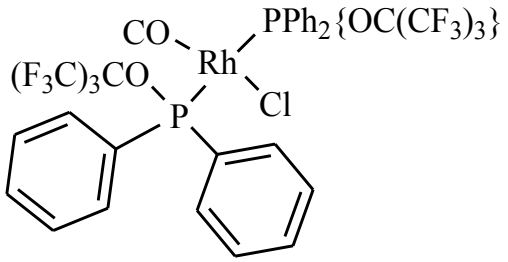

Di-μ-chloro-tetra-carbonyl dirhodium, $[Rh(CO)_2Cl]_2$ (19.44 mg, 0.05 mmol, 1 eq.) and CD_2Cl_2 (0.7 mL) were added to a PTFE J Young's NMR NMR tube in an inert-atmosphere glovebox. To this, di(perfluoro-*t*-butoxy)diphenyl phosphinite, $PPh_2\{OC(CF_3)_3\}$ (42 mg, 0.1 mmol, 2 eq.) was added. The red $[Rh(CO)_2Cl]_2$ solution turned orange instantly, and bubbles were observed, indicating that the reaction had occurred. The reaction mixture was then layered with hexane and left to crystallise. The mother liquor was removed *via* a canula transfer on the Schlenk line. The crystalline material was then washed with hexane, followed by another canula transfer to remove the solvent. The crystalline product in the NMR tube was dried *in vacuo* (1.5 x 10^{-2} mbar, for 30 min. at room temperature) on the Schlenk line. The orange crystalline product was treated as air-sensitive and stored in an inert-atmosphere glove box. Note, very few crystals grown were used for XRD and elemental analysis; hence the spectroscopic NMR analysis presented is before pure product is obtained *via* crystallisation.

^{1}H NMR (295 K, 400 MHz, $CDCl_3$): δ_H = 6.94-7.76 (m, Rh(CO)Cl(**Ph**$_2$P{$OC(CF_3)_3$}) ppm.

^{31}P{^{1}H} NMR (295 K, 161.8 MHz, $CDCl_3$): δ_P = 142.3 (br d, $^1J_{PRh}$ = 154 Hz, [Rh(CO)Cl(Ph_2**P**{$OC(CF_3)_3$}$_2$]) ppm. Peaks are likely to be broad due to fluorine coupling or possible ligand exchange.

Other peaks were observed at 37.9 (s, **P**Ph_2O**P**Ph_2), 22.6 (s, Ph_2**P**(O)H) ppm

^{19}F NMR (295 K, 376.2 MHz, $CDCl_3$): δ_F = -69.55 (br, Rh(CO)Cl(Ph_2P{$OC(C$**F**$_3)_3$}) ppm.

Other peaks were observed at -78.20 (br), -75.01 (br) and -71.23 (s) ppm.

The NMR spectra of this material also showed the presence of free $PPh_2\{OC(CF_3)_3\}$ ligand and DCM.

IR (CH_2Cl_2 solution): $\nu_{(CO)}$[cm^{-1}]: 2009.

EI-MS (MeCN): ($[Rh(CO)Cl(Ph_2P\{OC(CF_3)_3\})_2].NCCH_3$:$[M]^+$, observed mass 1047.91m/z.

Elemental Analysis: $RhCOCl(Ph_2P\{OC(CF_3)_3\})_2$: calculated. C(39.37) H(2.00), observed C(39.52) H(2.07).

Single-Crystal X-ray Diffraction Measurements: $C_{33}H_{20}ClF_{18}O_3P_2Rh$, M = 1006.79, tetragonal, crystal size/mm = 0.22 × 0.14 × 0.07, a = 26.6340(6) Å, c = 10.4926(4) Å, U = 7443.1(9) Å^3, T = 110.0 K, space group $P4_2/n$ (no. 86), Z = 8, μ(Mo Kα) = 0.742, ρ_{calc} mg/mm^3 = 1.797, 30074 reflections measured, 11662 unique (R_{int} = 0.0300) which were used in all calculations. The final $wR(F_2)$ was 0.0645 (all data) and R_1 was 0.0306, (>2sigma(I)).

6.4.26 Synthesis of Dibenzylideneacetone Bis(bis(hexafluoroisopropoxy phenylphosphonite) Palladium, [(dba)Pd(PhP{OCH(CF_3)$_2$}$_2$)$_2$], **[Pd(3)-2]**

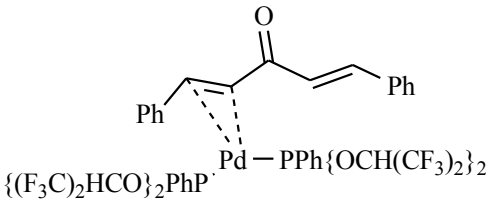

$Pd_2(dba)_3$ (46 mg, 0.05 mmol, 1 eq.) and deuterated toluene, C_7D_8 (0.6 mL) were added to a PTFE J Young's tap NMR tube in an inert-atmosphere glovebox. To this, bis(hexafluoroisopropoxy)phenyl phosphonite (88 mg, 0.20 mmol, 4 eq.) was added and immediately analysed using NMR spectroscopy. The solution changes from a deep red colour to a dark green, which indicates the reaction has occurred. The solution was treated as air- and light-sensitive and stored in an inert-atmosphere glove box in the dark. However, even in these conditions for periods longer than 3 weeks, the solution turned black in colour and no product was observed *via* $^{31}P\{^1H\}$ NMR spectroscopy.

^{1}H NMR (295 K, 500 MHz, toluene-d$_8$): δ_H = 4.48 (br, [(dba)Pd(PhP{OC**H**(CF_3)$_2$}$_2$)$_2$]), 6.81 -7.84(m, [(**dba**)Pd(**Ph**P{OCH(CF_3)$_2$}$_2$)$_2$]) ppm. The coordinated alkene protons from the dba ligand are presumably fluxional and are not observed.

$^{31}P\{^1H\}$ NMR (295 K, 202.5 MHz, toluene-d$_8$): δ_P = 183.4 (s, [(dba)Pd(PhP{OC**H**(CF_3)$_2$}$_2$)$_2$]) ppm.

^{19}F NMR (295 K, 376.2MHz, toluene-d$_8$): δ_F = -73.23 (br, [(dba)Pd(PhP{OCH(C**F**$_3$)$_2$}$_2$)$_2$]) ppm.

Other peaks were observed at -73.81 (d, J = 5.7 Hz), -75.97 (d) and -71.23 (d, J = 5.8 Hz) ppm.

The NMR sample of this material also contained free PPh{OCH(CF_3)$_2$} ligand, vacuum, grease, $[(CH_3CH_2)_3NH]^+[OCH(CF_3)_2]^-$ and diethyl ether solvent.

LIFDI-MS (MeCN): [^{106}(dba)Pd(PhP{OCH(CF_3)$_2$}$_2$)$_2$]: $[M]^+$: calculated mass 1224.06, m/z, observed mass 1224.01 m/z.

6.4.27 Synthesis of Dibenzylideneacetone Bis(hexafluoroisopropoxy diphenylphosphinite) Palladium, [(dba)Pd{$Ph_2POCH(CF_3)_2\}_2$], **[Pd(5)-2]**

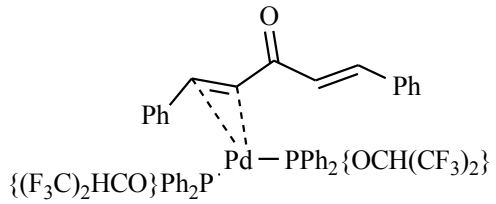

Tris(dibenzylideneacetone)palladium, $Pd_2(dba)_3$ (46 mg, 0.05 mmol, 1 eq.) and deuterated toluene, C_7D_8 (0.6 mL) were added to a PTFE J Young's tap NMR tube in an inert-atmosphere glovebox. To this, hexafluoroisopropoxydiphenylphosphinite (71 mg, 0.20 mmol, 4 eq.) was added and the mixture immediately analysed using NMR spectroscopy. The solution changes from a deep red colour to a dark green, which indicates the reaction has occurred. The solution was treated as air- and light-sensitive and stored in an inert-atmosphere glove box in the dark. However, even in these conditions for periods longer than 3 weeks, the solution turned black in colour and no product was observed *via* $^{31}P\{^1H\}$ NMR spectroscopy.

^{1}H NMR (295 K, 500 MHz, toluene-d_8): δ_H = 4.66 (br, [(dba)Pd{$Ph_2POCH(CF_3)_2\}_2$]) , 6.70-8.20 (m, [(**dba**)Pd{$\mathbf{Ph}_2POCH(CF_3)_2\}_2$]) ppm. The coordinated alkene protons from the dba ligand are presumably fluxional and are not observed.

$^{31}P\{^1H\}$ NMR (295 K, 202.5 MHz, toluene-d_8): δ_P = 150.2 (s, [(dba)Pd{$Ph_2\mathbf{P}OCH(CF_3)_2\}_2$]) ppm.

Other peaks were observed at -22.07 (s), -20.89 (s), 38.02 (s), 39.19 (s) and 40.08(s) ppm.

^{19}F NMR (295 K, 376.2 MHz, toluene-d_8): δ_F = -73.23 (br, [(dba)Pd{$Ph_2POCH(C\mathbf{F}_3)_2\}_2$]) ppm.

Other peaks were observed at -75.97 (d), -73.81 (d, J = 5.7 Hz), and -71.23 (d, J = 5.8 Hz) ppm.

The NMR spectra of this material also showed the presence of free $PPh_2\{OCH(CF_3)_2\}$ ligand, vacuum, grease, $[(CH_3CH_2)_3NH]^+[OCH(CF_3)_2]^-$ and diethyl ether.

LIFDI-MS (MeCN): [^{106}(dba)Pd{$Ph_2POCH(CF_3)_2\}_2$]: $[M]^+$: calculated mass 1044.1000 m/z, observed mass 1044.1194 m/z.

6.4.28 Synthesis of [1,1-Diphenyl-1-hexafluoroisopropoxy-1-methyl phosphonium Triflate, $[Ph_2P\{OCH(CF_3)_2\}Me]^+ [F_3CS(O)_2O]^-$, (**10**)

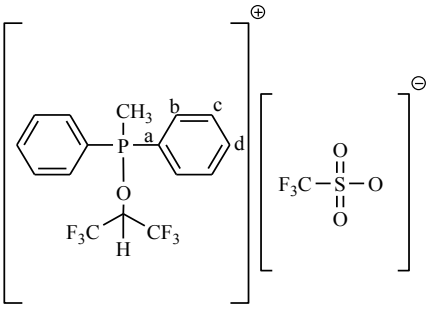

To 5 mL DCM in a Schlenk tube, hexafluoroisopropoxydiphenylphosphinite (352 mg, 1 mmol, 1 eq.) and methyl triflate (164 mg, 1 mmol, 1 eq.) were added in an inert-atmosphere glovebox. The DCM was removed *in vacuo* (10^{-2} mbar) and the solid material was washed with diethyl ether to remove any remaining free ligand. The solid was then dissolved in 2 mL DCM and layered with 5 mL hexane to crystallise *via* slow diffusion. A canula transfer was used to remove the mother liquor followed by a hexane wash (5 mL) and another canula transfer. The product was a colourless solid and was treated as air-sensitive and was stored in an inert-atmosphere glove box.

Yield: 150 mg (17 %)

^{1}H NMR (295 K, 400 MHz, CD_2Cl_2): δ_H = 3.06 (d, 3H, $[Ph_2P\{OCH(CF_3)_2\}\mathbf{Me}]^+$), 6.20 (m, 1H, $[Ph_2P\{O\mathbf{C}H(CF_3)_2\}Me]^+$), 7-47 – 8.10 (m, 10H, $[\mathbf{Ph}_2P\{OCH(CF_3)_2\}Me]^+$) ppm.

^{31}P{^{1}H} NMR (295 K, 161.8 MHz, CD_2Cl_2): δ_P = 85.0 (s, $[Ph_2\mathbf{P}\{OCH(CF_3)_2\}Me]^+$) ppm.

^{19}F NMR (295 K, 376.2 MHz, CD_2Cl_2): δ_F = -73.63 (d, 6F, $^4J_{FP}$ = 5 Hz $[Ph_2P\{OCH(C\mathbf{F}_3)_2\}Me]^+$), -79.13 (s, 3F, $[\mathbf{F}_3CS(O)_2O]^-$) ppm.

^{13}C NMR (295 K, 100.5 MHz, CD_2Cl_2): δ_C = 10.0 (d, $[Ph_2P\{OCH(CF_3)_2\}\mathbf{Me}]^+$), 71.6 (sept of d, $^2J_{CF}$ = 36, $^2J_{CP}$ = 7 Hz, $[Ph_2P\{O\mathbf{C}H(CF_3)_2\}Me]^+$),117.8 (d, $^1J_{CP}$ = 107 Hz, phenyl-a), 120.3 (q, $^1J_{CF}$ = 320 Hz, $[F_3\mathbf{C}S(O)_2O]^-$), 119.5 (q, $^1J_{CF}$ = 284 Hz, $[Ph_2P\{OCH(\mathbf{C}F_3)_2\}Me]^+$), 130.1 (d, $^1J_{CP}$ = 14 Hz, phenyl-b), 132.6 (d, $^1J_{CP}$ = 13 Hz, phneyl-c), 136.9 (d, $^1J_{CP}$ = 3 Hz, phenyl-d) ppm.

The NMR spectra of this material also showed the presence of vacuum grease and DCM and diethyl ether.

Melting Point: 114 °C (DSC)

EI-MS (MeCN): m/z = observed 367.4, 883.8 m/z (calculated for $[Ph_2P\{OCH(CF_3)_2\}Me]^+$and $[Ph_2P\{OCH(CF_3)_2\}Me]_2^+[F_3CS(O)_2O]^-$, $[M]^+$ respectively), 148.9526, $[M]^-$ (calculated 148.9523 m/z for $[OS(O)_2CF_3]^-$, 2.0 ppm).

Elemental Analysis: [$MePPh_2OCH\{CF_3\}_2]^+[OS(O)_2CF_3]^-$, calculated C(39.54) H(2.73), observed C(39.43) H(2.96).

Single-Crystal X-ray Diffraction Measurements: $C_{17}H_{14}F_9O_4PS$, M = 516.31, monoclinic, crystal size/mm = 0.27 × 0.21 × 0.16, a = 14.9344(10) Å, b = 13.5845(4) Å, c = 20.668(2) Å, β = 100.855(10)°, U = 4118.1(5) Å^3, T = 110.0 K, space group $P2_1/c$ (no. 14), Z = 8, μ(Mo Kα) = 0.338, ρ_{calc} mg/mm^3 = 1.666, 18510 reflections measured, 10389 unique (R_{int} = 0.0214) which were used in all calculations. The final $wR(F_2)$ was 0.0911 (all data) and R_1 was 0.0388 (>2sigma(I)).

6.4.29 Synthesis of $[MePPh\{OCH(CF_3)_2\}_2]^+[OS(O)_2CF_3]^-$, **(11)**

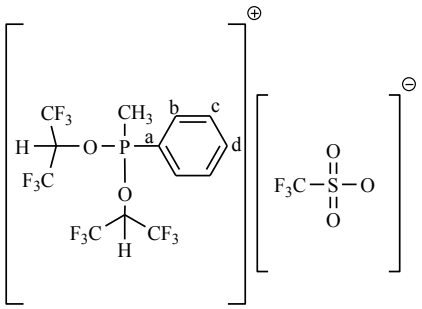

To 0.7 mL CD_2Cl_2 solvent in a Schlenk tube, bis(hexafluoroisopropoxy)phenylphosphonite, $PPh\{OCH(CF_3)_2\}_2$, (**3**) (88 mg, 0.20 mmol, 1 eq.) and methyl triflate, $MeOS(O)_2CF_3$ (33 mg, 0.20 mmol, 1 eq.) were added in an inert-atmosphere glovebox. The reaction mixture was heated (48 hr.at 50 °C). Removal of the CD_2Cl_2 solvent *in vacuo* (10^{-2} mbar) resulted in a clear oil.

^{1}H NMR (295 K, 400 MHz, CD_2Cl_2): δ_H = 3.22 (d, $^2J_{HP}$ = 13 Hz, $[\mathbf{Me}PPh\{OCH(CF_3)_2\}_2]^+$, 6.27 (m, $[MePPh\{OC\mathbf{H}(CF_3)_2\}_2]^+$), 7.01 – 8.30 (m, $[MeP\mathbf{Ph}\{OCH(CF_3)_2\}_2]^+$) ppm.

Signals are also observed at 1.18 (s), 1.25 (t, J = 7 Hz), 1.76 (d, J = 7 Hz), 1.91 (d, J = 8 Hz), 1.94 (d, J = 8 Hz), 2.19 (d, J = 4 Hz), 2.15 (d, J = 4 Hz), 2.15 (d, J = 16 Hz), 2.63 (d, J = 12 Hz), 2.88 (s), 3.06 (m), 3.77 (d, J = 12 Hz), 3.85 (s) ppm.

^{31}P{^{1}H} NMR (295 K, 161.8 MHz, CD_2Cl_2): δ_P = 92.4 (s, $[Me\mathbf{P}PH\{OCH(CF_3)_2\}_2$ ppm.

Signals were also observed at 24.8 (s, $Ph_2(O)\mathbf{P}H$), 32.7 (s, $Ph_2(O)\mathbf{PP}(O)Ph_2$), $]^+$), ppm.

^{19}F NMR (295 K, 376.2 MHz, CD_2Cl_2): δ_F = -79.32 (s, $[\mathbf{F}_3CS(O)_2O]^-$), -73.45 (m, $[MePPh\{OCH(C\mathbf{F}_3)_2\}_2]^+$), -73.70 (m, $[MePPh\{OCH(C\mathbf{F}_3)_2\}_2]^+$) ppm. Two environments were observed for each CF_3 group in the ^{19}F NMR, possibly indicating atropisomerism due to hindered rotation around either the P-O or O-C bond

^{13}C NMR (295 K, 100.5 MHz, CD_2Cl_2): δ_C = 9.0 (d, $[PhP\{OCH(CF_3)_2\}_2\mathbf{Me}]^+$), 71.3 (m, $[PhP\{O\mathbf{C}H(CF_3)_2\}_2Me]^+$),),116.5 (d, $^1J_{CP}$ = 143 Hz, phenyl-a), 119.9 (q, $^1J_{CF}$ = 290 Hz, $[PhP\{OCH(\mathbf{C}F_3)_2\}_2Me]^+$ and $[F_3\mathbf{C}S(O)_2O]^-$), 132.7 (d, $^1J_{CP}$ = 15 Hz, phenyl-b), 136.9 (d, $^1J_{CP}$ = 13 Hz, phneyl-c), 139.7 (d, $^1J_{CP}$ = 3 Hz, phenyl-d) ppm.

The NMR spectra of this material also showed the presence vacuum grease and free $PPh\{OCH(CF_3)_2\}$ ligand.

6.4.30 Synthesis of $[PPh_2\text{-}P\{OCH(CF_3)_2\}_3]^+[AlCl_4]^-$, (**12**)

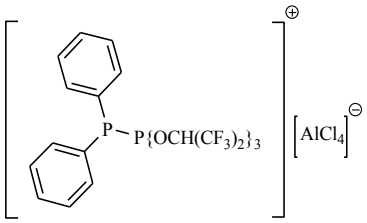

To 5 mL DCM in a J Young's ampoule, tris(hexafluoroisopropoxy)phosphite ligand (53 mg, 0.10 mmol, 1 eq.), chlorodiphenylphosphine (22 mg, 0.100 mmol, 1 eq.) and aluminium trichloride (66 mg, 0.50 mmol, 5 eq.) were added. Ultrasonic activation was used (room temperature, 1 hr.) to increase the solubility of the aluminium trichloride. Complete conversion of the chlorodiphenylphosphine was monitored by $^{31}P\{^1H\}$ NMR spectroscopy. The DCM was removed *in vacuo* (10^{-2} mbar) resulting in a transparent, pale-yellow oil.

^{1}H NMR (295 K, 400 MHz, $CDCl_{32}$): δ_H = 4.28 (m, 1H, $[PPh_2\text{-}P\{OC\mathbf{H}(CF_3)_2\}_3]^+$), 7.19-8.47 (m, 10H, **$[P\mathbf{Ph_2}\text{-}P\{OCH(CF_3)_2\}_3]^+$**) ppm.

$^{31}P\{^1H\}$ NMR (295 K, 161.8 MHz, $CDCl_3$): δ_P = -16.3 (d, $^1J_{PP}$ = 363 Hz, $[PPh_2\text{-}\mathbf{P}\{OCH(CF_3)_2\}_3]^+$), 87 (d, $^1J_{PP}$ = 370 Hz, $[\mathbf{P}Ph_2\text{-}P\{OCH(CF_3)_2\}_3]^+$) ppm.

Other peaks were observed at 1.1 (d, $^1J_{PP}$ = 393 Hz, $[PPh_2\text{-}\mathbf{P}Ph_2Cl]^+$, 41.6 (s, $\mathbf{P}Ph_2Cl\text{-}AlCl_3$, 66.2 (s, $\mathbf{P}\{OCH(CF_3)_2\}_3\text{-}AlCl_3$, 73.3 (d, $^1J_{PP}$ = 393 Hz, $[\mathbf{P}Ph_2\text{-}PPh_2Cl]^+$) ppm.

The NMR spectra of this material also showed the presence of free $P\{OCH(CF_3)_2\}_3$ ligand, sodium hexafluoroisopropoxide, DCM and a small amount of vacuum grease.

6.4.31 Synthesis of $[PPh_2\text{-}PPh\{OCH(CF_3)_2\}_2]^+[AlCl_4]^-$, (**13**)

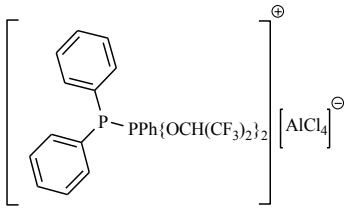

To 5 mL DCM in a Young's ampoule, bis(hexafluoroisopropoxy)phenylphosphinite (35 mg, 0.10 mmol, 1 eq.), chlorodiphenylphosphine (22 mg, 0.10 mmol, 1 eq.) and aluminium trichloride (66 mg, 0.50 mmol, 5 eq.) were added. Ultrasonic activation was used (room temperature, 1 hr.) to increase the solubility of the aluminium trichloride. Complete conversion of the chlorodiphenylphosphine was monitored by $^{31}P\{^1H\}$ NMR spectroscopy. The DCM was removed *in vacuo* (10^{-2} mbar), resulting in a transparent, pale-yellow oil.

^{1}H NMR (295 K, 400 MHz, $CDCl_{32}$): δ_H = 7.20-8.10 (m, **[P$\mathbf{Ph_2}$-P$\mathbf{Ph}$**$\{OCH(CF_3)_2\}_2]^+$) ppm.

$^{31}P\{^1H\}$ NMR (295 K, 161.8 MHz, $CDCl_3$): δ_P = 58.2 (d, $^1J_{PP}$ = 393 Hz [PPh_2-**P**$Ph\{OCH(CF_3)_2\}_2]^+$), 71.7 (d, $^1J_{PP}$ = 393 Hz [**P**Ph_2-$PPh\{OCH(CF_3)_2\}_2]^+$) ppm.

Other peaks were observed at 1.2 (d, $^1J_{PP}$ = 400 Hz, [PPh_2-**P**$Ph_2Cl]^+$, 41.5 (s, **P**Ph_2Cl-$AlCl_3$, 66.0 (s, **P**$Ph\{OCH(CF_3)_2\}_2$-$AlCl_3$), 73.4 (d, $^1J_{PP}$ = 376 Hz, [**P**Ph_2-$PPh_2Cl]^+$) ppm.

^{19}F NMR (295 K, 376.2 MHz, $CDCl_3$): δ_F = -71.06 (d, $^4J_{FP}$ = 9 Hz [PPh_2-$PPh\{OCH(C\mathbf{F}_3)_2\}_2]^+$).

Other peaks were also observed at -71.80 (d, J =7 Hz) and -71.50 (d, $^4J_{FP}$ = 6 Hz, $PPh\{OCH(C\mathbf{F}_3)_2\}_2$-$AlCl_3$) ppm.

The NMR spectra of this material also showed the presence of free $PPh\{OCH(CF_3)_2\}_2$ ligand, DCM and vacuum grease.

6.4.32 Synthesis of $[PPh_2\text{-}PPh_2\{OCH(CF_3)_2\}]^+[AlCl_4]^-$, (**14**)

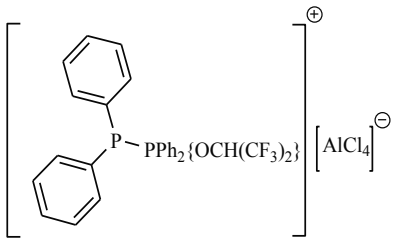

To 5 mL DCM in a Young's ampoule, hexafluoroisopropoxydiphenylphosphinite (35 mg, 0.10 mmol, 1 eq.), chlorodiphenylphosphine (22 mg, 0.10 mmol, 1 eq.) and aluminium trichloride (66 mg, 0.50 mmol, 5 eq.) were added. Ultrasonic activation was used (room temperature, 1 hr.) to increase the solubility of the aluminium trichloride. Complete conversion of the chlorodiphenylphosphine was monitored by $^{31}P\{^1H\}$ NMR spectroscopy. The DCM was removed *in vacuo* (10^{-2} mbar) resulting in a transparent, pale yellow oil.

^{1}H NMR (295 K, 400 MHz, $CDCl_3$): δ_H = 4.21 (sept, $^3J_{HF}$ = 5 Hz, **[**PPh_2-$PPh_2\{OC\mathbf{H}(CF_3)_2\}]^+$), 7.25-8.10 (m, **[**$P\mathbf{Ph_2}$-$P\mathbf{Ph}_2\{OCH(CF_3)_2\}]^+$) ppm.

$^{31}P\{^1H\}$ NMR (295 K, 161.8 MHz, $CDCl_3$): δ_P = -16.2 (d, $^1J_{PP}$ = 370 Hz, [PPh_2-$\mathbf{P}Ph_2\{OCH(CF_3)_2\}]^+$), 87.0 (d, (d, $^1J_{PP}$ = 364 Hz, [$\mathbf{P}Ph_2$-$PPh_2\{OCH(CF_3)_2\}]^+$) ppm.

Other lower intensity peaks were also observed at 1.1 (d, $^1J_{PP}$ = 393 Hz, $[PPh_2\text{-}\mathbf{P}Ph_2Cl]^+$, 66.0 (s, $\mathbf{P}Ph_2\{OCH(CF_3)_2\}$-$AlCl_3$) and 73.3 (d, $^1J_{PP}$ = 390 Hz, $[\mathbf{P}Ph_2\text{-}PPh_2Cl]^+$) ppm.

^{19}F NMR (295 K, 376.2 MHz, $CDCl_3$): δ_F = -72.70 (t, $^4J_{FP}$ = 6 Hz [PPh_2-$PPh_2\{OCH(C\mathbf{F}_3)_2\}]^+$).

Other lower intensity peak were also observed at -73.14 (d, J = 6 Hz), -72.79 (d, J = 6 Hz), -71.48 (d, J = 6 Hz), -71.04 (d, J = 6 Hz) ppm.

The NMR spectra of this material also showed the presence DCM, sodium hexafluoroisopropoxide and vacuum grease.

6.4.33 Synthesis of $[PPh_2\text{-}PPh_2\{OC(CF_3)_3\}]^+[AlCl_4]^-$, (**15**)

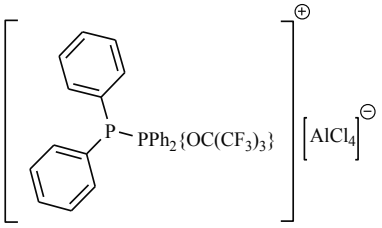

To 5 mL DCM in a Young's ampoule, perfluoro-*t*-butoxydiphenylphosphinite, (42 mg, 0.10 mmol, 1 eq.), chlorodiphenylphosphine (22 mg, 0.10 mmol, 1 eq.) and aluminium trichloride (66 mg, 0.50 mmol, 5 eq.) were added. Ultrasonic activation was used (room temperature, 1 hr.) to increase the solubility of the aluminium trichloride. Complete conversion of the chlorodiphenylphosphine was monitored by $^{31}P\{^1H\}$ NMR spectroscopy. The DCM was removed *in vacuo* (10^{-2} mbar) resulting in a transparent, pale-yellow oil.

^{1}H NMR (295 K, 400 MHz, $CDCl_{32}$): δ_H = 7.23-8.12 (m, **[P$\mathbf{Ph_2}$-P$\mathbf{Ph}_2${OC$(CF_3)_3$}]$^+$**) ppm.

$^{31}P\{^1H\}$ NMR (295 K, 161.8 MHz, $CDCl_3$): δ_P = -12.2 (d, $^1J_{PP}$ = 375 Hz, [PPh_2-**P**Ph_2{OC$(CF_3)_3$}]$^+$), 89.1 (d, (d, $^1J_{PP}$ = 375 Hz, [**P**Ph_2-PPh_2{OC$(CF_3)_3$}]$^+$) ppm.

Other lower intensity peaks were also observed at 1.1 (d, $^1J_{PP}$ = 393 Hz, [PPh_2-**P**$Ph_2Cl]^+$, 62.7 (s, **P**Ph_2{OC$(CF_3)_3$}-$AlCl_3$) and 73.4 (d, $^1J_{PP}$ = 393 Hz, [**P**Ph_2-$PPh_2Cl]^+$) ppm.

^{19}F NMR (295 K, 376.2 MHz, $CDCl_3$): δ_F = -70.13 (br, [PPh_2-PPh_2{OC(C**F**$_3)_3$}]$^+$).

A lower intensity peak was also observed at -69.78 (br, **P**Ph_2{OC$(CF_3)_3$}-$AlCl_3$) ppm.

The NMR spectra of this material also showed the presence DCM, sodium hexafluoroisopropoxide and vacuum grease.

6.4.34 Synthesis of Pentakis(hexafluoroisopropoxy)phosphorane, $P\{OCH(CF_3)_2\}_5$, **(16)**

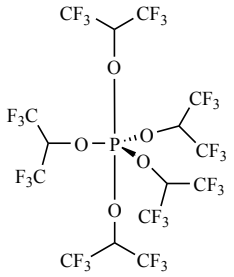

Phosphorus pentachloride (208 mg, 1 mmol, 1 eq.) and $NaOCH(CF_3)_2$ (950 mg, 5 mmol, 5 eq.) were added to an ampoule with DCM (10 mL) in an inert-atmosphere glovebox. Ultrasonic activation (room temperature, 1 hour) was used to increase the solubility of the $NaOCH(CF_3)_2$. The DCM was removed *in vacuo* (10^{-2} mbar) and the product redissolved in diethyl ether (10 mL). NMR spectroscopy was used to establish reaction completion. The reaction mixture was then filtered through Celite under an inert-atmosphere to remove NaCl. This filtrate was washed with 3 x 25 mL diethyl ether and was analysed by NMR spectroscopy to check the purity and for any hydrolysis of the products. The majority of the diethyl ether was removed *in vacuo* (10^{-2} mbar). The ampoule was then placed in a dewar filled with ethanol at room temperature and the dewar was placed in a refrigerator at 4 °C for crystallisation. The product was a white solid, treated as air-sensitive and stored in an inert-atmosphere glovebox. The crystals were air- and temperature-sensitive, stored at 4 °C.

Yield: 150 mg (17 %)

^{1}H NMR (295 K, 400 MHz, CD_2Cl_2): δ_H = 5.08 (br, $P\{OC\mathbf{H}(CF_3)_2\}_5$) ppm.

$^{31}P\{^{1}H\}$ NMR (295 K, 161.8 MHz, CD_2Cl_2): δ_P = -83.9 (s, $\mathbf{P}\{OCH(CF_3)_2\}_5$) ppm.

^{19}F NMR (295 K, 376.2 MHz, CD_2Cl_2): δ_F = -73.42 (br, $P\{OCH(C\mathbf{F}_3)_2\}_5$) ppm.

^{13}C NMR (295 K, 100.5 MHz, $CDCl_3$): δ_C = 74.23 (sept, $^{4}J_{CF}$ = 30 Hz, $P\{O\mathbf{C}H(CF_3)_2\}_5$), 120.8 (q, $^{1}J_{CF}$ = 288 Hz, $P\{OCH(\mathbf{C}F_3)_2\}_5$) ppm.

The NMR spectra of this material also showed the presence of vacuum grease and DCM and solvent.

ATR-IR: $\nu_{(CF)}$[cm^{-1}]: 1367, 1359, 1288, 1235, 1199, 1107.

EI-MS (Et_2O): m/z = 550.9535, $[M-\{OCH(CF_3)_2\}\{OCH(CF_3)CF_2\}]^+$ (calculated 550.9516 m/z for $[P\{OCH(CF_3)_2\}_3F]^+$, 3.4 ppm), 698.9491, $[M-OCH(CF_3)_2]^+$ (calculated 698.9464 m/z for $[P\{OCH(CF_3)_2\}_4]^+$, 3.9 ppm), 846.9412, $[M-F]^+$ (calculated 846.9412 m/z for $[P\{OCH(CF_3)_2\}_4\{OCH(CF_3)CF_2\}]^+$, 0.0 ppm).

Single-Crystal X-ray Diffraction Measurements: $C_{15}H_5F_{30}O_5P$, M = 866.16, triclinic, crystal size/mm = 0.09 × 0.06 × 0.04, a = 9.6035(8) Å, b = 10.6908(8) Å, c = 15.3222(9) Å, α = 77.230(6)°, β = 71.948(6)°, γ = 63.608(8)°, U = 1333.36(19) Å^3, T = 149.8 K, space group P-1 (no. 2), Z = 2, μ(Mo Kα) = 0.344, ρ_{calc} mg/mm^3 = 2.157, 5248 reflections measured, 4210 unique (R_{int} = 0.0181) which were used in all calculations. The final $wR(F_2)$ was 0.1133 (all data) and R_1 = 0.0493 (>2sigma(I)).

6.4.35 Synthesis of Tetrakis(acetonitrile)silver(I) monofluoropentakis-(hexafluoroisopropoxy)phosphate, $[Ag(NCMe)_4]^+[P\{OCH(CF_3)_2\}_5F]^-$, (**17**)

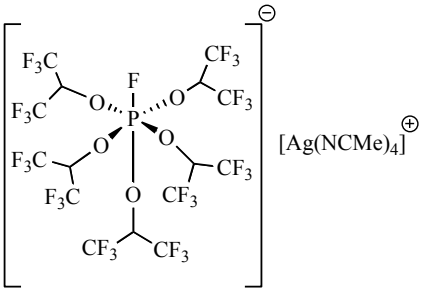

Phosphorus pentachloride (41 mg, 0.20 mmol, 1 eq.) and $NaOCH(CF_3)_2$ (190 mg, 1.0 mmol, 5 eq.) were added to an ampoule with DCM (10 mL) in an inert-atmosphere glovebox. Ultrasonic activation (room temperature, 1 hour) was used to increase the solubility of the $NaOCH(CF_3)_2$. NMR spectroscopy was used to establish reaction completion. The $P\{OCH(CF_3)_2\}_5$ reaction mixture was used *in situ;* AgF (26 mg, 0.20 mmol, 1 eq.) and MeCN (5 mL) were added, followed by further ultrasonic activation (room temperature, 1 hour). The reaction mixture was filtered through Celite under inert-atmosphere to remove the NaCl. The reaction mixture was washed with MeCN (20 mL) in the filtration step. Majority of the solvent was removed *in vacuo* (10^{-2} mbar), leaving ~ 2 mL solution. To this a hexane layer (5 mL) was added to aid crystallisation *via* slow diffusion of the solvents. However, the clear crystals were too fine and were not suitable for single-crystal X-ray diffraction. The product was treated as air-sensitive and stored in an inert-atmosphere glovebox.

^{1}H NMR (295 K, 400 MHz, CD_3Cl_3): δ_H = 4.77 (m, 1H, equatorial $[P\{OC\mathbf{H}(CF_3)_2\}_5F]^-$), 5.41 (m, 4H, axial $[P\{OC\mathbf{H}(CF_3)_2\}_5F]^-$) ppm.

^{31}P{^{1}H} NMR (295 K, 161.8 MHz, $CDCl_3$): δ_P = -147.4 ppm (d, $^1J_{PF}$ = 818 Hz, $[\mathbf{P}\{OCH(CF_3)_2\}_5F]^-$), -4.3 (s), -3.9 (s) ppm.

^{19}F NMR (295 K, 376.2 MHz, CD_2Cl_2): δ_F = -73.48 (s, equatorial $[P\{OCH(C\mathbf{F}_3)_2\}_5F]^-$), -73.25 (br, axial $[P\{OCH(C\mathbf{F}_3)_2\}_5F]^-$), -60.60 (d, 1F, $^1J_{FP}$ = 818 Hz, $[P\{OCH(CF_3)_2\}_5\mathbf{F}]^-$), ppm. Since the equatorial and axial peaks overlap, a combined integration was calculated to give 30F for the hexafluoroisopropoxy groups on the $[P\{OCH(C\mathbf{F}_3)_2\}_5F]^-$ anion.

Other weak intensity peaks present at -76.43 (d, $^3J_{FH}$ = 6 Hz, $NaOCH(C\mathbf{F}_3)_2$), -75.21 (d, J = 6 Hz) and -74.96 (s) ppm were also observed.

ESI-MS (MeCN): m/z observed mass = 109.9 $[M]^+$ for $[Ag]^+$, 885.0 $[M]^-$ for $[P\{OCH(CF_3)_2\}_5F]^-$.

6.4.36 Synthesis of Hexakis(acetonitrile)sodium(I) monofluoropentakis-(hexafluoroisopropoxy)phosphate, $[Na(NCMe)_6]^+[P\{OCH(CF_3)_2\}_5F]^-$ (**18**)

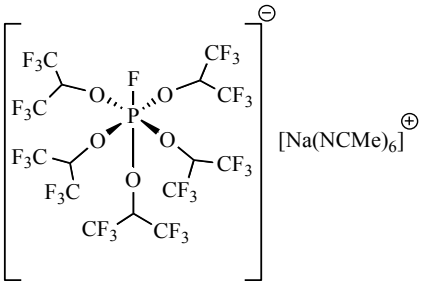

Phosphorus pentachloride (41 mg, 0.20 mmol, 1 eq.) and $NaOCH(CF_3)_2$ (190 mg, 1.0 mmol, 5 eq.) were added to an ampoule with DCM (10 mL) in an inert-atmosphere glovebox. Ultrasonic activation (room temperature, 1 hour) was used to increase the solubility of the $NaOCH(CF_3)_2$. NMR spectroscopy was used to establish reaction completion. The $P\{OCH(CF_3)_2\}_5$ reaction mixture was used *in situ*; NaF (8 mg, 0.20 mmol, 1 eq.) and MeCN (5 mL) were added, followed by further ultrasonic activation (room temperature, 1 hour). The reaction mixture was filtered through Celite under inert-atmosphere to remove the NaCl. The reaction mixture was washed with MeCN (20 mL) in the filtration step. The majority of the MeCN was removed *in vacuo* (10^{-2} mbar), leaving ~ 2 mL solution. To this a hexane layer (5 mL) was added to aid crystallisation *via* slow diffusion of the solvents. However, the clear crystals were too fine and were not suitable for single-crystal X-ray diffraction. The product was treated as air-sensitive and stored in an inert-atmosphere glovebox.

^{1}H NMR (295 K, 400 MHz, $CDCl_3$): δ_H = 4.78 (m, 24F, equatorial $[P\{OC\mathbf{H}(CF_3)_2\}_5F]^-$), 4.92 (m, 6F, axial $[P\{OC\mathbf{H}(CF_3)_2\}_5F]^-$) ppm.

A peak at 4.20 ppm (m, $NaOC\mathbf{H}(CF_3)_2\}_5$) was also observed.

^{31}P{^{1}H} NMR (295 K, 161.8 MHz, $CDCl_3$): δ_P = -147.7 (d, $^1J_{PF}$ = 818 Hz, $[\mathbf{P}\{OCH(CF_3)_2\}_5F]^-$) ppm.

Peaks were also observed at -147.1 (s, $[\mathbf{P}\{OCH(CF_3)_2\}_6]^-$), -84.0 (s, $\mathbf{P}\{OCH(CF_3)_2\}_5$), -4.5 (s, $O{=}\mathbf{P}\{OCH(CF_3)_2\}_3$) ppm.

^{19}F NMR (295 K, 376.2 MHz, $CDCl_3$): δ_F = -73.00 (br, axial $[P\{OCH(C\mathbf{F}_3)_2\}_5F]^-$), -72.75 (s, equatorial $[P\{OCH(C\mathbf{F}_3)_2\}_5F]^-$), -60.21 (d, 1F, $^1J_{FP}$ = 818 Hz, $[P\{OCH(CF_3)_2\}_5\mathbf{F}]^-$), ppm. Since the equatorial and axial peaks overlap, a combined integration was calculated to give 30F for the hexafluoroisopropoxy groups on the $P\{OCH(C\mathbf{F}_3)_2\}_5F]^-$ anion.

Peaks were also observed at -81.15 (s), -76.02 (br, $NaOCH(C\mathbf{F}_3)_2$), -74.75 (s), -73.23(s), -70.99 (s) ppm.

The NMR spectrum of this sample also contained a small amount of vacuum grease and DCM.

ESI-MS (CH_2Cl_2): m/z observed mass = 884.9421, $[M]^-$ (calculated 884.9385 m/z for $P\{OCH(CF_3)_2\}_5F]^-$, -4.1 ppm), m/z observed mass = 1032.9392 $[M]^-$ (calculated 1032.9333 m/z for $P\{OCH(CF_3)_2\}_6]^-$, -5.7 ppm).

6.4.37 Synthesis of Tris(triphenylphosphine)silver(I) monofluoropentakis-(hexafluoroisopropoxy)phosphate, $[Ag(PPh_3)_3]^+[P\{OCH(CF_3)_2\}_5F]^-$, **(19)**

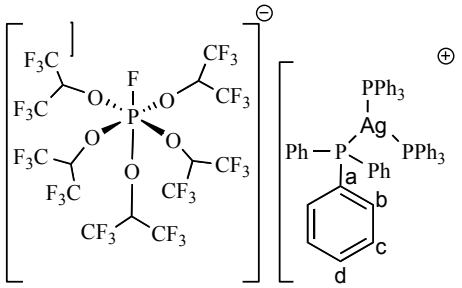

Phosphorus pentachloride (41 mg, 0.20 mmol, 1 eq.) and $NaOCH(CF_3)_2$ (190 mg, 0.20 mmol, 5 eq.) were added to an ampoule with DCM (10 mL) in an inert-atmosphere glovebox. Ultrasonic activation (room temperature, 1 hour) was used to increase the solubility of the $NaOCH(CF_3)_2$. NMR spectroscopy was used to establish reaction completion. The $P\{OCH(CF_3)_2\}_5$ reaction mixture was used *in situ*; AgF (26 mg, 0.20 mmol, 1 eq.) and PPh_3 (157 mg, 0.60 mmol, 3 eq.) were added to this, followed by further ultrasonic activation (room temperature, 1 hour). The reaction mixture was filtered through Celite under inert-atmosphere to remove the NaCl. The reaction mixture was washed with DCM (20 mL) in the filtration step. The majority of the DCM was removed *in vacuo* (10^{-2} mbar) followed by the addition of a hexane layer (5 mL) to aid crystallisation *via* slow diffusion of the solvents. The product was a white solid, treated as air-sensitive and stored in an inert-atmosphere glovebox.

Yield: 300 mg (84 %)

^{1}H NMR (295 K, 400 MHz, CD_2Cl_2): δ_H = 5.08 (m, 4H, equatorial $[P\{OC\mathbf{H}(CF_3)_2\}_5F]^-$), 5.21 (m, 1H, axial $[P\{OC\mathbf{H}(CF_3)_2\}_5F]^-$), 6.88 -7.70 (m, 45H, $[Ag(P\mathbf{Ph}_3)_3]^+$), ppm.

^{31}P{^{1}H} NMR (295 K, 161.8 MHz, CD_2Cl_2): δ_P = -147.5 (d, $^1J_{PF}$ = 818 Hz, $[\mathbf{P}\{OCH(CF_3)_2\}_5F]^-$), 11.5 (s, $[Ag(\mathbf{P}Ph_3)_3]^+$) ppm.

^{19}F NMR (295 K, 376.2 MHz, CD_2Cl_2): δ_F = -73.10 (br , axial $[P\{OCH(C\mathbf{F}_3)_2\}_5\mathbf{F}]^-$), -72.83 (s, equatorial $[P\{OCH(C\mathbf{F}_3)_2\}_5F]^-$), -59.85 (d, 1F, $^1J_{FP}$ = 818 Hz, $[P\{OCH(CF_3)_2\}_5\mathbf{F}]^-$) ppm. Since the equatorial and axial peaks overlap, a combined integration was calculated to give 30F for the hexafluoroisopropoxy groups on the $[P\{OCH(C\mathbf{F}_3)_2\}_5F]^-$ anion.

A weak intensity peak at -73.83 (d, J = 58.6 Hz) ppm was also observed.

^{13}C NMR (295 K, 100.5 MHz, CD_2Cl_2): δ_C = 71.86 (m, [P{O**C**H(CF_3)$_2$}$_5$F]$^-$), 122.9 (q, $^1J_{CF}$ =290 Hz, [P{OCH(**C**F_3)$_2$}$_5$F]$^-$), 129.8 (d, $^2J_{PF}$ = 10 Hz, phenyl-c), 131.1(d, $^1J_{PF}$ = 30 Hz, phenyl-a), 131.5 (s, phenyl-d) 134.1 (d, $^3J_{PF}$ = 16 Hz, phenyl-b), ppm.

Peaks at -76.86 (d, J = 7 Hz),-74.64 (d, J = 6 Hz),) and -73.50 (d, J = 6 Hz) ppm were also observed.

The NMR spectra of this material also showed the presence of vacuum grease.

ESI-MS (CH_2Cl_2): m/z = 631.0842 $[M]^+$ (calculated 631.0868 m/z for $[^{109}Ag(PPh_3)_2]^+$ 4.5 ppm), 884.9414, $[M]^-$ (calculated 884.9385 m/z P{OCH(CF_3)$_2$}$_5$F]$^-$, -3.3 ppm).

Elemental Analysis: $[Ag(PPh_3)_3]^+$[P{OCH(CF_3)$_2$}$_5$F]$^-$ calculated; C(46.57), H(2.83), observed; C(46.68), H(3.15).

Single-Crystal X-ray Diffraction Measurements: $C_{69}H_{50}AgF_{31}O_5P_4$, M = 1779.84, monoclinic, crystal size/mm = 0.19 × 0.16 × 0.09, a = 20.6438(10) Å, b = 17.9725(18) Å, c = 19.262(3) Å, β = 97.128(9)°, U = 7091.3(13) Å^3, T = 110.00(14) K, space group $P2_1/c$ (no. 14), Z = 4, μ(Mo Kα) = 0.507, ρ_{calc} mg/mm^3 = 1.667, 31419 reflections measured, 18980 unique (R_{int} = 0.0283) which were used in all calculations. The final $wR(F_2)$ was 0.0901 (all data) and R_1 was 0.0390 (>2sigma(I)).

6.4.38 Synthesis of Silver Tris(trimethylphosphine)silver(I) monofluoropentakis-(hexafluoroisopropoxy)phosphate, $[Ag(PMe_3)_3]^+[P\{OCH(CF_3)_2\}_5F]^-$, (**20**)

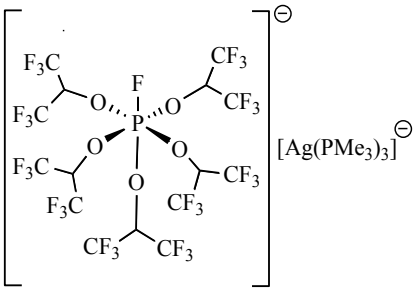

Phosphorus pentachloride (41 mg, 0.20 mmol, 1 eq.) and $NaOCH(CF_3)_2$ (190 mg, 1.0 mmol, 5 eq.) were added to a J Young's ampoule with DCM (10 mL) in an inert-atmosphere glovebox. Ultrasonic activation (room temperature, 1 hour) was used to increase the solubility of the $NaOCH(CF_3)_2$. NMR spectroscopy was used to establish reaction completion. The $P\{OCH(CF_3)_2\}_5$ reaction mixture was used *in situ*; AgF (26 mg, 0.20 mmol, 1 eq.) and PMe_3 (47 mg, 0.60 mmol, 3 eq.) were added, followed by further ultrasonic activation (room temperature, 1 hour). The reaction mixture was filtered through Celite under inert atmosphere to remove the NaCl. The reaction mixture was washed with DCM (20 mL) in the filtration step. The majority of the DCM was removed *in vacuo* (10^{-2} mbar), leaving ~ 2 mL solution. To this a hexane layer (5 mL) was added to aid crystallisation *via* slow diffusion of the solvents. However, the crystals were not suitable for single-crystal X-ray diffraction. The product was a white solid, treated as air-sensitive, and stored in an inert-atmosphere glovebox.

^{1}H NMR (295 K, 400 MHz, $CDCl_3$): δ_H = 1.52 (m, $[Ag(P\mathbf{Me}_3)_3)]^+$), 2.69 (m, $[Ag(P\mathbf{Me}_3)_3)]^+$), 4.45 (m, $[P\{OC\mathbf{H}(CF_3)_2\}_5F]^-$) ppm.

^{31}P{^{1}H} NMR (295 K, 161.8 MHz, $CDCl_3$): δ_P = -147.5 (d, $^1J_{PF}$ = 818 Hz, $[\mathbf{P}\{OCH(CF_3)_2\}_5F]^-$), -49.1 (s, $[Ag(\mathbf{P}Me_3)_3)]^+$) ppm.

Lower intensity peaks were observed at -4.5 (br, $O{=}P\{OCH(CF_3)_2\}_3$, 24.2 (s), 31.2 (s), 33.8 (s), 42.7 (s), 43.6 (s), 46.5 (s), 47.0 (s) ppm.

^{19}F NMR (295 K, 376.2 MHz, $CDCl_3$): δ_F = -73.00 (br, axial $[P\{OCH(C\mathbf{F}_3)_2\}_5F]^-$), -72.70 (s, equatorial $[P\{OCH(C\mathbf{F}_3)_2\}_5F]^-$), -60.07 (d, 1F, $^1J_{FP}$ = 818 Hz, $[P\{OCH(CF_3)_2\}_5\mathbf{F}]$), ppm. Since the equatorial and axial peaks overlap, a combined integration was calculated to give 30F for the hexafluoroisopropoxy groups on the $P\{OCH(C\mathbf{F}_3)_2\}_5F]^-$ anion.

Lower intensity peaks were observed at -83.57 (s), -81.37, (s), -78.31 (s), -75.73 (br, $NaOCH(CF_3)_2$), -74.75 (br), -73.64 (br) and -71.02 ppm.

The NMR spectrum of this sample also contained a small amount of vacuum grease and DCM.

ESI-MS (CH_2Cl_2): m/z = 884.9377, $[M]^-$ (calculated 884.9385 m/z $P\{OCH(CF_3)_2\}_5F]^-$, 1.1 ppm).

6.4.39 Synthesis of Tris(triisoproylphosphine)silver(I) monofluoro,pentakis-(hexafluoroisopropoxy)phosphate, $[Ag(P^iPr_3)_3]^+[P\{OCH(CF_3)_2\}_5F]^-$, (**21**)

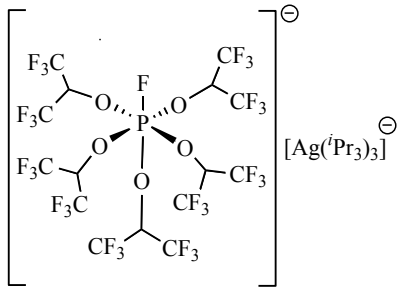

Phosphorus pentachloride (41 mg, 0.20 mmol, 1 eq.) and $NaOCH(CF_3)_2$ (190 mg, 1.0 mmol, 5 eq.) were added to a J Young's ampoule with DCM (10 mL) in an inert-atmosphere glovebox. Ultrasonic activation (room temperature, 1 hour) was used to increase the solubility of the $NaOCH(CF_3)_2$. NMR spectroscopy was used to establish reaction completion. The $P\{OCH(CF_3)_2\}_5$ reaction mixture was used *in situ*; AgF (26 mg, 0.20 mmol, 1 eq.) and P^iPr_3 (96 mg, 0.60 mmol, 3 eq.) were added, followed by further ultrasonic activation (room temperature, 1 hour). The reaction mixture was filtered through Celite under inert-atmosphere to remove the NaCl. The reaction mixture was washed with DCM (20 mL) in the filtration step. The DCM was removed *in vacuo* (10^{-2} mbar) to give a clear oil, which was treated as air-sensitive and stored in an inert-atmosphere glovebox.

^{1}H NMR (295 K, 400 MHz, CD_2Cl_2): δ_H = 1.21 (m, $P\{CH(C\mathbf{H}_3)_2\}_3$), 2.11 (m, $P\{C\mathbf{H}(CH_3)_2\}_3$), 4.44 (m, equatorial, $[P\{OC\mathbf{H}(CF_3)_2\}_5F]^-$), 5.21 (m, axial $[P\{OC\mathbf{H}(CF_3)_2\}_5F]^-$) ppm. An overlapping impurity multiplet similar to the chemical shift of the CH_3 hydrogens of the isopropyl group meant the integration equated to 10H relative to 1H for the isopropyl hydrogen atom.

^{31}P{^{1}H} NMR (295 K, 161.8 MHz, CD_2Cl_2): δ_P = -147.5 (d, $^1J_{PF}$ = 818 Hz, $[\mathbf{P}\{OCH(CF_3)_2\}_5F]^-$), 44.9 (s, $[Ag(\mathbf{P}^iPr_3)_3]^+$), 60.4 (s), 63.7 (s) ppm. Other signals of weak intensity (lower than 10 % of the intense signal) are not listed here.

^{19}F NMR (295 K, 376.2 MHz, CD_2Cl_2): δ_F = -72.95 (br, axial $[P\{OCH(C\mathbf{F}_3)_2\}_5F]^-$), -72.72 (s, equatorial $[P\{OCH(C\mathbf{F}_3)_2\}_5F]^-$), -59.95 (d, 1F, $^1J_{FP}$ = 818 Hz, $[P\{OCH(CF_3)_2\}_5\mathbf{F}]^-$) ppm. Since the equatorial and axial peaks overlap, a combined integration was calculated to give 30F for the hexafluoroisopropoxy groups on the $[P\{OCH(C\mathbf{F}_3)_2\}_5F]^-$ anion.

Peaks were also observed at -75.31 (br, $NaOCH(CF_3)_2$) and -74.31 (s). Other peaks of weak intensity (lower than 10 % of the intense signal) are not listed here.

The NMR spectrum of this sample also contained a small amount of vacuum grease and DCM.

ESI-MS (CH_2Cl_2): m/z = 884.9356, $[M]^-$ (calculated 884.9385 m/z $P\{OCH(CF_3)_2\}_5F]^-$, 3.3 ppm).

6.4.40 Synthesis of $[Na(NCMe)_2(O{=}P\{OCH(CF_3)_2\}_3)]^+[P\{OCH(CF_3)_2\}_5F]^-$, (**22**)

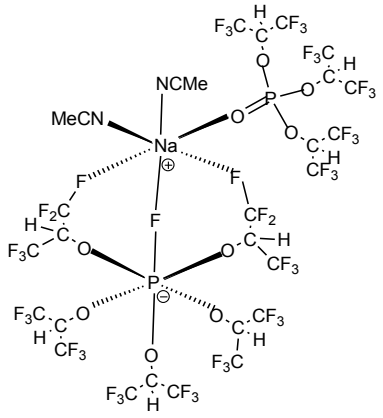

$P\{OCH(CF_3)_2\}_5$ was synthesised as described in 6.4.35 and used *in situ;* AgF (26 mg, 0.20 mmol, 1 eq.) and MeCN (5 mL) were added to this, followed by further ultrasonic activation (room temperature, 1 hour). The reaction mixture was filtered through Celite under inert atmosphere to remove the NaCl. The reaction mixture was washed with MeCN solvent (20 mL) in the filtration step. The majority of the solvent was removed under *vacuo* (~ 2 mL left), followed by the addition of a toluene layer (5 mL) to aid crystallisation *via* slow diffusion of the solvents at -16 ˚C. The clear solid product is treated as light- and air-sensitive and stored in the glovebox wrapped in foil. It appears a sodium ion from either $NaOCH(CF_3)_2$ or NaCl dissolved in solution coordinates to the anion. A fluorinated phosphate is also found in the reaction mixture, presumably from hydrolysis of the phosphorane. This fluorinated phosphate and two acetonitrile molecules are found to coordinate to the sodium ion, along with three fluorine atoms from the $[P\{OCH(CF_3)_2\}_5F]^-$ anion.

The reaction mixture was analysed by NMR spectroscopy as the crystals re-dissolved into solution after X-ray structural analysis.

^{1}H NMR (295 K, 400 MHz, $CDCl_3$): δ_H = 2.00 (s, coordinated NC**Me**), 4.30 (m). 4.80 (m, $O{=}P\{OC\mathbf{H}(CF_3)_2\}_3$), 4.97 (s, equatorial $[P\{OC\mathbf{H}(CF_3)_2\}_5F]^-$). 5.21 (m, axial $[P\{OC\mathbf{H}(CF_3)_2\}_5F]^-$) ppm.

$^{31}P\{^1H\}$ NMR (295 K, 161.8 MHz, $CDCl_3$): δ_P = -143.3 (t, $^1J_{PF}$ = 860 Hz, $[\mathbf{P}\{OCH(CF_3)_2\}_4F_2]^-$), -141.3 (d, $^1J_{PF}$ = 820, $[\mathbf{P}\{OCH(CF_3)_2\}_5F]^-$), -84.3 (s, $\mathbf{P}\{OCH(CF_3)_2\}_5$), -81.7 (d, $^1J_{PF}$ = 735 Hz, $\mathbf{P}\{OCH(CF_3)_2\}_4F$), -2.5 (s, $O{=}P\{OCH(CF_3)_2\}_3$) ppm.

^{19}F NMR (295 K, 376.2 MHz, CD_2Cl_2): δ_F = -74.23 (br), -74.13 (d, J = 30 Hz). -74.05 (br), -73.60 (br), -73.30 (br), -73.21 (br, axial $[P\{OCH(C\mathbf{F}_3)_2\}_5F]^-$), -72.10 (br, equatorial $[P\{OCH(C\mathbf{F}_3)_2\}_5F]^-$), -57.89 (d, $^1J_{FP}$ = 793 Hz) ppm.

The NMR spectrum of this sample also contained vacuum grease and toluene.

Single-Crystal X-ray Diffraction Measurements: $C_{28}H_{14}F_{49}N_2NaO_9P_2$, M = 1538.34, monoclinic, crystal size/mm = 0.28 × 0.20 × 0.11, a = 14.3172(4) Å, b = 19.3101(4) Å, c = 18.3073(5) Å, β = 90.176(3)°, U = 5061.3(2) Å^3, T = 109.95(10) K, space group $P2_1/n$ (no. 14), Z = 4, μ(Mo Kα) = 0.326, ρ_{calc} mg/mm^3 = 2.019, 19053 reflections measured, 9658 unique (R_{int} = 0.0263) which were used in all calculations. The final $wR(F_2)$ was 0.1253 (all data) and R_1 was 0.0500 (>2sigma(I)).

6.4.41 Synthesis of Triethylamine Coordinated Sodium(I) monofluoro, pentakis-(hexafluoroisopropoxy) phosphate, $[Na(NEt_3)_n]^+[P\{OCH(CF_3)_2\}_5F]^-$, (**23**)

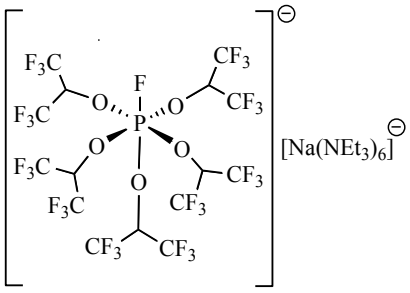

Phosphorus pentachloride (41 mg, 0.20 mmol, 1 eq.) and $NaOCH(CF_3)_2$ (190 mg, 1.0 mmol, 5 eq.) were added to a J Young's ampoule containing DCM (10 mL). Ultrasonic activation (room temperature, 1 hour) was used to increase the solubility of the $NaOCH(CF_3)_2$. NMR spectroscopy was used to establish reaction completion. The $P\{OCH(CF_3)_2\}_5$ reaction mixture was used *in situ*; NaF (8 mg, 0.20 mmol, 1 eq.) and triethylamine (122 mg, 0.60 mmol, 6 eq.) were added to this, followed by further ultrasonic activation (room temperature, 1 hour). The reaction mixture was filtered through Celite under inert-atmosphere to remove the NaCl. The reaction mixture was washed with DCM (20 mL) in the filtration step. The majority of the solvent was removed *in vacuo* (~ 2 mL remaining), followed by the addition of a hexane layer (5 mL) to aid crystallisation *via* slow diffusion of the solvents. However, the clear crystals were too fine and were not suitable for single-crystal X-ray diffraction. The product was treated as air-sensitive and stored in the glovebox.

^{1}H NMR (295 K, 400 MHz, $CDCl_3$): δ_H = 1.33 (m, $[Na(N\mathbf{Et}_3)_n]^+$), 3.46 (m, $[Na(N\mathbf{Et}_3)_n]^+$) ppm.

Peaks at 0.88 (t, $^3J_{HH}$ = 7Hz, $\mathbf{Et}_3$), 2.38 (q, $^3J_{HH}$ = 7Hz, $\mathbf{Et}_3$), 4.25 (m, $P\{OC\mathbf{H}(CF_3)_2\}_5$) ppm were also observed.

$^{31}P\{^1H\}$ NMR (295 K, 161.8 MHz, $CDCl_3$): δ_P = -147.6 (d, $^1J_{PF}$ = 818 Hz, $[\mathbf{P}\{OCH(CF_3)_2\}_5F]^-$), 146.9 (s, $[\mathbf{P}\{OCH(CF_3)_2\}_6]^-$), -84.0 (s, $\mathbf{P}\{OCH(CF_3)_2\}_5$), -2.0 (s, $O{=}\mathbf{P}\{OCH(CF_3)_2\}_3$) ppm.

^{19}F NMR (295 K, 376.2 MHz, $CDCl_3$): δ_F = -73.03 (br, axial $[P\{OCH(C\mathbf{F}_3)_2\}_5F]^-$), -72.69(s, equatorial $[P\{OCH(C\mathbf{F}_3)_2\}_5F]^-$), -58.48 (d, $^1J_{FP}$ = 818 Hz, $[P\{OCH(CF_3)_2\}_5\mathbf{F}]^-$) ppm.

Peaks at -75.82 (s, $\mathbf{P}\{OCH(CF_3)_2\}_6]^-$), -74.31 (s, $O{=}P\{OCH(C\mathbf{F}_3)_2\}_3$) -73.34 (s, $P\{OCH(C\mathbf{F}_3)_2\}_5$) ppm were also observed.

The NMR spectra of this material also showed the presence of DCM and vacuum grease.

ESI-MS (CH_2Cl_2): m/z observed mass = 884.9387, $[M]^-$ (calculated 884.9385 m/z $P\{OCH(CF_3)_2\}_5F]^-$, -0.2 ppm).

6.4.42 Synthesis of Tetraethylammonium monofluoropentakis-(hexafluoroisopropoxy)phosphate, $[NEt_4]^+[P\{OCH(CF_3)_2\}_5F]^-$, (**24**)

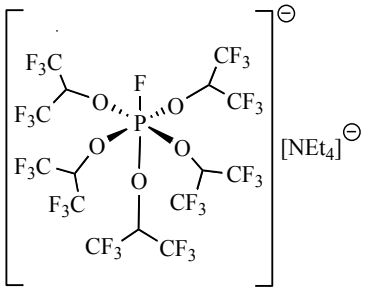

Phosphorus pentachloride (41 mg, 0.20 mmol, 1 eq.) and $NaOCH(CF_3)_2$ (190 mg, 1.0 mmol, 5 eq.) were added to a J Young's ampoule with DCM (10 mL) in an inert-atmosphere glovebox. Ultrasonic activation (room temperature, 1 hour) was used to increase the solubility of the $NaOCH(CF_3)_2$. The $P\{OCH(CF_3)_2\}_5$ reaction mixture was used *in situ*; tetra(ethyl)ammonium bromide, Et_4NBr (36 mg, 0.20 mmol, 1 eq.) was added, followed by further ultrasonic activation (room temperature, 1 hour). The reaction mixture was filtered through Celite under inert atmosphere to remove the NaBr. The reaction mixture was washed with DCM (20 mL) in the filtration step. The majority of the DCM was removed *in vacuo* (10^{-2} mbar), followed by the addition of a hexane layer (5 mL) to aid crystallisation *via* slow diffusion of the solvents. The product was a white solid, treated as air-sensitive and stored in an inert-atmosphere glovebox.

Yield: 35 mg (17 %)

^{1}H NMR (295 K, 400 MHz, $CDCl_3$): δ_H = 1.34 (m, $^1J_{HH}$ = 7Hz, $[N(CH_2C\mathbf{H}_3)_4]^+$), 3.24 (q, $^1J_{HH}$ = 7 Hz, $[N(C\mathbf{H}_2CH_3)_4]^+$), 4.61 (m, $P\{OC\mathbf{H}(CF_3)_2\}_5$) ppm.

Lower intensity peaks at 1.25 (s) and 0.87 (m) ppm were also observed.

$^{31}P\{^1H\}$ NMR (295 K, 161.8 MHz, $CDCl_3$): δ_P = -147.5 (d, $^1J_{PF}$ = 818 Hz, $[\mathbf{P}\{OCH(CF_3)_2\}_5F]^-$) ppm.

^{19}F NMR (295 K, 376.2 MHz, CD_2Cl_2): δ_F = -72.98 (br, axial $[P\{OCH(C\mathbf{F}_3)_2\}_5F]^-$), -72.71(s, equatorial $[P\{OCH(C\mathbf{F}_3)_2\}_5F]^-$), -59.67 (d, 1F, $^1J_{FP}$ = 818 Hz, $[P\{OCH(CF_3)_2\}_5\mathbf{F}]^-$) ppm. Since the equatorial and axial peaks overlap, a combined integration was calculated to give 30F for the hexafluoroisopropoxy groups on the $[P\{OCH(C\mathbf{F}_3)_2\}_5F]^-$ anion.

Lower intensity peaks at -75.63 (d, J = 7 Hz), -74.59 (d, J = 6 Hz), -74.34 (d, J = 5 Hz), -73.37 (s) and -71.02 (s) ppm were also observed.

^{13}C NMR (295 K, 100.5 MHz, CD_2Cl_2): δ_C = 7.6 (s, $[N(CH_2\mathbf{C}H_3)_4]^+$), 53.0 (s, $[N(\mathbf{C}H_2CH_3)_4]^+$), 71.6 (m, $[P\{O\mathbf{C}H(CF_3)_2\}_5F]^-$), 122.6 (q, $^1J_{CF}$ = 287 Hz, $[P\{OCH(\mathbf{C}F_3)_2\}_5F]^-$) ppm.

The NMR spectrum of this sample also contained vacuum grease and DCM.

Melting Point: 118 °C (DSC)

ESI-MS (CH_2Cl_2): m/z observed mass = 130.1592, $[M]^+$ (calculated 130.1590 m/z for $[N(CH_2CH_3)_4]^+$, -1.3 ppm), 884.9369, $[M]^-$ (calculated 884.9385 m/z $P\{OCH(CF_3)_2\}_5F]^-$, 1.9 ppm).

Elemental Analysis: $[N(CH_2CH_3)_4]^+[P\{OCH(CF_3)_2\}_5F]^-$ calculated ; C(27.19),H(2.48), N(1.38) observed; C(27.92), H(2.90), N(1.42). Trace amounts of grease observed in the ^{1}H NMR spectra for this sample is likely to have caused the higher C and H values found.

Single-Crystal X-ray Diffraction measurements: $C_{23}H_{25}F_{31}NO_5P$, M = 1015.41, triclinic, crystal size/mm = 0.35 × 0.23 × 0.12, a = 9.4138(6) Å, b = 9.9392(5) Å, c = 19.7741(10) Å, α = 97.902(4)°, β = 97.617(5)°, γ = 101.894(5)°, V = 1768.39(17) Å^3, T = 110.00(10) K, space group P-1 (no. 2), Z = 2, μ(MoKα) = 0.279, ρ_{calc} mg/mm^3 = 1.907, 35119 reflections measured, 9362 unique (R_{int} = 0.0296) which were used in all calculations. The final wR_2 was 0.2829 (all data) and R_1 was 0.0992 (>2sigma(I)).

6.5 REACTION CONDITIONS EMPLOYED IN SEARCH OF $[P(OR^F)_4]^+$ CATIONS (CHAPTER 4)

6.5.1 Attempted Synthesis of $[P\{OC(CF_3)_3\}_4]^+[N\{S(O)_2CF_3\}_2]^-$, **[(8)][Tf$_2$N]**

Phosphorus pentachloride (206 mg, 1 mmol, 1 eq.), lithium bis(trifluoromethanesulfonyl)imide, ($LiTf_2N$), $LiN\{S(O)_2CF_3\}_2$ (287 mg, 1 mmol, 1 eq.) and lithium perfluoro-*t*-butoxide (968 mg, 1 mmol, 4 eq.), were added to a double J Young's ampoule under an inert-nitrogen atmosphere. DCM (7.5 mL) and diethyl ether (2.5 mL) were added to the solid reagents and the reaction mixture was cooled to -78 K (to avoid side reactions on addition of the diethyl ether). Ultrasonic activation (room temperature, 30 min.) was used to increase the solubility of the reactants.

$^{31}P\{^1H\}$ NMR (295 K, 161.8 MHz, $CDCl_3$): δ_P = -33.0 (s, $\mathbf{P}\{OC(CF_3)_3\}_2Cl_3$), -12.7 (s, $\mathbf{P}\{OC(CF_3)_3\}Cl_4$), -3.5 (s, O=$\mathbf{P}\{OC(CF_3)_3\}_3$), 6.9 (s, proposed as potential $[\mathbf{P}\{OC(CF_3)_3\}_4]^+$), 147.0 (m, $^4J_{PF}$ = 21 Hz, $\mathbf{P}\{OC(CF_3)_3\}_3$) ppm.

^{19}F NMR (295 K, 376.2 MHz, $CDCl_3$): δ_F = -79.42 (s, $[N\{S(O)_2C\mathbf{F}_3\}_2]^-$), -74.51 (s, $LiOC(C\mathbf{F}_3)_3$), -71.37 (d, $^4J_{FP}$ = 23 Hz, $P\{OC(C\mathbf{F}_3)_3\}_3$), -71.20 (s), -71.12 (s) ppm.

Many other weak intensity peaks are present in the ^{19}F NMR spectrum.

After removal of solvent in vacuo (10^{-2}mbar):

$^{31}P\{^1H\}$ NMR (295 K, 161.8 MHz, $CDCl_3$): δ_P = -33.8 (s, $\mathbf{P}\{OC(CF_3)_3\}_2Cl_3$), -11.7 (s, proposed $[\mathbf{P}\{OC(CF_3)_3\}_4]^+$), -5.6 (s, proposed as potential $[\mathbf{P}\{OC(CF_3)_3\}_4]^+$), -3.9 (s, O=$\mathbf{P}\{OC(CF_3)_3\}_3$), 10.8 (s) ppm.

^{19}F NMR (295 K, 376.2 MHz, $CDCl_3$): δ_F = -80.05 (s, $[N\{S(O)_2C\mathbf{F}_3\}_2]^-$), -75.57 (s, $LiOC(CF_3)_3$), -71.49 (d, J = 8 Hz) ppm.

Many other weak intensity peaks are present in the ^{19}F NMR spectrum.

6.5.2 Attempted Synthesis of $[P\{OC(CF_3)_3\}_4]^+[N\{S(O)_2CF_3\}_2]^-$, **[(8)][Tf$_2$N]**

Phosphorus pentachloride (52 mg, 0.25 mmol, 1 eq.), lithium bis(trifluoromethanesulfonyl)imide, ($LiTf_2N$), $LiN\{S(O)_2CF_3\}_2$ (72 mg, 0.25 mmol, 1 eq.) and lithium perfluoro-*t*-butoxide (242 mg, 1 mmol, 4 eq.), were added to a double J Young's

ampoule under inert-nitrogen atmosphere. Diethyl ether (10 mL) was added to the solid reagents and the reaction mixture was cooled to -78 K (to avoid side reactions on addition of the diethyl ether). Ultrasonic activation (room temperature, 30 min.) was used to increase the solubility of the reactants. The reaction mixture was filtered to the other compartment of the double J Young's ampoule, by cooling this to -78 K to create a pressure gradient to aid the transfer.

$^{31}P\{^{1}H\}$ NMR (295 K, 161.8 MHz, $CDCl_3$): δ_P = 147.0 (m, $^4J_{PF}$ = 21 Hz, **P**$\{OC(CF_3)_3\}_3$) ppm.

^{19}F NMR (295 K, 376.2 MHz, $CDCl_3$): δ_F = -79.12 (s, $[N\{S(O)_2C\mathbf{F}_3\}_2]^-$), -72.02 (d, $^4J_{FP}$ = 23 Hz, $P\{OC(C\mathbf{F}_3)_3\}_3$) ppm.

Many other weak intensity peaks are present in the ^{19}F NMR spectrum.

The diethyl ether was removed *in vacuo* (10^{-2} mbar), and MeCN was added to the reaction mixture, followed by an inert-air filtration to remove the insoluble phosphite:

$^{31}P\{^{1}H\}$ NMR (295 K, 161.8 MHz, $CDCl_3$): δ_P = 7.7 (s), 9.7 (s) ppm. Either one of these is proposed as potentially the $[\mathbf{P}\{OC(CF_3)_3\}_4]^+$ product.

^{19}F NMR (295 K, 376.2 MHz, $CDCl_3$): δ_F = -79.12 (d, J = 26 Hz), -74.03 (d, J = 26 Hz) ppm.

Other very weak intensity peaks are present in the ^{19}F NMR spectrum.

6.5.3 Attempted Synthesis of $[P\{OC(CF_3)_3\}_4]^+[N\{S(O)_2CF_3\}_2]^-$, **[(8)][$Tf_2N$]**

Phosphorus pentachloride (52 mg, 0.25 mmol, 1 eq.), lithium bis(trifluoromethanesulfonyl)imide, ($LiTf_2N$), $LiN\{S(O)_2CF_3\}_2$ (144 mg, 0.25 mmol, 1 eq.) and lithium perfluoro-*t*-butoxide (175 mg, 1 mmol, 4 eq.), were added to a double J Young's ampoule under an inert-nitrogen atmosphere. Diethyl ether (10 mL) was added to the solid reagents and the reaction mixture was cooled to -78 K (to avoid side reactions on addition of the diethyl ether). Ultrasonic activation (room temperature, 30 min.) was used to increase the solubility of the reactants. The reaction mixture was filtered to the other compartment of the double J Young's ampoule, by cooling this to -78 K to create a pressure gradient to aid the transfer.

$^{31}P\{^{1}H\}$ NMR (295 K, 161.8 MHz, $CDCl_3$): δ_P = -13.5 (s), -12.5 (s, **P**$\{OC(CF_3)_3\}Cl_4$), -4.6 (s), 2.5 (s, O=**P**$\{OC(CF_3)_3)\}_3$ ppm.

^{19}F NMR (295 K, 376.2 MHz, $CDCl_3$): δ_F = -79.61 (s, Tf_2N), -74.86 (s, $NaOC(C\mathbf{F}_3)_3$), -71.40 (d, J = 26 Hz), -71.16 (s), -71.00 (s), 70.25 (s), ppm.

Many other weak intensity peaks are present in the ^{19}F NMR spectrum.

ESI-MS (MeCN): found mass; 970.7 m/z, $[M]^+$, $[P\{OC(CF_3)_3\}_4]^+$

6.5.4 Attempted Synthesis of $[P\{OCH(CF_3)_2\}_4]^+[PF_6]^-$, **[(9)][$PF_6$]**

Phosphorus pentachloride (52 mg, 0.25 mmol, 1 eq.), and lithium hexafluorisopropoxide, $LiOCH(CF_3)_2$ (175 mg, 1 mmol, 4 eq.), were added to a double J Young's ampoule under an inert-nitrogen atmosphere. DCM (10 mL) was added to the solid reagents and the reaction mixture was cooled to -78 K. The reaction was left stirring (room temperature, 48 hrs.). Potassium hexafluorophosphate, KPF_6 (183 mg, 0.25 mmol, 1 eq.) was added to the other compartment of the double J Young's ampoule. $P\{OCH(CF_3)_2\}_4Cl$ was filtered to the compartment containing KPF_6 by cooling this to -78 K to create a pressure gradient to aid the transfer of the solution. Ultrasonic activation (room temperature, 30 min.) was used to increase the solubility of the KPF_6. The DCM was removed *in vacuo* (10^{-2} mbar) and MeCN was added to the reaction mixture.

$^{31}P\{^{1}H\}$ NMR (295 K, 161.8 MHz, $CDCl_3$): δ_P = -144.0 (sept, $^1J_{PF}$ = 711 Hz, K**P**F_6), -81.0 (d. $^1J_{PF}$ = 803 Hz, **P**$\{OCH(CF_3)_2\}_4F$), -3.3 (s, O=**P**$\{OCH(CF_3)_2\}_3$) ppm.

Spectroscopic NMR analysis was repeated after 48 hrs. of stirring at room temperature.

$^{31}P\{^{1}H\}$ NMR (295 K, 161.8 MHz, $CDCl_3$): δ_P = -144.1 (t, $^1J_{PF}$ = 770 Hz, [**P**$\{OCH(CF_3)_2\}_4F_2]^-$), -81.0 (d. $^1J_{PF}$ = 803 Hz, **P**$\{OCH(CF_3)_2\}_4F$), -3.3 (s, O=**P**$\{OCH(CF_3)_2\}_3$), 34.5 (m, $^1J_{PF}$ = 1072 Hz, **P**F_5) ppm.

^{19}F NMR (295 K, 376.2 MHz, $CDCl_3$): δ_F = -88.34 (d, $^1J_{FP}$ = 1072 Hz, P**F**$_5$), -75.82 ($^3J_{FH}$ = 8 Hz, $NaOCH(C\mathbf{F}_3)_2$), -74.36 (d, J = 8 Hz), -74.24 (br, $P\{OCH(C\mathbf{F}_3)_2\}_4F$), -73.25 (d, $^1J_{FP}$ = 715Hz, K**F**$_6$),-55.9 (d, $^1J_{FP}$ = 805 Hz, $P\{OCH(CF_3)_2\}_4\mathbf{F}$).

Other weak intensity peaks are present in the ^{19}F NMR spectrum.

ESI-MS (MeCN): found mass; 589.3 m/z $[M]^-$, $[P\{OC(CF_3)_3\}_3F_3]^-$, 885.0 m/z, $[M]^-$, $[P\{OC(CF_3)_3\}_5F]^-$, 737.1m/z, $[M]^-$, $[P\{OC(CF_3)_3\}_4F_2]^-$. The positive mode consisted of intense peaks for $[K_{n+1}(PF_6)_n]^+$ clusters only.

6.5.5 Attempted Synthesis of $[P\{OCH(CF_3)_2\}_4]^+[Al\{OC(CF_3)_3\}_4]^-$, **[(9)][Al{OC(CF$_3$)$_3$}$_4$]**

Phosphorus pentachloride (52 mg, 0.25 mmol, 1 eq.), and lithium hexafluoroisopropoxide, $LiOCH(CF_3)_2$ (175 mg, 1 mmol, 4 eq.), were added to a double J Young's ampoule under an inert-nitrogen atmosphere. DCM (10 mL) was added to the solid reagents and the reaction mixture was cooled to -78 K. The reaction was left stirring (room temperature, 48 hrs.). Lithium perfluoro-*t*-butoxy aluminate, $LiAl\{OC(CF_3)_3\}_4$, (243 mg, 0.25 mmol, 1 eq.) was added to the other compartment of the double J Young's ampoule. $P\{OCH(CF_3)_2\}_4Cl$ was filtered to the compartment containing $LiAl\{OC(CF_3)_3\}$ by cooling this to -78 K to create a pressure gradient to aid the transfer of the solution. Ultrasonic activation (room temperature, 30 min.) was used to increase the solubility of the $LiAl\{OC(CF_3)_3\}$. The DCM was removed *in vacuo* (10^{-2} mbar) and CD_2Cl_2 (0.6 mL) was added. The solution was transferred to a J Young's tap NMR tube and the sample was analysed using NMR spectroscopy.

^{31}P{^{1}H} NMR (295 K, 161.8 MHz, CDCl$_3$): δ_P = -84.0 (s, **P**$\{OCH(CF_3)_2\}_5$), -80.5 (d, $^1J_{PF}$ = 784 Hz, **P**$\{OCH(CF_3)_2\}_4F$), -18.2 (s), -11.2 (s), 6.2 (br), 22.4 (s).

^{19}F NMR (295 K, 376.2 MHz, CDCl$_3$): δ_F = -78.95 (br), -76.33 (br), -74.49 (br, $P\{OCH(C\mathbf{F}_3)_2\}_4F$), -72.04 (br, $P\{OCH(C\mathbf{F}_3)_2\}_5$) ppm. Very poor shimming of this sample meant peak multiplicities are difficult to obtain.

PhF (0.5 mL) was added to the reaction mixture of the NMR tube, in hope to stabilize and cationic species formed. The sample was again analysed using NMR spectroscopy.

^{31}P{^{1}H} NMR (295 K, 161.8 MHz, CDCl$_3$): δ_P = -83.8 (s, **P**$\{OCH(CF_3)_2\}_5$), -81.9 (d, $^1J_{PF}$ = 796 Hz, **P**$\{OCH(CF_3)_2\}_4F$), -78.7 (d, $^1J_{PF}$ = 790 Hz), -10.8 (s), 5.5 (s) ppm.

^{19}F NMR (295 K, 376.2 MHz, CDCl$_3$): δ_F = -75.60 (br), -74.95 (br), -74.76 (br, $P\{OCH(C\mathbf{F}_3)_2\}_4F$), -73.86 (br, $P\{OCH(C\mathbf{F}_3)_2\}_5$), -57.9 (d, $^1J_{PF}$ = 827 Hz, $P\{OCH(CF_3)_2\}_4\mathbf{F}$) ppm. Very poor shimming of this sample meant peak multiplicities are difficult to obtain.

Other weak intensity peaks are present in the ^{19}F NMR spectrum.

6.5.6 Attempted Synthesis of $[P\{OC(CF_3)_2\}_4]^+[Al\{OC(CF_3)_3\}_4]^-$, **[(9)][Al{OC(CF$_3$)$_3$}$_4$]**

Phosphorus pentachloride (25 mg, 0.125 mmol, 1 eq.), and lithium perfluoro-*t*-butoxide (129 mg, 0.50 mmol, 4 eq.), were added to a double J Young's ampoule under inert-nitrogen atmosphere. Diethyl ether (5 mL) was added to the solid reagents and the reaction mixture was cooled to -78 K. The reaction was left stirring at room temperature for two days. Lithium perfluoro-*t*-butoxy aluminate, $LiAl\{OC(CF_3)_3\}_4$, (121 mg, 0.125 mmol, 1 eq.) was added to the other compartment of the double J Young's ampoule. $P\{OC(CF_3)_3\}_4Cl$ was filtered to the compartment containing $LiAl\{OC(CF_3)_3\}$ by cooling this to -78 K to create a vacuum. Ultrasonic activation (room temperature, 30 min.) was used to increase the solubility of the $LiAl\{OC(CF_3)_3\}$ reagent.

^{31}P{^{1}H} NMR (295 K, 161.8 MHz, CD$_3$CN): δ_P = -33.8 (s, **P**$\{OC(CF_3)_3\}_4Cl$), -10.6 (s), -3.9 (s, O=**P**$\{OC(CF_3)_3\}_3$), 147.3 (m. **P**$\{OC(CF_3)_3\}_3$) ppm.

^{19}F NMR (295 K, 376.2 MHz, CD$_3$CN): δ_F = -80.04 (s),-79.81(br), -75.93 (s), -75.87 (s), -75.71 (s), -75.08 (s) ppm.

6.5.7 Attempted Synthesis of $[P\{OC(CF_3)_3\}_4]^+[P\{OCH(CF_3)_2\}_5F]^-$, **[(8)][P{OCH(CF$_3$)$_2$}$_5$F]**

Phosphorus pentachloride (52 mg, 0.25 mmol, 1 eq.), and lithium perfluoro-*t*-butoxide (258 mg, 1 mmol, 4 eq.), were added to a J Young's ampoule under an inert-nitrogen atmosphere. PhF (10 mL) was added to the solid reagents and ultrasonic activation (room temperature, 30 min.) was used to increase the solubility of the reagents. $^{31}P\{^1H\}$ NMR spectroscopy was used to establish complete conversion of the phosphorus pentachloride. $[Ag(NCMe)_3]^+[P\{OCH(CF_3)_2\}_5F]^-$ (**17**) (0.25 mmol in 5 mL MeCN) was added to this phosphorane and analysed by NMR spectroscopy and ESI MS spectrometry.

^{1}H NMR (295 K, 400 MHz, CDCl$_3$): δ_H = 4.30 (m, potentially related to the -3.7 ppm in the $^{31}P\{^1H\}$ NMR), 4.80 (m, $[P\{OCH(C\mathbf{F}_3)_2\}_5F]^-$) ppm.

^{31}P{^{1}H} NMR (295 K, 161.8 MHz, CDCl$_3$): δ_P = -147.5 (d, $^1J_{PF}$ = 818 Hz, $[\mathbf{P}\{OCH(CF_3)_2\}_5F]^-$), -3.7 (s, either O=**P**$\{OCH(CF_3)_2\}_3$ or proposed to be the cation, $[\mathbf{P}\{OCH(CF_3)_2\}_4]^+$) ppm.

Lower intensity signals are present at -33.7 (s, **P**{OCH(CF_3)$_2$}$_4$Cl), -16.1 (s), -11.9 (s, **P**{OCH(CF_3)$_2$}Cl_4), -8.9 (s) ppm.

^{19}F NMR (295 K, 376.2 MHz, $CDCl_3$): δ_F = -76.27 (br), -74.82 (s), -74.71 (s), -73.35 (br, axial [P{OCH(C**F**$_3$)$_2$}$_5$F]$^-$), -73.13 (s), -71.49 (s, equatorial [P{OCH(C**F**$_3$)$_2$}$_5$F]$^-$), -60.50 (d, $^1J_{PF}$ = 818 Hz, [P{OCH(CF_3)$_2$}$_5$**F**]$^-$) ppm. Since the equatorial and axial peaks overlap, a combined integration was calculated to give 30F for the hexafluoroisopropoxy groups on the [P{OCH(C**F**$_3$)$_2$}$_5$F]$^-$ anion.

The NMR spectra of this material also showed the presence vacuum grease, DCM and PhF.

ESI-MS (MeCN): m/z observed mass 970.7, $[M]^+$ (calculated for 970.9 m/z for [P{OC(CF_3)$_3$}$_4$]$^+$).

6.5.8 Attempted Synthesis of [P{OCH(CF_3)$_2$}$_4$]$^+$[$AlCl_4$]$^-$, **[(9)][$AlCl_4$]**

Phosphorus pentachloride (21 mg, 0.10 mmol, 1 eq.), and lithium hexafluoroisopropoxide, NaOCH(CF_3)$_2$ (76 mg, 0.40 mmol, 4 eq.), were added to a J Young's ampoule under an inert-nitrogen atmosphere. PhF (5 mL) was added to the solid reagents and ultrasonic activation (room temperature, 30 min.) was used to increase the solubility of the reagents. ^{31}P{^{1}H} NMR spectroscopy was used to establish complete conversion of the phosphorus pentachloride. Aluminium trichloride, $AlCl_3$ (13 mg, 0.10 mmol, 1 eq.) was added to this phosphorane, followed by ultrasonic activation (room temperature, 30 min.).

^{1}H NMR (295 K, 400 MHz, CD_2Cl_2): δ_H = 4.38 (m) ppm.

^{31}P{^{1}H} NMR (295 K, 161.8 MHz, CD_2Cl): δ_P = -16.5 (s, proposed to potentially be the cation, [**P**{OCH(CF_3)$_2$}$_4$]$^+$) ppm.

^{19}F NMR (295 K, 376.2 MHz, CD_2Cl): δ_F = -73.67 (d, J = 8 Hz), -71.53 (d, J = 8 Hz) ppm.

Other weak intensity peaks are present in the ^{19}F NMR spectrum.

The NMR spectra of this material also showed the presence vacuum grease and PhF.

6.5.9 Attempted Synthesis of [P{OCH(CF_3)$_2$}$_4$]$^+$[$AlCl_4$]$^-$, **[(9)][$AlCl_4$]**

Phosphorus pentachloride (52 mg, 0.25 mmol, 1 eq.), and lithium hexafluoroisopropoxide, NaOCH(CF_3)$_2$ (174 mg, 1 mmol, 4 eq.), were added to a J Young's ampoule under inert-nitrogen atmosphere. DCM (5 mL) was added to the solid reagents and ultrasonic activation

(room temperature, 30 min.) was used to increase the solubility of the reagents. $^{31}P\{^{1}H\}$ NMR spectroscopy was used to establish complete conversion of the phosphorus pentachloride. Aluminium trichloride $AlCl_3$ (33 mg, 0.25 mmol, 1 eq.) was added to this phosphorane, followed by ultrasonic activation (room temperature, 30 min.). This resulted in an orange colour reaction mixture, which was analysed by NMR spectroscopy.

^{1}H NMR (295 K, 400 MHz, $CDCl_3$): δ_H = 4.45 (m) ppm.

$^{31}P\{^{1}H\}$ NMR (295 K, 161.8 MHz, $CDCl_3$): δ_P = -81.8 (d, $^{1}J_{PF}$ = 795 Hz, **P**$\{OCH(CF_3)_2\}_4F$), -21.7 (s), -16.2 (s, proposed to be the cation, $[\mathbf{P}\{OCH(CF_3)_2\}_4]^+$), 14.8 (s) ppm.

^{19}F NMR (295 K, 376.2 MHz, $CDCl_3$): δ_F = -74.25 (br), -73.63 (d, J = 8 Hz),-72.63 (d, J =8 Hz), -72.28 (br) ppm.

The NMR spectra of this material also showed the presence vacuum grease and DCM.

Repeated Reaction:

^{1}H NMR (295 K, 400 MHz, $CDCl_3$): δ_H = 4.45 (m) ppm.

$^{31}P\{^{1}H\}$ NMR (295 K, 161.8 MHz, $CDCl_3$): δ_P = -84.0 (s, **P**$\{OCH(CF_3)_2\}_5$), -64.7 (s, **P**$\{OCH(CF_3)_2\}_4Cl$), -21.7 (s), 14.8 (s) ppm.

The NMR spectra of this material also showed the presence vacuum grease and DCM.

6.5.10 Attempted Synthesis of $[P\{OCH(CF_3)_2\}_4]^+[AlCl_4]^-$, **[(9)][AlCl$_4$]**

Phosphorus pentachloride (52 mg, 0.25 mmol, 1 eq.) and lithium hexafluoroisopropoxide, $NaOCH(CF_3)_2$ (174 mg, 1 mmol, 4 eq.) were added to a J Young's ampoule under an inert-nitrogen atmosphere. DCM (5 mL) was added to the solid reagents and ultrasonic activation (room temperature, 30 min.) was used to increase the solubility of the reagents. $^{31}P\{^{1}H\}$ NMR spectroscopy was used to establish complete conversion of the phosphorus pentachloride. Aluminium trichloride $AlCl_3$ (33 mg, 0.25 mmol, 1 eq.) was added to this phosphorane, followed by ultrasonic activation (room temperature, 30 min.). This resulted in an orange solution, which was analysed by NMR spectroscopy.

$^{31}P\{^{1}H\}$ NMR (295 K, 161.8 MHz, $CDCl_3$): δ_P = -84.1 (s, **P**$\{OCH(CF_3)_2\}_5$), -16.7 (s) ppm.

^{19}F NMR (295 K, 376.2 MHz, $CDCl_3$): δ_F = -73.72 (br), -73.41 (br),-71.55 (br),-71.11 (br) ppm.

The NMR spectra of this material also showed the presence vacuum grease and DCM.

Repeated Reaction:

^{31}P{^{1}H} NMR (295 K, 161.8 MHz, $CDCl_3$): δ_P = -20.1 (s), -16.2 (s) ppm.

After the addition of PMe_3:

^{31}P{^{1}H} NMR (295 K, 161.8 MHz, $CDCl_3$): δ_P = -84.0 (s, **P**{$OCH(CF_3)_2$}$_5$), -4.1 (s, O=**P**{$OCH(CF_3)_2$}$_3$) ppm.

^{19}F NMR (295 K, 376.2 MHz, $CDCl_3$): δ_F = -75.55 (br, $NaOCH\{C\mathbf{F}_3\}_2$), -75.27 (br) ,-71.55 (s), -74.14 (s), -73.39 (d, J = 8 Hz), -72.95 (d, J = 8 Hz) ppm.

The NMR spectra of this material also showed the presence vacuum grease and DCM.

6.6 REACTION CONDITIONS FOR P(III) LIGAND OXIDATION REACTIONS

6.6.1 Attempted Synthesis of $[BrP\{OC(CF_3)_3\}_3]^+[NO_2C_4H_4]^-$

Perfluoro-*t*-butyl phosphite, $P\{OC(CF_3)_3\}_3$, (2) (39 mg, 0.05 mmol, 1 eq.) and *N*-Bromosuccinimide (NBS), (9 mg, 0.05 mmol, 1 eq.) were added to a Schlenk tube in an inert-atmosphere glovebox. Diethyl ether (10 mL) was added to this on the Schlenk line. Ultrasonic activation (room temperature, 30 min.) was used to increase the solubility of the reactants.

^{1}H NMR (295 K, 400 MHz, $CDCl_3$): δ_H = 2.52 (d, $^4J_{HP}$ = 8 Hz, proposed to be $(NC_4\mathbf{H}_4O_2)_2P\{OC(CF_3)_3\}_3$) ppm.

$^{31}P\{^1H\}$ NMR (295 K, 161.8 MHz, $CDCl_3$): δ_P = -30.0 (s, proposed to be $(NC_4H_4O_2)_2\mathbf{P}\{OC(CF_3)_3\}_3$), 14.7 (s), 147.3 (m, $\mathbf{P}\{OC(CF_3)_3\}_3$) ppm.

^{19}F NMR (295 K, 376.2 MHz, $CDCl_3$): δ_F = -74.85 (s, $LiOC(C\mathbf{F}_3)_3\}_3$), -72.00 (s),- 71.93 (br), -71.77 (d, $^4J_{HP}$ = 19 Hz, $P\{OC(C\mathbf{F}_3)_3\}_3$) -71.39 (s), -70.96 (s), -70.11 (br) ppm.

Many other weak intensity peaks are present in the ^{19}F NMR spectrum.

The NMR spectra of this material also showed the presence of diethyl ether.

Repeated reaction in MeCN solvent:

Perfluoro-*t*-butyl phosphite, $P\{OC(CF_3)_3\}_3$, (2) (39 mg, 0.05 mmol, 1 eq.) and N-Bromosuccinimide (NBS), (9 mg, 0.05 mmol, 1 eq.) were added to a Schlenk tube in an inert-atmosphere glovebox. MeCN (10 mL) was added to this on the Schlenk line. Ultrasonic activation (room temperature, 30 min.) was used to increase the solubility of the reactants.

^{1}H NMR (295 K, 400 MHz, $CDCl_3$): δ_H = 2.05 (s), 2.35 (s) ppm.

$^{31}P\{^1H\}$ NMR (295 K, 161.8 MHz, $CDCl_3$): δ_P = -29.9 (s, proposed to be $(NC_4H_4O_2)_2\mathbf{P}\{OC(CF_3)_3\}_3$), 14.7 (s), 147.3 (m, $\mathbf{P}\{OC(CF_3)_3\}_3$) ppm.

^{19}F NMR (295 K, 376.2 MHz, $CDCl_3$): δ_F = -74.65 (s, $LiOC(C\mathbf{F}_3)_3\}_3$),-71.29 (s) ppm.

Many other weak intensity peaks are present in the ^{19}F NMR spectrum.

The NMR spectra of this material also showed the presence of MeCN.

6.6.2 Attempted Synthesis of $[BrPPh_2\{OCH(CF_3)_2\}]^+[NO_2C_4H_4]^-$

Hexafluoroisopropoxy phosphinite, $PPh_2\{OCH(CF_3)_2\}$, (5) (18 mg, 0.05 mmol, 1 eq.) and *N*-Bromosuccinimide (NBS), (9 mg, 0.05 mmol, 1 eq.) were added to a Schlenk tube in an inert-atmosphere glovebox. Diethyl ether (10 mL) was added to this on the Schlenk line. Ultrasonic activation (room temperature, 30 min.) was used to increase the solubility of the NBS. The reaction mixture turned from colourless to orange, with a dark orange precipitate.

^{1}H NMR (295 K, 400 MHz, $CDCl_3$): δ_H = 0.4 (s), 1.56 (s, free NBS), 2.10 (s), 6.80 – 7.40 (m, Ph) ppm.

^{31}P{^{1}H} NMR (295 K, 161.8 MHz, $CDCl_3$): δ_P = 38.8 (s, $[Br\mathbf{P}Ph_2\{OCH(CF_3)_2\}]^+$), 61.5 (s), 71.5 (s), 141.4 (m, $\mathbf{P}Ph_2\{OCH(CF_3)_2\}$) ppm.

^{19}F NMR (295 K, 376.2 MHz, $CDCl_3$): δ_F = -76.79 (d, J = 4 Hz), -75.11 (t, J = 8 Hz), -74.73 (d, J = 8 Hz) ppm.

Many other weak intensity peaks are present in the ^{19}F NMR spectrum.

The NMR spectra of this material also showed the presence of vacuum grease and diethyl ether.

6.6.3 Synthesis of $[BrPPh_3]^+[NO_2C_4H_4]^-$

Triphenylphosphine, PPh_3 (67 mg, 0.25 mmol, 1 eq.) and *N*-Bromosuccinimide (NBS), (45 mg, 0.25 mmol, 1 eq.) were added to a Schlenk tube in an inert-atmosphere glovebox. DCM (10 mL) was added to this on the Schlenk line. Ultrasonic activation (room temperature, 30 min.) was used to increase the solubility of the reactants. The reaction mixture turned from colourless to orange. Sodium hexafluorisopropoxide, $NaOCH(CF_3)_2$ (48 mg, 0.25 mmol, 1 eq.) was added to this reaction mixture in an inert-atmosphere glovebox.

^{1}H NMR (295 K, 400 MHz, $CDCl_3$): δ_H = 2.60 (s), 4.16 (m, $NaOC\mathbf{H}(CF_3)_2$), 6.80 – 7.40 (m, Ph) ppm.

Many other weak intensity peaks not listed here are present in the ^{1}H NMR spectrum.

^{31}P{^{1}H} NMR (295 K, 161.8 MHz, $CDCl_3$): δ_P = -5.0 (s, $\mathbf{P}Ph_3$), 20.9 (s), 31.5 (s), 61.5 (s), 71.5 (s), 141.4 (m, $\mathbf{P}Ph_2\{OCH(CF_3)_2\}$) ppm.

^{19}F NMR (295 K, 376.2 MHz, $CDCl_3$): δ_F = -75.89 (d, $^3J_{FH}$ = 8 Hz, $NaOCH(CF_3)_2$), -73.51 (t, J = 8 Hz) ppm.

Many other weak intensity peaks not listed here are present in the ^{19}F NMR spectrum.

The NMR spectra of this material also showed the presence of vacuum grease and DCM.

6.7 REACTION CONDITIONS FOR $[PCL_4]^+[X]^-$ SYNTHESIS

6.7.1 Attempted Synthesis of $[PCl_4]^+[Tf_2N]^-$

Phosphorus pentachloride (206 mg, 1 mmol, 1 eq.) and lithium bis(trifluoromethanesulfonyl)imide, ($LiTf_2N$), $LiN\{S(O)_2CF_3\}_2$ (290 mg, 1 mmol, 1 eq.) were added to a double J Young's ampoule under an inert-nitrogen atmosphere. DCM (7.5 mL) and diethyl ether (2.5 mL) were added to the solid reagents and the reaction mixture was cooled to -78 K (to avoid side reactions on addition of the diethyl ether). Ultrasonic activation (room temperature, 30 min.) was used to increase the solubility of the reactants. The reaction mixture was filtered to the other compartment of the double J Young's ampoule, by cooling this to -78 K to create a vacuum, aiding the transfer.

^{31}P{^{1}H} NMR (295 K, 161.8 MHz, $CDCl_3$): δ_P = 5.3 (s), 5.5 (s), 39.8 (s), 86.4 (s, $[PCl_4]^+$), 93.6 (s), 219.9 (s, PCl_3) ppm.

^{19}F NMR (295 K, 376.2 MHz, $CDCl_3$): δ_F = -79.70 (s, Tf_2N) ppm.

6.7.2 Attempted Synthesis of $[PCl_4]^+[PF_6]^-$

Phosphorus pentachloride (52 mg, 0.25 mmol, 1 eq.) and potassium hexafluorophosphate, KPF_6 (46 mg, 0.25 mmol, 1 eq.) were added to a double J Young's ampoule under an inert-nitrogen atmosphere. MeCN (5 mL) was added to the solid reagents and the reaction mixture was cooled to -78 K. Ultrasonic activation (room temperature, 30 min.) was used to increase the solubility of the reactants. The reaction mixture was filtered under Celite using an inert-air-sensitive technique. The reaction mixture was washed with DCM (10 mL) in the filtration step.

^{31}P{^{1}H} NMR (295 K, 161.8 MHz, $CDCl_3$): δ_P = -35.0 (q, $^1J_{PF}$ = 1070 Hz, $\mathbf{P}Cl_2F_3$) ppm.

^{19}F NMR (295 K, 376.2 MHz, $CDCl_3$): δ_F = -88.32 (d, $^1J_{FP}$ = 1070 Hz, $PCl_2\mathbf{F}_3$), -84.63 (d, $^1J_{FP}$ = 978 Hz, $KPCl_3\mathbf{F}_3$), -73.16 (d, $^1J_{FP}$ = 1070 Hz, $KP\mathbf{F}_6$) ppm.

6.7.3 Synthesis of $[PCl_4]^+[AlCl_4]^-$

Phosphorus pentachloride (21 mg, 0.10 mmol, 1 eq.) and aluminium trichloride (13 mg, 0.10 mmol, 1 eq.) were added to a J Young's ampoule in an inert-atmosphere glovebox. DCM (10 mL) was added to the solid reagents and ultrasonic activation (room temperature, 30 min.) was used to increase their solubility.

$^{31}P\{^1H\}$ NMR (295 K, 161.8 MHz, $CDCl_3$): δ_P = 85.0 (br, $[\mathbf{P}Cl_4]^+$) ppm.

6.7.4 Attempted Synthesis of $[P\{OCH(CF_3)_2\}_4]^+[Al\{OCH(CF_3)_2\}_4]^-$, **[(9)][Al{OCH(CF$_3$)$_2$}$_4$]**

Sodium hexafluoroisopropoxide, $NaOCH(CF_3)_2$ (152 mg, 0.80 mmol, 8 eq.) was added to a sample of $[PCl_4]^+[AlCl_4]^-$ (as described above) followed by ultrasonic activation (room temperature, 30 min.).

^1H NMR (295 K, 400 MHz, $CDCl_3$): δ_H = 4.38 (m,$P\{OC\mathbf{H}(CF_3)_2\}_5$) ppm.

Many other weak intensity peaks are present in the ^1H NMR spectrum.

$^{31}P\{^1H\}$ NMR (295 K, 161.8 MHz, $CDCl_3$): δ_P = -84.0 (s, $\mathbf{P}\{OCH(CF_3)_2\}_5$), 3.7 (s, O=$\mathbf{P}\{OCH(CF_3)_2\}_3$) ppm.

^{19}F NMR (295 K, 376.2 MHz, $CDCl_3$): δ_F = -78.11 (br, $NaOCH(C\mathbf{F}_3)_2\}_5$), -74.34 (t, J = 8 Hz, $\mathbf{P}\{OCH(CF_3)_2\}_5$), -74.45 (d, J =4 Hz, O=$\mathbf{P}\{OCH(CF_3)_2\}_3$), -73.42 (s), -73.99 (s, d, J = 4 Hz) ppm.

The NMR spectra of this material also showed the presence vacuum grease and DCM.

6.7.5 Attempted Synthesis of $[P\{OCH(CF_3)_2\}_4]^+[AlCl_4]^-$, **[(9)][Al{OCH(CF$_3$)$_2$}$_4$]**

Phosphorus pentachloride (52 mg, 0.25 mmol, 1 eq.) and aluminium trichloride (33 mg, 0.25 mmol, 1 eq.) were added to a J Young's ampoule in an inert-atmosphere glovebox. DCM (10 mL) was added to the solid reagents and ultrasonic activation (room temperature, 30 min.) was used to increase their solubility. Sodium hexafluoroisopropoxide, $NaOCH(CF_3)_2$ (190 mg, 1 mmol, 4 eq.) was added to this sample of $[PCl_4]^+[AlCl_4]^-$ followed by ultrasonic activation (room temperature, 30 min.) $^{31}P\{^1H\}$ NMR spectroscopy indicated the presence of

$P\{OCH(CF_3)_2\}_4Cl$), hence extra aluminium trichloride (33 mg, 0.25 mmol, 1 eq.) was added, to abstract the chloride from the $P\{OCH(CF_3)_2\}_4Cl$ phosphorane.

^{1}H NMR (295 K, 400 MHz, $CDCl_3$): δ_H = 4.34 (m, $P\{OC\mathbf{H}(CF_3)_2\}_5$), 4.55 (m, $P\{OC\mathbf{H}(CF_3)_2\}_4Cl$), ppm.

Many other weak intensity peaks are present in the ^{1}H NMR spectrum.

$^{31}P\{^1H\}$ NMR (295 K, 161.8 MHz, $CDCl_3$): δ_P = -84.0 (s, $\mathbf{P}\{OCH(CF_3)_2\}_5$), -64.9 (s, $\mathbf{P}\{OCH(CF_3)_2\}_4Cl$), 85.5 (s, $[\mathbf{P}Cl_4]^+$) ppm.

The ^{19}F NMR consisted of many overlapping broad peaks due to poor shimming, hence this spectrum was difficult to characterise.

The NMR spectra of this material also showed the presence vacuum grease and DCM.

After the addition of more $AlCl_3$ (1 eq.):

^{1}H NMR (295 K, 400 MHz, $CDCl_3$): δ_H = 4.38 (m,$P\{OC\mathbf{H}(CF_3)_2\}_5$) ppm.

Many other weak intensity peaks are present in the ^{1}H NMR spectrum.

$^{31}P\{^1H\}$ NMR (295 K, 161.8 MHz, $CDCl_3$): δ_P = -84.0 (s, $\mathbf{P}\{OCH(CF_3)_2\}_5$), 0.0 (s, proposed as $[\mathbf{P}\{OCH(CF_3)_2\}_4]^+$), 85.2 (s, $[\mathbf{P}Cl_4]^+$) ppm.

^{19}F NMR (295 K, 376.2 MHz, $CDCl_3$): δ_F = -76.62 (d, J = 8 Hz, $NaOCH(C\mathbf{F}_3)_2\}$), 76.44 (d, J = 8 Hz), -73.39 (s) ppm.

The NMR spectra of this material also showed the presence vacuum grease and DCM.

6.7.6 Attempted Synthesis of $[P\{OCH(CF_3)_2\}_4]^+[AlCl_3Br]^-$, **[(9)][$AlCl_3Br$]**

Phosphorus pentabromide (43 mg, 0.10 mmol, 1 eq.) and aluminium trichloride (13 mg, 0.10 mmol, 1 eq.) were added to a J Young's ampoule in an inert-atmosphere glovebox. DCM (10 mL) was added to the solid reagents and ultrasonic activation (room temperature, 30 min.) was used to increase their solubility. Sodium hexafluoroisopropoxide, $NaOCH(CF_3)_2$ (72 mg, 0.4 mmol, 4 eq.) was added to this sample of $[PCl_4]^+[AlCl_4]^-$ followed by ultrasonic activation (room temperature, 30 min.).

$^{31}P\{^1H\}$ NMR (295 K, 161.8 MHz, $CDCl_3$): δ_P = -65.1 (s, $[\mathbf{P}Br_4]^+$), 228.6 (br, $\mathbf{P}Br_3$) ppm.

After the addition of $Na\{OCH(CF_3)_2\}$ (4 eq.):

^{1}H NMR (295 K, 400 MHz, $CDCl_3$): δ_H = 4.43 (m,P{OC**H**$(CF_3)_2$}$_5$) ppm.

^{31}P{^{1}H} NMR (295 K, 161.8 MHz, $CDCl_3$): δ_P = -84.0 (s, **P**{OCH$(CF_3)_2$}$_5$), -66.2 (s, [**P**Br_4]$^+$), -64.7 (s, **P**{OCH$(CF_3)_2$}$_4$Br), -3.2 (s,O=**P**{OCH$(CF_3)_2$}$_3$), 85.2 (s, [**P**Cl_4]$^+$) ppm.

^{19}F NMR (295 K, 376.2 MHz, $CDCl_3$): δ_F = -77.28 (d, J = 4 Hz), -75.95 (br, NaOCH(C**F**$_3)_2$}), -74.34 (d, J = 4 Hz), -73.49 (br), -73.41 (s) ppm.

The NMR spectra of this material also showed the presence vacuum grease and DCM.

6.7.7 Attempted Synthesis of [P{OC$(CF_3)_3$}$_4$]$^+$[$AlCl_4$]$^-$, **[(2)][$AlCl_4$]**

Phosphorus pentachloride (52 mg, 0.25 mmol, 1 eq.) and aluminium trichloride (33 mg, 0.25 mmol, 1 eq.) were added to a J Young's ampoule in an inert-atmosphere glovebox. DCM (10 mL) was added to the solid reagents and ultrasonic activation (room temperature, 30 min.) was used to increase their solubility. Sodium perfluoro-*t*-butoxide, NaOC$(CF_3)_3$ (256 mg, 1 mmol, 4 eq.) was added to this sample of [PCl_4]$^+$[$AlCl_4$]$^-$, followed by ultrasonic activation (room temperature, 30 min.).

^{31}P{^{1}H} NMR (295 K, 161.8 MHz, $CDCl_3$): δ_P = -8.6 (s, [**P**{OC$(CF_3)_3$}$_3$Cl]$^+$), 28.8 (s, [**P**{OC$(CF_3)_3$}$_2$$Cl_2$]$^+$), 61.8 (s, [**P**{OC$(CF_3)_3$}$Cl_3$]$^+$), 85.4 (s, [**P**$Cl_4$]$^+$) ppm.

^{19}F NMR (295 K, 376.2 MHz, $CDCl_3$): δ_F = -75.71 (s), -75.39 (s), -75.36 (s), -75.06 (s), -74.82 (s), -69.74 (s, [P{OC(C**F**$_3)_3$}$_3$Cl]$^+$), -69.34 (s, [P{OC(C**F**$_3)_3$}$_2$$Cl_2$]$^+$), -69.03 (s, [P{OC(C**F**$_3)_3$}$_3$Cl]$^+$) ppm.

The NMR spectra of this material also showed the presence vacuum grease and DCM.

6.8 REACTION CONDITIONS FOR THE SYNTHESIS OF P(III)-LIGAND STABILISED DIPHENYLPHOSPHENIUM SALTS

6.8.1 Attempted Synthesis of $[PPh_2\text{-}PPh\{OC(CF_3)_3\}_2]^+[AlCl_4]^-$

To 5 mL DCM in a J Young's ampoule, bis(perfluoro-*t*-butoxy)phenylphosphonite (58 mg, 0.10 mmol, 1 eq.), $PPh\{OC(CF_3)_3\}_2$, (**4**) chlorodiphenylphosphine (22 mg, 0.10 mmol, 1 eq.) and aluminium trichloride (70 mg, 0.50 mmol, 5 eq.) were added. Ultrasonic activation was used (room temperature, 1 hr.) to increase the solubility of the aluminium trichloride. Complete conversion of the chlorodiphenylphosphine was monitored by $^{31}P\{^1H\}$ NMR spectroscopy. The DCM was removed *in vacuo* (10^{-2} mbar) resulting in a transparent, pale-yellow oil.

^{1}H NMR (295 K, 400 MHz, $CDCl_{32}$): δ_H = 7.20 -8.30 (m, **[PPh_2-P**Ph**$\{OC(CF_3)_3\}_2]^+$**) ppm.

$^{31}P\{^1H\}$ NMR (295 K, 161.8 MHz, $CDCl_3$): δ_P = 75.5 (s, **[P**Ph_2-PPh$\{OC(CF_3)_3\}_2]^+$**)**, 55.3 (s, [PPh_2-**P**Ph$\{OC(CF_3)_3\}_2]^+$) ppm.

Other peaks were observed at 1.3 (d, $^1J_{PP}$ = 400 Hz, [PPh_2-**P**Ph_2Cl]$^+$, 41.5 (s, **P**Ph_2Cl-$AlCl_3$, 62.7 (s, **P**Ph$\{OC(CF_3)_3\}_2$-$AlCl_3$), 73.3 (d, $^1J_{PP}$ = 390 Hz, [**P**Ph_2-PPh_2Cl]$^+$) ppm.

^{19}F NMR (295 K, 376.2 MHz, $CDCl_3$): δ_F = -71.42 (d, $^4J_{FP}$ = 22 Hz [PPh_2-PPh$\{OC(C\mathbf{F}_3)_3\}_2]^+$).

A lower intensity peak was also observed at -70.26 (d, J = 6 Hz).

The NMR spectra of this material also showed the presence of free $PPh\{OC(CF_3)_3\}_2$ ligand, DCM and vacuum grease.

6.8.2 Attempted Synthesis of $[PPh_2\text{-}PPh_2\{OC(CF_3)_3\}]^+[OS(O)_2CF_3]^-$

To 5 mL DCM in a Young's ampoule, perfluoro-*t*-butoxydiphenylphosphinite, $PPh_2\{OC(CF_3)_3\}$, (**6**) (42 mg, 0.10 mmol, 1 eq.), chlorodiphenylphosphine, PPh_2Cl (22 mg, 0.10 mmol, 1 eq.) and trimethylsilyl triflate, $Me_3SiOS(O)_2CF_3$ (22 mg, 0.10 mmol, 1 eq.) were added in an inert-atmosphere glovebox. The DCM and trimethylsilyl chloride, Me_3SiCl were removed *in vacuo* (10^{-2} mbar) resulting in a transparent, pale-yellow oil.

^{1}H NMR (295 K, 400 MHz, $CDCl_3$): δ_H = 7.20-7.90 (m, **Ph**) ppm.

$^{31}P\{^{1}H\}$ NMR (295 K, 161.8 MHz, $CDCl_3$): δ_P = 1.3 (s), 36.3(s), 42.0 (s), 44.3 (br), 79.7 (s), 132.4 (m, **P**$Ph_2\{OC(CF_3)_3\}$) ppm.

^{19}F NMR (295 K, 376.2 MHz, $CDCl_3$): δ_F = -78.36 (s), -75.63(s), -74.34 (s), -71.60 (s), -71.54 (s), -71.16 (s), -71.11 (s) ppm.

The NMR spectra of this material also showed the presence of vacuum grease, DCM and hexane.

6.8.3 Attempted Synthesis of $[PPh_2\text{-}PPh_2\{OCH(CF_3)_2\}]^+[OS(O)_2CF_3]^-$

To 5 mL DCM in a Young's ampoule, hexafluoroisopropoxydiphenylphosphinite, $PPh_2\{OCH(CF_3)_2\}$, (**5**) (35 mg, 0.100 mmol, 1 eq.), chlorodiphenylphosphine, PPh_2Cl (22 mg, 0.100 mmol, 1 eq.) and trimethylsilyl triflate, $Me_3SiOS(O)_2CF_3$ (22 mg, 0.100 mmol, 1 eq.) were added in an inert-atmosphere glovebox. The DCM and trimethylsilyl chloride, Me_3SiCl were removed *in vacuo* (10^{-2} mbar) resulting in a transparent, pale-yellow oil.

^{1}H NMR (295 K, 400 MHz, $CDCl_3$): δ_H = 0.77 (br), 3.25 (m, $PPh_2\{OC\mathbf{H}(CF_3)_2\}$), 7.25-8.00 (m, **Ph**) ppm.

$^{31}P\{^{1}H\}$ NMR (295 K, 161.8 MHz, $CDCl_3$): δ_P = 41.6 (s), 59.1 (d, $^1J_{PP}$ = 378 Hz), 66.2 (s), 71.7 (d, $^1J_{PP}$ = 391 Hz) ppm.

^{19}F NMR (295 K, 376.2 MHz, $CDCl_3$): δ_F = -74.87 (br), -71.74(m), -71.01 (t, J = 4 Hz), -71.45 (m), -70.27 (s) ppm.

The NMR spectra of this material also showed the presence of vacuum grease, DCM and hexane.

6.8.4 Attempted Synthesis of $[PPh_2\text{-}PPh_2\{OCH(CF_3)_2\}]^+[GaCl_4]^-$

To 5 mL DCM in a Young's ampoule, hexafluoroisopropoxydiphenylphosphinite, $PPh_2\{OCH(CF_3)_2\}$, (**5**) (35 mg, 0.10 mmol, 1 eq.), chlorodiphenylphosphine, PPh_2Cl (22 mg, 0.10 mmol, 1 eq.) and gallium, trichloride, $GaCl_3$ (53 mg, 0.30 mmol, 1 eq.) were added in an inert-atmosphere glovebox. The DCM was removed *in vacuo* (10^{-2} mbar) resulting in a transparent, pale-yellow oil.

^{1}H NMR (295 K, 400 MHz, $CDCl_3$): δ_H = 0.80 (br), 1.40 (s), 4.22 (m, $PPh_2\text{-}PPh_2\{OC\mathbf{H}(CF_3)\}_2]^+$), 7.20-8.00 (m, **Ph**) ppm.

$^{31}P\{^{1}H\}$ NMR (295 K, 161.8 MHz, $CDCl_3$): δ_P = -16.1 (d, $^{1}J_{PP}$ = 370 Hz, [PPh_2-**P**$Ph_2\{OCH(CF_3)\}_2]^+$), 1.0 (d, $^{1}J_{PP}$ = 394 Hz, [PPh_2-**P**$Ph_2Cl]^+$), 36.5 (s), 51.3 (s), 65.5 (s, **P**$Ph_2\{OCH(CF_3)_2\}$-$GaCl_3$). 73.4 (d, $^{1}J_{PP}$ = 390 Hz, [**P**Ph_2-$PPh_2Cl]^+$), 81.0 (d, $^{1}J_{PP}$ = 361 Hz, [**P**Ph_2-$PPh_2\{OCH(CF_3)_2\}]^+$) ppm.

^{19}F NMR (295 K, 376.2 MHz, $CDCl_3$): δ_F = -75.84 (d, $^{3}J_{FH}$ = 4 Hz, $NaOCH(CF_3)_2$), -74.34 (s), -73.17 (d, J = 4 Hz), -72.85 (d, J = 4 Hz), -72.74 (br) ppm.

The NMR spectra of this material also showed the presence of vacuum grease and DCM.

6.8.5 Attempted Synthesis of $[PPh_2\text{-}PPh\{OCH(CF_3)_2\}_2]^+[GaCl_4]^-$

To 5 mL DCM in a Young's ampoule, bis(hexafluoroisopropoxy)phenylphosphonite, $PPh\{OCH(CF_3)_2\}_2$, (**3**) (44 mg, 0.10 mmol, 1 eq.), chlorodiphenylphosphine, PPh_2Cl (22 mg, 0.10 mmol, 1 eq.) and gallium, trichloride, $GaCl_3$ (53 mg, 0.30 mmol, 1 eq.) were added in an inert-atmosphere glovebox. The DCM was removed *in vacuo* (10^{-2} mbar) resulting in a transparent, pale-yellow oil.

^{1}H NMR (295 K, 400 MHz, $CDCl_3$): δ_H = 0.80 (br), 1.40 (s), 3.33 (m, PPh_2-$PPh\{OCH(CF_3)_2\}_2]^+$), 7.20-8.50(m, **Ph**) ppm.

$^{31}P\{^{1}H\}$ NMR (295 K, 161.8 MHz, $CDCl_3$): δ_P = -2.0 (br, [PPh_2-**P**$Ph_2Cl]^+$), 41.6 (s), 66. 8 (s, **P**$Ph\{OCH(CF_3)_2\}_2$-$GaCl_3$), 62. 8 (s), 64.3 (br) 74.0 (br, [**P**Ph_2-$PPh_2Cl]^+$), 109.1 (s) ppm.

^{19}F NMR (295 K, 376.2 MHz, $CDCl_3$): δ_F = -75.60 (d, $^{3}J_{FH}$ = 4 Hz, $NaOCH(CF_3)_2$), -74.70 (d, J = 4 Hz), -73.59 (br), -73.33 (br), -72.70 (d, $^{4}J_{FP}$ = 30 Hz, $PPh\{OCH(CF_3)_2\}_2$), -72.23 (br), -71.69 (br) ppm.

The NMR spectra of this material also showed the presence of vacuum grease and DCM.

6.8.6 Attempted Synthesis of $[PPh_2\text{-}P\{OCH(CF_3)_2\}_3]^+[GaCl_4]^-$

To 5 mL DCM in a Young's ampoule, tris(hexafluoroisopropoxy)phosphite, $P\{OCH(CF_3)_2\}_2$, (**2**) (53 mg, 0.100 mmol, 1 eq.), chlorodiphenylphosphine, PPh_2Cl (22 mg, 0.100 mmol, 1 eq.) and gallium, trichloride, $GaCl_3$ (53 mg, 0.300 mmol, 1 eq.) were added in an inert-atmosphere glovebox. The DCM was removed *in vacuo* (10^{-2} mbar) resulting in a transparent, pale-yellow oil.

^{1}H NMR (295 K, 400 MHz, $CDCl_3$): δ_H = 4.87 (m, $P\{OCH(CF_3)_2\}_3$), 7.10-8.30 (m, **Ph**) 8.30 (s), 9.73 (s) ppm.

Many other weak intensity peaks are present in the ^{1}H NMR spectrum.

^{31}P{^{1}H} NMR (295 K, 161.8 MHz, $CDCl_3$): δ_P = 8.6 (s), 11.4 (s), 41.7 (s, [**P**Ph_2Cl-$GaCl_3$]$^+$), 61.0 (s, [**P**{$OCH(CF_3)_2$}$_3$-$GaCl_3$]$^+$), 73.6 (d, $^1J_{PP}$ = 386 Hz, [**P**Ph_2-PPh_2Cl]$^+$), 93.0 (d, $^1J_{PP}$ = 322 Hz, [**P**Ph_2-P{$OCH(CF_3)_2$}$_3$]$^+$), 140.4 (m, **P**{$OCH(CF_3)_2$}$_3$) ppm.

Many other weak intensity peaks are present in the ^{31}P{^{1}H} NMR spectrum.

^{19}F NMR (295 K, 376.2 MHz, $CDCl_3$): δ_F = -75.66 (d, $^3J_{FH}$ = 8 Hz, NaOCH(C**F**$_3$)$_2$),-74.39 (d, J = 8 Hz), -73.85 (d, J = 8 Hz), -73.50 (m), -72.23 (d, J = 8 Hz), -72.00 (m) ppm.

Many other weak intensity peaks are present in the ^{19}F NMR spectrum.

The NMR spectra of this material also showed the presence of vacuum grease.

6.8.7 Attempted Synthesis of $[PPh_2\text{-}PPh_2\{OC(CF_3)_3\}]^+[GaCl_4]^-$

To 5 mL DCM in a Young's ampoule, perfluoro-*t*-butoxydiphenylphosphinite, $PPh_2\{OC(CF_3)_3\}$, (**6**) (42 mg, 0.10 mmol, 1 eq.), chlorodiphenylphosphine, PPh_2Cl (22 mg, 0.100mmol, 1 eq.) and gallium, trichloride, $GaCl_3$ (53 mg, 0.30 mmol, 1 eq.) were added in an inert-atmosphere glovebox. The DCM was removed *in vacuo* (10^{-2} mbar) resulting in a transparent, pale-yellow oil.

^{1}H NMR (295 K, 400 MHz, $CDCl_3$): δ_H = 7.15-8.25 (m, Ph) ppm.

^{31}P{^{1}H} NMR (295 K, 161.8 MHz, $CDCl_3$): δ_P = 43.6 (s, **P**Ph_2Cl-$GaCl_3$]$^+$), 64.4 (m), 52.6 (br), 90.9 (d, J = 374 Hz), 95.2 (br)

^{19}F NMR (295 K, 376.2 MHz, $CDCl_3$): δ_F = -75.60 (s),-73.84 (s) -70.38 (s), -70.11(d, J = 8 Hz), -70.04 (d, J = 4 Hz), -69.65 (d, J = 4 Hz) ppm.

Many other weak intensity peaks are present in the ^{19}F NMR spectrum.

The NMR spectra of this material also showed the presence of vacuum grease.

6.8.8 Crystal Structure of the Phosphonate-Alcohol Complex, $\{OC(CF_3)_3\}_3P{=}O\cdots HOC(CF_3)_3$

Single-Crystal X-ray Diffraction Measurements: $C_{16}HF_{36}O_5P$, M = 988.14, monoclinic, crystal size/mm = 0.12 × 0.09 × 0.04, a = 23.505(3) Å, b = 13.1280(15) Å, c = 20.743(2) Å, β = 114.601(2)°, V = 5819.8(11) Å^3, T = 110.15 K, space group $P2_1/c$ (no. 14), Z = 8,

μ(MoKα) = 0.359, ρ_{calc} mg/mm^3 = 2.256, 45911 reflections measured, 10346 unique (R_{int} = 0.0885) which were used in all calculations. The final wR_2 was 0.1339 (all data) and R_1 was 0.0569 (>2sigma(I)).

6.9 REACTION CONDITIONS USED FOR "OTHER" REACTIONS DESCRIBED IN CHAPTER 5

6.9.1 Attempted Synthesis of $[\{Et_2O\}_2H]^+[P\{OCH(CF_3)_2\}_5F]^-$

Phosphorus pentachloride (41 mg, 0.20 mmol, 1 eq.) and $NaOCH(CF_3)_2$ (190 mg, 1.0 mmol, 5 eq.) were added to a J Young's ampoule with DCM (10 mL) in an inert-atmosphere glovebox. Ultrasonic activation (room temperature, 1 hour) was used to increase the solubility of the $NaOCH(CF_3)_2$. NMR spectroscopy was used to establish reaction completion. This reaction mixture was then used *in situ;* NaF (8 mg, 0.20 mmol, 1 eq.) and $\{Et_2O\}_2HCl$ (0.05 mL of 1M solution, 0.05 mmol, 0.25 eq.) were added, followed by ultrasonic activation (room temperature, 1 hour) to increase the solubility of NaF.

^{1}H NMR (295 K, 400 MHz, $CDCl_3$): δ_H = 1.09 (t, J = 8 Hz, $\{Et_2O\}_2HCl$), 1.90 (s), 3.37 (q, J = 8 Hz, $\{Et_2O\}_2HCl$), 4.30 (m, $P\{OC\mathbf{H}(CF_3)_2\}_5$), ppm.

^{31}P{^{1}H} NMR (295 K, 161.8 MHz, $CDCl_3$): δ_P = -84.0 (s, $\mathbf{P}\{OCH(CF_3)_2\}_5$), -64.9 (s, $\mathbf{P}\{OCH(CF_3)_2\}_4Cl$), -2.0 (s, O=$\mathbf{P}\{OCH(CF_3)_2\}_3$) ppm.

^{19}F NMR (295 K, 376.2 MHz, $CDCl_3$): δ_F = -75.96 (t, J = 6 Hz, $P\{OC\mathbf{H}(CF_3)_2\}_5$), -74.43 (s), -74.42 (br), 74.33 (s), -73.52 (s) ppm.

The NMR spectra of this material also showed the presence of vacuum grease and DCM.

6.9.2 Reactivity of $[Ag(NCMe)_4]^+[P\{OCH(CF_3)_2\}_5F]^-$, (**17**) with Ph_3CCl

Recrystallised tritylchloride, Ph_3CCl (3 mg, 0.01 mmol, 1 eq.), $[Ag(NCMe)_3]^+[P\{OCH(CF_3)_2\}_5F]^-$, (**17**) (0.2 mmol, 1 eq.), and CD_2Cl_2 (0.6 mL) were added to a J Young's tap NMR tube in an inert-atmosphere glovebox. This sample was analysed using NMR spectroscopy.

^{31}P{^{1}H} NMR (295 K, 161.8 MHz, $CDCl_3$): δ_P = -83.8 (s, $\mathbf{P}\{OCH(CF_3)_2\}_5$), -81.8 (d, $^1J_{FP}$ = 794 Hz, $\mathbf{P}\{OCH(CF_3)_2\}_4F$), -80.8 (t, $^1J_{FP}$ = 775 Hz, $\mathbf{P}\{OCH(CF_3)_2\}_3F_2$), -27.6 (s), -21.2 (s), -14.8 (s), -13.9 (s), -7.6 (s), -5.3 (s), -2.4 (s, O=$\mathbf{P}\{OCH(CF_3)_2\}_3$) ppm.

^{19}F NMR (295 K, 376.2 MHz, $CDCl_3$): δ_F = -81.20 (br), -76.15 (br), -74.86 (m), -74.54 (br), -72.59 (br) ppm.

6.9.3 Synthesis of $Ph_3COCH(CF_3)_2$

$NaOCH(CF_3)_2$ (10 mg, 0.05 mmol, 1 eq.) and DCM (10 mL) were added to a J Young's tap NMR tube in an inert-atmosphere glovebox. Recrystallised tritylchloroide, Ph_3CCl (14 mg, 0.05 mmol, 1 eq.) was added to this, followed by ultrasonic activation (room temperature, 1 hour) to increase the solubility of the $NaOCH(CF_3)_2$. This sample was analysed using NMR spectroscopy.

^{1}H NMR (295 K, 400 MHz, $CDCl_3$): δ_H = 3.36 (m, 1H, $Ph_3COC\mathbf{H}\{CF_3\}_2$), 7.17 – 7.60 (m, 15H, $\mathbf{Ph}_3COCH(CF_3)_2$) ppm.

^{19}F NMR (295 K, 376.2 MHz, $CDCl_3$): δ_F = -72.34 (d, J = 7 Hz, $Ph_3COCH\{C\mathbf{F}_3\}_2$) ppm.

The NMR spectra of this material also showed the presence of vacuum grease and DCM.

6.9.4 Synthesis of $[PPh_3\text{-}CPh_3]^+[PF_6]^-$

$[Ph_3C]^+[PF_6]^-$ (19 mg, 0.05 mmol, 1 eq.) and CD_2Cl_2 (0.6 mL) were added to a J Young's tap NMR tube in an inert-atmosphere glovebox. Triphenylphosphine, PPh_3 (13 mg, 0.05 mmol, 1 eq.) was added to this and a colour change from deep orange to almost colourless was observed. This sample was analysed using NMR spectroscopy.

^{1}H NMR (295 K, 400 MHz, $CDCl_3$): δ_H = 6.60 -7.80 (m, $[P\mathbf{Ph}_3\text{-}C\mathbf{Ph}_3]^+$) ppm.

^{31}P{^{1}H} NMR (295 K, 161.8 MHz, $CDCl_3$): δ_P = -143.9 (sept, $^1J_{PF}$ = 711 Hz, $[\mathbf{P}F_6]^-$), -5.5 (br, $\mathbf{P}Ph_3$), 24.9 (s, $[\mathbf{P}Ph_3\text{-}CPh_3]^+$) ppm.

^{19}F NMR (295 K, 376.2 MHz, $CDCl_3$): δ_F = -73.36 (d, $^1J_{FP}$ = 711 Hz, $[P\mathbf{F}_6]^-$) ppm.

The NMR spectra of this material also showed the presence of vacuum grease and DCM.

6.9.5 Reactivity of $[Ag(PPh_3)_3]^+[P\{OCH(CF_3)_2\}_5F]^-$, (**19**) with Ph_3CCl

Recrystallised tritylchloride, Ph_3CCl (3 mg, 0.01mmol, 1 eq.), $[Ag(PPh_3)_3]^+[P\{OCH(CF_3)_2\}_5F]^-$, (**19**) (18 mg, 0.01 mmol, 1 eq.), and CD_2Cl_2 (0.6 mL) were added to a J Young's tap NMR tube in an inert-atmosphere glovebox. Ultrasonic activation (room temperature, 30 min.) was used to increase the solubility of the reagents. A hexane layer (0.7 mL) was used to aid crystallisation *via* slow diffusion of the solvents. The clear crystals, suitable for single-crystal X-ray diffraction were found to consist of $(PPh_3AgCl)_2$.

The reaction mixture before crystallisation and the mother liquor after crystallisation were both analysed by NMR spectroscopy.

^{1}H NMR (295 K, 400 MHz, $CDCl_3$): δ_H = 2.01 (br), 6.80 -7.70 (br, $[Ag(P\mathbf{Ph}_3)_3]^+$), 8.60-9.90 (br), ppm. The shimming of this sample was poor, hence the multiplicity of the peaks was difficult to obtain.

^{31}P{^{1}H} NMR (295 K, 161.8 MHz, $CDCl_3$): δ_P = -145.5 (d, $^{1}J_{PF}$ = 818 Hz, $[\mathbf{P}\{OCH(CF_3)_2\}_5F]^-$), 10.3 (s, $[Ag(\mathbf{P}Ph_3)_3]^+$), 25.5 (s, $[Ph_3C\text{-}\mathbf{P}Ph_3]^+$), 26.7 (s, $(\mathbf{P}Ph_3AgCl)_2$) ppm.

^{19}F NMR (295 K, 376.2 MHz, $CDCl_3$): δ_F = -70.98 (br, axial $[P\{OCH(C\mathbf{F}_3)_2\}_5F]^-$), -70.77 (s, equatorial $[P\{OCH(C\mathbf{F}_3)_2\}_5F]^-$), -58.15 (d, $^{1}J_{FP}$ = 818 Hz, $[P\{OCH(CF_3)_2\}_5\mathbf{F}]^-$) ppm. Since the equatorial and axial peaks overlap, a combined integration was calculated to give 30F for the hexafluoroisopropoxy groups on the $[P\{OCH(C\mathbf{F}_3)_2\}_5F]^-$ anion.

Weak intensity peaks at -73.70 (t, J = 8 Hz), -72.36 (br), -72.26 (br), -71.85 (br), -71.70 (br), ppm were also observed.

The NMR spectra of this material also showed the presence of vacuum grease and DCM.

NMR spectra of mother liquor:

^{1}H NMR (295 K, 400 MHz, $CDCl_3$): δ_H = 7.02 -7.83 (m, $[Ag(P\mathbf{Ph}_3)_3]^+$) ppm.

^{31}P{^{1}H} NMR (295 K, 161.8 MHz, $CDCl_3$): δ_P = -147.5 (d, $^{1}J_{PF}$ = 818 Hz, $[\mathbf{P}\{OCH(CF_3)_2\}_5F]^-$), 7.7 (s, $[Ag(\mathbf{P}Ph_3)_3]^+$), 23.6 (s, $[Ph_3C\text{-}\mathbf{P}Ph_3]^+$) ppm.

^{19}F NMR (295 K, 376.2 MHz, $CDCl_3$): δ_F = -75.42 (d, J = 7Hz), -74.50 (d, J = 5 Hz), -73.78 (br), -73.60 (br, axial $[P\{OCH(C\mathbf{F}_3)_2\}_5F]^-$), -72.72 (s, equatorial $[P\{OCH(C\mathbf{F}_3)_2\}_5F]^-$), -60.30 (d, $^{1}J_{FP}$ = 818 Hz, $[P\{OCH(CF_3)_2\}_5\mathbf{F}]$) ppm. Since the equatorial and axial peaks overlap, a combined integration was calculated to give 30F for the hexafluoroisopropoxy groups on the $[P\{OCH(C\mathbf{F}_3)_2\}_5F]^-$ anion.

The NMR spectra of this material also showed the presence of vacuum grease, hexane and DCM.

6.9.6 Reactivity of $[Ag(PPh_3)_3]^+[P\{OCH(CF_3)_2\}_5F]^-$, (**19**) with MeI

$[Ag(PPh_3)_3]^+[P\{OCH(CF_3)_2\}_5F]^-$, (**19**) (10 mg, 0.005 mmol, 1 eq.) and CD_2Cl_2 (0.6 mL) were added to a J Young's tap NMR tube in an inert-atmosphere glovebox. Methyl iodide,

MeI (1 mg, 0.07mmol, 14 eq.) was added to this, followed by ultrasonic activation (room temperature, 30 min.). A hexane layer (0.7 mL) was used to aid crystallisation *via* slow diffusion of the solvents. The colourless crystals suitable for single-crystal X-ray diffraction were found to consist of $[PPh_3Me]^+[I_4Ag_3]^-$.

^{1}H NMR (295 K, 400 MHz, $CDCl_3$): δ_H = 2.09 (s, **Me**I), 2.91 (d, J = 14 Hz, $[PPh_3\mathbf{Me}]^+$), 6.55 -7.83 (m, $[P\mathbf{Ph}_3Me]^+$) ppm.

^{31}P{^{1}H} NMR (295 K, 161.8 MHz, $CDCl_3$): δ_P = -147.5 (d, $^1J_{PF}$ = 818 Hz, $[\mathbf{P}\{OCH(CF_3)_2\}_5F]^-$), 21.8 (s, $[PPh_3Me]^+$) ppm.

^{19}F NMR (295 K, 376.2 MHz, $CDCl_3$): δ_F = -75.39 (d, J = 8 Hz, NaOCH(C**F**$_3$), -73.04 (br, axial $[P\{OCH(C\mathbf{F}_3)_2\}_5F]^-$), -72.77 (s, equatorial $[P\{OCH(C\mathbf{F}_3)_2\}_5F]^-$), -59.85 (d, $^1J_{FP}$ = 818 Hz, $[P\{OCH(CF_3)_2\}_5\mathbf{F}]^-$) ppm. Since the equatorial and axial peaks overlap, a combined integration was calculated to give 30F for the hexafluoroisopropoxy groups on the $[P\{OCH(C\mathbf{F}_3)_2\}_5F]^-$ anion. Five other weak intensity signals were observed in the spectrum.

The NMR spectra of this material also showed the presence of vacuum grease and DCM.

6.9.7 Reactivity of $[Ag(PPh_3)_3]^+[P\{OCH(CF_3)_2\}_5F]^-$, (**19**) with $\{Et_2O\}_2HCl$

$[Ag(PPh_3)_3]^+[P\{OCH(CF_3)_2\}_5F]^-$, (**19**) (10 mg, 0.005 mmol, 1 eq.) and CD_2Cl_2 (0.6 mL) were added to a PTFE J Young's tap NMR tube in an inert-atmosphere glovebox. $\{Et_2O\}_2HCl$ (0.05 mL of 1M solution, 0.05 mmol, 0.25 eq.) was added on the Schlenk line, followed by ultrasonic activation (room temperature, 1 hour). The reaction mixture was then layered with hexane and left to crystallise. Crystals suitable for single-crystal X-ray diffraction were observed to consist of a $Ag_4Cl_4(PPh_3)_4$ type cluster.

^{1}H NMR (295 K, 400 MHz, $CDCl_3$): δ_H = 1.07 (t, J = 8 Hz, $\{\mathbf{Et}_2O\}_2HCl$), 3.36 (q, J = 8 Hz, $\{\mathbf{Et}_2O\}_2HCl$), 4.28 (m, NaOC**H**$(CF_3)_2\}_5$), 7.10-7.50 (m, $[Ag(\mathbf{P}Ph_3)_3]^+$) ppm.

^{31}P{^{1}H} NMR (295 K, 161.8 MHz, $CDCl_3$): δ_P = -10.6 (d, J = 1021 Hz), -10.1 (d, J = 927 Hz), -3.3 (s, O=**P**$\{OCH(CF_3)_2\}_3$), -2.6 (s). 8.77 (br, $Ag_4Cl_4(\mathbf{P}Ph_3)_4$), 23.1 (s) ppm.

^{19}F NMR (295 K, 376.2 MHz, $CDCl_3$): δ_F = -83.45 (d, J = 21 Hz), -76.04 (d, J = 8 Hz), -75.70 (d, J = 977 Hz), -74.94 (d, J = 4 Hz), -74.75 (d, J = 5Hz), -74.65 (m), -74.50 (d, J = 5Hz), -73.31 (s) ppm.

The NMR spectra of this material also showed the presence of vacuum grease and DCM.

6.9.8 Reactivity of $[Ag(PPh_3)_3]^+[P\{OCH(CF_3)_2\}_5F]^-$, (**19**) with Water

D_2O (0.4 mL) was added to 5 mg of solid $[Ag(PPh_3)_3]^+[P\{OCH(CF_3)_2\}_5F]^-$, (**10**) in a non-air tight NMR tube. The salt was found to be insoluble in D_2O, so wet THF was added and the sample was analysed by $^{31}P\{^1H\}$, ^{19}F and ^1H NMR spectroscopy. The solubility of (**19**) in D_2O/THF was poor. However, the characteristic peaks of the $[P\{OCH(CF_3)_2\}_5F]^-$ anion were present in the ^{19}F NMR spectrum. This suggests hydrolysis of the $[P\{OCH(CF_3)_2\}_5F]^-$ anion does not occur.

^{1}H NMR (295 K, 400 MHz, D_2O): δ_H = 4.70 (br, H_2O), 5.10 (s, $[P\{OC\mathbf{H}(CF_3)_2\}_5F]^-$), 7.00-7.38 (m, $[Ag(P\mathbf{Ph}_3)_3]^+$) ppm.

$^{31}P\{^1H\}$ NMR (295 K, 161.8 MHz, D_2O): δ_P = -147.5 (d, $^1J_{PF}$ = 818 Hz, $[\mathbf{P}\{OCH(CF_3)_2\}_5F]^-$), 11.8 (s, $[Ag(\mathbf{P}Ph_3)_3]^+$).

^{19}F NMR (295 K, 376.2 MHz, D_2O): δ_F = -73.12 (br, axial $[P\{OCH(C\mathbf{F}_3)_2\}_5F]^-$), -72.83(s, equatorial $[P\{OCH(C\mathbf{F}_3)_2\}_5F]^-$), -59.85 (d, 1F, $^1J_{FP}$ = 818 Hz, $[P\{OCH(CF_3)_2\}_5\mathbf{F}]^-$) ppm. Since the equatorial and axial peaks overlap, a combined integration was calculated to give 30F for the hexafluoroisopropoxy groups on the $[P\{OCH(C\mathbf{F}_3)_2\}_5F]^-$ anion.

Lower intensity signals were observed at -75.99 (d, J = 8 Hz), -73.90 (br) and -73.75 (s) ppm.

The NMR spectra of this material also showed the presence of vacuum grease.

6.9.9 Attempted Synthesis of $[Na(NCMe)_6]^+[P\{OCH(CF_3)_2\}_6]^-$

Phosphorus pentachloride (41 mg, 0.20 mmol, 1 eq.) and $NaOCH(CF_3)_2$ (190 mg, 1.0 mmol, 5 eq.) were added to a J Young's ampoule with DCM (10 mL) in an inert-atmosphere glovebox. Ultrasonic activation (room temperature, 1 hour) was used to increase the solubility of the $NaOCH(CF_3)_2$. NMR spectroscopy was used to establish reaction completion. This reaction mixture was then used *in situ,* for reaction of $P\{OCH(CF_3)_2\}_5$ with $NaOCH(CF_3)_2\}$ (38 mg, 0.20 mmol, 1 eq.) followed by ultrasonic activation (room temperature, 1 hour). The ESI-MS analysis (in MeCN solution) indicated the presence of $[P\{OCH(CF_3)_2\}_6]^-$ in the negative mode, although spectroscopic NMR analysis did not confirm the presence of this anion in the condensed phase.

^{1}H NMR (295 K, 400 MHz, $CDCl_3$): δ_H = 4.30 (m, $P\{OC\mathbf{H}(CF_3)_2\}_5$) ppm.

$^{31}P\{^{1}H\}$ NMR (295 K, 161.8 MHz, $CDCl_3$): δ_P = -83.4 (s, **P**$\{OCH(CF_3)_2\}_5$), -3.1 (s, O=**P**$\{OCH(CF_3)_2\}_3$) ppm.

^{19}F NMR (295 K, 376.2 MHz, $CDCl_3$): δ_F = -75.98 (t, J = 7 Hz, P$\{OCH(CF_3)_2\}_5$), -75.55 (d, J = 6 Hz, Na$\{OCH(CF_3)_2\}$), -73.43 (br, O=**P**$\{OCH(CF_3)_2\}_3$) ppm.

The NMR spectra of this material also showed the presence of vacuum grease, DCM and MeCN.

EI-MS (MeCN): m/z observed 884.9349 m/z, $[M]^-$ (calculated 884.9385 m/z for $[P\{OCH(CF_3)_2\}_5F]^-$, 4.1 ppm), m/z observed 1032.9349 m/z, $[M]^-$ (calculated 1032.9333 m/z for $[P\{OCH(CF_3)_2\}_6]^-$, -1.5ppm).

7 ABBREVIATIONS

General Chemical:

$[M]^+$	molecular ion
˚C	degrees Celcius
Å	Angstrom
Ar	aryl
cm^{-1}	centimeter
Cp	cyclopentadienyl
DCM	dichloromethane
DFT	density functional theory
dm^{-3}	decimeter cubed
DSC	differential scanning calorimetry
EI	electron ionisation
eq.	equivalents
ESI	electrospray ionisation
Et_2O	diethyl ether
FTIR	Fourier Transform Infrared
g	grams
GC	Gas Chromotography
hr.	hour
IL	ionic liquid
^{i}Pr	isopropyl
IR	infrared
J	Joules
K	Kelvin
kcal	kilocalories
kJ	kilojoules
LIFDI	Liquid Injection Field Desorption Ionisation
m/z	mass/charge
Me	methyl
MeCN	acetonitrile
Mesityl	2,4,6 trimethylphenyl
mg	milligrams
min.	minute
mL	millilitre
mmol	milimole
MS	mass spectrometry
o	*ortho*
OR	alkoxy group
OR^F	fluorinated alkoxy group
p	*para*
Ph	phenyl
PTFE	polytetrafluoroethylene

R	alkyl group	WCC	weakly coordinating cation
ref.	reference	$\Delta G^{\ddagger}$	Gibbs free energy
R^F	fluorinated alkyl group	$\Delta H^{\ddagger}$	enthalpy
^{t}Bu	tert-butyl	$\Delta S^{\ddagger}$	entropy
THF	tetrahydrofuran	µL	microlitre
WCA	weakly coordinating anion		

In relation to nuclear magnetic resonance spectroscopy

br	broad	ppm	parts per million
d	doublet	q	quartet
Hz	Hertz	quin	quintet
J	coupling constant	s	singlet
m	complex multiplet	sept	septet
MHz	megaHertz	t	triplet
NMR	nuclear magnetic resonance	δ	chemical shift (in ppm)

8 REFERENCES

1. Q. C. Mir, R. W. Shreeve and J. M. Shreeve, *Phosphorus Sulfur and Silicon and the Related Elements*, 1980, **8**, 331-333.
2. D. Dakternieks, G. V. Roschenthaler and R. Schmutzler, *Journal of Fluorine Chemistry*, 1978, **11**, 387-398.
3. D. G. Gusev, *Organometallics*, 2009, **28**, 763-770.
4. C. J. Willis, *Coordination Chemistry Reviews*, 1988, **88**, 133-202.
5. F. Swarts, *Recueil Des Travaux Chimiques Des Pays-Bas Et De La Belgique*, 1909, **28**, 166-170.
6. C. J. Bradaric, A. Downard, C. Kennedy, A. J. Robertson and Y. H. Zhou, Green Solvents for Catalysis Meeting, Bruchsal, Germany, 2002.
7. G. Keglevich, Z. Baan, I. Hermecz, T. Novak and I. L. Odinets, *Current Organic Chemistry*, 2007, **11**, 107-126.
8. J. J. Tindale and P. J. Ragogna, *Chemical Communications*, 2009, 1831-1833.
9. J. Dupont, R. F. de Souza and P. A. Z. Suarez, *Chemical Reviews*, 2002, **102**, 3667-3691.
10. N. Burford, T. S. Cameron, J. A. C. Clyburne, K. Eichele, K. N. Robertson, S. Sereda, R. E. Wasylishen and W. A. Whitla, *Inorganic Chemistry*, 1996, **35**, 5460-5467.
11. K. Eichele, R. E. Wasylishen, R. W. Schurko, N. Burford and W. A. Whitla, *Canadian Journal of Chemistry-Revue Canadienne De Chimie*, 1996, **74**, 2372-2377.
12. P. G. Gassman, J. R. Sowa, M. G. Hill and K. R. Mann, *Organometallics*, 1995, **14**, 4879-4885.
13. M. G. Hill, W. M. Lamanna and K. R. Mann, *Inorganic Chemistry*, 1991, **30**, 4687-4690.
14. P. G. Gassman and P. A. Deck, *Organometallics*, 1994, **13**, 1934-1939.
15. G. Erre, S. Enthaler, K. Junge, S. Gladiali and M. Beller, *Coordination Chemistry Reviews*, 2008, **252**, 471-491.
16. T. Hayashi, *Accounts of Chemical Research*, 2000, **33**, 354-362.
17. C. A. Fleckenstein and H. Plenio, *Chemical Society Reviews*, 2010, **39**, 694-711.
18. M. R. Wilson, H. Y. Liu, A. Prock and W. P. Giering, *Organometallics*, 1993, **12**, 2044-2050.
19. M. Yamashita and J. F. Hartwig, *Journal of the American Chemical Society*, 2004, **126**, 5344-5345.
20. C. A. Tolman, *Chemical Reviews*, 1977, **77**, 313-348.
21. T. E. Muller and D. M. P. Mingos, *Transition Metal Chemistry*, 1995, **20**, 533-539.
22. B. J. Dunne, R. B. Morris and A. G. Orpen, *Journal of the Chemical Society-Dalton Transactions*, 1991, 653-661.
23. K. D. Cooney, T. R. Cundari, N. W. Hoffman, K. A. Pittard, M. D. Temple and Y. Zhao, *Journal of the American Chemical Society*, 2003, **125**, 4318-4324.
24. E. Burello and G. Rothenberg, *International Journal of Molecular Sciences*, 2006, **7**, 375-404.

25. A. L. Seligson and W. C. Trogler, *Journal of the American Chemical Society*, 1991, **113**, 2520-2527.
26. C. A. Tolman, W. C. Seidel and L. W. Gosser, *Journal of the American Chemical Society*, 1974, **96**, 53-60.
27. T. L. Brown and K. J. Lee, *Coordination Chemistry Reviews*, 1993, **128**, 89-116.
28. L. Stahl and R. D. Ernst, *Journal of the American Chemical Society*, 1987, **109**, 5673-5680.
29. K. A. Bunten, L. Z. Chen, A. L. Fernandez and A. J. Poe, *Coordination Chemistry Reviews*, 2002, **233**, 41-51.
30. D. Evans, J. A. Osborn and Wilkinso.G, *Journal of the Chemical Society a - Inorganic Physical Theoretical*, 1968, 3133-3142.
31. K. A. P. Aaron M. Gillespie, Thomas R. Cundari, and David P. White, *Internet Electron. J. Mol. Des.*, 2002, **1**, 242-251.
32. N. Fey, A. C. Tsipis, S. E. Harris, J. N. Harvey, A. G. Orpen and R. A. Mansson, *Chemistry-a European Journal*, 2006, **12**, 291-302.
33. J. Jover, N. Fey, J. N. Harvey, G. C. Lloyd-Jones, A. G. Orpen, G. J. J. Owen-Smith, P. Murray, D. R. J. Hose, R. Osborne and M. Purdie, *Organometallics*, 2010, **29**, 6245-6258.
34. R. A. Mansson, A. H. Welsh, N. Fey and A. G. Orpen, *Journal of Chemical Information and Modeling*, 2006, **46**, 2591-2600.
35. S. Kozuch and S. Shaik, *Journal of Molecular Catalysis a-Chemical*, 2010, **324**, 120-126.
36. A. Immirzi and A. Musco, *Inorganica Chimica Acta*, 1977, **25**, L41-L42.
37. I. A. Guzei and M. Wendt, *Dalton Transactions*, 2006, 3991-3999.
38. L. N. Zakharov, Y. N. Safyanov and G. A. Domrachev, *Inorganica Chimica Acta*, 1989, **160**, 77-82.
39. N. J. Coville, M. S. Loonat, D. White and L. Carlton, *Organometallics*, 1992, **11**, 1082-1090.
40. D. P. White, J. C. Anthony and A. O. Oyefeso, *Journal of Organic Chemistry*, 1999, **64**, 7707-7716.
41. D. White, B. C. Taverner, P. G. L. Leach and N. J. Coville, *Journal of Computational Chemistry*, 1993, **14**, 1042-1049.
42. T. L. Brown, *Inorganic Chemistry*, 1992, **31**, 1286-1294.
43. M. G. Choi and T. L. Brown, *Inorganic Chemistry*, 1993, **32**, 5603-5610.
44. M. G. Choi and T. L. Brown, *Inorganic Chemistry*, 1993, **32**, 1548-1553.
45. M. G. Choi, D. White and T. L. Brown, *Inorganic Chemistry*, 1994, **33**, 5591-5594.
46. N. Fey, A. G. Orpen and J. N. Harvey, *Coordination Chemistry Reviews*, 2009, **253**, 704-722.
47. C. A. Tolman, *Journal of the American Chemical Society*, 1970, **92**, 2953-2956.
48. J. Chatt and F. A. Hart, *Journal of the Chemical Society*, 1960, 1378-1389.
49. A. G. Orpen and N. G. Connelly, *Organometallics*, 1990, **9**, 1206-1210.
50. F. A. Cotton and G. Wilkinson, *Advanced Inorganic Chemistry 5th Edition*, Wiley-Interscience, New York, 1988.
51. L. Perrin, E. Clot, O. Eisenstein, J. Loch and R. H. Crabtree, *Inorganic Chemistry*, 2001, **40**, 5806-5811.
52. C. H. Suresh and N. Koga, *Inorganic Chemistry*, 2002, **41**, 1573-1578.

53. J. Mathew, T. Thomas and C. H. Suresh, *Inorganic Chemistry*, 2007, **46**, 10800-10809.
54. Bonaccor.R, E. Scrocco and J. Tomasi, *Journal of Chemical Physics*, 1970, **52**, 5270-5284.
55. Bonaccor.R, E. Scrocco and J. Tomasi, *Theoretica Chimica Acta*, 1971, **21**, 17-27.
56. H. Berthod and A. Pullman, *Chemical Physics Letters*, 1975, **32**, 233-235.
57. C. Giessnerprettre and A. Pullman, *Theoretica Chimica Acta*, 1975, **37**, 335-339.
58. G. Dive and D. Dehareng, *International Journal of Quantum Chemistry*, 1993, **46**, 127-136.
59. P. Politzer and J. S. Murray, *Journal of Physical Chemistry A*, 1998, **102**, 1018-1020.
60. K. D. Sen and P. Politzer, *Journal of Chemical Physics*, 1989, **90**, 4370-4372.
61. G. Narayszabo and G. G. Ferenczy, *Chemical Reviews*, 1995, **95**, 829-847.
62. B. Pullman, *International Journal of Quantum Chemistry*, 1990, 81-92.
63. S. R. Gadre and I. H. Shrivastava, *Journal of Chemical Physics*, 1991, **94**, 4384-4390.
64. R. N. Shirsat, S. V. Bapat and S. R. Gadre, *Chemical Physics Letters*, 1992, **200**, 373-378.
65. C. H. Suresh, *Inorganic Chemistry*, 2006, **45**, 4982-4986.
66. W. P. Giering, A. Prock and A. L. Fernandez, *Inorganic Chemistry*, 2003, **42**, 8033-8037.
67. O. Kuhl, *Coordination Chemistry Reviews*, 2005, **249**, 693-704.
68. J. Tiburcio, S. Bernes and H. Torrens, *Polyhedron*, 2006, **25**, 1549-1554.
69. D. J. M. Snelders, G. van Koten and R. J. M. K. Gebbink, *Chemistry-a European Journal*, 2011, **17**, 42-57.
70. A. D. Burrows, G. Kociok-Kohn, M. F. Mahon and M. Varrone, *Comptes Rendus Chimie*, 2006, **9**, 111-119.
71. A. L. Fernandez, M. R. Wilson, A. Prock and W. P. Giering, *Organometallics*, 2001, **20**, 3429-3435.
72. R. L. Harlow, D. L. Thorn, R. T. Baker and N. L. Jones, *Inorganic Chemistry*, 1992, **31**, 993-997.
73. A. L. Fernandez, C. Reyes, A. Prock and W. P. Giering, *Journal of the Chemical Society-Perkin Transactions 2*, 2000, **5**, 1033-1041.
74. D. Woska, A. Prock and W. P. Giering, *Organometallics*, 2000, **19**, 4629-4638.
75. P. G. Edwards, B. M. Kariuki, M. Limon, L.-L. Ooi, J. A. Platts and P. D. Newman, *European Journal of Inorganic Chemistry*, 2011, 1230-1239.
76. A. K. Brisdon and C. J. Herbert, *Chemical Communications*, 2009, 6658-6660.
77. K. K. Banger, A. K. Brisdon, C. J. Herbert, H. A. Ghaba and I. S. Tidmarsh, *Journal of Fluorine Chemistry*, 2009, **130**, 1117-1129.
78. C. L. Pollock, G. C. Saunders, E. Smyth and V. I. Sorokin, *Journal of Fluorine Chemistry*, 2008, **129**, 142-166.
79. A. B. Burg and W. Mahler, *Journal of the American Chemical Society*, 1958, **80**, 2334-2334.
80. R. G. Peters, B. L. Bennett, R. C. Schnabel and D. M. Roddick, *Inorganic Chemistry*, 1997, **36**, 5962-5965.

81. G. R. Dobson, *Advances in Inorganic Chemistry*, 1966, **8**, 1.
82. H. J. Emeleus and J. D. Smith, *Journal of the Chemical Society*, 1959, 375-381.
83. M. F. Ernst and D. M. Roddick, *Inorganic Chemistry*, 1989, **28**, 1624-1627.
84. L. D. Field and M. P. Wilkinson, *Tetrahedron Letters*, 1992, **33**, 7601-7604.
85. P. Cooper, R. Fields and Haszeldi.Rn, *Journal of the Chemical Society C-Organic*, 1971, 3031-3035.
86. I. G. Phillips, R. G. Ball and R. G. Cavell, *Inorganic Chemistry*, 1988, **27**, 4038-4045.
87. C. A. Mcauliffe, *Comprehensive Coordination Chemistry*, 1987, **2**, CH14.
88. W. Levason, *In The Chemistry of Organophosphorus Compounds*, 1990, **1**, CH15.
89. V. I. Losilkina, M. N. Estekhina, N. K. Baranetskaya and V. N. Setkina, *Journal of Organometallic Chemistry*, 1986, **299**, 187-195.
90. M. B. Murphy-Jolly, L. C. Lewis and A. J. M. Caffyn, *Chemical Communications*, 2005, 4479-4480.
91. J. J. Kampa, J. W. Nail and R. J. Lagow, *Angewandte Chemie-International Edition in English*, 1995, **34**, 1241-1244.
92. V. Y. Semenii, V. A. Stepanov, N. V. Ignatev, G. G. Furin and L. M. Yagupolskii, *Zhurnal Obshchei Khimii*, 1985, **55**, 2716-2720.
93. K. K. Banger, R. P. Banham, A. K. Brisdon, W. I. Cross, G. Damant, S. Parsons, R. G. Pritchard and A. Sousa-Pedrares, *Journal of the Chemical Society-Dalton Transactions*, 1999, 427-434.
94. N. A. Barnes, A. K. Brisdon, F. R. W. Brown, W. I. Cross, I. R. Crossley, C. Fish, J. V. Morey, R. G. Pritchard and L. Sekhri, *New Journal of Chemistry*, 2004, **28**, 828-837.
95. N. A. Barnes, A. K. Brisdon, F. R. W. Brown, W. I. Cross, C. J. Herbert, R. G. Pritchard and G. Sadiq, *Dalton Transactions*, 2008, 101-114.
96. N. A. Barnes, A. K. Brisdon, M. J. Ellis and R. G. Pritchard, *Journal of Fluorine Chemistry*, 2001, **112**, 35-45.
97. H. G. Horn, F. Kolkmann, H. C. Marsmann and R. Kontges, *Zeitschrift Fur Naturforschung Section B-a Journal of Chemical Sciences*, 1978, **33**, 1422-1426.
98. A. Roodt, S. Otto and G. Steyl, *Coordination Chemistry Reviews*, 2003, **245**, 121-137.
99. S. Serron, S. P. Nolan and K. G. Moloy, *Organometallics*, 1996, **15**, 4301-4306.
100. I. T. Horvath and J. Rabai, *Science (Washington D C)*, 1994, **266**, 72-75.
101. E. de Wolf, G. van Koten and B. J. Deelman, *Chemical Society Reviews*, 1999, **28**, 37-41.
102. P. Bhattacharyya, D. Gudmunsen, E. G. Hope, R. D. W. Kemmitt, D. R. Paige and A. M. Stuart, *Journal of the Chemical Society-Perkin Transactions 1*, 1997, 3609-3612.
103. D. J. Adams, J. A. Bennett, D. J. Cole-Hamilton, E. G. Hope, J. Hopewell, J. Kight, P. Pogorzelec and A. M. Stuart, *Dalton Transactions*, 2005, 3862-3867.
104. D. J. Adams, D. Gudmunsen, J. Fawcett, E. G. Hope and A. M. Stuart, *Tetrahedron*, 2002, **58**, 3827-3834.
105. D. J. Adams, D. Gudmunsen, E. G. Hope, A. M. Stuart and A. West, *Journal of Fluorine Chemistry*, 2003, **121**, 213-217.

106. P. Bhattacharyya, B. Croxtall, J. Fawcett, D. Gudmunsen, E. G. Hope, R. D. W. Kemmitt, D. R. Paige, D. R. Russell, A. M. Stuart and D. R. W. Wood, *Journal of Fluorine Chemistry*, 2000, **101**, 247-255.
107. B. Croxtall, J. Fawcett, E. G. Hope and A. M. Stuart, *Journal of the Chemical Society-Dalton Transactions*, 2002, 491-499.
108. J. Fawcett, E. G. Hope, R. D. W. Kemmitt, D. R. Paige, D. R. Russell, A. M. Stuart, D. J. ColeHamilton and M. J. Payne, *Chemical Communications*, 1997, 1127-1128.
109. D. Gudmunsen, E. G. Hope, D. R. Paige and A. M. Stuart, *Journal of Fluorine Chemistry*, 2009, **130**, 942-950.
110. E. G. Hope, D. Gudmunsen, R. D. W. Kemmitt, D. R. Paige and A. M. Stuart, *Abstracts of Papers of the American Chemical Society*, 1998, **216**, U825-U825.
111. A. M. B. Osuna, W. P. Chen, E. G. Hope, R. D. W. Kemmitt, D. R. Paige, A. M. Stuart, J. L. Xiao and L. J. Xu, *Journal of the Chemical Society-Dalton Transactions*, 2000, 4052-4055.
112. G. Pozzi, F. Montanari and S. Quici, *Chemical Communications*, 1997, 69-70.
113. J. M. Vincent, A. Rabion, V. K. Yachandra and R. H. Fish, *Angewandte Chemie-International Edition in English*, 1997, **36**, 2346-2349.
114. R. Kling, D. Sinou, G. Pozzi, A. Choplin, F. Quignard, S. Busch, S. Kainz, D. Koch and W. Leitner, *Tetrahedron Letters*, 1998, **39**, 9439-9442.
115. D. Rutherford, J. J. J. Juliette, C. Rocaboy, I. T. Horvath and J. A. Gladysz, *Catalysis Today*, 1998, **42**, 381-388.
116. J. J. J. Juliette, I. T. Horvath and J. A. Gladysz, *Angewandte Chemie-International Edition in English*, 1997, **36**, 1610-1612.
117. J. J. J. Juliette, D. Rutherford, I. T. Horvath and J. A. Gladysz, *Journal of the American Chemical Society*, 1999, **121**, 2696-2704.
118. C. P. Casey, E. L. Paulsen, E. W. Beuttenmueller, B. R. Proft, L. M. Petrovich, B. A. Matter and D. R. Powell, *Journal of the American Chemical Society*, 1997, **119**, 11817-11825.
119. D. B. Denney, D. Z. Denney, P. J. Hammond, L. T. Liu and Y. P. Wang, *Journal of Organic Chemistry*, 1983, **48**, 2159-2164.
120. D. E. Young and W. B. Fox, *Inorganic & Nuclear Chemistry Letters*, 1971, **7**, 1033-1036.
121. D. Dakternieks, G. V. Roschenthaler and R. Schmutzler, *Journal of Fluorine Chemistry*, 1978, **12**, 413-426.
122. P. Vanleeuwen and C. F. Roobeek, *Tetrahedron*, 1981, **37**, 1973-1983.
123. V. F. Mironov and I. V. Konovalova, *Zhurnal Obshchei Khimii*, 1993, **63**, 2537-2541.
124. J. M. Shreeve and S. M. Williamson, *Journal of Organometallic Chemistry*, 1983, **249**, C13-C15.
125. O. Sakatsume, H. Yamane, H. Takaku and N. Yamamoto, *Tetrahedron Letters*, 1989, **30**, 6375-6378.
126. A. J. M. Caffyn and K. M. Nicholas, *Journal of the American Chemical Society*, 1993, **115**, 6438-6439.
127. M. Murakami, M. Ubukata, K. Itami and Y. Ito, *Angewandte Chemie-International Edition*, 1998, **37**, 2248-2250.
128. R. S. Jolly, G. Luedtke, D. Sheehan and T. Livinghouse, *Journal of the American Chemical Society*, 1990, **112**, 4965-4966.

129. K. S. Shen and T. Livinghouse, *Synlett*, 247-249.
130. C. Cativiela, J. I. Garcia, J. A. Mayoral and L. Salvatella, *Chemical Society Reviews*, 1996, **25**, 209-218.
131. D. J. R. O'Mahony, D. B. Belanger and T. Livinghouse, *Organic & Biomolecular Chemistry*, 2003, **1**, 2038-2040.
132. S. Yanagisawa, T. Sudo, R. Noyori and K. Itami, *Tetrahedron*, 2008, **64**, 6073-6081.
133. S. Yanagisawa, T. Sudo, R. Noyori and K. Itami, *Journal of the American Chemical Society*, 2006, **128**, 11748-11749.
134. S. Yanagisawa, K. Ueda, H. Sekizawa and K. Itami, *Journal of the American Chemical Society*, 2009, **131**, 14622-+.
135. K. Ueda, S. Yanagisawa, J. Yamaguchi and K. Itami, *Angew Chem Int Ed Engl*, **49**, 8946-8949.
136. B. Liegault, D. Lapointe, L. Caron, A. Vlassova and K. Fagnou, *Journal of Organic Chemistry*, 2009, **74**, 1826-1834.
137. R. A. Baber, M. L. Clarke, K. M. Heslop, A. C. Marr, A. G. Orpen, P. G. Pringle, A. Ward and D. E. Zambrano-Williams, *Dalton Transactions*, 2005, 1079-1085.
138. L. O. Muller, R. Scopelitti and I. Krossing, *Zeitschrift Fur Anorganische Und Allgemeine Chemie*, 2008, **634**, 1035-1040.
139. J. B. Tong, S. L. Liu, S. W. Zhang and S. S. Z. Li, *Spectrochimica Acta Part a-Molecular and Biomolecular Spectroscopy*, 2007, **67**, 837-846.
140. A. D. DeBellis, S. D. Pastor, G. Rihs, R. K. Rodebaugh and A. R. Smith, *Inorganic Chemistry*, 2001, **40**, 2156-2160.
141. H. Stadtmuller and P. Knochel, *Organometallics*, 1995, **14**, 3163-3166.
142. S. O. Grim, McAllist.Pr and R. M. Singer, *Journal of the Chemical Society D-Chemical Communications*, 1969, 38-39.
143. M. Elmottaleb, *Journal of Molecular Structure*, 1976, **32**, 203-205.
144. E. O. Fischer, J. G. Verkade, L. Knauss and R. L. Keiter, *Journal of Organometallic Chemistry*, 1972, **37**, C7-C10.
145. F. Nief, F. Mercier and F. Mathey, *Journal of Organometallic Chemistry*, 1987, **328**, 349-355.
146. W. A. Schenk and W. Buchner, *Inorganica Chimica Acta-Articles*, 1983, **70**, 189-196.
147. T. J. Malosh, S. R. Wilson and J. R. Shapley, *Inorganica Chimica Acta*, 2009, **362**, 2849-2855.
148. F. Mercier, F. Mathey, C. Afiongakpan and J. F. Nixon, *Journal of Organometallic Chemistry*, 1988, **348**, 361-367.
149. E. Moser, E. O. Fischer, W. Bathelt, W. Gretner, L. Knauss and E. Louis, *Journal of Organometallic Chemistry*, 1969, **19**, 377-381.
150. G. Frenking, K. Wichmann, N. Frohlich, J. Grobe, W. Golla, D. Le Van, B. Krebs and M. Lage, *Organometallics*, 2002, **21**, 2921-2930.
151. S. O. Grim, Wheatlan.Da and McFarlan.W, *Journal of the American Chemical Society*, 1967, **89**, 5573-5577.
152. J. Apel, R. Bacher, J. Grobe and D. Levan, *Zeitschrift Fur Anorganische Und Allgemeine Chemie*, 1979, **453**, 39-52.
153. K. Tanaka, T. Tanaka and I. Kawafune, *Inorganic Chemistry*, 1984, **23**, 516-518.
154. F. A. Cotton and C. S. Kraihanz, *Journal of the American Chemical Society*, 1962, **84**, 4432-4438.

155. V. Jonas and W. Thiel, *Journal of Physical Chemistry A*, 1999, **103**, 1381-1393.
156. D. Karakas and C. Kaya, *Journal of Organometallic Chemistry*, 2001, **640**, 37-40.
157. F. T. Delbeke, E. G. Claeys and G. P. Vanderke, *Journal of Organometallic Chemistry*, 1970, **25**, 219-222.
158. N. Burford, D. E. Herbert, P. J. Ragogna, R. McDonald and M. J. Ferguson, *Journal of the American Chemical Society*, 2004, **126**, 17067-17073.
159. A. C. Diz, R. H. Contreras, M. A. Natiello and H. O. Gavarini, *Journal of Computational Chemistry*, 1985, **6**, 647-651.
160. J. F. Nixon and J. R. Swain, *Journal of the Chemical Society-Dalton Transactions*, 1972, 1038-1043.
161. A. W. Verstuyft, D. A. Redfield, L. W. Cary and J. H. Nelson, *Inorganic Chemistry*, 1976, **15**, 1128-1133.
162. R. L. Keiter, J. W. Benson, E. A. Keiter, T. A. Harris, M. W. Hayner, L. L. Mosimann, E. E. Karch, C. A. Boecker, D. M. Olson, J. VanderVeen, D. E. Brandt, A. L. Rheingold and G. P. A. Yap, *Organometallics*, 1997, **16**, 2246-2253.
163. J. M. Slattery and S. Hussein, *Dalton Transactions*, 2012, **41**, 1808-1815.
164. B. Breit, *Angewandte Chemie-International Edition*, 2005, **44**, 6816-6825.
165. P. R. E. C. F. Macrae, P. McCabe, E. Pidcock, G. P. Shields, R. Taylor, M. Towler and J. van de Streek, *J. Appl. Cryst.*, 2006, **39**, 453-457
166. F. H. Allen, *Acta Cryst.*, 2002, **B58**, 380-388.
167. J. C. C. I. J. Bruno, P. R. Edgington, M. Kessler, C. F. Macrae, P. McCabe, J. Pearson and R. Taylor, *Acta Crystallogr.*, 2002, **B58**, 389-397.
168. D. A. Fletcher, McMeeking, R.F., Parkin, D., *J. Chem. Inf. Comput. Sci.*, 1996, **36**, 746-749.
169. B. E. Mann, C. Masters and B. L. Shaw, *Journal of the Chemical Society a - Inorganic Physical Theoretical*, 1971, 1104-1106.
170. C. E. Dykstra and H. F. Schaefer, *Journal of the American Chemical Society*, 1978, **100**, 1378-1382.
171. M. I. Bruce, *Chemical Reviews*, 1991, **91**, 197-257.
172. J. Silvestre and R. Hoffmann, *Helvetica Chimica Acta*, 1985, **68**, 1461-1506.
173. E. Ruba, W. Simanko, K. Mauthner, K. M. Soldouzi, C. Slugovc, K. Mereiter, R. Schmid and K. Kirchner, *Organometallics*, 1999, **18**, 3843-3850.
174. C. S. Yi, J. R. Torres-Lubian, N. H. Liu, A. L. Rheingold and I. A. Guzei, *Organometallics*, 1998, **17**, 1257-1259.
175. M. Tokunaga and Y. Wakatsuki, *Angewandte Chemie-International Edition*, 1998, **37**, 2867-2869.
176. T. Suzuki, M. Tokunaga and Y. Wakatsuki, *Organic Letters*, 2001, **3**, 735-737.
177. C. Bruneau and P. H. Dixneuf, *Angewandte Chemie-International Edition*, 2006, **45**, 2176-2203.
178. C. Bruneau and P. H. Dixneuf, *Accounts of Chemical Research*, 1999, **32**, 311-323.
179. J. M. Lynam, *Chemistry-a European Journal*, 2010, **16**, 8238-8247.
180. Y. Arikawa, H. Yamasaki, M. Yamaguchi, K. Umakoshi and M. Onishi, *Organometallics*, 2009, **28**, 5587-5589.
181. J. M. Lynam, C. E. Welby and A. C. Whitwood, *Organometallics*, 2009, **28**, 1320-1328.

182. C. Grunwald, M. Laubender, J. Wolf and H. Werner, *Journal of the Chemical Society-Dalton Transactions*, 1998, 833-839.
183. F. De Angelis, A. Sgamellotti and N. Re, *Organometallics*, 2002, **21**, 2715-2723.
184. F. De Angelis, A. Sgamellotti and N. Re, *Dalton Transactions*, 2004, 3225-3230.
185. M. Tokunaga, T. Suzuki, N. Koga, T. Fukushima, A. Horiuchi and Y. Wakatsuki, *Journal of the American Chemical Society*, 2001, **123**, 11917-11924.
186. M. Olivan, E. Clot, O. Eisenstein and K. G. Caulton, *Organometallics*, 1998, **17**, 3091-3100.
187. P. D. Christian Bruneau, Jun Zhu, Zhenyang Lin, *Metal Vinylidenes and Allenylidenes in Catalysis: From Reactivity to Applications in Synthesis*, 2008.
188. E. Amigues, C. Hardacre, G. Keane, M. Migaud and M. O'Neill, *Chemical Communications*, 2006, 72-74.
189. B. Dutta, B. F. E. Curchod, P. Campomanes, E. Solari, R. Scopelliti, U. Rothlisberger and K. Severin, *Chemistry-a European Journal*, 2010, **16**, 8400-8409.
190. K. Kirchner, *Monatshefte Fur Chemie*, 2008, **139**, 337-348.
191. J. A. Varela and C. Saa, *Journal of Organometallic Chemistry*, 2009, **694**, 143-149.
192. Y. Yamamoto, T. Arakawa, R. Ogawa and K. Itoh, *Journal of the American Chemical Society*, 2003, **125**, 12143-12160.
193. K. Kirchner, M. J. Calhorda, R. Schmid and L. F. Veiros, *Journal of the American Chemical Society*, 2003, **125**, 11721-11729.
194. E. Elakkari, B. Floris, P. Galloni and P. Tagliatesta, *European Journal of Organic Chemistry*, 2005, 889-894.
195. E. Negishi, A. O. King and N. Okukado, *Journal of Organic Chemistry*, 1977, **42**, 1821-1823.
196. R. F. Heck and J. P. Nolley, *Journal of Organic Chemistry*, 1972, **37**, 2320-2322.
197. N. Miyaura, K. Yamada and A. Suzuki, *Tetrahedron Letters*, 1979, **20**, 3437-3440.
198. A. G. Myers, N. J. Tom, M. E. Fraley, S. B. Cohen and D. J. Madar, *Journal of the American Chemical Society*, 1997, **119**, 6072-6094.
199. P. Wipf and S. Lim, *Journal of the American Chemical Society*, 1995, **117**, 558-559.
200. C. Y. Hong, N. Kado and L. E. Overman, *Journal of the American Chemical Society*, 1993, **115**, 11028-11029.
201. S. J. Danishefsky, J. J. Masters, W. B. Young, J. T. Link, L. B. Snyder, T. V. Magee, D. K. Jung, R. C. A. Isaacs, W. G. Bornmann, C. A. Alaimo, C. A. Coburn and M. J. DiGrandi, *Journal of the American Chemical Society*, 1996, **118**, 2843-2859.
202. D. Mc Cartney and P. J. Guiry, *Chemical Society Reviews*, 2011, **40**, 5122-5150.
203. Y. Bendavid, M. Portnoy, M. Gozin and D. Milstein, *Organometallics*, 1992, **11**, 1995-1996.
204. K. Kikukawa and T. Matsuda, *Chemistry Letters*, 1977, 159-162.
205. S. Liu, O. Saidi, N. Berry, J. Ruan, A. Pettman, N. Thomson and J. Xiao, *Letters in Organic Chemistry*, 2009, **6**, 60-64.
206. Q. W. Yao, E. P. Kinney and Z. Yang, *Journal of Organic Chemistry*, 2003, **68**, 7528-7531.

207. C. Amatore, E. Carre, A. Jutand and Y. Medjour, *Organometallics*, 2002, **21**, 4540-4545.
208. A. Jutand, *Pure and Applied Chemistry*, 2004, **76**, 565-576.
209. C. Amatore, S. Bensalem, S. Ghalem, A. Jutand and Y. Medjour, *European Journal of Organic Chemistry*, 2004, 366-371.
210. A. F. Littke and G. C. Fu, *Angewandte Chemie-International Edition*, 2002, **41**, 4176-4211.
211. C. Amatore, A. Jutand, F. Khalil, M. A. Mbarki and L. Mottier, *Organometallics*, 1993, **12**, 3168-3178.
212. I. J. S. Fairlamb, A. R. Kapdi and A. F. Lee, *Organic Letters*, 2004, **6**, 4435-4438.
213. Y. Mace, A. R. Kapdi, I. J. S. Fairlamb and A. Jutand, *Organometallics*, 2006, **25**, 1795-1800.
214. P. Sehnal, H. Taghzouti, I. J. S. Fairlamb, A. Jutand, A. F. Lee and A. C. Whitwood, *Organometallics*, 2009, **28**, 824-829.
215. S. Maurer, C. Burkhart and G. Maas, *European Journal of Organic Chemistry*, 2010, 2504-2511.
216. F. A. Jalon, B. R. Manzano, F. Gomez-de la Torre, A. M. Lopez-Agenjo, A. M. Rodriguez, W. Weissensteiner, T. Sturm, J. Mahia and M. Maestro, *Journal of the Chemical Society-Dalton Transactions*, 2001, 2417-2424.
217. S. M. Reid, J. T. Mague and M. J. Fink, *Journal of Organometallic Chemistry*, 2000, **616**, 10-18.
218. I. Krossing, J. M. Slattery, C. Daguenet, P. J. Dyson, A. Oleinikova and H. Weingartner, *Journal of the American Chemical Society*, 2006, **128**, 13427-13434.
219. A. A. H. Padua, M. F. C. Gomes and J. N. A. C. Lopes, *Accounts of Chemical Research*, 2007, **40**, 1087-1096.
220. J. Qu, J. J. Truhan, S. Dai, H. Luo and P. J. Blau, *Tribology Letters*, 2006, **22**, 207-214.
221. K. Tsunashima and M. Sugiya, *Electrochemistry Communications*, 2007, **9**, 2353-2358.
222. H. Sawada, S. Kodama, K. Tsunashima and M. Sugiya, 4th Meeting of the Brazilian-Society-for-Materials-Research, Recife, BRAZIL, 2005.
223. T. Sato, G. Masuda and K. Takagi, *Electrochimica Acta*, 2004, **49**, 3603-3611.
224. H. Matsumoto, H. Sakaebe and K. Tatsumi, 12th International Meeting on Lithium Batteries, Nara, JAPAN, 2004.
225. Z. B. Zhou, H. Matsumoto and K. Tatsumi, *Chemistry-a European Journal*, 2005, **11**, 752-766.
226. X. M. Wang, E. Yasukawa and S. Kasuya, *Journal of the Electrochemical Society*, 2001, **148**, A1058-A1065.
227. X. M. Wang, E. Yasukawa and S. Kasuya, *Journal of the Electrochemical Society*, 2001, **148**, A1066-A1071.
228. B. E. Smart, W. J. Middleton and W. B. Farnham, *Journal of the American Chemical Society*, 1986, **108**, 4905-4907.
229. W. B. Farnham, B. E. Smart, W. J. Middleton, J. C. Calabrese and D. A. Dixon, *Journal of the American Chemical Society*, 1985, **107**, 4565-4567.
230. I. A. Koppel, R. Schwesinger, T. Breuer, P. Burk, K. Herodes, I. Koppel, I. Leito and M. Mishima, *Journal of Physical Chemistry A*, 2001, **105**, 9575-9586.
231. R. Schwesinger, R. Link, P. Wenzl, S. Kossek and M. Keller, *Chemistry*, 2005, **12**, 429-437.

232. A. Pleschke, A. Marhold, M. Schneider, A. Kolomeitsev and G. N. Roschenthaler, *Journal of Fluorine Chemistry*, 2004, **125**, 1031-1038.
233. V. R. Fantin, M. J. Berardi, L. Scorrano, S. J. Korsmeyer and P. Leder, *Cancer Cell*, 2002, **2**, 29-42.
234. R. Schwesinger, R. Link, P. Wenzl and S. Kossek, *Chemistry*, 2005, **12**, 438-445.
235. R. Noyori, I. Nishida and J. Sakata, *Tetrahedron Letters*, 1981, **22**, 3993-3996.
236. M. Henrich, A. Marhold, A. A. Kolomeitsev, N. Kalinovich and G. V. Roschenthaler, *Tetrahedron Letters*, 2003, **44**, 5795-5798.
237. G. M. Kosolapoff, *Organic Reactions*, 1951, **6**, 273-338.
238. H. R. Hudson, R. W. Matthews, M. McPartlin, M. A. Pryce and O. O. Shode, *Journal of the Chemical Society-Perkin Transactions 2*, 1993, 1433-1440.
239. H. R. Hudson, R. G. Rees and J. E. Weekes, *Journal of the Chemical Society-Perkin Transactions 1*, 1974, 982-985.
240. J. H. Finley, D. Z. Denney and D. B. Denney, *Journal of the American Chemical Society*, 1969, **91**, 5826-5831.
241. J. S. Cohen, *Journal of the American Chemical Society*, 1967, **89**, 2543-2547.
242. G. A. Olah, J. S. McIntyre, I. J. Bastien, W. S. Tolgyesi, E. B. Baker and J. C. Evans, *Journal of the American Chemical Society*, 1964, **86**, 1360-1373.
243. G. Hilgetag and H. Teichmann, *Chemische Berichte-Recueil*, 1963, **96**, 1465-1469.
244. M. J. H. Teichmann, G. Hilgetag, *Angewandte Chemie-International Edition*, 1967.
245. R. M. LV. Nesterev, *Tetrahedron Letters*, 1968.
246. E. S. Lewis and K. S. Colle, *Journal of Organic Chemistry*, 1981, **46**, 4369-4372.
247. C. Emnet, K. M. Weber, J. A. Vidal, C. S. Consorti, A. M. Stuart and J. A. Gladysz, *Advanced Synthesis & Catalysis*, 2006, **348**, 1625-1634.
248. J. A. Gladysz, I. T. Horvath and D. P. Curran, *Handbook of Fluorous Chemsitry*, Wiley-VCH, Weinham, 2004.
249. C. S. Consorti, M. Jurisch and J. A. Gladysz, *Organic Letters*, 2007, **9**, 2309-2312.
250. S. H. Hausner, C. A. F. Striley, J. A. Krause-Bauer and H. Zimmer, *Journal of Organic Chemistry*, 2005, **70**, 5804-5817.
251. M. Gonsior, I. Krossing, L. Muller, I. Raabe, M. Jansen and L. van Wullen, *Chemistry-a European Journal*, 2002, **8**, 4475-4492.
252. I. Krossing and I. Raabe, *Angewandte Chemie-International Edition*, 2004, **43**, 2066-2090.
253. C. J. Price, H.-Y. Chen, L. M. Launer and S. A. Miller, *Angewandte Chemie-International Edition*, 2009, **48**, 956-959.
254. K. B. Dillon, M. P. Nisbet and T. C. Waddington, *Polyhedron*, 1982, **1**, 123-127.
255. M. B. Gazizov, S. N. Ibragimov, D. B. Bagautdinova, R. F. Karimova, O. D. Khairullina and O. G. Sinyashin, *Doklady Chemistry*, 2008, **418**, 17-18.
256. J. E. Nycz and R. Musiol, *Heteroatom Chemistry*, 2006, **17**, 310-316.
257. V. Chauzov, *Žurnal obŝej himii* 1991, **61**, 2128.
258. F. H. Hu, L. S. Wang and S. F. Cai, *Journal of Chemical and Engineering Data*, 2010, **55**, 492-495.

259. N. A. Bondarenko, A. V. Kharlamov and A. G. Vendilo, *Russian Chemical Bulletin*, 2009, **58**, 1872-1885.
260. E. Evangelidou-Tsolis and R. Fausto, *Phosphorus and the Related Group V Elements* 1974, **4**, 121-127.
261. L. O. Muller, D. Himmel, J. Stauffer, G. Steinfeld, J. Slattery, G. Santiso-Quinones, V. Brecht and I. Krossing, *Angewandte Chemie-International Edition*, 2008, **47**, 7659-7663.
262. J. Mitra and C. Ramakrishnan, *International Journal of Peptide and Protein Research*, 1977, **9**, 27-48.
263. I. Krossing, *Journal of the Chemical Society-Dalton Transactions*, 2002, 500-512.
264. I. Krossing and I. Raabe, *Angewandte Chemie-International Edition*, 2001, **40**, 4406-4409.
265. N. Burford, P. J. Ragogna, R. McDonald and M. J. Ferguson, *Journal of the American Chemical Society*, 2003, **125**, 14404-14410.
266. A. H. Cowley and R. A. Kemp, *Chemical Reviews*, 1985, **85**, 367-382.
267. C. A. Dyker and N. Burford, *Chemistry-an Asian Journal*, 2008, **3**, 28-36.
268. M. H. Holthausen, C. Richter, A. Hepp and J. J. Weigand, *Chemical Communications*, 2010, **46**, 6921-6923.
269. J. J. Weigand, M. Holthausen and R. Froehlich, *Angewandte Chemie-International Edition*, 2009, **48**, 295-298.
270. J. Slattery, University of Bristol, 2005.
271. M. B. Abrams, B. L. Scott and R. T. Baker, *Organometallics*, 2000, **19**, 4944-4956.
272. N. J. Hardman, M. B. Abrams, M. A. Pribisko, T. M. Gilbert, R. L. Martin, G. J. Kubas and R. T. Baker, *Angewandte Chemie-International Edition*, 2004, **43**, 1955-1958.
273. C. A. Reed, *Accounts of Chemical Research*, 2010, **43**, 121-128.
274. T. Kato and C. A. Reed, *Angewandte Chemie-International Edition*, 2004, **43**, 2908-2911.
275. C. A. Reed, *Accounts of Chemical Research*, 1998, **31**, 133-139.
276. S. H. Strauss, *Chemical Reviews*, 1993, **93**, 927-942.
277. K. O. Christe, D. A. Dixon, D. McLemore, W. W. Wilson, J. A. Sheehy and J. A. Boatz, *Journal of Fluorine Chemistry*, 2000, **101**, 151-153.
278. N. Burford, T. S. Cameron, D. J. LeBlanc, P. Losier, S. Sereda and G. Wu, *Organometallics*, 1997, **16**, 4712-4717.
279. N. Burford, T. S. Cameron, P. J. Ragogna, E. Ocando-Mavarez, M. Gee, R. McDonald and R. E. Wasylishen, *Journal of the American Chemical Society*, 2001, **123**, 7947-7948.
280. N. Burford, P. Losier, P. K. Bakshi and T. S. Cameron, *Journal of the Chemical Society-Dalton Transactions*, 1993, 201-202.
281. N. Burford, P. Losier, S. V. Sereda, T. S. Cameron and G. Wu, *Journal of the American Chemical Society*, 1994, **116**, 6474-6475.
282. J. J. Weigand, N. Burford and A. Decken, *European Journal of Inorganic Chemistry*, 2008, 4343-4347.
283. H. Althaus, H. J. Breunig and E. Lork, *Chemical Communications*, 1999, 1971-1972.
284. C. Symmes and L. D. Quin, *Journal of Organic Chemistry*, 1978, **43**, 1250-1253.

285. A. J. Lupinetti and S. H. Strauss, *Chemtracts: Inorganic Chemistry*, 1998, **11**, 565-595.
286. I. Krossing and A. Reisinger, *Coordination Chemistry Reviews*, 2006, **250**, 2721-2744.
287. N. J. Patmore, C. Hague, J. H. Cotgreave, M. F. Mahon, C. G. Frost and A. S. Weller, *Chemistry-a European Journal*, 2002, **8**, 2088-2098.
288. E. Y. X. Chen and T. J. Marks, *Chemical Reviews*, 2000, **100**, 1391-1434.
289. J. C. W. Chien, W. M. Tsai and M. D. Rausch, *Journal of the American Chemical Society*, 1991, **113**, 8570-8571.
290. X. M. Yang, C. L. Stern and T. J. Marks, *Organometallics*, 1991, **10**, 840-842.
291. J. A. Ewen, *Catalyst Design for Tailor-Made Polyolefins*, 1994, **89**, 405-410.
292. L. Jia, X. M. Yang, A. Ishihara and T. J. Marks, *Organometallics*, 1995, **14**, 3135-3137.
293. Y. M. Sun, M. V. Metz, C. L. Stern and T. J. Marks, *Organometallics*, 2000, **19**, 1625-1627.
294. J. J. Eisch, S. I. Pombrik and G. X. Zheng, *Organometallics*, 1993, **12**, 3856-3863.
295. H. Bohnen, C. Fritze and F. Kuber *Compounds Having An Ionic Structure used as Constituent of An Olefin Polymerisation Catalyst*, 1999.
296. W. Leitner, M. Solinas, E. Janssen, G. Francio, P. Wasserscheid and A. Boesmann, *Abstracts of Papers of the American Chemical Society*, 2002, **224**, U630-U630.
297. S. M. Ivanova, B. G. Nolan, Y. Kobayashi, S. M. Miller, O. P. Anderson and S. H. Strauss, *Chemistry-a European Journal*, 2001, **7**, 503-510.
298. F. Kita, H. Sakata, S. Sinomoto, A. Kawakami, H. Kamizori, T. Sonoda, H. Nagashima, J. Nie, N. V. Pavlenko and Y. L. Yagupolskii, *Journal of Power Sources*, 2000, **90**, 27-32.
299. V. Aravindan, J. Gnanaraj, S. Madhavi and H. K. Liu, *Chemistry-a European Journal*, 2011, **17**, 14326-14346.
300. J. van den Broeke, B. J. Deelman and G. van Koten, *Tetrahedron Letters*, 2001, **42**, 8085-8087.
301. K. Fujiki, J. Ichikawa, H. Kobayashi, A. Sonoda and T. Sonoda, *Journal of Fluorine Chemistry*, 2000, **102**, 293-300.
302. A. G. Massey and A. J. Park, *Journal of Organometallic Chemistry*, 1964, **2**, 245-250.
303. J. H. Golden, P. F. Mutolo, E. B. Lobkovsky and F. J. Disalvo, *Inorganic Chemistry*, 1994, **33**, 5374-5375.
304. J. M. Zhou, S. J. Lancaster, D. A. Walker, S. Beck, M. Thornton-Pett and M. Bochmann, *Journal of the American Chemical Society*, 2001, **123**, 223-237.
305. R. E. LaPointe, G. R. Roof, K. A. Abboud and J. Klosin, *Journal of the American Chemical Society*, 2000, **122**, 9560-9561.
306. D. Vagedes, G. Erker and R. Frohlich, *Journal of Organometallic Chemistry*, 2002, **641**, 148-155.
307. M. Bochmann, *Coordination Chemistry Reviews*, 2009, **253**, 2000-2014.
308. S. J. Lancaster, A. Rodriguez, A. Lara-Sanchez, M. D. Hannant, D. A. Walker, D. H. Hughes and M. Bochmann, *Organometallics*, 2002, **21**, 451-453.
309. E. Bernhardt, G. Henkel, H. Willner, G. Pawelke and H. Burger, *Chemistry-a European Journal*, 2001, **7**, 4696-4705.

310. D. J. Brauer, H. Burger, Y. Chebude and G. Pawelke, *Inorganic Chemistry*, 1999, **38**, 3972-3977.
311. G. Pawelke and H. Burger, *Coordination Chemistry Reviews*, 2001, **215**, 243-266.
312. M. Finze, E. Bernhardt, A. Terheiden, M. Berkei, H. Willner, D. Christen, H. Oberhammer and F. Aubke, *Journal of the American Chemical Society*, 2002, **124**, 15385-15398.
313. E. Bernhardt, M. Finze, H. Willner, C. W. Lehmann and F. Aubke, *Angewandte Chemie-International Edition*, 2003, **42**, 2077-2079.
314. V. V. Bardin, S. G. Idemskaya and H. J. Frohn, *Zeitschrift Fur Anorganische Und Allgemeine Chemie*, 2002, **628**, 883-890.
315. H. J. Frohn, N. Y. Adonin, V. V. Bardin and V. F. Starichenko, *Journal of Fluorine Chemistry*, 2002, **117**, 115-120.
316. H. J. Frohn and V. V. Bardin, *Zeitschrift Fur Anorganische Und Allgemeine Chemie*, 2002, **628**, 1853-1856.
317. H. J. Frohn and V. V. Bardin, *Journal of Fluorine Chemistry*, 2003, **123**, 43-49.
318. N. Y. Adonin, V. V. Bardin and H. J. Frohn, *Organometallics*, 2004, **23**, 535-539.
319. L. A. Shundrin, V. V. Bardin and H. J. Frohn, *Zeitschrift Fur Anorganische Und Allgemeine Chemie*, 2004, **630**, 1253-1257.
320. V. V. Bardin, N. Y. Adonin and H. J. Frohn, *Organometallics*, 2005, **24**, 5311-5317.
321. N. Y. Adonin, H.-J. Frohn and V. V. Bardin, *Organometallics*, 2007, **26**, 2420-2425.
322. K. Shelly, C. A. Reed, Y. J. Lee and W. R. Scheidt, *Journal of the American Chemical Society*, 1986, **108**, 3117-3118.
323. Z. W. Xie, T. Jelinek, R. Bau and C. A. Reed, *Journal of the American Chemical Society*, 1994, **116**, 1907-1913.
324. Z. W. Xie, J. Manning, R. W. Reed, R. Mathur, P. D. W. Boyd, A. Benesi and C. A. Reed, *Journal of the American Chemical Society*, 1996, **118**, 2922-2928.
325. C. A. Reed, *Accounts of Chemical Research*, 1998, **31**, 325-332.
326. Y. Zhang, F. S. Tham and C. A. Reed, *Inorganic Chemistry*, 2006, **45**, 10446-10448.
327. D. Stasko and C. A. Reed, *Journal of the American Chemical Society*, 2002, **124**, 1148-1149.
328. T. Kato, E. Stoyanov, J. Geier, H. Grutzmacher and C. A. Reed, *Journal of the American Chemical Society*, 2004, **126**, 12451-12457.
329. Y. Zhang and C. A. Reed, *Dalton Transactions*, 2008, 4392-4394.
330. M. G. Fete, Z. Havlas and J. Michl, *Journal of the American Chemical Society*, 2011, **133**, 4123-4131.
331. D. M. Vanseggen, P. K. Hurlburt, M. D. Noirot, O. P. Anderson and S. H. Strauss, *Inorganic Chemistry*, 1992, **31**, 1423-1430.
332. H. P. A. Mercier, J. C. P. Sanders and G. J. Schrobilgen, *Journal of the American Chemical Society*, 1994, **116**, 2921-2937.
333. T. S. Cameron, I. Krossing and J. Passmore, *Inorganic Chemistry*, 2001, **40**, 4488-4490.
334. D. M. Vanseggen, P. K. Hurlburt, O. P. Anderson and S. H. Strauss, *Inorganic Chemistry*, 1995, **34**, 3453-3464.

335. K. Moock and K. Seppelt, *Zeitschrift Fur Anorganische Und Allgemeine Chemie*, 1988, **561**, 132-138.
336. A. Bihlmeier, M. Gonsior, I. Raabe, N. Trapp and I. Krossing, *Chemistry-a European Journal*, 2004, **10**, 5041-5051.
337. T. S. Cameron, A. Decken, I. Dionne, M. Fang, I. Krossing and J. Passmore, *Chemistry-a European Journal*, 2002, **8**, 3386-3401.
338. I. Krossing and A. Reisinger, *Angewandte Chemie-International Edition*, 2003, **42**, 5919-5919.
339. T. J. Barbarich, S. T. Handy, S. M. Miller, O. P. Anderson, P. A. Grieco and S. H. Strauss, *Organometallics*, 1996, **15**, 3776-3778.
340. I. Raabe, K. Wagner, K. Guttsche, M. Wang, M. Graetzel, G. Santiso-Quinones and I. Krossing, *Chemistry-a European Journal*, 2009, **15**, 1966-1976.
341. T. Drews, S. Seidel and K. Seppelt, *Angewandte Chemie-International Edition*, 2002, **41**, 454-456.
342. S. Seidel and K. Seppelt, *Science*, 2000, **290**, 117-118.
343. I. C. Hwang and K. Seppelt, *Angewandte Chemie-International Edition*, 2001, **40**, 3690-3693.
344. R. Schmutzler, *Journal of the Chemical Society*, 1964, 4551-4557.
345. D. U. Robert, G. N. Flatau, A. Cambon and J. G. Riess, *Tetrahedron*, 1973, **29**, 1877-1885.
346. D. H. Brown, K. D. Crosbie, G. W. Fraser and D. W. A. Sharp, *Journal of the Chemical Society a -Inorganic Physical Theoretical*, 1969, 872-875.
347. G. V. Roschenthaler, *Angewandte Chemie-International Edition in English*, 1977, **16**, 862-862.
348. T. Kubota, K. Yamamoto and T. Tanaka, *Chemistry Letters*, 1983, 167-168.
349. C. Lichtenberg, M. Elfferding and J. Sundermeyer, *European Journal of Inorganic Chemistry*, 2010, 3117-3124.
350. G. A. Bowmaker, A. Camus, B. W. Skelton and A. H. White, *Journal of the Chemical Society-Dalton Transactions*, 1990, 727-731.
351. T. Koga and H. Kobayashi, *Journal of Chemical Physics*, 1985, **82**, 1437-1439.
352. P. Pulay, *Chemical Physics Letters*, 1980, **73**, 393-398.
353. P. Csaszar and P. Pulay, *Journal of Molecular Structure*, 1984, **114**, 31-34.
354. R. Ahlrichs, M. Bar, M. Haser, H. Horn and C. Kolmel, *Chemical Physics Letters*, 1989, **162**, 165-169.
355. O. Treutler and R. Ahlrichs, *Journal of Chemical Physics*, 1995, **102**, 346-354.
356. M. von Arnim and R. Ahlrichs, *Journal of Chemical Physics*, 1999, **111**, 9183-9190.
357. F. Weigend, *Physical Chemistry Chemical Physics*, 2006, **8**, 1057-1065.
358. K. Eichkorn, O. Treutler, H. Ohm, M. Haser and R. Ahlrichs, *Chemical Physics Letters*, 1995, **240**, 283-289.
359. P. Deglmann and F. Furche, *Journal of Chemical Physics*, 2002, **117**, 9535-9538.
360. P. Deglmann, F. Furche and R. Ahlrichs, *Chemical Physics Letters*, 2002, **362**, 511-518.
361. P. Deglmann, K. May, F. Furche and R. Ahlrichs, *Chemical Physics Letters*, 2004, **384**, 103-107.